

ICCT

INTERNATIONAL CONFERENCE
ON CHEMICAL TECHNOLOGY

9. mezinárodní chemicko-technologická konference 9th International Conference on Chemical Technology

25. – 27. 4. 2022
Mikulov, Czech Republic

www.icct.cz

proceedings



MAIN PARTNER



SPONSORS



MEDIA PARTNERS

Chemické listy

CHEMAGAZÍN

Proceedings of the 9th International Conference on Chemical Technology

1st edition, October 2022

EDITORS

Martin Veselý

University of Chemistry and Technology, Prague
Technická 5
166 28 Prague 6, Czech Republic

Zdeněk Hrdlička

University of Chemistry and Technology, Prague
Technická 5
166 28 Prague 6, Czech Republic

Jiří Hanika

Institute of Chemical Process Fundamentals of the CAS, Prague
Rozvojová 1/135
165 02 Prague 6, Czech Republic

Jaromír Lubojacký

Jistebník 242
742 82 Jistebník, Czech Republic

All communications submitted were duly reviewed by the scientific committee.

PUBLISHED AND DISTRIBUTED BY

Czech Society of Industrial Chemistry
Novotného Lávká 5
116 68 Prague, Czech Republic

in cooperation with
Czech Chemical Society
Novotného Lávká 5
116 68 Prague, Czech Republic

ISBN 978-80-88307-11-2

Copyright © 2022 Czech Society of Industrial Chemistry

SCIENTIFIC COMMITTEE

Assoc. Prof. Ing. Jaromír Lederer, Ph.D. | UniCRE Litvínov (President)
Prof. Ing. Jiří Hanika, Ph.D. | ICPF of the CAS, Prague (Vice-President)
Prof. Dr. Ing. Karel Bouzek | UCT Prague
Assoc. Prof. Ing. Tomáš Hlinčík, Ph.D. | UCT Prague
Prof. Ing. Milan Hronec, Ph.D. | STU Bratislava
Prof. Ing. Ľudovít Jelemenský, Ph.D. | STU Bratislava
Prof. Ing. Tomáš Jirout, Ph.D. | CTU in Prague
Prof. Ing. Jan John, Ph.D., FJFI, CTU in Prague
Prof. Ing. Petr Kalenda, Ph.D. | FCHT University of Pardubice
Assoc. Prof. Ing. Milan Králik, Ph.D. | VUChT Bratislava
Prof. Flavia Marinelli | University of Insubria, Varese, Italy
Dr. Agustín Martínez | Universidad Politécnica de Valencia
Prof. Ing. Petr Mikulášek, Ph.D. | FCHT University of Pardubice
Ing. Jozef Mikulec, Ph.D. | VÚRUP Bratislava
Prof. Dimitry Murzin | Åbo Akademi University, Turku, Finland
Prof. Ing. Lucie Obalová, Ph.D. | VŠB TU Ostrava
Prof. Ing. Josef Pašek, Ph.D. | UCT Prague
Prof. Dr. Ing. Petra Patáková | UCT Prague
Ing. Ivan Souček, PhD. | Association of Chemical Industry of the Czech Republic
Prof. Ing. Ján Šajbidor, Ph.D. | FCHPT STU Bratislava
Prof. RNDr. Pavel Šajgalík, DrSc. | Slovak Academy of Sciences, Bratislava
Prof. RNDr. Jitka Ulrichová, Ph.D. | UP Olomouc
Prof. Ing. Kamil Wichterle, Ph.D. | VŠB TU Ostrava
Prof. Ing. Petr Zámstný, Ph.D. | UCT Prague

PROGRAM COMMITTEE

Ing. Jaromír Lubojacký, MBA | Ixa Consulting Jistebník (President)
Assoc. Prof. Ing. Jaromír Lederer, Ph.D. | UniCRE Litvínov (Vice-President)
Prof. Ing. Jiří Hanika, Ph.D. | ICPF of the CAS, Prague (Vice-President, Best Poster Award)
Prof. Ing. Petr Zámstný, Ph.D. | UCT Prague (Petrochemicals and Organic Technology)
Assoc. Prof. Ing. Jaromír Lederer, Ph.D. | UniCRE Litvínov (Gas, Coal, Fuel)
Prof. Dr. Ing. Karel Bouzek | UCT Prague (Inorganic Technology)
Prof. Dr. Ing. Petra Patáková | UCT Prague (Biotechnology)
Ing. Barbora Branská, Ph.D. | UCT Prague (Biotechnology)
Prof. RNDr. Bohumil Kratochvíl, DSc. | UCT Prague (Pharmaceutical Technology)
Prof. Ing. Kamila Kočí, Ph.D. | VŠB TU Ostrava (Waste Processing, Air and Water Protection, Technologies for the Decontamination of Soils)
Prof. Ing. Lucie Obalová, Ph.D. | VŠB TU Ostrava (Waste Processing, Air and Water Protection, Technologies for the Decontamination of Soils)
Prof. Dr. Ing. Dalibor Vojtěch | UCT Prague (Material Engineering)
Assoc. Prof. Ing. Pavel Novák, Ph.D. | UCT Prague (Material Engineering)
Ing. Ivan Souček, PhD. | Association of Chemical Industry of the Czech Republic (Economy of Chemical Industry)
Prof. Ing. Tomáš Jirout, Ph.D. | CTU in Prague (Chemical Processes and Devices)
Ing. Hugo Kittel, Ph.D., MBA | UCT Prague (Oil, Petrochemicals, Biofuels)
Assoc. Prof. Ing. Antonín Kuta, Ph.D. | UCT Prague (Polymers, Composites)

CONTENTS

OIL, PETROCHEMICALS, BIOFUELS

INFLUENCE OF PYROLYSIS OIL FROM PLASTICS ON PRODUCT STRUCTURE IN FLUID CATALYTIC CRACKING

Pšenička M., Vráblik A., Vondrášková K.

PYROLYSIS OF PLASTICS: DEHALOGENATION VIA STEPWISE PYROLYSIS AND METAL SORBENTS

Hubáček J., Lederer J., Kuráň P., Kašpárek A.

CARBON CAPTURE IN STEAM METHANE REFORMING THROUGH TECHNO-ECONOMIC, SAFETY AND ENVIRONMENTAL OPTICS

Janošovský J., Šandor R., Mišún P., Řežucha M., Jelemenský L.

THE FUTURE OF JET FUEL AS AN IMPORTANT REFINERY PRODUCT

Kittel H., Horský J.

EMPIRICAL MODEL FOR PREDICTION OF VISBREAKING PRODUCT YIELDS

Jíša P., Černý R.

COMPREHENSIVE MULTI-CRITERIA PROCESS DESIGN METHODOLOGY

Kraviarová D., Janošovský J.

GAS, COAL, FUEL

C3MR LNG PROCESS OPTIMIZATION: AN ENVIRO-ECONOMIC STUDY

Furda P., Variny M.

C3MR LNG PROCESS OPTIMIZATION: PARALLEL GENETIC ALGORITHM INTERFACE

Furda P., Variny M.

CO-FIRING MULTIPLE FUELS IN VOJANY THERMAL POWER PLANT

Variny M., Stričík M., Štofová L.

RCAT SHORT-TERM AGEING OF BITUMINOUS BINDERS IN PRESENCE OF MASTIC

Matoušek L., Jíša P., Černý R.

CONCEPTUAL DESIGN OF GASIFIER PROCESSING HEAVY OIL FRACTIONS

Podolský S., Variny M.

ENERGY AND ENVIRONMENTAL ASPECTS OF INDUSTRIAL HEAT SAVING IN VARIOUS SITUATIONS

Variny M., Kšiňanová M., Furda P.

MATERIAL ENGINEERING

MINERAL ADMIXTURES REACTIVITY DETERMINATION

Šídllová M., Doležal T., Šulc, R.², Pulcová K.

THERMAL INSULATION COMPOSITE BLOCKS BASED ON GEOPOLYMER

Kohout J., Soukup A., Kohoutová E., Koutník P., Hájková P.

PROPERTIES OF HYDRAULIC BINDER PREPARED FROM METAKAOLIN, ANHYDRITE AND LIME

Šulc R., Škvára F., Šídllová M., Trefný J., Králová K., Pulcová K., Formáček P.

INFLUENCE OF THE ADDITION OF VARIOUS TYPES OF MINERAL ADMIXTURES ON THE ALKALI-SILICA REACTION IN CONCRETE

Šídlová M., Mauermann L., Šulc R., Pulcová K.

ANALYSIS OF ECOLOGICAL ENERGETIC MATERIALS

Olšovský M., Budzák Š., Krištof M., Kuna P.

DETERMINATION OF THE OPTIMAL COMPOSITION OF THE NEW HYDRAULIC BINDER PREPARED FROM METAKAOLIN, ANHYDRITE AND LIME

Pulcová K., Šídlová M., Šulc R., Škvára F., Kohoutková M., Sedlářová I.

POROSITY OF DIFFERENT ROCKS IN RELATION TO CAPTURING/MOVING OF GASES AND LIQUIDS

Římnáčová D., Vöröš D., Natherová V., Příkryl R., Lokajíček T.

ORGANIC TECHNOLOGY

REDUCTION OF 3-PHENYLPROPANOIC ACID

Kotova M., Mušková J., Vyskočilová E., Červený L.

A METHOD FOR PRE-TREATMENT OF WASTE PLASTIC PYROLYSIS OIL ALLOWING THE EVALUATION BY PYROLYSIS GAS CHROMATOGRAPHY

Le T.A., Karaba A., Patera J., Zámotný P.

PYRIDINIUM-BASED CATALYST FOR α -PINENE OXIDE ISOMERIZATION

Zítová K., Bulavina V., Vyskočilová E.

CE-MODIFIED BETA ZEOLITES AS CATALYSTS FOR B-PINENE OXIDE ISOMERIZATION

Paterová I., Gorlova O., Příbylová P., Červený L.

REDUCED SENSITIVITY RDX AND HMX CRYSTALLIZED AND SPHERIODIZED IN PROPYLENE CARBONATE

Skácel R., Šabach J., Zikmundová M., Kožená V., Kubíček M., Fryš O.

STUDY OF SPECIFIC PROPERTIES OF COBALT CATALYST FOR APPLYING IN A NEW LARGE-SCALE CAPACITY UNIT FOR THE CYCLOHEXYLAMINE PRODUCTION

Valeš R., Krupka J.

POLYMERS, COMPOSITES

GOALS AND CHALLENGES OF RUBBER SUSTAINABILITY

Brejcha J., Hrdlička Z., Krmela J., Beneš L., Hittlová M.

ALTERNATIVE BIO-BASED PLASTICIZERS FOR RUBBER INDUSTRY

Hrdlička Z., Brejcha J., Hittlová M., Alexová C.

MATERIALS RECYCLING IN THE PRODUCTION OF POROUS POLYMERIC MOLDS

Pokorný J., Motýčková J., Riedelová K., Sedlářová I., Urbánek J., Blažek Z.

PREPARATION OF STRONG CATION EXCHANGE RESIN ON THE BASE OF STYRENE – DIVINYLBENZENE COPOLYMER FOR WATER TREATMENT

Skálová H., Jelínek L., Štěpánková Z.

PREPARATION AND POTENTIAL APPLICATIONS OF LIGNIN-BASED NANOSYSTEMS

Maršík D., Thoresen P.P., Kulišová M., Masák J., Rova U., Christakopoulos P., Matsakas L.

SINTERING OF PTFE-PEEK POLYMER BLEND IN AIR ATMOSPHERE

Melichar J., Foitlová A., Mészáros M., Steiner V.

ECONOMICS OF CHEMICAL INDUSTRY

THE ACCOMPLISHMENT OF THE DIGITAL WELL-BEING IN COMPANIES

Botek M., Charvátová D., Dvořáková Z.

IMPORTANCE OF AN ECO-LABEL FOR THE CUSTOMER

Branská L., Paták M., Pecinová Z., Kocmanova A.

DECENT WORK IN THE GREEN ECONOMY

Dvorakova Z., Polents I.

MODELLING STEAM METHANE REFORMER OPERATION WITH HYDROGEN-ENRICHED FEEDSTOCK

Hoppej D., Variny M., Kondáš R.

CHANGES IN MANAGING HUMAN RESOURCES IN THE POST COVID ERA IN THE CZECH REPUBLIC

Charvatova D., Botek M.

CAPACITY CALCULATIONS USING QUANTITATIVE METHODS IN CHEMICAL OPERATIONAL MANAGEMENT

Kostalek J., Kotatkova Stranska P.

MATHEMATICAL MODELING OF HEAT AND MASS TRANSFER IN A ROTARY KILN

Kozakovic M., Cada J., Kokavcova A., Havlica J., Huchet F.

CONSUMER BEHAVIOUR IN THE GERMAN BREAD MARKET

Kutnohorská O., Strachotová D.

PRODUCTIVE ECONOMIC VIEW OF THE BAKERY INDUSTRY

Strachotová D., Kutnohorská O.

USE OF DIGITIZATION IN CHEMICAL ENTERPRISES

Vávra J., Spáčil P., Bakeš O.

LOWERING THE ENERGY AND WATER FOOTPRINT OF A LAUNDRY FACILITY

Čížmár M., **Variny M.**

SELECTED OPTIONS TO INCREASE THE EFFICIENCY OF A STEAM METHANE REFORMER

Hoppej D., Variny M., Kondáš R.

ASSESSING VARIANTS OF LOW-GRADE HEAT VALORIZATION IN THE REFINING INDUSTRY

Rybár P., **Variny M.**

THE DYNAMICS OF THE PRODUCTION OF THERMAL INSULATION MATERIALS USED IN THE CONSTRUCTION INDUSTRY

Vytlačil D.

SYNTHESIS AND PRODUCTION OF DRUGS

TECHNOLOGY TRANSFER FOR THE DRY GRANULATION PROCESS AIMING AT KEEPING IDENTICAL RIBBON PROPERTIES

Petr J., Zamostný P., Stasiak P.

EFFECT OF THE MIXING STRATEGY ON THE UNIFORMITY OF POWDER MIXTURES FOR DIRECT COMPRESSION

Römerová S., Novák D., Zámotný P.

PREDICTING BULK DENSITY OF BINARY POWDER MIXTURES FROM PURE COMPONENT PROPERTIES

Komínová P., Smrčka D., Gajdošová M., Zámotný P.

SOLID DISPLACEMENT METHOD TO DETERMINE ENVELOPE DENSITY OF ROLLER COMPACTED RIBBONS

Marinko N., Zámotný P., Gajdošová M.

DRUGS PRODUCTION BY UNIAXIAL COMPACTION OF POWDER MATERIAL

Peciar P., Gušťařík A., Jezsó K., Fekete R., Peciar M.

DETERMINATION OF HANSEN SOLUBILITY PARAMETERS OF BINARY MIXTURES OF POLYMERS

Petříková E., Čerňová M., Adamska K., Voelkel A., Dammer O., Krejčík L., Patera J.

EFFECT OF POWDER PROPERTIES AND COMPACTION PRESSURE ON PARTICLE SIZE OF ROLL-COMPACTED GRANULATE

Švehla O., Zámotný P.

WASTE TREATMENT, WATER PROTECTION

ONE-STEP DIRECT CATALYTIC SEWAGE SLUDGE LIQUEFACTION OVER A SULFIDED METAL CATALYST

Hidalgo Herrador J.M., Babor M., Brablíková M., Moghaddam M.A., Vráblík A.

CHEMICAL PRETREATMENT OF INDUSTRIAL LIGNIN BY DISSOLVING IN ORGANIC SOLVENTS

Kafková V., Ondrejčíková P., Hruška M.

POSSIBILITIES OF HYDRODEBROMINATION OF BROMINATED AROMATIC COMPOUNDS USING Cu-BASED CATALYSTS

Kamenická B., Weidlich T.

BIOTECHNOLOGY AND BIOREFINERY

OPTIMIZATION OF CULTIVATIONS OF CAROTENOGENIC YEASTS ON POULTRY WASTE SUBSTRATES

Holub J., Chujanov O., Szotkowski M., Šimanský S., Schildová V., Dzurická L., Márová I.

STABILITY AND ANTIOXIDANT ACTIVITY OF MONASCUS PIGMENTS IN COMPLEX RED YEAST RICE EXTRACTS

Husakova M., Patakova P.

GENOMIC AND FUNCTIONAL ANALYSIS OF POLYHYDROXYALKANOATES PRODUCER *RHODOSPIRILLUM RUBRUM* DSM 467

Jureckova K., Nykrynova M., Slaninova E., Bezdicek M., Obruca S., Skutkova H., Sedlar K.

DIVERSITY OF SCHLEGELELLA THERMODEPOLYMERANS REVEALED WITH NANOPORE SEQUENCING

Sedlar K., Musilova J., Kourilova X., Bezdicek M., Obruca S.

OPTIMIZATION OF EXTRACTION, PURIFICATION AND STABILIZATION OF BIOLOGICALLY ACTIVE COMPOUNDS FROM YEAST AND MICROALGAE BIOMASS

Šimanský S., Szotkowski M., Holub J., Obračaj H., Dzurická L., Schildová V., Márová I.

DETERMINATION OF METHODOLOGY FOR MONITORING BIOFILM FORMATION OF FILAMENTOUS MICROSCOPIC FUNGI

Kulišová M., Kolouchová I.

SIDEROPHORES – THE ACTIVE COMPONENT OF THE BIOPESTICIDE PREPARATION

Mach J., Halecký M.

ANTIMICROBIAL ACTIVITY OF SILVER NANOPARTICLES PREPARED BY GREEN APPROACH

Miškovská A., Čejková A.

CHEMICAL PROCESSES AND DEVICES

THE VERIFICATION OF MATERIAL FLOW IN A BREWERY MALT TANK USING THE DEM METHOD

Likavčan A., Peciar M., Peciar, P.

INORGANIC TECHNOLOGY

DIFFERENCES IN COMPOSITION OF NAPLES YELLOW AND SYNTHESIS OF ITS MAIN PHASES

Dohnalová Ž., Luxová J., Šulcová P., Šefců R., Antušková V.

OIL, PETROCHEMICALS, BIOFUELS

INFLUENCE OF PYROLYSIS OIL FROM PLASTICS ON PRODUCT STRUCTURE IN FLUID CATALYTIC CRACKING

Pšenička M.¹, Vráblik A.¹, Vondrášková K.¹

¹ORLEN UniCRE, Revoluční 1521/84, 400 01 Ústí nad Labem, Czech Republic
Martin.Psenicka@orlenunicre.cz, Ales.Vrablik@orlenunicre.cz

Abstract

The chemical recycling is currently a very hot topic. In this respect, the possibility of using oils from the pyrolysis of waste plastics for petrochemical production is often discussed and studied. The most problematic from this point of view is the processing of the distillation fraction above 280 °C. One option is to use this fraction as a component for co-processing on fluid catalytic cracking (FCC) technology. However, some specific properties of this alternative component could be very problematic. In particular the content of nitrogen, oxygen and polyaromatics compounds. This can have a negative effect on the yields as well as life cycle of the FCC catalyst. Therefore, the aim of this work was to determine the effect of adding pyrolysis oil to the standard feedstock in the level of 10 and 20 wt%. The comparison of the obtained yield structures was performed in the laboratory scale using the ACE[®] R+MM unit. The possibility of eliminating the negative properties of pyrolysis oil was also tested. The addition of hydrocracked vacuum distillate (HCVD) was studied for this purpose. The negative effect of the addition of pyrolysis fraction on the yields of the required product was confirmed. On the other hand, a very positive role of HCVD addition was found. This fact can help process of problematic materials, especially from the economic point of view.

Introduction

The European Union is working to reduce greenhouse gas emissions in the fight against climate change. All EU countries are set to be climate neutral by 2050¹. They consider the production of greenhouse gases, especially CO₂, to be the main reason. A comparison of CO₂ emissions between thermolytic treatment and incineration of mixed waste plastics shows that CO₂ production from waste incineration is approximately doubled. Thermolytic treatment of waste, especially plastics, leads not only to savings in greenhouse gas production, but also to a lower burden on the natural environment by landfilling. Last but not least, natural resources are being saved. The quality of sorted waste plastic pyrolysis oils often achieves very good properties, from which monomers can again be produced in the required quality. In addition, with the nickname "recycled". Pyrolysis oil from unsorted waste may contain substances from contaminated packaging. Mainly from plant and animal products.

Pyrolysis is therefore the best process for processing plastics waste (and biodegradable plastics). Gaseous, liquid and solid products can be obtained by pyrolysis^{2,3}. The most valuable of the pyrolysis products is its liquid phase. The pyrolysis oil produced can be used for fuel production or other co-processing in units in the petrochemical and refining industries. Due to the different quality of the input material, the quality of the products also changes and therefore its price cannot simply be calculated. There are several ways to increase a quality of product for the best final price. By using the FCC catalyst already in the pyrolysis of plastics, the proportion of gasoline in the pyrolysis oil itself is higher and thus the price for this desired material increases.^{4,5} In terms of processing on FCC technology, this may prove appropriate. The treatment of recycled low-density polyethylene plastic waste on an FCC riser simulator revealed higher material conversion and higher gasoline production. In this case, however, it is a pure raw material, which is more suitable for using in the petrochemical processes. In the case of a raw material with the required properties, the addition of HCVD can be used to the raw material⁶. HCVD is standardly used in refineries as a raw material to dilute process raw materials. It reduces the negative impact of non-standard oils so that they can be processed without a significant impact on technology. It is a particularly high quality raw material and there is no purpose to add it in too much excess. Using the ACE unit, the minimum amount required to eliminate the side effects of the "bad" raw material can be determined. However, the biggest advantage of co-processing pyrolysis oil in FCC units is the effort to minimize investment costs for the refurbishment or construction of new refinery units. The next phase of testing pyrolysis oils must therefore take place on pilot units to determine the effect of the particular plastic pyrolysis oil available on the required product yield structure and whether the processing of such material is cost-effective. The ACE unit is used for this purpose.

Experimental

Materials and methods

For the purposes of this testing, real feedstock materials used for processing on FCC technology at the Kralupy nad Vltavou refinery (KPY) were used. This is the FCC reference feedstock (reference, R), distillation residue from the atmospheric distillation of West Texas Medium crude oil. Hydrocracked distillation residue from crude oil IB REB and CPC 70:30 (HCVD), is used to improve FCC feedstock performance when processing substandard oil. In our case, the addition of pyrolysis oil from the pyrolysis of unsorted plastics with a distillation cut above 280 °C (WPPO 280) will be tested. The catalyst used for the tests is an equilibrium FCC catalyst taken from the operating unit in KPY. Analyzes of used raw materials and products were performed - Density (EN ISO 12185), Total nitrogen (ASTM D 4629), Total sulphur (ASTM D 5453), Simdist (ASTM D 2887), MCRT (ASTM D 4530), GC – RGA (ASTM D 7833), Metals content (EN ISO 11885), Content C, H, S (ISO 29541, EN 15104), water content (ISO 12937), Chlorine content (ASTM D7536), SARA (IP 469). Simdis, GC-RGA and SERVOPRO 1440D for coke production are used to evaluate the products. Tests of the effect of WPPO 280 addition were performed on an ACE® R + MM laboratory unit, which is used to simulate the FCC process, including the fluidized bed. The results of distillation analyzes are shown in Figure 1a, aromates in figure 1b and other analyzes of feedstocks are shown in Table I. In Figure 1a can be seen, that distillation curves of WPPO 280 and HCVD are lighter than reference feedstock. It should be precursor for making lighter fraction like gasoline.

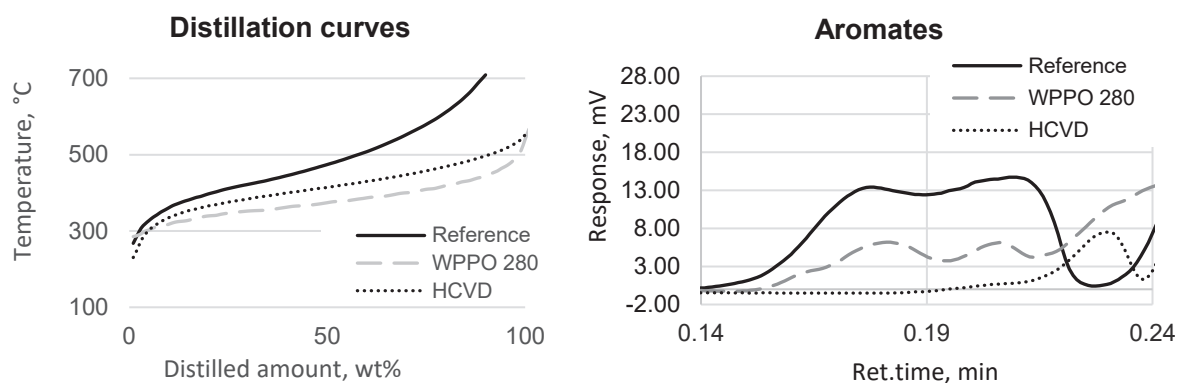


Figure 1a. Distillation curves, 1b. Aromates

Table 1
Properties of used input raw materials and their mixtures

	R	WPPO >280 °C	HCVD	R+ 10 wt% WPPO 280	R + 20 wt% WPPO 280	R + 10 wt% WPPO 280 + 10 wt% HCVD	R + 20 wt% WPPO 280 + 20 wt% HCVD
Density@15°C (kg·m ³)	918.2	876.7	847.7	914.1	909.9	907.0	895.8
Aromates (wt%)	39.9	17.2	8.9	37.6	35.4	34.5	29.2
Asphaltenes (wt%)	3.3	0.5	0.4	3.0	2.7	2.7	2.2
Saturated (wt%)	47.5	54.6	89.9	48.2	48.9	52.5	57.4
Resins (wt%)	10.0	27.7	0.9	11.8	13.5	10.9	11.7
Chlorine (mg·kg ⁻¹)	<0.1	4.0	<0.1	0.4	0.8	0.4	0.8
Sodium (mg·kg ⁻¹)	0.4	<0.1	<0.1	0.4	0.3	0.3	0.2
Calcium (mg·kg ⁻¹)	0.7	0.1	0.1	0.6	0.6	0.6	0.5
Iron (mg·kg ⁻¹)	4.6	0.8	1.0	4.2	3.8	3.9	3.1
Vanadium (mg·kg ⁻¹)	1.5	<0.1	<0.1	1.4	1.2	1.2	0.9

	R	WPPO >280 °C	HCVD	R+ 10 wt% WPPO 280	R + 20 wt% WPPO 280	R + 10 wt% WPPO 280 + 10 wt% HCVD	R + 20 wt% WPPO 280 + 20 wt% HCVD
Nickel (mg·kg ⁻¹)	5.5	<0.1	<0.1	5.0	4.5	4.4	3.3
Sulphur (mg·kg ⁻¹)	4900	177	12	4428	3955	3939	2978
Nitrogen (mg·kg ⁻¹)	993	10200	1.0	1914	2834	1815	2663
Carbon (wt%)	86.8	83.9	86.8	86.5	86.2	86.5	86.2
Hydrogen (wt%)	12.6	12.6	13.2	12.6	12.6	12.7	12.7
Oxygen (wt%)	<0.1	2.5	<0.1	0.3	0.5	0.2	0.5
C / H	6.9	6.7	6.6	6.9	6.8	6.8	6.8
Water (mg·kg ⁻¹)	<1	200	79	20	40	28	56
MCRT (wt%)	3.5	0.3	<0.1	3.2	2.9	2.8	2.2

Table I lists the properties of the materials used and their laboratory-prepared mixtures. From the point of view of the density of substances, the density decreases in the direction R > WPPO 280 > HCVD. The amount of aromates in the raw material decreases in the same direction as the density and is also one of the indicators of possible increased coke formation. The content of saturated substances, on the other hand, increases in the direction R > WPPO 280 > HCVD. The metal content of WPPO 280 and HCVD is similar and lower than the reference raw material. After the feedstocks were prepared, the test conditions were set according to the FCC operating unit.

Test conditions are: reaction temperature 536 °C, preheating of the feedstock material 90 °C, C/O ratio: 9.0; 7.5; 6.0; 4.5; 3.0. Catalyst loading is for each C/O 9.0 grams, so feedstock injection is 1.0; 1.2; 1.5; 2.0; 3.0 grams.

The testing was performed on an advanced laboratory unit ACE® R+MM, which provides data on testing equilibrium FCC catalysts to determine the conversion, or to test possible alternative raw materials possible for processing on FCC technology. The layout of the ACE unit is shown in Figure 2.

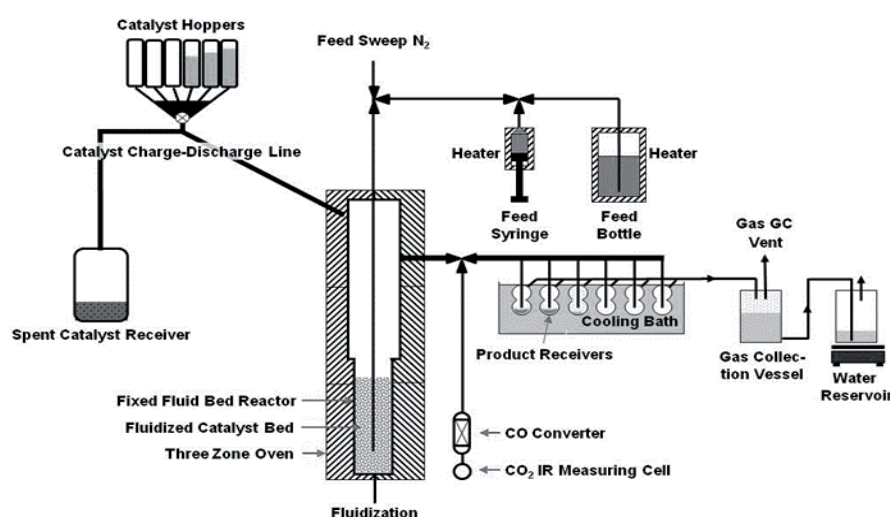


Figure 2. ACE unit diagram

Results and discussion

Figure 3 shows a graphical representation of the feedstock material conversion as a function of the C/O ratio. It can be seen that with the increasing addition of only WPPO 280, the conversion and thus the yields of the desired products decrease. With the increasing addition of WPPO 280 along with HCVD, the conversion increases. To achieve the required conversion, it is necessary to add HCVD during WPPO 280 processing.

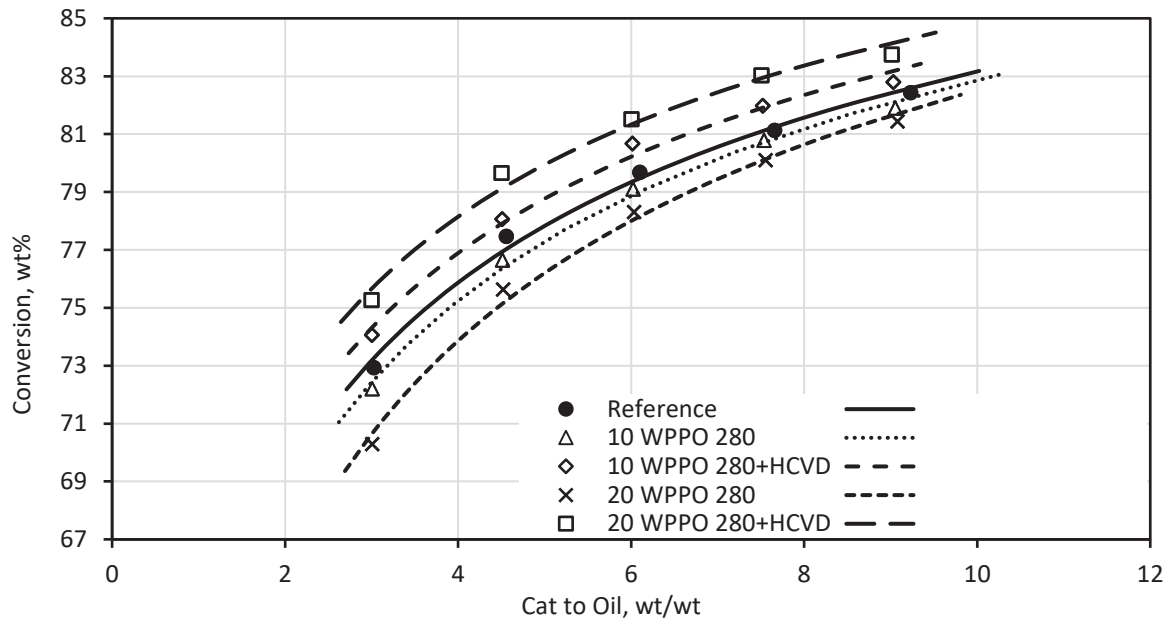


Figure 3. Feedstock conversion

Figure 4 shows coke production as a function of material conversion. Coke production affects the FCC's heat balance and is therefore a very important value in terms of operating economy. Coke production can be monitored by the amount of MCRT, which shows the ability of substances to pass into coke, or to a number of aromatic compounds, especially polyaromatic ones. According to Table 2, the MCRT value for both WPPO 280 and HCVD is significantly lower than for the reference raw material. However, the difference in the mixtures is not so obvious and most of them tend to show nitrogen contamination. Probably the amount of polyaromatic substances in WPPO 280 lead to the formation of coke. Their reduced content in a mixture with HCVD leads to lower coke production and higher yields of the desired products. Thus, it can be observed that with the addition of WPPO 280, coke production increases and with the addition of WPPO 280 together with HCVD, coke production decreases. From the point of view of the FCC unit, it is again better to process WPPO 280 together with HCVD.

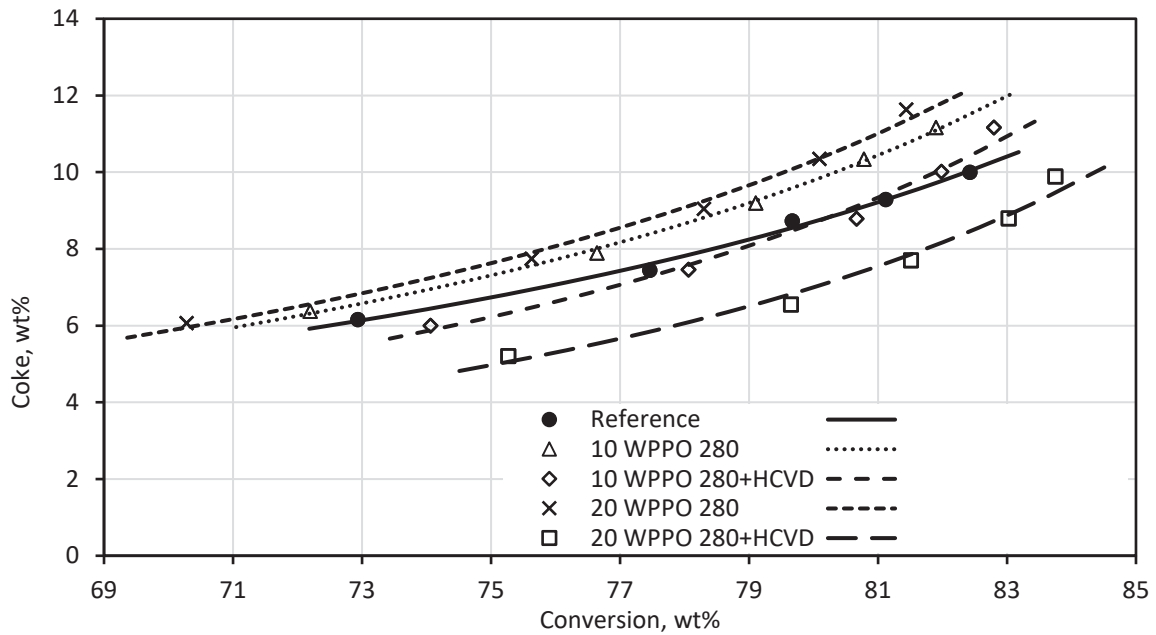


Figure 4. Coke production

Figure 5 shows the production of gasoline fraction as a function of feedstock conversion. Gasoline production is the main activity of FCC units, as is the production of monomers for petrochemical use. With the increasing addition of WPPO 280, there is no difference in gasoline production at lower conversions. The difference increases with increasing conversion, so that gasoline production decreases with the addition of WPPO 280. With the addition of WPPO 280 and with HCVD, there is an increase in gasoline production. This is due to the amount of "lighter" substances during the distillation of all the feedstock materials, which were used. So from the third point of view, treatment with HCVD is recommended.

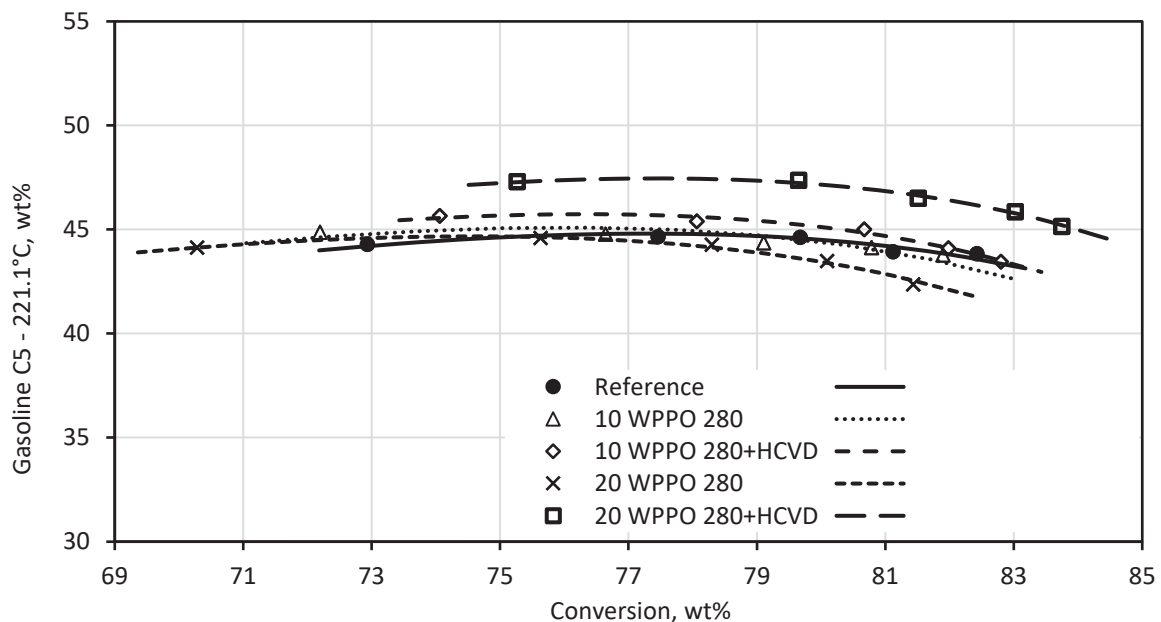


Figure 5. Gasoline production

From a comparison of the effect of WPPO 280 without and with HCVD at C/O ratios, ratios of 6.0 and 7.5 were chosen because they were located in the center of the obtained dependence. In terms of conversion, it is possible to calculate how much HCVD must be added to the FCC reference feed mixture with WPPO 280 to neutralize the negative effect of WPPO 280 on material conversion. From the calculation in Figure 6, it can be

seen that a half addition of HCVD to the addition of WPPO 280 is sufficient to keep the feedstock material conversion at the value for the reference material. In the future, better quality of fluids from pyrolysis processes is expected and thus to increased profits by processing them on FCC without the addition of HCVD.

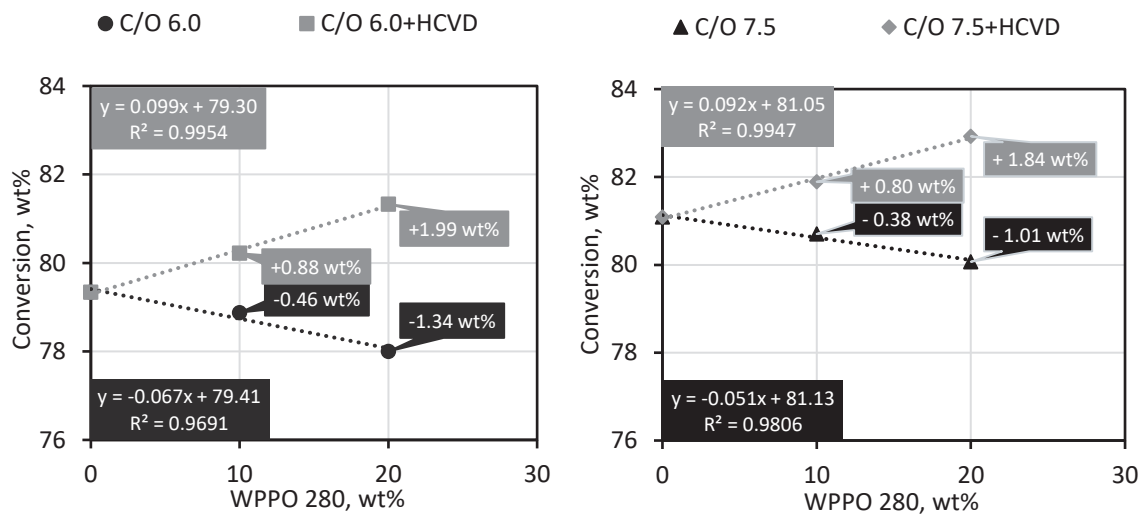


Figure 6. Dependence of conversion on the addition of WPPO 280 and HCVD at C/O 6.0 and 7.5.

Conclusion

When processing non-traditional raw materials at the FCC, it is necessary to monitor metal concentrations. Metals such as iron, vanadium and nickel acts as a catalytic poison when deposited on a catalyst. The nitrogen content is another catalytic poison and their amount in WPPO 280 is ten times higher compared to the reference feedstock. Unlike metals, the nitrogen content of the catalyst can be removed in the catalyst regenerator. Another possible problem is the presence of chlorine in WPPO 280. In our case, it is a small amount that does not exceed $2 \text{ mg}\cdot\text{kg}^{-1}$ in the mixtures. This is the limit value for the concentration in the processed raw material within the refinery operation. During long-term processing, chlorine destroys materials. In addition, WPPO 280 contains oxygenates and CO_2 is formed in the processes. The MCRT shows the value of the Conradson residue, and this value indicates the amount of carbon that is converted to coke. The higher the value, the more coke the raw material forms, and from a operational point of view, this behavior is limited and rigorously monitored. In this case, however, the MCRT value for WPPO 280 and HCVD is significantly lower than for the reference feedstock.

In the case of co-processing of only WPPO 280, undesirable lower feedstock conversions, lower gasoline fraction production and higher coke production were found. These reasons lead to lower profits from the operation of the FCC unit. The chance to influence this negative trend is the possibility of adding HCVD to the mixture. According to tests at the ACE unit, the addition of HCVD to the reference feedstock at a ratio of 1: 1 to the addition of WPPO 280 proved to be a very good way to reduce the negative effect of the addition of WPPO 280 itself. Based on the calculation, only half the amount of HCVD can be added to the WPPO 280 addition do reference feedstock o neutralize the negative impact of WPPO 280.

Acknowledgement

The result was achieved using the infrastructure included in the project *Efficient Use of Energy Resources Using Catalytic Processes (LM2018119)* which has been financially supported by MEYS within the targeted support of large infrastructures.

References

1. Paris Agreement, adopted by the United Nations in December 2015.
2. S. Kartik, B. Hermant, S. Manisha, S. Agus, J. K. Rakesh, J. B. Jyeshtharaj and S. Abhishek, *Thermal Science and Engineering Progress*, 28 April (2022).
3. K. Saeaug, N. Phusunti, W. Phetwarotai, S. Assabumrumgrat and B. Cheirsilp, "Catalytic pyrolysis of petroleum-based and biodegradable plastic waste to obtain high-value chemicals," *Waste management*, pp. 101-111, 21, (2021).
4. E. T. Aisien, I. C. Otuya and F. A. Aisien, "Thermal and catalytic pyrolysis of waste polypropylene plastic using spent FCC catalyst," *Environmental Technology & Innovation*, 13 March (2021).
5. R. Palos, E. Rodríguez, A. Gutiérrez, J. Bilbao, J. M. Arandes, Cracking of plastic pyrolysis oil over FCC equilibrium catalysts to produce fuels: Kinetic modeling, *Fuel*, 316, (2022), 123341
6. A. Karaba, J. Rozhon, L. Filip and P. Zámstný, *8th ICCT*, Mikulov, (2021).

PYROLYSIS OF PLASTICS: DEHALOGENATION VIA STEPWISE PYROLYSIS AND METAL SORBENTS

Hubáček J.^{1,2}, Lederer J.¹, Kuráň P.², Kašpárek A.¹

¹ ORLEN UniCRE a.s., Revoluční 1521/84, 400 01 Ústí nad Labem, Czech Republic, Our Street 7, 879 49, Prague 6

² Faculty of Environment, Jan Evangelista Purkyně University, Pasteurova 3632/15, Ústí nad Labem, 400 96, Czech Republic

Jan.Hubacek@orlenunicre.cz

Abstract

In order to process pyrolysis products into new polymers, it is necessary to remove halogens, especially Cl and Br, that may cause corrosion of technology, inactivation of catalysts, and deterioration of products. This study used different pyrolysis settings and sorbents to decrease the Cl content below the set limit of 10 ppm. It was observed that it is not feasible to use sorbents directly in the reactor (in-situ) as the captured Cl is released over higher temperatures yielding even more Cl in the products. Introducing the step at 350 °C (stepwise pyrolysis) proved to be a crucial part of the process. Required Cl content was reached via a combination of stepwise pyrolysis, reflux extension, and sorbents (Ca(OH)₂, Fe₃O₄-Si) in a separated bed (ex-situ) at 300 °C. Results have direct implications for designing an efficient pilot plant or modifying current technologies without a dehalogenation procedure.

Introduction

Plastic waste is something that humanity has not yet been able to cope with properly. To gain perspective, the production of plastic materials reached 368 Mt in 2019, and it is constantly growing.¹ According to Plastics Europe, most post-consumer plastics (40%) in 2019 were used for packaging, which usually has a short lifespan and quickly enters waste streams. In 2010 the main proportion of these plastics was as follows: LDPE (27.9%), PP (17.5%), HDPE (14%), PET (11.9%), PVC (8%) and PS (7.6%).² Also, when comparing European production of plastics in 2018, which was 61.8 Mt, with plastics collected in post-consumer waste, it accounts only for 47%, of which another 25% was sent to landfills.¹

⁴Chemical recycling offers the option of producing new virgin polymers, thereby dealing with the disadvantages of currently most used and misused³ mechanical recycling. Among chemical recycling technologies, pyrolysis is often considered the most suitable option.⁵ The main advantage of the process is the possibility of gaining high yields of liquid product that differ in aromatics, alkanes, and alkenes.⁶ It is possible to treat these liquids in the framework of standard refinery or petrochemical processes.⁷ However, the problem arises when feedstock contains halogen atoms such as Cl and Br that may cause severe corrosion of steel structures during pyrolysis and in the following treatments.⁸ Therefore, dehalogenation procedures are necessary when pyrolyzing materials such as PVC that contains a considerable amount of Cl (~57%) in the structure of the polymer.

It is well-known that the thermal degradation of PVC can be broadly divided into two partially overlapping steps. 1. step up to ~360 °C is dehydrochlorination, where most of the chlorine (~99%) leaves in the form of HCl. In the 2. step above 360 °C remaining polyene structure undergoes intramolecular cyclization and cross-linking that lead to the formation of mainly aromatic compounds. It is an important feature of PVC that can be utilized in the dehalogenation process called stepwise pyrolysis. This method has been studied extensively, and authors usually report the high dehalogenation efficiency.^{9,10} However, not all halogen atoms are naturally released during pyrolysis as HCl, which raises the significance of removing halogens from organohalogen compounds. Therefore, it is crucial to look for both catalysts that would mediate these reactions and methods that can prevent secondary reactions of HCl that lead to the creation of new chlorinated hydrocarbons.¹⁰

The majority of studies used sorbents or catalysts in a pyrolysis reactor (in-situ) which includes mixing the catalyst with the feed material or placing it on a separated bed in contact with the vapors. The placement of sorbents outside the reactor (ex-situ) is less mentioned in the literature.¹¹ Also, there are contradictory results when comparing conventional, catalytic, and stepwise/catalytic pyrolysis and dehalogenation efficiency varies with used catalysts/sorbents and parameters of pyrolysis.¹² However, it is not always clear what causes the differences in dehalogenation efficiency. Authors also report catalyst deactivation and increased Cl content in the liquid, suggesting that catalytic and dehalogenation steps should be separated.¹³

This report presents a summary of recently published research,¹⁴ the goal of which was to address the dehalogenation of a liquid product during pyrolysis of a model plastic mixture, including 10% PVC. In addition, the aim was to identify appropriate reliable procedures necessary to decrease the halogen content below the estimated limit of 10 ppm¹⁵ among the wide spectrum of possible approaches that often give contradictory

results. For this purpose, we conducted conventional pyrolysis with different residence times mediated by reflux extension of pyrolysis reactor, stepwise pyrolysis, pyrolysis with sorbents both in-situ and ex-situ, and a combination of these approaches.

Materials and methods

Sorbent preparation

Preparation of Ca(OH)₂-extrudate

About 67 wt% of Ca(OH)₂ was mixed and mechanically kneaded with 33 wt% tetraethyl orthosilicate. The extrusion was done on a Caleva extruder with 2.5 mm diameter slits. The resulting extrudate was kept in a desiccator. The tetraethyl orthosilicate was removed during the drying sequence before pyrolysis. Ca(OH)₂ powder was obtained from Lhoist - Vápenka Čertovy schody, a.s under the tradename Sorbacal H90. Properties of sorbents are listed in Tab II.

Preparation of Fe₃O₄-Si

The preparation involved precipitation of silica gel from potassium water glass with 21.7% HNO₃ solution. 400 g of water glass with a composition of 26.5% SiO₂; 24% K₂O; 0.4% Na₂O, and 0.02% Al was mixed with 2 l of distilled water, and the HNO₃ solution was added while stirring until the pH reached 5. The resulting silica gel was filtered off and washed with distilled water up to neutral pH. Silica gel was then mixed with Fe₃O₄ powder so that the Fe₃O₄ constituted 50% of the dry weight of silica gel. The mixture was left at 60 °C for two days and then extruded with the addition of tetramethylammonium hydroxide (25% aqueous solution), the weight of which corresponded to 17% of dry silica gel. The extrusion was done as above, and the extrudate was then dried overnight at 90 °C following 2 hours at 135 °C. Fe₃O₄ powder was obtained from PRECHEZA a.s (trademark Fepren B630).

Experimental procedure

Based on data from Villanueva and Eder, the model mixture (5P) resembling real waste composition was prepared, containing LDPE (35%), PP (25%), HDPE (20%), PS (10%), and PVC (10%).²

Pyrolysis was carried out in a batch pyrolysis unit described elsewhere.¹⁴ In all experiments, 300 g of 5P was placed into the reactor in a steel cylinder (id: 60 mm; height: 250 mm). Sorbents were either mixed with feedstock (Ca(OH)₂), placed in the upper 1/3 of the reactor (Fe₃O₄-Si) – A setting, or ex-situ in the first condenser – B setting. The weight of sorbents accounted for 10% of the batch material. Before the experiment, a pressure test was performed to detect system leaks. After proper sealing was ensured, all components except the pyrolysis reactor were heated to their respective temperatures under N₂ flow to remove any residues of cleaning solvents and moisture. Total pyrolysis time was set to 4 h to ensure completion of pyrolysis processes, and it was extended to 5 h in the case of stepwise pyrolysis for this reason. The final temperature was, in all cases, at 500 °C (10 °C/min). The N₂ flow (5 l/h) was increased to 60 l/h during step 1 of stepwise pyrolysis to reduce the residence time of HCl in the system. The first step lasted 60 min counted after reaching 350 °C, and the temperature in the reactor did not exceed 360 °C during this step. An overview of experiments is shown in Table I. Liquid, wax, and char product yields were determined by weighing, while gas was considered the remaining weight percentage to 100%. All experiments were conducted in triplicates, and the results are presented as the average of measured values with standard deviation.

Table I

Overview of discussed experiments

setting	conditions
A (without reflux)	conventional
	stepwise
	Ca(OH) ₂ (in-situ)
	Fe ₃ O ₄ -Si (in-situ)
B (with reflux)	conventional
	stepwise
	stepwise/Ca(OH) ₂ -extr. (ex-situ)
	stepwise/Fe ₃ O ₄ -Si (ex-situ)

Analytical methods

The total chlorine content in liquid products was determined directly via Sindie monochromatic wavelength dispersive x-ray fluorescence analyzer by XOS. The Cl in gases was determined by argentometry from Cl- content

in the scrubbers. Sorbents were characterized by gas porosimetry with BET method (Autosorb iQ, Quantachrome Instruments), Hg porosimetry (AutoPore 9510, Micromeritics), and XRD analysis (D8 Advanced, Bruker).

Results and discussion

Chlorine in gases

Generally, most Cl was found in the gaseous product, especially after the first step of the stepwise pyrolysis (Fig. 1), and the yield of Cl in gases from step 2 was negligible. Cl content in the scrubbers also increased by approximately 6% after introducing reflux extension. However, the same increase was not observed in conventional pyrolysis, which suggests that the effect of the reflux attachment on dehalogenation was associated with a longer residence time of the material in the reactor during stepwise pyrolysis. When sorbents were used in-situ (A setting), they significantly reduced Cl content in gases, but at the same time, it led to higher Cl content in the liquid, which is discussed below. Sorbent placement in the B setting could not affect step 1 of the pyrolysis, and the results correspond with the stepwise pyrolysis.

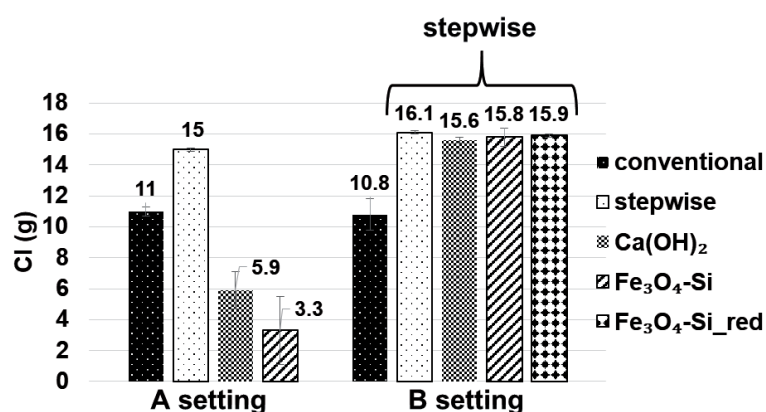


Figure 1. Cl content in scrubbers – gas products

Chlorine in liquid

From the comparison of individual settings, it can be seen that there was a 36% reduction of Cl content in the liquid product upon introduction of reflux extension during conventional pyrolysis (Fig. 2). It was probably caused by the longer residence time of heavier compounds mediated by reflux extension and slower reactor heating in the B setting that allowed HCl evolution without secondary reactions. Previously, it was found that high heating rates cause a shift of dechlorination reactions to higher temperatures and also widen the temperature range of HCl release.¹⁶ Results suggest that for dehalogenation purposes is worthwhile to consider the properties of a particular technology and pyrolysis parameters, focusing on sufficient residence time.

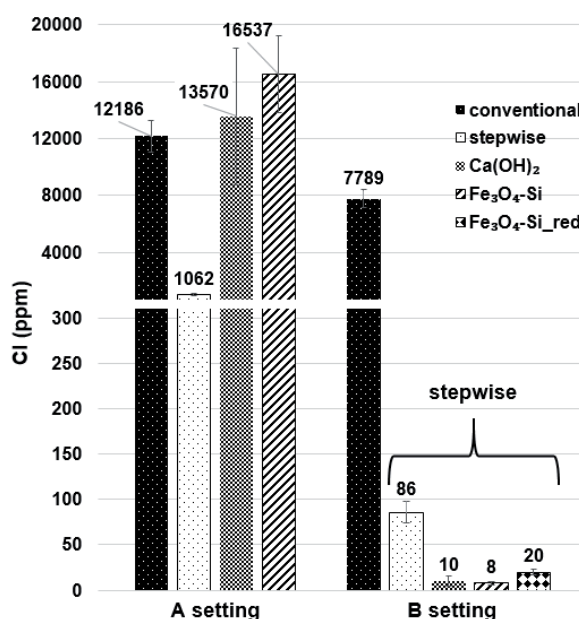


Figure 2. Cl content in liquid products

Regarding stepwise pyrolysis, there was about a 90% decrease in Cl content upon introduction of stepwise pyrolysis in the A setting, and 98.9% efficiency was achieved in the B setting. This result correlates with the increase of Cl found in the scrubbers and suggests an undeniable effect of reflux extension on the dechlorination efficiency. The temperature is another critical variable. For example, when Park et al. conducted 10 min long step1 in an auger reactor at 300 °C, they reached approximately 18% dehalogenation efficiency.¹¹ At the same time, Bhaskar et al. reported 100% efficiency with a solid bed reactor at 330°C and a 2hour-long first step.¹⁷ The amount of Cl in the liquid products from conventional pyrolysis was 425 ppm and 390 ppm, respectively, while in this study, we obtained liquid with as much as 12186 ppm in the A setting and 7789 ppm in the B setting. It follows that Cl content in the feedstock also needs to be considered to set the time of the first step appropriately.

In the case of sorbent efficiency, major differences were found between individual settings. Most importantly, results suggest that it is not suitable to use sorbents directly in the pyrolysis reactor, as Ca(OH)₂ and Fe₃O₄-Si in-situ increased the Cl content in liquid products in the A setting (Fig. 2). It was most likely caused by the mechanism when the Cl was initially successfully adsorbed by sorbents. As the temperature increased, part of Cl was desorbed, re-entered the stream where it reacted with hydrocarbons or ended up in the liquid product in the form of HCl. Results that support these findings were obtained, for example, by López et al., who reported a decrease of Cl in the gas product but a significant increase in Cl content in the liquid product upon introduction of CaCO₃ in-situ.¹² XRD analysis showed that the Cl bound to the sorbents formed hydrated FeCl₂ and CaCl₂ (Tab. II). However, no chlorine species were detected after most experiments at the B setting because only a small amount of Cl remained for the reaction with the sorbent after the first pyrolysis step.

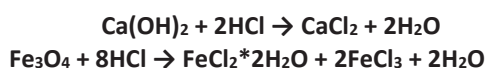
Table II

Sorbent properties before (new) and after pyrolysis (used) in setting with (B) and without reflux extension (A)

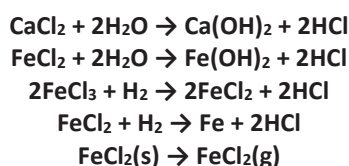
catalyst/ sorbent	surface area (m ² /g)	pore volume (cm ³ /g)	average pore diameter (nm)	composition (XRD)		
				new	used (A)	used (B)
Ca(OH) ₂ (in-situ)		powder		Ca(OH) ₂ , CaCO ₃	CaCl ₂ ·Ca(OH) ₂ ·H ₂ O, CaCl(OH), CaO, Ca(OH) ₂ , CaCO ₃	-
Fe ₃ O ₄ -Si (in-situ)	178.0	0.49	7.5	Fe ₃ O ₄	FeCl ₂ ·2H ₂ O, FeCl ₂ ·4H ₂ O, Fe ₂ SiO ₄ , Fe(OH) ₂ , Fe	Fe ₃ O ₄
Ca(OH) ₂ - extr.	29.4	0.39	46.4	Ca(OH) ₂	-	Ca(OH) ₂ , CaCl(OH)
Fe ₃ O ₄ -Si	178.0	0.49	7.5	Fe ₃ O ₄	-	Fe ₃ O ₄

It has been described recently by Sophonrat et al. that at temperatures above 400 °C, CaCl₂ can undergo several reactions in the presence of water that leads to the HCl desorption,¹⁸ and evaporation or reduction of FeCl₂ at this temperature is also documented by Ye et al.¹⁹ The latter mechanisms were confirmed by ICP and XRD analysis, as we found a significant amount of Fe in the liquid and partially reduced Fe in the sorbent. The desorption described by Sophonrat et al. also seems plausible as XRD of Ca(OH)₂ residue after pyrolysis showed CaO and Ca(OH)Cl, formed by releasing water. Furthermore, Li et al. described CaO as an active agent for the dechlorination of stable chlorinated compounds such as chlorobenzene produced during pyrolysis of PVC.²⁰ Based on the confrontation of XRD and ICP results with literature, sorbents could have acted both as sorbents and catalysts for the dechlorination of organohalogen compounds, but they underwent desorption upon increasing temperature. We propose the following examples of possible Cl pathways during in-situ dehalogenation which is relevant for the rejection of in-situ dehalogenation:

1. Chloride formation by reaction with HCl at temperatures up to 400 °C.



2. Chloride formation by reaction with HCl at temperatures up to 400 °C.



This finding also has potential implications for the pyrolysis of municipal plastic waste, as CaCO_3 , Fe_2O_3 , ZnO , and Sb_2O_3 are widely used as plastic additives²¹ and could hinder stepwise pyrolysis by a similar mechanism, creating respective chlorides during the first pyrolysis step. The resulting outcome would be that more Cl is retained in the reactor forming chlorinated hydrocarbons. Nevertheless, the stepwise pyrolysis reduces the portion of Cl that is susceptible to form HCl, protecting the apparatus from corrosion and decreasing the liquid Cl content. It can also decrease the water and oxygenate content formed from organic impurities,¹⁸ which makes it an essential first part of dehalogenation technology.

Previously, authors have used similar sorbents/catalysts in an in-situ setting with mixed results, and the negative effect of using sorbents in this setting has not yet been emphasized. Authors reported both an increase in Cl content after the introduction of sorbents in-situ^{11,12} and also a decrease and even complete dehalogenation²². Following results from in-situ sorbent placement, subsequent experiments with sorbents ex-situ were done in the B setting in combination with stepwise pyrolysis to utilize the best possible approach according to our knowledge. Results in Fig. 2 clearly show that the combination of stepwise pyrolysis with the placement of sorbent ex-situ further decreased the Cl content in the liquid products to 3-23 ppm, which is a sufficient level for the introduction of the liquid into the refinery.

Conclusion

Batch pyrolysis utilizing different system settings and sorbents was investigated to establish optimal conditions for the dehalogenation of liquid products. Stepwise pyrolysis was an effective dehalogenation tool that significantly reduced Cl content prior to the final pyrolysis step. Further dehalogenation was achieved by increasing residence time through the introduction of the designed reflux extension. Regarding the sorbents, their placement had a key role in dehalogenation. The results showed that it is not viable to use sorbents in-situ if the main objective is the dehalogenation of liquid products. Implications for municipal plastic waste pyrolysis were drawn, considering similar sorbents being present as additives in plastics. Among used sorbents, the best results were achieved when Fe_3O_4 with silica gel was placed ex-situ.

By combining stepwise pyrolysis with sorbents placed ex-situ, the resulting chlorine content in the liquid from the model plastic mixture containing 10% PVC was around the limit of 10 ppm for subsequent refinery treatment.

Acknowledgment

This publication is a result of the project CACTU, Reg. No. CZ.02.1.01/0.0/0.0/17_049/0008397, co-financed by the European Union from the European Regional Development Fund through the Operational Programme Research, Development and Education. The project CACTU has been integrated into the National Sustainability Programme I of the Ministry of Education, Youth and Sports of the Czech Republic (MEYS) through the project Development of the UniCRE Centre (LO1606). The project was carried out within the financial support of the Ministry of Industry and Trade of the Czech Republic with institutional support for the long-term conceptual development of the research organization. The result was achieved using the infrastructure included in the project Efficient Use of Energy Resources Using Catalytic Processes (LM2018119), which has been financially supported by MEYS within the targeted support of large infrastructures. The authors also acknowledge the assistance provided by the Research Infrastructure NanoEnviCz, supported by MEYS under Project No. LM2018124.

References

1. PlasticsEurope, Plastics -The Facts 2020: An analysis of European plastics production, demand and waste data. 2020. Available from: https://plasticseurope.org/wp-content/uploads/2021/09/Plastics_the_facts- WEB-2020_versionJun21_final.pdf.
2. Villanueva, A. and P. Eder, End-of-waste criteria for waste plastic for conversion. Institute for Prospective Technological Studies, 2014. <https://data.europa.eu/doi/10.2791/13033>.
3. Guzzonato, A., F. Puype, and S.J. Harrad, Evidence of bad recycling practices: BFRs in children's toys and food-contact articles. Environmental Science: Processes & Impacts, 2017. 19(7): p. 956-963. <https://doi.org/10.1039/C7EM00160F>.
4. Maris, J., Bourdon, S., Brossard, J., Cauret, L., Fontaine, L., Montembault, V., Mechanical recycling: Compatibilization of mixed thermoplastic wastes. Polymer Degradation and Stability, 2018. 147: p. 245-266. <https://doi.org/10.1016/j.polymdegradstab.2017.11.001>.
5. Kunwar, B., Cheng, H.N., Chandrashekar, S.R., Sharma, K.B., Plastics to fuel: a review. Renewable and Sustainable Energy Reviews, 2016. 54: p. 421-428. <https://doi.org/10.1016/j.rser.2015.10.015>.

6. Pinto, F., Costa, P., Gulyurtlu, I., Cabrita, I., Pyrolysis of plastic wastes. 1. Effect of plastic waste composition on product yield. *Journal of Analytical and Applied Pyrolysis*, 1999. 51(1): p. 39-55. [https://doi.org/10.1016/S0165-2370\(99\)00007-8](https://doi.org/10.1016/S0165-2370(99)00007-8).
7. Buekens, A., Introduction to feedstock recycling of plastics. *Feedstock Recycling and Pyrolysis of Waste Plastics: Converting Waste Plastics into Diesel and Other Fuels* 2006. 6(7): p. 1-41. Available from: <https://www.academia.edu/download/53303494/0470021527.pdf>.
8. Nagu, M., N. Alanazi, and F. Adam, Organochloride Contamination in a Refinery Naphtha Hydrotreater Unit. *Materials performance*, 2017. 56.
9. Miranda, R., Pakdel, H., Roy, CH., Darmstadt, H., Vasile, C., Vacuum pyrolysis of PVCII: Product analysis. *Polymer Degradation and Stability*, 1999. 66(1): p. 107-125. [https://doi.org/10.1016/S0141-3910\(99\)00060-9](https://doi.org/10.1016/S0141-3910(99)00060-9).
10. Miranda, R., Pakdel, H., Roy, C., Vasile, C., Vacuum pyrolysis of commingled plastics containing PVC II. Product analysis. *Polymer Degradation and Stability*, 2001. 73(1): p. 47-67. [https://doi.org/10.1016/S0141-3910\(01\)00066-0](https://doi.org/10.1016/S0141-3910(01)00066-0).
11. Park, K., Oh, S., Begum, G., Kim, J., Production of clean oil with low levels of chlorine and olefins in a continuous two-stage pyrolysis of a mixture of waste low-density polyethylene and polyvinyl chloride. *Energy*, 2018. 157: p. 402-411. <https://doi.org/10.1016/j.energy.2018.05.182>.
12. López, A., de Marco, I., Caballero, B.M., Laresgoiti, M.F., Adrados A., Dechlorination of fuels in pyrolysis of PVC containing plastic wastes. *Fuel Processing Technology*, 2011. 92(2): p. 253-260. <https://doi.org/10.1016/j.fuproc.2010.05.008>.
13. Lopez-Urionabarrenechea, A., de Marco, I., Caballero, B.M., Laresgoiti, M.F., Adrados A., Catalytic stepwise pyrolysis of packaging plastic waste. *Journal of Analytical and Applied Pyrolysis*, 2012. 96: p. 54-62. <https://doi.org/10.1016/j.jaap.2012.03.004>.
14. Hubáček, J., Lederer, J., Kuráň, P., Koutník, P., Gholami, Z., Zbuzek, M., Bačiak, M., Dechlorination During Pyrolysis of Plastics: The Potential of Stepwise Pyrolysis in Combination with Metal Sorbents. *Fuel Processing Technology*, 2022, 231. <https://dx.doi.org/https://doi.org/10.1016/j.fuproc.2022.107226>.
15. Kaminsky, W., Recycling of polymers by pyrolysis. *Le Journal de Physique IV*, 1993. 3(C7): p. C7-1543-C7-1552. <https://doi.org/10.1051/jp4:19937241>.
16. Cao, Q., Yuan, G., Yin, L., Chen, D., He, P., Wang, H., Morphological characteristics of polyvinyl chloride (PVC) dechlorination during pyrolysis process: Influence of PVC content and heating rate. *Waste Management*, 2016. 58: p. 241-249. <https://doi.org/10.1016/j.wasman.2016.08.031>.
17. Bhaskar, T., Negoro, R., Muto, A., Sakata, Y., Prevention of chlorinated hydrocarbons formation during pyrolysis of PVC or PVDC mixed plastics. *Green Chemistry*, 2006. 8(8): p. 697-700. <https://doi.org/10.1039/B603037H>.
18. Sophonrat, N., Sandström, L., Svanberg, R., Han, T., Dvinskikh, S., Lousada, C. M., Yang, W., Ex Situ Catalytic Pyrolysis of a Mixture of Polyvinyl Chloride and Cellulose Using Calcium Oxide for HCl Adsorption and Catalytic Reforming of the Pyrolysis Products. *Industrial & Engineering Chemistry Research*, 2019. 58(31): p. 13960-13970. <https://doi.org/10.1021/acs.iecr.9b02299>.
19. Ye, L., T. Li, and L. Hong, Co-pyrolysis of Fe₃O₄-poly(vinyl chloride) (PVC) mixtures: Mitigation of chlorine emissions during PVC recycling. *Waste Management*, 2021. 126: p. 832-842. <https://doi.org/10.1016/j.wasman.2021.04.021>.
20. Li, Y.-X., H. Li, and K.J. Klabunde, Destructive Adsorption of Chlorinated Benzenes on Ultrafine (Nanoscale) Particles of Magnesium Oxide and Calcium Oxide. *Environmental Science & Technology*, 1994. 28(7): p. 1248-1253. <https://doi.org/10.1021/es00056a011>.
21. Hahladakis, J. N., Velis, C. A., Weber, R., Iacovidou, E., Purnell, P., An overview of chemical additives present in plastics: migration, release, fate and environmental impact during their use, disposal and recycling. 2018. 344: p. 179-199. <https://doi.org/10.1016/j.jhazmat.2017.10.014>.
22. Bhaskar, T., et al., Pyrolysis studies of PP/PE/PS/PVC/HIPS-Br plastics mixed with PET and dehalogenation (Br, Cl) of the liquid products. 2004. 72(1): p. 27-33. <https://doi.org/10.1016/j.jaap.2004.01.005>.

CARBON CAPTURE IN STEAM METHANE REFORMING THROUGH TECHNO-ECONOMIC, SAFETY AND ENVIRONMENTAL OPTICS

Janošovský J., Šandor R., Mišún P., Řežucha M., Jelemenský Ľ.

*Institute of Chemical and Environmental Engineering FCHPT STU, Radlinského 9, 812 37 Bratislava, Slovakia
jan.janosovsky@stuba.sk*

Abstract

Carbon dioxide emissions associated with hydrogen production are expected to rise with continuous transition to hydrogen economy. The steam methane reforming as the most frequently used technology was heavily investigated in this work for options to reduce its carbon footprint. Three possible carbon capture (CC) approaches for steam reforming of natural gas are studied from techno-economic, safety and environmental point of view. The considered CC techniques are post-combustion CC of flue gases, pre-combustion CC of offgases from pressure swing adsorption (PSA) and oxyfuel combustion. For each investigated CC technology, mathematical model and process simulation were developed in Aspen Plus. Simulation data supplemented by safety data sheet data were used to assess all simulated case studies by multiple criteria – economic feasibility, use of resources, environmental impact, and inherent safety. Oxyfuel combustion was identified as the best option considering all criteria simultaneously.

Introduction

One of the main priorities of today's industrial growth is the reduction of environmental burden of production processes. To achieve this goal, many robust policies have been introduced on worldwide level such as the "Fit for 55" package which was adopted to implement core strategy of the European Green Deal. Industrial sustainability reflecting these issues consists of multiple coexisting criteria that impact each other positively or negatively^{1,2}. It is extremely difficult to monitor all criteria and to reveal all synergy effects in processes with high level of complexity, e.g. highly intensified processes in chemical industry.

One of such processes is hydrogen production via steam methane reforming (SMR). Hydrogen is currently promoted as a clean fuel that can replace conventional fossil fuels in practically all applications due to its very low environmental footprint as water is its only emission during combustion. It is expected that transition towards hydrogen economy will lead to less environmentally damaging industries, job creation, cleaner transportation, etc.³ Although multiple hydrogen production ways are being investigated^{4,5}, SMR process remains the dominant technology in the global market.

During the SMR, hydrogen is produced from methane via high-temperature medium-pressure catalytic process in the presence of excess water. Main production units are steam reformer and temperature shift reactors (one or two). Usual components in product stream are hydrogen, carbon dioxide, carbon monoxide, methane and water. Product stream is led into pressure swing adsorption (PSA) unit where high-purity hydrogen is separated from the mixture. PSA offgases are combusted with air to provide heat necessary for reactions in steam reformer. If the heat obtained by combustion of PSA offgases is not sufficient, additional fuel can be combusted. Flue gas containing carbon dioxide, nitrogen, water and oxygen can be further treated before its release into atmosphere. In our work, three possible alternatives for carbon footprint reduction of SMR process were simulated and assessed. Commercial Aspen Plus was used as the simulation tool. The assessment consisted of four main criteria – economic feasibility, use of resources, environmental impact, and inherent safety. Analytical hierarchy process (AHP) was utilized to combine all criteria simultaneously and to select the best overall option.

Methodology and simulation

Aspen Plus models of four hydrogen production states were developed and simulated. First one (Figure 1) represents base process configuration of hydrogen production plant (HPP). In the next step, three modifications by adding carbon capture (CC) were simulated:

- Post-combustion CC by monoethanolamine absorption of carbon dioxide from flue gas
- Pre-combustion CC by monoethanolamine absorption of carbon dioxide from tail gas, i.e. PSA offgases
- Oxyfuel combustion as a substitution of combustion with air and consequent cooling and condensation separation step

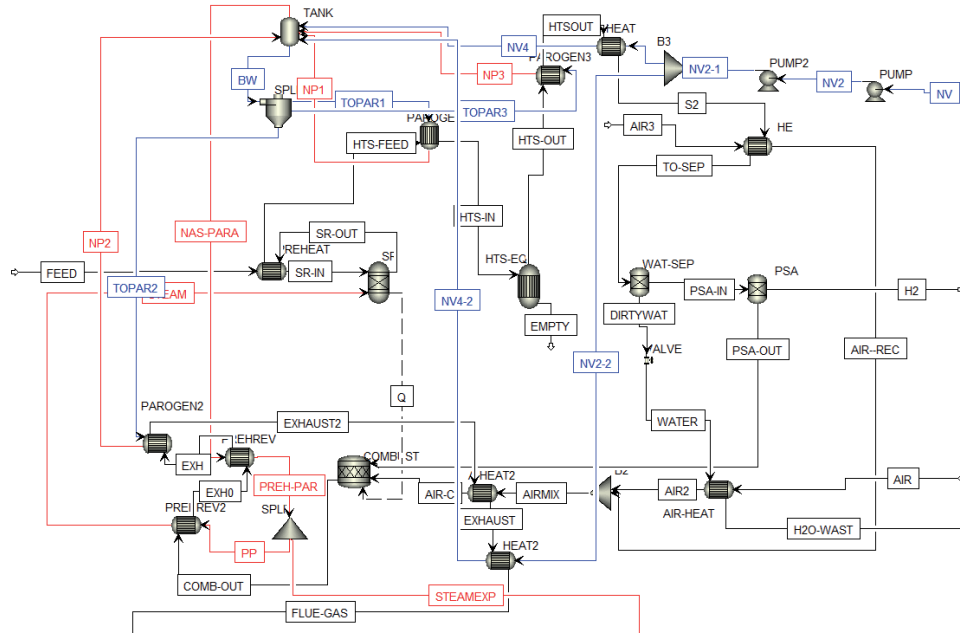


Figure 1. Aspen Plus simulation flowsheet of base hydrogen production plant (HPP)

Simulation data were supplemented by safety data sheets and price levels to create input data-pool for process feasibility assessment and ranking via AHP which is a sophisticated technique to subdivide complex decisions into its components and arrange them into an ascending order. The output of AHP is set of priorities which can be used to rank different options and to investigate strengths and weaknesses of each decision alternative. Four main criteria (each divided into two subcriteria) were selected to assess feasibility of studied processes from multiple viewpoints (Table 1). All subcriteria were selected based on their calculation suitability and maturity of use in industrial practice. Capital expenditures (CAPEX) were calculated utilizing Aspen Process Economic Analyzer and literature guidance⁶. Equation 1 provides calculation procedure for second “Economics” subcriterion of Total Production Costs (TPC) utilizing CAPEX, operating expenditures (OPEX), selected payback period (PP) and annual hydrogen production. Environmental impact was determined by subcriteria C factor (Equation 2)⁷ and Eco-Indicator 99 (Equation 3) where δ_d is a normalisation factor and ω_d is the damage weighting for damage of category d , β_b is the amount of chemical b released by direct emission and $\alpha_{b,k}$ is the damage in category k per unit of chemical b released to the environment⁸. For use of resources, energy efficiency was evaluated separately from material utilisation efficiency. Energy efficiency was assessed by Specific Energy Consumption (SEC, see Equation 4)⁹ and material utilisation efficiency was calculated by E factor (Equation 5)⁷. Inherent safety was determined by simplified Process Route Index (PRI) method and more complex Comprehensive Inherent Safety Index (CISI) method. PRI data inputs can be directly extracted from Aspen Plus environment. Its calculation procedure is presented by Equation 6 where $\bar{\rho}$ is average density, \bar{P} average pressure, $\bar{H}\bar{V}$ average heating value and ΔFL_{mix} average difference between upper and lower flammability limits for all streams in the examined system¹⁰. Calculation procedure of CISI is schematically depicted by Figure 2. It combines properties of chemicals, character of reactions in unit operations, process conditions and stream interconnections within the examined system¹¹.

$$TPC = \frac{OPEX + \frac{CAPEX}{PP}}{\text{annual hydrogen production}} \quad (1)$$

$$C \text{ factor} = \frac{\text{mass of emitted carbon dioxide equivalents}}{\text{mass of products}} \quad (2)$$

$$EI99 = \sum_b \sum_d \sum_{k \in K} \delta_d \times \omega_d \times \beta_b \times \alpha_{b,k} \quad (3)$$

$$SEC = \frac{\text{annual energy consumption}}{\text{annual hydrogen production}} \quad (4)$$

$$E \text{ factor} = \frac{\text{mass of generated waste}}{\text{mass of products}} \quad (5)$$

$$PRI = \bar{\rho} \times \bar{P} \times \overline{HV} \times \overline{\Delta FL_{mix}} \times 10^{-8} \quad (6)$$

Table I
Assessment criteria for feasibility ranking

Criterion	Subcriterion
Economics	CAPEX
	TPC
Environmental impact	C factor
	EI99
Use of resources	E factor
	SEC
Inherent safety	PRI
	CISI

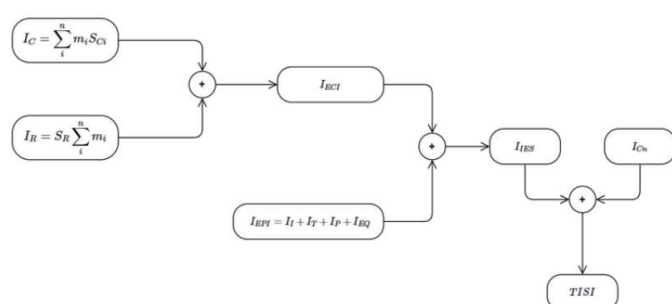


Figure 2. Calculation procedure schematics for CISI taken from Gangadharan et al (2013)¹¹ where I_C represents chemical index related to chemicals properties, I_R reactivity index related to character of reactions, I_{EPI} equipment index related to process conditions and I_{CN} connection index characterizing stream interconnections

Decision-making procedure is depicted in Figure 3. In the first step, simulation data supplemented by manual input of other relevant data were used to evaluate all eight subcriteria. In the next step, process routes ranking was generated by scoring system where the best process route in one criterion (e.g. process route with lowest CAPEX and TPC) has scored one point and the worst process route one quarter of a point. After single criterion rankings were established, AHP was applied for different weights of each criterion to determine overall best process route. In the final step, all possible combinations of criterion weights were studied and global feasibility rankings were generated.

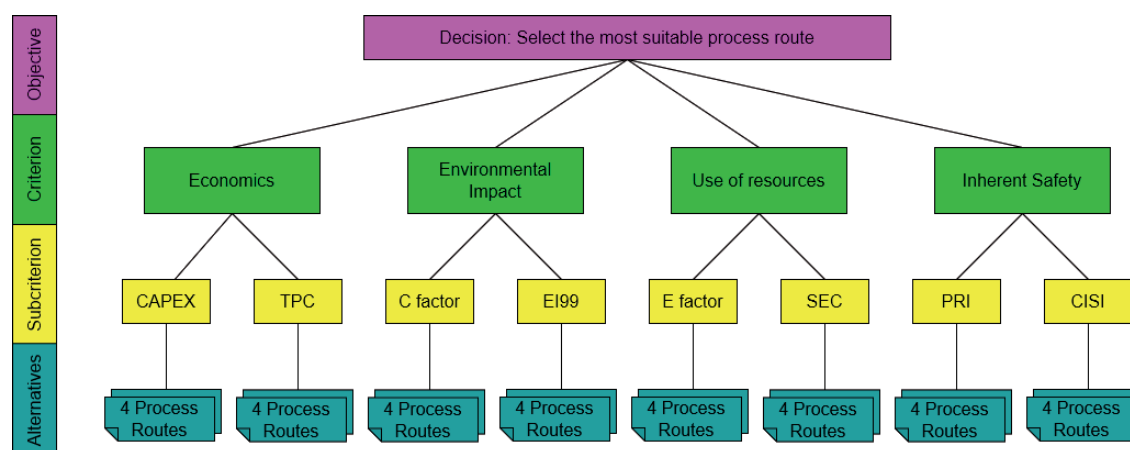


Figure 3. Diagram of MCDA employed in this study

Results and discussion

The main output of methodology proposed in this paper is viability map. It is a complex visualisation of process feasibility ranking using three-dimensional space where one dimension is represented by colour (Figure 4). On x axis, all studied process routes are located. Y axis represents specific placement in the ranking (from 1st to 4th). Colour (z axis) corresponds to percentage of occurrence of specific process route at specific placement, e.g. original HPP process route was ranked first for 67.4 % of decision scenarios, i.e. combinations of weights of main criteria. Viability maps can be decomposed into smaller fragments. Figure 5 depicts two viability maps, one for prioritised economics criterion and second one for prioritised environmental impact criterion.

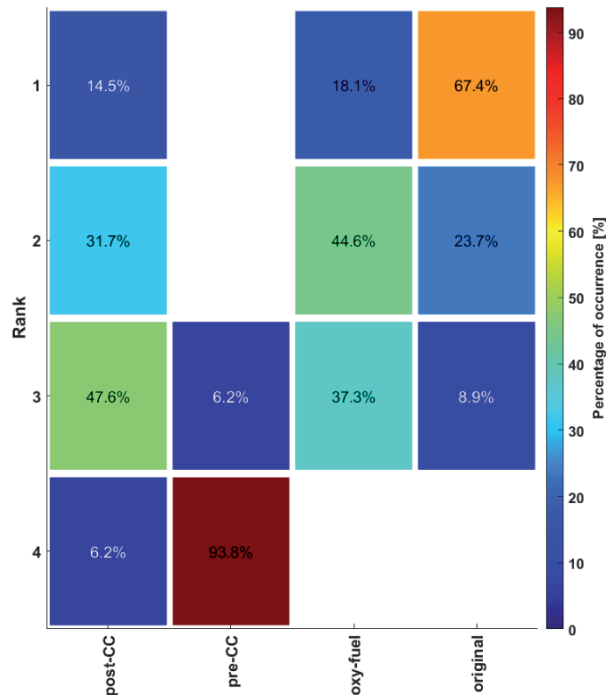


Figure 4. Global process feasibility ranking

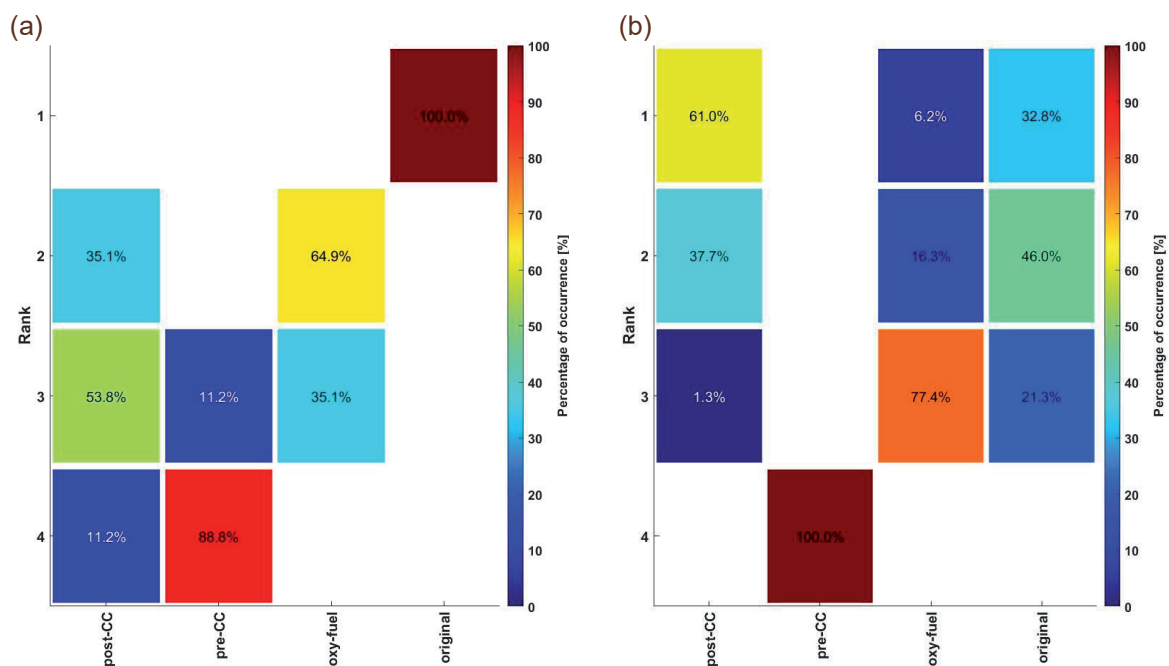


Figure 5. Process feasibility rankings: economics prioritised (a) and environmental impact prioritised (b)

Studied alternatives of CC were identified as inferior to original HPP process route if process economics was the main decision criteria (Figure 5a). However, if the importance was shifted towards environmental impact (Figure 5b), post-combustion CC was ranked as the overall best alternative in more than half of the examined decision scenarios. Such analysis allows to study synergy effects of different aspects of process design and recognize important patterns for enhanced decision-making.

According to global feasibility ranking (Figure 4), it was revealed that installation of CC technology was generally not feasible as the original HPP process route was the best rated alternative for majority of decision scenarios. Oxyfuel combustion was identified as the most suitable option for CC technology (first place for 18.1 % of decision scenarios) and pre-combustion CC as the least preferred one (last place for 93.8 % of decision scenarios).

Conclusion

Three carbon capture alternatives for steam reforming of natural gas were investigated. Firstly, simulation case files were developed and verified in Aspen Plus. Simulation data supported by necessary manual inputs (such as safety data sheet information) were used to assess their performance from various points of view and create feasibility rankings. According to the proposed assessment, oxyfuel combustion was identified as the best option for carbon capture considering all criteria simultaneously. However, for over 60 % of decision scenarios, original hydrogen plant without carbon capture technology was ranked as the best overall process route indicating low feasibility of studied carbon capture alternatives and necessity to improve studied processes, mainly in economic indicators which strongly prefer original plant that was ranked first in 100 % of decision scenarios with prioritised economics criterion.

The proposed methodology of multiple criteria assessment can be successfully employed in selection of the most suitable process route considering variable societal needs and industrial trends. Its flexibility allows application in early design stage for selection of appropriate plant configurations as well as in optimisation of existing plants when improving or extending already operating production units. Due to the general character of used subcriteria, developed methodology is not limited to carbon capture techniques and can be applied to other production and separation processes in chemical industry. Currently investigated future improvements are input data sensitivity analysis, substitution and upgrade of assessment criteria, and possible use for process benchmarking.

Acknowledgement

This work was supported by the Slovak Research and Development Agency [Grant No. APVV-18-0134] and by the Slovak Scientific Agency [Grant No. VEGA 1/0511/21].

References

1. Kumar A., Singh A.R., Deng Y., He X., Kumar P., Bansal R.C.: *Energy Convers Manage.* 180, 442 (2019).
2. Šulgan B., Labovský J., Labovská Z.: *Processes* 8, 1618 (2020).
3. Acar C., Dincer I.: *J Cleaner Prod.* 218, 835 (2019).
4. Baykara S.Z.: *Int J Hydrogen Energy* 43, 10605 (2018).
5. Wijayasekera S.C., Hewage K., Siddiqui O., Hettiaratchi P., Sadiq R.: *Int J Hydrogen Energy* 47, 5842 (2022).
6. Woods D. R.: *Rules of Thumb in Engineering Practice.* Wiley, Weinheim 2007.
7. Woodley J.M.: *Curr Opin Green Sustainable Chem.* 21, 22 (2020).
8. Goedkoop M. J., Spriensma R.: *The Eco-Indicator 99. A Damage Oriented Method for Life Cycle Impact Assessment.* PRé, Amersfoort, Netherlands 2001.
9. Šulgan B., Labovský J., Labovská Z.: *Processes* 8, 1618 (2020).
10. Leong C.T., Shariff A.M.: *J Loss Prev Process Ind.* 22, 216 (2009).
11. Gangadharan P., Singh R., Cheng F., Lou H.H.: *Ind. Eng. Chem. Res.* 52, 5921 (2013).

THE FUTURE OF JET FUEL AS AN IMPORTANT REFINERY PRODUCT

Kittel H., Horský J.

*University of Chemistry and Technology, Technická 1905, 166 28 Prague
hugo.kittel@vscht.cz*

Abstract

Jet fuel is a widely available and uniformly standardized product of oil refineries. In 2019, it accounted for 8.1 vol% of crude oil consumption. It is characterized by a projected increasing market demand of 3.7% per year by 2050 and a very good refinery margin. At present, there is virtually no alternative to aircraft turbines similar to electric motors in the case of cars, which means that there is no threat to jet fuel in the long term. Although the basic characteristics of jet fuel will not change significantly, it will be reformulated with an increasing addition of sustainable aviation fuels (SAF), to contribute to carbon dioxide emissions savings. Various feedstocks (oil crops, lignocellulose, sugar and starch, algae, waste plastics and scrapped tires), platforms (vegetable virgin and used oils, pyrolysis oil, bioalcohols, synthesis gas, and bioalkenes), and technologies (pyrolysis, hydrogenation, hydrocracking, synthesis gas production, Fischer-Tropsch synthesis, oligomerization, modified Methanol-to-Gasoline process, and isomerization) are now targeted for production of jet fuel. The EU, EIA, IATA, and other organizations started important initiatives in this direction. Major aircraft manufacturers are currently testing the use of various blends of SAF with mineral kerosene as well as pure SAF. Related driving forces and barriers to this development are discussed in this paper.

Introduction

In the second decade of the 21st century, air traffic increased by 5% and jet fuel consumption by 2.6% ·yr⁻¹ [1].

Jet fuel is a conventional product of oil refineries. Global consumption in 2019, the last pre-pandemic year, was 472 million m³ (372 Mt), representing 13.2 vol% of the consumption of motor fuels and 8.1 vol% of the consumption of crude oil [1]. It is responsible for 2.5% of carbon dioxide emissions. Consumption in the Czech Republic in 2019 was 448 kt [2]. As regards origin, jet fuel is divided into four categories: non-, mildly, severely hydroprocessed, and synthetic. Although the first two categories currently dominate, future attention will focus on the last category. Jet fuel is uniformly standardized and available under the name JET A-1 (Table 1) [3].

Table 1

JET A-1 quality requirements

Property	Method	Limit
Aromatics content (vol%)	ASTM D 6379 (A)	max 26.5
Sulfur total (wt%)	ASTM D 5453 (A)	max 0.3
Distillation profile (°C)	ASTM D 86 (A)	
10 vol% distilled by		max 205
End of distillation		max 300
Distillation residue (vol%)	ASTM D 86 (A)	max 1.5
Distillation loss (vol%)	ASTM D 86 (A)	max 1.5
Density at 15 °C (kg·m ⁻³)	ASTM D 7566	775-840
Freezing point (°C)	ASTM D 5972	max -47
Viscosity at -20 °C (mm ² ·s ⁻¹)	ASTM D 445	max 8
Calorific value (MJ·kg ⁻¹)	ASTM D 3338	min 42.8
Smoke point (mm)	ASTM D 1322	
Naphthalenes > 3 vol%		min 25
Naphthalenes max 3 vol%		min 18
Flash point (°C)	ASTM D 56 (A)	min 40

The Joint Inspection Group (JIG) jet fuel list refers to a total of 24 standardized properties. The high sulfur content (0.3 wt%) is in contrast to clean fuels, the density range (775-840 kg·m⁻³) and the distillation limited to only two points are very liberal. Viscosity is measured at -20 °C instead of the usual 40 °C for petroleum products. The freezing point of maximum -47 °C and the aromatic content of maximum 26.5 vol% can be

considered as critical quality requirements for the product. No major changes in the quality of jet fuel are expected to occur in the near future.

The following may be considered as the main driving forces for the further use of jet fuel ^[4]:

- There is no serious alternative to aircraft turbines similar to electric motors in cars. Batteries and hydrogen power cells are considered an energy source for regional commuter flights only by 2030.
- An improved network operational efficiency (more direct flights), modernization of airlines' fleets, focus on future modern airplane technology (aircraft design and new construction materials).
- A long-term growth in market demand. It will grow by 3.7% ·yr⁻¹ by 2050 according to the US Energy Information Administration (EIA) ^[5].
- A generally better refinery margin for jet fuel in comparison to diesel.
- Air transport is also required to reduce its contribution to carbon dioxide emissions. The reformulation of jet fuel is in progress. The SAF content in jet fuel will continue to grow from current <0.1% to 40 wt% (445 Mt) expected by 2050 ^[6].
- A possibility of using a variety of feedstocks, including niche feedstocks.

There are also certain barriers that will be important to overcome, mainly related to the reformulation of jet fuel:

- A limited availability of alternative feedstocks compared to crude oil.
- Low energy density of most alternative feedstocks.
- Immature feedstock supply chains: a need for proper policies.
- High capital expenditures (CAPEX) of SAF technologies. These now range from 1 US\$·gal⁻¹ (hydrogenated esters and fatty acids, HEFA) to 30 US\$·gal⁻¹ (Power-to-Jet fuel, PtL) of SAF capacity ^[7].
- The high price of SAF. For example, HEFA was three times more expensive than JET A-1 in July 2021.
- The negative social impact of jet fuel reformulation.

Currently, a great number of scientific and technical publications and projects on this topic are published, for example, ^[8-12].

To overcome the existing barriers to the implementation of SAF in jet fuel production, appropriate policies, legislation, and a commitment to participate will be necessary. In the United States, the "California Low Carbon Fuel Standard" opted for aviation in 2018 and the "US Renewable Fuels Standard" included SAF ^[13]. The Sustainable Aviation Buyers Alliance (SABA) seeks to create an SAF credits trading system, analogous to the trading of carbon dioxide emission allowances. The Roundtable on Sustainable Biomaterials (RSB) developed a pilot scheme to apply this ^[14]. The "Sustainable Skies Act" proposed a tax credit for SAF blenders of 1.5-2.0 US\$·gal⁻¹ ^[15]. Current fuel specifications allow for up to 50 vol% blends of SAF with JET-A in the US; however, an ASTM committee is already developing a specification strategy for 100 vol% ^[4]. Sixteen organizations have committed to fly with zero carbon dioxide emissions by 2050 ^[16]. In the EU, a mandate for SAF is ready for a 63 vol% share of SAF in jet fuel by 2050 (Figure 1) ^[17, 18].

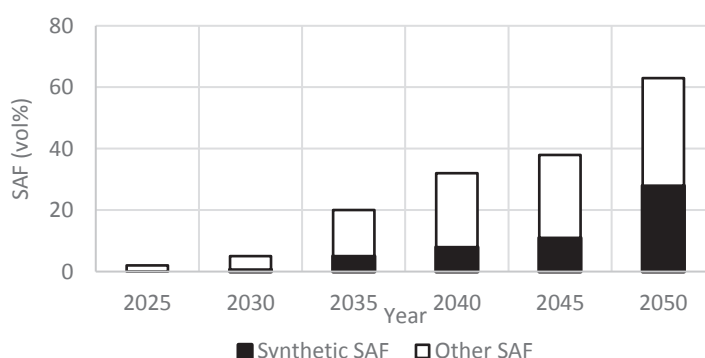


Figure 1. EU mandate for SAF

Stakeholders' engagement will be key in overcoming the existing barriers to SAF implementation – connecting organizations of different types, collaborating on policy-making, creating roadmaps, organizing various initiatives, participating in projects, mobilizing capital, collecting and publishing data, organizing conferences and webinars, etc. In this context, it is important to mention the World Economic Forum (WEF) ^[10, 19], the US

Energy Information Administration (EIA) ^[20], the International Energy Agency (IEA) Bioenergy subsidy ^[4, 21-27], the International Air Transport Association (IATA) ^[28, 29], the International Civil Aviation Organization (ICAO) ^[30-32], the Air Transport Action Group (ATAG) ^[33] and its Commercial Aviation Alternative Fuels Initiative (CAAFI) ^[26] activities.

Similar to the production of alternative components for automotive fuels, a wide variety of feedstocks can be used for the production of SAF:

- Oil crops – the 1st (rapeseed) and 2nd generation (camelina, jatropha, carinata, Salicornia, oil seed trees, etc.).
- Sugar and starch plants (sugar beet, sugar cane, lignocellulose, potatoes, etc.).
- Green juice (grasses, green apple, parsley, spinach, cucumber, lemon, ginger, etc.)
- Algae, also called the 3rd generation. They contain oil and sugar.
- Wastes of various origin (used cooking oils, animal fats, plastics, scrapped tires, municipal solid waste and residues, as well as carbon monoxide and dioxide).

For global material balance of feedstocks, see a WEF analysis ^[19] and a CAAFI presentation ^[26]. The various feedstocks can be converted to semiproducts called platforms ^[34], which open a direct path to jet fuel. These are biooil, synthesis gas, pyrolysis liquids, alcohols (methanol, ethanol, n- and i-butanol), alkanes (propene and butenes), and synthetic alkanes (farnesene). The most important technologies to produce jet fuel and components are (Table 2 and Figure 2).

Table 2

Technologies to produce jet fuel

Technology	Feed	Catalyst	T (°C)	P (MPa)
MEROX	Virgin kerosene	Active carbon, NaOH, ftalocyanine	40-60	<1
HYDROTREATING	Virgin kerosene	Co/Mo sulfides on γ -alumina	300-330	3-6
HYDROCRACKING	Vacuum distillates	Ni/Mo or Ni/W sulfides on	380-430	15-25
	Vegetable oils & animal fats	alumosilicates		
GASIFICATION	Various biofeeds, wastes	Non catalytic	>900	3
REVERSE WATER GAS SHIFT REACTION (PtL)	Carbon dioxide + hydrogen	Metal oxides on solid support	200-600	0.1
PYROLYSIS	Various biofeeds, wastes	Non catalytic or catalytic	350-900	<1
HYDROTHERMAL LIQUEFACTION (HTL)	Various biofeeds (wet)	Non catalytic	350	20
	Water			
FISHER-TROPSH SYNTHESIS (FTS)	Syngas	Fe oxides	300-350	2.5-6
		Co oxides on alumina	200-250	
METHANOL SYNTHESIS	Syngas	Cu/Zn/Cr ₂ O ₃ oxides on alumina	250	5-10
METHANOL-TO- JET	Methanol	ZSM-5	480	0.1
DEHYDRATATION	Alcohols	Strong acids	180-300	0.4
FERMENTATION	Lignocellulose, sugars	Enzymes (acetogenic bacterium)	40	0.1
OLIGOMERIZATION	Ethylene, propylene, i-butene	Resins	180-230	4-8
		H ₃ PO ₄ on solid support		
		Alkylaluminium (homogenous)		
HYDROGENATION	Alkenes	Pt on γ -alumina	250-300	3
ISOMERIZATION	n-Alkanes	Pt on γ -alumina + Cl	120-150	2-3

The standard technologies used to produce jet fuel from crude oil in oil refineries are Merox ^[35], hydrotreatment, and hydrocracking ^[36-39]. Hydrocracking vegetable oil processes are called NexBTL (Neste Oil) ^[40] and Ecofining (UOP&ENI) ^[41], originally developed to produce a component of diesel (hydrogenated vegetable oil, HVO). Each HVO facility can produce 15 vol% (without CAPEX) to 50 vol% (high CAPEX) of HEFA. Gasification, pyrolysis, and FT synthesis are mature processes. The combination of gasification, FT synthesis, and hydrocracking is used by Fulcrum Bioenergy, the Sierra Nevada project (capacity 175 kt·y⁻¹ of wastes, produces 32 kt·y⁻¹ jet fuel) ^[42-44]. The use of synthesis gas and FT synthesis is also the basis for the currently highly promoted Power-to-Liquid (PtL) technology. The German government is the main stakeholder of this technology. It plans to invest 10 billion Euros in it. A PtL roadmap has been developed in Germany ^[45]. A mandatory use from 2030 and significant shares from 2050 are considered. Pyrolysis is extremely flexible as regards feeds, reaction conditions, and product yields. HTL takes place at lower temperatures but at much higher pressures than pyrolysis and is suitable for wet feedstocks. The HyFlexFuel project uses this technology to produce jet fuel ^[46]. Oligomerization has matured as a technology to produce high octane gasoline, for example, INALK (UOP) ^[47] or DIMERSOL (Axens) ^[48], and can easily be used for the production of jet fuel. There are several sources of light olefins as feed for these technologies. The Methanol-to-Jet (MtJ) technology is

based on the Mobil Methanol-to-Gasoline (MTG) process operated in New Zealand between the years 1985-1997 (capacity $1,640 \text{ kt}\cdot\text{y}^{-1}$ of methanol to $620 \text{ kt}\cdot\text{y}^{-1}$ of gasoline) [49]. The leaders in the use of fermentation to produce ethanol to jet fuel are Lanza [50] and of biobutanol Gevo [30]. These alcohols are dehydrated, alkenes oligomerized, and hydrogenated. The specific application of enzymatic hydrolysis and fermentation is the conversion of sugars to $\text{C}_{15}\text{H}_{24}$ (α -farnesene) and $\text{C}_{15}\text{H}_{26}$ (β -farnesene) hydrocarbons, as in the Amyris & Renmatix & Total MegaBio Project [51]. Although most of the individual processes are proven, most jet fuel production schemes are not. An overview of current projects focused on the production of SAF was published [26].

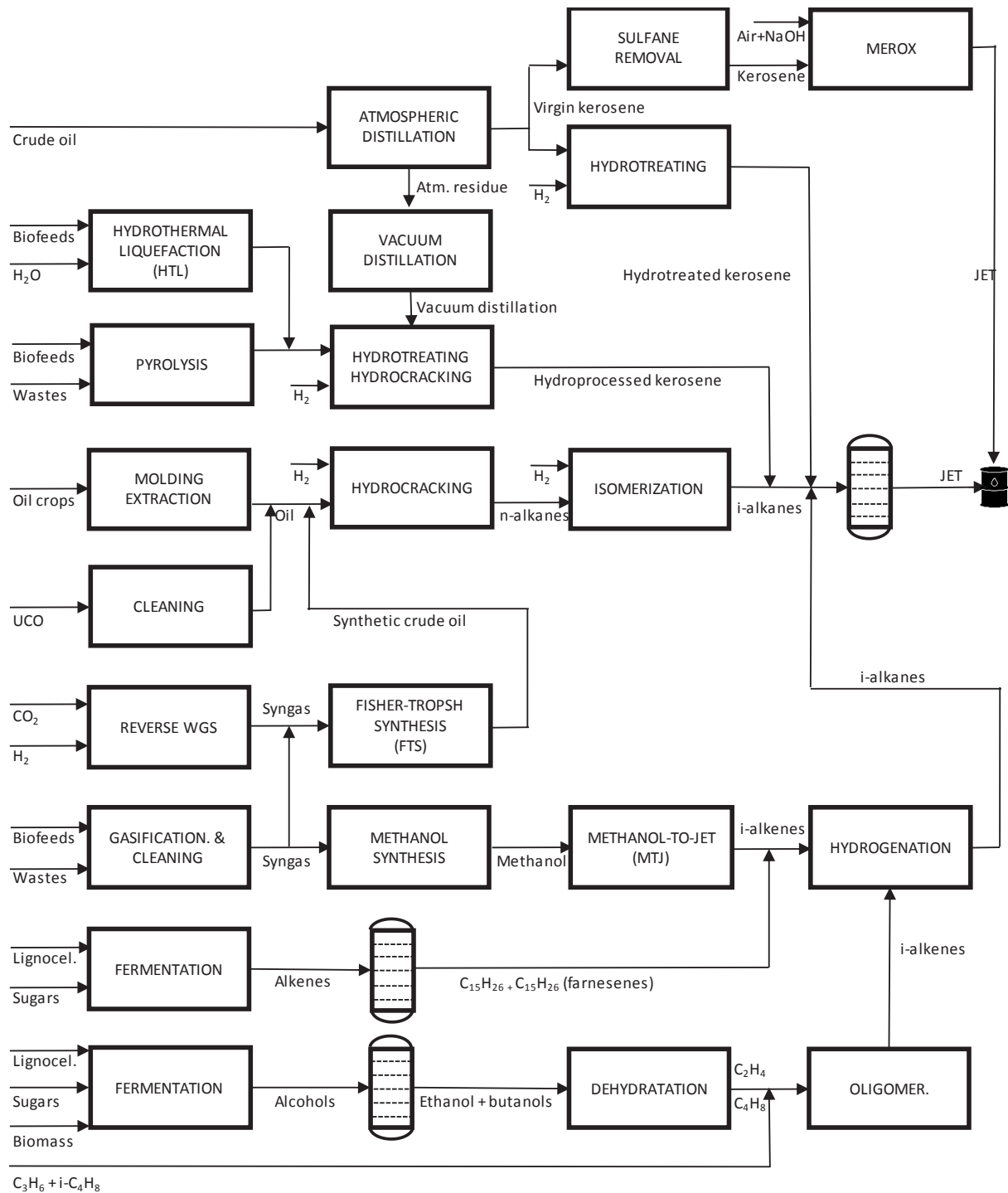


Figure 2. Overview of the most important technologies for jet fuel production

Co-processing of alternative feedstocks/platforms with mineral oil fractions is often emphasized as the recommended path, first of all, for vegetable oils, biooils, and FT waxes. Hydrocracking and FCC are the

technologies considered for this path. Co-processing of petroleum and alternative fractions is important with regard to CAPEX reduction, utilizing existing facilities, and actively involving the refining sector in the production of low-carbon-intensity products. On the other hand, this will require changes in refinery metallurgy and process parameters. The ^{14}C tracking of biocomponents in mixtures with mineral oil fractions will be important.

Only HEFA has been fully commercialized as a drop-in component (can be blended with mineral jet fuel and the final product requires no infrastructure or equipment changes) in jet fuel up to now and it will continue to be a dominant SAF to jet production over the next 10 years. Various scenarios forecast SAF consumption in 2050 at 330-445 $\text{Mt}\cdot\text{yr}^{-1}$ [4], or 50-100 vol% in jet fuel.

SAF testing in real operation has been underway since 2012 as one of the major developments in air transport. The two main airplane producers, Airbus [52, 53] and Boeing [4], in cooperation with aircraft turbine manufacturers (for example, Rolls Royce) [54] are committed in this direction. In the US, organizations such as the Federal Aviation Administration (FAA), the National Aeronautics and Space Administration (NASA), and the National Oilheat Research Alliance (NORA) are also contributing to testing with their knowledge, experience, and skills.

Discussion

Considering the 3.7% annual increase in jet fuel consumption as estimated by the EIA forecast means that about 1,110 Mt of jet fuel will be consumed in 2050. Therefore, the requirements to replace mineral kerosene with SAF must be understood in terms not of the current ($372 \text{ Mt}\cdot\text{yr}^{-1}$), but of the future jet fuel consumption ($1,110 \text{ Mt}\cdot\text{yr}^{-1}$). With a projected SAF consumption of 445 Mt in 2050 [4], petroleum-based kerosene would account for 665 Mt, almost double the current consumption. Can this be true?

Mineral feedstocks are chemical continua that contain thousands of compounds. Some platforms such as pyrolysis oils or waxes from FT synthesis are similarly complex; however, in comparison to mineral feedstocks, pyro- and biooils (HTL) contain oxygen, nitrogen, sulfur compounds, aromatics, and water in high concentration, which is difficult to process. On the other hand, other feedstocks/platforms, such as alkenes, alcohols, and vegetable oils, are chemically much simpler than mineral feedstocks.

Chemical technologies are about the conversion of feedstocks by chemical reactions under suitable conditions into the required reaction products. A range of mature refinery and petrochemical technologies are being considered to produce SAF (Table 2), for example, hydrotreating, hydrocracking, oligomerization, and isomerization. Most jet fuel is currently produced using a very simple MEROX reaction scheme. Hydrotreating and hydrocracking are also based on relatively simple chemical reactions. In contrast, the processing of alternative feedstocks is mostly based on complex chemical transformations and a very complicated reaction scheme, which necessarily means higher CAPEX and OPEX. As far as fermentation technologies are concerned, the disadvantage will be the low reaction rate, which does not allow the technology to be directly integrated with refinery or petrochemical processes. Furthermore, the desired products are present in low concentrations and thus require costly purification (alcohols). Green hydrogen can be used in all hydrogen-consuming technologies.

To produce mildly hydroprocessed mineral jet fuel, a typical hydrotreating unit capacity is $500 \text{ kt}\cdot\text{yr}^{-1}$. For SAF with CAPEX of 1 to 30 $\text{US}\$\cdot\text{gal}^{-1}$ such a grassroots unit will cost from 165 to 5,000 million US\$, i.e. 1.5-45 times more than a standard hydrotreating unit [7]. No one will invest without an adequate return on investment, which will be related to the sale price of the SAF produced, which will be high. Moreover, as the experience with HVO production shows, securing sufficient feedstocks for such a capacity will be extremely difficult.

Mineral jet fuel is a mixture of i-alkanes, cykloalkanes, aromatics. N-alkanes are present in low concentration only due to the low freezing point. However, SAFs are characterized by a significant concentration of one type of hydrocarbon. Most SAFs have a much simpler chemical composition than mineral jet fuel (farnesenes, for example), most of them contain i-alkanes, while hydrotreated kerosene from waste tires contains a high concentration of aromatics. The dominant hydrocarbons give jet fuel specific qualities. When SAF is implemented, it will be useful to look at synergies with mineral fractions and other SAFs.

Because the basic quality characteristics of jet fuel listed in Table 1 will not change, the completely different molecules of alternative feedstocks/platforms have to be transformed to the current molecules in jet fuel. This will require a more chemical approach than is usual in crude oil processing. This means that jet fuel will require research from the crude oil chemical continuum down to the molecular level. As a result, no changes in infrastructure or equipment for jet fuel supply will be necessary, resulting in billions of dollars worth of savings.

Conclusions

Even in 2050, mineral oil fractions will still play a significant role in the production of jet fuel. However, the upcoming policies and legislation will force the production and blending of sustainable aviation fuels (SAF) regardless of the real cost and price. SAF technologies will compete for feedstocks with other solutions. SAF technology schemes are not fully matured now, which means that all schemes studied can be considered promising as for now. However, the high CAPEX and OPEX and the resulting high sales prices of SAF will be serious barriers. Therefore, co-processing of alternative feedstocks with mineral oil fractions and using existing assets in oil refineries will be beneficial. HEFA pioneered the use of SAF and will be also the dominant drop-in fuel for the next decade. There is exceptional potential for further scientific research and testing of the properties and technologies of SAF. The optimistic plans for air transport and jet fuel consumption growth will be in conflict with the forthcoming extremely expensive SAF policies, and certainly both will have to be revised.

Acknowledgement

The work was supported by the Ministry of Education, Youth and Sports of the Czech Republic from the institutional support of the research organization (CZ60461373)

References

1. BP Statistical Review of World Energy 2021. 2021 [cited 2022 Mar. 15]; 70th:[Available from: <https://www.bp.com/content/dam/bp/business-sites/en/global/corporate/pdfs/energy-economics/statistical-review/bp-stats-review-2021-full-report.pdf>]
2. Loula, V. Vývoj spotřeby pohonných hmot v ČR za rok 2020. 2021 [cited 2022 Apr. 17]; Available from: <https://www.cappo.cz/aktuality-a-media/aktuality/vyvoj-spotreby-pohonnnych-hmot-v-cr-za-rok-2020>
3. The Aviation Fuel Quality Requirements for Jointly Operated Systems (AFQRJOS) in JIG Product Specification Bulletin. 2020, The Joint Inspection Group.
4. Newsum, S., The path to sustainable aviation, in The IEA Bioenergy Conference 2021. 2021, Dec. 1, The IEA Bioenergy.
5. Hanson, S., EIA projects energy consumption in air transportation to increase through 2050. 2019 [cited 2021 Nov. 15]; Available from: <https://www.eia.gov/todayinenergy/detail.php?id=41913>
6. The Sustainable Aviation Buyers Alliance (SABA). 2022 [cited 2022 Apr. 1]; Available from: <https://rmi.org/saba/>
7. Blanshard, A., et al., Fueling Net Zero. 2021, Sep., ICS International Inc.: Fairfax, US.
8. Waypoint 2050. 2020, Sep., The Air Transport Action Group (ATAG).
9. Destination 2050. A Route to Net Zero European Aviation. 2021, Feb., The Royal Netherland Aerospace Centre: Amsterdam.
10. Soubly, K., C. Wolf, and L. Uppink, Clean Skies for Tomorrow Sustainable Aviation Fuels as a Pathway to Net-Zero Aviation. 2020, Nov., The World Economic Forum.
11. Decarbonisation Road-map: A Path to Net Zero. A plan to decarbonise UK aviation. 2020, sustainableaviation.co.uk.
12. Ten critical insights on the path to a net-zero aviation sector. 2021, Oct., Mission Possible Partnership.
13. Renewable Fuel Standard Program. Approved Pathways for Renewable Fuel. 2021 [cited 2022 Apr. 17]; Available from: <https://www.epa.gov/renewable-fuel-standard-program/approved-pathways-renewable-fuel>
14. RSB - Advancing the transition to a bio-based and circular economy. 2022 [cited 2022 Apr. 2]; Available from: <https://rsb.org/>
15. U.S. Airlines Applaud Introduction of Sustainable Skies Act. 2021, May 20 [cited 2022 Apr. 17]; Available from: <https://www.prnewswire.com/news-releases/us-airlines-applaud-introduction-of-sustainable-skies-act-301296418.html>
16. Commitment to Fly Net Zero 2050. 2021, Oct. 5 [cited 2022 Apr. 15]; Available from: <https://aviationbenefits.org/media/167501/atag-net-zero-2050-declaration.pdf>
17. COMMUNICATION 2021/ 561 final proposal for a regulation of the European Parliament and of the Council on ensuring a level playing field for sustainable air transport. 2021, The European Commission: Brussels.
18. COMMUNICATION 2021/ 561 Annex to the proposal for regulation of the European Parliament and of the Council on ensuring a level playing field for sustainable air transport. 2021, Jul. 14, The European Commission: Brussels.

19. Gibbs, A., et al., Clean Skies for Tomorrow – Sustainable Aviation Fuel Policy Toolkit, D. Carpenter, Editor. 2021, Nov., The World Economic Forum: Geneva.
20. International Energy Outlook 2021 with projection to 2050. 2021 [cited 2022 Feb. 2]; Available from: https://www.eia.gov/outlooks/ieo/pdf/IEO2021_Narrative.pdf
21. The IEA Bioenergy Task 39 – Biofuels to Decarbonize Transport. 2022 [cited 2022 Apr. 12]; Available from: <https://task39.ieabioenergy.com/>
22. van Dyk, S., et al., Drop-in: The key role that co-processing will play in its production. 2019, Jul., The IEA Bioenergy.
23. The IEA Bioenergy Webinar - Sustainable Aviation Fuel/Biojet Technologies - Commercialization Status, Opportunities and Challenges. 2021 [cited 2022 Apr. 17]; Available from: <https://www.ieabioenergy.com/blog/publications/iea-bioenergy-webinar-sustainable-aviation-fuel-biojet-technologies-commercialisation-status-opportunities-and-challenges/>
24. The IEA Bioenergy Conference 2021. 2021 [cited 2021 Dec. 9]; Available from: <https://www.ieabioenergyconference2021.org/>
25. van Dyk, S. and J. Saddler, Progress in Commercialisation of Biojet fuels/SAF, in The IEA Bioenergy Conference 2021. 2021, The IEA Bioenergy.
26. Csonka, S., Sustainable Aviation Fuel (SAF) U.S. Progress and Direction Overview, in The IEA Bioconference 2021. 2021, Dec. 1, The IEA Bioenergy.
27. Tauvette, G., The development of C-SAF, and progress in establishing a Canadian biojet/SAF supply chain, in The IEA Bioconference 2021. 2021, Dec. 1, The IEA Bioenergy.
28. IATA Guidance Material for Sustainable Aviation Fuel Management. 2015, The International Air Transport Association (IATA): Montreal-Geneve.
29. IATA Sustainable Aviation Fuel Roadmap. 2015, International Air Transport Association (IATA): Montreal.
30. Johnston, G., Alcohol to Jet - Isobutanol, in ICAO Seminar on Alternative Fuels, 2017, Feb. 8-9, Montreal. 2017, The International Civil Aviation Organization (ICAO): Montreal.
31. Carbon Offsetting and Reduction Scheme for International Aviation (CORSA). 2019 [cited 2022 Apr. 21]; Available from: <https://www.icao.int/environmental-protection/CORSIA/Pages/default.aspx>
32. ICAO 2019 Environmental Report. Destination Green. The Next Chapter. 2019, The International Civil Aviation Organization (ICAO): Montreal.
33. Waypoint 2050. 2021, Sep., The Air Transport Action Group (ATAG).
34. Task 42: Biorefining in a Circular Economy. 2020 [cited 2020 Dec. 3]; Available from: <https://task42.ieabioenergy.com/>
35. Honeywell-UOP. Diesel & Jet. Refining 2022 [cited 2022 Mar 10]; Available from: <https://uop.honeywell.com/en/industry-solutions/refining/diesel-and-jet>
36. Robinson, P.R., Hydroconversion processes and technology for clean fuel and chemical production, in Advances in Clean Hydrocarbon Fuel Processing, R.M. Khan, Editor. 2011, Sep., Woodhead Publishing: Sawston. p. 287-325.
37. Hydrocracking is an important source of diesel and jet fuel. 2013 [cited 2022 Feb. 9]; Available from: <https://www.eia.gov/todayinenergy/detail.php?id=9650>
38. Christensen, P., A. Hearn, and T. Yeung. The future for hydrocracking: part 1. 2017 [cited 2021 Nov. 15]; Available from: <https://cdn.digitalrefining.com/data/articles/file/1103141712.pdf>
39. Christensen, P., A. Hearn, and T. Yeung. The future for hydrocracking: part 2. 2018 [cited 2021 Nov. 15]; Available from: <https://cdn.digitalrefining.com/data/articles/file/1754709570.pdf>
40. NexBTL technology. 2022 [cited 2022 Apr. 25]; Available from: <https://www.neste.com/about-neste/innovation/nexbtl-technology>
41. Honeywell Green Diesel. 2022 [cited 2022 May 5]; Available from: <https://uop.honeywell.com/en/industry-solutions/renewable-fuels/green-diesel>
42. BP and Johnson Matthey licence Fischer-Tropsch technology to waste-to-biofuels producer Fulcrum BioEnergy for biojet. 2018, Sep. 28 [cited 2022 Apr. 20]; Available from: <https://www.greencarcongress.com/2018/09/20180928-bp.html>
43. SK Inc. Invests in Fulcrum BioEnergy to Accelerate Production of Low-Carbon Fuel from Waste. 2021, Dec. 16 [cited 2022 Apr. 20]; Available from: <https://www.prnewswire.com/news-releases/sk-inc-invests-in-fulcrum-bioenergy-to-accelerate-production-of-low-carbon-fuel-from-waste-301446673.html>
44. Clean, Low-Cost, Sustainable-Low-carbon fuel made from trash reduces reliance on imported oil. 2022 [cited 2022 Apr. 1]; Available from: <https://fulcrum-bioenergy.com/contact-us/>
45. Pfeiffer, U.M. and M. Spöttle, PtL roadmap. Sustainable aviation fuel from renewable energy sources for aviation in Germany. 2021, Apr., Nordicelectrofuel.

46. The HyFlexFuel Project. 2022 [cited 2022 Apr. 5]; Available from: <https://www.hyflexfuel.eu/technologies/>
47. The Isoalky Process Solution. 2021 [cited 2021 Oct. 28]; Available from: <https://www.digitalrefining.com/videos/209/the-isoalky-process-solution>
48. Jones, D. and P.R. Pujado, Dimersol, in Handbook of Petroleum Processing 2006, Springer The Netherlands p. 389-391.
49. Hindman, M., Exxon Mobil methanol to gasoline (MTG), in Syngas Technology Conference. 2017, Global Syngas Technologies Council: Colorado Spring, CO, USA.
50. Hede, K. Faster and Cheaper Ethanol-to-Jet-Fuel on the Horizon. 2021, Aug. 19 [cited 2022 Apr. 7]; Available from: <https://www.pnnl.gov/news-media/faster-and-cheaper-ethanol-jet-fuel-horizon>
51. Mitrovich, Q. MegaBio: Integrated process for production of farnesene, a versatile platform chemical, from domestic lignocellulosic feedstock. 2019, Mar. 6 [cited 2022 Apr. 10]; Available from: https://www.energy.gov/sites/prod/files/2019/03/f61/Integrated%20process%20for%20commercial%20production%20of%20farnesene%20a%20versatile%20platform%20chemical%20from%20domestic_EE000772_9_v2.pdf
52. A319neo takes off on 100% Sustainable Aviation Fuels. 2021 [cited 2021 Nov. 5]; Available from: <https://www.youtube.com/watch?v=qF1IOX7H5t8>
53. This A380 is the latest to test 100% SAF. 2022, Mar. 28 [cited 2022 Apr. 24]; Available from: <https://www.airbus.com/en/newsroom/news/2022-03-this-a380-is-the-latest-to-test-100-saf>
54. Chui, S. Flying the Rolls Royce B747 Test Bed - An Experimental Flight with 100% SAF. 2021 [cited 2022 Mar. 23]; Available from: <https://www.youtube.com/watch?v=4gSKbmODNxl>

EMPIRICAL MODEL FOR PREDICTION OF VISBREAKING PRODUCT YIELDS

Jíša P., Černý R.

ORLEN UniCRE a.s., Revoluční 1521/94, Ústí nad Labem, 400 01

petr.jisa@orlenuicre.cz

ABSTRACT

Prediction of visbreaking conversion and product yields may be carried out using various kinetic models. The kinetic models can be very accurate but they require high amount of input parameters. In fact, the overall amount and diversity of the input parameters can limit the model precision. Therefore, empirical models can become a more suitable tool in many cases. In our study we present our empirical model for prediction of visbreaking product yields from the feedstock input vector at two fixed severity levels. At any process conditions, the yields of all visbreaking fractions are determined by a linear interpolation using the yields, calculated for the fixed severity levels. Verification of the model showed that it could be applied instead of the kinetic models, providing an advantageous combination of simplicity and sufficient prediction accuracy.

INTRODUCTION

Refining technologies are usually simulated by kinetic models. These models can offer a precise prediction of the yield vectors for the technologies. However, they have also disadvantages. One of them is the necessity of carrying out the kinetic study, to obtain a relevant data for development of the model. Another disadvantage is that these models have high demands on the amount and diversity of the input data, such that it can limit the usage of these models.

Especially, simulation of visbreaking¹ and other processes for manufacturing of the crude oil residues can be a challenge. There are not many studies, dealing with modelling of visbreaking. And furthermore, the possibilities of chemical analysis of the feedstocks for visbreaking is limited due to the properties of these materials. Last but not least, the simulation of visbreaking process on a pilot unit, as a key part of the kinetic study, may also be difficult due to the coking phenomenon and severe reaction conditions.

Nevertheless, there are still a few studies, dealing with kinetic modelling of visbreaking process^{1,2}. The models from these studies have the aforementioned disadvantages – to use them, it is necessary to dispose with high amount of input parameters and the usage is very difficult. Another study³ deals with estimation of visbreaking yield vector from the limited amount of feedstock properties (content of carbonization residue, results from SARA analysis) and basic processing parameters (feedstock residence time, reaction temperature). The demands on input parameters are significantly lower and acceptable. However, it still requires to be equipped with thin layer chromatography, to carry out SARA analysis. Moreover, this method may also be too slow and difficult for frequent analyses of visbreaking feedstock, to obtain sufficient amount of input data.

The goal of our study was to develop a simple empirical model for prediction of visbreaking yield vectors. Input parameters of the model are only transformed simulated distillation curve of the visbreaking feedstock, feedstock residence time and reaction temperature. Verification of the model showed that it could be applied instead of the kinetic models, providing an advantageous combination of simplicity and sufficient prediction accuracy.

ARCHITECTURE, FITTING AND VERIFICATION OF THE MODEL

The basic assumption

The basic assumption for the model development is the existence of a linear dependence of the yield vector on the shape of the feedstock distillation curve at visbreaking reference state (equivalent operating conditions). If this assumption is valid, the relationship between the yield vector and the vectorized representation of the feedstock distillation curve at fixed visbreaking reference state is able to be expressed by equation (1):

$$\vec{w}^T = A \cdot \vec{u}^T \quad (1)$$

where

$$\begin{aligned} \vec{w} &= (w_1, \dots, w_m) && \text{Yield vector} \\ \vec{u} &= (u_1, \dots, u_n) && \text{Feedstock composition vector} \\ A &= \begin{pmatrix} a_{1,1} & \dots & a_{1,n} \\ \vdots & \ddots & \vdots \\ a_{m,1} & \dots & a_{m,n} \end{pmatrix} && \text{Distribution matrix (m x n)} \end{aligned}$$

In principle, the yield vector and feedstock composition vector may be defined variously. In our study, the yield vector coordinates are defined by Table I and the feedstock composition vector coordinates are defined by Table II.

Table I. The yield vector coordinates

m	1	2	3	4	5
Product yield [wt %]	Gas	Gasoline	Gas oil	Vacuum distillate	Vacuum residue

Table II. The feedstock composition vector coordinates

n	1	2	3	4	5	6	7	8	9
Content of fraction [wt %]	< 400 °C	400 – 450 °C	450 – 500 °C	500 – 550 °C	550 – 600 °C	600 – 650 °C	650 – 700 °C	> 700 °C	1

Visbreaking reference states

In our work, the visbreaking reference states were defined as the states at which visbreaking residue of given viscosity (η_{REF}) is produced from the feedstock of given viscosity (η_{FEED}).

In general, it is suitable to find at least two various reference states. These states should represent various visbreaking conversion levels, to enable interpolative calculation of visbreaking yield vectors at the process conditions that do not correspond with the process conditions at reference states. In our work, two reference states are used, representing low conversion level and high conversion level of visbreaking. The definition of these states are in Table 3.

Table III. Visbreaking reference states

Reference state	Conversion level	η_{FEED} (at 100 °C)	η_{REF} (at 150 °C)
REF 1	Low	1300	300
REF 2	High	1300	500

Equivalent operating conditions

Filtration of visbreaking processing data using the criteria from Table III returns the equivalent operating conditions for the reference states REF 1 and REF 2, at which the visbreaking unit achieves the specific conversion levels. It was found out that the equivalent operating conditions can be expressed as linear relationships between feedstock flow and reaction temperature.

For REF 1 and REF, different relationship is found out (Figure 1). These relationships enable to obtain information, what reaction temperature must be achieved at given feedstock flow, to reach the visbreaking reference state (whether REF 1 or REF 2), and vice versa.

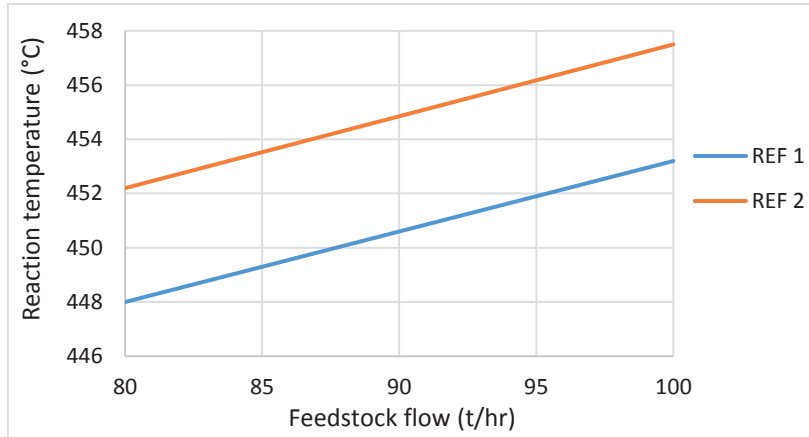


Fig. 1. Equivalent operating conditions for visbreaking reference states (REF 1 and REF 2)

Distribution matrix for the visbreaking reference states

As a next step in the model development, it is possible to filtrate the data that correspond with reaching the defined visbreaking reference states – REF 1 or REF 2. This step can easily be done by filtration of data according to combination of feedstock flow and reaction temperature. Then the data that are found for the feedstocks with available viscosity at combinations of feedstock flow and reaction temperature, corresponding with the reference states according to the relationships in Figure 1, create the data set for REF 1 and REF 2. On this filtered data set for REF 1 and REF 2, it is possible to apply the equation (1) and to determine the distribution matrix for these reference states using the least squares method, according to the equation (2) and equation (3).

$$\overrightarrow{w_{REF1}^T} = A_{REF1} \cdot \overrightarrow{u^T} \quad (2)$$

$$\overrightarrow{w_{REF2}^T} = A_{REF2} \cdot \overrightarrow{u^T} \quad (3)$$

Calculation of visbreaking yield vector

Using the equation (2) and (3), it is possible to calculate the theoretical visbreaking yield vectors at both reference states REF 1 and REF 2. From these yield vectors, it is possible to calculate the real visbreaking yields, using the linear interpolation according to the equation (4):

$$\overrightarrow{w_{REAL}} = \overrightarrow{w_{REF1}} + \frac{T_{REAL} - T_{REF1}}{T_{REF2} - T_{REF1}} \cdot (\overrightarrow{w_{REF2}} - \overrightarrow{w_{REF1}}) \quad (4)$$

Figure 2 explains obtaining the determination of temperatures T_{REF1} and T_{REF2} for the equation (4) in detail. At the actual feedstock flow, the corresponding temperatures T_{REF1} is found as temperature, at which the reference state REF 1 is reached at the actual feedstock flow. T_{REF2} is determined similarly, but for the reference state REF 2.

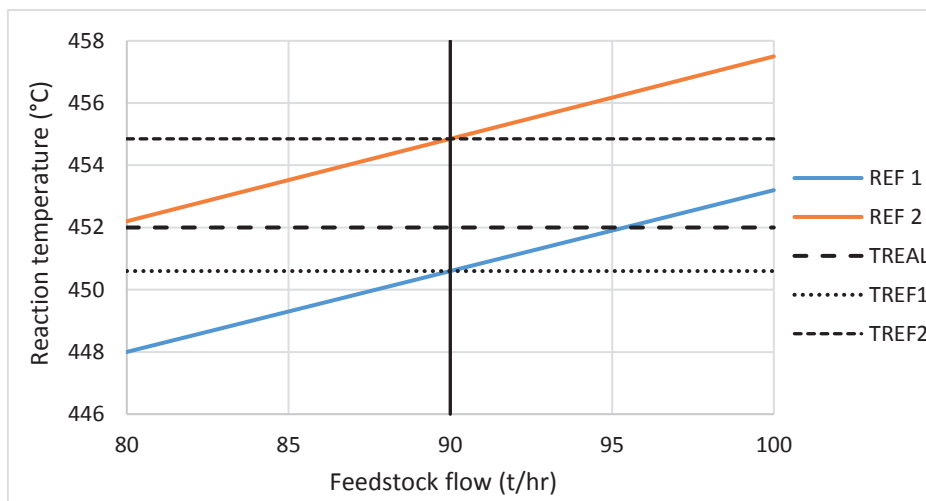


Fig. 2. Calculation of T_{REF1} and T_{REF2}

At the conditions, corresponding to actual feedstock flow and calculated temperatures T_{REF1} and T_{REF2} , reference visbreaking yield vectors \vec{w}_{REF1} and \vec{w}_{REF2} are calculated using the distribution matrix for REF 1 and distribution matrix for REF 2, according to equations (2) and (3). In the end, a simple linear interpolation using the relationship between real temperature and temperatures T_{REF1} and T_{REF2} is used to calculate the real visbreaking yield vector from reference visbreaking yield vectors \vec{w}_{REF1} and \vec{w}_{REF2} .

Model fitting and verification

The available visbreaking data were divided into three groups:

- data for low conversion reference state (REF 1)
- data for high conversion reference state (REF 2)
- remaining data

The data for low conversion reference state (REF 1) and for high conversion reference state (REF 2) were used as the training dataset. From these data, the distribution matrix A_{REF1} and distribution matrix A_{REF2} were determined by a least squares method according to equation (2) and equation (3). The remaining data were used as a verification dataset – they were used for calculation of visbreaking yield vector, using the equation (4).

RESULTS AND DISCUSSION

The verification of the model was carried out by comparison of the calculated yield vectors with the real yield vectors. To simplify the vectors comparison, the calculated yields of the visbreaking products were compared with the real yields of these products.

The yields of gases were not significantly influenced neither by feedstock nor by the process conditions – most frequently, they were in the range from 2.5 wt % and 3 wt %. The yields of other products were more different and the relationships between the calculated yields were discussed.

Figure 3 contains comparison of calculated and real yields of gasoline, gas oil, vacuum distillate and vacuum residue. In general, the prediction of all products yields was carried out with less than 2 wt % error. For the prediction of gas oil, there was a slightly higher tendency to overestimate the yield (higher amount of cases when the calculated yield was more than 2 wt % higher compared to the real yield), which was compensated by an opposite tendency to underestimate the yield of vacuum residue. Nevertheless, these errors occurred in minor cases. For gasoline, the prediction was the most accurate – the difference between calculated and real

yield did not exceed 1 wt % in most cases. On the other hand, this higher accuracy also corresponds with narrower range of the real gasoline yields, compared to the range of real yields of other visbreaking products.

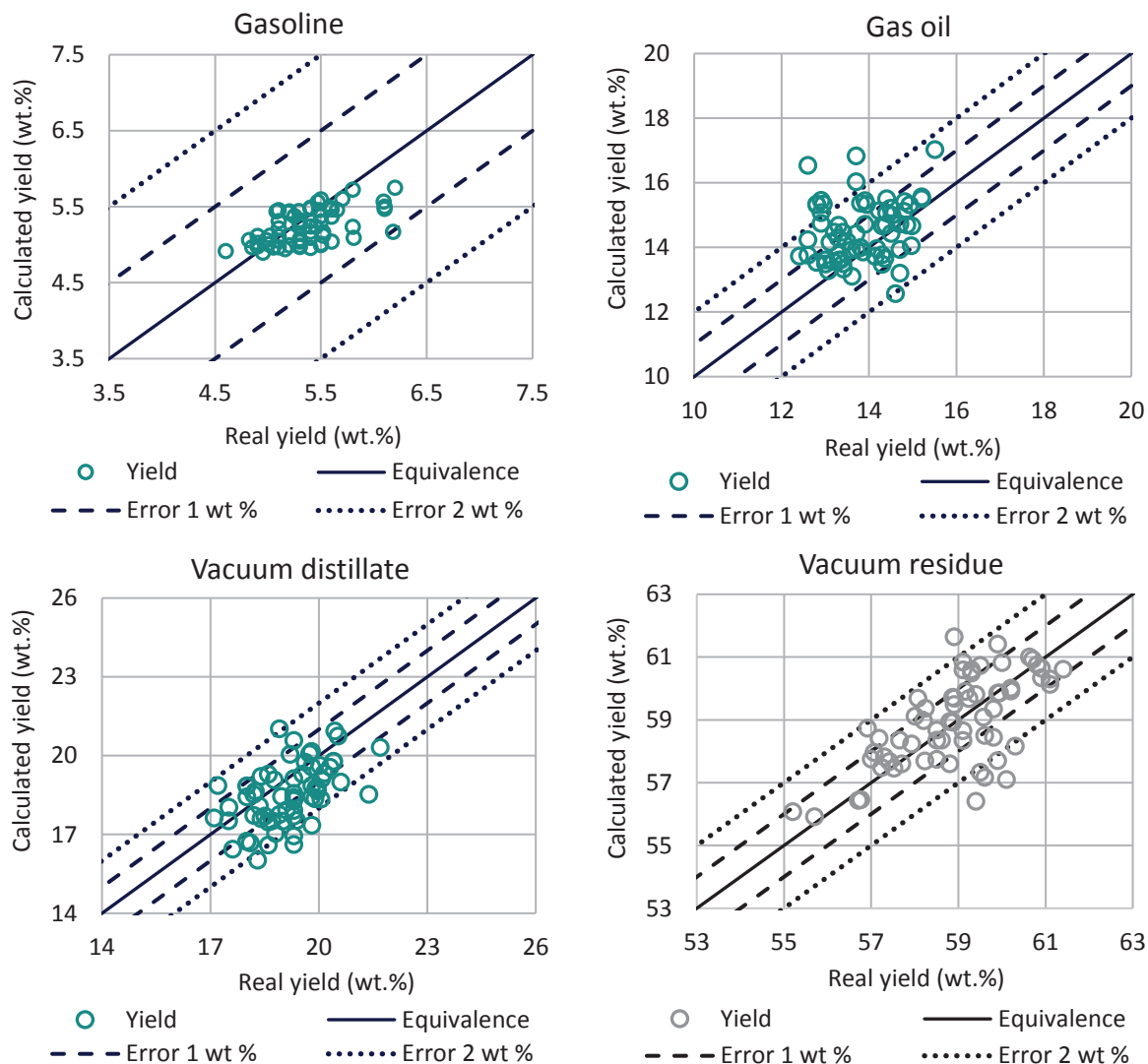


Fig 3. Model verification – yields of gasoline, gas oil, vacuum distillate and vacuum residue

CONCLUSIONS

Empirical model for prediction of visbreaking yield structure was developed. The main benefit of this model is that it does not require to carry out the kinetic study of visbreaking - it is easy to be created only from the processing data, using two reference states that correspond with different visbreaking conversion levels. Moreover, the model is not too demanding on the input parameters – it only requires the feedstock simulated distillation curve, reaction temperature and feedstock flow to carry out the calculation of visbreaking yield vector. The accuracy of the model is up to 2 wt % for all visbreaking products in most cases.

REFERENCES

1. Mohaddecy, S. R. S., & Sadighi, S. (2011). Simulation and kinetic modeling of vacuum residue soaker-visbreaking. *Petroleum & Coal*, 53(1), 26-34.
2. Joshi, Jyeshtharaj B., et al. "Petroleum residue upgradation via visbreaking: A review." *Industrial & Engineering Chemistry Research* 47.23 (2008): 8960-8988.
3. Kataria, K. L., Kulkarni, R. P., Pandit, A. B., Joshi, J. B., & Kumar, M. (2004). Kinetic studies of low severity visbreaking. *Industrial & engineering chemistry research*, 43(6), 1373-1387.

ACKNOWLEDGEMENT

The publication is a result of the project which was carried out within the financial support of the Ministry of Industry and Trade of the Czech Republic with institutional support for long-term conceptual development of research organisation.

Kraviarová D.¹, Janošovský J.¹

¹*Institute of Chemical and Environmental Engineering, Faculty of Chemical and Food Technology, Slovak University of Technology in Bratislava, Radlinského 9, 812 37, Bratislava, Slovak Republic
jan.janosovsky@stuba.sk*

Abstract

Multi-criteria decision analysis (MCDA) is a very important tool nowadays. Using MCDA can comprehensively compare several of chosen process design alternatives and reduce their number for the future realisation. In this work, eight alternatives of hydrogen production were compared by four criteria: economics, material use and energy efficiency, safety and environmental aspect. We applied this method on the hydrogen production by steam reforming. The subject of this analysis was set of eight representative process design alternatives. Ranking of process design alternatives was constructed for all possible criteria combination. Our attention was also aimed at two often communicated topics nowadays: importance of economics or environmental aspect of the chosen alternatives. The impact of each criterion's dominance to the final ranking was also studied. Interesting result of this study was the change of final ranking if different criterion was considered as the most important. NG and NG LTS alternatives were dominant in economic case. Their positions decreased in the middle of the ranking if environmental aspect was the most important. Biogas alternative with addition of LTS and post-combustion carbon capture was the best alternative in this case.

Introduction

Economic analysis is usually the main prerequisite for identification if introduced process design is suitable and can be realized into industrial scale. Except of economics, important aspect is also safety of the process. When more process design alternatives are available, plant management's attention is paid to comparative criteria, mainly economics, to find the most feasible alternative. Nowadays, chemical processes are evolving fast and with use of multiple criteria we can find advantages and disadvantages of single processes. It is the main goal of multi-criteria decision analysis (MCDA)¹, principles of which have been applied in this work. More complex results are achieved as opposed to comparison according to only one criterion. At the present, environmental aspect has more and more important position in introducing new technology. Rating of process design alternatives could totally change final ranking or get different trends in results when comparison is done by environmental or economic aspect separately. Combination of more criteria provided us complex overview of presented alternatives, but this method has to be applied carefully to avoid incorrect conclusions. In this work, four main criteria were chosen: economics, material use and energy efficiency, safety and environmental aspect. The goal was to compare eight created process design alternatives. We can create any weighting of these criteria by using analytic hierarchy process (AHP) methodology. AHP is the most popular and powerful method for group decision making used in project selection, which simplifies complex problems by decision criteria¹. Problems are simplified by defining sub-criteria whose priorities are calculated. The main principle of AHP application is creation of comparison pair-wise matrixes by user decision of criteria preference. Evaluation of decision preferences is converted to numerical values. Final ranking of presented alternatives is achieved by connecting the weights of sub-criteria with the score of decision alternatives².

Methodology of MCDA and AHP was applied to hydrogen production. Nowadays almost all hydrogen is produced by steam reforming of hydrocarbons or the water electrolysis^{3,4}. The most frequently used technology in industrial hydrogen production is catalytic steam reforming, which was also considered in our study.

Hydrogen production by steam reforming

Heart of the technology consists of two reactors. Reaction with overall endothermic effect run in the first reactor called a steam reformer (SR). Main portion of hydrogen is produced there. Second reaction is exothermic and takes place in high temperature shift reactor (HTS). Additional hydrogen together with carbon dioxide is produced in this step⁵. Scheme of hydrogen production by steam reforming is depicted in Figure 1. Process design alternatives differed in types of processed feedstocks. Two different types of raw material were used, natural gas (NG) representing traditional feedstock and on the other hand more environmentally friendly alternative – biogas (BG). Operation temperature in steam reformer (SR) is 825 °C to all alternatives with natural gas as a

feedstock and 700 °C to biogas alternative. Improvement in basic technology was done by addition of low temperature shift reactor (LTS) after HTS. An advantage of this addition is increase in hydrogen yield with simultaneous reduction of carbon monoxide in outlet flow. Environmental improvement was achieved by extension of post-combustion carbon capture (CC) which is a requirement for reclassification of produced hydrogen from grey to blue. By-product of the second reaction section, carbon dioxide, is captured by added absorber/desorber unit.

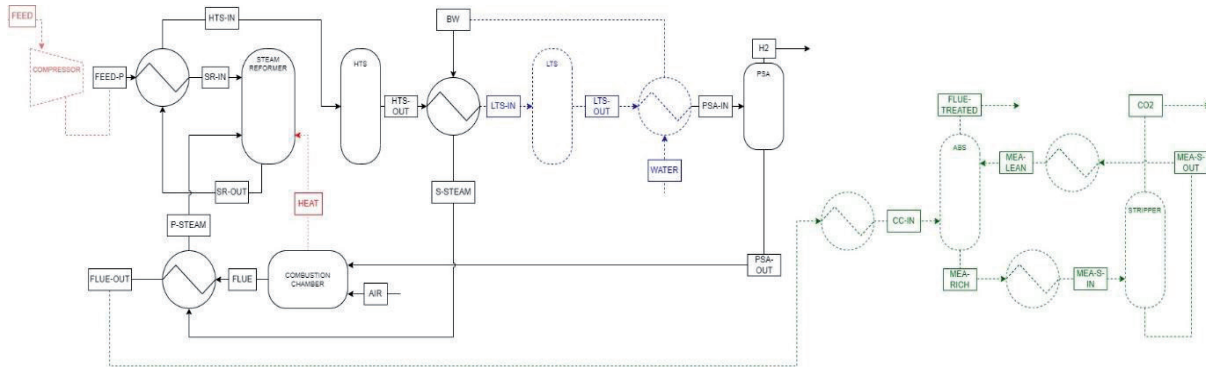


Figure 1. Scheme of hydrogen production by steam reforming; basic process with NG feedstock (black), basic process with BG feedstock (red+black), addition of LTS reactor (blue), addition of post-combustion carbon capture (green)

Presented specific processes of hydrogen production were divided to eight representative process design alternatives (characterisation of each alternative is shown in Table I) and they were simulated in Aspen Plus.

Table I
Basic characteristics of process design alternatives

Process design alternative		LTS	CC
Biogas	Natural gas		
BG	NG	×	×
BG LTS	NG LTS	✓	×
BG CC	NG CC	×	✓
BG LTS+CC	NG LTS+CC	✓	✓

MCDA and AHP principles

MCDA is an analytic method that connects several criteria to make ranking and find the best of presented alternatives¹. Schematic procedure of our employed MCDA is shown in Figure 2. Decision-making requires the evaluations of different sub-criteria, which are calculated simultaneously. We can usually divide sub-criteria to three groups, represented by main criteria, that are economic, environmental, and social dimension which is described by safety of processes⁶. The fourth criterion in our study was material use and energy efficiency for assessment of process energy requirements.

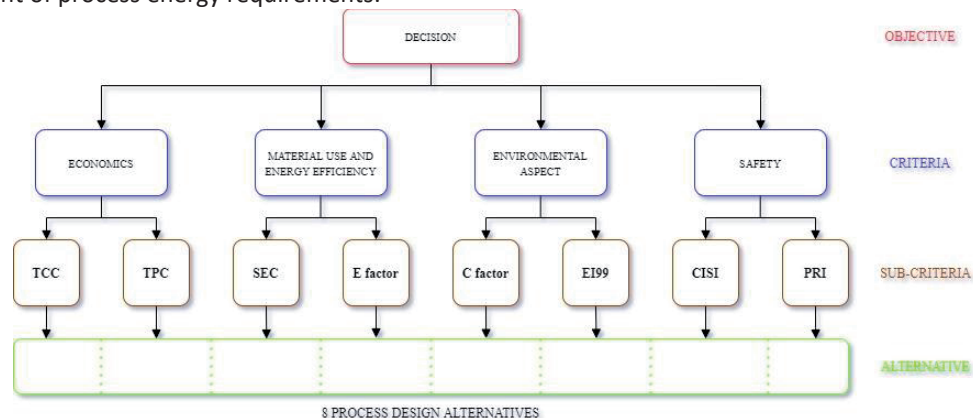


Figure 2. Scheme of MCDA methodology

Final ranking is conclusion of MCDA technology, which is preceded by several calculation steps. Firstly, appropriate indicators (sub-criteria) were found for description of compared criteria. In this study two sub-criteria characterised each criterion. Their values were calculated for every process design alternative separately. Sub-criteria weights were determined based on their complexity. Total Capital Cost (TCC) and Total Production Cost (TPC) were chosen as economic indicators. Costs of devices were calculated using built-in simulator economic tool and index methods from literature⁷. Material use and energy efficiency was described by specific energy consumption (SEC) and E factor. SEC was calculated as ratio of energy consumption to mass of the product. E factor characterised amount of waste per amount of product. Environmental indicators were C factor and massive Eco-indicator 99 (EI99). C factor represented quantity of produced carbon dioxide equivalents per mass of product. EI99 included three types of environmental damages that affect human health, natural resources, and ecosystem quality. Principals of EI99 calculation are to impose penalties for each of the three aspects of environmental damage. Final value of EI99 is obtained by counting all penalties⁸. Safety was characterised by Comprehensive Inherent Safety Index (CISI) and Process Route Index (PRI). CISI includes both toxicity and flammability potential. Value of CISI represent overall process hazard index which is calculated with score of multiple indexes. PRI depends on basic process parameters which are directly proportional to explosion potential and can be directly exported from simulation tool. Two main parameters are mass release defined by average density and pressure and energy release defined by average heating value. Common method for solving MCDA is AHP and it is comprised from five steps. Basic characterization of each step of our study is described below:

1. Define the decision problem:
 - create the ranking of process design alternatives with different preferences of criteria
2. Find out criteria priorities:
 - choose preferences between four criteria – typically odd numbers from 1 to 9 (1 is equally preferred and 9 is extremely preferred)
 - create a pair-wise comparison matrix – it is based on preferences from point 2. a)
 - assess the consistency of the matrix – matrix is acceptable as consistent if consistency index does not exceed value of 0.1
 - calculate the priority of each criterion – we obtained four values of priorities
3. Assign importance of sub-criteria:
 - in this study two sub-criteria describe one criterion, and their importance was determined by their complexity
4. Find out process design alternatives priorities (specific to every criterion):
 - calculate values of sub-criteria
 - determine a sub-criterion score (position 1st-8th)
 - determine a criterion score (position 1st-8th) – multiply importance and score of sub-criteria
 - create a pair-wise matrix – one matrix for each presented criterion
 - calculate the weights of process design alternatives corresponding to each criterion – weights are same during all AHP calculation, and they are connected to presented process design alternatives
5. Create ranking:
 - multiply weights of criteria with priorities of criteria – final ranking of eight chosen process design alternative is create with position from the first to the eighth place

We can create n possible pair-wise comparison matrixes (step 2) which correspond with n rankings for different preferences of criteria. Our study identified 9 027 logical decision scenarios with usage of odd numbers from 1 to 9 of preferences between four criteria. It was found by cyclic calculation of the second step where consistency index represented condition which must be fulfilled.

Simulation of described AHP methodology was conducted in MATLAB environment. Values of presented sub-criteria were calculated separately and algorithm of AHP in MATLAB used these values as input data.

Comparison of economics and environmental aspect

For better understanding of introduced AHP principles, two specific results of this method are shown (Figure 3) in comparison of two dominant criteria: economics and environmental aspect. Firstly, we create two pair-wise comparison matrixes, examples of both are illustrated in Figure 3. Preferences between criteria were odd numbers from 1 to 7. Dominant preference was characterised by number 7, decreasing preference represents number 5 and 3.

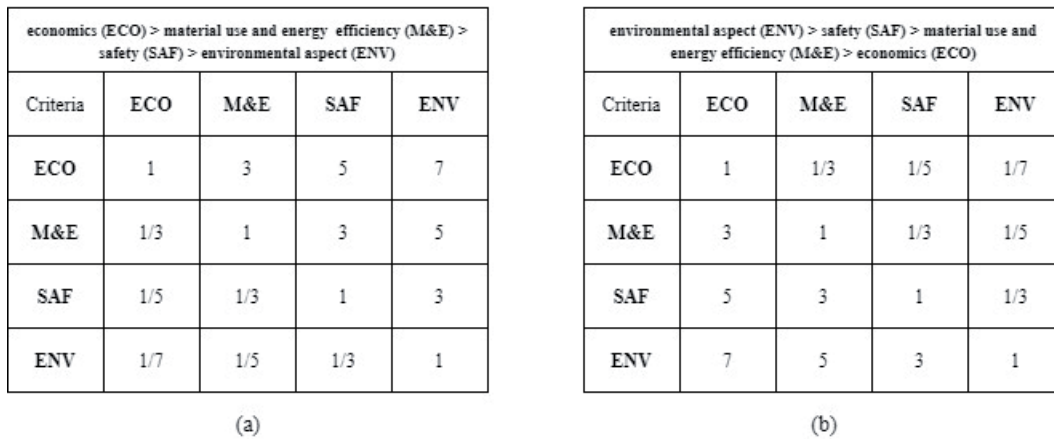


Figure 3. Pair-wise matrices: dominant criterion is economics (a) and environmental aspect (b)

We have found out that the final ranking changes dramatically with substitution of the criteria importance. If economics was the dominant criterion, the ranking of criteria is presented in Figure 3a. Concrete ascending ranking of criteria were economics, material use and energy efficiency, safety, and environmental aspect. The exact opposite importance was associated with the environmental aspect as the key criterion. Pair-wise matrix also with criteria ranking of this example is shown in Figure 3b. Condition of consistency was fulfilled for both matrixes. Final ranking of process design alternatives for both decision scenarios is illustrated in Figure 4.

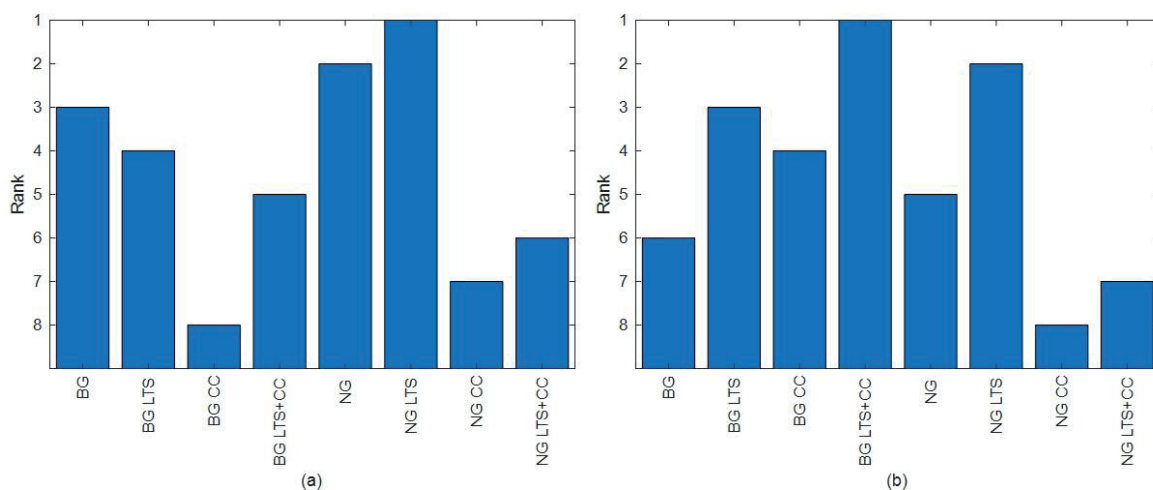


Figure 4. Ranking of process design alternatives if the most important criterion is economics (a) and environmental aspect (b)

The assumption that better positions for BG alternatives are achieved if the environmental impact is the most important criterion was fulfilled. The best alternative for economics being the dominant criterion was NG feedstock with addition of LTS. High positions of NG and NG LTS alternatives in this case confirm common technology used for hydrogen production in the industry. Basic production processes with both types of feedstocks (BG and NG) have better positions in the economic case (Figure 4a). Their positions decrease to the second half of the ranking in the case of environmental importance (Figure 4b). Using biogas and inclusion of carbon capture and LTS in hydrogen production made this process the best alternative from environmental point of view.

Overall ranking of processes

Second part of this work was comparing alternatives by overall ranking. We created all consistent combinations in criteria preferences what represented 9 027 decision scenarios. The results were presented in graphs by percentage of occurrence of each alternative in 1st-8th place which is shown in Figure 5a. Values in y axis presented position in ranking of the process design alternatives. Percentage of occurrence represents value how many times each process design alternative was in specific rank if all possible combinations of criteria preferences was considered (Figure 5a). The graphs in Figure 5b-5c considered only such combinations of preferences, when the most important criterion was always the same one.

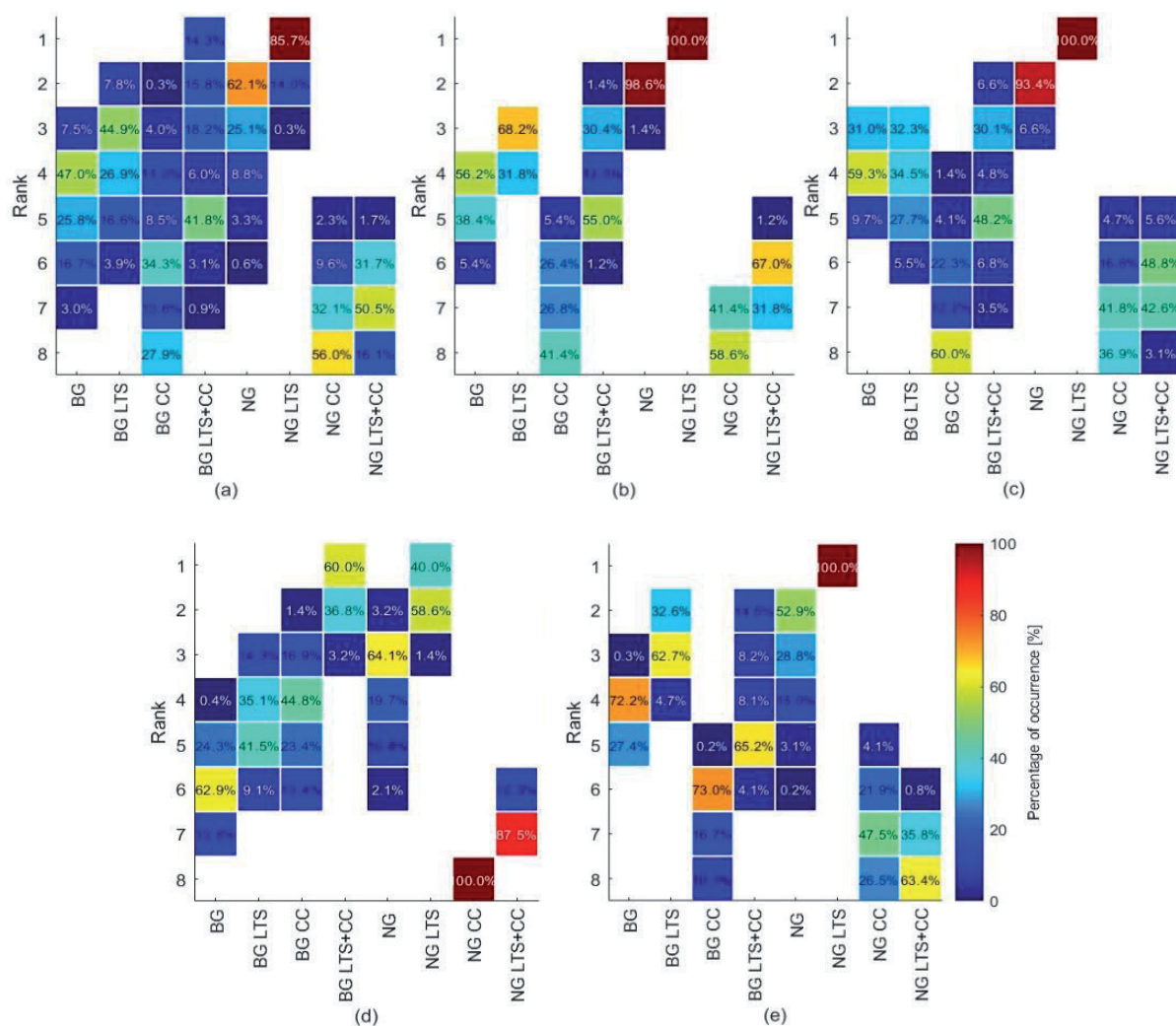


Figure 5. Percentage ranking of process design alternatives: all possible criteria combination (a), dominant criterion is material use and energy efficiency (b), economics (c), environmental aspect (d) and safety (e)

Trends in the best alternatives of all decision scenarios (Figure 5a) suggest preferability of NG as feedstock and the interesting result was reached by addition of LTS to the basic process. The best alternative for more environment friendly possibility (Figure 5d) was found to be biogas as feedstock with addition of CC and LTS, it was identified also as a best option if environmental aspect has the highest preference. On the other hand, usage of the BG as a feedstock and the addition of post-combustion CC were placed in the bottom of ranking (Figure 5a-c). The combination of NG feedstock with addition of CC and both CC and LTS addition was placed in 88 % and 66 % of scenarios in the last two positions. Positions in the middle of the ranking in overall preference of criteria were occupied mainly by biogas process design alternatives.

A comparison of BG and environmental dominance was also made for all consistent scenarios (Figure 5c and 5d). It was an undoubted victory of NG feedstock alternative with 100 % of occurrence in scenarios with economics dominance (Figure 5c). If the environmental aspect is dominant, occurrence of this alternative in the first position was decreased to 40 %. First place, in this case, was reached by using BG feedstock with addition of LTS and CC with 60 % of occurrence (Figure 5d). NG feedstock with post-combustion CC was identified as the worst alternative, if we combined rankings for both compared criteria.

Conclusion

We compared in our study eight process design alternatives using MCDA methodology for hydrogen production. Alternatives can be divided into two groups by different type of feedstock. Basic process technology used natural gas and slightly modified technology used biogas as a feedstock. Other modifications of the basic process were

similar in both feedstock alternatives. The best alternative of all 9 027 decision scenarios was found as natural gas feedstock with addition of LTS. Dominance in the first position of this process design was found out in three of four considered criteria. Only environmental aspect importance decreased its position of the best alternative of all others. Comparable more environmentally friendly alternative was biogas feedstock with addition of LTS and post-combustion CC. Final process rankings can be largely influenced by changing preference of different criteria. This preference impact was shown in comparison of economics and environmental aspect in one concrete example (Figure 3) as well as in all related decision scenarios (Figure 4). Overall ranking showed why MCDA can be beneficial in comparison to more traditionally used one criterion decision analysis. The NG LTS alternative would be undoubtedly the best option if the environmental aspect is not included to analysis. This criterion decreased its leader position. It is the big advantage of MCDA, that overall ranking could connect all criteria preferences and find the best and the worst alternative and also alternatives in the middle of the ranking. The interesting result of this study is demonstration of MCDA ability to find for example the worst process design alternative that can be omitted from consideration in the future realization. Furthermore, the best alternatives were also identified that should be studied in more detail. Identification of alternatives placed in the middle of the ranking can be helpful guide if decision priorities will be changed in the future.

Acknowledgement

This work was supported by the Faculty of Chemical and Food Technology STU in Bratislava, Grant No. APVV-18-0134 and Grant No. VEGA 1/0511/21.

References

1. Pirdashti M., Ghadi A., Mohammadi M., Shojatalab G.: *Int. J. Chem. Mol. Eng.* **3**, 54 (2009).
2. Saaty, T.L.: *The Analytic Hierarchy Process: Planning, Priority Setting, Resource Allocation*. McGraw-Hill, New York 1980.
3. Nnabuife S. G., Ugbeh-Johnson J., Okeke N., E., Ogbonnaya Ch.: *Carbon Capture Sci. Technol.* **3**, 100042 (2022).
4. Liu K., Song Ch., Subramani V.: *Hydrogen and Syngas Production and Purification Technologies*. Wiley, New York 2009.
5. Mosinska M., Szynkowska M. I., Mierczynski P.: *Catalysts* **10**, 896 (2020).
6. Serna J., Martinez E. N. D., Rincón P. C. N., Camargo M., Gálvez D., Orjuela Á.: *Chem. Eng. Res. Des.* **113**, 28 (2016).
7. Woods D. R.: *Rules of Thumb in Engineering Practice*. Wiley, Weinheim 2007.
8. Goedkoop M. J., Spriensma R.: *PRé*, Amersfoort (2001).

GAS, COAL, FUEL

C3MR LNG PROCESS OPTIMIZATION: AN ENVIRO-ECONOMIC STUDY

Furda P.¹, Variny M.¹

¹ *Department of Chemical and Biochemical Engineering, Faculty of Chemical and Food Technology, Slovak University of Technology in Bratislava, Radlinského 9, 812 37 Bratislava, Slovak republic
patrik.furda@stuba.sk*

Abstract

Since the global energy requirements are expected to rise and the world-wide energy demand is still supplied mostly by fossil fuels, a search for a suitable transition fuel is a high priority. The natural gas is considered the cleanest fossil fuel and is commonly recognized as the best option. However, because the natural gas is usually extracted at remote locations, suitable means of transport are vital in the gas industry. Liquefied natural gas (LNG) is suitable for long-distance transport and is already one of the pillars of secure energy supply in many countries. In this work, a 3.5 MTPA propane-precooled mixed-refrigerant (C3MR) LNG plant is modeled in Aspen Plus and subjected to a robust dual-objective optimization using the genetic algorithm (GA/NSGA-II) and a novel Aspen Plus – Matlab interface. For the optimization study, 18 process variables were chosen and varied in a $\pm 75\%$ interval. Thanks to the novel optimization interface, up to 1000 optimization individuals and 500 generations could be used. To choose the most suitable individual from the 1000 individuals in the final Pareto front, four decision making methods: Euclidean distance, fuzzy non-dimensionalized distance, and two statistical methods have been used and the results have been compared and discussed. The optimization results document approx. 76 mil. USD/year decrease in the total annual processing costs and an over 76 KTPA decrease in the carbon dioxide emissions. Furthermore, the in-optimization behavior of parameters was studied: only 6 out of 18 parameters underwent significant changes throughout the process while the others converged to optimum in the first iterations. Finally, the results of the dual-objective optimization were confronted with the single-objective ones. The conclusion is that dual-objective optimization should be generally favored as the single-objective optimization yields only marginal decrease in the respective objective function while significantly increasing the other one.

Introduction

The energy-intensive industry accounts for 33% of the anthropogenic carbon dioxide emissions worldwide¹ and for two thirds of emissions in Europe². In a response, the European Union committed itself to reducing the CO₂ emissions by 80%–95% by 2050³. However, global energy requirements are expected to further increase by 56% between 2010 and 2040⁴ and because the use of renewable resources is still under development, it is expected that 76% of the world-wide energy demand will be still supplied by fossil fuels until 2040⁵. These predictions initiated the search for a suitable transition fuel to bridge the gap between conventional fossil fuels and renewables.

Natural gas is an attractive candidate amongst the conventional sources of energy because of its low carbon emissions and high heating value. These attributes make it the cleanest fossil fuel with the lowest contribution to climate change^{6,7}. Therefore, natural gas is expected to outperform coal as an energy source by 2035⁸. However, natural gas is usually extracted at remote locations. In Figure 1 there are 157 most important gas fields located world-wide: most of the fields are located in the Gulf of Persia and Iran, continental Russia, and former Soviet republics such as Uzbekistan and Turkmenistan, continental United States, and in the seas of Australia and Indonesia. While pipeline transport is still prevalent, the transport of the natural gas in its liquefied form is undergoing substantial development. The reason for this is that liquefied natural gas or LNG is suitable for long-distance transport and is generally considered safer than pipeline transport. Furthermore, it enables countries such as the United States to trade gas with Europe. Therefore, it is expected to surpass pipeline transport by late 2020s⁹. However, natural gas liquefaction is a very energy-intensive process (Table I) and comes with a considerable carbon footprint.

The actual situation regarding the natural gas liquefaction can be seen in Figure 2 which displays location and capacities of 42 most important LNG facilities around the world. When compared with the locations of the gas fields, it is only understandable that most of the facilities are located in the Gulf of Persia, on the coast of the United States and around Australia and Indonesia. Russia with only two liquefaction facilities relies mainly on the pipeline transport nowadays but a number of new projects are planned for the upcoming years.

Table I
Specific energy consumption of various LNG technologies¹⁰

Technology	Specific energy consumption / kJ kg ⁻¹
Cascade	1180-1390
SMR	1240-1490
C3MR	1050-1370
Single N2 expander	2370-3450
Double N2 expander	1420-2020



Figure 1. Most important natural gas fields



Figure 2. Most important LNG facilities

There are several LNG technologies, however, the APCI C3MR LNG technology developed by Air Products and Chemicals, Inc. is the most used one. At the moment, it produces more LNG than all other technologies combined¹¹. The Air Products and Chemicals, Inc. is responsible for almost three quarters of the world-wide production, followed by ConocoPhillips, Royal Dutch Shell plc., and Linde plc. Therefore, in this study, the C3MR APCI LNG technology was chosen as the object of study.

Simulation framework

The APCI C3MR LNG Process stands for Air Products and Chemicals' propane pre-cooled mixed-refrigerant natural gas liquefaction process. The process consists of two cycles – the propane cycle and the mixed-refrigerant cycle. The pre-treated natural gas (NG) which enters the system at approximately 25°C and 60 bar is first pre-cooled in the propane cycle to approximately -33 °C. It then enters the mixed-refrigerant (MR) cycle where it is liquefied at approximately -139°C and its pressure is drastically decreased to 2 bar which causes the natural gas to subcool to approximately -160°C.

A more detailed layout of the process is displayed in Figure 3. Propane in the precooling cycle is compressed in a four-stage compressor and condensed in an air-cooler. Then, it is sequentially expanded and partially evaporated thus cooling the NG and MR. Compressed MR, after partial condensation in the precooling section, passes through a flash drum and enters the coil-wound heat exchanger. Here, its liquid part is subcooled to approximately -127°C and expanded in a throttling valve. The vapor is cooled to -139 °C and liquefied, and subsequently expanded in a throttling valve. Finally, MR vapors are collected and compressed in a two-stage compressor.

The described system was modelled in Aspen Plus software for production of 3.5 MTPA LNG or processing of 160 kg/s of natural gas which is a standard capacity of a single C3MR LNG train.

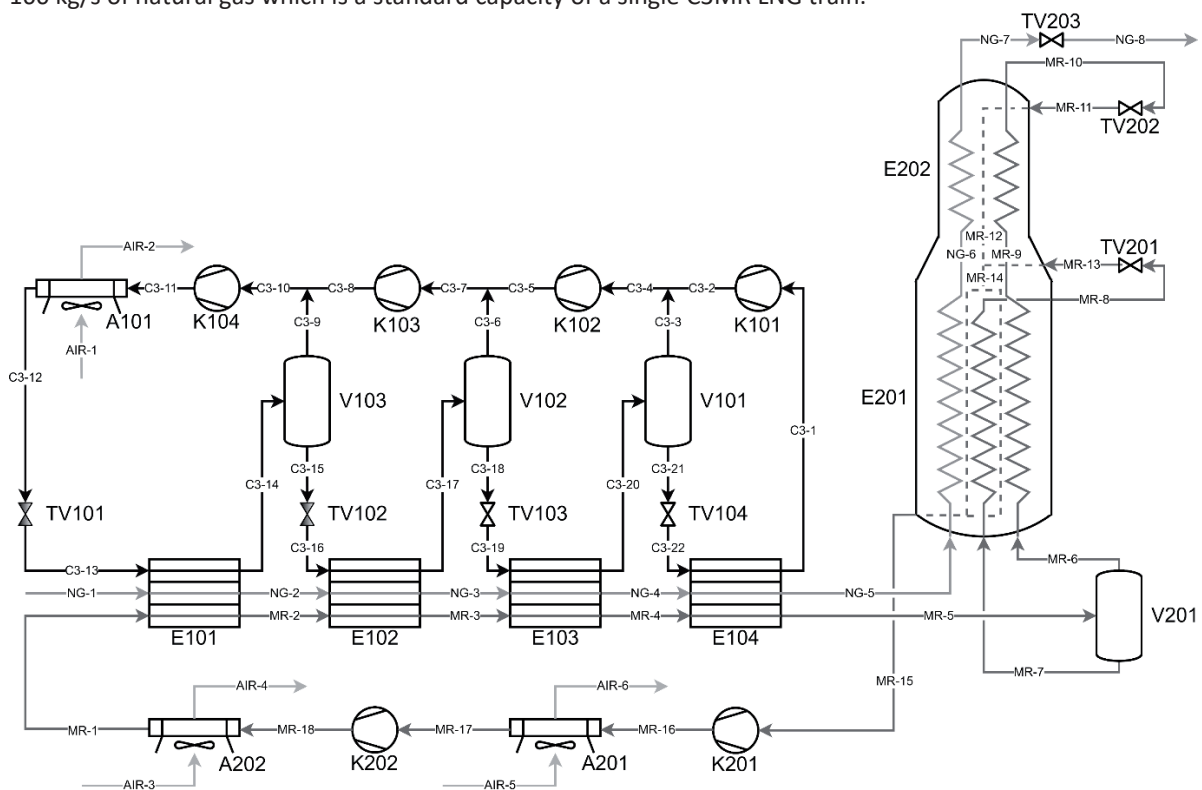


Figure 3. APCI C3MR process flow diagram.

Optimization study

The presented process is very energy-intensive, and the associated carbon footprint is also substantial. Even though the exact figures differ depending on the utilized technology, the liquefaction process accounts for 30–40% of LNG cost¹². Contrary to other studies which set specific or total energy consumption, annualized profit, period of return, or various efficiencies as the objective function¹³, this study uses levelized processing cost as the first objective function because it provides a single number which encompasses CAPEX, OPEX, and the plant economic life. Environmental objectives are not usually incorporated in optimization studies of LNG processes, although, in this study, carbon footprint is calculated as the second objective function based on the total energy consumption and the associated marginal emission factor. However, with lowering of the capital expenses and consequently the levelized costs, the operational expenses typically increase. Also, the total energy consumption increases which causes the carbon emissions to increase. The objectives are therefore conflicting, and a dual-objective optimization needs to be executed. To minimize the two objectives, 18 process parameters were optimized. These parameters are listed in Table II.

Table II

Optimization variables

Parameter	Range
Precooling cycle	
Propane mass flow / kg s^{-1}	$110.7 \leq \dot{m}_{\text{C3-11}} \leq 774.7$
K101 discharge pressure / bar	$1.1 \leq P_{\text{C3-2}} \leq 4.4$
K102 discharge pressure / bar	$1.3 \leq P_{\text{C3-5}} \leq 8.9$
K103 discharge pressure / bar	$1.8 \leq P_{\text{C3-8}} \leq 12.6$
K104 discharge pressure / bar	$3.75 \leq P_{\text{C3-11}} \leq 25.0$
TV104 discharge pressure / bar	$1.1 \leq P_{\text{C3-22}} \leq 2.3$
Mixed refrigerant cycle	
MR mass flow rate / kg s^{-1}	$75.5 \leq \dot{m}_{\text{MR-11}} \leq 528.2$
K201 discharge pressure / bar	$4.4 \leq P_{\text{MR-16}} \leq 30.6$
K202 discharge pressure / bar	$16.3 \leq P_{\text{MR-18}} \leq 113.8$
TV202 discharge pressure / bar	$1.1 \leq P_{\text{MR-11}} \leq 5.3$
E201 outlet temperature (NG) / K	$140 \leq T_{\text{NG-6}} \leq 150$
E201 outlet temperature (MR, l) / K	$140 \leq T_{\text{MR-8}} \leq 150$
E201 outlet temperature (MR, g) / K	$140 \leq T_{\text{MR-9}} \leq 150$
E202 outlet temperature (MR) / K	$130 \leq T_{\text{MR-10}} \leq 140$
Mixed refrigerant composition	
Propane / mass fraction	$0.0868 \leq x_{\text{C}_3\text{H}_8} \leq 0.6076$
Nitrogen / mass fraction	$0.0181 \leq x_{\text{N}_2} \leq 0.1269$
Methane / mass fraction	$0.0620 \leq x_{\text{CH}_4} \leq 0.4338$
Ethane / mass fraction	$0.0831 \leq x_{\text{C}_2\text{H}_6} \leq 0.5817$

In summary, the optimization problem consists of 2 conflicting objective functions and 18 process parameters. Because traditional optimization techniques such as sequential quadratic programming or similar would not be able to solve such system, the non-dominated sorting genetic algorithm (NSGA-II) was used. What this algorithm does is that it creates a variety of combinations of parameter values that are called individuals. The algorithm created 1000 combinations and evaluated the processing costs and carbon emissions for each of the combinations (or individuals). The best combinations were kept, the worst discarded, and the rest was combined so that a new 1000 combinations was created. This process was repeated 500 times. Because such process is extremely exhausting and time-consuming, a novel Parallel Genetic Algorithm Interface (PAGAN)¹⁴ was used.

Results and discussion

Results of the optimization, i.e., all combinations based on the processing costs and carbon emissions are displayed in Figure 4. The so-called Pareto front consists of the top 30% of combinations which gave the lowest values of objective functions. To choose the best solution from the 300 Pareto-optimal solutions, four decision-making techniques were utilized: the Euclidean-distance, the normalized distance, the linear programming technique for multi-dimensional analysis of performance (LINMAP), and the technique for order performance by similarity to ideal solution (TOPSIS). First, the Euclidean distance calculates the distance from a fictive point consisting of the lowest values of both functions. However, this method provides biased results as the objective functions do not reach values of the same order of magnitude. Also, this method assesses both objectives as equally important and provides no statistical evaluation. By employing fuzzy normalization, the effect of different orders of magnitude is erased. However, even though the result is more objective, neither this method provides any statistical evaluation. LINMAP and TOPSIS methods utilize different method of normalization and statistical weights of individual objective functions. These methods assess the distance of solutions to the best and worst weighted normalized points and rank the solutions according to their performance scores.

From Figure 4 it is evident that different methods consider different values as the best solutions. While geometric methods favor minimizing of the levelized costs, statistical methods favor minimization of the carbon emissions. The final choice of the exact parameters must be done based on experience. According to the current situation, however, considering the TOPSIS solution is strongly recommended.

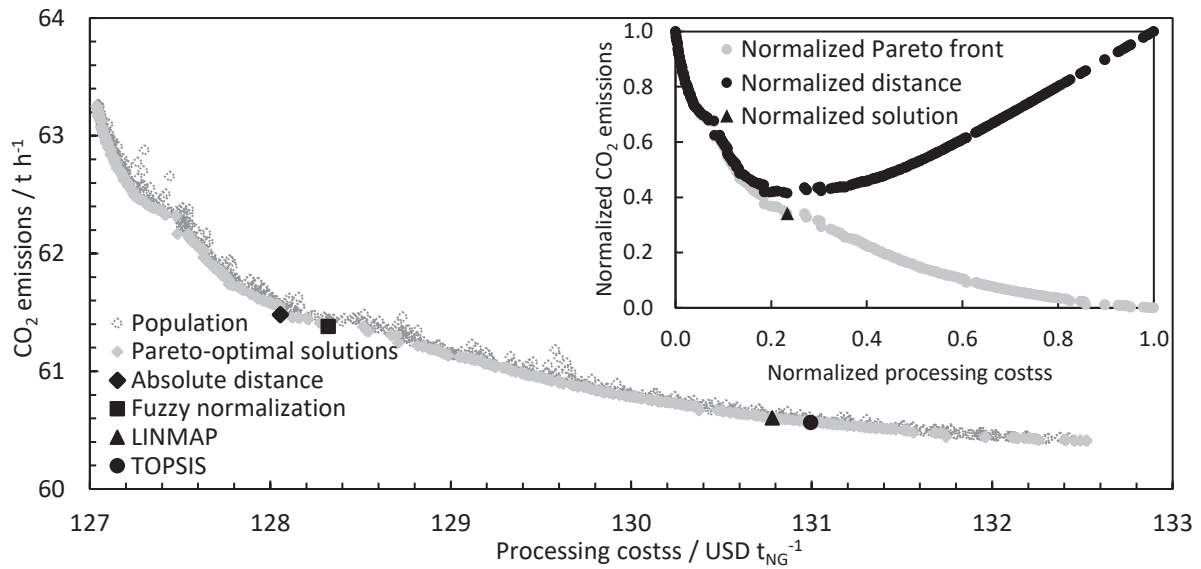


Figure 4. Dual-objective optimization results. Enclosed figure: Pareto-optimal results and their respective distance from zero, non-dimensionalized by fuzzy normalization.

Table III summarizes the actual values of process parameters as well as the results chosen by each of the decision-making techniques. In the first column there are base-case values of the process parameters. In the other columns there are optimized values of the respective parameters.

Table III
Optimized process parameters

Parameter	Dual-objective					Single-objective	
	Base case	Absolute distance	Fuzzy norm.	LINMAP	TOPSIS	min(PC)	min(G_{CO_2})
Precooling cycle							
Propane mass flow / $kg\ s^{-1}$	442.7	446.0	446.1	446.2	446.1	445.8	448.6
K101 discharge pressure / bar	2.500	1.851	1.903	2.437	2.433	1.526	2.532
K102 discharge pressure / bar	5.100	3.761	3.801	4.012	4.007	2.933	4.631
K103 discharge pressure / bar	7.200	6.470	6.684	6.803	6.802	5.739	7.438
K104 discharge pressure / bar	14.30	14.73	14.72	15.00	15.01	14.36	15.05
TV104 dis. pressure / bar	1.300	1.230	1.258	1.510	1.539	1.100	1.715
Mixed refrigerant cycle							
MR mass flow rate / $kg\ s^{-1}$	301.8	291.2	291.2	291.5	291.5	290.1	291.1
K201 discharge pressure / bar	17.50	30.59	30.58	30.59	30.59	30.63	30.56
K202 discharge pressure / bar	65.00	74.74	74.68	74.55	74.55	75.76	73.31
TV202 dis. pressure / bar	3.000	4.987	4.970	4.992	4.992	4.639	5.250
E201 outlet temp. (NG) / K	146.0	142.8	142.8	142.9	142.9	141.4	145.9
E201 outlet temp. (MR, l) / K	146.0	147.2	147.2	147.4	147.4	147.1	146.6
E201 outlet temp. (MR, g) / K	146.0	149.0	149.0	149.0	149.0	149.3	147.4
E202 outlet temp. (MR) / K	134.0	139.4	139.4	139.4	139.5	140.0	130.0
Mixed refrigerant composition							
Propane / mass fraction	0.3472	0.3204	0.3205	0.3207	0.3208	0.3198	0.3200
Nitrogen / mass fraction	0.0725	0.0733	0.0733	0.0733	0.0743	0.0736	0.0731
Methane / mass fraction	0.2479	0.2375	0.2376	0.2384	0.2370	0.2378	0.2377
Ethane / mass fraction	0.3324	0.3688	0.3686	0.3676	0.3679	0.3688	0.3692
Results							
Processing costs / $USD.t_{NG}^{-1}$	146.0	128.1	128.3	130.8	131.0	126.9	143.7
CO_2 emissions / $t.h^{-1}$	70.35	60.98	60.88	60.10	60.07	63.22	58.56
Decrease against base case							
Processing costs / %	-	-12.26	-12.12	-10.41	-10.27	-13.08	-1.575
CO_2 emissions / %	-	-13.32	-13.46	-14.57	-14.61	-10.14	-16.76

Total decrease in processing costs reached 10 to 12%. At the same time, a 13 to 14% decrease in the carbon dioxide emissions was achieved. To further compare the results, a single-objective optimization, aimed either on lowering the processing costs or the carbon emissions, was carried out. Unsurprisingly, when aiming solely on the processing costs, these can be lowered slightly more although the decrease in carbon emissions would be lower. This aspect of the single-objective optimization is even more evident when aiming only on the carbon emissions. While these could be theoretically lowered by almost 17%, the associated processing cost would be lowered much less, by only 1.5%. It can be therefore stated that the single-objective optimization yields only marginal decrease in the respective objective function while significantly increasing the other one and so the dual-objective optimization is favored.

Conclusion

In conclusion, the achieved decrease in processing costs can be roughly translated into 76 million dollars per year in savings. The associated carbon footprint of this process can be potentially lowered by approximately 76 thousand tons of carbon dioxide per year. Furthermore, dual-objective optimization was proven to be superior to single-objective one.

Acknowledgement

This study was supported by the Slovak Research and Development Agency under contract nos. APVV-18-0134 and APVV-19-0170, and by the Slovak Scientific Agency, grant no. VEGA 1/0511/21.

References

1. Rissman J., Bataille C., Masanet E., Aden N., Morrow W. R., Zhou N., Elliott N., Dell R., Heeren N., Huckestein B., Cresko J., Miller S. A., Roy J., Fennell P., Cremmins B., Koch Blank T., Hone D., Williams E. D., de la Rue du Can S., Sisson B., Williams M., Katzenberger J., Burtraw D., Sethi G., Ping H., Danielson D., Lu H., Lorber T., Dinkel J., Helseth J. *Appl. Energy*. **266**, 114848 (2020).
2. Gerres T., Chaves Á., José P., Llamas P. L., San Román T. G. *Journal of Cleaner Production*. **210**, 585 (2019).
3. Mikulčić H., Baleta J., Klemeš J. J. *Cleaner Prod.* **251**, 119727 (2020).
4. Chong Z. R., Yang S. H. B., Babu P., Linga P., Li. X. *Appl. Energy*. **162**, 1633 (2016).
5. Qyyum M. A., Yasin M., Nawaz A., He T., Ali W., Haider J., Qadeer K., Nizami A., Moustakas K., Lee M. *Energies*. **13**, 1732 (2020).
6. Rogala Z., Brenk A., Malecha Z. *Energies*. **8**, 1426 (2019).
7. Koo J., Oh S., Choi Y., Jung J., Park K. *Energies*. **12**, 1933 (2019).
8. Lee I., Tak K., Kwon H., Kim J., Ko D., Moon I. *Ind. Eng. Chem. Res.* **53**, 10397 (2014).
9. International Energy Agency: *Gas Market Report Q3-2021*, 2021. <https://www.iea.org/reports/gas-market-report-q3-2021> (accessed 3. 10. 2021)
10. Song R., Cui M., Liu J. *Energy*. **124**, 19 (2017).
11. Air Products and Chemicals, Inc.: *Large to Mega-Scale Plant Processes and Equipment*, 2021. <https://www.airproducts.com/equipment/large-scale-lng-plants> (accessed 26. 10. 2021).
12. Vikse M., Watson H. A. J., Kim D., Barton P. I., Gundersen T. *Energy*. **196**, 116999 (2020).
13. Sabbagh O., Fanaei M. A., Arjomand A., Hossein Ahmadi M. *Sustain. Energy Technol. Assess.* **47**, 101493 (2021).
14. Furda P., Variny M., Labovská Z. *Energy Convers. Manag.* **260**, 115602 (2022).

C3MR LNG PROCESS OPTIMIZATION: PARALLEL GENETIC ALGORITHM INTERFACE

Furda P.¹, Variny M.¹

¹ *Department of Chemical and Biochemical Engineering, Faculty of Chemical and Food Technology, Slovak University of Technology in Bratislava, Radlinského 9, 812 37 Bratislava, Slovak republic
patrik.furda@stuba.sk*

Abstract

Environmental protection and sustainable development, emissions, energy efficiency, and economic profits have become important considerations in the present industrial studies. These considerations are now being simultaneously included as multiple optimization objectives. To this day, the non-dominated sorting genetic algorithm (NSGA-II) is the most widely utilized multi-objective optimization algorithm in real-world applications. A significant effort has been made to connect the NSGA-II algorithm with modern process simulators such as Aspen Plus. However, Aspen Plus-based genetic optimization suffers from extensive computation time. To tackle this problem, a novel approach, the Parallel Genetic Algorithm Interface, is proposed. As opposed to the traditional approach, the PAGAN algorithm makes use of the fact that fitness functions can be vectorized in Matlab-based GA, and that Aspen Plus simulations can be run asynchronously. Thanks to the accelerated algorithm, extensive optimization studies were made possible. For our studies, the propane-precooled mixed-refrigerant (C3MR) liquefaction process was chosen. A standard C3MR 3.5 MTPA LNG production process scheme was set up in Aspen Plus environment with 18 process parameters selected for single- and dual-objective optimization of both the processing costs and the associated CO₂ emissions, with the process parameter deviation range of $\pm 75\%$. The PAGAN algorithm achieved a seven-fold decrease in the computation time which enabled increasing the number of individuals in the optimization runs up to 1000, while achieving a 12% decrease in processing costs and 14% decrease in CO₂ emissions. The difference in the Pareto front position between the runs led to the conclusion that the number of individuals needed to approach the optimal conditions in C3MR LNG production is much higher than the 200 commonly used in studies.

Introduction

Real-world multi-objective optimization problems include several criteria that need to be optimized simultaneously while the objective functions are often conflicting. The process parameters may often be imprecise, and the objective functions may have many extremes. Therefore, the process of multi-objective optimization is very exhausting and traditional methods usually fail when trying to solve such problems¹.

Nowadays, the most widely utilized optimization methods are modern stochastic methods and namely genetic algorithms and their variations. These algorithms are very robust, they do not break easily, and they are good for solving multi-modal and multi-dimensional problems. Moreover, the multi-objective non-dominated sorting genetic algorithm² (NSGA-II) has been directly included in the Matlab Optimization toolbox since 2007 and is thus a ready-to-use algorithm.

This work aims for improvement of a multi-objective optimization interface providing broadened possibilities of optimization of Aspen Plus-based process simulations. The object of study was the APCI C3MR LNG process closer explained in conference paper "C3MR LNG Process Optimization: Enviro-economic study" presented at the ICCT 2022 conference.

Methodology: Parallel Genetic Algorithm Interface

Genetic algorithm is a global optimization method derived from evolution and natural selection. And nature follows an interesting path to select an optimum solution to any problem. By generations, nature chooses and keeps the best and fittest individuals which it lets to reproduce, and it discards the rest. In this work, two objective functions were evaluated: levelized processing costs and carbon dioxide emissions, both associated with production of LNG via propane-precooled mixed-refrigerant (C3MR) process. For optimization, 18 process variables were altered. From the algorithm's point of view, these variables create the genome of an individual, i.e., one individual consists of a random combination of values of these 18 parameters. The algorithm creates a population, which is a series of combinations of the parameter values. For each individual, a simulation of the process is carried out in Aspen Plus software. Based on the objective function values, the algorithm chooses the best individuals which are those with the lowest values of the objective functions and applies no changes to these individuals. In the nature, if the evolution is slow, random changes may occur to genes. The algorithm

therefore finds the weakest individuals and applies random changes to them for a chance to randomly create something better. For the rest of the individuals, the algorithm combines their genes to create potentially stronger individuals. This way a whole new population is obtained which is potentially better than the previous one. The algorithm then ranks the new generation, chooses the best, the worst, and repeats the entire process. This procedure is repeated until the population cannot be more improved. In this work, 1000 individuals were used, and the cycle was repeated 500 times.

To link the genetic algorithm with Aspen Plus software, the ActiveX technology was used. It is a technology developed by Microsoft for sharing information across various platforms and it provides virtually unlimited control over selected software. It is compatible with Matlab and enables the user to gain almost unlimited control over practically any simulation software, for example Aspen HYSYS, Aspen Plus, gPROMS, PRO/II and so forth. When working with Aspen Plus, this technology enables the user to write a code that can run simulations, alter the settings, read and write data, etc.

An obvious problem with the Aspen-linked genetic-algorithm optimization is that the simulation needs to be run for each individual in each generation, i.e., in this case $1000 \times 500 = 5 \times 10^5$ simulations need to be run. Considering just one second per simulation this results in a computation time of 5×10^5 seconds or 5.8 days.

To solve this common recurring problem with optimization using Aspen Plus, a novel optimization interface dubbed the Parallel Genetic Algorithm Interface or PAGAN³ was proposed. This interface makes use of two aspects:

1. In Matlab-based GA the objective function can be called on the entire population at once⁴.
2. Any number of Aspen Plus simulations can be running simultaneously, provided that they have a different name, and they can be run asynchronously, i.e., the algorithm does not wait for a running simulation to finish and continues to the next step⁵.

The traditional genetic algorithm creates the population and sends individuals one by one into just one simulation. To evaluate G individuals, the algorithm needs G cycles. On the other hand, PAGAN creates copies of the original simulation. If the number of copies is N, the number of necessary cycles is G/N as shown in Figure 1. Detailed layout of this algorithm is displayed in Figure 2.

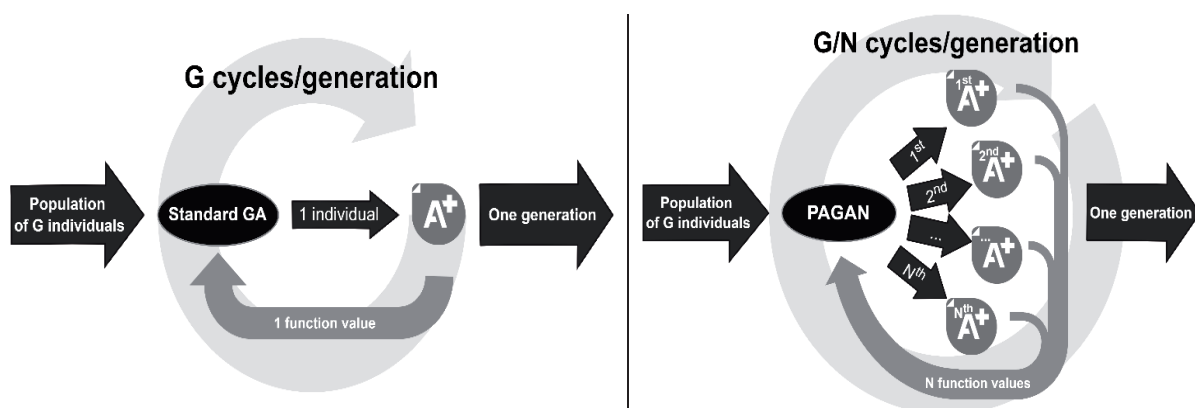


Figure 1. Comparison of standard and proposed algorithm

Results and discussion

Performance of the proposed interface was evaluated using a desktop computer with an AMD Ryzen 9 3900X 3.80 GHz 12-core processor and a 48 GB RAM. Several test runs were executed, each with a different number of simultaneous simulations (N). To avoid unnecessarily extensive computation times during the performance test, the population was reduced to 100 individuals and 50 generations were generated. To guarantee reproducibility, each test run was initiated with identical initial population. Absolute computation times are shown in Figure 3. A great reduction in computation time can be observed with increasing number of simultaneous simulations. In Figure 3, the relative computation rate is the ratio of computation time using one simulation to the computation time using the respective number of simultaneous simulations. The trend is linear up to $N = 4$ and then gradually flattens. Nonetheless, a relative computation rate of approximately 7.5 was achieved with 24 simultaneous simulations. This, however, is strongly dependent on the performance of the processor and the capacity of the RAM.

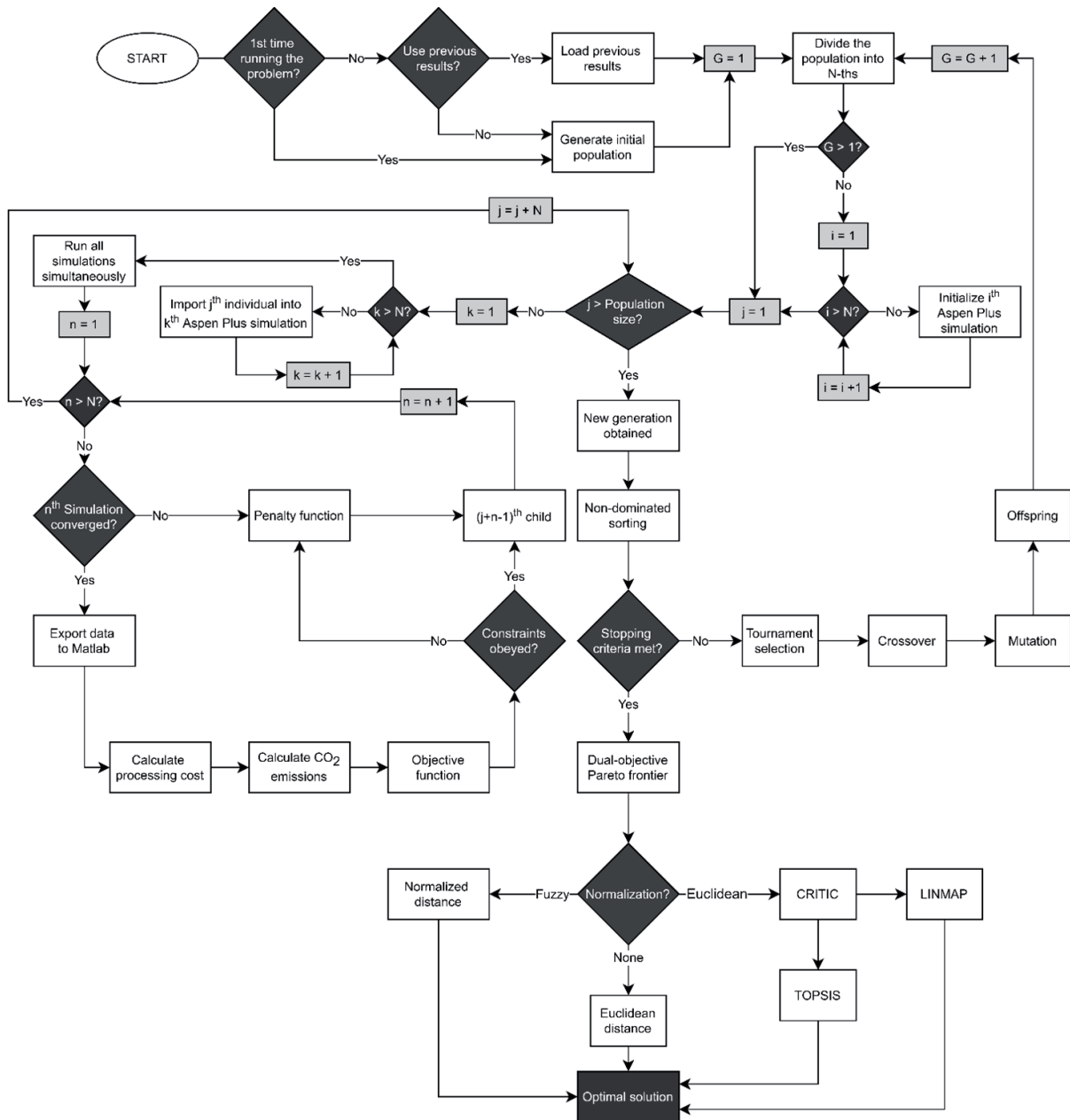


Figure 2. PAGAN algorithm for NSGA-II optimization.

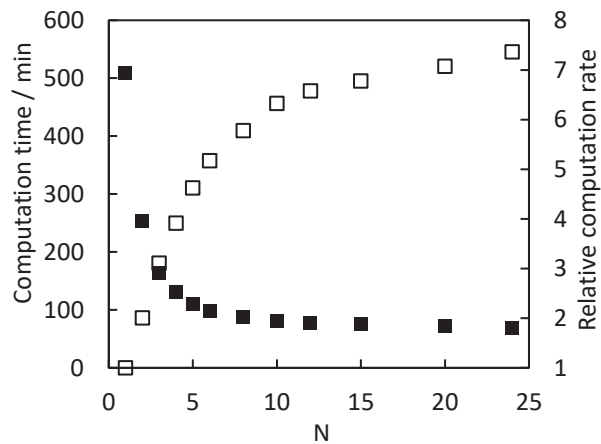


Figure 3. Absolute computation time and relative computation rate for various numbers of simultaneous simulations

As a direct consequence of the 750% increase in computation speed, sequential dual-objective optimization of the C3MR LNG process was made possible. The optimization procedure was initiated with a population of 200 individuals over 200 generations. The results of the first run were used as the initial population for the second run. This was repeated in eight runs, hence the term sequential optimization. The number of individuals was gradually increased to final number of 1000 individuals. In the eighth run, optimization boundaries regarding the two objective functions were found and later confirmed by two single-objective optimization runs. From Figure 4 it is evident how the optimization progressed throughout the individual runs. This underlines the need for repeated optimization. A 10-12% decrease in processing costs and a 13-14% decrease in carbon dioxide emissions were achieved.

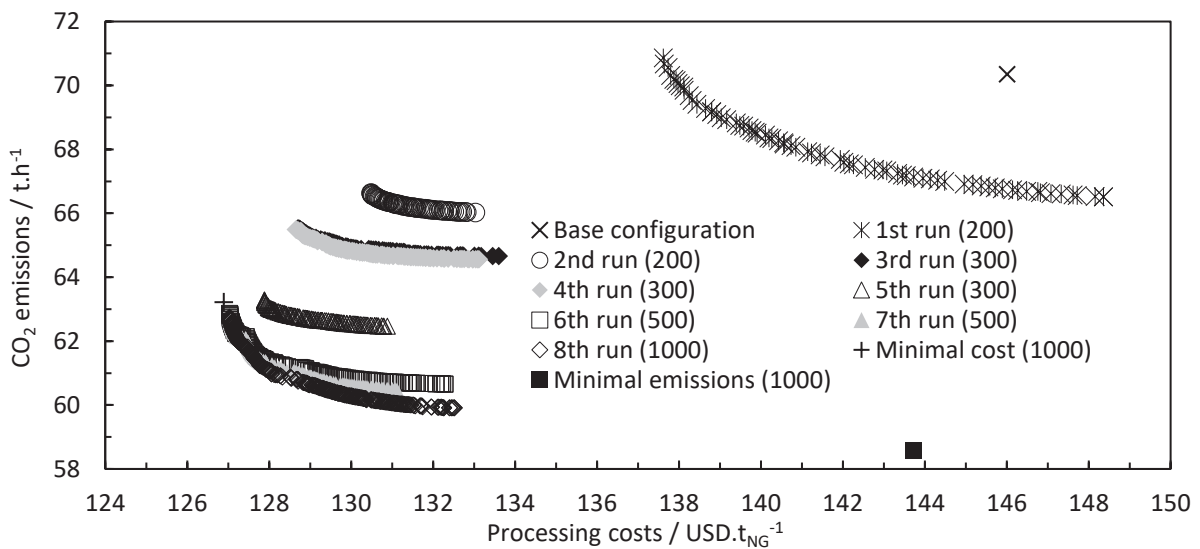


Figure 4. Single- and dual-objective optimization results (Number of individuals displayed in parentheses.)

In addition to dual-objective optimization of the C3MR process, the in-optimization behavior of parameters was studied. First, evolution of parameters was analyzed. Average values of each of the parameters in individual runs is displayed in Figure 5. The evolution of parameters shows how much the process parameters changed between individual runs. Moreover, the evolution is a direct indicator of the optimization results' quality – the more parameters remain unchanged between runs (or change slightly), the closer to the global optimum the optimization is. Based on the parameters' evolution, one can see which parameters cause the initial decrease in the objective function values (e.g., P_{K201}) and which affect the last runs (e.g., P_{TV202}).

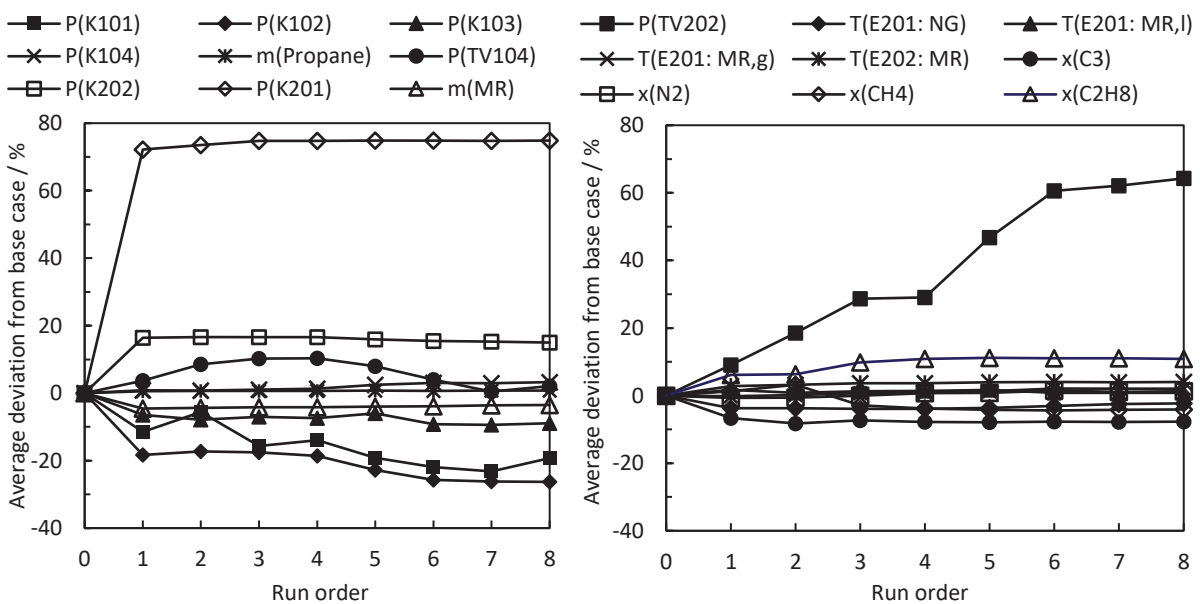


Figure 5. Evolution of process parameters throughout optimization runs.

Secondly, the interest was focused on the parameter variance which defines the shape of the Pareto front. The parameter ranges (or the ratios of maximal-to-minimal values) for each of the optimization runs were calculated and displayed in Figure 6. Some parameters, such as P_{K202} reported almost identical values throughout the optimization process. Hence, these parameters affect the shape of the Pareto front minimally. This implies that certain values of these parameters can satisfy both objective functions simultaneously. On the contrary, parameters such as P_{TV104} were reported in a wide range of values and, therefore, it can be deduced that such parameters cannot be optimized to a single value simultaneously satisfying both objectives.

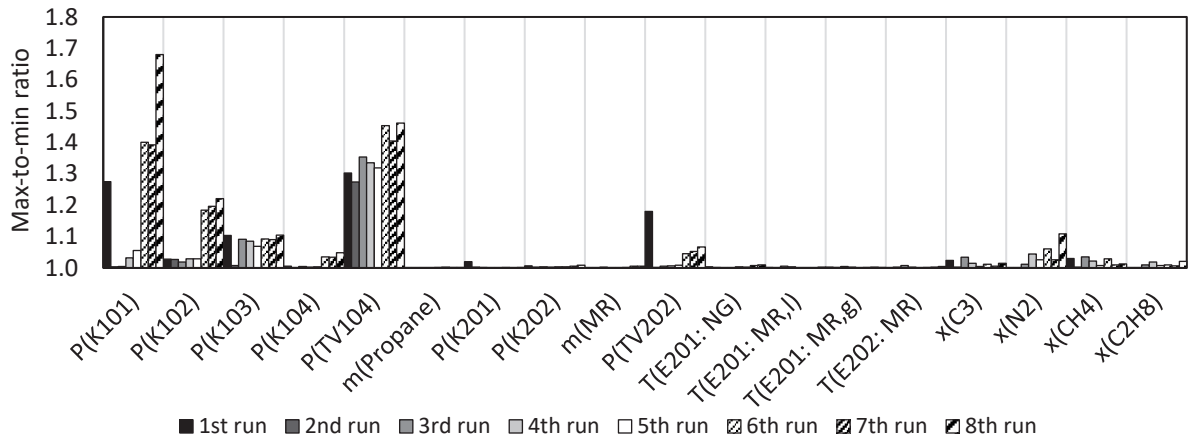


Figure 6. Parameter variance throughout optimization runs.

Values of the most crucial parameters based on their variance were normalized and plotted against normalized values of the objective functions in Figure 7. The figure shows that the trends of function values of all parameters are well developed and that the trends regarding the two objectives are approximately inverse to each other. An exception to this is P_{TV104} which shows slightly different behavior.

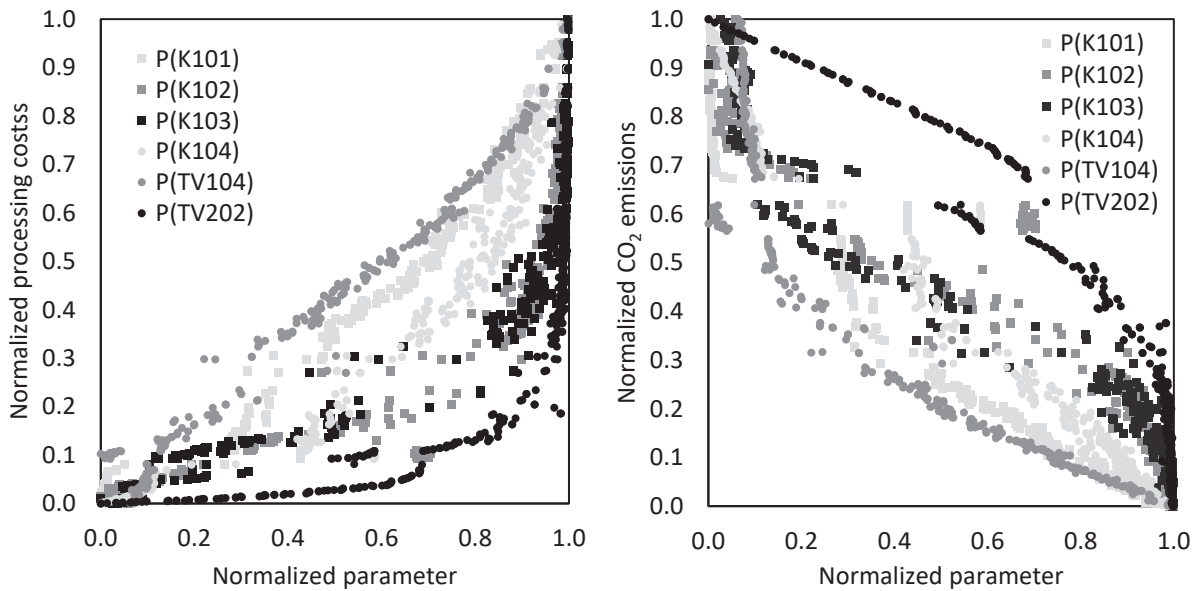


Figure 7. Fuzzy-normalized relations between values of the objective functions and optimized parameters

Conclusion

The main contribution of this work lies in the development of an advanced optimization interface which achieved 750% increase in the optimization rate. However, this value is strongly dependent on the used hardware. On the other hand, with the current rate of development of information technology it can be assumed that this value will increase overtime. The sequential dual-objective optimization revealed the

behavior of the process parameters and optimization boundaries. In the end, it has been proven that, by selecting the crucial parameters, an even more effective optimization can be done.

Acknowledgement

This study was supported by the Slovak Research and Development Agency under contract nos. APVV-18-0134 and APVV-19-0170, and by the Slovak Scientific Agency, grant no. VEGA 1/0511/21.

References

1. Cui Y., Geng Z., Zhu Q., Han Y. *Energy*. 125, 681 (2017)
2. Deb K., Pratap A., Agarwal S., Meyarivan T. *IEEE Trans. Evol. Comput.* 6, 182 (2002).
3. Furda P., Variny M., Labovská Z. *Energy Convers. Manag.* 260, 115602 (2022).
4. Aspen Technology, Inc.: *Aspen Plus User Guide*, Version V10.2.
5. The MathWorks, Inc.: *Genetic Algorithm Options*, 2021. <https://uk.mathworks.com/help/gads/genetic-algorithm-options.html#f17234> (accessed: 21. 2. 2022)

CO-FIRING MULTIPLE FUELS IN VOJANY THERMAL POWER PLANT

Variny M.¹, Stričík M.², Štofová L.³

¹*Institute of Chemical and Environmental Engineering, Faculty of Chemical and Food Technology, Slovak University of Technology in Bratislava, Radlinského 9, 812 37 Bratislava, Slovak Republic*

²*Department of Economics, Faculty of Business Economics with seat in Košice, University of Economics in Bratislava, Tajovského 13, 041 30 Košice, Slovak Republic*

³*Department of Management, Faculty of Business Economics with seat in Košice, University of Economics in Bratislava, Tajovského 13, 041 30 Košice, Slovak Republic*
miroslav.variny@stuba.sk

Abstract

Rising fuel prices and the steady costs increase of carbon dioxide emissions force the thermal power plants to search for alternative feedstock. Finding a way of cleaner power production is an imperative if a definitive shutdown of ageing coal power plants is to be avoided. Vojany power plant responded to this need a few years ago and started its transformation from a coal power plant to a multi-fuel power source. Positive experiences of coal-wood chips mixture combustion in plant's boilers since 2009 served as a basis for a far more ambitious goal – to gradually replace coal by alternative fuels. Successful tests with solid recovered fuel combustion in 2019 and the permit to use this alternative fuel for power production granted thereafter constituted a breakthrough in the effort to produce cleaner power. Since then, the long-term experiences confirmed the feasibility of plant's operation as multi-fuel power source. In this contribution, the underlying operation experiences are discussed, and basic performance figures are provided, highlighting the plant's transformation as an example that could inspire other power plants in the region to proceed likewise.

Introduction

The issue of ageing fossil power plant fleet in Central and Eastern Europe deserves a sustainable and economically feasible solution¹. Their retirement option is not good news for the power grid stability, as they serve as baseload providers but, at the same time, are flexible enough to support the grid in case of longer lasting imbalances. Repowering of coal power plant with natural gas-based technologies might prolong their lifetime but does not solve the issue of greenhouse gases emissions as natural gas is perceived only as a transition fuel, though substantially cleaner than coal or oil^{2,3}. Additional incentive supporting repowering and reconstruction projects, including those to enrich fuel mix with alternative fuels is related to public health and environmental impacts of power generation and the associated costs that are not internalized (are not part of electricity market price)⁴. Those costs are termed externalities and can amount to tens of €/MWh⁵. Recent studies quantified externalities related to power production from gas to 10 to 20 €/MWh while those resulting from power production from coal amounted to over 40 €/MWh^{6,7}.

Waste management in Central Europe region differs significantly country by country⁸. In Slovakia, landfilling is still the most prominent way of dealing with waste and substantial effort has to be developed to reach a significant cut in it, complying with the European Union regulations⁹. Landfilled waste releases methane, which is a by far more intense greenhouse gas than carbon dioxide. Even if captured and used for power and heat production, it is too diluted to be economically feasible and represents mostly a way how to convert methane to a less harmful gas (carbon dioxide). Waste processing capacities in Slovakia are underdeveloped, with only two large municipal waste incineration plants being in operation¹⁰. At the same time, several hundred thousand tons per annum of processed and sorted waste are used in clinker and cement plants in Slovakia, the majority of which has to be supplied from other countries.

Both the issue of ageing power plant and the untapped potential for local fuel source has prompted Slovenské elektrárne, a.s., the Vojany thermal power plant owner, to test refuse-derived fuel as a possible coal replacement in future. The aim of this study is to analyze the power plant operation before and after fuel mix change, to analyze fuel parameters and to assess the feasibility of refuse-derived fuel inclusion in and of biomass share increase in the power plant fuel mix from technical, energy, economic and environmental points of view.

Materials and methods

Vojany thermal power plant is located in Eastern Slovakia. It is a subcritical coal power plant with an installed power output of 2x110 MW. It was designed to combust black coal from Russia and Ukraine as there are no black coal seam in Slovakia. Natural gas serves only during power boiler start-ups and for stabilization of combustion process. Since 2009 biomass was included in the fuel mix but with a comparatively low share on fuel energy input (a few %).

Tables I and II sum up the basic power plant operation parameters in the period 2016 to 2020. Total power production exceeded 400, even 600 GWh per year till 2018 and then it gradually decreased to 314 GWh per year in 2019 and even to less than 75 GWh per year in 2020. This resulted from decreased amount of combusted coal, while co-combusted biomass amount increased and that of natural gas did not vary too significantly. Refuse-derived fuel (RDF) was tested as alternative feedstock for power generation in 2019 and 2020 but its share on total annual fuel energy input was low.

Table I

Basic operation parameters of Vojany thermal power plant

Parameter/year	2016	2017	2018	2019	2020
Net power generated from alternative feedstock, GWh	5.89	20.99	21.64	20.67	12.91
Total net power generated, GWh	431.44	607.08	693.94	313.70	74.20
Average net output per block when in service, MW	61.86	66.49	60.22	61.90	57.20

Table II

Fuel balance of Vojany thermal power plant

Fuel type/year	2016	2017	2018	2019	2020
Biomass (tons)	6,035	20,974	20,263	20,666	12,906
RDF (tons)	-	-	-	1,550	4,900
Coal, 10 ³ tons	208	282	331	151	33
Natural gas, 10 ³ m ³	539	833	625	404	349

Table III

Relative fuel prices per GJ lower heating value (coal = 100 %)

Fuel type/year	2016	2017	2018	2019	2020
Biomass	147	116	98	119	104
RDF	-	-	-	40	31
Natural gas	1285	654	705	444	376

Data in Table III elucidate the economic incentives for such power plant operation. Apart from CO₂ costs that increased significantly over the analyzed period, coal became an expensive fuel in comparison with biomass or with RDF. Given the low power prices, power production from coal became infeasible and plant managers faced the option either to shut the plant down or seek for alternative fuels that would be more sustainable. RDF price, together with reasonable biomass content in it, made it a promising candidate to be tested for longer operation in co-combustion mode with coal and biomass. Data from conducted tests are analyzed in Results and discussion section.

To complete the description of the situation, it must be stated that Slovenské elektrárne, a.s. operate one more thermal power plant, located in Upper Nitra region in Western Slovakia. This power plant fires local brown coal. Coal mining in the region will stop at the end of 2022 and this power plant will retire consecutively.

Results and discussion

Table IV provides insight into several quality parameters of fuels forming the Vojany power plant fuel mix. Natural gas is not used during normal operation. Lower heating value of natural gas is by far the highest, followed by coal. Biomass and RDF have lower heating values lower than 20 MJ kg⁻¹, due to their chemical composition. This is partly reflected in carbon content as well. It is interesting to compare CO₂ emissions released by complete combustion of fuels listed in Table IV expressed per mass and per energy unit. Natural gas exhibits the highest CO₂ emissions per mass unit but the lowest ones per energy unit, given its very high calorific value. On the other hand, biomass releases least CO₂ per mass unit, but most of it per energy unit. After CO₂ emissions recalculation giving credit to renewable carbon content in fuels, the highest fossil CO₂ emissions are attributable to coal. CO₂

emissions released by RDF combustion stem partly from its non-renewable constituents and partly from its renewable part; nevertheless, they are much lower than those from coal combustion. This clearly underlines the effort developed by Vojany power plant in phasing coal out and replacing it by fuels with lesser carbon footprint. Comparison of dry stoichiometric flue gas amount per energy unit delivers important findings, too. Biomass, coal and RDF produce approximately the same flue gas amount per energy unit, meaning that the flue gas path in the boiler is loaded with similar flue gas volumetric flow at given boiler thermal output, regardless of fuel fired. Natural gas is used only during boiler start-ups and for stabilization of combustion process, so that the fact, that it forms less flue gas per energy unit has no serious impact on totally produced flue gas.

Table IV

Comparison of individual fuels in recent fuel mix. LHV = lower heating value. * = 6 % vol. O₂ in dry flue gas; @ = 3 % vol. O₂ in dry flue gas

Fuel/average parameter value	LHV, GJ t ⁻¹	Carbon content, % wt.	CO ₂ emissions, t t ⁻¹	CO ₂ emissions kg GJ ⁻¹	Fossil CO ₂ emissions, kg GJ ⁻¹	Dry stoichiometric flue gas, Nm ³ GJ ⁻¹
Biomass (as received)	11.4	37	1.36	119	0	390*
Coal	24.6	58	2.12	86	86	370*
RDF	19.5	35	1.3	67	47	300-400*
Natural gas	48.9	72	2.65	54	54	280@

Recent and planned fuel mix of Vojany power plant is summed up in Table V. The change in combusted fuel amounts is clearly visible, with plant's management striving to phase coal completely out, replacing it with RDF and, partly, by biomass. This is a long-term issue, coupled with several operational tests and with optimizing process conditions for its successful implementation, including an investment in a new, fluid steam boiler with circulating fluid bed. Apart from economic and environmental reasons, current geopolitical situation strongly favors the use of fuels that can be produced locally. What remains somewhat unclear is whether local biomass resources suffice to cover the ambitious plan for 2022. Regarding RDF, its domestic production capacities are underdeveloped at the moment and significant part of the fuel must be transported over longer distance. It makes sense to support and create local RDF production capacities to stabilize its share in Vojany fuel mix on one hand and to boost circular economy in the region on the other one.

Table V

Recent and planned fuel mix. * = planned value

Fuel type/year	2018	2019	2020	2021	2022*
Biomass (tons)	20,263	20,666	12,906	30,030	49,643
RDF (tons)	-	1,550	4,900	88,940	150,000
Coal, 10 ³ tons	331	151	33	61.3	0

Table VI

Average concentrations of selected pollutants in dry flue gas

Concentration, mg Nm ⁻³	CO	NO _x	Particulate matter	SO _x
2018	182	63	8.8	167
2019	189	47	6.7	166
2020	161	67	5.6	119
2021	188	62	7.0	147

Data shown in Table VI have to be analysed along with the dry stoichiometric flue gas formation values listed in Table IV. Concentration profiles on individual air pollutants over the years 2018 to 2021 indicate that, regardless of the actual fuel mix, neither have the emission limits been violated, nor has the total amount of released pollutants changes significantly as a result of it. This provides additional justification for enriching the fuel mix with both biomass and RDF. 2020 values fall out of the observed trend. It should, though, be remembered that overall power production fell to a minimum in that year and the share of natural gas on totally combusted fuels was significant – see Table I and II. This was reflected in slightly lower emissions of CO, particulate matter and of SO_x, compared to the corresponding values in the other three years.

Data trends observed in Table VII resemble those in Table VI closely and yield a similar explanation as well. No significant influence of RDF inclusion in and biomass share increase in the fuel mix over years can be observed.

Carbon content in bed ash is below 1 % wt. during the whole period, with the lowest values reached in 2019 and 2020. Fly ash contained approximately the same amount of carbon, except in 2020 which, similarly to the minima in air pollutant in 2020 can be attributed to lower coal share in the fuel mix. As results from Table VI and VII, enrichment of the Vojany fuel mix by RDF and by larger biomass share did neither lead to higher emissions of air pollutants nor to worsened fuel burnout, leading to the conclusion that boiler thermal efficiency did not vary significantly with the fuel mix changes.

Table VII
Average values of carbon content in ash

Carbon content, % wt.	Bed ash	Fly ash
2018	0.53	7.60
2019	0.21	7.04
2020	0.35	3.13
2021	0.77	6.65

Additional information from Vojany power plant include the fact that produced steam parameters were invariant to changes in fuel mix, providing additional proof that fuel mix enrichment by RDF and by larger biomass share is feasible both from technical, energy and environmental point of view. Furthermore, fuel cost relations indicated in Table III clearly exhibit the trend of coal becoming a too expensive fuel which becomes even more obvious if CO₂ costs were added to fuel costs. Phasing coal out of the fuel mix is thus perceived as the only option how to avoid the power plant retirement and, at the same time, RDF is deemed as a suitable replacement for coal both from quality, costs and availability point of view.

Refuse-derived fuel is produced in waste management plants and is rich in paper and plastic wastes; in addition, it contains some other constituents such as of biomass, textile, and other components^{11,12}. Experiences with its combustion and co-combustion in thermal power plants in Western and Northern Europe are documented in several studies^{13,14}. Besides serving as alternative fuel for heat and power production, it is known to successfully replace fossil fuels in clinker and cement production^{15,16} or in iron and steel industry¹⁷. This provides sufficient evidence that choosing RDF as part of the fuel mix in Vojany power plant might be a good decision.

Conclusion

This contribution analyses the feasibility of fuel mix changes in Vojany thermal power plant resulting from the economic necessity and environmental incentives. Inclusion of refuse-derived fuel in the fuel mix was tested in 2019 and, later, in 2020, followed by its increased share in the fuel mix in 2021. Fuel data analysis yielded that RDF is compatible with other fuels such as coal and biomass and can be co-combusted without serious technical, energy and environmental issues. Although these findings are promising, longer testing is necessary. A successful inclusion of RDF in the fuel mix of Vojany thermal power plant might inspire other ageing power plants in Central and Eastern Europe to consider choosing similar path. A boost in regional circular economy can be anticipated as a result, developing waste processing capacities, lowering waste landfilling share and creating new job opportunities. In addition, stable but flexible power sources will be maintained which will allow to include additional renewable energy (wind, solar) based power sources to be phased in the European power grid without an increased risk of blackout.

Acknowledgement

This work was financially supported by the Slovak Research and Development Agency, Grant No. APVV-15-0148 and APVV-19-0170. The authors would like to thank the KEGA grant agency, project KEGA 035EU-4/2022, for supporting research work and financing.

References

1. Qvist S., Gładysz P., Bartela Ł., Sowizdżał, A.: *Energies* 14, 120 (2020).
2. Kefford B.M., Ballinger B., Schmeda-Lopez D. R., Greig C., Smart S.: *Energy Policy* 119, 294 (2018).
3. Variny M., Kšiňanová M.: *Pol. J. Environ. Stud.* 31(3), 2861 (2022).
4. Cole-Hunter T., Johnston F. H., Marks G. B., Morawska L., Morgan G. G., Overs M., Porta-Cubas A., Cowie C. T.: *Environ. Res. Lett.* 15, 123006 (2020).
5. Krupnick A. J., Burtraw D.: *Resour. Energy Econ.* 18, 423 (1996).
6. Rabl A., Spadaro J. V.: *J. Sol. Energy Eng.* 138, 1 (2016).

7. Streimikiene D.: *Econ. Sociol.* 14(1), 89 (2021).
8. Iacovidou E., Hahladakis J., Deans I., Velis C., Purnell P.: *Waste Manage.* 73, 535 (2018).
9. Stričík M., Bačová M., Čonková M., Kršák B.: *Udržateľné nakladanie s komunálnym odpadom*. Vysoká škola báňská - Technická univerzita Ostrava, Ostrava 2019.
10. Pobožná M.: *Odpady v Slovenskej republike 2019*. Štatistický úrad Slovenskej republiky. Bratislava 2020.
11. Šuhaj P., Haydary J., Husár J., Steltenpohl P., Šupa I.: *Waste Manage.* 85, 1 (2019).
12. Januszewski J., Brzezińska D.: *Sustainability* 13, 12718 (2021).
13. Mlonka-Mędrala A., Dziok T., Magdziarz A., Nowak W.: *Energy* 234, 121229 (2021).
14. Badyda K., Krawczyk P., Pikoń K.: *Energy* 100, 425 (2016).
15. Del Zotto L., Tallini A., Di Simone G., Molinari G., Cedola L.: *Energy Procedia* 81, 319 (2015).
16. Abu-Elyazeed O. S. M., Nofal M., Ibrahim K., Yang J.: *Waste Disposal Sustainable Energy* 3, 257 (2021).
17. Han J., Huang Z., Qin L., Chen W., Zhao B., Xing F.: *J. Cleaner Prod.* 278, 123594 (2021).

RCAT SHORT-TERM AGEING OF BITUMINOUS BINDERS IN PRESENCE OF MASTIC

Matoušek L., Jíša P., Černý R.

ORLEN UniCRE a.s., Revoluční 1521/94, Ústí nad Labem, 400 01

lubos.matousek@orlenunicre.cz

ABSTRACT

The resistance of bituminous binders to ageing is one of the main factors influencing the lifetime of pavement. During the pavement construction and lifetime the bituminous binder oxidizes, which has a negative effect on the pavement durability. The first phase of ageing process includes rapid short-term ageing that occurs during production, storage and field application of a binder. The second phase of ageing process is slow and long-term ageing during the whole pavement lifetime. Several methods are used in laboratory scale to simulate the ageing of bituminous binders.

In this study, short-time ageing of bituminous binders was performed using methods RTFOT, RCAT, and mainly RCAT with mastic at standardized temperature of 163 °C. The method RCAT with mastic should be closer to real conditions in the asphalt plant compared to the standard RTFOT or RCAT methods, because the mastic can influence the reaction mechanisms during oxidation. The influence of mastic on the bitumen ageing was studied by comparison of the results from ageing with and without mastic, using two neat bituminous binders.

INTRODUCTION

One of the most important factors determining the lifetime of a pavement are changes in the physico-mechanical properties of the bituminous binders. These changes are caused by ageing of bituminous binders. The ageing process of bituminous binders is caused by oxidation of the material at higher temperatures.¹ The most important factors contributing the ageing of the bituminous binders include heating, atmospheric oxygen and ultraviolet electromagnetic radiation.² After ageing process the bituminous binders become harder and more brittle, thus increasing risk of pavement failure.

Ageing of bituminous binders is divided into two basic types. The first, short-term ageing process, is characterized by coating aggregate with bituminous binder to produce the mixture at higher temperature during plant mixing, production, transportation and construction. The next type of ageing, long-term ageing, takes place during pavement in-service. The mechanism of the bituminous binders ageing is divided into two types.³ In the first case, it is irreversible ageing mechanism. This mechanism is characterized by chemical changes in the bituminous binder, which affect its physical and mechanical properties. It is caused by the loss of volatile components during the oxidation process and migration of oil components from the bituminous binder to the aggregate.^{3,4} In the second case, it is reversible process called physical hardening. The molecules are reorganized that the resulting structure is as close as possible to the optimal thermodynamic state in this process.⁵

To simulate ageing of bituminous binders in laboratory, various methods are used. These methods apply the optimized conditions to simulate bitumen ageing in shorter time compared to the ageing in real conditions. There are 4 standardized methods to simulate short-term ageing at high temperatures:⁶

- Rolling thin-Film Oven Test (RTFOT, EN 12607-1)
- Thin Film Oven Test (TFOT, EN 12607-2)
- Rotating Flask Test (RFT, EN 12607-3)
- Rotating Cylinder Test (RCAT, ČSN EN 15323)

Short-term ageing by method RCAT can be modified for ageing of the bituminous binder and aggregate in their mixture. With this modification, the presence of the aggregates is involved in the procedure, and therefore the conditions during ageing simulation are closer to the condition on the plant, compared to the situation when only bituminous binder is used.

The objectives of this study are to compare different types of short-term ageing RTFOT, RCAT and modified RCAT with mastic using basalt as an aggregate.

MATERIALS AND METHODS

Materials

Two unmodified bituminous binders were used in this study. Both bituminous binders had similar properties in original unaged form. Both binders were obtained from standard bitumen production and they have a penetration grade 70/100. The main difference between the selected binders was their thermal stability. The basic properties of the binders are in table I.

Table I

Basic properties of tested binders

	Bitumen binder 1	Bitumen binder 2
Softening point R&B (°C)	44.8	45.4
Penetration at 25 °C (0.1 mm ⁻¹)	89	77
Complex shear modulus G* at 60 °C; 0.1 Hz (Pa)	81.9	105.8
Dynamic viscosity at 100 °C (mPa.s)	2280	2560
RESISTANCE TO AGEING - RTFOT		
Softening point increase (°C)	3.3	7.6
Penetration decrease (0.1 mm ⁻¹)	29	33
Complex shear modulus – ageing index (-)	1.71	2.77
Relative increase in viscosity at 100 °C (-)	1.42	2.01
RESISTANCE TO AGEING - PAV		
Softening point increase (°C)	8.5	13.9
Penetration decrease (0.1 mm ⁻¹)	37.2	50.8
Complex shear modulus – ageing index (-)	10.22	17.93
Relative increase in viscosity at 100 °C (-)	4.08	6.21

Ageing procedures

To simulate the bitumen changes during ageing, standardized methods were used for short-term ageing - RTFOT (Rolling Thin Film Oven Test) and RCAT (Rotating Cylinder Ageing Test). Furthermore, the modified method RCAT with addition of the mastic to the ageing cylinder was used. Conditions of standards and modified laboratory ageing methods are summarised in table II.

Table II

Methods for bitumen ageing

Method	Conditions (Temperature and time of ageing)
RTFOT	163 °C, 75 minutes
RCAT	163 °C, 4 hours
RCAT with mastic	163 °C, 4 hours, with mastic

The short-term ageing by RCAT method was used to simulate ageing of the asphalt mixture (binder with mastic) to approach the conditions that are on the mixing plants. As a mastic, basalt was used. Basic properties of basalt are shown in table III. The mixture was blended from 300 g of bitumen and 600 g of mastic. The influence of mastic on binder ageing was evaluated.

Table III

Basic properties of mastics used for mixture ageing

	Basalt
Density (g/ml)	1.305
Characteristic	Acidic
Size (mm)	8 - 16

Test Methods

Softening point increase: softening point was determined according to EN 1427. The increase of softening point was calculated according to the equation (1):

$$\Delta SP = SP_{after\ ageing} - SP_{original} \quad (1)$$

Penetration at 25 °C decrease: penetration was determined according to EN 1426. The decrease of penetration was calculated according to the equation (2):

$$\Delta PE = SP_{original} - SP_{origiafter ageing} \quad (2)$$

Complex shear modulus ageing index: the rheology tests were carried out on dynamic shear rheometer. These tests were based on the application of oscillating shear stress on the loaded samples at 60 °C, oscillation frequency 0.1 Hz and constant strain amplitude 1 %. Complex modulus ageing index (G_i^*) showed the ageing resistance. G_i^* was calculated according to the equation (3):

$$G_i^* = \frac{G_{after ageing}^*}{G_{original}^*} \quad (3)$$

Relative increase in viscosity: the dynamic viscosity was determined according to ČSN EN 13302. The dynamic viscosity was measured for 4 temperatures and the ageing index was calculated according to the equation (4):

$$\eta_i = \frac{\eta_{i,after ageing}}{\eta_{i,original}} \quad i = \text{temperature (80 °C, 100 °C, 135 °C and 150 °C)} \quad (4)$$

RESULTS AND DISCUSSION

The methods RTFOT and RCAT were selected for the simulation of short-term ageing. The RTFOT ageing was performed according the standard EN 12607-1 and the RCAT ageing according the standard EN 15323. The RCAT ageing was modified by addition of mastic.

Figure 1 illustrates the increase in softening point for both bituminous binders. Methods RTFOT and RCAT give very similar results according to softening point increase. Values of softening point increase for both binders do not show difference higher than 1 °C when the binders are aged by methods RTFOT and RCAT, but the softening point increase are higher for both binders after ageing by the RCAT method with mastic.

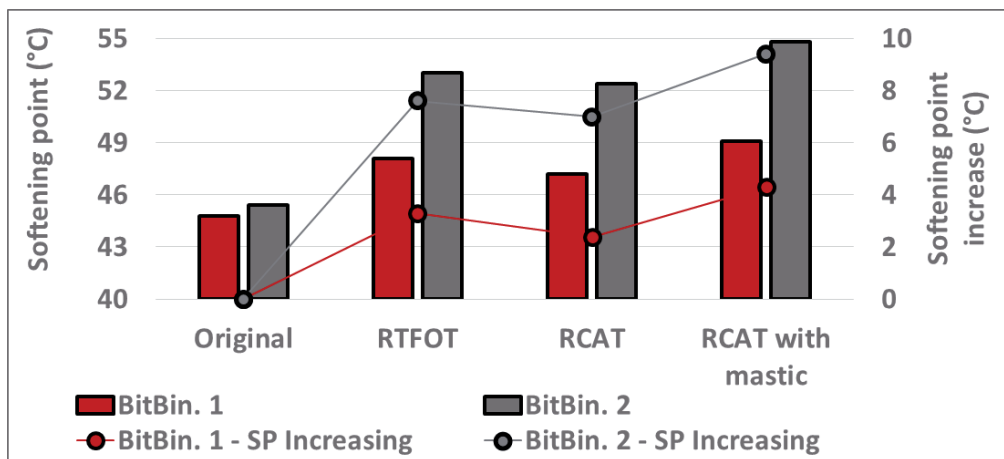


Figure 1. Comparison of three methods for laboratory ageing (RTFOT, RCAT and RCAT with mastic) by softening point for bituminous binders with penetration grade 70/100.

The next figure 2 illustrates the decrease in the penetration at 25 °C. After short-term ageing by standard methods RTFOT and RCAT the penetration of both bituminous binders decrease very similarly. The range of the penetration decrease was 29 – 33 p.u. More significant penetration decrease in bitumen penetration was recorded for bituminous binders that were aged by the method RTFOT, compared to the bituminous binders that were aged by the method RCAT. For bituminous binders that were aged by the method RCAT with mastic, the decrease in penetration was higher in comparison to decrease in penetration for the bituminous binders that

were aged by the standard methods RTFOT and RCAT (without mastic). It was 35 p.u for binder 1 and 37 p.u. for binder 2.

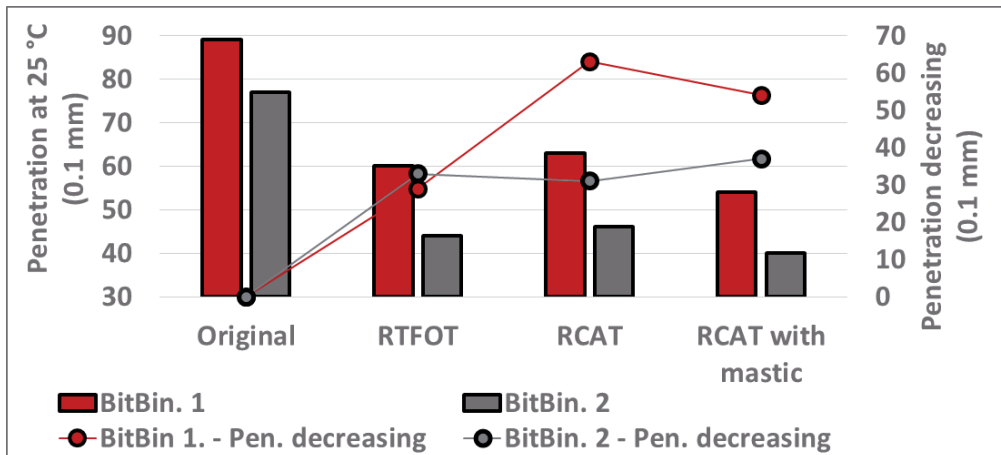


Figure 2. Comparison of three methods laboratory ageing (RTFOT, RCAT and RCAT with mastic) by penetration at 25 °C for bituminous binders with penetration grade 70/100.

Figure 3 illustrates the change in complex shear modulus for both bituminous binders. Ageing index of the complex shear modulus (G^*) for binders aged by method RTFOT are similar to values of binders aged by RCAT. It is 1.71 (RTFOT), resp. 1.51 (RCAT) for bituminous binder 1 and 2.77 (RTFOT), resp. 2.67 (RCAT) for bituminous binder 2. However, the ageing index of complex shear modulus is higher after ageing and even after ageing by method RCAT with mastic and it is 1.99 for bituminous binder 1 and 3.20 for bituminous binder 2.

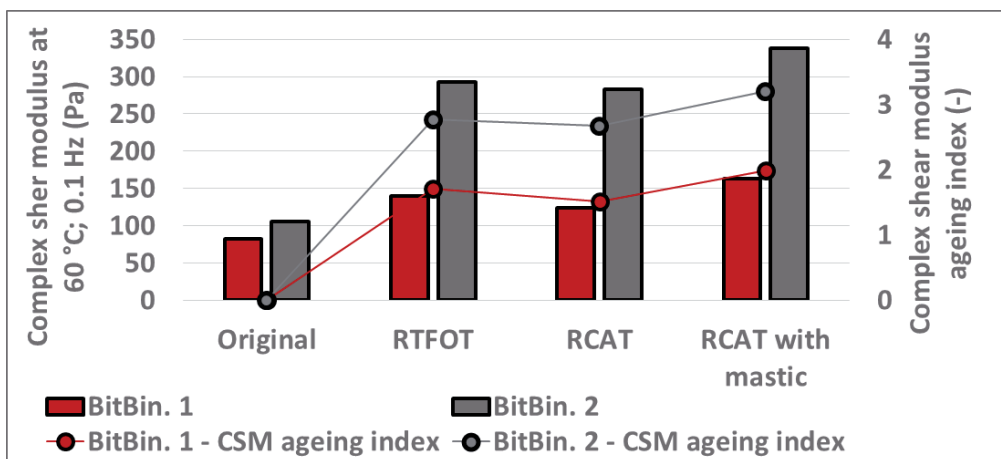


Figure 3. Comparison of three methods laboratory ageing (RTFOT, RCAT and RCAT with mastic) by complex shear modulus for bituminous binders with penetration grade 70/100.

Figure 4 illustrates decreasing of the upper critical temperature. Values of upper critical temperatures decrease after RTFOT ageing for both bituminous binders approximately of about 2 °C. After RCAT, ageing lead to decrease in the upper critical temperature of about 2.7 °C (resp. 2.6 °C). The highest decrease in the upper critical temperature was for both bituminous binders after ageing using method RCAT with mastic. The decrease was of about 3 °C for bituminous binder 1 and of about 3.6 °C for bituminous binder 2.

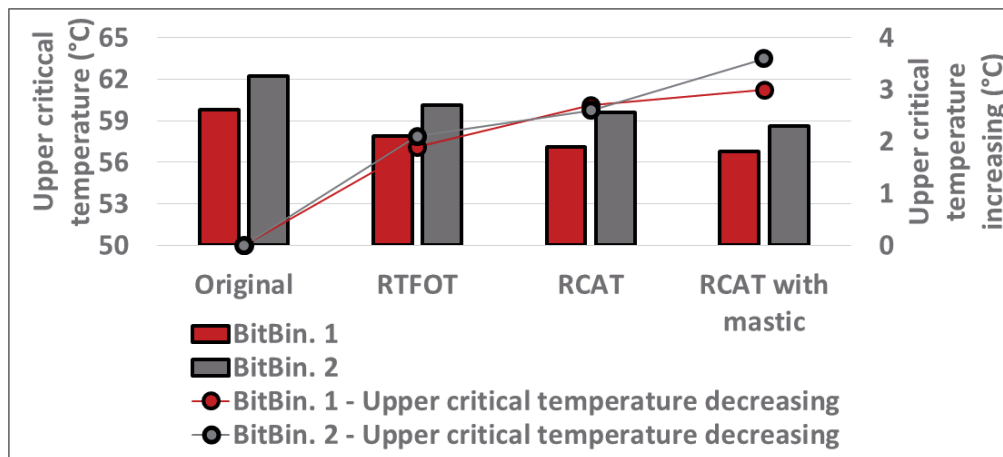


Figure 4 Comparison of three methods laboratory ageing (RTFOT, RCAT and RCAT with mastic) by upper critical temperature for bituminous binders with penetration grade 70/100.

Figure 5 illustrates increase in the lower critical temperature. Values of upper critical temperatures after RTFOT and RCAT ageing for bituminous binders increase approximately of about 0.5 °C. For bituminous binder 1 it is a little less, of about 0.2 °C. The highest increase in the lower critical temperature was for both bituminous binders after ageing using method RCAT with mastic. The increase was little more than 0.5 °C for bituminous binder 2 and ca 0.5 °C for bituminous binder 1.

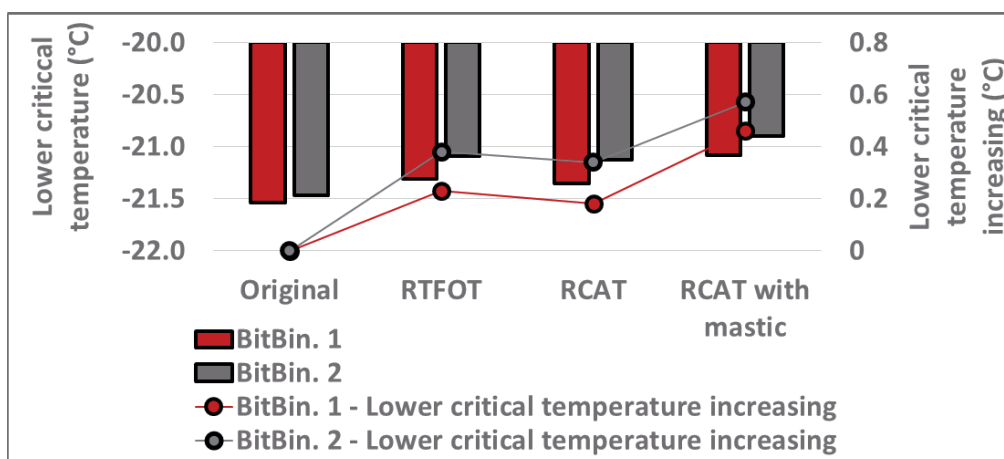


Figure 5 Comparison of three methods laboratory ageing (RTFOT, RCAT and RCAT with mastic) by lower critical temperature for bituminous binders with penetration grade 70/100.

CONCLUSIONS

This study shows results of methodology RCAT that is designed for simulating both short-term and long-term ageing of bituminous binders, and can be used for ageing of binders mixed with mastic. The simulation of laboratory bitumen short-term ageing was performed by the methods RTFOT, RCAT and RCAT with mastic. For the ageing characterization of the bituminous binders, various criterions were used – softening point increase, penetration decrease, relative increase in viscosity, relative increase in complex modulus, as well as changes in upper critical temperatures and low critical temperatures. Based on the results from our study, the following conclusions can be drawn:

- For the RTFOT and RCAT, the ageing of binders is simulated by creation and movement of thin film of binder. The standard methods of laboratory short-term ageing (RTFOT and RCAT) gave very similar changes in the evaluated properties (softening point, penetration at 25 °C, complex shear modulus, upper critical temperature, lower critical temperature, and dynamic viscosity).
- Both binders reached higher changes in their properties by the method RCAT with mastic and aggregate accelerated the process of ageing.
 - In the presence of mastic the film of binder was thinner and it supported the oxygen transfer in binder. Simultaneously, there is an effect of basalt acidity which speeded up the ageing.

- The ageing was observed for both, the traditional and the rheological properties.
- The method with mastic should be used to describe the ageing of bituminous binders closer to real conditions.

ACKNOWLEDGEMENT

The publication is a result of the project which was carried out within the financial support of the Ministry of Industry and Trade of the Czech Republic with institutional support for long-term conceptual development of research organisation.

REFERENCES

1. Saoula, S.; Khedoudja, S.; Haddadi, S.; Munoz, M.; Santamaria, A. Analysis of the Rheological Behavior of Aging Bitumen and Predicting the Risk of Permanent Deformation of Asphalt. *Materials Sciences and Applications* 2013, 4, 312–318.
2. Lu, X., Talon, Y., & Redelius, P. (2008, May). Aging of bituminous binders—laboratory tests and field data. In *Proceedings of the 4th Eurasphalt & Eurobitume Congress, Copenhagen* (pp. 21-23).
3. Petersen JC. Chemical composition of asphalt as related to asphalt durability: state of the art. *Transport. Res. Record* 1984; 999:13-30
4. O'connell, J., & Steyn, W. J. (2017). An overview of the ageing of bituminous binders. Southern African Transport Conference.
5. Pipintakos, G., Ching, H. V., Soenen, H., Sjövall, P., Mühlich, U., Van Doorslaer, S., ... & Lu, X. (2020). Experimental investigation of the oxidative ageing mechanisms in bitumen. *Construction and Building Materials*, 260, 119702.
6. European Standard. "Bitumen and bituminous binders – Determination of the resistance to hardening under the influence of heat and air – Part 1: RTFOT method (EN 12607-1); Part 2: TFOT method (EN 12607-2); Part 3: RFT method (EN 12607-3)"

CONCEPTUAL DESIGN OF GASIFIER PROCESSING HEAVY OIL FRACTIONS

Podolský S.¹, Variny M.¹

¹ *Institute of Chemical and Environmental Engineering, Faculty of Chemical and Food Technology, Slovak University of Technology in Bratislava, Radlinského 9, 812 37, Bratislava, Slovak Republic*
miroslav.variny@stuba.sk

Abstract

Maximization of material and energy efficiency is imperative for the refining and petrochemical industries to succeed on the competitive market. Searching for suitable solutions, refineries often focus on the “bottom of the barrel”, striving to upgrade the heavy oil residues from hydrocracking processes. Such materials are typically sold as low-cost ship fuels or serve for internal heat and power production. One of the possible alternatives is to route such feedstock to a gasifier, where it is broken down into small molecules with the help of a suitable gasifying agent (air, oxygen, steam). Gasifier effluent is then treated in a series of steps, optimized for its energy content recovery as well as for removal of undesired fractions (tars). The produced cleaned syngas is suitable as fuel or can undergo further treatment to recover hydrogen or other valuable components. This study presents the results of a conceptual design of a gasifier processing heavy oil fractions. Advantages of integrating the gasifier within a refinery are pointed out.

Introduction

Heavy oil residues belong to refining by-products with lower value, usable as ship fuels or as calorific fuels for steam and power plants. This material consists of large hydrocarbon molecules (asphaltenes) with heteroatoms embedded in their structure¹ and is difficult to be upgraded with conventional refining techniques. Its material utilization by thermochemical conversion^{2,3} poses a challenge but is, on the other hand, a promising means for increasing its market value^{4,5}, especially if its use as fuel would be banned due to environmental regulations becoming steadily more stringent.

Gasification is a promising alternative to valorize various liquid and solid by-products and wastes by converting them into syngas⁶ which, on being cleaned, can further be utilized as a source of hydrogen⁷, or for highly efficient heat and power cogeneration^{8,9}. Coal, biomass, or various waste fractions represent just a part of possible feedstock for gasification units¹⁰⁻¹². Gasifying agents include air, steam and/or oxygen^{9,13}. Syngas cleaning is considered as one of the crucial issues impacting the viability of gasifiers¹⁴, its design being still case-dependent and, despite a lot of research undertaken¹⁵, still incurring significant operational expenses to the plant^{16,17}.

Standalone thermochemical feedstock valorization projects (either by pyrolysis or gasification) cope with a multitude of issues to comply with the related legislation, leading to extra capital investment and operation expenses to deal with all by-products and wastes generated in the process¹⁸. In addition, their social acceptance is usually low¹⁹ which repeatedly prevented such units to be built either in Slovakia or elsewhere in Central Europe. On the contrary to that, incorporating a gasifier in an existing industrial enterprise poses a possibility to exploit its existing infrastructure²⁰ and spare capacities of auxiliary units capable to clean the produced syngas and wastewaters. Moreover, material and heat integration are made possible which, taken altogether, should lead to a decrease in capital expenses and an increase in revenue of gasification projects due to exploited synergies²¹.

This is a pilot study focusing on heavy oil residues gasifier unit design, to be placed in an existing refining complex^{22,23}. Possibilities for plant integration are pointed out along with utilization of the spare capacities of plant's gas desulphurization systems. Further research will aim at techno-economic studies comparing standalone and integrated gasification plants.

Materials and methods

Typical heavy oil residue gasification plant integrated in oil refinery consists of three main blocks, that are coupled together. Considered process flow diagram is shown in Figure 1. The main three blocks are block of heavy oil residue gasification and syngas generation, block of syngas cleaning and cooling and block of steam and power generation. Syngas generation block includes oxygen compressor (**KOM**) and gasification reactor (**REA**). Syngas cooling and cleaning block includes heat exchanger and condenser joined in series (**VT6**, **VT7**), section of acid gas absorption and regeneration of absorbent (**ABS**, **DES**) and PSA section (**PSA**). Steam and power generation block includes steam boiler (**KOT**), deaerator (**ODP**), condensate and fresh chemically treated water

preheaters (VT4, VT5) and steam condensation turbine with power generator (KPT). Main material and energy inputs and outputs are heavy oil residues (T1), oxygen (O1), chemically treated water (U1, U2, U3), return condensates (K4), hydrogen gas (G12), PSA off-gas (G11), steam export (P12) and produced power. Waste gas from acid gas adsorption is rich in H₂S (G7) and was not considered in overall energy balance.

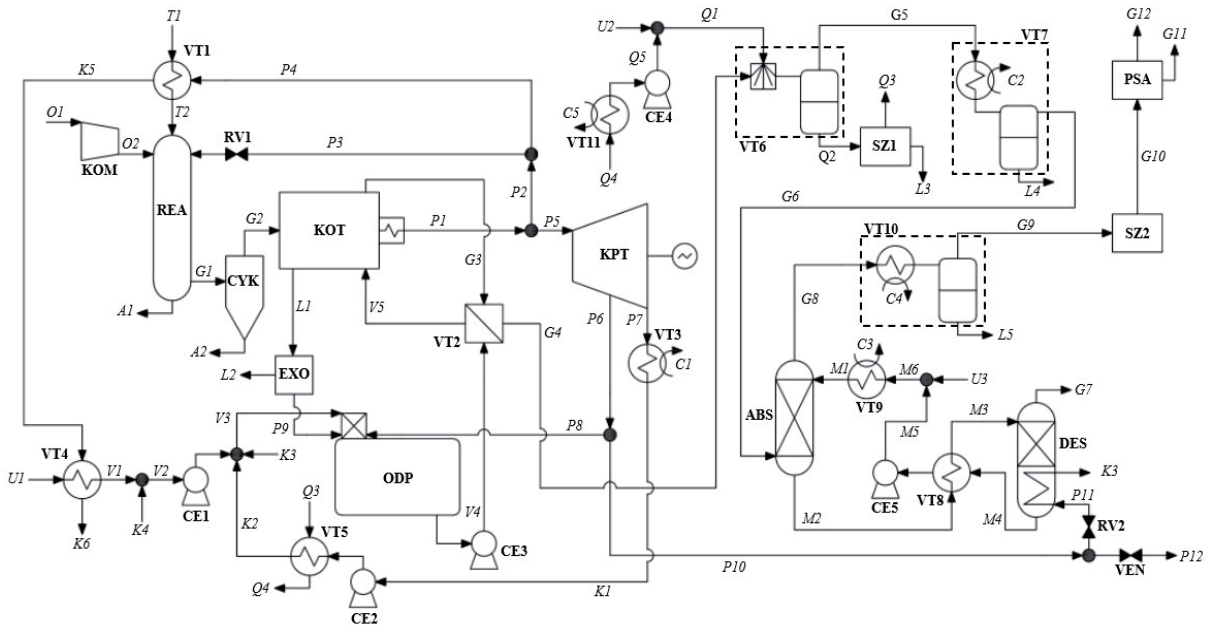


Figure 1. Considered flow diagram of heavy oil residue gasification plant

Flow scheme of reactor is shown in Figure 2. Type of reactor considered in this study is entrained-flow reactor, that was approximated as CSTR reactor with perfect dispersion (spray) of heavy oil residue.

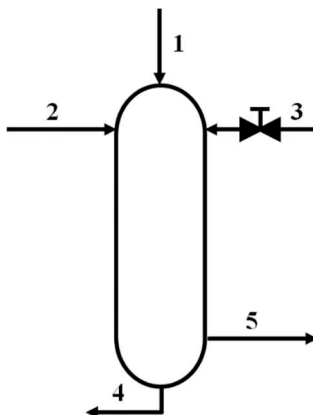


Figure 2. Flow scheme of reactor (1 – Heavy oil residue, 2 – Compressed oxygen, 3 – Steam with pressure reduction, 4 – Ash, 5 – Syngas)

Composition of heavy oil residue depends on oil composition², therefore, reactor processing rate of 60 t/h was assumed. Heavy oil residue's w composition (mass %) and LHV (lower heating value, MJ kg⁻¹) is shown in Table I.

Table I
Heavy oil residue properties²⁴

Dry heavy oil residue					Ash	Moisture	LHV
C	H	O	N	S			
86.25	11.05	0	0.40	2.20	0.10	0.30	40.5

Further assumptions include the following quantities and qualities of single inlet flows and process parameters of reactor, shown in Table II.

Table II

Process parameters (* – preliminary results)

Parameter	Value	Reference
t_1 , °C	200	25
t_2 , °C / P_2 , MPa	415.6 / 3	*
t_3 , °C / P_3 , MPa	460 / 6	*
$m_1 : m_2 : m_3$	1 : 1.1 : 0.35	26
P_{reactor} , MPa	3	26
τ_5 , s	12	27
w_5 , m s^{-1}	1.5	23

As the pressure of inlet steam is higher than pressure in gasifier, isenthalpic pressure reduction is also needed (from 6 MPa to 3 MPa). Complete conversion of carbon was assumed; reactions of gasification are presented in equations (1) – (5)^{2,26}.



Reactions (1) – (3) are deemed to be instant, reaction rates of (4) and (5) are presented in equations (6) – (9)^{25,28}.

$$r_4 = 2700 \exp\left(-\frac{1510}{T}\right) \left[C_{\text{CO}} C_{\text{H}_2\text{O}} - \frac{C_{\text{CO}_2} C_{\text{H}_2}}{K_{C4}} \right] \quad (6)$$

$$K_{C4} = 0.0265 \exp\left(\frac{3968}{T}\right) \quad (7)$$

$$r_5 = 1.585 \times 10^7 \exp\left(-\frac{24157}{T}\right) \left[C_{\text{CO}} C_{\text{H}_2} - \frac{C_{\text{CH}_4} C_{\text{H}_2\text{O}}}{K_{C5}} \right] \quad (8)$$

$$K_{C5} = T^{-6.567} \exp\left(\frac{7082.848}{T} + \frac{7.466 \times 10^{-3}}{2} T - \frac{2.164 \times 10^{-6}}{6} T^2 + \frac{0.701 \times 10^5}{2T^2} + 32.541\right) \quad (9)$$

Reactor dimensions are calculated via equation (10).

$$\dot{V}_5 = \frac{V_R}{\tau_5} = \pi D_R^2 w_5 = \frac{\pi D_R^2 L_R}{4\tau_5} \quad (10)$$

Discussion and result analysis

This system represents a set of several non-linear equations, that consist of material balances of each component, overall enthalpy balance and reactor size equation, what was solved by using MATLAB. Results are shown in Table III.

The results indicate that outlet syngas is energy-rich, which can be further utilized. Main components of syngas are hydrogen and carbon monoxide. Considering the acid gas content, mainly H₂S, it is necessary to separate these gases out of the syngas, otherwise they would act corrosively. Simultaneously, rapid syngas flow in reactor entrains solid phase pieces (mainly tars, soot, heavy metals), which can shorten the equipment's life in operation and solid phase separation is also necessary. Reactor is 18 m high, and its diameter is 3.1 m, representing reactor volume 134.3 m³.

Table III

Results of calculations (# - physical enthalpy, reference conditions: 0°C, gaseous state)

Parameter		Value
n_s , kmol s ⁻¹		2.44
t_s , °C		1 384
P_s , kPa		3 000
Composition, mol. %	H ₂ O	7.51
	CO	46.11
	CO ₂	2.40
	H ₂	41.88
	CH ₄	0.33
	N ₂	1.29
	H ₂ S	0.47
h_s , kJ kmol ⁻¹ #		45 656
LHV, MJ kmol ⁻¹		236.9

Main product of gasification is hydrogen, most frequently. As was mentioned, component separation is needed, preceded by syngas cooling and vapour condensation. First of all, solid phase pieces are separated using cyclone, then syngas physical energy content is utilized by high pressure steam production, that can be coupled with cogeneration. Before acid gas absorption is used, syngas temperature must be further decreased by cooling (and simultaneous vapour condensation) using water injection and subsequent tubular heat exchanger. Acid gas absorption unit is coupled with absorbent regeneration section. Chemisorption by alkaline absorbents is used, mostly employing aqueous solutions of alkanolamines. Last step of hydrogen production is its separation from purified syngas. This operation can be realized by membrane or cryogenic separation, but most conveniently by adsorption. Because of many components, PSA adsorption is used. Products of this process are high purity hydrogen and PSA off-gas, further used as fuel.

Summer and winter regime are distinguished in plant's operation. Winter operation enables excess steam export to the refinery with steam condensates return assumed. In this regime, steam turbine minimizes the share of condensing power production; thus, it lowers its electric output to generate low pressure steam for export instead. In summer, steam export option is not considered, and all excess steam is used to produce electric energy surplus. Individual features of both operation regimes can be followed in Table IV showing the obtained energy balance of the gasification plant.

Table IV

Proposed energy balance of the gasification plant in summer and winter regime

Energy content, MW	Winter	Summer
Feeds		
VR	676	676
Oxygen	1	1
Chemically treated water (U1)	2	2
Return condensates (K4)	7	0
Products		
Hydrogen (G12)	186	186
PSA off-gas (G11)	389	389
Excess electric energy	8	18
Steam export	59	0
Losses and waste streams	44	86

Polygeneration operation with steam export in winter lowers the production of waste heat. Waste heat production in summer as almost twice compared to winter, mostly due to condensing turbine steam condenser load.

Conclusions

Purpose of this study was to estimate basic design and operation parameters of HOR gasification reactor processing 60 t/h of HOR. The obtained syngas represents a source of usable materials (as hydrogen) as well as a source of technically usable energy for cogeneration. Locating the gasifier in existing oil refinery enterprise with existing infrastructure and spare capacities for syngas and wastewaters cleaning can enhance the gasification plant's flexibility and make it an environmentally friendly method of vacuum residue valorization following the concept of polygeneration. Apart from hydrogen, the plant exports both calorific offgases, excess electric energy and excess steam (in winter). The possibility of offgases and steam export to the refinery improves the plant's energy efficiency substantially and is expected to improve its economic feasibility, compared to a standalone gasification plant. This will be subject of further research.

Acknowledgement

This work was financially supported by the Slovak Research and Development Agency, Grant No. APVV-15-0148 and APVV-19-0170 as well as by the Faculty of Chemical and Food Technology, Slovak University of Technology in Bratislava.

References

1. Seljeskog M., Sevault A., Ditaranto M.: *Energy Procedia* 37, 7231 (2013).
2. Furimsky E.: *Oil Gas Sci. Technol* 54, 597 (1999).
3. Gulyaeva L. A., Vinogradova N. Y., Bitiev G. V., Gorlov E. G., Shumovskii A. V.: *Chem. Technol. Fuels Oils* 52, 469 (2016).
4. Marcantonio V., Müller M., Bocci E.: *Energies* 14, 6519 (2021).
5. Al-Samhan M., Al-Fadhli J., Al-Otaibi A. M., Al-Attar F., Bouresli R., Rana M. S.: *Fuel* 310, 122161 (2022).
6. Yang Y., Liew R. K., Tamothran A. M., Foong S. Y., Yek P. N. Y., Chia P. W., Van Tran T., Peng W., Lam S. S.: *Environ. Chem. Lett.* 19, 2127 (2021).
7. Materazzi M., Taylor R., Cairns-Terry M.: *Waste Manage.* 94, 95 (2019).
8. Zaporowski B.: *Appl. Energy* 74, 297 (2003).
9. Yu P., Luo Z., Wang Q., Fang M.: *Energy Convers. Manage.* 198, 111801 (2019).
10. Gabbar H. A., Aboughaly M., Russo S.: *Sustainability* 9, 1474 (2017).
11. Šuhaj P., Husár K., Haydari J., Steltenpohl P., Šupa I.: *Waste Manage.* 85, 1 (2019).
12. Zelenak S., Skvarekova E., Senova A., Wittenberger G.: *Energies* 14, 3718 (2021).
13. Ebrahimi A., Ziabasharhagh M.: *Energy Convers. Manage.* 209, 112624 (2020).
14. Richardson Y., Blin J., Julbe A.: *Prog. Energy Combust. Sci.* 38, 765 (2012).
15. Moiola S., Giuffrida A., Romano M. C., Pellegrini L. A., Lozza G.: *Appl. Energy* 183, 1452 (2016).
16. Kheiriniq M., Rahmanian N., Farsi M., Garmsiri M.: *J. Nat. Gas Sci. Eng.* 55, 534 (2018).
17. Zhu W., Ye H., Zou X., Yang Y., Dong H.: *Sep. Purif. Technol.* 276, 119301 (2021).
18. Puig-Gamero M., Argudo-Santamaria J., Valverde J. L., Sánchez P., Sanchez-Silva L.: *Energy Convers. Manage.* 177, 416 (2018).
19. Upham P., Shackley S.: *Biomass Bioenergy* 31, 433 (2007).
20. Meratizaman M., Monadizadeh S., Tohidi Sardasht M., Amidpour M.: *Energy* 83, 1 (2015).
21. Neves A., Godina R., Azevedo S. G., Matias J. C. O.: *J. Cleaner Prod.* 247, 119113 (2020).
22. Fasih H. F., Ghassemi H., Shahi H. K. M.: *Pet. Chem.* 61, 162 (2020).
23. Cao Z., Wu Q., Zhou H., Chen P., You F.: *Energy* 197, 117220 (2020).
24. Vaezi M., Passandideh-Fard M., Moghiman M., Charmchi M.: *Fuel* 90, 878 (2011).
25. Choi Y.C., Lee J.G., Yoon S.J., Park M.H.: *Korean J. Chem. Eng.* 24, 60 (2007).
26. Blažek J., Rábl. V.: *Základy zpracování a využití ropy*, Vysoká škola chemicko-technologická v Praze, Praha 2006.
27. Ashizawa M., Hara S., Kidoguchi K., Inumaru J.: *Energy* 30, 2194 (2005).
28. Miao Q., Zhu J., Barghi S., Wu C., Yin X., Zhou Z.: *Renewable Energy* 50, 655 (2013).

ENERGY AND ENVIRONMENTAL ASPECTS OF INDUSTRIAL HEAT SAVING IN VARIOUS SITUATIONS

Variny M.¹, Kšiňanová M.¹, Furda P.¹

¹ *Institute of Chemical and Environmental Engineering, Faculty of Chemical and Food Technology, Slovak University of Technology in Bratislava, Radlinského 9, 812 37, Bratislava, Slovak Republic
miroslav.variny@stuba.sk*

Abstract

Large industrial facilities and industrial clusters traditionally operate a combined heat and power unit serving as a marginal heat source. This unit can consist of either a steam Rankine cycle unit or comprise a Combined Cycle-based cogeneration unit. These distinctive designs differ by both heat to power ratio and delivered heat quality (temperature); both parameters being further impacted by the unit's operation. A change in heat quantity exported from the combined heat and power unit can thus have various impacts on cogenerated electric energy quantity and released greenhouse gas emissions. This contribution aims at elucidating this aspect of industrial heat saving projects with the goal to deliver valuable input for industrial energy managers and decision makers. Rankine and combined cycle units are modelled, providing a realistic assessment of energetic and environmental impact variability of their operation change due to the variable heat export. Greenhouse gas emissions generated in external power sources are considered as well.

Introduction

Industrial complexes and clusters tend to have complex energy supply systems, employing central and decentralised sources of energies and utilities^{1,2}, interconnected by an extensive system of pipelines. Among these, steam networks belong to most frequently studied and optimised systems³. Steam systems often comprise three or even four pressure levels that are interconnected, supplied by several sources producing steam on purpose or generating it from waste heat streams⁴. Extensive steam systems were modelled and optimised in case of steel and iron production plants⁵, petrochemical and refining enterprises⁶, pulp and paper mills⁷ as well as in other energy-intensive industries⁸. Complexity of the studies varies from assessing selected parts of the steam systems to multi-period analysis and operation optimization of whole systems^{9,10}.

Conditions securing a stable and efficient steam system operation are influenced by a multitude of factors. Transported steam quality and amount, steam system topology and technical state of pipelines, including insulation efficiency, can be counted among the most important ones¹¹. These are further impacted by plant's production load, products' structure, possible renovation and refurbishment activities, implementation of new technologies and many more, which result from the plant's development and strategical decisions made over decades¹². Any innovation activities impacting the plant's steam balance inevitably change the operation of the plant's marginal steam source – in most cases it is the central steam and power plant. To correctly assess the techno-economic dimensions of any such change, a deep understanding of the system's operation and limitations is required^{13,14}.

In this study, three distinctive case studies are considered, comprising changes in the plant's steam demand at two pressure levels and a change in condensates return to the central steam and power plant. Evaluation of each of the case studies is performed for A. a typical steam and power plant equipped with an extraction-condensing steam turbine and B. for a plant repowered by a gas turbine. The aim of this study is to highlight common trends and differences in obtained fuel consumption, CO₂ emissions and power production and to make the readers aware of system operation constraints likely to be approached in some scenarios.

Study objectives

The main goals of this study are:

- Analysis of seasonal variations of an industrial steam and power plant (ISPP), either as Rankine unit, or repowered by a gas turbine
- Evaluation of different exported heat load changes in terms of fuel consumption, power production and emitted CO₂

Combined heat and power unit description

This section provides description of the plant model scheme (displayed in Figure 1., where repowering and studied scenarios are depicted in dark grey and black). The plant combusts heavy fuel oil in a boiler, which transforms pre-heated feed water (stream no. 20) into a superheated high-pressure steam at the temperature of 530 °C. (stream no. 1). The steam flows to an extraction-condensing turbine (ECT), where the steam expands. ECT produces not only electricity but also extraction steam is produced. In repowered mode, the plant combusts natural gas with compressed air in a combustion chamber of the gas turbine. Because of the high rate of excess air used in the combustion, flue gas from the gas turbine contains high amount of unused oxygen, which created an opportunity to reuse the flue gas mixed with fresh air in combustion in the original boiler. As mentioned above, feed water used in the boiler undergoes the process of pre-heating, which takes place in the series of low temperature water heaters (by 30 °C), a degasser (by 30 °C) and high temperature water heaters (by 40 °C). Condensate loss caused by export is compensated with chemically treated water addition to a condenser.

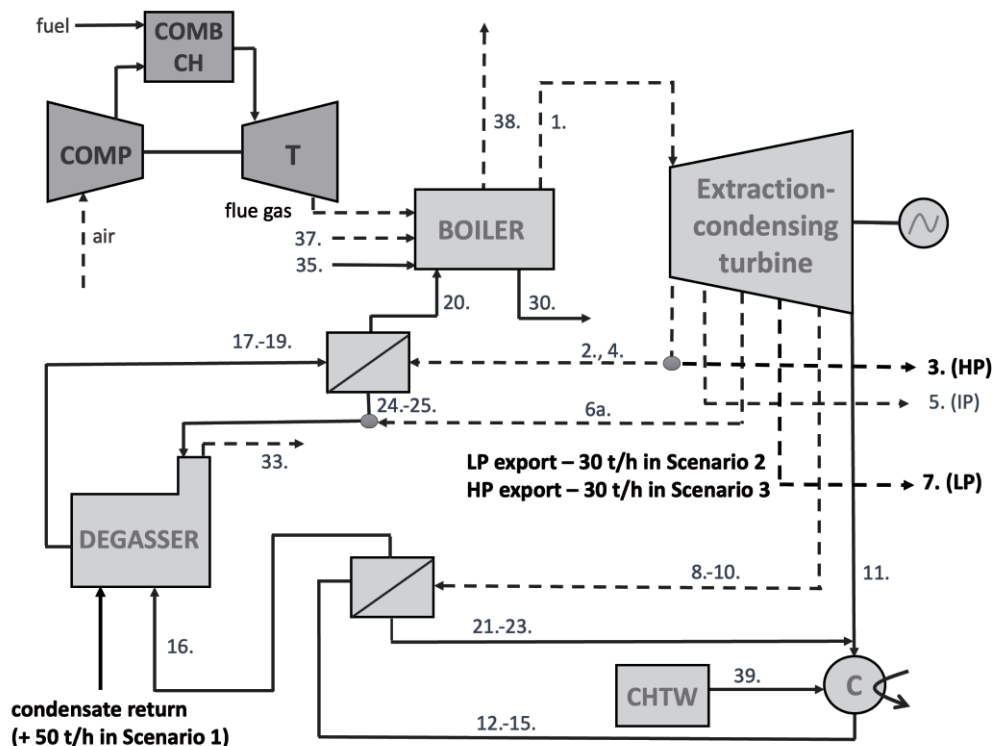


Figure 1. Simplified schematics of thermal power plant, where streams in gaseous state are depicted by dashed lines, solid lines represent liquid streams. Legend: C = condenser; COMB CH = combustion chamber; COMP = compressor; CHTW = chemically treated water; T = turbine.

Calculation assumptions are:

- to produce at least 60 MW of electric energy (either extraction-condensing turbine (ECT) alone or ECT and gas turbine (GT) together),
- to produce high-, intermediate- and low-pressure (HP, IP, LP) extraction steam for export as well as for its own consumption,
- minimal mass flow of vapour-liquid mixture (stream no. 11) is 10 t/h
- unit is studied in two modes – non-repowered and repowered,
- calculations are divided, based on season into winter and summer production,
- gas turbine electric efficiency in repowered mode is 30%,
- gas turbine mechanic efficiency is 95%,
- lower heat value of heavy oil is 40.496 MJ/kg both in winter and summer, for natural gas it is 48.609 MJ/kg in winter and 48.931 MJ/kg in summer,

- different temperatures of humid air are considered – 4 °C (winter), 22 °C (summer) and in both cases, the air is pre-heated to 100 °C,
- relative air humidity in winter is 80 % and 65 % in summer.

In addition, three different scenarios both for repowered and non-repowered ISPP including seasonal changes in winter and summer were proposed. In Scenario 1, 50 t/h of condensate return at the temperature of 100 °C is included, Scenario 2 includes lowered consumption of low-pressure extraction steam by 30 t/h and Scenario 3 includes lowered consumption of high-pressure extraction steam by 30 t/h.

Mathematical model

In this section, the most important steps of calculation and the mathematical model development is described. Basis of the calculation is to assemble material and enthalpic balances of ISPP units as shown in equation (1) and equation (2).

$$\sum \dot{m}_{in} = \sum \dot{m}_{out} \quad (1)$$

$$\sum h_{in} \dot{m}_{in} = \sum h_{out} \dot{m}_{out} \quad (2)$$

$$(3)$$

where \dot{m} = mass flow, h = enthalpy, lower index in = inlet output, lower index out = outlet output.

Important step is to determine stream enthalpies either from literature or based on calculations. After acknowledging all assumptions mentioned in previous section, the results of mass flows for original non-repowered ISPP are obtained.

Next step is to compile material and enthalpy balances for the gas turbine based on the same principle and reconstruct the original balances for a boiler to include the flue gas from the gas turbine as a part of the combustion air. Subsequently, the results for repowered ISPP are obtained.

In addition, the electrical efficiency of ISPP and CO₂ production is calculated based on equation (3) and equation (4).

$$\eta_{el} = \frac{P_{el,total}}{Q_{fuel}} \quad (4)$$

where η_{el} = electrical efficiency of ISPP, $P_{el,total}$ = produced electricity obtained from the enthalpy balance and Q_{fuel} = total heat obtained by burning fuel.

$$\dot{m}_{CO_2} = \dot{m}_{38} \cdot w_{CO_2} \quad (5)$$

where \dot{m}_{CO_2} = mass flow of CO₂ produced in combustion, \dot{m}_{38} = mass flow of the flue gas from the boiler and w_{CO_2} = mass fraction of CO₂ produced in combustion.

Model results

This section is dedicated to the results of the mathematical model. In the Figure 2. and Figure 3., production of electric energy before and after repowering can be observed. As mentioned in the previous section, different initial states were chosen for winter and summer, which resulted in variable electricity production.

Consumption of fuel (heavy oil and natural gas separately) and CO₂ production are displayed in Table I and Table II. In this case, different values are observed for different seasons as well. When production of electric energy rises, fuel consumption and CO₂ production goes up too, which is an expected trend, but the dependency of those values is not necessarily a continual proportion.

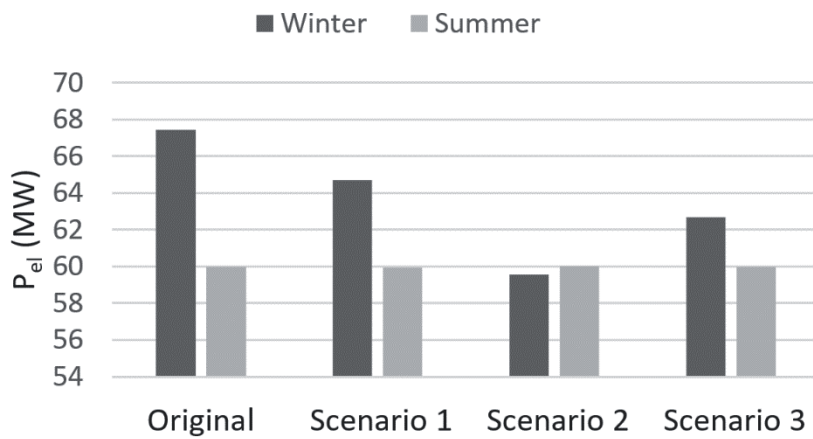


Figure 2. Electricity production – non-repowered option

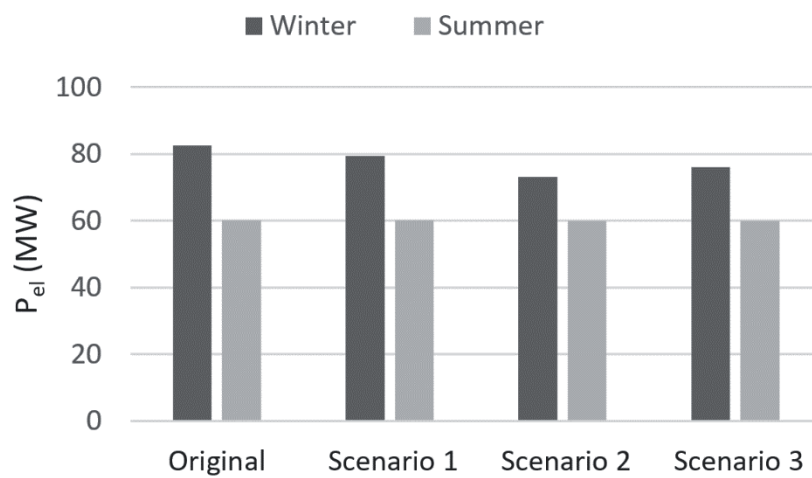


Figure 3. Electricity production – repowered option

Table I
CHP operation comparison – before repowering proposal

Non-repowered		Original		Scenario 1		Scenario 2		Scenario 3	
		Winter	Summer	Winter	Summer	Winter	Summer	Winter	Summer
Fuel consumption (t/h)	Heavy oil	29	25.3	28.16	25.13	25.99	24.24	25.99	23.42
	Natural gas	-	-	-	-	-	-	-	-
CO ₂ production (t/h)		92.59	80.57	89.92	80.01	82.98	77.18	82.98	74.58

Table II
CHP operation comparison – repowering proposal included

Repowered		Original		Scenario 1		Scenario 2		Scenario 3	
		Winter	Summer	Winter	Summer	Winter	Summer	Winter	Summer
Fuel consumption (t/h)	Heavy oil	25.31	19.26	24.56	19.14	22.68	18.41	22.67	17.82
	Natural gas	4.26	3.3	4.13	3.29	3.81	3.16	3.81	3.06
CO ₂ production (t/h)		92.59	92.48	70.55	89.75	70.13	82.86	67.46	82.84

Discussion and Conclusions

Data presented in Figure 2, Figure 3 and in Table I and Table II lead to the following observations:

- Winter operation requires more fuel and generates more electricity, resulting from higher exported heat load, compared to summer operation.
- Repowered ISPP fulfills the required power production and heat export with less CO₂ emissions than the non-repowered one.
- Condition of minimum 60 MW power production causes an adequate increase in condensing power production in summer if exported heat load decreases (Scenarios 2 and 3); low pressure steam export decrease leads to less fuel saving than the same decrease in high pressure steam export.
- Smallest fuel saving and CO₂ emissions decrease is observed in case of condensates return (Scenario 1 = internal heat consumption decrease).
- Repowered ISPP performs better than the non-repowered one, in all scenarios, but the observed trends are similar. Extra power from the gas turbine decreases condensing power production and contributes to cleaner power production and overall CO₂ emissions decrease.

This demonstrates the need for individual assessment of heat saving projects in industry when an ISPP operation change is involved.

Acknowledgement

This work was financially supported by the Slovak Research and Development Agency, Grant No. APVV-15-0148 and APVV-18-0134 as well as by the Faculty of Chemical and Food Technology, Slovak University of Technology in Bratislava.

References

1. Rehfeldt M., Fleiter T., Worrell E.: *J. Cleaner Prod.* **187**, 98 (2018).
2. Hassiba R. J., Linke P.: *Appl. Therm. Eng.* **127**, 81 (2017).
3. Zhu Q., Lu X., Zhang B., Chen Y., Mo S.: *Energy* **97**, 191 (2016).
4. Jouhara H., Khordehgah N., Almahmoud S., Delpech B., Chauhan A., Tassou S. A.: *Therm. Sci. Eng. Prog.* **6**, 268 (2018).
5. Zhang Q., Zhao T., Ni T., Gao J.: *Energy Sources, Part A* **43**, 1100 (2021).
6. Marton S., Svensson E., Subiaco R., Bengtsson F., Harvey S.: *J. Sustainable Dev. Energy Water Environ. Syst.* **4**, 560 (2017).
7. Cortés E., Rviera W.: *Energy* **35**, 1289 (2010).
8. Halasz T., Nagy A. B., Ivicz T., Friedler F., Fan L.T.: *Appl. Therm. Eng.* **22**, 939 (2002).
9. Liu Y., Liu Q., Wang W., Zhao J., Leung H.: *Inf. Sci.* **193**, 104 (2012).
10. Li Z., Du W., Zhao L., Qian F.: *Ind. Eng. Chem. Res.* **53**, 11021 (2015).
11. Zhong W., Feng H., Wang X., Wu D., Xue M., Wang J.: *Energy* **87**, 566 (2015).
12. Hanus K., Variny M., Illés P.: *Processes* **8**, 622 (2020).
13. Sun L., Doyle S., Smith R.: *Appl. Energy* **161**, 647 (2016).
14. Bungener S. L., Van Eetvelde G., Maréchal F.: *Front. Energy Res.* **4**, 1 (2016).

MATERIAL ENGINEERING

MINERAL ADMIXTURES REACTIVITY DETERMINATION

Šídllová M.¹, Doležal T.¹, Šulc, R.², Pulcová K.¹

¹University of Chemistry and Technology Prague, Department of Glass and Ceramics, Technická 5, 166 28, Prague 6, Czech Republic

²Czech Technical University in Prague, Faculty of Civil Engineering, Thákurova 7, 166 29, Prague 6, Czech Republic

Martina.Sidlova@vscht.cz

Abstract

Sustainability and new greening measures bring new challenges to the construction industry within the European Union. Reducing CO₂ emissions is forcing the market to find new ways and use new materials as admixtures in cement or concrete. Lower quality clays could undoubtedly be such materials. Fly ashes from co-combustion of biomass are also beginning to appear on the market. They have different composition and properties compared to conventional fly ashes. In addition, it cannot be forgotten that there is the potential use of power plant bottom ashes. In this work, the pozzolanic activity and reactivity of various types of mineral admixtures, both traditional and new ones, were compared. The reactivity of the admixtures was determined using the Frattini test and the electrical conductivity test. The 8-day Frattini test proved the pozzolanic activity of all raw materials except for one sample of fly ash from biomass. The shortened 1-day Frattini test showed a different reactivity of the materials after one day of hydration in comparison to 8-day Frattini test. Nevertheless, the quantitative agreement between the results of the 1-day Frattini test and the electrical conductivity test was not clearly demonstrated. It was further confirmed that the pozzolanic activity of the supplied substances is determined by their grain size as well.

Introduction

Cement is one of the most produced materials in the world, including the Czech Republic. Its role in civil engineering is irreplaceable but its production also contributes to 5-8 % of world CO₂ emissions¹. Other problems concerning cement production are lack of natural resources and landscape changes caused by mining. These problems can be partially solved by replacing a part of the cement by pozzolans such as fly ash, slag or calcined clays². A material with pozzolanic activity (pozzolan) reacts with portlandite, a cement hydration product, forming additional C-S-H binding phase³. Pozzolans can even increase compressive strength⁴, but their advantage is also in replacing part of the clinker in cement, thus reducing CO₂ emissions, saving natural resources and solving the problem with their landfilling.

Various materials with pozzolanic properties have already been used for decades³. Fly ash (FA) and blast furnace slag are the most frequently used and their usage in construction is in Czech Republic regulated by standards ČSN EN 450-1⁵ and ČSN EN 450-2⁶. Coal power plants are also to be closed as a part of fulfilling GreenDeal agreement. Fresh FA will thus be unavailable and the issue of FA recovery from landfills will arise⁷. FA is often deposited not in pure form, but in mixture with other coal combustion products such as gypsum, produced by flue gas desulfurization. New materials such as calcined clays or oil shales are thus subjected to research⁴. Calcined clays and fly ashes have been examined by various authors in the world and in the Czech Republic^{8,9}.

Measuring strength activity index of the mixture is advantageous but relatively time-consuming. Methods of pozzolanic activity assessment are thus mostly based on determining Ca²⁺ ions consumption¹⁰ by the examined material. Comparisons of pozzolanic activity test methods are offered e.g. by Donatello¹¹ or Parashar¹².

Materials and methods

The input materials for the pozzolanic activity tests were bottom ashes from power plant Počeradý (ST 5 C) and Tušimice (ST 6 C), fly ash from power plant Tušimice (VP 8 C), biomass combustion ash from energetics centre Jindřichův Hradec (BM 1 C) and biomass co-combustion ash from power plant Hodonín (BM 27 C). In addition, five different calcinated clays from companies Keraclay (AW, WBS, WS) and LB Minerals (GEP, VIŽ) were studied.

The calcined clays were heated at the temperature of 850°C for 1 hour. While the clay WS is suitable as a raw material for ceramics, other clays are supposed to have lower quality and they could be potentially used as cement admixture.

X-ray diffraction analysis (XRD) was performed for phase composition of samples (Table I). With the addition of 10 wt. % ZnO the amount of amorphous phase was determined. θ - θ powder diffractometer with Bragg-Brentan parafocusing geometry X'Pert3 Powder diffractometer (PANalytical, Netherlands) was used.

X-ray fluorescence analysis (XRF) was used for the oxide composition determination of samples (Table II) using wave-dispersive X-ray spectrometer ARL 9400 XP (Thermo ARL, Switzerland), equipped with X-ray lamp with 4GN type Rh anode with Be window of 50 μ m thickness. Spectral lines intensities were measured in vacuum by software WinXRF.

Table I

Phase composition of the samples (XRD %), AP = amorphous phase

Sample	AP*	quartz	kaolinite	muscovite	mullite	sylvite	orthoclase	akranite	anotrite	albite	others
WBS	34	5	57	4	-	-	-	-	-	-	-
GEP	52	3	27	18	-	-	-	-	-	-	-
VIŽ	11	74	2	13	-	-	-	-	-	-	-
WS	37	4	57	2	-	-	-	-	-	-	-
ST 5 C	66	10	-	-	18	-	-	-	5	-	1
ST 6 C	70	7	-	-	20	-	-	-	-	-	3
VP 8 C	54	9	-	-	35	-	-	-	-	-	2
BM 1 C	75	2	-	-	-	13	-	6	-	-	4
BM 27 C	48	38	-	-	-	-	6	-	-	4	4

Table II

Oxide composition of the samples (XRF %)

Sample	SiO ₂	Al ₂ O ₃	Fe ₂ O ₃	CaO	MgO	Na ₂ O	K ₂ O	TiO ₂	SO ₃	P ₂ O ₅	Cl ⁻	MnO	others
AW	50.92	42.06	2.51	0.45	0.43	0.20	1.70	1.34	0.07	0.09	-	0.04	0.18
WBS	51.10	43.65	1.59	0.21	0.23	-	1.18	1.31	-	-	-	-	0.73
GEP	56.28	26.42	10.30	1.08	1.77	0.06	2.42	1.09	0.15	0.14	-	0.04	0.26
VIŽ	68.24	25.23	1.51	0.25	0.62	0.19	2.36	1.28	0.03	0.09	-	-	0.20
WS	50.04	46.07	0.82	0.17	0.13	0.03	0.73	1.56	0.20	0.06	-	-	0.20
ST 5 C	52.24	31.94	8.84	1.21	1.17	0.34	2.30	1.27	-	0.16	0.03	0.11	0.39
ST 6 C	49.89	32.97	8.48	2.02	1.23	0.54	1.72	1.29	1.22	0.19	0.06	0.08	0.32
VP 8 C	49.76	33.93	8.86	1.75	1.02	0.60	1.65	1.19	0.60	0.20	-	-	0.45
BM 1 C	39.10	0.82	0.64	13.53	2.89	0.31	25.72	0.09	5.05	2.20	9.31	0.14	0.21
BM 27 C	43.13	5.93	2.61	28.17	4.87	0.80	7.04	0.36	0.90	3.49	-	1.99	0.72

Particle size distribution (PSD) was measured by Bettersizer ST (Dandong Bettersize Instruments Ltd., China) in isopropanole as the carrier medium. Specific density of the samples was measured by pycnometric method. Specific surface area was determined by Blaine's apparatus JIP-TECH MATEST (MATEST S.p.A., Italy). The following Table III shows PSD quantiles, specific density and specific surface (based on the standard ČSN EN 196-6¹³).

Table III

Specific density, specific area and PSD quantiles of samples

Sample	d10 [μm]	d50 [μm]	d90 [μm]	specific density [$\text{g}\cdot\text{cm}^{-3}$]	specific area [$\text{m}^2\cdot\text{kg}^{-1}$]
AW	3.2	43.3	254.9	2.691	480
WBS	2.6	12.2	48.2	2.859	850
GEP	2.4	19.0	78.4	2.653	826
VIŽ	2.0	10.7	54.7	2.695	817
WS	1.9	10.6	54.6	2.643	1004
ST 5 C	56.3	188.2	400.3	2.053	157
ST 6 C	94.8	251.8	557.8	1.630	128
VP 8 C	1.7	12.2	66.5	2.059	461
BM 1 C	8.4	64.3	268.5	2.036	600
BM 27 C	124.7	231.9	424.3	2.649	101

According to Frattini test, described in ČSN EN 196-5¹⁰, 5 g of the sample were mixed with 15 g of Portland cement and put into 500 ml PE bottle with 100 ml of re-boiled distilled water. The bottles were kept at 40 °C for 8 days. Apart from this time, selected samples were kept just for 1 day to see whether the results could be obtained in shorter time period. Resulting mixture was filtered. In the solution, total alkalinity and Ca^{2+} content were determined by titration with 0.1 M HCl and 0.03 M EDTA respectively.

Electric conductivity test was described by Sinthaworn and Nimityongskul¹⁴. The test consisted of preparing an extract of Portland cement suspension by 30 minutes of leaching. The filtrate was then diluted to conductivity of roughly $10 \text{ mS}\cdot\text{cm}^{-1}$ and heated to 80 °C. 1 g of the tested material was added and the electric conductivity was being monitored for 24 hours accompanied by constant mixing of the suspension.

Results and Discussion

Diagrams for pozzolanic activity assessment are shown in Figure 1 (8-day Frattini test) and Figure 2 (1-day Frattini test). The horizontal axes represent total alkalinity and the vertical axes show Ca^{2+} content in the samples. As the pozzolan reacts with Ca^{2+} ions from the filtrate, Ca^{2+} concentration in the solution decreases. Dependence of $\text{Ca}(\text{OH})_2$ solubility on sample alkalinity as to be taken into account. Therefore, position of each point representing one sample has to be compared with the curve of theoretical solubility of $\text{Ca}(\text{OH})_2$, as defined in ČSN EN 196-5¹⁰. The further below the curve the point is, the higher the pozzolanic activity is.

It can be seen that calcined clay VIŽ, both power plant bottom ashes (ST 5 C, ST 6 C) and power plant fly ash VP 8 C have close pozzolanic activity. Clays AW and GEP show higher pozzolanic activity. Clays WS and WBS are the most reactive ones. Biomass ash BM 1 C is not shown in the graph, as the test showed $19.2 \text{ mmol}\cdot\text{l}^{-1} \text{Ca}^{2+}$ ions and $100.94 \text{ mmol}\cdot\text{l}^{-1}$ total alkalinity. However, the Frattini test is not suitable for materials with high calcium content, including also BM 27 C. Position of the control cement sample (Cem) should be exactly on the curve of theoretical Ca^{2+} ions solubility. The higher Ca^{2+} content is probably caused by some portlandite crystals passing through filter and getting suspended into the titrated solution.

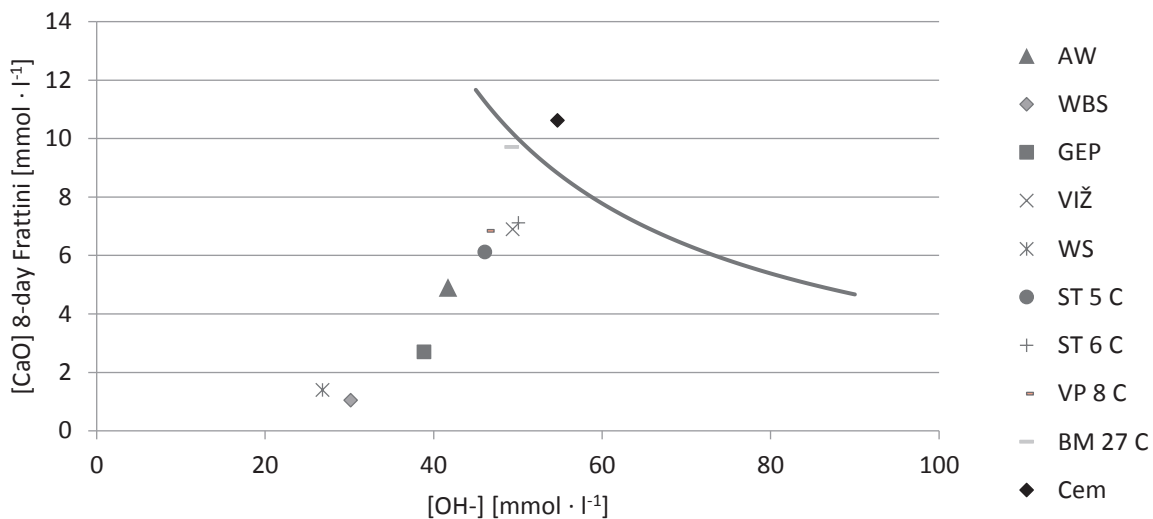


Figure 1. Results of the 8-day Frattini test

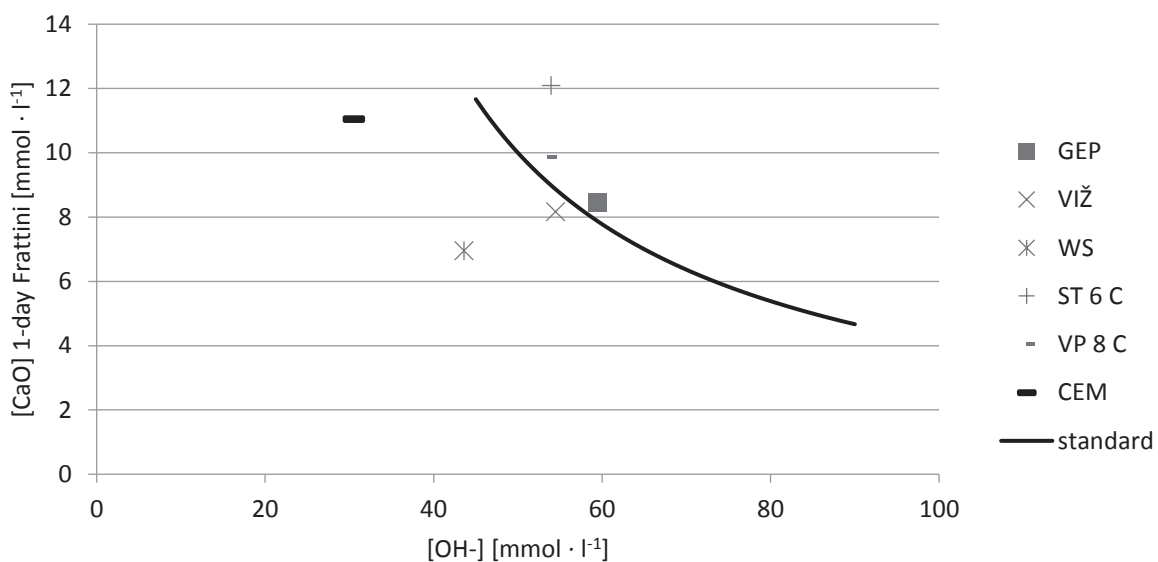


Figure 2. Results of the 1-day Frattini test

When Figure 1 and Figure 2 are compared, it can be seen that one day is mostly not enough for pozzolanic assessment by the Frattini test. Even the alkalinity of the control cement sample (Cem) did not reach its expected value. For example, sample VP 8 C, which exhibits lower, but clear pozzolanic activity by 8-day test version, is not proven to be pozzolan by 1-day version. Nevertheless, good pozzolans such as VIŽ and WS may already be recognized by the shortened Frattini test version, despite the fact that their Ca^{2+} consumption is much lower after 1 day than after 8 days.

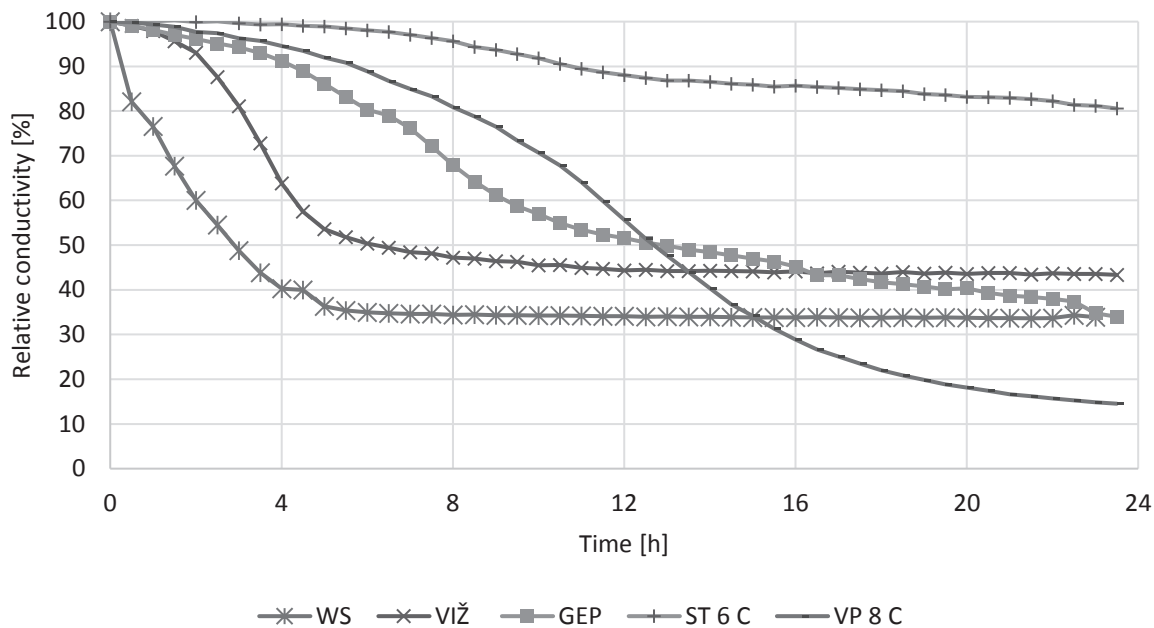


Figure 3. Time-dependent relative electric conductivity in the electric conductivity test

During the electric conductivity test, Ca^{2+} ions are also consumed by the pozzolanic reaction. This decreases the overall solution conductivity which is measured. It can thus be stated that clays WS and VIŽ mostly reacts during first 4 hours of the experiment, while clay GEP and fly ash VP 8 C react more slowly. Reaction of bottom ash ST 6 C is much slower, which confirms the results of the 1-day Frattini test.

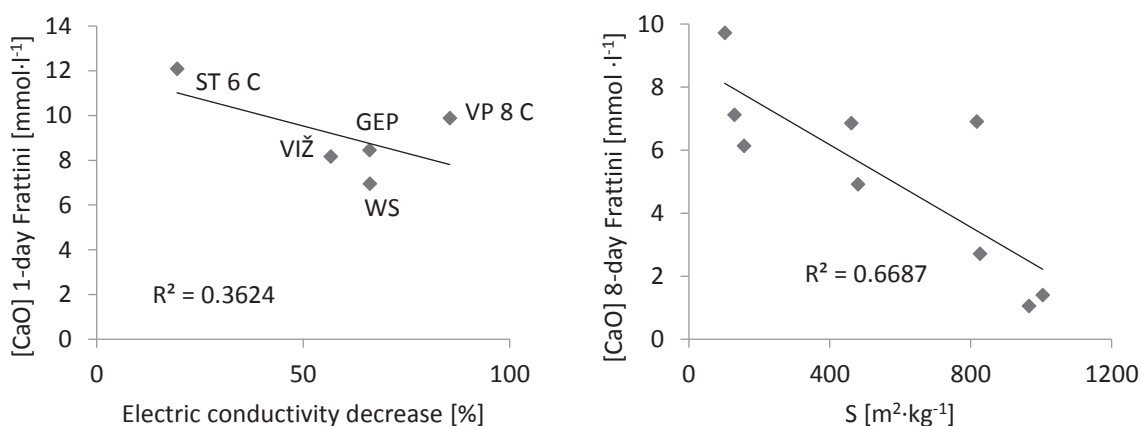


Figure 4. Correlation between electrical conductivity decrease after 24 hours and 1-day Frattini test (left), correlation between specific surface area and 8-day Frattini test (right)

In Figure 4 there is no significant correlation between electrical conductivity decrease and 1-day Frattini test. It can be caused by high diversity of the samples. However, many more measurements should be conducted in order to reach statistically significant conclusions. Nevertheless, moderate correlation between specific surface area and 8-day Frattini test has been confirmed.

Conclusion

It can be concluded that calcined clays, fly ash and bottom ash show significant pozzolanic activity. It was found that all of the examined calcined clays are pozzolans according to the 8-day Frattini test, whereas clays WS and WBS are the most reactive ones. On the other hand, biomass combustion ashes are problematic due to elemental

composition and hardly detectable pozzolanic activity; Frattini test is thus not suitable for pozzolanic activity assessment of biomass combustion ashes due to their high Ca^{II} and Mg^{II} content.

Shortened 1-day Frattini test could be used for preliminary screening of large amounts of different samples as it detects the biggest differences of Ca²⁺/OH⁻ in much shorter time, but it is not sufficient for getting conclusive results. The results of the 1-day Frattini test did not match the results of the standard 8-day Frattini test. Shortened test version discovered the pozzolanic activity only for calcinated clays WS 850 °C and VIŽ 850 °C, which responded most quickly when measuring conductivity.

Electrical conductivity test after 24 hours confirmed the results of 1-day Frattini test in most cases and it revealed different time courses of the reactions.

Acknowledgement

This project was co-financed by the Technology Agency of the Czech Republic as a part of programme TREND FW01010195.

References

1. Andrew R. M.: *Earth Syst. Sci. Data*, *11*, 1675 (2019).
2. Siddique R., Cachim P.: *Waste and Suppl. Cem. Mat. in Concrete*. Woodhead Publishing 2018.
3. Sprung S.: *Cement. Ullmann's Encyc. of Ind. Chem.* Wiley 2018.
4. Wang B., Zhang Y., Li M.: *Eng. Materials*, *539*, 230 (2013).
5. ČSN EN 450-1 Fly ash for concrete - Part 1: Definition, specifications and conformity criteria. Czech Office for Standards, Metrology and Testing, Prague 2013.
6. ČSN EN 450-2 Fly ash for concrete - Part 2: Conformity evaluation. Czech Office for Standards, Metrology and Testing, Prague 2005.
7. Šulc R., Šídlová M., Formáček P., Snop R., Škvára F., Polonská A.: *Materials*, *15(10)*, 3653 (2022).
8. Charbuský J.: *Úprava popelovin pro využití ve stavebním průmyslu*. CTU Prague, 2020.
9. Sokolová K.: *Vlastnosti deponovaných elektrárenských popílků*. CTU Prague, 2018.
10. ČSN EN 196-5 Methods of testing cement – Part 5: Pozzolanicity test for pozzolanic cement. Czech Office for Standards, Metrology and Testing, Prague 2011.
11. Donatello S., Tyrer M., Cheeseman C.R.: *Cement and Concrete Composites*, *32*, 121 (2010).
12. Parashar A., Bishnoi S.: *Construction and Building materials*, *256* (2020).
13. ČSN EN 196-6 Methods of testing cement – Part 6: Determination of fineness. Czech Standardization Agency, Prague 2019.
14. Sinthaworn S., Nimityongkul P.: *Waste Management*, *29 (5)*, 1526 (2009).

THERMAL INSULATION COMPOSITE BLOCKS BASED ON GEOPOLYMER

Kohout J.^{1,2}, Soukup A.^{1,2}, Kohoutová E.^{1,2}, Koutník P.¹, Hájková P.^{1,2}

¹ ORLEN UniCRE a.s., Ústí nad Labem, Czech Republic

² Technical University of Liberec, Faculty of Mechanical Engineering, Department of Material Science, Liberec, Czech Republic

Jan.Kohout@orlenunicre.cz

Abstract

Thermal insulation composite blocks consisted from two types of different geopolymer boards with different properties. One board was a foamed geopolymer with low bulk density and thermal conductivity and second board, also based on a geopolymer binder, was characterized by high bulk density and excellent mechanical properties. The composite block was prepared by pouring a geopolymer containing a foaming agent onto a prefabricated compact board prepared by pressing a mixture of a refractory filler with a geopolymer binder. The function of the pressed board is the mechanical protection of the foamed board. The basic mechanical and thermal insulation properties of both cast and pressed boards were determined. The thermal insulation properties of composite blocks were investigated using a high-temperature gas chamber. It was verified that the composite blocks had comparable thermal insulation properties as a commercial thermal insulation board (polycrystalline mullite/alumina wool).

Introduction

Geopolymer binders are based on the partial dissolution of aluminosilicates in an alkaline medium and the subsequent polycondensation reaction of the resulting precursors, which leads to hardening of the binder^{1,2}. Geopolymers are characterized by excellent mechanical properties, resistance to high temperatures, resistance to chemicals and great variability of properties and possibilities of applications in industrial practice^{3,4}. Geopolymers have attracted attention as a material whose production is associated with low CO₂ emissions and low energy consumption compared to materials based on Portland cement and ceramics^{5,6}.

The aim of this work was to develop thermal insulation composite blocks without fibers based on geopolymer with good mechanical and chemical resistance. The development of these composite blocks was started based on the requirements of the heating and waste industry as a more mechanically resistant alternative to traditional furnace linings.

Experimental

Composite blocks consisted from two types of different geopolymer boards (pressed and foamed board).

Materials

Raw materials used for the preparation of pressed board were all commercial products: metakaolinite-rich material Mefisto L₀₅ produced by the calcination of kaolinic claystone at about 750 °C in rotary kiln (České lupkové závody, a.s., Czech Republic), potassium hydroxide flakes (Lach-Ner, s.r.o., Czech Republic) and commercial potassium silicate (Vodní sklo, a.s., Czech Republic). Chamotte (České lupkové závody, a.s., Czech Republic), corundum (Korund Benátky, s.r.o., Czech Republic) or silicon carbide (Korund Benátky, s.r.o., Czech Republic) of grain size 0–2 mm were used as a different fillers for the preparation of the pressed board.

Starting materials used for the preparation of foamed board were commercial Mefisto L₀₅, potassium silicate Baucis L_K (České lupkové závody, a.s., Czech Republic), calcium hydroxide Čerták (Vápenka Čertovy schody, a.s., Czech Republic) and aluminium powder AIPRA (PK Chemice, Czech Republic). Mixture of chamotte with a grain size of 0–0.5 mm and Liapor with a grain size of 1–4 mm (Lias Vintířov, LSM k.s., Czech Republic) was used as a filler for the preparation of foamed board.

Commercial thermal insulation board (CB, polycrystalline mullite/alumina fibre wool) was used as a comparative material.

Sample preparation

Raw materials for the preparation of geopolymer binder of pressed board were mixed together. The geopolymer binder were chosen on the basis of the results of our previous works, where the geopolymer binder based on Mefisto L₀₅ provided binders with very low viscosity and excellent mechanical properties⁷. The

filler was added after homogenization of geopolymer binder and the weight ratio of the geopolymer binder to filler was 5.3 for corundum and silicon carbide and 3.6 for chamotte. The mixture of geopolymer were poured into a compression mould and loaded with a force of 100 kN for 5 minutes. Compression mould with the pressed board sample were cured at 60 °C for 4 hours in electric oven.

The production of the foamed board had a similar process as the preparation of the pressed board. Firstly the components for the preparation of the geopolymer binder were mixed and then the fillers were added. The weight ratio of the geopolymer binder to filler was 1.7. Mixture of foamed board was poured onto cured pressed board placed in the compression mould. The composite block was removed from the mould after the foamed board had solidified. The composite block was sealed into polyethylene bags and cured at 60 °C for 4 hours in an electric oven.

A simplified scheme for preparing a composite blocks is shown in the Figure 1. Prepared composite blocks are shown in Figure 2.



Figure 1. Scheme for preparation of a composite blocks

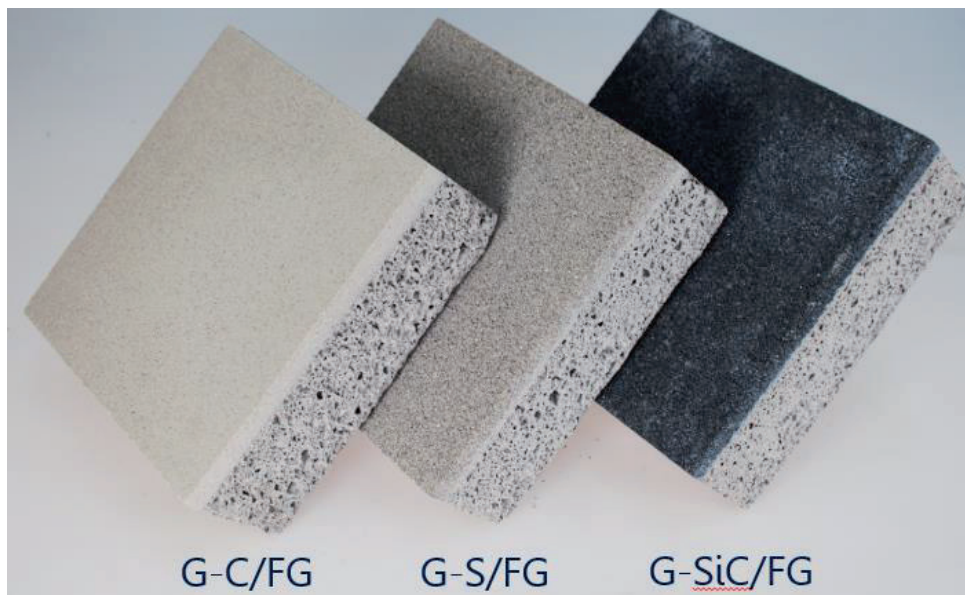


Figure 2. Photo of three prepared composite blocks

Results and discussion

The flexural strength was measured on the 40 x 40 x 160 mm samples for commercial and foamed board and on 10 x 10 x 120 mm samples for pressed boards. The results are shown in Figure 3. It was found that the pressed boards have a significantly higher flexural strengths than the foamed board. Visible differences in flexural strength of pressed boards are due to the use of different fillers. The bulk density of the foamed board had an effect on the low flexural strength. The flexural strengths of the foamed board are comparable to those of commercial board.

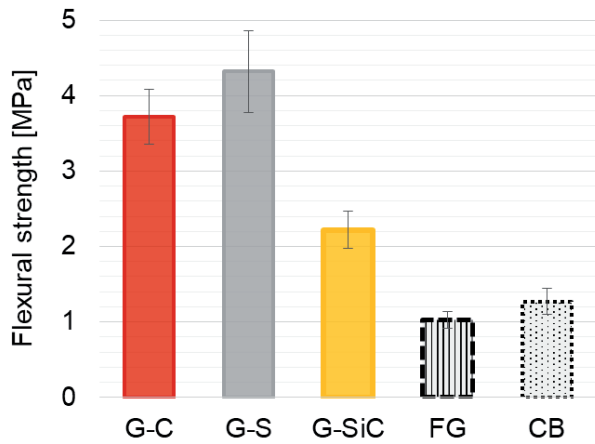


Figure 3. Flexural strength of prepared boards and commercial thermal insulation board (CB)

The thermal conductivity was measured on the 150 x150 x 35 mm samples for commercial and foamed board and on 200 x 200 x 100 mm samples for pressed boards. The thermal conductivity results are given in Figure 4. The measured data showed that pressed boards were more thermally conductive than the foamed board and were able accumulate more heat. Notable differences in the thermal conductivity of the pressed boards were caused by the use of filler and the weight ratio of binder to filler.

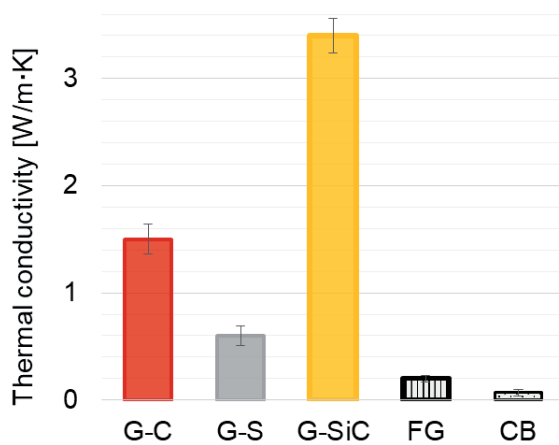


Figure 4. Thermal conductivity of prepared boards and commercial thermal insulation board

The ability to resist high temperatures (refractoriness) was examined on samples cut from prepared boards and CB (cube with a side length of 10 mm) by heat microscopy. The samples were heated up to 1600 °C at a rate of 10° C/min. The behaviour of prepared boards at 800 and 1600 °C is visible in Figure 5. It is evident that prepared samples from the pressed boards were thermally stable throughout the heating up to 1600 °C. Sample prepared from foamed board was also very durable, but less than samples from pressed boards (1400 °C).

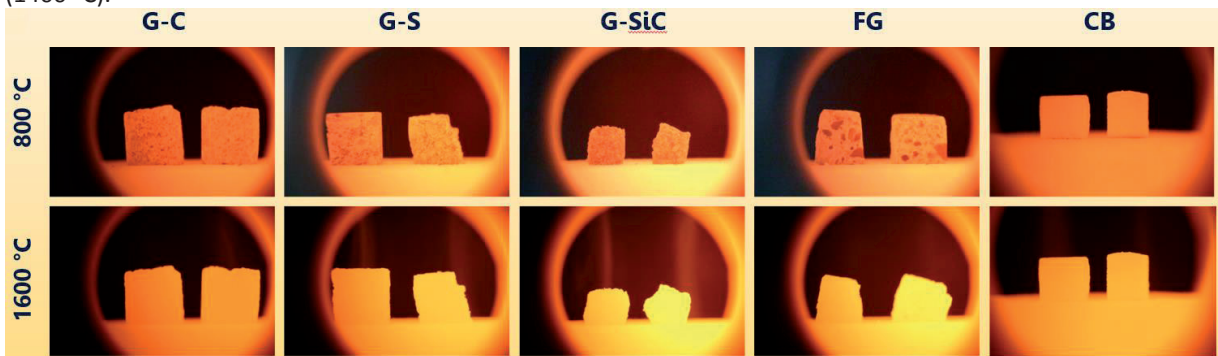


Figure 5. Heat microscopy of prepared boards and commercial thermal insulation board (CB)

Figure 6 shows the dilatometric curves of the prepared boards and CB within the range from 30 to 1200 °C with a heating rate of 5 °C/min. The dilatometric curves showed that all examined samples expanded in the temperature range between 30 to 1200 °C and that the determining factor was the used filler. The pressed board filled with corundum showed the highest expansion during heating compared to other pressed boards. It can be observed that the total shrinkage of geopolymer boards were in the range of 0–0.2% from their total length after the run of heating and cooling.

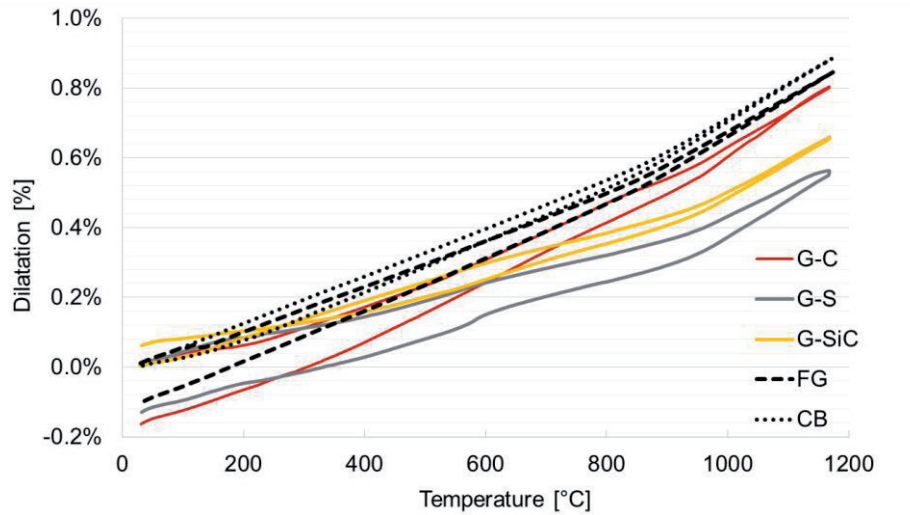


Figure 6. Dilatometry of prepared boards and commercial thermal insulation board (CB)

The thermal insulation properties of the composite blocks were investigated using a high-temperature gas chamber displayed on Figure 7. Temperature profiles in time measured during heating and cooling of the composite block and the commercial thermal insulation board (A – surface of the tested samples and B – in the middle of the tested samples) in the high- temperature gas chamber at 1200 °C for 30 minutes are shown in Figure 8. It can be seen that the thermal insulation properties measured on the surface and in the middle of the composite blocks were comparable to a commercial thermal insulation board with regard to its height. The commercial board was about 20 mm lower than the composite blocks. The maximum measured temperatures were therefore 200 °C higher for a commercial board at both measured locations. There were no visible differences between the individual composite blocks.

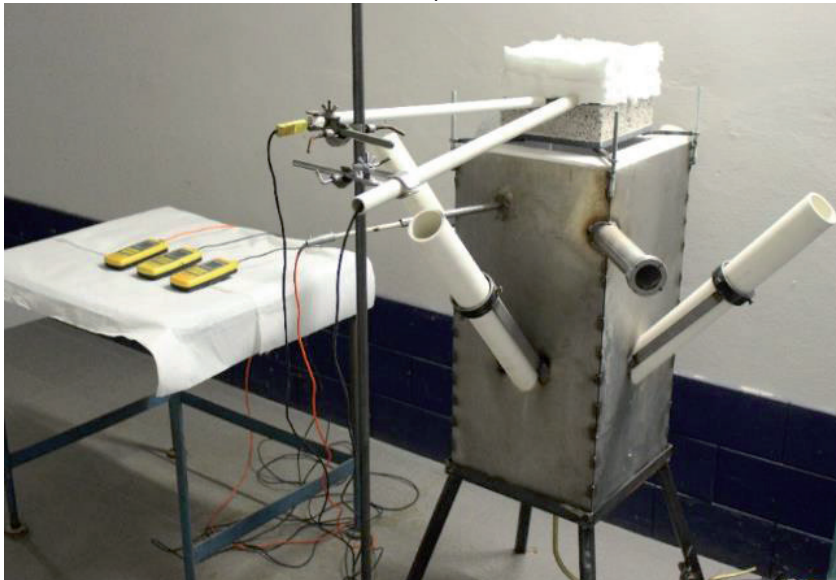


Figure 7. High-temperature gas chamber

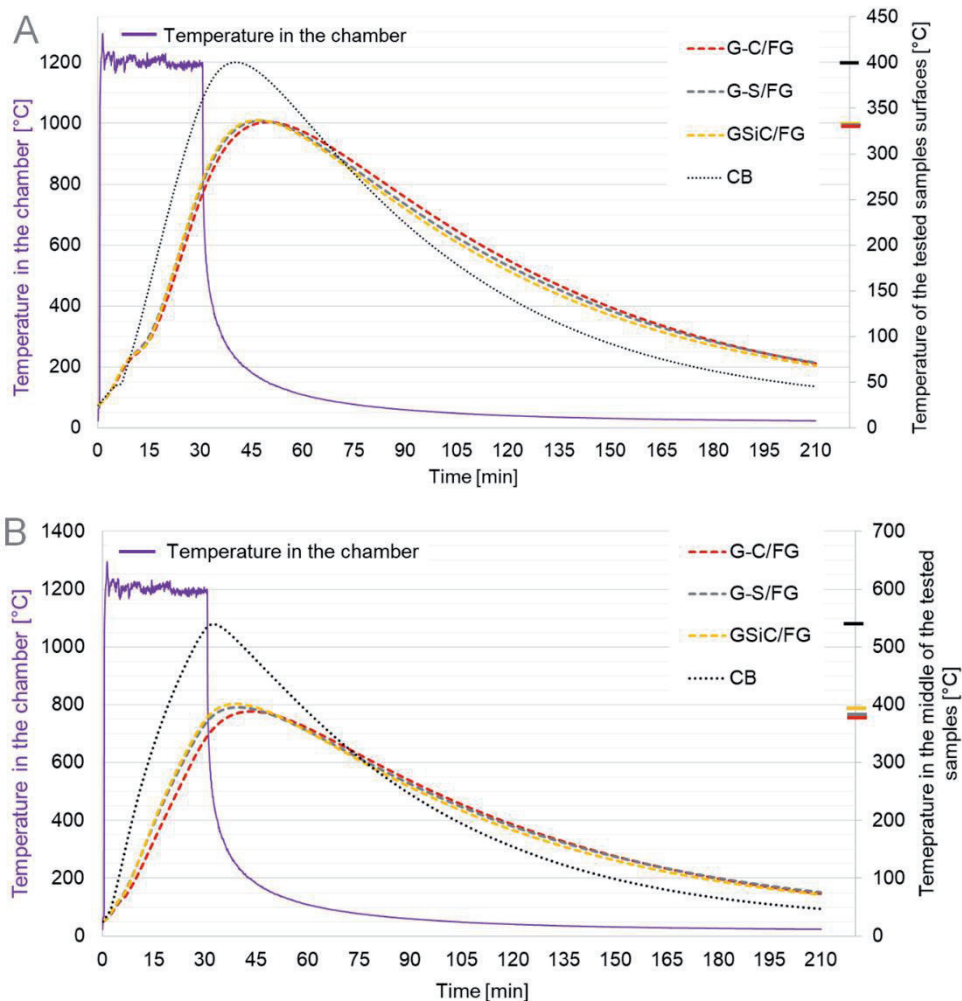


Figure 8. Temperature profiles in time measured during heating and cooling of the composite block and the commercial thermal insulation board (A – surface of the tested samples and B – in the middle of the tested samples) in the high- temperature gas chamber at 1200 °C for 30 minutes

Conclusion

Thermal insulation composite blocks based on geopolymer were prepared by pouring the foamed geopolymer onto geopolymer pressed board. Three types of pressed boards with different types of filler (chamotte, corundum, silicon carbide) were prepared. Good mechanical and thermal insulation properties of the prepared composite blocks were verified. The individual boards of the composite block were thermally stable up to 1400 °C and did not show any significant length changes during heating and cooling. The monitored values of thermal insulation of the composite block were comparable to measured values of the commercial thermal insulation board.

Acknowledgement

The publication is a result of the project which was carried out within the financial support of the Ministry of Industry and Trade of the Czech Republic with institutional support for long-term conceptual development of research organization. The result was achieved using the infrastructure included in the project Efficient Use of Energy Resources Using Catalytic Processes (LM2018119) which has been financially supported by MEYS within the targeted support of large infrastructures.

The results of the project entitled "Reduction of noise pollution from linear transport structures using active and passive elements", registration number CZ.01.1.02/0.0/0.0/20_321/0025218, were obtained through the financial support of the Ministry of Industry and Trade of the Czech Republic within the targeted program support "Application, Call VIII ", the project of the OP PIK.

References

1. Lahoti M., Wong K.K., Yang E-H., Tan K.H.: *Ceramics int.* **44**, 5726 (2018).
2. Zhang H.-y., Kodur V., Cao L., Qi S.-l.: *Procedia Eng.* **71**, 153 (2014).
3. Kohout J., Koutník P., Hájková P., Kohoutová E., Soukup A.: *Polymers* **13**, 3754 (2021).
4. Sabbatini A., Vidal L., Pettinari C., Sobrados I., Rossignol S.: *Materials and Design* **116**, 347 (2017).
5. Davidovits J.: Institut Géopolymère, Saint-Quentin, 285 (2008).
6. Duxson P., Fernández-Jiménez A., Provis J.L., Lukey G.C., Palomo A., van Deventer J.S.J.: *Journal of Mat. Sci.* **42**, 2917 (2007).
7. Koutník, P.; Soukup, A.; Bezucha, P.; Šafář, J.; Kohout, J.: *Construction and Building Materials* **230**, 116978 (2020).

PROPERTIES OF HYDRAULIC BINDER PREPARED FROM METAKAOLIN, ANHYDRITE AND LIME

Šulc R.¹, Škvára F.², Šídlová M.², Trefný J.¹, Králová K.², Pulcová K.², Formáček P.¹

¹Czech Technical University in Prague, Faculty of Civil Engineering, Thákurova 7, 166 29, Prague 6, Czech Republic

²University of Chemistry and Technology Prague, Department of Glass and Ceramics, Technická 5, 166 28, Prague 6, Czech Republic

rostislav.sulc@fsv.cvut.cz

Abstract

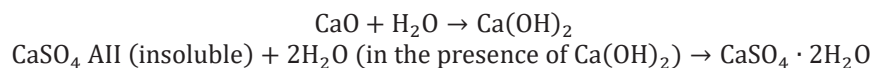
The paper deals with the property verification of the newly designed hydraulic binder based on metakaolin, anhydrite and lime. Two types of mixtures were prepared, and the influence of the preparation method was observed. The resulting mechanical properties of the hardened binder in the horizon of up to 90 days were monitored. The change in composition over time was further studied on all hardened binder using X-ray diffraction analysis. In addition, the porosity of the hardened binder was determined for 90-day samples and scanning electron microscope images were taken. It was found that after 90 days the hardened binders reached the strengths comparable to hardened Portland cement and were in the range of 40 – 61 MPa. No decrease in strength was noted over time. The main crystalline phase of the hardened binder was ettringite, which is formed at the beginning of the hydration process. With increasing time its amount remained constant or decreased slightly.

Introduction

Today, cement is still one of the most widely used materials in the world. However, its production is demanding, especially in terms of CO₂ emissions. The best way to improve the sustainability of cement and concrete is to mix cement clinker with pozzolan based supplementary cementitious materials (SCM). Nevertheless, the most common SCMs such as slag and fly ash are becoming more inaccessible today, and calcined clays are the most promising source of other SCMs that can significantly contribute to a further reduction in environmental impacts¹. Scrivener et al. deal with the preparation of such a mixed binder containing partially cement clinker and calcined clays called LC³ in works^{2,3}.

Another possibility is to replace cement clinker completely with another type of binder. According to new scientific research, such a clinker-free binder could be based on calcined clays⁴. Although calcined clays are not industrial waste, they are still more environmentally friendly than cement, as their production requires much lower temperatures and thus total energy⁵.

This new composite hydraulic binder⁴ contains a combination of 25 – 85 wt.% of aluminosilicate metakaolin-based component, 5 – 30 wt.% of anhydrous calcium component (CaO), and 8 – 45 wt.% of anhydrous calcium sulphate component (CaSO₄ anhydrite II). The reaction of the binder with water is based on the calcium sulphate activation of aluminosilicate. This is done using the anhydrous components of the binder CaO + CaSO₄ anhydrite II in their reaction with H₂O:



Aluminosilicate amorphous anhydrous substance under the reaction of Ca(OH)₂ and SO₄²⁻ ions gives the binder phases as C-A-S-H, C-S-H and ettringite. There is no CaO in this hardened binder, which could cause undesirable expansion phenomena⁴.

This work presents the preparation of a newly designed hydraulic binder based on metakaolin, anhydrite and lime. It also studies the influence of grinding time and the firing method of mixtures on the compressive strength of hardened binders and the phase composition changes.

Materials and methods

Four input raw materials were used for the preparation of the mixtures – flue gas desulfurization gypsum (FGD-CaSO₄·2H₂O) from the coal power plant Tušimice CZ (EGS), metakaolin Mefisto from ČLUZ a.s. CZ (Mk), quick lime (CaO) and limestone (CaCO₃) from Čertovy schody CZ. All input raw materials were characterized by X-ray fluorescence (Table I), X-ray diffraction (Table II), and granulometry (Table III).

X-ray fluorescence (XRF) determines the chemical composition of the sample and was performed on an X-ray spectrometer ARL 9400 XP (Thermo ARL, Switzerland). X-ray diffraction determines the phase composition of the sample. The measurement was performed on a θ - θ X'Pert3 Powder diffractometer (PANalytical, Netherlands). Samples for XRD were measured by semi-quantitative analysis, but also by quantitative Rietveld analysis. The semi-quantitative analysis does not consider the amorphous binder phase, while the quantitative Rietveld analysis also determines the amorphous binder phase using internal standard ZnO (10%). The results were evaluated using a HighScore Plus 4.0 software.

The particle size distribution (PSD) was measured on a laser particle size analyzer Bettersizer ST (Dandong Bettersize Instruments Ltd., China). The porosity of the samples was determined by measurements on AutoPore IV 9500 (Micromeritics, Georgia, USA) instrument. The basic part of the research was the measurement of compressive strength using compressive strength testing machine (VEB Thüringer Industriewerk Rauenstein, Germany). Scanning electron microscope images were taken on Hitachi S 4700 (Hitachi, Japan) for completion.

Table I. Chemical composition of input materials [%]

Material	CaO	SiO ₂	Al ₂ O ₃	Fe ₂ O ₃	K ₂ O	Na ₂ O	MgO	SO ₃	TiO ₂	P ₂ O ₅	CO ₂	Others
EGS	43.77	1.94	1.05	0.31	1.05	0.14	1.01	50.49	-	-	-	0.24
Mk	0.26	51.15	42.93	2.75	1.09	-	-	-	1.13	0.16	-	0.53
CaO	98.07	0.01	0.01	0.01	-	-	0.08	0.01	-	-	-	1.81
CaCO ₃	54.46	1.10	0.24	0.05	0.03	0.04	0.54	0.04	0.01	0.15	43.3	0.04

Table II. Phase composition of input materials [%]

Material	Quartz	Mullite	Hematite	Muscovite	Lime	Portlandite	Calcite	Gypsum	Amorph.
EGS	-	-	-	-	-	-	-	100	-
Mk	10	3	1	4	-	-	-	-	82
CaO	-	-	-	-	90	8	2	-	-
CaCO ₃	-	-	-	-	-	1	99	-	-

Table III. PSD quantiles of input materials [μ m]

Material	D10	D50	D90
EGS	19.05	46.12	83.42
Mk	1.32	5.42	21.30
CaO	1.31	12.46	78.45
CaCO ₃	2.67	146.90	355.80

Firstly, to find an optimal recipe for the preparation of the new binder, several types of mixtures with different ratios of input materials were mixed. Based on the mechanical-physical properties, two series labelled 18 and 23 were selected as optimal and their recipes are presented in Table IV.

For the preparation of series 18 and 23, EGS was fired at 850 °C for 1 hour to form anhydrous CaSO₄ anhydride All. This was followed by homogenization by grinding of metakaolin, lime, and CaSO₄ All in a Tencan QM-15 ball mill (TENCAN, China) at 200 rpm for 60 min (V) or 180 min (VII). Cubes with an edge size of 20 mm were prepared from the mixtures.

The 18P and 23P series were chosen as the second binder preparation variant (recipe Table IV), where all input materials were fired together - metakaolin, limestone, and CaSO₄·2H₂O at 850 °C for 1 hour. This was followed by homogenization in the ball mill at 200 rpm for 60 min (V) and 180 min (VII) and the preparation of cubes with an edge size of 20 mm.

The binders were prepared by mixing with water and placing them into a form. For all series, the water to binder ratio was adjusted so that comparable consistency may have been achieved. Therefore, the water to binder ratio

is varying in both series (Table IV). 5 days after mixing the cubes were removed from the forms and placed into a humidity cabinet with a temperature of 22 ± 1 °C. Binders were stored for 7, 14, 28 and 90 days in a stable environment.

Table IV. Recipes of mixtures 18, 18P, 23, 23P in [%], (w = water to binder ratio)

Mixture	Mk	CaO	Ca(CO ₃)	CaSO ₄ All	CaSO ₄ .2H ₂ O	w
18	58.8	17.7	-	23.5	-	0.60
18 - V	58.8	17.7	-	23.5	-	0.59
18 - VII	58.8	17.7	-	23.5	-	0.59
18P - V	45.8	-	24.5	-	29.7	0.56
23	60.0	20.0	-	20.0	-	0.64
23 - V	60.0	20.0	-	20.0	-	0.60
23 - VII	60.0	20.0	-	20.0	-	0.60
23P - V	46.9	-	27.9	-	25.3	0.67

Results and discussion

The compressive strength was tested on both types of series 18 and 23. The influence of sample preparation on the final mechanical properties was observed. The following graphs (Figure 1) compare the compressive strength of samples with different grinding times. It was found that the grinding of the input raw materials (18 - V, 18 - VII, 23 - V, 23 - VII) increases the strength of hardened binders compared to the unground samples (18 and 23). Both V and VII ground series had almost identical strengths after 90 days, series 18 (52 – 54 MPa) and series 23 (59 – 61 MPa). On the other hand, it is necessary to take into account the different values of the water to binder ratio of the prepared binders, which could affect the results.

Furthermore, the influence of the firing method of input raw materials on the final compressive strength was investigated (Figure 2). Hardened binders are prepared by the separate firing of input raw materials (18 - V and 23 - V) achieved higher compressive strengths compared to binders whose input materials were fired together (18P - V and 23P - V).

In addition, it is evident in all samples that the strengths of the hardened binders do not prove a significant decrease in strengths between 7 and 90 days.

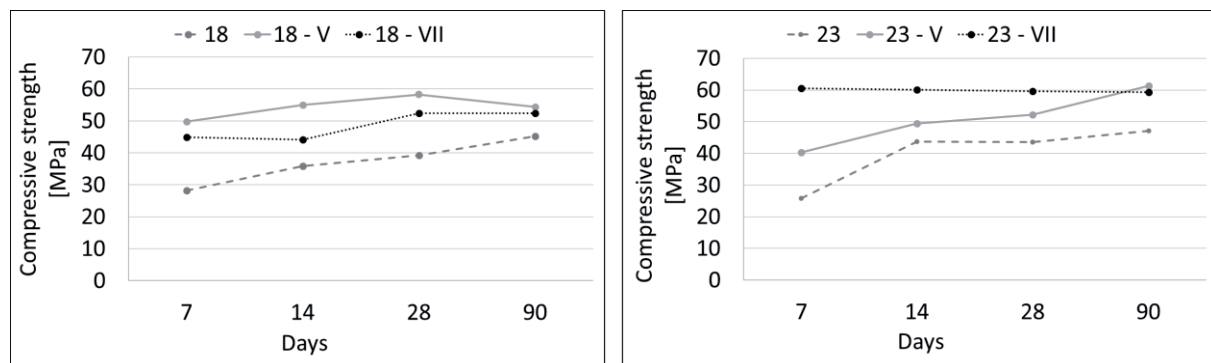


Figure 1. Influence of grinding time on the strength of hardened binders (18 left, 23 right)

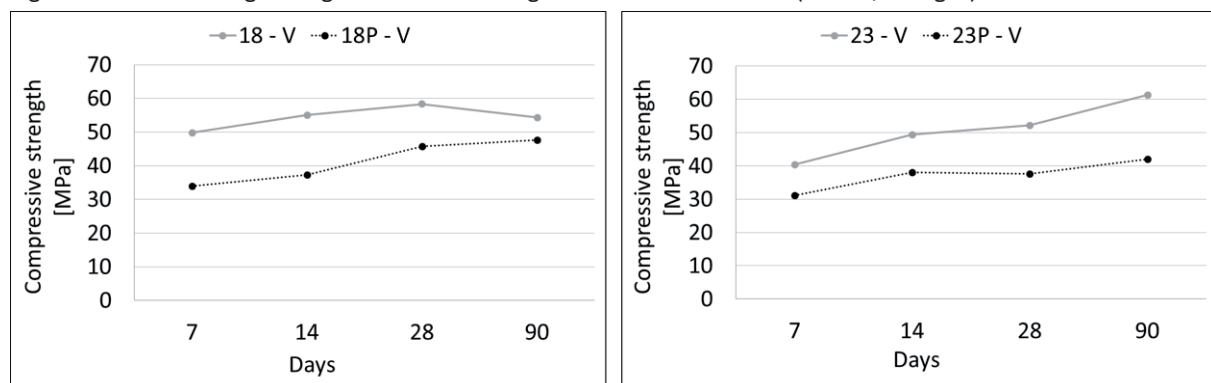


Figure 2. Influence of firing method on the compressive strength of hardened binders (18 left, 23 right)

The samples were analysed by XRD for the phase changes during the hydration (Table V). The phase composition of the hardened binders confirmed the presence of the main crystalline phase, ettringite⁴. In addition, it was found that the content of the amorphous binder phase is in the range of 42 – 61%. For samples 18P and 23P a higher content of anhydrite in comparison to 18 and 23 samples was found. The higher amount of anhydrite in the input raw materials resulted in the formation of higher content of ettringite in the hardened binder and concurrently to lower content of the amorphous binder phase. The lower content of the binder phase was probably the main influence on the lower strength of the hardened binder (Figure 1 and Figure 2). The strength of the hardened binder in the prepared hardened samples was influenced by the different compositions of the input material as well as by the different water to binder ratio and in addition by the different preparation methods of the input materials. Therefore, further research needs to focus on reducing the variables to could be determined definite conclusions. The presence of the ettringite crystalline phase was also confirmed by SEM analysis images (Figure 3).

Table V. Phase composition of the input mixtures and hardened binders after 14, 28 and 90 days [%] by XRD analysis

Sample	Amorph.	Ettringite	Anhydrite	Lime	Portlandite	Calcite	Quartz
18	50	-	28	14	2	-	6
18-V - 14d	48	48	-	-	-	1	3
18-V - 28d	47	49	-	-	-	1	3
18-V - 90d	51	43	-	-	-	2	4
18P	51	-	32	11	-	-	6
18P-V - 14d	40	56	-	-	-	1	3
18P-V - 28d	40	55	-	-	-	-	5
18P-V - 90d	42	52	1	-	-	1	4
23	53	-	24	15	2	-	6
23-V - 14d	58	36	-	-	-	1	5
23-V - 28d	61	33	-	-	-	2	4
23-V - 90d	58	36	-	-	-	2	4
23P	49	-	30	8	-	7	6
23P-V - 14d	47	45	-	-	-	5	3
23P-V - 28d	45	48	-	-	-	4	3
23P-V - 90d	42	48	-	-	-	6	4

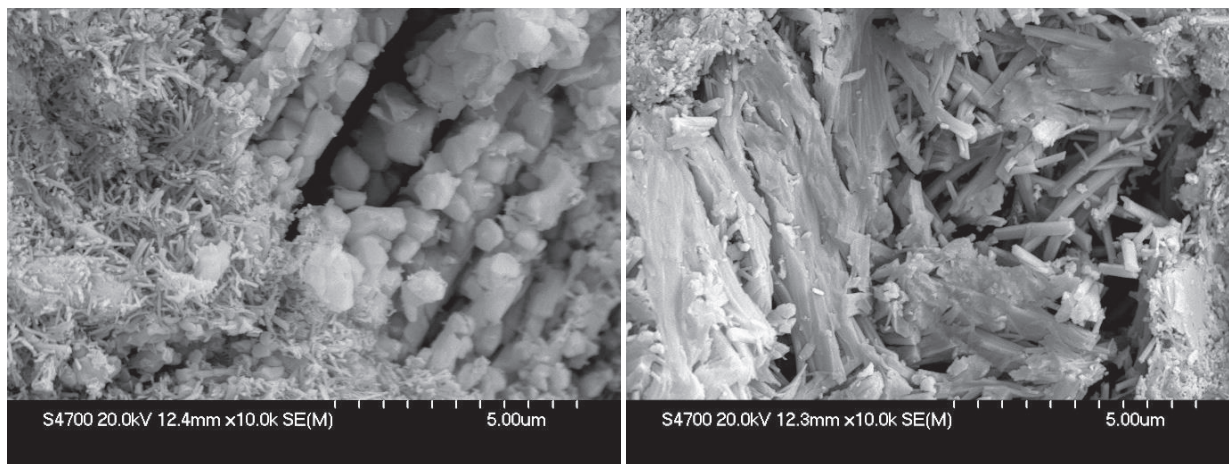


Figure 3. SEM images of hardened binders 18P - V (left) a 23 - V (right) after 90 days of hydration, magnified 10000 x

Porosimetry results for selected binders 23 - V and 23P - V after 90 days of hydration are shown in Figure 4. It has been proven that hardened binders with a higher water to binder ration (higher capilar porosimetry) and also higher ettringite content exhibit higher porosity. The same results were obtained for the 18 and 18P samples.

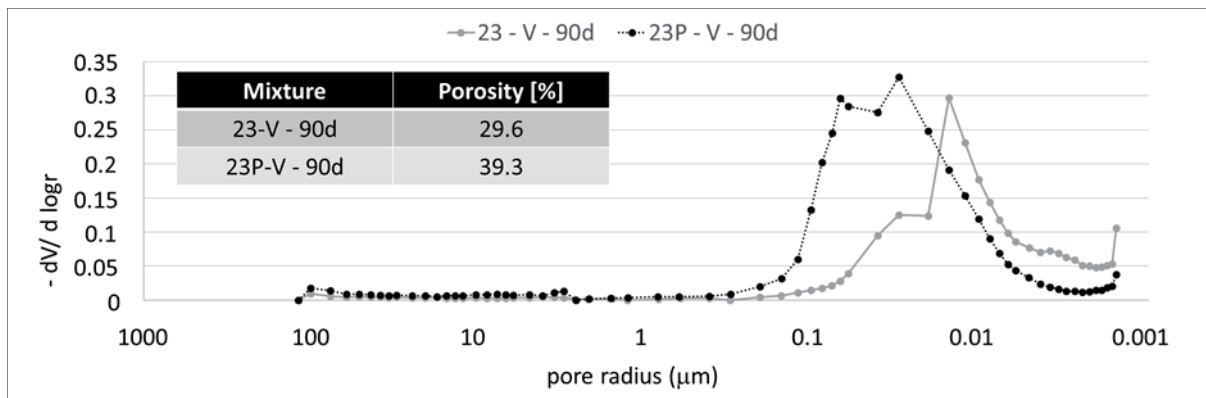


Figure. 4. Porosity of hardened binders 23 and 23P after 90 days of hydration

Conclusion

Based on the obtained results it was found that the grinding of the input raw materials increases the strength of hardened binders. It has also been found that the strengths of the hardened binders in the range from 7 to 90 days do not show a significant decrease in strengths. Hardened binders prepared by the separate firing of input raw materials (18 and 23) achieved higher compressive strengths compared to binders whose input materials were fired together (18P and 23P). Due to the different ratios of the input raw materials and the different water to binder ratio of the prepared mixtures, the influence of the methods of preparation of the mixtures on the resulting strengths of the hardened binders cannot be clearly proved. The phase composition of the hardened binders as well as the SEM images confirmed the presence of the main crystalline phase, i.e. ettringite. In addition, it was found that the content of the amorphous binder phase is in the range of 42 – 61%.

Acknowledgement

This work was supported from TAČR FW01010195 Advanced and innovative processing technologies for strategic utilization and storing of coal combustion products (CCPs); 2020 – 2023

References

1. Bishnoi S.: Calcined clays for sustainable concrete. Springer Verlag, Singapore 2020.
2. Scrivener K., Martirena F., Bishnoi S., Maity S.: Cem. Concr. Res., 114, 49 (2018).
3. Sharma M., Bishnoi S., Martirena F., Scrivener K.: Cem. Concr. Res., 149 (2021).
4. Škvára F., Šídlová M., Polonská A.: Composite hydraulic binder, producing and using it. CZ patent 308850 (2021).
5. Siddique R., Cachim P.: Waste and supplementary cementitious material in concrete. Woodhead Publishing 2018.

INFLUENCE OF THE ADDITION OF VARIOUS TYPES OF MINERAL ADMIXTURES ON THE ALKALI-SILICA REACTION IN CONCRETE

Šídllová M.¹, Mauermann L.¹, Šulc R.², Pulcová K.¹

¹University of Chemistry and Technology Prague, Department of Glass and Ceramics, Technická 5, 166 28, Prague 6, Czech Republic

²Czech Technical University in Prague, Faculty of Civil Engineering, Thákurova 7, 166 29, Prague 6, Czech Republic

Martina.Sidlova@vscht.cz

Abstract

The work deals with the alkali-silica reaction (ASR) in concretes and mortars, which is one of the possible causes of failures of concrete structures. The aim of the work was to study the effect of different supplementary cementitious materials (SCMs) on ASR. The results were evaluated using an accelerated expansion test according to ASTM 1260. Firstly, it was necessary to solve the issue of the low-reactive aggregate. These aggregates did not allow a clear evaluation of the effect of SCMs on ASR. This problem was solved by replacing a part of the aggregate with glass shards, which led to an increase in the reactivity. In addition, the effects of different amount and different glass fractions on ASR were studied. A subsequent experiment with SCMs showed a positive effect on ASR elimination for all tested SCMs. The greatest effect on ASR elimination was detected for fly ash together with metakaolin followed by the Sorfix binder. The least effective was a blast furnace slag.

Introduction

ASR represents one of the most common destructive mechanisms in concrete. ASR is based on the solubility of silicate-rich aggregates in highly concentrated alkali solutions in concrete ¹. The dissolution of silicates is initiated by nucleophilic attack by OH⁻ ions. This reaction produces hygroscopic silica gel, which subsequently causes stress in the concrete by swelling, which can result in cracking ². The formation of ASR depends mainly on three factors; sufficient environmental humidity, the existence of alkalis in the environment or in concrete and the presence of reactive SiO₂ in the aggregate ³. The most important factor in preventing the formation of ASR is to select a suitable aggregate with a minimum of reactive phases SiO₂ ⁴. It is also possible to eliminate the formation of ASR with various admixtures such as fly ash, metakaolin, silica fume, various lithium-based inhibitors or using suitable aggregate grain sizes ^{1, 5, 6}.

The aim of the work was to assess the suitability of mineral admixtures in concrete to suppress ASR. For this purpose, samples (prisms-shape) were prepared and subjected to a dilatometric test according to ASTM 1260 ⁷.

Upon completion of the dilatation tests, some of the prisms were observed with a scanning electron microscope (SEM). The result of the work was the evaluation of the expandability of prisms based on their influence on the formation of alkali-silica reaction.

Materials and methods

The input raw materials for preparing prisms were cement CEM 42,5 R (Českomoravský cement, plant Mokrý), natural aggregates fraction 0-4 mm (Dobříň), fly ash – ETU (power plant Tušimice), blast furnace slag – VS (Kotouč Štramberk), metakaolin – MET (České lupkové závody a.s.), calcium-sulphate binder Sorfix – SFX based on FBC ash ⁸, float glass shards – GLASS (TGK – Technika, sklo a umění s.r.o.), all materials from the Czech Republic. Table I depicts chemical composition of input raw materials obtained by X-ray fluorescence.

X-ray fluorescence analysis (XRF) was performed with an ARL 9400 XP (Thermo ARL, Switzerland) sequential wave-dispersive X-ray spectrometer. The spectrometer is equipped with an X-ray lamp with Rh, an anode type 4GN and a Be window terminal window 50 μm thick. All element spectral line intensities were measured in vacuum with WinXRF. The obtained intensities were processed by the Uniquant software without the need to measure standards. The analyzed powder samples were compressed into tablets with a thickness of 5 mm and a diameter of 40 mm. The measurement time of one sample was approximately 15 min.

Table I

Chemical composition of input raw materials (XRF)

Raw materials	Percentage by mass [%]									
	Na ₂ O	MgO	K ₂ O	CaO	SiO ₂	Al ₂ O ₃	Fe ₂ O ₃	TiO ₂	SO ₃	Rest
CEM	0.4	1.3	0.9	65.0	18.6	4.8	3.5	0.3	4.7	0.5
ETU	0.6	1.0	1.7	1.8	49.8	33.9	8.9	1.2	0.6	0.5
VS	0.5	9.1	0.5	41.7	36.5	9.6	0.2	0.5	0.0	1.4
MET	0.3	0.1	0.7	0.2	51.1	45.3	0.8	1.5	0.00	0.0
SFX	0.1	0.7	0.6	21.6	33.8	26.6	4.6	2.5	9.0	0.5
GLASS	15.6	4.0	0.4	9.5	69.1	1.1	0.1	0.0	0.2	0.0

The phase composition of the raw materials CEM, ETU, VS, MET and SFX is given in Table II. X-ray diffraction analysis (XRD) was performed at room temperature on a θ - θ powder diffractometer X'Pert3 Powder (PANalytical, Netherlands) using the wavelength of CuK α radiation ($\lambda = 1.5418 \text{ \AA}$, U = 40 kV, I = 30 mA). The data were scanned with an ultrafast linear detector PIXCEL in the angular range 15-78 ° with a measurement step of 0.013 ° and with a counting time of 180 s step⁻¹. A fixed aperture was used for the measurement. Qualitative and quantitative analysis was then performed by evaluation in HighScore Plus 4.0 (PANalytical, Netherlands). The amorphous content was determined by the indirect internal standard method. 7.5% ZnO was added to the samples.

Table II

Phase composition of the raw materials (XRD), AP = amorphous phase, percentage by mass [%]

Phase	AP	Hatruite	Larnite	Brownmillerite	Tricalcium aluminate	Gypsum	Rest
CEM	10	56	19	11	2	2	0
Phase	AP	Quartz	Mullite	Magnetite	Hematite	Hercynite	
VP	54	9	34	1	1	1	0
Phase	AP	Calcite	Akermanite	Kalcium magnezium silicate			
VS	91	3	3	3			0
Phase	AP	Quartz	Mullite	Anatase	Muscovite	Kaolinite	
MET	85	7	3	1	2	2	0
Phase	AP	Quartz	Anhydrite	Anatase	Lime	Portlandite	
SXF	58	8	15	2	6	6	5

Following Table III shows characterization of raw materials by quantiles D10, D50, D90. The measurement of particle sizes (PSD) of the samples for research purposes was performed by a laser analyzer (Dandong Bettersize Instruments Ltd., China) and took place in the laboratory of Korund Benátky s.r.o., Czech Republic.

Table III

PSD quantiles D10, D50 and D90 of input raw materials

Quantiles	D10	D50	D90
	[μm]	[μm]	[μm]
CEM	2.5	14.1	44.2
ETU	1.7	12.2	66.5
VS	2.1	14.0	43.5
MET	1.1	3.8	12.2
SFX	1.8	18.3	122.0

The following two tables relate to the composition of the individual mixtures. Table IV shows the composition of the prisms with different amounts of glass, Table V shows the composition of the prisms with different amounts of admixtures.

Table IV

Composition of the reference prism (AST s0) and prisms containing glass, GF = glass fraction, AF = aggregate fraction

Prism	Cement [g]	Aggregate [g]	Glass [g]	Glass [%]	Water [g]	Note
AST s0	500	1125	0	0	235	
AST s5	500	1069	56	5	235	GF corresponds to the aggregate granulometry
AST s10	500	1013	112	10	235	
AST s15	500	956	169	15	235	
AST s10 (2)	500	1013	112	10	235	GF 4-2 mm
AST s10 (63)	500	1013	112	10	235	GF 125-63 μm
AST k10 (2)	500	1125	0	0	235	10% AF 4-2 mm
AST s20 (2)	500	900	225	20	235	GF 4-2 mm

Table V

Composition of prisms with admixtures

Prism	Type of admixture	Admixture [g]	Cement [g]	Aggregate [g]	Glass [g]	Water [g]
ETU 30	Fly ash	150	350	1013	112	235
VS 30	Blast furnace slag	150	350	1013	112	235
MET 30	Metakaolin	150	350	1013	112	235
SFX 30	Sorfix	150	350	1013	112	235
ETU 10	Fly ash	50	450	1013	112	235
ETU 20	Fly ash	100	400	1013	112	235

Preparation of mortar prisms for expansion tests (ASTM 1260) and measurement of prisms:

- Weighing of raw materials according to recipes – Table IV and Table V, dry homogenization approximately 1 minute in mortar mixer, addition of water, mixing 3 minutes
- Pouring the mortars into forms of sizes 25 x 25 x 285 mm, storing in a moist cabinet (20 ± 2 °C)
- After 24 hours removing the forms with mortar prisms from the moist cabinet, demolding the prisms
- Placing the prisms into the containers with water, placing the containers with submerged prisms into the drying oven (80 ± 2 °C)
- After 24 hours – zero value reference measurement, placing the prisms into the containers with 1 M NaOH solution
- Storage of containers with submerged prisms in the 1M NaOH solution in the drying oven (80 ± 2 °C)
- The following values of length changes are ideally measured every 24 hours for 28 days
- Individual measurement of every prism lasted less than 15 seconds

The measurement result is the relative expansion of the prisms calculated by the relation:

$$L = \frac{L_x - L_0}{G_x \times 100},$$

where L_x is the length of the prism read from the display of the x-th measurement, L_0 is the value of the zero measurement and $G_x = 285$ mm, which represents the length of the prism determined for the ASTM 1260 standard⁷. Measurements were performed on dilatometric device mod. S382-01 (MATEST S.p.A., Italy).

Observation and imaging of prisms (after 28 days of testing) was performed with a Hitachi S 4700 (Hitachi, Japan) cold cathode scanning electron microscope. The microscope is equipped with two secondary electron detectors and one reflected electron detector. For the measurement a resolution of 1.5 nm was selected, with magnification of 20 x - 500000 x and with accelerating voltage from 0.5 to 30 kV.

Results and discussion

Figure 1 shows the results of dilatometric tests for mixtures prepared with different addition of glass instead of aggregate, with glass addition of 0% (AST s0), 5% (AST s5), 10% (AST s10) and AST 15% (AST s15). Figure 1 shows the linear expansion of the prisms as a function of time over a period of 28 days.

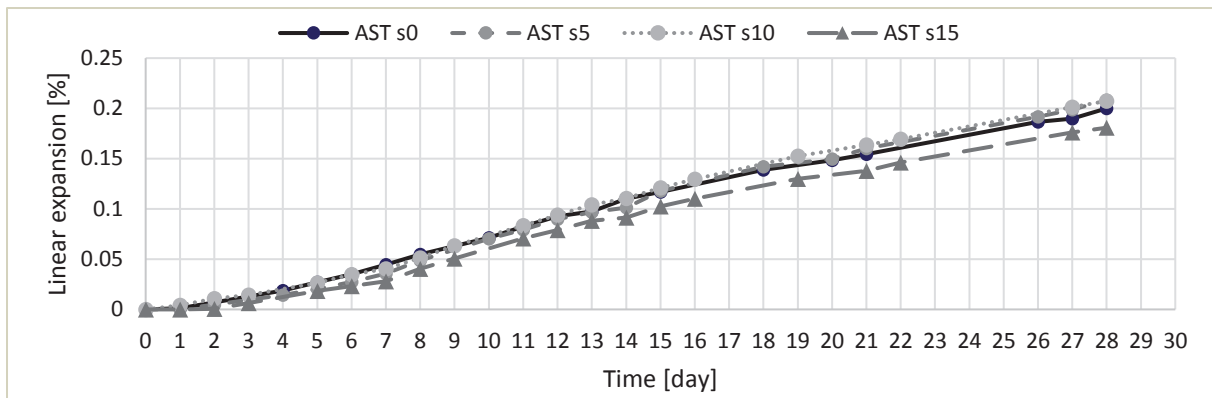


Figure 1. Expansion of the prisms for time, mixtures prepared with glass with the same granulometric curve as aggregate AST s0, AST s5, AST s10, AST s15 – composition see Table III

In case of prisms AST s0, AST s5, AST s10, AST s15 – Figure 1, length changes were not registered with increasing amount of glass in the prisms compared to the reference prism without added glass. Paradoxically, the prism with the highest amount of glass exhibited the lowest expansion. This may be due to the dominant amount of fine glass fraction, which is in accord with the works of D. Serpa et al., Shuhua et al. suppresses ASR^{9, 10}.

In Figure 2 results of mixtures AST s10 (2), AST s10 (63) and AST s10 are listed. It is possible to observe the dependence of expansion prisms on the different fraction of added glass. ASR was suppressed in the prism with the addition of fine glass (63 μm). The prism with the coarse glass fraction (2-4 mm) reached the highest expansion values. It corresponds to the results of Shuhua's et al. work, that fine glass suppresses ASR and coarse glass causes ASR¹⁰.

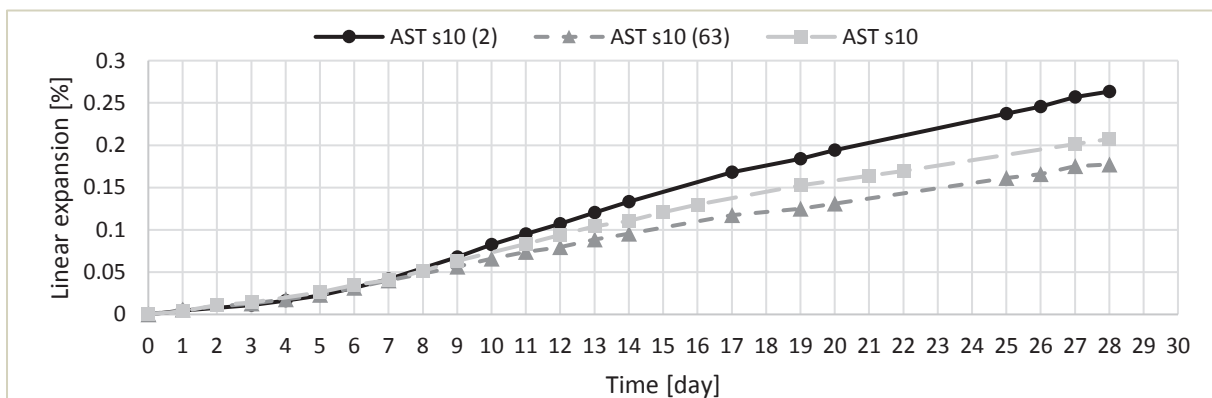


Figure 2. Expansion of the prisms for time, mixtures prepared with different glass fraction AST s10 (2), AST s10 (63), AST s10 – composition see Table III

Following Figure 3 shows the results of dilatometric tests for mixtures prepared with admixtures – 30 % fly ash (ETU 30), 30 % blast furnace slag (VS 30), 30 % metakaolin (MET 30), 30 % binder Sorfix (SFX 30) and referential prism AST s10 (2) without admixture. All admixtures used had a positive effect on reducing ASR expansion. It was found that the prisms with fly ash (ETU 30) had the greatest effect on the suppression of ASR in the prepared mortars (0.014 % after 28 days). After 14 days of measurement, visible expansion was measured only for prisms SFX 30 (0.031 %), VS 30 (0.063 %). Values of linear expansion of prims ETU 30 and MET 30 after 14 days were 0.000 % and 0.009 %. After 28 days, a slight increase in the value of linear expansion of the prism ETU 30 matched the value of the prism MET 30 (0.015 %). Regarding the effectiveness of individual admixtures in suppressing expansion ASR, the results obtained correspond to the results of the working group of Pertold et al., where blast furnace slag had the least effect on the formation of the expansion gel and metakaolin was the most effective⁴. An explanation of why ash and metakaolin are such effective admixtures against ASR is offered by XRF analysis. It was found that they contain a large amount of SiO₂ and, conversely, a small amount of alkali and calcium. It is the reason for higher efficiency against the formation of expansive ASR gel according to a study by Michael Thomas¹. In the case of metakaolin also plays an important role small size of particulars. According to Kizhakkumodoma Venkatanarayanan and Rangarajua, smaller particles have a positive effect on the elimination of ASR¹¹.

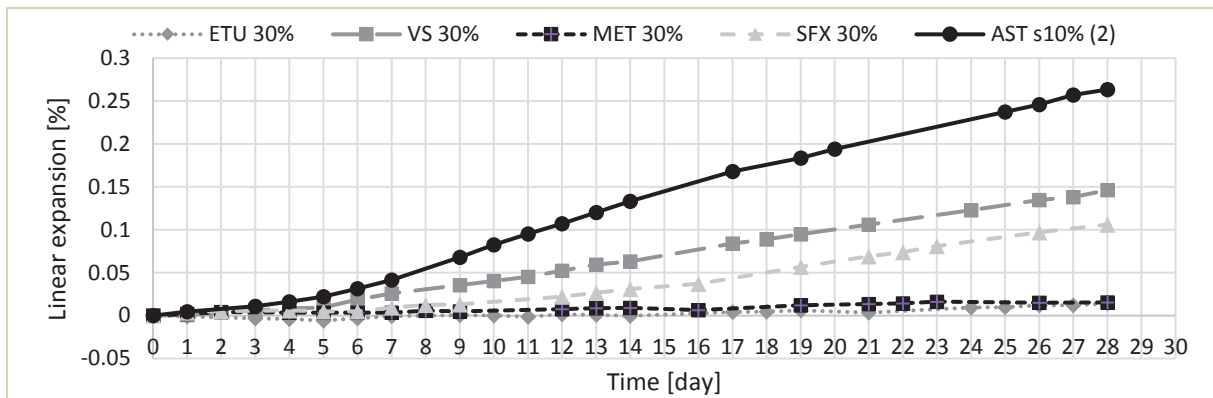


Figure 3. Expansion of the prisms for time, prisms prepared with different admixtures ETU 30, VS 30, MET 30, SFX 30, AST s10 (2) – composition see Table III, IV

In the last Figure 4 there are results of mixtures listed with the weight representation 10 %, 20 % and 30 % of fly ash (ETU 10, ETU 20 and ETU 30) and referential prism AST s10 without admixture. From these results, it is possible to conclude that with increasing ETU content (10 - 30%) the effectiveness of ASR suppression increases as well, which confirms the findings from the study of Pertold et al. ⁴.

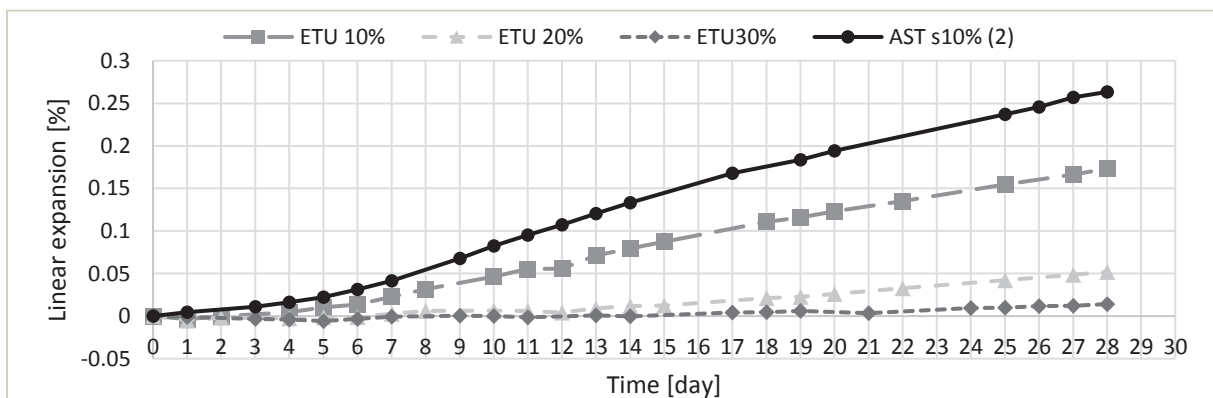


Figure 4. Expansion of the prisms for time, prisms prepared with different amount fly ash ETU 10, ETU 20, ETU 30, AST s10 (2) – composition see Table III, IV

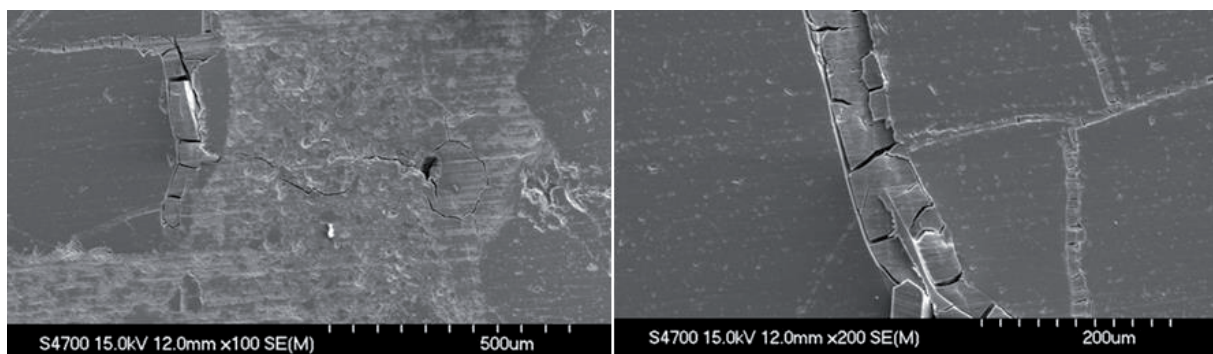


Figure 5. SEM images of the crack across the glass grain of the AST s10 (2), left 100x, right 200x

Figure 5 shows cracks across the glass grain, which were identified by SEM in the prism AST s10 (2) after 28 days of measurement. These cracks did not appear in natural aggregates. The presence of silica-calcium hydrate was found in the crack from EDX analysis, which, according to the literature, may be a consequence of ASR ¹². Compared to the glass composition from XRF and EDX analyses, the crack had a significantly higher content of calcium ions.

Conclusion

The Replacement of a part of the aggregate with glass (5%, 10% and 15%), in which glass fraction corresponded with the aggregate fraction (sieves analysis), did not result in the final expansion of the prisms in the dilatometric

test according to ASTM 1260. These prisms did not show higher values of expansion during the measurement compared to the prisms without added glass. The addition of the coarse glass fraction 2-4 mm increased the linear expansion of the prisms, which was caused by the expansion of ASR gel. The fine glass of the 63-125 µm fraction used as a replacement for part of the aggregate, on the other hand, reduced the expansion of the prisms. All used admixtures in the amount of 30% as a cement substitute - fly ash, blast furnace slag, Sorfix binder, metakaolin - had a positive effect on the elimination of ASR. The most effective admixtures in the measurement were fly ash and metakaolin. Their effectiveness is probably related to their composition and, in the case of metakaolin, also to its small particle size. With increasing fly ash content (10 - 30%) the effectiveness of ASR suppression increases as well.

Acknowledgement

This project was co-financed by the Technology Agency of the Czech Republic as a part of programme TREND FW01010195.

References

- (1) Thomas M.: Cement and Concrete Research, 41, 1224 (2011).
- (2) Rajabipour F., Giannini E., Dunant C., Ideker J. H., Thomas M.: Cement and Concrete Research, 76, 130 (2015).
- (3) Lukschová Š., Přikryl R., Pertold Z.: Construction and Building Materials, 23, 734 (2009).
- (4) Pertold Z. et al.: Materiály a technologie, 2., (2014).
- (5) Mo X.: Cement and Concrete Research, 35, 499 (2005).
- (6) Multon S., Cyr M., Sellier A., Diederich P., Petit L., Struct J. C., Ke G., Li W., Li R., Li Y., Wang G.: International Journal of Concrete Structures and Materials, 40, 508 (2010).
- (7) ASTM C1260-21, Standard Test Method for Potential Alkali Reactivity of Aggregates (Mortar-Bar Method); ASTM International, West Conshohocken, 2021.
- (8) Škvára F., Šulc R., Snop R., Peterová A., Šídlová M.: Cement and Concrete Composites, 93, 118 (2018).
- (9) Serpa D., Santos Silva A., De Brito J., Pontes J., Soares D.: Construction and Building Materials, 47, 489 (2013).
- (10) Liu S., Wang S., Tang W., Hu N., Wei J.: Materials, 8, 6849 (2015).
- (11) Kizhakkumodom Venkatanarayanan H., Rangaraju P. R.: Cement and Concrete Composites, 43, 54 (2013).
- (12) Winter N. B.: *Understanding Cement*; WHD Microanalysis Consultants Ltd., Woodbridge 2012.

ANALYSIS OF ECOLOGICAL ENERGETIC MATERIALS

Olšovský M.¹, Budzák Š.², Krištof M.¹, Kuna P.³

¹ZVS Impex, Štúrova 925/27, 018 41, Dubnica nad Váhom

²Faculty of Natural Science Matej Bel University, Tajovského 40, 974 01, Banská Bystrica

³STC, Hlinky 505/18, Brno

milan.olsovsky@msm.sk

Abstract

Detection of the composition of energy materials (explosives) is important not only in forensic and environmental applications, but also in evaluating the quality of production and analysis of raw materials. Knowing the exact composition of the produced ecological pyrotechnic compositions and explosives is extremely important for determining the correct function, as well as predicting the effect in the products.

Most of the analysis methods used so far are based on time-consuming titration, precipitation and redox methods and reagents. Even in these cases, some compounds are eliminated. Therefore, it is necessary to look for new modern methods of analysis of energetic materials.

Introduction

With the increase in the number of analytical areas used for explosives and the development of new types of explosives, the use of different methods and techniques for the analysis of explosives has been tried with varying degrees of success. Although the scope of this work does not allow to analyze all existing analytical methods, we have tried to summarize the most used methods.

It is well known that most explosives undergo „color reactions“, in particular chemical reactions with reagents. One or more drops of reagent solution are applied to a small amount of the analyzed sample, resulting in colored reaction products. Identification by the calorimetric method is based on the fact that the resulting color is characteristic of a particular compound or defined group of compounds. The main disadvantage of this method lies in its reliability. Although some reactions are quite specific, this is largely unsatisfactory. Nevertheless, these tests are still widely used in many explosives laboratories, mainly due to their simplicity and low cost. The set of said tests and thin layer chromatography are examples of preliminary color tests that are often used in laboratory screening of explosive residues. Longer analysis time, the need to prepare different amounts of chemical in the development chamber, and low portability are major weaknesses of these methods.

One of the most widely used and methods for explosives analysis is spectroscopy. The principle of spectroscopy is the interaction between matter and electromagnetic radiation. The ionized samples are then separated by an electric field according to ion mobility or mass to charge ratio before being detected by a spectrometer detector. An example of a spectroscopic method is Raman spectroscopy, atomic absorption spectroscopy, infrared spectroscopy, nuclear magnetic resonance spectroscopy, mass spectroscopy, ion mobility spectroscopy and others. Spectroscopy methods have high selectivity and sensitivity, but each instrument itself is very expensive^[1-3].

Other known methods include high performance liquid chromatography, ion chromatography, gas chromatography or X-ray fluorescence.

Experimental part

The aim of the work was to identify and test a modern analytical method for determining the composition of pyrotechnic compositions. All standards and pyrotechnic compositions were analyzed by X-ray fluorescence. The aim of the practical part was to determine whether the selected X-ray fluorescence is a suitable method in the production and quality control of pyrotechnic compositions. Our goal was to get closer and get an idea of the level at which the selected method works in quality control. All analyzes were performed on a hand-held analyzer, type VANTA. In the following section, we will further describe the methodology and procedures that were used in the analysis of the samples and the subsequent evaluation of the samples.

Materials and methodology

We analyzed a total of 21 pure chemicals and 5 samples of pyrotechnic compositions produced in ZVS IMPEX. We did not modify the samples in any way before analysis. This fact of not modifying the samples is a great advantage of the analysis.

The following table (Table 1) lists all the components of the tested pyrotechnic compositions and the associated alternative compounds with a similar elemental composition that we had at our disposal.

Table 1: List of chemical substances used in the analysis

Components of tested pyrotechnic compositions	Alternative compounds
BaCrO ₄	K ₂ CrO ₄ ; BaSO ₄
BaMoO ₄	(NH ₄) ₆ Mo ₇ O ₂₄ · 4H ₂ O; Na ₂ MoO ₄ · 2H ₂ O
Pb ₃ O ₄	PbI ₂ ; Pb
Bi ₂ O ₃	BiI ₃
S	S (powder)
KClO ₄	KCl; NaCl; KI
Zr	Zr(NO ₃) ₄ ·5H ₂ O
Nitrocellulose	NH ₄ Cl
Fluoro rubber	-
Ti	-
FeSiMn	Fe ₂ O ₃ ; SiO ₂ ; MnSO ₄ ; MnO ₂

Instrument technology

The practical part was performed using the VANTA device. The instrument is used for X-ray fluorescence analysis. We performed measurements on 26 samples, while we analyzed each sample in two different modes, so we performed a total of 42 analyzes. The first of the two modes is AlloyMode. This mode is used mainly for the analysis of metal elements, used in practice most often for metal alloys. AlloyMode mode libraries are calibrated directly from the manufacturer to 26 elements, which are as follows: Al, Mg, Si, P, S, Ti, V, Cr, Mn, Fe, Co, Ni, Cu, Zn, Zr, Nb, Mo, Hf, Ta, W, Re, Pb, Ag, Sn, Bi and Sb.

The second mode in which we analyzed the samples was the GeoMode mode, which was calibrated directly from the manufacturer to 35 elements, which are as follows: Mg, Al, Si, P, S, Cl, K, Ca, Ti, V, Cr, Mn, Fe, Co, Ni, Cu, Zn, As, Se, Rb, Sr, Y, Zr, Nb, Mo, Ag, Cd, Sn, Sb, W, Hg, Tl, Pb, Bi, Th, U. serves mainly for the analysis of soils, rocks and light matrices.

The technical settings of the device are:

- 4 watt X-ray lamp with voltage from 40 kV to 50 kV
- SDD detector (Silicon Operation Detector)
- Linux operating system
- 5-megapixel panoramic camera with auto focus

Sample analysis

Each sample was poured into a plastic container with a cellophane foil at the bottom before analysis. Subsequently, we attached the VANTA device to a stand and placed a platform on top of the device to hold the sample. We placed a sample container on the platform and placed a protective sheath on top, which served to prevent the escape of X-rays. The first analysis was always run in AlloyMode mode, which lasted 36 s. After analyzing the sample, we reattached the instrument to the stand and analyzed the sample in Geo mode in the same way. Geo mode analysis took 96 s. After each analysis of the sample, we cleaned the plastic container with distilled water and wiped it with a paper towel to prevent contamination of the sample. We then lost the results in the VantaDataMnager program, in which we observed not only the results of the analysis but also the graphs provided by the instrument. We also transcribed all the results into the MicrosoftExcel program, where we also performed calculations to verify the quantitative analysis. The calculations were mainly focused on finding the expected percentage of the element in the samples.

Table 2: Results of the practical part analysis

Sample	Qualitative analysis	Quantitative analysis
BaCrO ₄	yes	not
K ₂ CrO ₄	yes	not
BaSO ₄	yes	no (sulfur only)
(NH ₄) ₆ Mo ₇ O ₂₄	yes	not
Na ₂ MoO ₄ · 2H ₂ O	yes	not
Pb ₃ O ₄	yes	not
PbI ₂	yes	not
Pb	yes	yes (at the level of 99.886 %)
Bi ₂ O ₃	yes	not
BiI ₃	yes	not
S (powder)	yes	yes (at the level of 99.929 %)
NaCl	yes	not
KCl	yes	yes (deviation below 1 %)
KI	yes	not
Zr(NO ₃) ₄ · 5H ₂ O	yes	no (deviation below 3.5 %)
NH ₄ Cl	yes	not
SiO ₂	yes	yes (deviation below 1.2 %)
Fe ₂ O ₃	yes	not
Ti	yes	yes (at the level of 99.413 %)
MnO ₂	yes	not
MnSO ₄	yes	yes (deviation below 1.7 %)
Pyrotechnic composition 1	yes	not
Pyrotechnic composition 2	yes	not
Pyrotechnic composition 3	yes	not
Pyrotechnic composition 4	no (missing potassium)	not
Pyrotechnic composition 5	no (missing potassium)	not

Conclusion

In this work, based on the performed research, we chose the X-ray fluorescence method (with the VANTA device, which is a commonly available commercial device) as the most suitable method for the possible analysis of the prepared pyrotechnic compositions. We used the method to analyze various formulations of samples of pyrotechnic compositions (5 samples) intentionally selected with different elements, respectively, compounds. Although it has not been possible to reliably identify all the elements (compounds) due to the limitations of the instrument, the measured results are a very good basis for further research in the field of quantitative and qualitative analysis of pyrotechnic compositions.

The achieved results can be used directly in the production process, but especially in the input control of components in pyrotechnic compositions. In industrial practice, the VANTA device can be used to check whether it is a given raw material to be used in the production process. By a simple method, where the worker has a matrix of the results of the analysis of the required raw material, he can check whether it is the right raw material to be used in the production process. As part of the input control, the device can also be used to control the quality of the supplied raw materials, whether there is only the necessary substance in the supplied raw materials or whether it is contaminated directly from the supplier.

The device is very useful in the output control. As we found out from the practical part that the exact representation of individual components cannot be achieved with the VANTA device, it is possible to perform quality control using a graphical display, but also software evaluation of the results as far as possible.

Regarding the quality control of the measurement of individual final products using the VANTA device, we found that the determination of individual components is not the most accurate, as the device is more accurate within pure substances.

The results presented by us show that the VANTA device and the X-ray fluorescence method are suitable for application in the process of production of pyrotechnic compositions, as well as in input and output quality control. Measurement portability and analysis speed with VANTA equipment can have practical applications in many areas of industrial production.

Acknowledgement

This work was supported by European Regional Development Fund – INTERREG V-A SK-CZ No. NFP304010X023 “Ecologically acceptable energy materials meeting the requirements of REACH”.



INTERREG V-A
SLOVENSKÁ REPUBLIKA
ČESKÁ REPUBLIKA



EURÓPSKA ÚNIA
EURÓPSKY FOND
REGIONÁLNEHO ROZVOJA

SPOLOČNE BEZ HRANÍC

References

1. Huri M. A. M., Ahmad U. K., Ibrahim R., Omar M.: *Malaysian Journal of Analytical Sciences*, 21, 2 (2017).
2. Yinon J.: *Explosives - Handbook of Analytical Separations*. Elsevier, Amsterdam 2000.
3. Marshall M., Oxley J.: *The Detection Problem - Aspects of Explosives Detection*. Elsevier, Amsterdam 2009.

DETERMINATION OF THE OPTIMAL COMPOSITION OF THE NEW HYDRAULIC BINDER PREPARED FROM METAKAOLIN, ANHYDRITE AND LIME

Pulcová K.¹, Šídlová M.¹, Šulc R.², Škvára F.¹, Kohoutková M.¹, Sedlářová I.¹

¹University of Chemistry and Technology Prague, Technická 5, 166 28, Prague 6, Czech Republic

²Czech Technical University in Prague, Faculty of Civil Engineering, Thákurova 7, 166 29, Prague 6, Czech Republic

Klara.Pulcova@vscht.cz

Abstract

This work investigates the preparation of a new hydraulic binder based on metakaolin, anhydrite and free lime, which may in the future become an alternative to Portland cement. A series of 26 mixtures with varying amounts of calcined metakaolin clay (50–80 wt.%), anhydrite (10–30 wt.%) and lime (5–35 wt.%) were prepared. The mixtures had the same water to binder ratio of 0.35 and contained a superplasticizer. The compressive strength of the mixtures was assessed after 7 and 28 days. Furthermore, on selected 28-day samples of hardened binders the phase composition and porosity were determined and also scanning electron microscope images were taken. Compressive strengths exceeding 60 MPa after 7 and 28 days of wet storage were measured for the selected optimal compositions. These results are comparable to the characteristics of Portland cement. In addition, these optimal mixtures did not display any potentially dangerous expansive behaviour. Expansion behaviour was observed only for samples with high lime content, especially in the mixture containing 35 wt.% of lime. Furthermore, it was found that ettringite is the main crystalline phase in hardened binder mixtures.

Introduction

Today, the price of cement is rising worldwide due to the environmental requirements and the reduction of CO₂ emissions produced in cement industry. For these reasons, there is a tendency to partially replace cement by admixtures such as fly ash, blast furnace slag, silica fume, etc.^{1, 2}. Another possibility is to replace cement as a binder in general with non-clinker binder which does not produce as high CO₂ emissions. Currently, many works^{3, 4, 5, 6} deal with the production of low-emission binders or cement additives based on calcined clays. Adherence to the required properties such as strength, volume stability, corrosion resistance, etc. proves to be essential³.

One of the right options may be the preparation of FCB ash-based binders, which are formed as a secondary coal combustion product (CCP) in the dry flue gas desulphurisation process when burning coal in the presence of limestone. Upon reaction with water, this FBC ash hardens due to the reaction of metakaolin with CaSO₄ anhydrite II and CaO^{7, 8}. Clays and other aluminosilicates in their original crystalline form cannot be practically activated by the addition of lime activators; it is only after calcination at a temperature of 500-900 °C that they acquire reactive pozzolanic properties. Calcination dehydrates the kaolinite and forms amorphous metakaolin⁹. The advantage of calcination temperatures is that they are still significantly lower compared to cement clinker production temperatures above 1450 °C. A detailed examination of the hydration currents of the FBC ash binder revealed that the system of calcined metakaolin, calcium oxide and anhydrous CaSO₄ in the form of anhydrite II acts as a clinker-free hydraulic binder in which CaO and CaSO₄ anhydrite II act as an effective activator in metakaolin hydration. The subsequent hardened binder phase contains amorphous C-A-S-H and C-S-H phases and crystalline phases, especially ettringite, CaCO₃, Ca(OH)₂ and CaSO₄.2H₂O^{7, 8}.

Another hydraulic binder called LC³ cement, which contains calcined clay, limestone and partly Portland cement, works by a similar mechanism¹⁰. Further use of calcined clays as an additive to Portland cement is reported in Bishnoi³. This work builds on previous research on hydration systems associated with FCB ash^{7, 8}. Based on these previous works, a binder¹¹ was designed from pure components containing a similar composition of metakaolin from Czech calcined kaolinitic clay, anhydrite II from flue gas desulphurisation processes and pure lime.

Materials and methods

Raw materials characterization

The input raw materials used in this work were: calcined aluminosilicate metakaolin clay called Mefisto (labelled L05) (České lupkové závody, CZ), CaSO₄ - anhydrite (labelled AII) (Anhydritec GmbH, DE) and lime CaO (Vápenka Čertovy schody, CZ). The basic characteristics of these materials, including X-ray diffraction (XRD), X-ray fluorescence (XRF) and particle size distribution (PSD), are given in the following Tables I-III.

Table I

Frequency quantiles D10, D50, D90 of PSD [μm]

Material	D10	D50	D90
L05	1.24	5.58	19.51
All	1.60	18.43	68.93
CaO	1.31	12.46	78.45

Table II

Oxide composition of raw materials, XRF analysis [wt.%], (LOI = loss on ignition)

Material	SiO ₂	Al ₂ O ₃	CaO	K ₂ O	SO ₃	Fe ₂ O ₃	TiO ₂	MgO	Others	LOI
L05	48.0	45.4	0.2	0.8	0.0	1.4	1.6	0.2	0.2	2.2
All	0.4	0.1	44.4	0.0	54.6	0.1	0.0	0.1	0.0	0.3
CaO	0.1	0.1	98.6	0.0	0.1	0.1	0.0	0.8	0.1	0.1

Table III

Quantitative phase composition of raw materials, XRD analysis [wt.%], Rietveld method (error R_w <5%)

Material	Amorph. phase	Anhydrite	Lime	Quartz	Mullite	Muscovite	Calcite	Portlandite	Anatase
L05	90	0	0	5	2	2	0	0	1
All	0	100	0	0	0	0	0	0	0
CaO	0	0	97	0	0	0	2	1	0

Preparation of pastes

26 mixtures were prepared according to ternary diagram in Figure 1. These mixtures, labelled as K1–K26, contained varying amount of L05 (50–80 wt.%), All (10–30 wt.%) and CaO (5–35 wt.%). The preparation of the pastes was as follows. After weighing, the dry ingredients were homogenized in a mortar mixer (ELE International, United Kingdom) for 1 minute, followed by the addition of water and a polycarboxylate-based superplasticizer. The water to binder ratio was $w=0.35$ for all mixtures. The mixing time varied according to the composition, maintaining the same consistency of the mixtures, and ranged from 1 to 6 minutes in the presence of water. Cubic specimens with an edge of 20 mm were prepared from the mixtures and, after demolding, were placed in a curing cabinet (95% relative humidity, temperature 20–23 °C) to be cured.

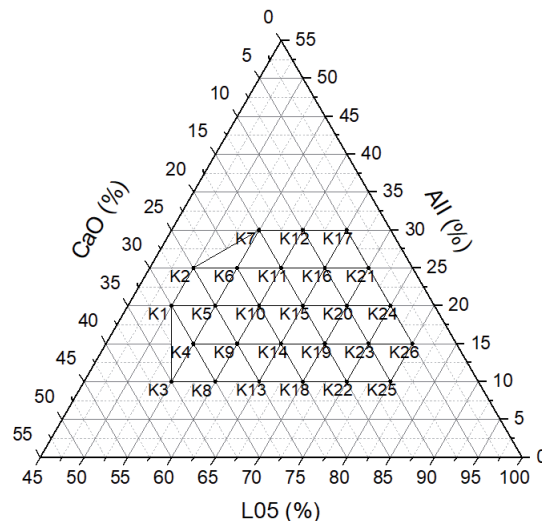


Figure 1. Mixtures composition ternary diagram

Methods and instrumentation

The X-ray diffraction analysis (XRD) was performed on a θ - θ X'Pert3 Powder diffractometer (PANalytical, Netherlands) in a Bragg-Brentan parafocusing geometry using CuK α radiation wavelength ($\lambda = 1.5418 \text{ \AA}$, $U = 40 \text{ kV}$, $I = 30 \text{ mA}$). Samples were scanned with an ultrafast linear detector PIXCEL in the angular range 15–78 ° (2θ) with a measurement step of 0.013 ° (2θ), counting time of 180 s step⁻¹. Qualitative and quantitative analysis was evaluated using HighScore Plus 4.0 software, Rietveld method. The amorphous content was determined

indirectly using internal standard 10 wt.% ZnO. The morphology of selected hydration products was also monitored by SEM and EDX analysis on a Hitachi S 4700 (Hitachi, Japan) scanning electron microscope.

To measure the X-ray fluorescence analysis (XRF), sequential wave-dispersive X-ray spectrometer ARL 9400 XP (Thermo ARL, Switzerland) with an X-ray lamp with Rh anode type 4GN was used. The intensities of the spectral lines were measured in vacuum using the WinXRF software. The intensities were processed using the Uniquant 4 software. The analyzed powder samples were compressed into 5 mm thick tablets. The measurement time was about 15 min.

The particle size distribution (PSD) was determined by a laser particle size analyzer Bettersizer ST (Dandong Bettersize Instruments Ltd., China). The laboratory measurement was performed in Korund Benátky, s.r.o. Czech Republic.

In addition, AutoPore IV 9500 (Micromeritics, Georgia USA) was used to measure mercury intrusion porosimetry (MIP) of open pores. The evaluation of the porosity took place in the range of tissue 101.325 kPa - 400 MPa with a corresponding range of pore radius size of about $6 \times 10^{-6} - 1.5 \times 10^{-9}$ m.

To measure compressive strength, concrete compressive strength testing machine (VEB Thüringer Industriewerk Rauenstein, Germany) was used.

Results and discussion

Compressive strength

Compressive strengths shown in the following ternary diagrams in the Figure 2 ranged between 24–62 MPa after 7 days and 28–67 MPa after 28 days. Samples K16 (62 MPa), K15 (61 MPa) and K19 together with K20 (60 MPa) had the highest compressive strength. The lowest strengths were recorded for samples K17 (24 MPa), K21, K24 (27 MPa), K3 (28 MPa) and finally K26 (32 MPa). This marked decrease in strength is related to the CaO content of the mixture, where 5 wt.% of CaO was used. The K3 mixture, on the other hand, was prepared from 35% CaO and this value proved to be unsatisfactory both in terms of strength and in terms of preparation. The K3 mixture reacted very strongly exothermically and solidified rapidly.

In the strength diagram after 28 days, it is possible to observe a slight increase in strength compared to the strength after 7 days. The lowest strength values were again recorded for samples K17 (28 MPa), K24 (29 MPa), K26 (31 MPa) and finally K3 together with K21 (32 MPa). The highest strengths were identified for the K9 and K16 mixture (67 MPa). This was followed by K15 and K23 (65 MPa) and K10 with K11 (64 MPa). From these results, it may be concluded that the ideal composition of the proposed binder is around 60–65% calcined clay, 15–25% anhydrite and 10–25% CaO.

Similarly to the LC³ binder from Scrivener et al.¹⁰, the presented binder achieves excellent strengths, with the difference that it does not contain cement clinker at all, making it a more environmentally friendly variant.

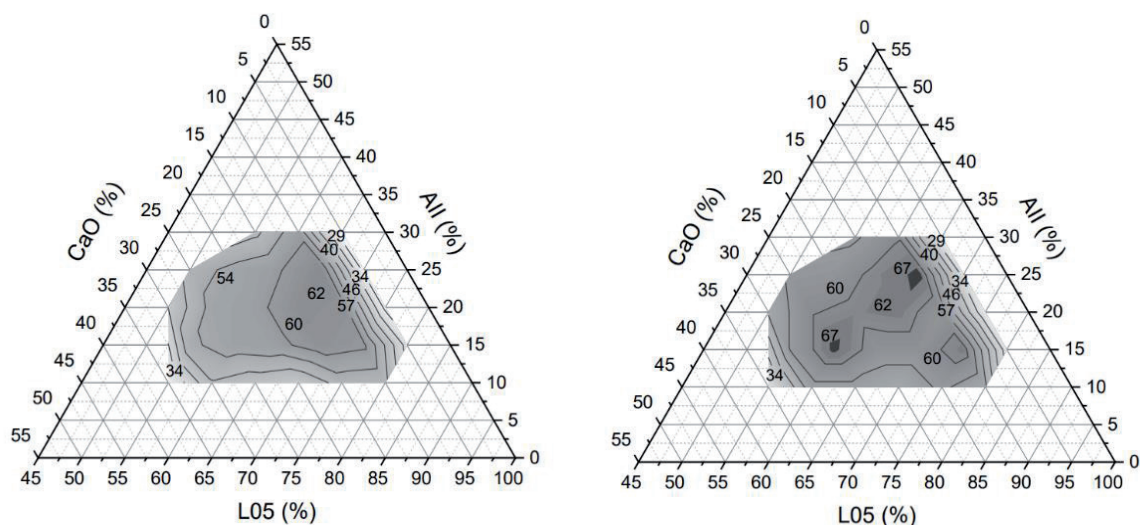


Figure 2. Compressive strength [MPa] after 7 days (left) and after 28 days (right)

Although the research was not focused on measuring the expansion of the samples, it should be added that eye-visible expansion in comparison with the others was noted for K3 sample, as seen in Figure 3. The reason is probably the highest CaO content (35 wt.%) of this mixture. Observations of expansion and corrosion behaviour are needed and will be part of further research.



Figure 3. Visible expansion of sample K3 after 7 days

Porosity

In the next step, the open-pore porosity of all 28-day samples was measured using MIP. Porosity, shown in Figure 4, ranged between 19–33%. The measurement can be compared with the results of Caré¹², who measured MIP cement slurries with the same water to binder ratio ($w = 0.35$) and obtained a porosity of 13.8%.

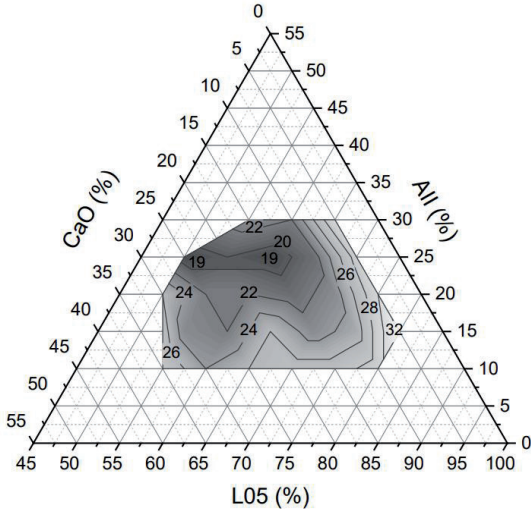


Figure 4. Porosity after 28 days, MIP [%]

It also could be seen that there is a slight correlation with 28-day compressive strength showed in Figure 5. With higher porosity, a decrease in compressive strength was observed with a coefficient of determination $R^2=0.6997$.

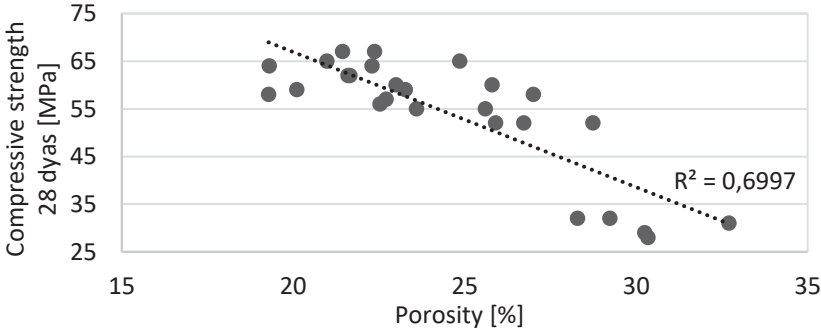


Figure 5. Correlation between compressive strength and porosity after 28 days

XRD analysis

By XRD analysis after 28 days of hydration, the mixtures were found to contain the following phases: amorphous phase, ettringite, portlandite, anhydrite, calcite, quartz and trace amount of muscovite. The amount of the individual phases varied depending on the proportion of the input raw material during mixing.

Portlandite began to appear in mixtures that were prepared from more than 10 wt.% CaO. Subsequently, with increasing CaO content the amount of portlandite in the hydrated mixtures increased linearly. The largest amount of portlandite contained the K3 mixture (18%). Similarly, for increasing amounts of All in preparation, the hydrated samples contained higher amounts of anhydrite. Most of the anhydrite contained K17 (22%), which was prepared from 30 wt.% All. The sum of quartz and calcite content was up to 5% for all samples.

The amorphous content ranged from 39-74 wt.% and a slight dependence of the amorphous phase increase was observed with the increasing amount of L05 clay, which itself contains 90 wt.% amorphous phase. The amount of ettringite ranged from 17-40 wt.%. Interestingly, although no direct correlation was observed between the amount of ettringite and 28-day compressive strengths, the highest strength (67 MPa) was measured for K16 with the highest amount of ettringite (40%). The selected optimal K16 mixture had the composition shown in the following Table IV.

Table IV

Quantitative phase composition K16 after 28 days, XRD analysis [wt.%], Rietveld method (error $R_w < 5\%$)

Sample	Amorph. phase	Ettringite	Anhydrite	Quartz	Calcite	Portlandite
K16	50	40	8	1	1	0

SEM

SEM image of the selected optimal sample K16 after 28 days confirmed the existence of needle-like crystals of ettringite.

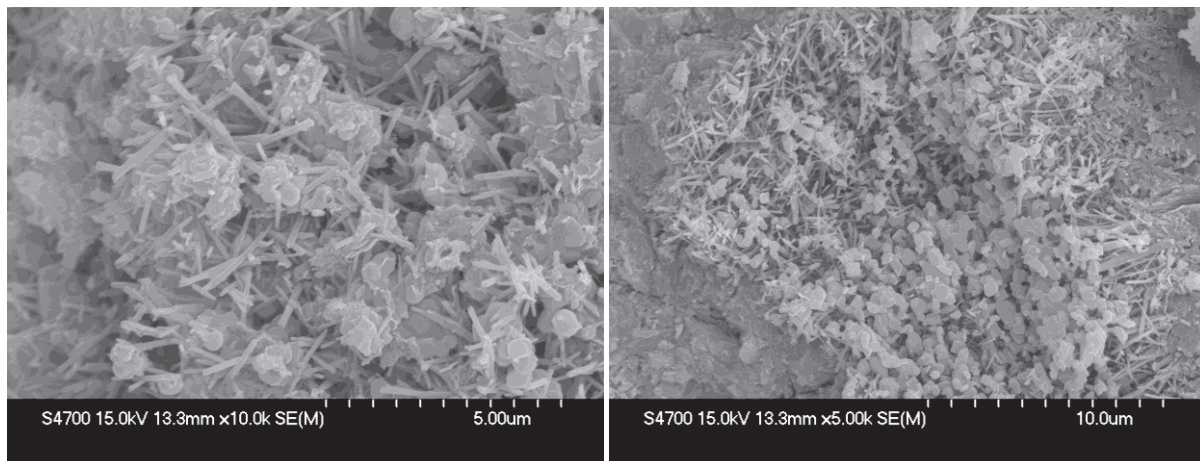


Figure 6. Fracture surface of hardened paste K16 after 28 days - SEM 10000x (left) 5000x (right)

Conclusion

Compressive strengths exceeding 60 MPa after 7 and 28 days in wet storage were measured for the selected optimal compositions of a new hydraulic binder based on calcined metakaolin clay, anhydrite and free lime. In addition, optimal mixtures did not display any potentially dangerous expansive behaviour after 28 days. Visible expansion behaviour was observed only for samples with high lime content, especially in the mixture K3 containing 35 wt.% of lime. Furthermore, it was found that ettringite is the main crystalline phase in all hardened binder mixtures. With proper optimal composition, this new hydraulic binder has the potential to partly substitute cement in the future although further research is needed.

Acknowledgement

This work was supported from TAČR FW01010195 Advanced and innovative processing technologies for strategic utilization and storing of coal combustion products (CCPs); 2020 – 2023

This work was supported from the grant of Specific university research – grant No A1: FCHT_2022_002

References

1. Siddique R., Cachim P.: *Waste and supplementary cementitious material in concrete*. Woodhead Publishing 2018.
2. Lothenbach B., Scrivener K., Hooton R.D.: *Cem. Concr. Res.*, 41, 1244 (2011).
3. Bishnoi S.: *Calcined clays for sustainable concrete*. Springer Verlag, Singapore 2020.
4. Ayati B., Newport D., Wong H., Cheeseman Ch.: *Cleaner Materials*, 5 (2022).
5. Krishnan S., Bishnoi S.: *Cem. Concr. Res.*, 138 (2020).
6. Sharma M., Bishnoi S., Martirena F., Scrivener K.: *Cem. Concr. Res.*, 149 (2021).
7. Škvára F., Šulc R., Snop R., Cílová Z., Peterová A., Kopecký L., Formáček P.: *Ceram. – Silikaty*, 60, 344 (2016).
8. Škvára F., Šulc R., Snop R., Peterová A., Šídlová M.: *Cem. Concr. Compos.*, 93, 118 (2018).
9. Hollander S., Adriaens R., Skibsted J., Cizer Ö., Elsen J.: *Applied Clay Science*, 132–133, 552 (2016).
10. Scrivener K., Martirena F., Bishnoi S., Maity S.: *Cem. Concr. Res.*, 114, 49 (2018).
11. Škvára F., Šídlová M., Polonská A.: Composite hydraulic binder, producing and using it. CZ patent 308850 (2021).
12. Caré S.: *Construction and Building Materials*, 22 (7), 1560 (2008).

POROSITY OF DIFFERENT ROCKS IN RELATION TO CAPTURING/MOVING OF GASES AND LIQUIDS

Řimnáčová D.¹, Vöröš D.¹, Natherová V.^{1,2}, Příkryl R.², Lokajíček T.³

¹*Institute of Rock Structure and Mechanics, Academy of Sciences of the Czech Republic, V Holešovičkách 41, 182 09, Prague 8, Czech Republic*

²*Institute of Geochemistry, Mineralogy and Mineral Resources, Faculty of Science, Charles University in Prague, Albertov 6, 128 43, Prague 2, Czech Republic*

³*Institute of Geology, Academy of Sciences of the Czech Republic, Puškinovo náměstí 447/9, 160 00, Praha 6 - Bubeneč, Czech Republic*

rimnacova@irms.cas.cz

Abstract

Variability in the porosity of natural rocks and waste have been investigated in relation to the influence on the permeability of gases and water. The samples were of sedimentary or igneous rocks, carbon-rich rocks, and solid porous waste material after thermal conversion. Using mercury intrusion porosimetry, porosity values and pore size distribution varied with the origin of materials. These results have been compared and a connection between the origin and porosity of material was observed. Total porosity values of selected samples ranged from ca. 0.2% for granite to 55% for waste porous material. Lower porosity values demonstrate the connectivity between mesopores or micropores and are related to the capturing of greenhouse gases, while higher porosity is caused predominantly by the presence of macropores and coarse pores, which serve as pathways for permeability of gases and liquids.

Introduction

Nowadays, we are able to study in detail not only the structure but also the textural parameters of various solid porous materials, and this helps us understand the ongoing physical processes in the material mass. Many processes depend on the porosity and active surface area of porous solid materials, which influence the physical and mechanical properties of materials. There is a network of different types of pores. The surface area, volume and size distribution of pores in solid materials are variable, and the number and type depend on their origin, geophysical processes during their genesis, the age of the rock and its chemical composition. These factors, altogether, influence the permeability of rocks and the trapping of compounds such as gases and liquids in their porous system. All these factors are closely interrelated.

Each rock constituent and geophysical process can affect the formation of the pore network, which is closely related to the formation/adsorption/motion of thermogenic gases (CO₂ and CH₄). Gases migrating from the site of injectage through fractures and coarse pores have been trapped in pores of a suitable size by physical adsorption. Adsorption of gases is closely related to micropores and smaller mesopores, while permeability depends on the presence of macropores and coarse pores that serve as transport pathways for liquids and macromolecular compounds; these can be called seepage pores.

The amount of captured gases depends on the presence of micropores, small-dimensional mesopores and on the types and shapes of pores. Better knowledge of the maximum amount of gas that can be captured in material pores is important for characterization of the surface properties of solid porous materials and for a better understanding of possible migration into the pores of a porous network of materials.

Some studies have focused on evaluating the CH₄ reservoir in rich organic deposits¹⁻⁶, and in coal deposits in USCB⁷. The adsorption capacity of CO₂, an equally important gas in relation to the search for geological sites suitable for its sequestration, has been studied less frequently until now (e.g. ^{8, 9}).

The broad goal now is to obtain information on the connection between texture, permeability and adsorption capacity, not only of coal-bearing rocks but also of source rocks and waste porous materials.

The gas-tightness and the possibility of adsorption of gaseous substances in different types of porous environments are currently two important parameters for the use of rocks or waste porous materials for storing of CO₂ gas below the surface of the Earth. Well-researched structures with a sufficient volume of pore space to allow adsorption of molecules are necessary for CO₂ storage at depths greater than 800 m. Sufficient rock permeability to allow the movement of CO₂ and an impermeable overlying sealing layer, usually clay rocks or non-altered igneous rocks, ensure retention of stored CO₂ in the repository.

Samples and experiment

Studied materials

Natural rocks with the potential ability to capture gases were studied, as well as waste material slag. Their textural parameters were compared. If the measurement of CO₂ adsorption was significant, its determination was carried out. The basic description of materials demonstrates the main differences between them.

- Black coal with a dry matter carbon content of 83%.
- Coal-bearing rock is a basic rock with interlayers of high carbon content, up to 40 wt%. The drill core sample on the basis of bulk characterization and XRF analysis exhibits a low (3 wt%) content of carbon in the dry matter compared to a high content of SiO₂ - 53.9 wt%, and Al₂O₃ 11.2 wt%.
- Sandstone is a consolidated sediment from turron and cenoman which contains at least 25 wt% grains of the silicate fraction (0.6 – 2 mm). Samples contain gypsum and feldspar as well. Two samples from different depths, the bedrock layer and the continuous layer, were studied.
- Granite is a relatively homogenous non-altered igneous rock, and fine-grained granite has a content of quartz (24%), orthoclase (24%), plagioclase (43%) and biotite (5%) and other oxides and minerals¹⁰.
- Cordierite is a natural mineral with a content of Fe, Mg, and Al oxides, and is a typical cyclosilicate, resistant to temperature changes.
- Shale is a sedimentary rock from the Barrandien basin with low organic carbon content < 2.5 wt% and high content of clay minerals (> 64 wt%) and plagioclase (18 wt%)⁹.
- Slag is the waste residue from combustion of lignite at a thermal power plant. It is a non-homogenous and changeable material, depending on the burning sources of fuel, seasons etc. There is a low content of organic carbon, up to 5 wt%, relatively high level of CaO (>20 wt%), 30 - 35 wt% of SiO₂, and Al₂O₃ > 20 wt% and other oxides.

Measurement

The first type of determination of textural parameters was based on the adsorption of gases. The gas molecules were adsorbed onto the solid material surface by physisorption. Under real conditions, adsorption takes place in more than 1 layer, with a relatively infinite ability to form these layers. In addition, the individual layers of the adsorbate do not interact with each other. This fact enabled us to evaluate textural quantities.

Micropore (< 2 nm) parameters were obtained by low-pressure CO₂ adsorption into pores of ground materials at 25 °C and pressure up 0.1 MPa, using the IGA-100 precise gravimetric sorption analyser, Hiden Isochema^{11,12}. This kind of measurement was provided only for selected materials, rocks and sediments with an organic carbon content and for slag. The CO₂ adsorption capacities and isotherms were also obtained.

The important textural parameter for solid materials was the specific surface area (S_{BET}) calculated using the Brunauer-Emmett-Teller equation. S_{BET} was determined for all materials studied and is the main low-scale mesopore parameter measured by low-pressure physisorption of N₂ at -196 °C and up to 100 kPa, using the SURFER volumetric sorption device, Thermo Fisher Scientific¹³.

The second principle for obtaining textural parameters, mercury intrusion porosimetry, was used to determine the porosity and pore size distribution. Mesopore (2 – 60 nm), macropore (60 – 200 nm) and coarse pore (> 200 nm) parameters were measured by the mercury intrusion porosimeter, composed of two devices, Pascal EVO 140 and 440, Thermo Fisher Scientific¹⁴; the low-pressure unit was for pressures of mercury up 200 kPa and the high-pressure unit was for pressures up 400 MPa.

The method is based on increasing the pressure of the non-wetting intrusion fluid, mercury in this case, and gradually filling the pores from largest to smallest. This method therefore allows the determination of a wide range of pore distributions. The pore size distribution (Figure 1 A, B) is calculated from the displaced volume at a given pressure according to Washburn's equation:

$$d = \frac{-4\gamma\cos\theta}{p}$$

where d is the pore diameter, p is the applied pressure, γ the surface tension of mercury, and θ is the contact angle¹⁴.

Results and discussion

Characterization of materials

Textural parameters and the CO₂ adsorption capacity point to differences between materials (see Table I, Figures 1, 2). The main difference was in the pore size distribution (Figure 1 A, B) and ratio of size classes obtained by mercury porosimetry. In Figure 1A the difference between coal and coal-bearing rocks is clearly seen and between sandstones. Coal and sandstone 2 contained higher ratios of mesopores than the coal-bearing rock and sandstone 1, which had very low ratios of mesopores as opposed to coarse pores.

In the detailed view in Table I and Figure 1B it is clear that the slag had the highest content of mesopores and macropores, and the highest porosity, which is typical for that kind of material. On the other hand, the low porosity showed carbon-rich samples and compacted rocks such as sandstone 2 and granite, which had a very low content of all pores. The samples with organic carbon had the higher micropore content, which contributed minimally to porosity. The ratio of mesopores, macropores and coarse pores in each sample are shown in Figure 2. Macropores and coarse pores dominated in most samples with the exception of granite and sandstone 2, where the mesopores prevailed.

When slag is cooling, it typically releases gas bubbles, which result in high porosity. Granite had the lowest porosity, confirming the fact that lower porosity is typical for igneous rocks. Most pores in igneous or metamorphic rocks are the products of subsequent weathering processes.

Table I

Basic textural parameters of samples

Sample	S_{micro} [m ² /g]	V_{micro} [cm ³ /g]	S_{BET} [m ² /g]	$S_{\text{me+ma}}$ [m ² /g]	$V_{\text{me+ma}}$ [cm ³ /g]	P [%]	n [mmol/g]
Slag	7.43	0.0026	7.96	43.67	615.02	55.6	0.027
Coal	17.46	0.0607	12.03	4.49	35.47	4.6	0.239
Coal-bearing rock	7.57	0.0026	4.26	0.59	17.11	4.3	0.028
Sandstone 1	*	*	0	18.19	103.48	21.0	*
Sandstone 2	*	*	9.57	2.80	23.05	5.7	*
Granite	< 0.0005	0	0	0.19	0.27	0.2	-
Cordierite	< 0.0005	0	1	10	107	21.8	-
Shale	38.26	0.0137	12.92	6.18	53.11	12.2	0.244

$S_{\text{micro}} / V_{\text{micro}}$ – surface / volume of micropores, S_{BET} - specific surface area, $S_{\text{me+ma}} / V_{\text{me+ma}}$ – surface / volume of mesopores and macropores by Hg porosimetry, P - porosity, n – CO₂ adsorption, * – not measured.

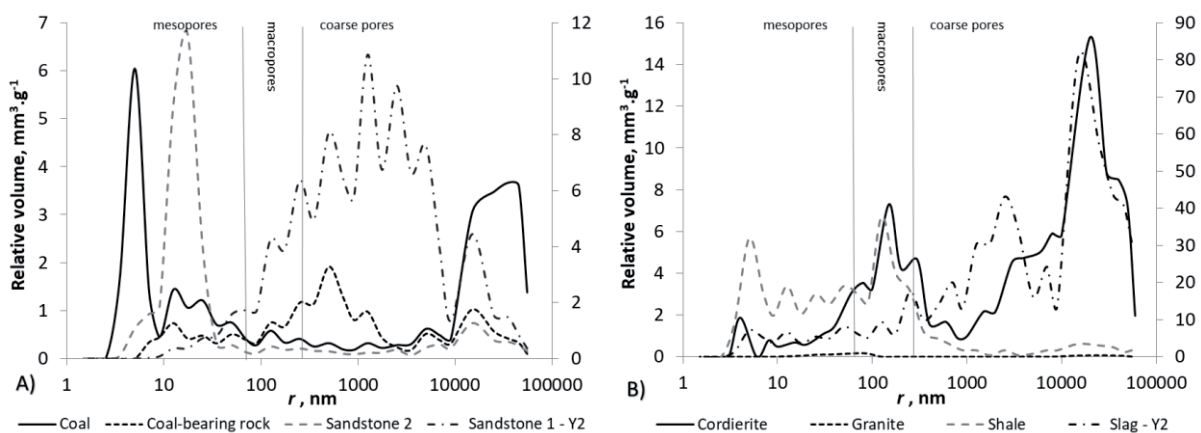


Figure 1. Pore size distribution of studied samples obtained by Hg porosimetry, A) Coal rocks and sandstones, sandstone 1 on the Y2 axis, B) Other rocks and slag, which is on the Y2 axis

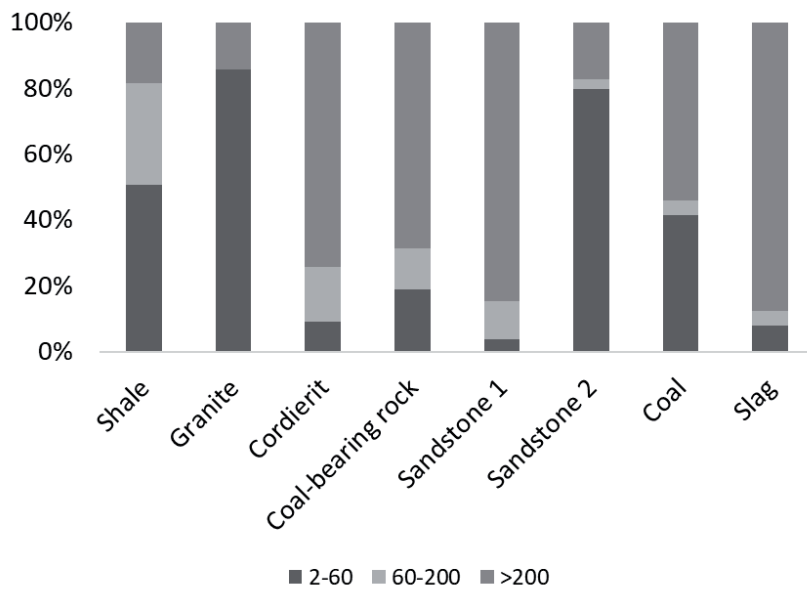


Figure 2. Ratio of pores in different size classes obtained by Hg porosimetry

The maximum CO₂ adsorption capacity for samples was assumed to be achieved at pressures between 4-6 MPa, with the exception of shale. In this work, the maximum adsorption capacity was achieved at 10 MPa, which is evident from the rising trend of isotherms (Figure 3) and the Langmuir model for CO₂ adsorption, according to adsorption in a monolayer on a homogeneous surface. The increase in adsorption capacity with increasing pressure, and the values of maximal adsorption capacities are shown in Table I. The adsorption capacity of coal and shale were about 10 times higher than in slag and coal-bearing rock and there was a clear dependence on micropore content and CO₂ adsorption capacity.

On the basis of pore content, coal, sandstone 2 and shale may capture gases due to their textural properties, whereas coal-bearing rock, sandstone 1, Cordierite or slag are permeable and can serve as transport corridors for gas and water molecules, thus being used for drainage. Shale is a sedimentary rock, more or less transformed by environmental conditions. It can be assumed to have adsorption capacities for CO₂ capture and can act as isolating underlay materials for ground water reservoirs. The properties of granite allow it to be used as an insulating material in gas reservoirs or as a barrier to water penetration. Both materials, as well as slag, will be the subject of further studies.

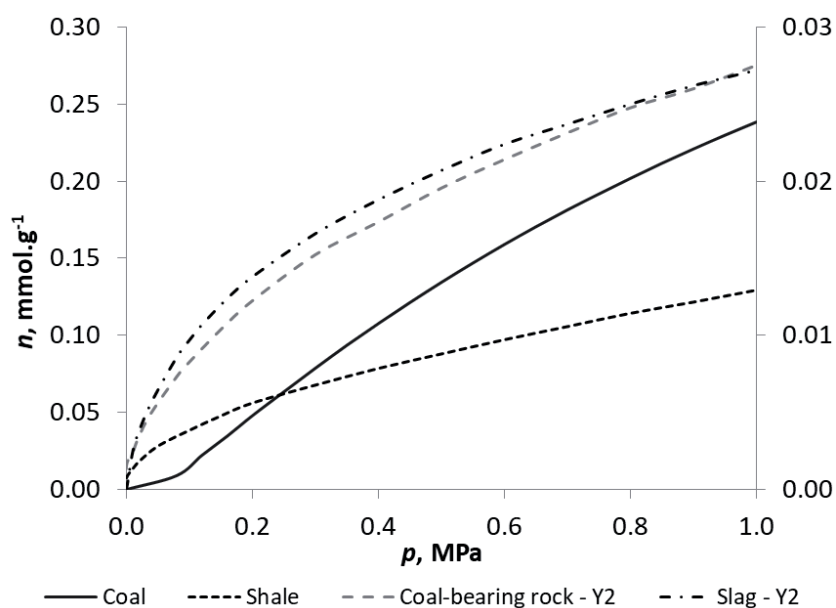


Figure 3. CO₂ adsorption isotherms for selected samples obtained by gravimetric sorption.

MATERIAL ENGINEERING

MATERIAL ENGINEERING

ORGANIC TECHNOLOGY

REDUCTION OF 3-PHENYLPROPANOIC ACID

Kotova M., Mušková J., Vyskočilová E., Červený L.

*Department of Organic Technology, University of Chemistry and Technology Prague, Technická 5, Prague 6 166 28, Czech Republic
maria.kotova@vscht.cz*

Abstract

The reduction of carboxylic acids to alcohols is an interesting synthetic transformation for pharmaceutical, food and fine chemical industries. This reaction can be performed using strong reducing agents. The use of these agents is associated with considerable disadvantages in terms of occupational safety and isolation of the obtained product. On the other side stands the selective catalytic hydrogenolysis of carboxylic acids. This reaction is a direct and efficient way to obtain alcohols avoiding the mentioned problems.

This work was focused on the reduction of 3-phenylpropanoic acid. Catalysts Re/TiO₂, Pd/C, Pt/Al₂O₃ and Ru/C were tested for the reduction. The influence of the reaction conditions on the rate of hydrogenation or hydrogenolysis and selectivity to individual products was studied. The hydrogenolysis of 3-phenylpropanoic acid to 3-phenylpropan-1-ol proceeded only in the presence of Re/TiO₂ in *n*-dodecane. The higher value of selectivity towards 3-phenylpropan-1-ol were achieved using 20 wt. % Re/TiO₂ at 150 °C, 5 MPa. The conversion achieved after five hours was 100 % and the selectivity to the desired product was 41 %.

Introduction

The development of efficient methods for the selective reduction of carboxylic acids to alcohols presents a formidable challenge. This challenge is associated predominantly with the fact that the carboxylic group is thermodynamically and kinetically stable due to the low electrophilicity of the carbonyl carbon¹. The reduction of carboxylic acids can be carried out in the presence of strong reducing agents such as lithium triethylborohydride or lithium aluminum hydride, but the use of these strong agents has significant disadvantages in terms of product isolation and occupational safety².

Homogeneous catalysts were used for the selective hydrogenation of aromatic carboxylic acids. For example, selective hydrogenation of benzoic acid to benzyl alcohol³ was described in the presence of Ru(triphos)(TMM) (triphos=1,1,1-tris(diphenylphosphinomethyl)ethane; TMM=trimethylene methane). The hydrogenolysis of 3-phenylpropionic acid⁴ was performed using homogeneous Ru- and Re-complexes. A homogeneous Co-complex, consisting of Co(BF₄)₂·6H₂O and a triphos ligand⁵, was prepared and used for the hydrogenolysis of benzoic acid, 3-hydroxybenzoic acid and succinic acid to the corresponding alcohols. Hydrogenolysis using mentioned catalysts proceeded with high selectivity; however, homogeneous catalysts generally suffer from challenging product separation and catalyst recycling. Harsh reaction conditions are usually required to perform the hydrogenolysis of carboxylic acids to alcohols using heterogeneous catalysts. For example, hydrogenolysis of carboxylic acids using Ru based catalysts⁶ took place at T=260 °C and p=10 MPa. Harsh reaction conditions often lead to low selectivity to the desired product. It has been found that the hydrogenolysis of carboxylic acids bearing a benzene ring often results in undesired hydrogenation of the aromatic ring or the hydroxyl group is cleaved off and aromatic hydrocarbons are formed (Fig. 1). The yield of the required alcohol is often so low that it is negligible compared to other products. In solving this problem, the use of rhenium-based catalysts, which are known for their ability to catalyze the reduction of a carboxyl group to alcohol in high yields, appears to be a suitable way.

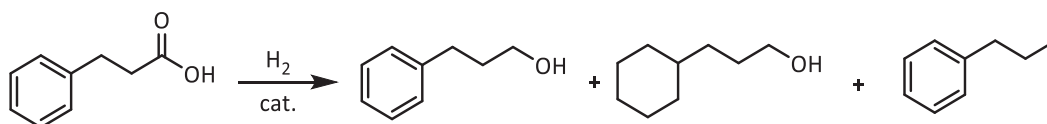


Figure 1. Reduction of carboxylic acids containing an aromatic ring

Currently, there are only a few articles describing the selective hydrogenolysis of aromatic carboxylic acids to alcohols, and therefore the study of carboxyl group reduction is still relevant.

Experiment

Catalysts

Supported catalysts, 5% ruthenium on active carbon 605 type, 5% platinum on alumina (supplied by Johnson & Matthey), 5% palladium on active carbon (supplied by Montecatini) and 2% rhenium on titanium dioxide (prepared at UCT Prague) were used. The catalysts were in a form of fine powders.

Chemicals

3-Phenylpropanoic acid, ammonium perrhenate and titanium dioxide were purchased from Merck. Methanol (Penta), *n*-octane (Merck), decane (Merck) and *n*-dodecane (Merck) were used as solvents.

Preparation of Re/TiO₂ catalyst

The Re/TiO₂ catalyst was prepared⁷ by the impregnation method employing NH₄ReO₄ and TiO₂. Ammonium perrhenate (0.72 g) was added to a round bottom flask with deionized water (100 ml). The flask was placed in an ultrasonic bath for one minute. After complete dissolution of NH₄ReO₄, TiO₂ (9.2 g) was added to the solution and the mixture was stirred on a magnetic stirrer at 300 rpm for 15 minutes at room temperature. This was followed by evaporation to dryness at 50 °C and drying at 90 °C under ambient pressure for 12 hours. The prepared material was calcined under oxygen (80 % N₂, 20 % O₂) at 500 °C for 3 hours and subsequently reduced at 500 °C under a hydrogen/nitrogen atmosphere (80 % H₂, 20 % N₂) for 2 hours.

Hydrogenation

Reductions of 3-phenylpropanoic acid were carried out in a stainless steel autoclave (100 ml). 3-Phenylpropanoic acid (0.5 g), supported catalyst and solvent (50 ml) were introduced into the autoclave. The reaction conditions were set to *p* = 5 MPa, *T* = 150 °C, the catalyst amount was 10 wt. % of the amount of 3-phenylpropanoic acid. Methanol, *n*-octane, decane, *n*-dodecane were used as solvents. Samples were analyzed using GC (column: ZB-5, length: 60 m, diameter: 0.32 mm, thickness: 0.25 μm). Selected samples were also analyzed by GC – MS (column: DB-5-MS, length: 35 m, diameter: 0.20 mm, thickness: 0.33 μm) in order to identify the by-products. The obtained data were used for the calculation of selectivity.

$$\text{Selectivity: } S = \frac{C_{\text{desired product}}}{\sum C_{\text{all products}}} * 100 [\%]$$

Discussion and result analysis

In this work, the reduction of 3-phenylpropanoic acid on various supported catalysts was studied. 3-Phenylpropan-1-ol (I), 3-cyclohexylpropan-1-ol (II), methyl ester of 3-phenylpropanoic acid (III), methyl ester of 3-cyclohexylpropanoic acid (IV), 3-cyclohexylpropanoic acid (V) and 3-cyclohex-3-enopropanoic acid (VI) were detected in reaction mixtures (Fig. 2). The composition of the reaction mixture was significantly influenced by the type of catalyst and used solvent.

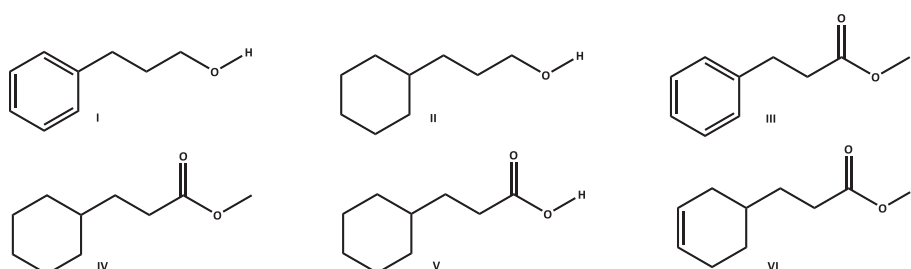


Figure 2. Compounds detected in reaction mixtures

Catalysts Re/TiO₂, Pd/C, Pt/Al₂O₃ and Ru/C were tested for the reduction of 3-phenylpropanoic acid. Methanol was used as a solvent. The conversion of the starting material and the selectivity to the individual reaction products were monitored. The influence of catalyst type on the conversion of 3-phenylpropionic acid is shown in Figure 3. It can be seen from the figure that the total conversion of starting materials was achieved using Ru/C and Pd/C catalysts. The conversion of 69 % and 46 % was achieved after five hours of reaction using Pt/Al₂O₃ and Re/TiO₂ catalysts, resp.

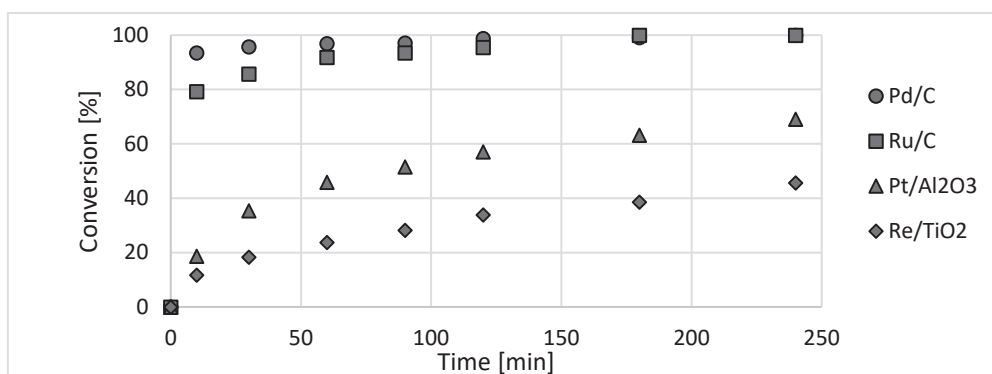


Figure 3. Influence of catalyst type on the conversion of 3-phenylpropionic acid (150 °C, 5 MPa, 50 ml methanol, catalyst amount – 10 wt.% of the amount of acid)

Hydrogenolysis of 3-phenylpropanoic acid to 3-phenylpropan-1-ol did not take place under chosen reaction conditions. Using Pd/C catalyst, esterification of 3-phenylpropanoic acid took place and methyl ester **III** was the major product (Fig. 4). Hydrogenation of ester **III** gave product **IV**. Using the Ru/C catalyst, the aromatic ring was hydrogenated to give product **V**. At the same time, esterification of 3-phenylpropanoic acid took place and ester **III** was formed in a small amount. When Pt/Al₂O₃ was used as a catalyst, a larger amount of 3-cyclohex-3-enpropanoic acid (**VI**) was formed. The main products in the presence of Re/TiO₂ were ester **III** and acid **V** (Fig.4). It is known from the literature⁸, that metallic rhenium has low activity in the dearomatization of the benzene ring. Hydrogenation of the benzene ring in the presence of Re/TiO₂ can be explained by the presence of rhenium oxides on the catalyst surface. X-ray photoelectron spectroscopy (XPS) analysis confirmed that the catalyst was only partially reduced to metallic rhenium and rhenium is also present on the surface in oxidation states Re⁺⁶ and Re⁺⁷.

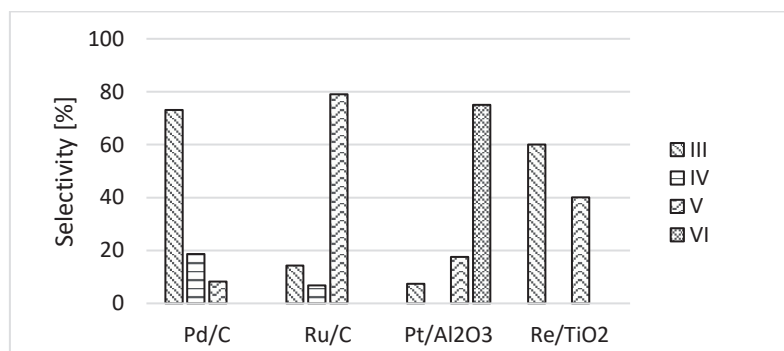


Figure 4. Influence of catalyst type on the selectivity (reaction time – 30 minutes, 150 °C, 5 MPa, 50 ml methanol, catalyst amount – 10 wt.% of the amount of 3-phenylpropionic acid)

Non-polar solvent *n*-dodecane was used to study the influence of the type of solvent on the reaction course. When the reaction was performed in the presence of Pd/C, Ru/C and Pt/Al₂O₃, the conversion values were lower, than when the reaction was performed in methanol. Conversion of 3-phenylpropanoic acid was higher compared to values achieved in methanol and reached 97 % when the reaction took place in the presence of Re/TiO₂ (Fig. 5).

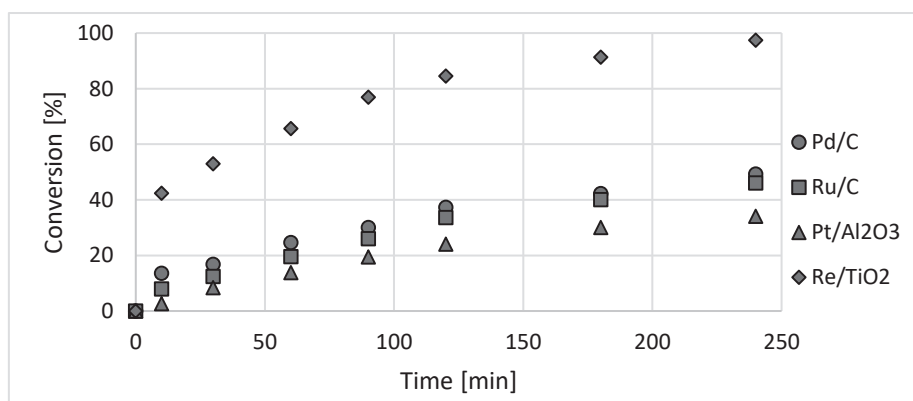


Figure 5. Influence of catalyst type on the conversion of 3-phenylpropionic acid (150 °C, 5 MPa, 50 ml *n*-dodecane, catalyst amount – 10 wt.% of the amount of acid)

Hydrogenation of the benzene ring and formation of product **V** took place when Pd/C, Ru/C, Pt/Al₂O₃ and Re/TiO₂ were used as catalysts (Fig. 6). Hydrogenolysis of the C-O bond occurred only in the presence of Re/TiO₂ and 3-phenylpropan-1-ol (**I**) was formed in the reaction mixture. Subsequent hydrogenation of benzene ring in **I** occurred and 3-cyclohexylpropan-1-ol (**II**) was also formed.

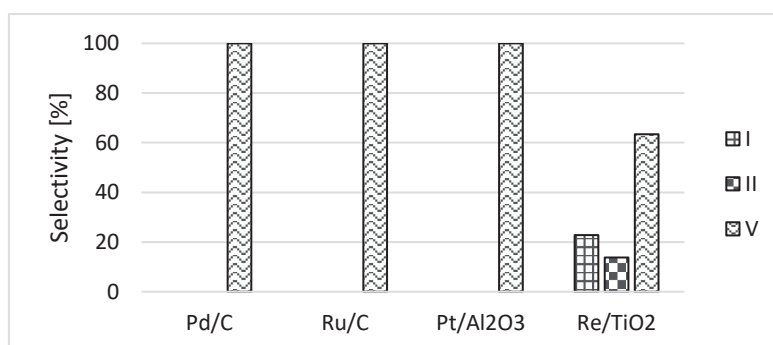


Figure 6. Influence of catalyst type on the selectivity (reaction time – 120 minutes, 150 °C, 5 MPa, 50 ml *n*-dodecane, catalyst amount – 10 wt.% of the amount of 3-phenylpropionic acid)

The reduction of 3-phenylpropionic acid was also performed in *n*-octane a decane using Pd/C, Ru/C, Pt/Al₂O₃ and Re/TiO₂. Hydrogenation of benzene ring and the formation of product **V** took place in all cases. The product of hydrogenolysis of the C-O bond was not detected in the reaction mixtures. Conversion of the starting material was lower compared to reactions performed in *n*-dodecane.

The influence of pressure, temperature and amount of catalyst on the reduction in the presence of Re/TiO₂ catalyst in *n*-dodecane was monitored. The results are summarized in table I.

Table I

The influence of reaction conditions on the reduction of 3-phenylpropionic acid (reaction time – 300 minutes, 50 ml *n*-dodecane)

Entry	Temperature, °C	Pressure, MPa	Catalyst amount, wt. %	Conversion, %	Selectivity, %		
					I	II	V
1	50	5	10	30	0	0	100
2	100	5	10	64	0	0	100
3	120	5	10	86	12	8	80
4	150	5	10	97	23	14	63
5	150	7	10	100	27	20	53
6	150	10	10	100	37	31	32
7	150	5	20	100	41	33	26

The temperature had a significant influence on the course of reduction. Selectivity to the hydrogenolysis product **I** increased with increasing temperature (entries 1-4). It was demonstrated, that a temperature of 100°C and lower was not enough to perform the hydrogenolysis of the C-O bond. With increasing pressure (entries 4-6) and amount of catalyst (entries 4,7) selectivity to the product **I** also increased. Hydrogenation of 3-phenylpropan-1-ol (**I**) to 3-cyclohexylpropan-1-ol (**II**), and 3-phenylpropionic acid to 3-cyclohexylpropanoic acid (**V**) took place in all cases. Best results in terms of selectivity to 3-phenylpropan-1-ol (**I**) was obtained when the reaction was performed under a temperature of 150°C, pressure of 5 MPa and the amount of catalyst was 20 wt.% of the amount of starting material (entry 7).

Conclusion

This work deals with the reduction of 3-phenylpropanoic acid using supported catalysts based on palladium, platinum, ruthenium and rhenium. The conversion of the starting material and the selectivity to the individual reaction products were monitored depending on the selected reaction conditions. It has been found that depending on the type of catalyst used in the reduction of 3-phenylpropanoic acid the complete or partial hydrogenation of the benzene ring or hydrogenolysis of the C-O bond occurred. At the same time, when the reaction was performed in methanol using all catalysts, esterification took place to give methyl ester of 3-phenylpropanoic acid. When the reduction was carried out at 150 °C and 5 MPa in methanol, total conversion of the starting material was achieved only when Ru/C and Pd/C catalysts were used.

Hydrogenolysis of 3-phenylpropanoic acid to 3-phenylpropan-1-ol took place only in the presence of Re/TiO₂ in *n*-dodecane. When using 20 wt. % of Re/TiO₂ at 150 °C, 5 MPa, in *n*-dodecane, 100 % conversion was achieved after 5 hours and the selectivity to 3-phenylpropan-1-ol was 41 %.

References

1. Dub P. A., Ikariya T.: ACS Catal. 2, 1718 (2012).
2. Brown H. C., Krishnamurthy S.: Tetrahedron 35, 567 (1979).
3. Vom Stein T., Meuresch M., Limper D., Schmitz M., Holscher M., Coetzee J., Cole-Hamilton D. J., Klankermayer J., Leitner W.: J. Am. Chem. Soc. 136, 13217 (2014).
4. Naruto M., Saito S.: Nat. Commun. 6, 8140 (2015).
5. Korstanje T. J., Ivar van der Vlugt J., Elsevier C. J., de Bruin B.: Science 350, 298 (2015).
6. Carnahan J. E., Ford T. A., Gresham W. F., Grigsby W. E., Hager G. F.: J. Am. Chem. Soc. 77, 3766 (1955).
7. Toyao T., Hakim Siddiki S. M. A., Touchy A. S., Onodera W., Kon K., Morita Y., Kamachi T., Kazunari Y., Ken-ichi S.: Chem.Eur.J. 23, 1001, (2017).
8. Broadbent H.S., Campbell G.C., Bartley W.J., Johnson J.H.: J. Org. Chem. 24, 1847 (1959).

A method for pre-treatment of waste plastic pyrolysis oil allowing the evaluation by pyrolysis gas chromatography

Le T.A., Karaba A., Patera J., Zámostný P.

University of Chemistry and Technology Prague, Technická 5, 166 28 Prague 6 – Dejvice, Czech Republic

Abstract

Waste plastic pyrolysis is one of many studied alternative technologies that offer a possible solution to the waste plastic problem. One of its material stream, pyrolysis oil, is currently blended with fuels and used as part of waste-to-energy technology, but our objective is to evaluate its possible utilization in steam-cracking. Three samples from our industrial partner were analyzed via pyrolysis gas chromatography method ($T = 815\text{ }^{\circ}\text{C}$, $p = 4\text{ bar}$, $F = 65\text{ ml}\cdot\text{min}^{-1}$). Unfortunately, original samples deactivated parts chromatography capillary column. In order to protect the analytical apparatus, a multiple step distillation method was developed. It was found that the method not only protected the chromatography apparatus but gave a possibility to examine the samples even more complex. Thereafter, experiments were conducted via pyrolysis gas chromatography with the treated samples and it was determined that some waste plastic pyrolysis oils produce a comparable product composition as traditional steam-cracking feedstock – primary naphtha.

Introduction

Nowadays, plastic material is a very popular material to use. Due to low production cost, easy and varied applicability, popularity and production of plastic material is still rising worldwide and waste plastic consequently as well. Only a smaller part of the waste plastic is mechanically recycled ⁽¹⁾, a part of it is used as feedstock in a waste-to-energy technology and the rest is being dumped for the time being. Topic of waste plastic utilization is currently a frequently discussed problem. A common idea of utilization is the before mentioned waste-to-energy technology ⁽²⁾ especially through pyrolysis ⁽³⁾.

Waste plastic pyrolysis product can be categorized into three material streams ⁽⁴⁾ – non-condensable gas, pyrolysis oil (or condensate) and char. From the perspective of further material utilization, the pyrolysis oil is the most interesting one. Physical properties of waste some plastic pyrolysis oil are comparable to those of primary naphtha ⁽⁵⁾, therefore a large part of the studies in literature is devoted to utilizing waste plastic pyrolysis oil as feedstock for diesel engines ⁽⁶⁾. Although direct injection of waste plastic pyrolysis oil into diesel engines is not possible, there are several studies claiming that indeed its blends with certain petroleum fractions are subject to direct use in diesel engines ⁽⁸⁻¹⁰⁾. Other pyrolysis reactors offer a possibility of producing pyrolysis oil with properties more similar to those of gasoline ⁽¹¹⁾. And as the previous type of pyrolysis oil, it is possible to use this one in blends as feedstock for combustion engines ⁽¹²⁾.

There is little to be found on the topic of further material utilization of waste plastic pyrolysis oil. A few patents are available in French ⁽¹⁴⁾ and English ⁽¹⁵⁾. The biggest hurdles along the way of material utilization of waste plastic utilization are the large variety of hydrocarbons, the amount of impurity and number of heteroatoms in the mixture ranging from nitrogen, sulphur, oxygen, halogens to all kinds of metals. Alternatively, the steam-cracking process could be a strong candidate for further material utilization, because the technology is capable processing a larger variety of hydrocarbons as feedstock, although the impurities have to be dealt with either way and it is unlikely that the pyrolysis oil would be used without any modifications ⁽¹⁶⁾. But before the introduction of the material steam as a feedstock for the steam-cracking process, an amount of question must be resolved or at least pre-solved. Between the most important, there is consideration about the steam-cracking products distribution and how much would be the yields of products influenced by an addition of the considered material into a feedstock. Is the distribution significantly different from the typical distribution obtained by the steam-cracking of standard feedstock? To answer this, we decided to evaluate experimentally pyrolysis product distribution of several samples of waste plastics pyrolysis oils and compare them to the yields obtain from traditional feedstock. We decided to use a pyrolysis gas chromatography ⁽¹⁷⁾, a technique very sensitive to the feedstock composition and relatively easy to use. But, after some preliminary experiments, we found that the samples of waste plastics pyrolysis oil seriously influenced the apparatus of pyrolysis gas chromatography. Specifically, they deactivated significant part of chromatographic columns, which would lead to future inability of the analytical system to separate individual pyrolysis products and then evaluate their yields. We assumed, there is a sort of compounds contained in the samples of waste plastics pyrolysis oils, their presence manifests by the deactivation of chromatographic columns. Assuming that this is caused by the heaviest part of the sample, we decided to develop a distillation-based method, which would pre-treat the sample and protect the equipment of pyrolysis chromatography from the observed undesired effects.

Materials and methods

All the pyrolysis oil samples (AdiOil M. Pedersen - 14/5/20, Pyrolysis condensate - 8/6/20 and CrUD - 31/3/20) available in this study were acquired by our industrial partner from various industrial companies, who understandably did not share any details about the technology that produced the samples. Because of that there is very little known about the samples. Information provided to us was that the samples were already treated and should only contain negligible amount of impurities. Material origin nor technological settings were not disclosed.

In order to pre-treat the samples, a three-step distillation method has been suggested. Firstly, the samples are distilled at atmospheric pressure at 80 °C. Secondly, the pressure is lowered to 50 torr and then distilled at 80 °C. Lastly, the pressure of the system is brought down to 10 torr and the mixture is distilled at 240 °C (with fraction cuts at 80 °C and 160 °C) or almost to a drought. Because the heavy aromatic hydrocarbons are detrimental to the gas chromatography capillary columns, the objective is to never distillate to a drought. Distillation was carried out in a distillation apparatus compiling of a 50 ml distillation flask (half filled with the sample) in an oil bath with a magnetic stirrer, thermometer (250 °C), condenser, distillation receiver with 3 round bottom flasks allowing to obtain 3 separate distillates, a cooling bath with ethanol and dry ice, and a vacuum pump.

The apparatus for laboratory study of hydrocarbon pyrolysis is composed of a pyrolysis unit Pyr-4A Shimadzu and two gas chromatography units GC 17A Shimadzu. The reactor is a micro-pulse tube reactor, which is 180 mm long and has 3 mm wide inside diameter. The reactor was heated up to 815 °C via an electric furnace, nitrogen gas flow rate was set to 65 ml.min⁻¹ and pressure was set to 300 kPa pressure gauge. 0.2 µl of sample was injected per analysis into the pyrolysis reactor and the composition of the products were determined by a set of 3 FID detectors. A more detailed description of the method is provided elsewhere ⁽¹⁷⁾.

Results and discussion

Pyrolysis gas chromatography experiments were carried out on every single fraction generated by the distillation except the heaviest vacuum residue. It was found that distillates obtained did not exhibit the

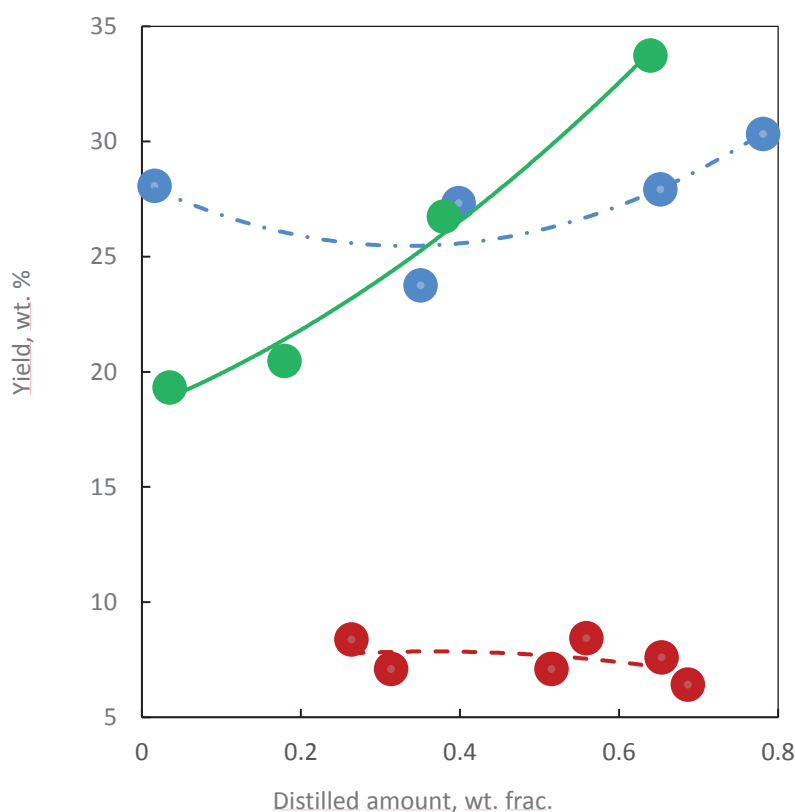


Figure 1. Ethylene dependency on distilled amount: ● AdiOil M. Pedersen - 14/5/20, ● Pyrolysis condensate - 8/6/20 and ● CrUD - 31/3/20; T = 815 °C, p = 4 bar, F = 65 ml.min⁻¹

undesired behaviour mentioned above - the deactivation of chromatographic columns. Each pyrolysis product yield was then examined as a dependency on the distilled amount. That dependency of ethylene is showcased in figure 1. It is clearly visible that the individual samples waste plastics pyrolysis oils are of a very different nature. The ethylene yield of CrUD – 31/3/20 is increasing with the distilled amount. In contrast, the samples AdiOil M. Pedersen – 14/5/20 and Pyrolysis condensate – 8/6/20 show a minimum and maximum. These characteristics are important especially for industrial practices because it provides a certain advantage in strategy planning. Industrial partner is able based on these data make specific distillation fraction cuts, which would provide even more valuable yields. For example, ethylene is a desired product of steam cracking and based on observations made from figure 1 the optimal feedstock for steam-cracking from the sample AdiOil M. Pedersen – 14/5/20 would be the heavier fraction. In contrary, the desired fraction of Pyrolysis condensate – 8/6/20 would be the lighter one.

Trends in figure 1 also offer the possibility to estimate the missing data of product composition of the distillation residue.

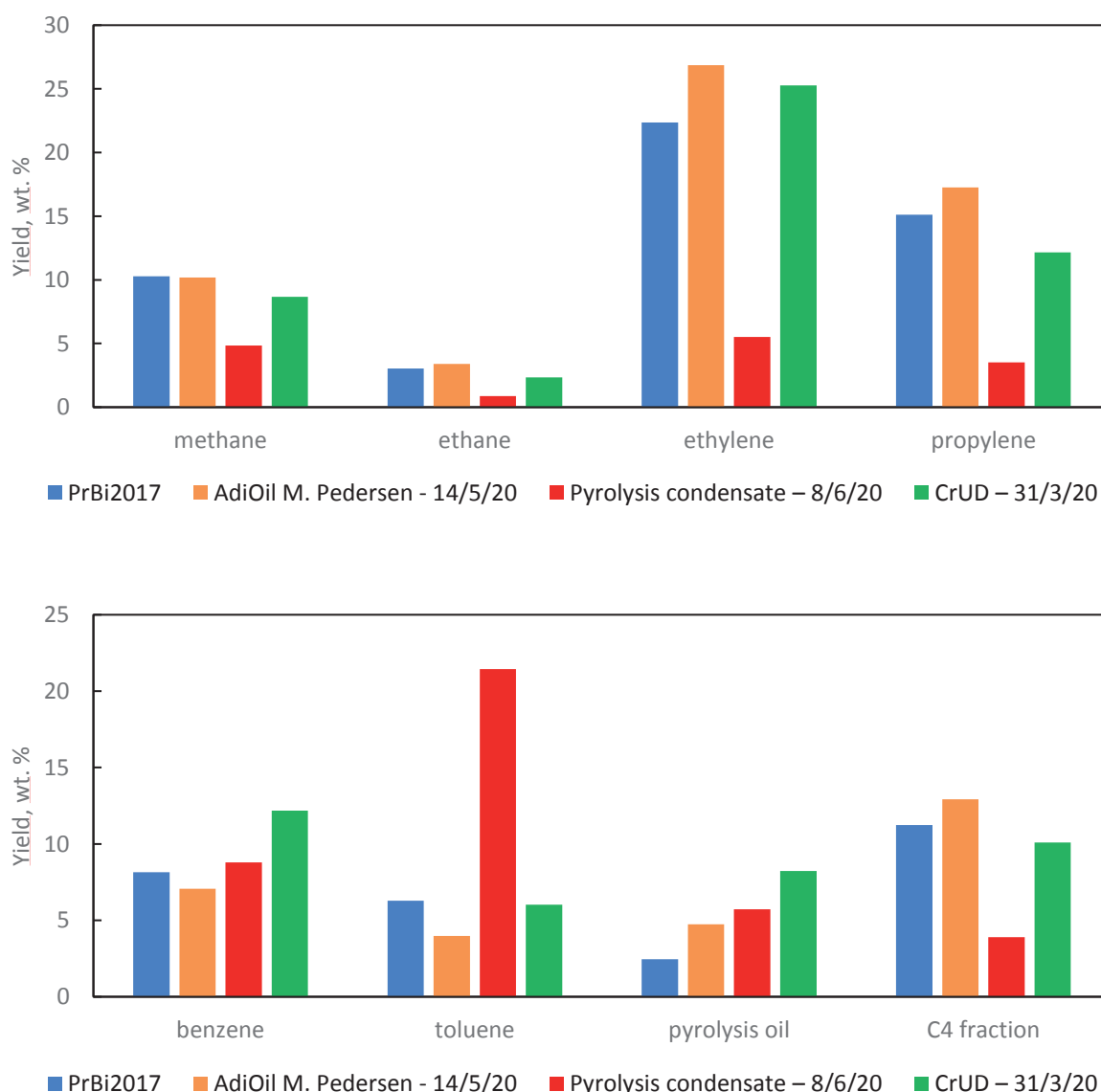


Figure 2. Comparison of composition of steam cracking products of waste plastic pyrolysis oils with traditional feedstock naphtha (PrBi2017); T = 815 °C, p = 4 bar, F = 65 ml.min⁻¹

Distillation residue could not be subject of pyrolysis experiments via gas chromatography. Since the distillation obviously removed the cause of distillation columns deactivation (probably the presence of the heaviest part of the sample), it is reasonable to assume that the compounds original causing problems with experiment were concentrated into the distillation residue. But, their contribution to the composition of steam cracking products cannot be ignored. Steam cracking product yield of the heaviest part of the sample can be extrapolated from the trends shown in figure 1. Extrapolated yield of each product of the distillation residues were later combined via weighted sum with the experiment yields of the rest of the sample. The results are shown in the figure 2 in comparison to products composition of steam cracking product of traditional feedstock, specifically primary naphtha. It has been observed that waste plastic pyrolysis oils such as AdiOil M. Pedersen - 14/5/20 and CrUD – 31/3/20 have a similar product distribution as the traditional feedstock. The product yield of Pyrolysis condensate – 8/6/20 is less favourable in lighter products such as ethylene and propylene but benzene and toluene are still very desirable products. Pyrolysis oil from steam cracking is an undesired product, thus it can be assumed that CrUD – 31/3/20 might not be advantageous to utilize as a feedstock for steam-cracking as a whole and specific fraction would be selected from this type of waste plastic pyrolysis oil.

Conclusion

The suggested three-step distillation method proved to be effective in order to protect the gas chromatography apparatus from any damage. Moreover, it also offered a possibility for a more complex examination of the samples. Information gained provide a choice of specific fractions, which would be more valuable as feedstock for industrial steam-cracking. The data also gives the possibility of extrapolation of product composition of the distillation residue, which could not be analysed with gas chromatography. Lastly, it was observed that some of the waste plastic pyrolysis oils are in fact a promising feedstock for steam-cracking compared to traditional feed, such as primary naphtha, while some of them are less promising. And this highlights even more the needs of experimental evaluation of each candidate feedstock, to select appropriate variety of them, which could take place in the industrial scale.

Acknowledgement

This work was supported from the grant of Specific university research – grant No A1_FCHT_2022_010.

References

1. Thiounn, T.; Smith, R. C. Advances and Approaches for Chemical Recycling of Plastic Waste. *J. Polym. Sci.* 2020, 58 (10), 1347–1364. <https://doi.org/10.1002/pol.20190261>.
2. Singhabhandhu, A.; Tezuka, T. The Waste-to-Energy Framework for Integrated Multi-Waste Utilization: Waste Cooking Oil, Waste Lubricating Oil, and Waste Plastics. *Energy* 2010, 35 (6), 2544–2551. <https://doi.org/10.1016/j.energy.2010.03.001>.
3. Erdogan, S. Recycling of Waste Plastics into Pyrolytic Fuels and Their Use in IC Engines; IntechOpen, 2020. <https://doi.org/10.5772/intechopen.90639>.
4. Khan, M. Z. H.; Sultana, M.; Al-Mamun, M. R.; Hasan, M. R. Pyrolytic Waste Plastic Oil and Its Diesel Blend: Fuel Characterization. *J. Environ. Public Health* 2016, 2016, e7869080. <https://doi.org/10.1155/2016/7869080>.
5. Mangesh, V. L.; Padmanabhan, S.; Tamizhdurai, P.; Ramesh, A. Experimental Investigation to Identify the Type of Waste Plastic Pyrolysis Oil Suitable for Conversion to Diesel Engine Fuel. *J. Clean. Prod.* 2020, 246, 119066. <https://doi.org/10.1016/j.jclepro.2019.119066>.
6. Ananthakumar, S.; Jayabal, S.; Thirumal, P. Investigation on Performance, Emission and Combustion Characteristics of Variable Compression Engine Fuelled with Diesel, Waste Plastics Oil Blends. *J. Braz. Soc. Mech. Sci. Eng.* 2017, 39 (1), 19–28. <https://doi.org/10.1007/s40430-016-0518-6>.
7. Van de Beld, B.; Holle, E.; Florijn, J. The Use of Pyrolysis Oil and Pyrolysis Oil Derived Fuels in Diesel Engines for CHP Applications. *Appl. Energy* 2013, 102, 190–197. <https://doi.org/10.1016/j.apenergy.2012.05.047>.
8. Lee, S.; Yoshida, K.; Yoshikawa, K. Application of Waste Plastic Pyrolysis Oil in a Direct Injection Diesel Engine: For a Small Scale Non-Grid Electrification. *Energy Environ. Res.* 2015, 5 (1), p18. <https://doi.org/10.5539/eer.v5n1p18>.
9. Chandran, M.; Tamilkolundu, S.; Murugesan, C. Investigation of the Performance, Combustion Parameters and Emissions Analysis on DI Engine Using Two Staged Distilled Waste Plastic Oil-Diesel Blends. *Therm. Sci.* 2018, 22 (3), 1469–1480.
10. Kumar, S.; Prakash, R.; Murugan, S.; Singh, R. K. Performance and Emission Analysis of Blends of Waste Plastic Oil Obtained by Catalytic Pyrolysis of Waste HDPE with Diesel in a CI Engine. *Energy Convers. Manag.* 2013, 74, 323–331. <https://doi.org/10.1016/j.enconman.2013.05.028>.

11. Ratnasari, D. K.; Nahil, M. A.; Williams, P. T. Catalytic Pyrolysis of Waste Plastics Using Staged Catalysis for Production of Gasoline Range Hydrocarbon Oils. *J. Anal. Appl. Pyrolysis* 2017, 124, 631–637. <https://doi.org/10.1016/j.jaap.2016.12.027>.
12. Khairil; Riayatsyah, T. M. I.; Bahri, S.; Sofyan, S. E.; Jalaluddin, J.; Kusumo, F.; Silitonga, A. S.; Padli, Y.; Jihad, M.; Shamsuddin, A. H. Experimental Study on the Performance of an SI Engine Fueled by Waste Plastic Pyrolysis Oil–Gasoline Blends †. *Energ.* 19961073 2020, 13 (16), 4196. <https://doi.org/10.3390/en13164196>.
13. Lee, K.-H. Thermal and Catalytic Degradation of Pyrolytic Oil from Pyrolysis of Municipal Plastic Wastes. *J. Anal. Appl. Pyrolysis* 2009, 85 (1), 372–379. <https://doi.org/10.1016/j.jaap.2008.11.032>.
14. Weiss, W.; Bonnardot, J. Method for Processing Plastic Pyrolysis Oils with a View to Their Use in a Steam-Cracking Unit. WO2021110395 (A1), June 10, 2021.
15. Bitting, D.; Parker, K.; Polasek, M.; Slivensky, D.; Wu, X.; Stavinoha, J. Optimized Cracker Conditions to Accept Pyrolysis Oil. WO2020242917 (A1), December 3, 2020.
16. Kusenberg, M.; Eschenbacher, A.; Djokic, M. R.; Zayoud, A.; Ragaert, K.; De Meester, S.; Van Geem, K. M. Opportunities and Challenges for the Application of Post-Consumer Plastic Waste Pyrolysis Oils as Steam Cracker Feedstocks: To Decontaminate or Not to Decontaminate? *Waste Manag.* 2022, 138, 83–115. <https://doi.org/10.1016/j.wasman.2021.11.009>.
17. Zamostny, P.; Belohlav, Z.; Starkbaumova, L. A Multipurpose Micro-Pulse Reactor for Studying Gas-Phase Reactions. *Chem. Biochem. Eng. Q.* 2007, 21 (2), 105–113.

AVAILABLE METHODS ENABLING CHEMICAL UTILIZATION OF ANTHROPOGENIC CO₂ FOR PRODUCTION OF CYCLIC CARBONATES USING HOMOGENEOUS NON-METALLIC CATALYSTS

Weidlich T.¹, Kamenická B.¹

¹University of Pardubice, Faculty of Chemical Technology, Chemical Technology Group, Studentska 95, 532 10 Pardubice,
tomas.weidlich@upce.cz

Abstract

Cyclic carbonates are utilizable as green solvents, electrolytes in Li-ion batteries, intermediates for fine chemicals and monomers for polyesters or polyurethanes production. Cyclic carbonates are available by cycloaddition of CO₂ into the epoxide (oxirane) ring. This reaction enables significant utilization of greenhouse carbon dioxide as the chemical building block. The synthetic pathways for both sustainable epoxides and cyclic carbonates production are described in this full text. This paper is focused mainly on description of applicable homogeneous non-metallic catalysts available for described CO₂ cycloaddition. The most effective cycloaddition catalysts contain sources of nucleophile such as onium salt, structural moiety working as hydrogen bond donors and/or amino group(s) working as epoxide ring activators and CO₂ scavengers for smooth CO₂ addition and subsequent ring closure. In case of terminal oxiranes such as epichlorohydrin, even the flue gas (diluted CO₂) is applicable for effective production of appropriate cyclic carbonates.

1. Introduction

CO₂ capture and utilization (CCU) technologies has been recognized as the cost-effective way to significantly reduce worldwide greenhouse gas emissions. Due to this reason, the use of CO₂ as a raw material in chemical synthesis is a research area of great scientific, economic and ecological interest [1–14].

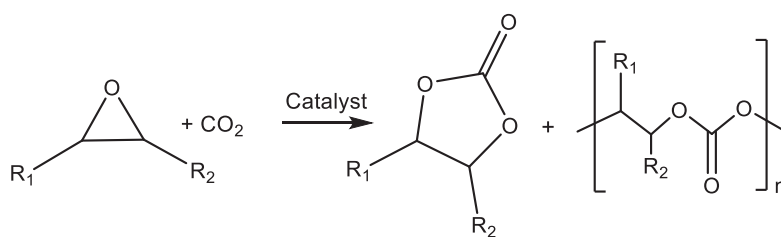
The plenty of CO₂, which is simply available, nontoxic and nonflammable makes it a very attractive and cheap C1-synthon in chemical technology. Thermodynamically stable CO₂ ($\Delta G^0 = -394.228$ kJ/mol)[10], however, needs activation and corresponding reactive agent(s) for its possible fixation into the organic molecules.

Three-membered heterocyclic rings such as oxiranes (epoxides) serve as ideal reactant for CO₂ fixation producing cyclic carbonates or polycarbonates (Figure 1, Scheme 1). Cyclic carbonates are applicable for polymer production, production of dialkyl carbonates, as electrolytes in lithium-ion batteries, polar aprotic (ethylene or propylene carbonate) or protic solvents (glycerol carbonate) and as chemical intermediates in organic fine chemicals production (Scheme 2). As North et al. have mentioned, only two reactions of CO₂: dry reforming of methane (for fuel production) and production of cyclic carbonates could consume up to 25% of the anthropogenic CO₂ produced annually [12].

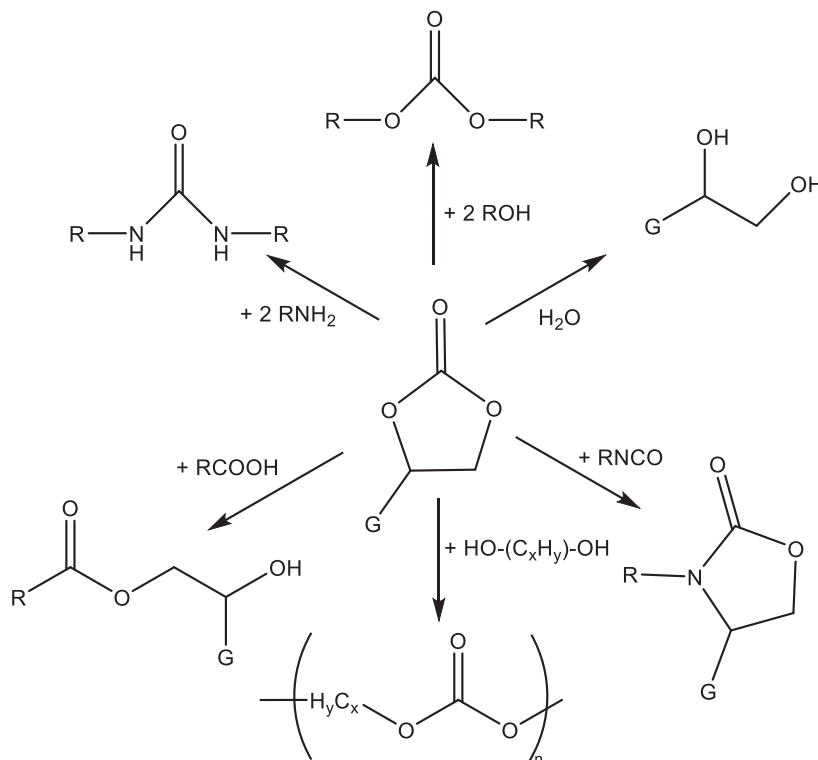
The epoxides available for carbonation can be classified according to their bound substituents as terminal epoxides (containing at least one unsubstituted CH₂ group in the oxirane ring) and internal epoxides (containing substituents on both carbon atoms of the oxirane ring, Figure 1).



Figure 1. Epoxides available for cycloaddition reactions.

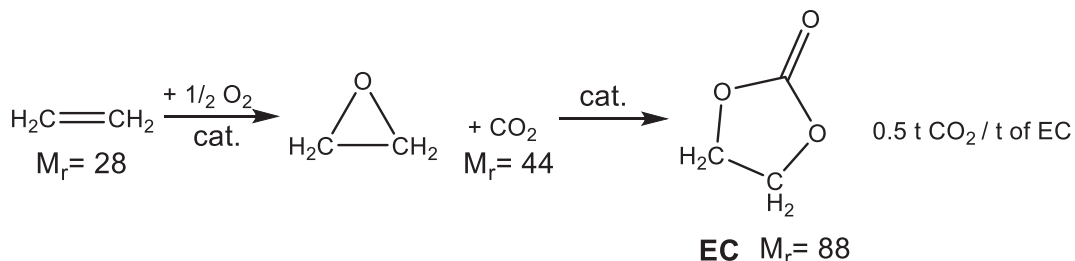


Scheme 1. Catalyzed reaction of carbon dioxide with epoxides (oxiranes).



Scheme 2. Possibilities for the chemical transformation of cyclic carbonates to linear (poly)carbonates, esters, ureas, ethyleneglycols and urethanes (carbamates) [1,2,5,13,15].

The reaction of CO₂ with oxiranes, which are available mainly from corresponding olefins (see Chapter , producing cyclic carbonates is highly attractive because these reactions are free of any side products (proceeds with 100% atom-economy, Scheme 3). In particular, the connection of direct air oxidation and carbonation of ethylene oxide serves as a simple and effective technology that is useful for the subsequent utilization of anthropogenic CO₂ (Scheme 3). In case of ethylene carbonate (EC) produced from ethylene, 44 g of CO₂ is utilized per mol of produced EC (1/2 of EC molecular weight creates CO₂) according to the stoichiometry of this reaction.



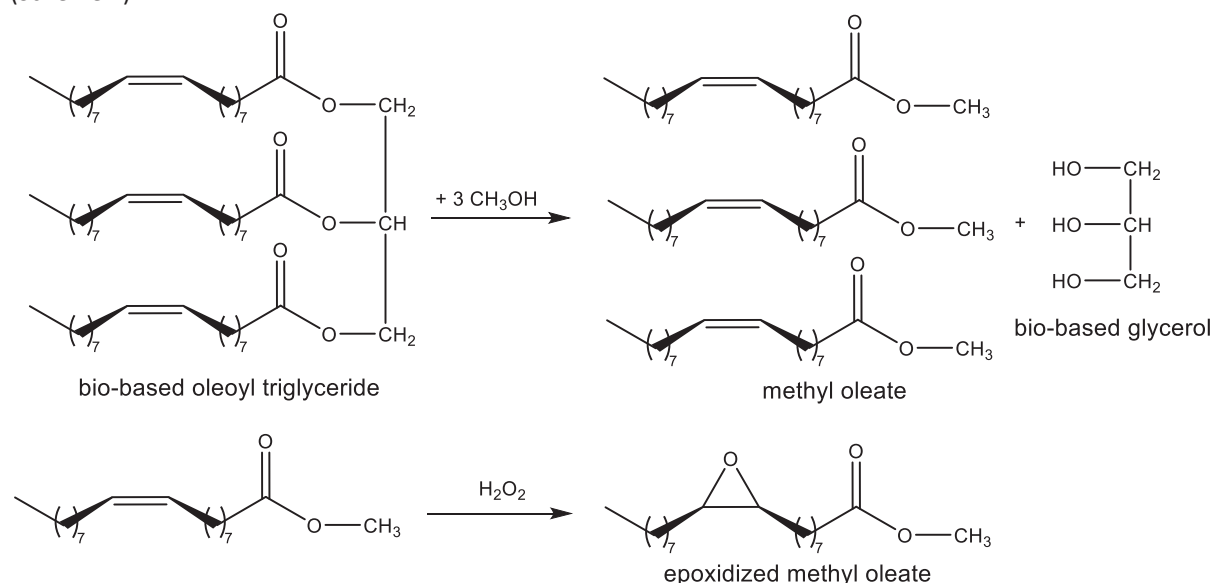
Scheme 3. Production of ethylene carbonate (EC) consumes 500 kg of CO₂ per ton of EC.

2. Sustainable sources of epoxides

Epoxides are accessible utilizing the oxidation of the C=C double bond in olefins (using peroxides or O₂/Ag-based reaction) or by the dehydrohalogenation of geminal halogenoethanols [5].

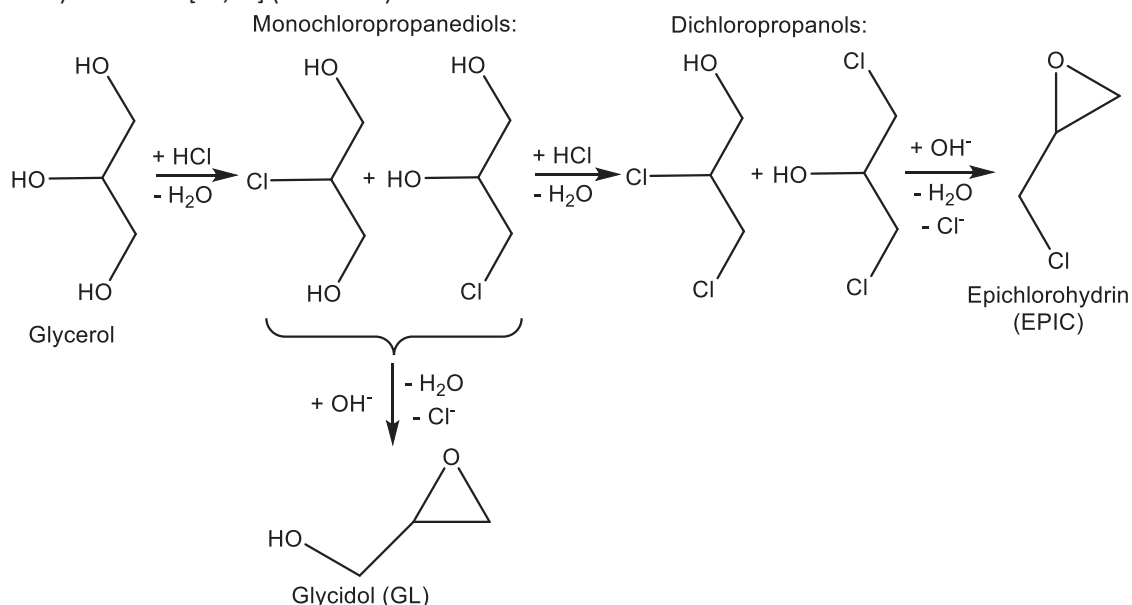
Especially terminal epoxides such as glycidol (GL), epichlorohydrin (EPIC), propylene oxide (PO) and ethylene oxide (EO) are mostly studied oxiranes for the CO₂/epoxide coupling reactions.

EPIC and GL are recently produced from bio-glycerol obtained from the fatty acids methyl esters production (Scheme 4).



Scheme 4. Production of epoxidized methyl oleate and glycerol from lipids.

The treating of OH groups in the glycerol structure with HCl enables the formation of monochloropropanediols or dichloropropanols, in the presence of a catalyst, usually a carboxylic acid [2,5,16–18], as the crucial intermediate for EPIC or GL production. The subsequent ring closure induced by an base enables oxirane (epoxide) formation [19,20] (Scheme 5).



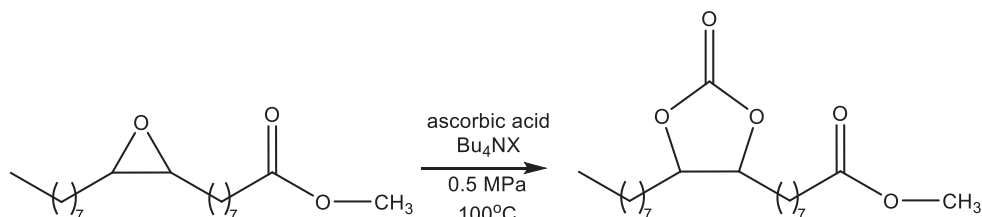
Scheme 5. Production of EPIC and GL via corresponding chloroethanols hydrodechlorination.

EO and PO are produced from ethylene and propylene produced by the cracking of petrochemical feedstock or potentially from plastic waste with subsequent silver-catalyzed direct air oxidation [3] (Schemes 1 and 6). The development of sustainable olefins production is based on bio-based syngas (CO + H₂) utilization obtained by the gasification of waste biomass [21]. The most promising pathway for alkene production exploits methanol as a crucial intermediate simply available from CO + H₂ mixture with its subsequent dehydrogenation/coupling. This mentioned reaction is catalysed by zeolites (methanol-to-olefins technology, MTO) [21]. The catalytic cracking of vegetable oils (lipids) may produce propylene, too [21].

Table II.

Comparison of various HBD/Bu₄Ni catalytic systems for the carbonation of EPIC.

Entry	Catalyst	Catalyst Amount (mol%)	CO ₂ Pressure (MPa)	Temp. (°C)	Reaction Time (h)	Conv. (%)	Ref.
1	L-Ascorbic acid	2	0.1	25	23	70	[23]
2	L-Ascorbic acid	2	0.1	40	23	94	[23]
3	Lactic acid	2	0.1	25	23	59	[23]
4	DBU/PhCH ₂ Br	2	0.1	25	23	93	[23,24]
5	Tetraethylene glycol/KI	2	0.1	40	23	92	[23,25]
6	Bu ₄ Ni	4	0.1	25	23	31	[23]



Scheme 9. Carbonation of epoxidized methyl oleate producing corresponding cyclic carbonate.

Table III.

Carbonation of methyl oleate using ascorbic acid (HBD) and different sources of nucleophile (Bu₄NX) [26].

Entry	Catalyst	Catalyst Amount (mol%)	CO ₂ Pressure (MPa)	Temp. (°C)	Reaction time (h)	Conversion (%)	Selectivity (%)
1	[Bu ₄ N]I	5	0.5	100	24	70	59
2	[Bu ₄ N]Br	5	0.5	100	24	83	87
3	[Bu ₄ N]Cl	5	0.5	100	24	44	>99
4	L-ascorbic acid/[Bu ₄ N]I	0.5/5	0.5	100	24	>99	20
5	L-ascorbic acid/[Bu ₄ N]Br	0.5/5	0.5	100	24	91	83
6	L-ascorbic acid/[Bu ₄ N]Cl	0.5/5	0.5	100	24	61	>99
7	L-ascorbic acid/[Bu ₄ N]Cl	1/5	0.5	100	24	62	>99
8	L-ascorbic acid/[Bu ₄ N]Cl	1.5/5	0.5	100	24	69	>99
9	L-ascorbic acid/[Bu ₄ N]I	1.5/5	0.5	100	24	>99	74
10	L-ascorbic acid/[Bu ₄ N]Br	1.5/5	0.5	100	24	98	>99
11	L-ascorbic acid/[Bu ₄ N]Cl	1.5/5	0.5	100	24	69	>99
12	L-ascorbic acid/[Bu ₄ N]Cl	1.5/5	0.5	100	24	59	>99
13	L-ascorbic acid/[Bu ₄ N]Cl	1.5/5	0.5	100	24	57	>99
14	L-ascorbic acid/[Bu ₄ N]Cl	2/5	0.5	100	24	49	>99
15	L-ascorbic acid/[Bu ₄ N]Cl	5/5	0.5	100	24	15	>99
16	L-ascorbic acid/[Bu ₄ N]Cl	1.5/5	0.5	100	48	>99	>99
17 ^a	L-ascorbic acid/[Bu ₄ N]Cl	1.5/5	0.5	100	24	38	>99
18	L-ascorbic acid/[Bu ₄ N]Cl	1.5/5	1	100	24	92	>99

^a Using recovered catalysts.

As is documented in Table III, the mentioned Bu₄NX/ascorbic acid mixture was effective even for the carbonation of internal epoxides at an elevated temperature (100 °C) and 2 MPa CO₂ pressure [15]. The most effective catalytic mixture found contains Bu₄NBr/ascorbic acid.

5. Conclusions

The carboxylation of epoxides is a sustainable pathway for the fixation of CO₂ into valuable chemicals, considering the industrial utilization of cyclic and polymeric carbonates. Hopefully, the next development of homogeneous catalysts, including organocatalysts (e.g., organic salt and ILs), will facilitate the expanding of the spectrum of available metal-free catalysts applicable for the reaction of CO₂ with terminal epoxides even at CO₂ pressures of 0.1 MPa and reaction temperatures of less than around 50 °C. Except high catalytic activity, the simple catalyst separability should be profitable because of the necessity of high catalytic loading for the effective course of

cycloaddition reaction. The bulky tetrabutylammonium cations in Bu₄NX enable the high nucleophilic activity of the appropriate naked anions of X⁻, such as bromide or iodide, in most cases. Onium salts are widely applied as part of multicomponent catalytic systems in the research and development of epoxides' carbonation processes. The most effective halide free IL-based homogeneous catalyst was recognized to be the Bu₄N-halides with ascorbic acid [26,27]. Searching for simple and cheap catalytic systems that are active at mild reaction conditions is attractive not only due to the environmental point of view (lower energy consumption) but even due to the thermodynamic reasons. As the formation the cyclic carbonate is exothermic, the lower reaction temperature affects the shifting of the reaction equilibrium in the products.

The utilization of tandem reactions such as the one-pot production of cyclic carbonates starting directly from bio-based unsaturated fatty acids esters [8], the one-pot production of ethylene carbonate from ethylene produced by low-energy-demanding methods [2].

It is evident from the recently published results that both the possible utilization of CO₂ from flue gas and the carbonation of internal bio-based epoxides such as epoxidized fatty acid esters are the main developing areas of research focused on CO₂ capture and utilization. However, the mild reaction conditions and lower catalytic loading are still challenging for both the carboxylation of internal epoxide substrates such as epoxidized fatty acid esters as well as for the direct utilization of waste CO₂ from power plant flue gas.

Acknowledgement

This research was funded by Faculty of Chemical Technology, University of Pardubice, with the support of excellent research.

References

1. Artz, J.; Müller, T.E.; Thenert, K.: *Chem. Rev.* **2018**, *118*, 434–504.
2. Aresta, M.; Dibenedetto, A.; Angelini, A.: *Chem. Rev.* **2014**, *114*, 1709–1742.
3. Shaikh, R.R.; Pornpraprom, S.; D'Elia, V.: *ACS Catal.* **2018**, *8*, 419–450.
4. Cui, S.; Borgemenke, J.; Liu, Z.; Li, Y.: *J. CO₂ Util.* **2019**, *34*, 40–52.
5. Kiatkittipong, K. Green Pathway in Utilizing CO₂ via Cycloaddition Reaction with Epoxide-A Mini Review. *Processes* **2020**, *8*, 548–570.
6. Cahugule, A.A.; Tamboli, A.H.; Kim, H. Ionic liquid as a catalyst for utilization of carbon dioxide to production of linear and cyclic carbonate. *Fuel* **2017**, *200*, 316–332.
7. Darensbourg, D.J.: *Chem. Rev.* **2007**, *107*, 2388–2410.
8. Calmanti, R.; Sargentoni, N.; Selva, M.; Perosa, A.: *J. CO₂ Util.* **2021**, *11*, 1477.
9. Coates, G.W.; Moore, D.R.: *Angew. Chem. Int. Ed.* **2004**, *43*, 6618.
10. Weidlich, T.; Kamenicka, B.: *Catalysts* **2022**, *12*, 298.
11. Rehman, A.; Saleem, F.; Javed, F.; Ikhlaq, A.; Ahmad, S.W.; Harvey, A.: *Environ. Chem. Eng.* **2021**, *9*, 105113.
12. Guo, L.; Lamb, K.J.; North, M.: *Green Chem.* **2021**, *23*, 77–118.
13. Sakakura, T.; Choi, J.C.; Yasuda, H.: *Chem. Rev.* **2007**, *107*, 2365.
14. You, H.; Wang, E.; Cao, H.; Zhuo, C.; Liu, S.; Wang, X.; Wang, F.: *Angew. Chem. Int. Ed.* **2022**, *61*, e202113152.
15. Padelkova, Z.; Weidlich, T.; Cisarova, I.; Ruzicka, A. *Appl. Organometal. Chem.* **2009**, *23*, 253–257.
16. Lari, G.M.; Pastore, G.; Mondelli, C.; Pérez-Ramírez, J.: *Green Chem.* **2018**, *20*, 148–159.
17. Vitiello, R.; Tesser, R.; Santacesaria, E.; Di Serio, M.: *Ind. Eng. Chem. Res.* **2016**, *55*, 1484–1490.
18. Morodo, R.; Gerardy, R.; Petit, G.; Monbaliu, J.M.: *Green Chem.* **2019**, *21*, 4422–4433.
19. Kubicek, P.; Sladek, P.: U.S. Patent EP 1663924 B1, 23 August 2004.
20. Cespi, D.; Cucciniello, R.; Ricciardi, M.; Capacchione, C.; Vassura, I.; Passarini, F.; Proto, A.: *Green Chem.* **2016**, *18*, 4559–4570.
21. Phung, T.K.; Pham, T.L.M.; Vu, K.B.; Busca, G.: *J. Environ. Chem. Eng.* **2021**, *9*, 105673.
22. Lin, W.; Koichi, K.; Takuji, H.: *Catal. Sci. Technol.* **2016**, *6*, 3872–3877.
23. Arayachukiat, S.; Kongtes, C.; Barthel, A.; Vummaleti, S.V.C.; Poater, A.; Wannakao, S.; Cavallo, L.; D'Elia, V.: *ACS Sustain. Chem. Eng.* **2017**, *5*, 6392–6397.
24. Wang, L.; Lin, L.; Zhang, G.; Kodama, K.; Yasutake, M.; Hirose, T.: *Chem. Commun.* **2014**, *50*, 14813–14816.
25. Kaneko, S.; Shirakawa, S.: *ACS Sustain. Chem. Eng.* **2017**, *5*, 2836–2840.
26. Natongchai, W.; Pornpraprom, S.; D'Elia, V.: *Asian J. Org. Chem.* **2020**, *9*, 801–810.
27. Schäffner, B.; Blug, M.; Kruse, D.; Polyakov, M.; Köckritz, A.; Martin, A.; Rajagopalan, P.; Bentrup, U.; Brückner, A.; Jung, S.: *ChemSusChem* **2014**, *7*, 1133–1139.

PYRIDINIUM-BASED CATALYST FOR α -PINENE OXIDE ISOMERIZATION

Zítová K.¹, Bulavina V.¹, Vyskočilová E.¹

¹Department of Organic Technology, UCT Prague, Technická 5, 166 28, Prague 6, Czech Republic
katerina.zitova@vscht.cz

Abstract

Pyridinium-based material supported on MCM-41 were prepared as a heterogeneous catalysts for isomerization of α -pinene oxide. The desired products were campholenic aldehyde and *trans*-carveol. The influence of catalyst amount and the type of solvent on the reaction course was studied. The total conversion of α -pinene oxide was achieved using 5 wt.% of MCM-I-py with *N,N*-dimethylformamide within 3 hours of the reaction. Under these conditions the selectivity to *trans*-carveol reached 53% and the selectivity to campholenic aldehyde 29%. This study shows that MCM-I-py as a metal-free catalyst is suitable for the isomerization of α -pinene oxide.

Introduction

α -Pinene oxide is a widely used precursor for the synthesis of fragrances and flavors¹. This epoxide does not occur in nature, but can be easily prepared by oxidation of α -pinene – a biomass product². α -Pinene oxide can be converted to approximately 200 different compounds by acid-catalyzed transformations³. However, the most valuable products of its isomerization are campholenic aldehyde and *trans*-carveol (Figure 1). Campholenic aldehyde find its utilization especially in perfume and flavor industry as an aroma chemical but also as an intermediate for the preparation other important compounds like santanol (sandalwood fragrance)^{4,5}. *trans*-Carveol is also a desirable and expensive component in perfumes for its pleasant scent¹. The selectivity to campholenic aldehyde and *trans*-carveol can be affected by the reaction conditions, especially catalyst type and a type of solvent^{2,6}. α -Pinene oxide isomerization has been studied using a number of homogeneous and heterogeneous catalysts. However, the usage of heterogeneous catalysts has many advantages such as easy separation of the catalyst from the reaction mixture and the possibility of reuse. The most commonly described heterogeneous catalysts for this type of reaction are metal-modified zeolites^{2,4} and metal-modified silicates⁷. Other possibilities are supported ionic liquids⁸, acid-modified clays⁹, or metal-organic frameworks¹⁰. This work is focused on pyridinium-based materials as a metal-free catalysts. These materials were already discussed as catalysts for cycloaddition reactions¹¹, reduction of carbon dioxide to methanol¹² or synthesis of pyranopyrazole derivatives¹³.

Experimental

Materials

Pyridine (99.8%), 3-iodopropyltrimethoxysilane (95%), tetraethoxysilane (98%) and *N,N*-dimethylacetamide (DMA) (p.a.) were purchased from Sigma-Aldrich. Dichloromethane (p.a.) and toluene (p.a.) were obtained from Lach:ner. Ammonia (26% aqueous solution), hexadecyltrimethylammonium bromide (99%), *N,N*-dimethylformamide (DMF) (p.a.), cyclohexane (p.a.) and dimethylsulfoxide (DMSO) (p.a.) were purchased from Penta and α -pinene oxide (APO) (95%) was purchased from TCI. Demineralized water was taken from UCT Prague sources (< 1 μ S/mL).

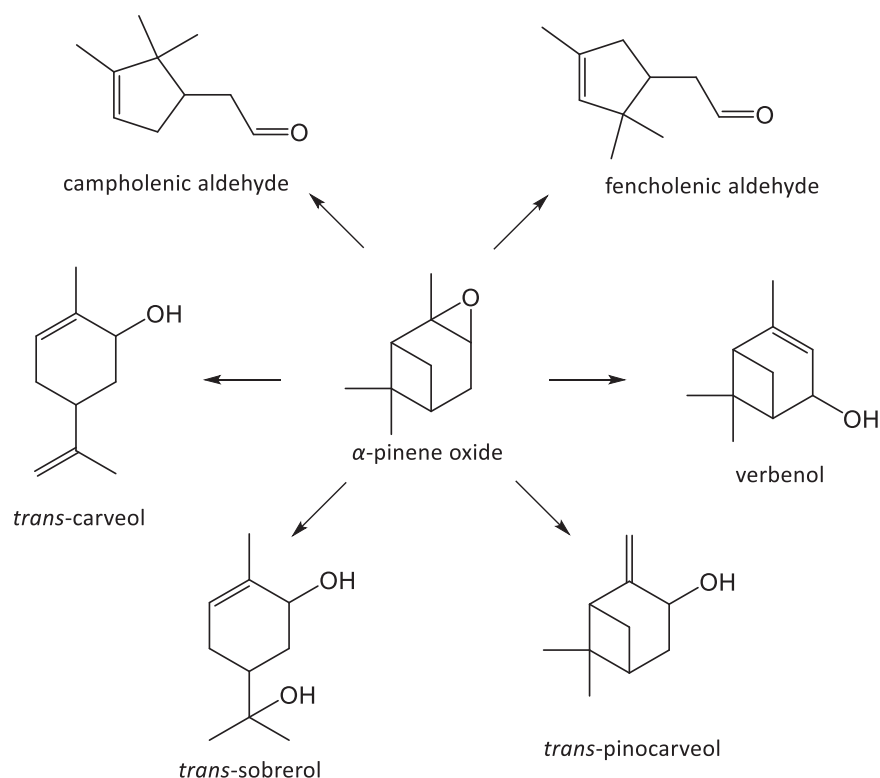


Figure 1. Products of isomerization of α -pinene oxide

Preparation of MCM-41

Support material MCM-41 was prepared following the standard procedure. First, 2.4 g of hexadecyltrimethylammonium bromide was dissolved in demineralized water (120 mL) preheated to 35 °C. After dissolution, 10 mL of 26% aqueous ammonia solution was added. After approximately 5 minutes, 10 mL of tetraethoxysilane was added and the resulting suspension was subsequently stirred for 24 hours at room temperature. After 24 hours the suspension was filtered and the solid was washed by demineralized water (3 x 10 mL), and ethanol (3 x 10 mL), and dried at 100 °C for 1 hour. This was followed by calcination at 550 °C under nitrogen atmosphere (2 h) and then in the air (18 h). Subsequently, the product was stirred in demineralized water for 20 h in order to increase the amount of hydroxyl groups. The solid was filtered and dried at 100 °C for 24 h.

Preparation of MCM-41 supported pyridinium iodide (MCM-I-py)

The surface modification of MCM-41 was performed by anchoring iodine in the form of 3-iodopropyltrimethoxysilane (Figure 2). First, 6 mmol of silane and 20 mL of toluene were mixed. Then 1 g of MCM-41 was added and the suspension was stirred under reflux (120 °C) for 2 h. The solid phase was filtered and washed with toluene (3 x 10 mL).

Subsequently, 1 g of modified MCM-41 was added to 10 mL of toluene and finally 4.2 mmol of pyridine was added to the flask. The suspension was stirred under the reflux (120 °C) for 24 hours. The final product (MCM-I-py) was filtered and washed by toluene (3 x 10 mL) and dichloromethane (3 x 10 mL).

Characterization of catalyst (MCM-I-py)

Elemental analysis (EA) (C,H,N) was performed using Elementar Vario EL Cube. The halogen content (I) was determined by the classic argentometric titration analysis modified for low sample loading. The presence of pyridinium ions was verified by FTIR, which was performed using Nicolet Magna IR 760 in the regime of DR. The samples were diluted by potassium bromide before analysis.

Isomerization of α -pinene oxide

α -Pinene oxide (APO) (5 mmol) was inserted into round bottom flask (25 mL) with 5 mL of solvent. Then, a catalyst (MCM-I-py) (5 wt.% based on the weight of APO) was added. The reaction mixture was heated to reflux and stirred. The samples taken in chosen intervals were analyzed by GC. Gas chromatograph Agilent equipped with FID and a non-polar column. The identification of the products was performed using GC/MS.

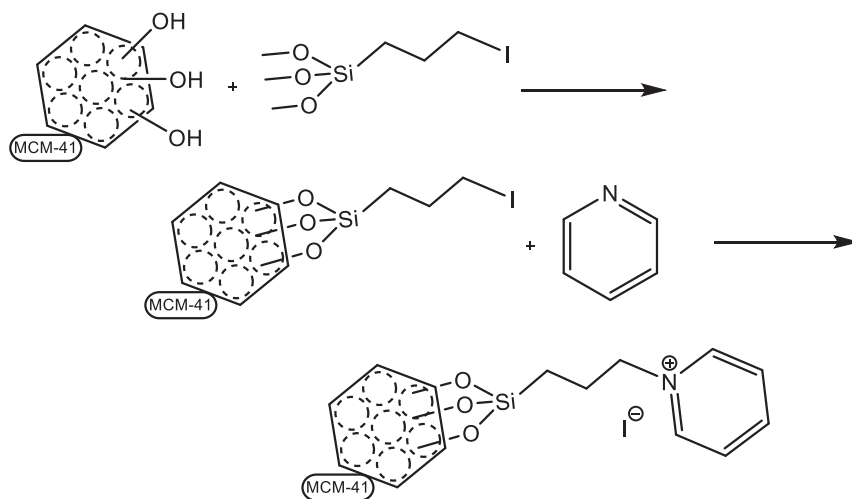


Figure 2. Preparation of catalyst MCM-I-py

Results and discussion

Characterization of catalyst

Elemental analysis confirmed the presence and the amount of halogen in the material and the amount of pyridine attached to the material after quaternization (Table I). The surface modification of MCM-41 was successful. We observed a slight decrease in the amount of C and H, which we explained by the elution the haloopropylsilane during the second preparation step. At the same time, we observed an increase in the amount of iodine supposing that iodine could remain in the structure in a form other than the ion.

Table I

The composition of prepared materials (in wt.%) from elemental analysis

Material	% C	% H	% N	% I
MCM-I	17.5	2.7	-	6.4
MCM-I-py	16.6	2.2	0.9	6.9

Isomerization of α -pinene oxide

The catalytic activity of the prepared material was verified in the isomerization of α -pinene oxide. The desired products were campholenic aldehyde and *trans*-carveol (Figure 1).

Influence of the catalyst amount

Firstly, the influence of the catalyst amount on reaction course was studied. For these experiments the amounts of 1, 5 and 10 wt.% of catalyst based on the amount of APO were tested. The conversion of APO increased as expected with the increasing amount of catalyst (Figure 3). Using 10 wt.% of catalyst the total conversion of APO

was achieved around 1 h of the reaction. In the case of 5 wt.% of catalyst the total conversion was achieved after 3 h of the reaction. The highest conversion of APO using 1 wt.% of catalyst was 17% after 5 h of the reaction. The initial reaction rate based on the weight of the catalyst increased in row $0.029 \text{ mmol}\cdot\text{mg}^{-1}\cdot\text{h}^{-1}$ (1 wt.%) < $0.087 \text{ mmol}\cdot\text{mg}^{-1}\cdot\text{h}^{-1}$ (10 wt.%) < $0.092 \text{ mmol}\cdot\text{mg}^{-1}\cdot\text{h}^{-1}$ (5 wt.%). The highest reaction rate was observed using 5 wt.% of catalyst. For this purpose, it was not desirable to increase the amount of catalyst to 10 wt.%. Dealing the selectivity, the catalyst amount did not significantly affected this parameter.

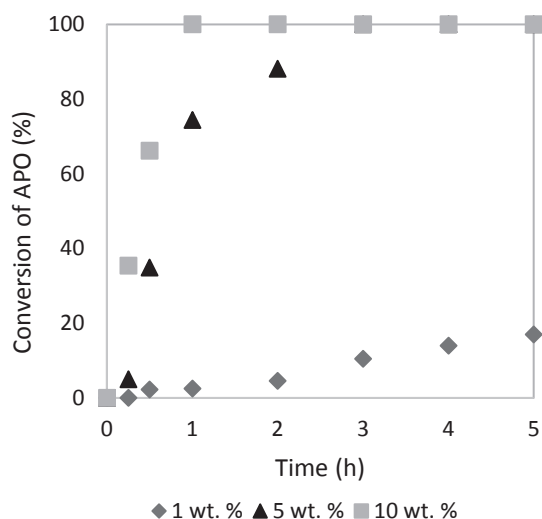


Figure 3. Dependence of conversion of APO on reaction time. Conditions: APO (5 mmol), catalyst: MCM-I-py (1, 5, 10 wt.%), solvent: DMA (5 mL), 140 °C.

Influence of the solvent type

The type of solvent can affect the reaction course of isomerization of α -pinene oxide, especially the selectivity. The selected solvents included non-polar solvents (cyclohexane, toluene) and polar aprotic solvents (DMF, DMA and DMSO). The polarity of the solvents was indicated by the dielectric constant (Table II). Another important property of solvent is basicity. The basicity was described by the donor number (Table II).

Table II
Properties of chosen solvents^{14,15}.

Solvent	Solvent type	Dielectric constant (-)	Donor number (kJ/mol)	Boiling point (°C)
Cyclohexane	Non-polar	2.0	0	81
Toluene	Non-polar	2.4	0.1	110
<i>N,N</i> -Dimethylformamide	Polar aprotic	36.7	26.6	152
<i>N,N</i> -Dimethylacetamide	Polar aprotic	37.8	27.8	165
Dimethylsulfoxide	Polar aprotic	46.7	29.8	189

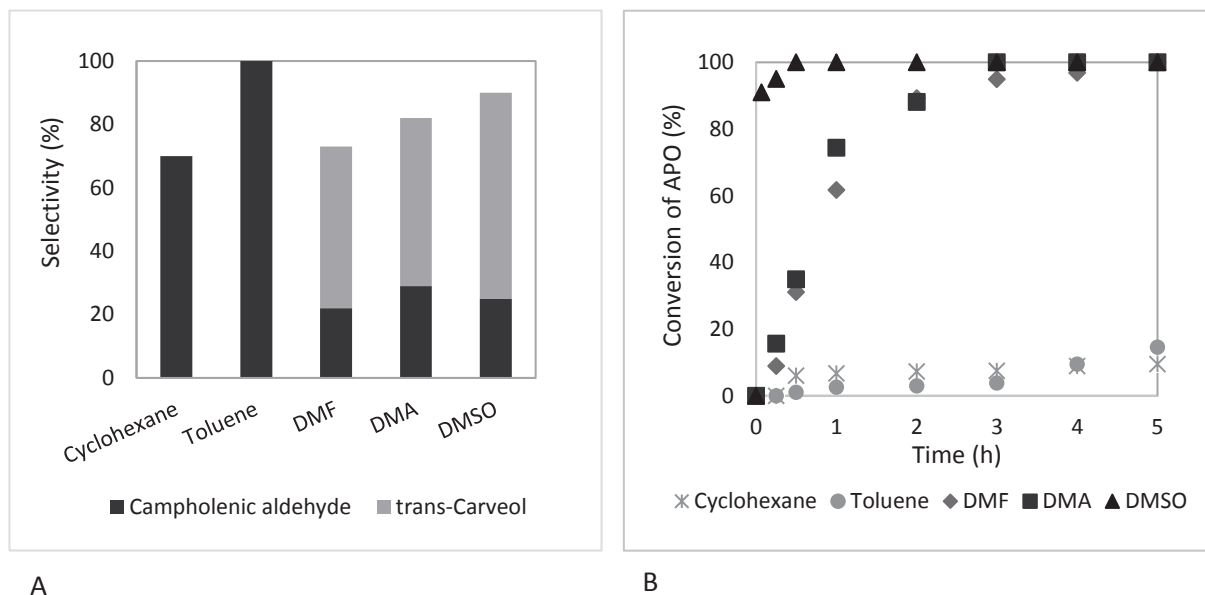


Figure 4. A: Selectivity to campholenic aldehyde and trans-carveol using different solvents, 5 h, B: Dependence of conversion of APO on reaction time. Conditions: APO (5 mmol), catalyst: MCM-I-py (5 wt.%), solvent (5 mL), reflux.

From the results of the experiments, it is obvious that the choice of solvent significantly affected the selectivity (Figure 4A). The more polar and basic solvent signified the higher selectivity to *trans*-carveol. Among the solvents with high basicity and polarity belonged DMF, DMA and DMSO. In their case, the selectivity to *trans*-carveol reached up to 65%. The selectivity to campholenic aldehyde was lower using these solvents. The formation of campholenic aldehyde was promoted using low polar or non-polar solvents with low basicity such as toluene and cyclohexane. However, in their case, the selectivity could be also affected by the low conversions of α -pinene oxide (Figure 4B). In addition to *trans*-carveol and campholenic aldehyde, pinocarveol and verbenol were also identified in the reaction mixture using DMF, DMA or DMSO as solvents. Figure 4B shows that solvent also affected the conversion of APO. The total conversion of APO was achieved in the reactions using DMF, DMA and DMSO as a basic polar aprotic solvents. The conversion of APO achieved using toluene and cyclohexane was 15% resp. 10% after 5 hours.

Conclusion

MCM-41 supported pyridinium iodide were successfully prepared in this work. The catalytic activity of this material was verified in isomerization of α -pinene oxide. The conversion of α -pinene oxide increased with the increasing amount of catalyst as expected. Nevertheless, the highest reaction rate was observed using 5 wt.% of MCM-I-py. It was confirmed that the polarity and basicity of solvent influenced the reaction course. The selectivity to *trans*-carveol and the reaction rate represented by the conversion of α -pinene oxide increased with increasing basicity and increasing polarity of the solvent. The combination of the ability of stabilize carbocation with the metal-free catalyst was efficient for the preferable formation of *trans*-carveol. The highest selectivity to *trans*-carveol (65%) was observed using 5 wt.% of MCM-I-py and dimethylsulfoxide as a solvent. Using dimethylsulfoxide the total conversion of α -pinene oxide was achieved within the first hour of reaction. The prepared catalyst, MCM-I-py, showed a good catalytic activity in this reaction, especially using basic polar solvents. This metal-free catalyst may present the possible alternative for the often described pinene oxide isomerization.

Acknowledgement

This work was supported from the grant of Specific university research - grant No A1_FCHT_2022_010. We also acknowledge grant project GACR 21-02183S.

References

1. Panchenko V. N., Kirillov V. L., Gerasimov E. Yu., Martyanov O. N., Timofeeva M. N.: *Reac. Kinet. Mech. Cat.*, **130**, 919 (2020).
2. Vrbková E., Vyskočilová E., Lhotka M., Červený L.: *Catalysts*, **10**, 1244 (2020).
3. Volcho K. P., Salakhutdinov N. F.: *Mini-Rev. Org. Chem.*, **5**, 345 (2008).
4. Mäki-Arvela P., Shcherban N., Lozachmeur Ch., Russo V., Wärnå J., Murzin D. Yu.: *Catal. Lett.*, **149**, 203 (2019).
5. da Silva Rocha K. A., Hoehne J. L., Gusevskaya E. V.: *Chem. Eur. J.*, **14**, 6166 (2008).
6. Vyskočilová E., Hašková L., Červený L.: *Chem. Pap.*, **73**, 1621 (2019).
7. Stekrova M., Kumar N., Aho A., Sinev I., Grünert W., Dahl J., Roine J., Arzumanov S. S., Mäki-Arvela P., Murzin D. Yu.: *Appl. Catal. A: Gen.*, **470**, 162 (2014).
8. Salminen E., Mäki-Arvela P., Virtanen P., Salmi T., Mikkola J.-P.: *Top. Catal.*, **57**, 1533 (2014).
9. Sidorenko A. Yu., Kravtsova A. V., Aho A., Heinmaa I., Kuznetsova T. F., Murzin D. Yu., Agabekov V. E.: *Mol. Catal.*, **448**, 18 (2018).
10. Dhakshinamoorthy A., Alvaro M., Chevreau H., Horcajada P., Devic T., Serre Ch., Garcia H.: *Catal. Sci. Technol.*, **2**, 324 (2012).
11. Vyskočilová E., Šafařík D., Zítová K., Vrbková E., Dimitrov R., Vagenknechtová A., Červený L.: *Catal. Lett.* (2022)
12. Barton Cole E. E., Baruch M. F., L'Esperance R. P., Kelly M. T., Lakkaraju P. S., Zeitler E. L., Bocarsly A. B.: *Top. Catal.*, **58**, 15 (2015).
13. Moosavi-Zare A. R., Zolfigol M. A., Salehi-Moratab R., Noroozizadeh E.: *J. Mol. Catal. A: Chem.*, **415**, 144 (2016).
14. Gutmann Acceptor and Donor number. Available online: <http://www.stenutz.eu/chem/solv21.php> (accessed on 15 June 2022).
15. Solvent Properties Chart. Available online: https://depts.washington.edu/eo optic/linkfiles/dielectric_chart%5B1%5D.pdf (accessed on 15 June 2022).

Paterová I.¹, Gorlova O.¹, Příbylová P.¹, Červený L.¹

¹Department of Organic Technology, UCT Prague, Prague, Czech Republic
iva.paterova@vscht.cz

Abstract

β -Pinene oxide (BPO) is a highly reactive molecule. Even under mild conditions, it can be transformed into several isomeric forms. The most important forms include myrtenol and myrtanal (M products group), and perillyl alcohol (P products group).

The Beta-type zeolite, β -38, modified by impregnation of CeO₂ on its surface, was tested as β -pinene oxide isomerization catalysts. The influence of CeO₂ amount impregnated on catalyst on the reaction course was tested. In addition, the effect of the chosen solvent, temperature and possible catalyst reuse was also studied. Under studied reaction conditions, the highest conversion of 90 % and selectivity of 83 % to P products was achieved in dimethylsulfoxide as a solvent with 10 wt. % of β -38 catalyst modified with 7 % of CeO₂.

Introduction

β -Pinene oxide (BPO) is one of the starting substances for the preparation of important components used mainly in the production of fine chemicals. By its rearrangement a large number of products can be obtained^{1,2}. Some emerging products can be divided into two groups - M and P products (**Figure 1**). M products include myrtenol and myrtanal. P products include perillyl alcohol, anthemol and isoperillyl alcohol. A formation of several byproducts, such as *p*-cymene, nopinone, *p*-menth-1-ene-7,8-diol and 1,3-*p*-menthadien-7-al, has been noted. These substances find their utilization in the chemical industry as well. Among the most important products used in the pharmaceutical industry belong myrtanal, which has antibacterial effect and also some fragrant properties³, myrtenol, with its anti-inflammatory and anxiolytic effects^{4, 5} and perillyl alcohol, which has antitumor properties and inhibits a number of carcinogens⁶. Isomerization of β -pinene oxide can be influenced by some reaction conditions, such as the chosen solvent, temperature, and, last but not least, the catalyst^{1,2}.

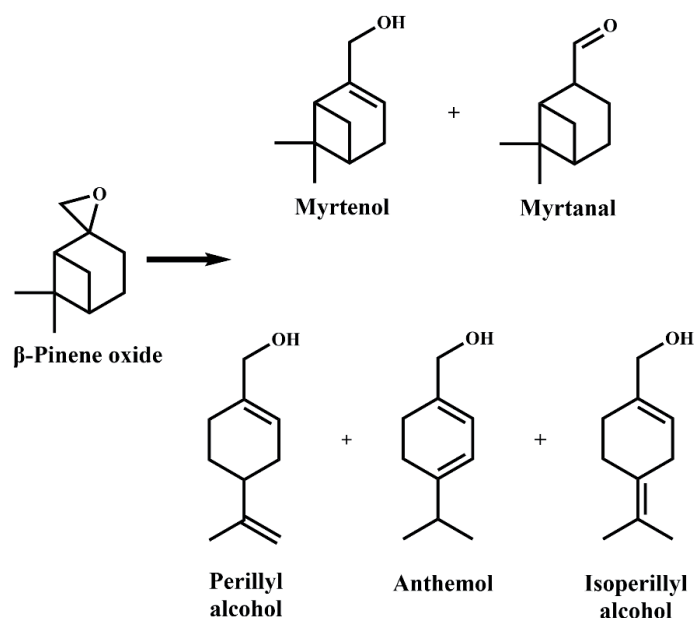


Figure 1. Formation of M and P products by BPO isomerization

Vyskočilová et al. described the solvent effect². In this work, the selectivity to perillyl alcohol depending on the selected solvents was tested. All solvents used belonged to the group of basic polar aprotic solvents. Suitable solvent choice helps to transfer protons from Brønsted's acidic surface sites to reactants, and Lewis sites can interact with polar molecules to form a proton.

A chosen solvent-catalyst combination played an important role in these experiments. A specific trend was observed; higher basicity of the selected solvent promoted the formation of perillyl alcohol and less basic solvent

favoured the formation of myrtanal. To form perillyl alcohol with high selectivity the use of dimethylsulfoxide (DMSO) as the solvent seemed to be the best choice. In DMSO, the reaction proceeded with a high reaction rate too. This fact is due to the highest basicity of DMSO of all selected solvents and is also supported by the stronger polar interaction of the DMSO oxygen atom with the metal occupied in the catalyst².

Both homogeneous and heterogeneous catalysts can be used for β -pinene oxide isomerization. ZnBr_2 ⁷ or *p*-toluene sulfonic acid⁸ can be used as a homogeneous catalyst. However, heterogeneous catalysts are more advantageous to use due to their easier separation and reuse. Heterogeneous catalysts include, for example, modified Beta zeolites⁹, USY², or MCM-41⁷. These are hexagonal mesoporous materials. Incorporating the metal into the structure increases the acidity of the catalyst. The activity of a material is affected by its properties, the type of metal incorporated, the acidity of the catalyst and the morphology of the metal oxide on its surface¹⁰.

The acidity of the catalyst is very important property. The resulting isomerization products are affected not only by the type of acid sites but also by its strength. When using a catalyst with Lewis acid sites (Sn-MCM-41), the main reaction product is myrtanal⁷. On the other hand, when catalysed by Brønsted acid sites, isomerization yielded mainly perillyl alcohol and myrtenol⁷. Especially for the second type, it is important to use weak acids. When catalysed by strong Brønsted acid, low conversions and mixtures containing many products were achieved⁷.

The preparation of myrtenol and myrtanal is described very often using many different types of catalysts containing Lewis acid sites, e.g. Sn-modified MCM-41⁷ or Zr-, Sn-, Ti-, Ta-, Nb-, Al- or Ge-modified zeolites⁹. The use of CeO_2 as Lewis acid or Ce-modified catalyst has not yet been described. We would like to present the results obtained with such a catalyst in combination with different solvents. Our findings could extend the knowledge about the studied reaction.

Experimental

Chemicals used

β -Pinene oxide (83%) was obtained from Aroma a.s. and was distilled before use to get purity of at least 96 %. All other chemicals were used as obtained from the producer. The unmodified zeolite β -38 catalyst was purchased from Zeolyst International. Cerium dioxide was prepared in the laboratories of the Institute of Chemical Technology in Prague. Cerium nitrate hexahydrate (99%) and *N,N'*-dimethylacetamide (DMA, p.a.) were obtained from Sigma-Aldrich. Other solvents, including acetonitrile (p.a.), dimethylsulfoxide (DMSO, p.a.), acetone (p.a.), toluene (p.a.), 1,4-dioxane (p.a.), *N,N*-dimethylformamide (DMF, p.a.), were purchased from Penta and used without other purification.

Modification of catalyst

Modification of zeolite β -38 was performed by impregnation with cerium dioxide using solution of cerium nitrate hexahydrate in water. Before impregnation, the zeolite was calcined in an air atmosphere at 450 °C for 6 hours. The mixture of calcined zeolite and cerium salt was stirred at 60 °C for 24 hours. The resulting modified catalyst was calcined at 450 °C. Thus, catalysts containing 1, 4, 7, and 15 wt. % of CeO_2 were prepared.

During recycling, the catalyst isolated from the reaction mixture was dried at 120 °C for 2 hours before the calcination.

Catalysts characterization

To determine the composition of catalysts ARL 9400 XP sequential WD-XRF spectrometer (Thermo ARL, Ecublens, Switzerland) equipped with an Rh anode end-window X-ray tube of type 4GN fitted with a 75 μm Be window was used to perform X-ray fluorescence analysis (XRF).

The measurement of the specific surface area was performed on a commercial Pulse Chemisorb 2700 instrument from Micromeritics. The specific surface area of catalysts was determined from the measured nitrogen physisorption data at three different partial pressures in the area of validity of the BET equation and a temperature of 77 K.

Acid properties were evaluated from temperature-programmed desorption (TPD) of pyridine using a Micromeritics Instrument, AutoChem II 2920. For desorbed pyridine detection both a thermal conductivity detector and quadrupole mass spectrometer (MKS Cirrus 2 Analyzer) with a capillary coupling system was used. Prior to the adsorption of pyridine, the catalyst was heated under a helium flow up to 450 °C and kept at this temperature for 60 min. Measured pulses of pyridine were injected into the helium gas and carried through the catalyst sample until adsorption saturation at 150 °C. Then the sample was purged with helium for 120 min to remove physisorbed pyridine. The linear temperature program (10 °C min^{-1}) was started, and the sample was heated up to a temperature of 700 °C. The amounts of desorbed pyridine were determined by calibration.

BPO isomerization

BPO isomerization was performed in a round bottom glass flask with a side sampling neck equipped with a reflux condenser and a magnetic stirrer. 5 ml of the solvent and 1 g of BPO were added to a flask. The mixture was stirred and warmed to the desired temperature. The reaction was started by adding 10 wt. % of catalyst. Samples of the reaction mixture were taken at regular intervals. The samples were analysed on a gas chromatograph (GC 2010 Shimadzu) equipped with FID and non-polar ZB-5 column (60 m, 0.32 mm diameter, 0.25 μm film).

Results and discussion

Characterization of prepared catalysts

Catalyst β -38 was modified according to the procedure described in the experimental part. The content of impregnated CeO_2 was determined by XRF analysis and corresponded to the desired amount (Table I). It can be seen from Table I that the impregnation of the increasing amount of CeO_2 on the surface of β -38 zeolite led to a decrease in the total surface area, probably by blocking the pores of the catalyst. A similar trend can be observed for the total acidity determined by TPD-pyridine; the amount of acid sites decreases significantly with increasing CeO_2 content. This is probably also due to blocking the acidic sites of zeolite beta, especially the strong ones.

Table I

XRF, TPD a S_{BET} analysis of prepared catalysts

wt.% CeO_2 + catalyst	CeO_2 (%)	S_{BET} (m^2/g)	Total acidity ($\mu\text{mol g}_{\text{cat}}^{-1}$)	Acid sites		Ratio of strong : weak acid sites
				Weak ($\mu\text{mol g}_{\text{cat}}^{-1}$)	Strong ($\mu\text{mol g}_{\text{cat}}^{-1}$)	
CeO_2	100	-	25*	25	0	0
β -38	0	710	479	186	292	1.6
1% β -38	1.3	552	374	155	219	1.4
4% β -38	4.1	530	336	189	147	0.8
7% β -38	6.9	479	346	166	180	1.1
15% β -38	14.6	422	281	152	129	0.9

* Only weak acid sites (T=260 $^{\circ}\text{C}$)

BPO isomerization

The following graph (Figure 2) shows the course of a typical BPO isomerization experiment. Of the products formed in the reaction mixture, myrtanal and perillyl alcohol were present in the largest amount. For both substances, a rise in the relative concentration at the beginning of the reaction was observed. Subsequently, the reaction rate expressed as the dependence of BPO conversion on time slowed down, the relative concentration of both products was around 20 %. BPO conversion of 56 % was achieved after 3 h of the reaction.

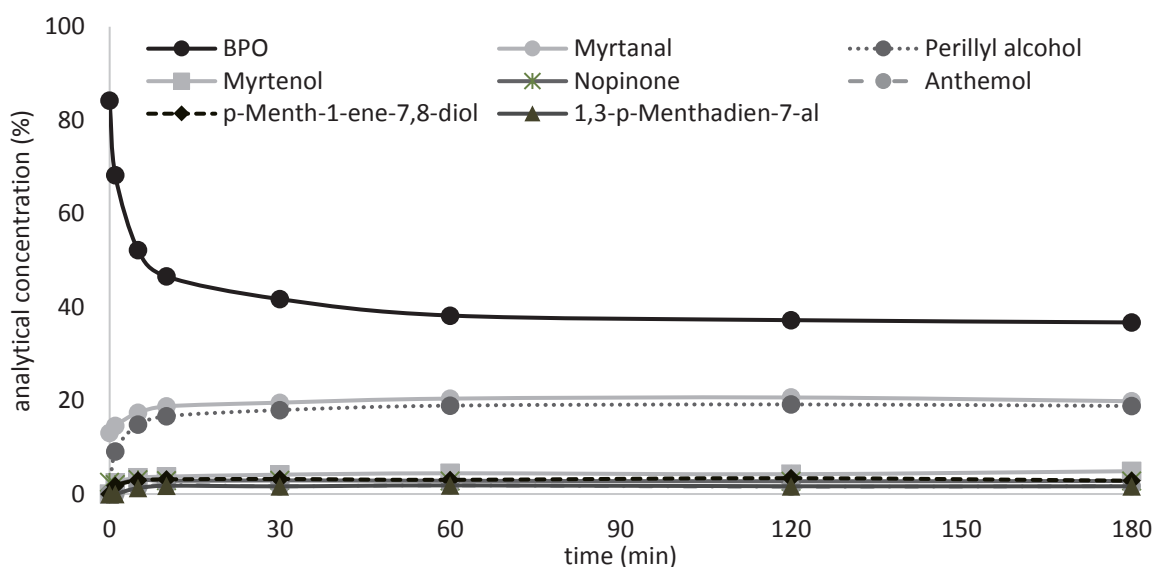


Figure 2. The course of a typical experiment. Reaction conditions: $m_{\beta\text{-pinene oxide}} = 1 \text{ g}$; $V_{1,4\text{-dioxane}} = 5 \text{ ml}$; catalyst (7 % CeO_2 β -38) = 10 wt. %; T = 70 $^{\circ}\text{C}$

The first parameter studied was the effect of temperature on BPO conversion and selectivity to M and P products. DMSO was chosen as the solvent. At low temperature (70 °C), data in **Table II** clearly show the low reaction rate expressed by the conversion (X) of BPO, even after one hour of the reaction conversion did not exceed 40 %. With increasing reaction temperature, a sharp increase in BPO conversion was observed at the beginning of the reaction. At the highest temperature (140 °C), the conversion raised to 90 % when the first sample was taken after 1 minute of reaction, and subsequently almost has not changed throughout the reaction.

Table II

Influence of reaction temperature. Reaction conditions: $m_{\beta\text{-pinene oxide}} = 1 \text{ g}$; $V_{\text{DMSO}} = 5 \text{ ml}$; catalyst (7 % CeO_2 $\beta\text{-38}$) = 10 wt. %; reflux; $t = 4 \text{ h}$

T (°C)	t = 1 min			t = 1 h		
	X (%)	S _P (%)	S _M (%)	X (%)	S _P (%)	S _M (%)
70	5.7	40.2	45.6	39.1	54.1	31.7
110	39.5	47.6	25.2	76.7	52.3	24.8
130	66.4	57.2	19.4	79.0	58.0	13.9
140	90.8	83.8	3.0	89.6	86.4	0

It can be seen from **Table II** that at the beginning of the reaction at 70 °C the selectivity to the M and P products was approximately the same, but over time the ratio of P to M products changed in favour of P products. With increasing temperature, an increase in selectivity to P products compared to M products can be observed, and this ratio has not changed much during the reaction. These results are in good agreement with data presented by Vyskocilova et.al² as the presence of DMSO rather contributes to perillyl alcohol formation.

It is known from the literature^{1,2} that the chosen solvent has a significant effect on the course of isomerization. Individual solvents were characterized in terms of polarity expressed by relative permittivity (ϵ_R), Lewis basicity expressed by donor number (DN) and acidity expressed by the negative decadic logarithm of pKa (**Table III**).

Table III

Influence of solvent type. Reaction conditions: $m_{\beta\text{-pinene oxide}} = 1 \text{ g}$; $V_{\text{solvent}} = 5 \text{ ml}$; catalyst (7 % CeO_2 $\beta\text{-38}$) = 10 wt. %; reflux; $t = 4 \text{ h}$

Solvent	ϵ_R (-)	pKa (-)	DN (kJ mol ⁻¹)	X (%)	S _P (%)	S _M (%)
Toluene	2.4	40.9	0.4	34.8	29.4	45.5
Acetonitrile	37.5	25.0	59.0	18.7	9.2	65.9
1,4-Dioxane	2.2	-3.9	62.0	51.6	40.3	28.2
Acetone	20.7	19.3	71.0	52.1	38.8	4.3
DMF	36.7	-0.3	111.0	31.6	92.9	0
DMA	37.8	10.7	116.0	47.5	57.1	2.5
DMSO	46.7	35.0	125.0	89.7	88.5	0

The lowest conversion was achieved in acetonitrile, only 19 %. In the case of acetonitrile and toluene, the reaction proceeded more selectively to M products; using other solvents, formation of P products has been preferred.

The relationship between any of the above solvent properties and the achieved conversion and selectivity was sought. Except for the results obtained in acetonitrile, it can be concluded that with increasing basicity, there was observed an increase in selectivity to P products and a decrease in selectivity to M products. Although low BPO conversion was achieved in acetonitrile; the highest selectivity to M products was noticed.

To determine the effect of the amount of CeO_2 impregnated on the $\beta\text{-38}$ zeolite support, BPO isomerization was performed in 3 selected solvents: acetonitrile, DMSO, and 1,4-dioxane.

Acetonitrile was chosen because it was the only solvent in which were formed almost only M products. It can be seen from **Table IV** that the highest values of selectivity to M products (98 %) were achieved using CeO_2 itself. However, after one hour of reaction, the conversion did not exceed 13 %. The reaction performed in the presence of unmodified $\beta\text{-38}$ with a similar conversion showed a decrease in selectivity to M products of up to 70 %. Modification of zeolite by only 1 wt. % of CeO_2 showed very similar results with unmodified $\beta\text{-38}$. Increasing the content of CeO_2 impregnated on the zeolite support led to a decrease in BPO conversion but growth in selectivity to M products. It can be related to the decrease of strong acid site amount in the catalysts (**Table I**). The positive

effect of weak Lewis acid such as CeO₂ in combination with acetonitrile as the solvent on selectivity do M products has been unambiguously confirmed.

Table IV

Influence of catalysts. Reaction conditions: $m_{\beta\text{-pinene oxide}} = 1 \text{ g}$; $V_{\text{solvent}} = 5 \text{ ml}$; catalyst = 10 wt. %; $T = 70 \text{ }^\circ\text{C}$ (in acetonitrile and 1,4-dioxane) and $140 \text{ }^\circ\text{C}$ (in DMSO); $t = 1 \text{ h}$

Catalyst	Acetonitrile			DMSO			1,4-Dioxane		
	X (%)	S _P (%)	S _M (%)	X (%)	S _P (%)	S _M (%)	X (%)	S _P (%)	S _M (%)
CeO ₂	12.5	0	98.4	88.1	85.1	1.3	4.8	76.4	0
$\beta\text{-38}$	16.8	10.1	69.6	86.9	87.1	0	51.9	41.9	25.6
1% $\beta\text{-38}$	15.2	11.1	68.0	88.0	86.1	0.2	58.7	41.0	17.4
4% $\beta\text{-38}$	-	-	-	-	-	-	57.2	41.6	19.7
7% $\beta\text{-38}$	11.8	11.0	75.3	87.6	86.4	0	54.7	41.0	21.6
15% $\beta\text{-38}$	-	-	-	-	-	-	50.6	39.0	20.6

It was evident from **Table III** that the highest values of BPO conversion and very high values of selectivity to P products were achieved in DMSO as solvent. It can be seen from **Table IV** that using both CeO₂ and zeolite $\beta\text{-38}$, modified and unmodified, the values of both BPO conversion and selectivity to P products were almost the same. The presence of M products was almost not recorded. From this it can be concluded that neither the acidity of the catalyst nor the amount of impregnated CeO₂ has a significant effect on the course of the reaction compared to the strong influence of DMSO as the used solvent.

Both M and P products were formed in 1,4-dioxane and toluene, but due to higher conversion values, 1,4-dioxane was chosen as an another solvent to compare the effect of the amount of CeO₂ impregnated on the zeolite support. It can be seen from **Table IV** that in the presence of CeO₂ itself, the isomerization of BPO in 1,4-dioxane proceeded selectively to M products but with conversion lower than 5 %. However, impregnation of a small amount of CeO₂ (up to 7 wt. %) on zeolite $\beta\text{-38}$ led to a slight increase in the conversion values above the value obtained when using unmodified zeolite. The selectivity to P products was not affected by the amount of CeO₂. As M products were not formed when catalysed by CeO₂, the decrease in their selectivity compared to unmodified zeolite can be attributed to the presence of CeO₂.

Finally, the possibility of reusing the catalyst was assessed. Zeolite $\beta\text{-38}$ modified by 1 wt. % of CeO₂ was used for such an experiment. Reactions were performed in 1,4-dioxane at 70 °C. After the termination of the reaction, the catalyst was filtered, washed, dried, and finally calcined at 450 °C.

As can be seen from **Table V**, there was no loss of catalytic activity in either cycle 2 or 3. In addition, a slight increase in the reaction rate expressed by conversion over time at the beginning of the reaction compared to the 1st reaction cycle was observed in both solvents. It was considered whether the slight increase in reaction rate was due to the release of CeO₂ from the impregnated catalyst. However, this assumption was disproved by XRF analysis of the sample after 3 reaction cycles.

Table V

Recycling of catalyst. Reaction conditions: $m_{\beta\text{-pinene oxide}} = 1 \text{ g}$; $V_{\text{solvent}} = 5 \text{ ml}$; catalyst (1 % CeO₂ $\beta\text{-38}$) = 10 wt. %; $T = 70 \text{ }^\circ\text{C}$

	Cycle	10 min			180 min		
		X (%)	S _P (%)	S _M (%)	X (%)	S _P (%)	S _M (%)
1,4-Dioxane	1.	27.9	48.3	21.9	47.3	41.3	24.4
	2.	40.1	43.7	32.7	52.3	40.7	29.7
	3.	36.8	46.5	28.9	50.6	40.2	28.4

After the 2nd and 3rd reaction cycles, after 3 hours, the selectivity to M and P products remained unchanged. Based on the results obtained, it can be concluded that the $\beta\text{-38}$ catalyst modified with CeO₂ is reusable and can be used at least 3 times without loss of activity.

Conclusions

This work was focused on the isomerization of β -pinene oxide, a very reactive molecule that can be converted into many isomeric forms. The most important forms are myrtenol, myrtanal and perillyl alcohol.

The studied parameters of BPO isomerization were temperature, type of solvent, amount of CeO₂ impregnated on the zeolite support, and also the possibility of reusing the catalyst.

The chosen solvent combined with the catalyst had the most significant effect on the selectivity to M and P products. With increasing solvent basicity, BPO conversion and selectivity to P products increased, and selectivity to M products decreased.

For acetonitrile, a slightly positive effect of increasing selectivity to M products with increasing CeO₂ content can be observed. In DMSO, similar results were obtained using both CeO₂ itself and modified or unmodified zeolite β -38. However, the positive influence of CeO₂ content on M products selectivity was found out in acetonitrile as the solvent.

The possibility of reusing the β -38 catalyst with 1 wt. % of CeO₂ in 1,4-dioxane was studied. In general, it has been found that reuse is possible without loss of catalyst activity in terms of conversion, and the selectivity to both M and P products remained unchanged.

Under studied reaction conditions, the highest conversion of 90 % and selectivity of 83 % to P products was achieved in DMSO as a solvent with 10 wt. % of β -38 catalyst modified with 7 % of CeO₂.

Acknowledgement

This work was supported from the grant of Specific university research – grant No A1_FCCHT_2022_010

References

1. Vyskocilova, E., Sekerova, L., Vrbkova, E., Paterova, I., Trejbal, J., Cervený, L., *Solvent Effects in Biomass Processing: α - and β -Pinene Oxide Rearrangements*. Nova Science Publishers: New York, 2020.
2. Vyskočilová, E.; Malý, M.; Aho, A.; Krupka, J.; Červený, L., The solvent effect in β -pinene oxide rearrangement. *Reaction Kinetics, Mechanisms and Catalysis* **2016**, *118*.
3. Mäki-Arvela, P.; Kumar, N.; Diáz, S. F.; Aho, A.; Tenho, M.; Salonen, J.; Leino, A.-R.; Kordás, K.; Laukkanen, P.; Dahl, J.; Sinev, I.; Salmi, T.; Murzin, D. Y., Isomerization of β -pinene oxide over Sn-modified zeolites. *Journal of Molecular Catalysis A: Chemical* **2013**, *366*, 228-237.
4. Gomes, B. S.; Neto, B. P. S.; Lopes, E. M.; Cunha, F. V. M.; Araújo, A. R.; Wanderley, C. W. S.; Wong, D. V. T.; Júnior, R. C. P. L.; Ribeiro, R. A.; Sousa, D. P.; Venes R Medeiros, J.; Oliveira, R. C. M.; Oliveira, F. A., Anti-inflammatory effect of the monoterpene myrtenol is dependent on the direct modulation of neutrophil migration and oxidative stress. *Chemico-Biological Interactions* **2017**, *273*, 73-81.
5. Moreira, M. R. C.; Salvadori, M. G. d. S. S.; de Almeida, A. A. C.; de Sousa, D. P.; Jordán, J.; Satyal, P.; de Freitas, R. M.; de Almeida, R. N., Anxiolytic-like effects and mechanism of (-)-myrtenol: A monoterpene alcohol. *Neuroscience Letters* **2014**, *579*, 119-124.
6. Jung YA, R. K., Separation of perillyl alcohol from korean orange peel by solvent extraction and chromatography. *Korean Journal of Chemical Engineering* **1998**, *15* (5), 538-543.
7. Corma, A.; Renz, M.; Susarte, M., Transformation of Biomass Products into Fine Chemicals Catalyzed by Solid Lewis- and Brønsted-acids. *Topics in Catalysis* **2009**, *52* (9), 1182-1189.
8. Carr, G.; Dosanjh, G.; Millar, A. P.; Whittaker, D., Ring opening of α -pinene epoxide. *Journal of the Chemical Society, Perkin Transactions 2* **1994**, (7), 1419-1422.
9. de la Torre, O.; Renz, M.; Corma, A., Biomass to chemicals: Rearrangement of β -pinene epoxide into myrtanal with well-defined single-site substituted molecular sieves as reusable solid Lewis-acid catalysts. *Applied Catalysis A: General* **2010**, *380* (1), 165-171.
10. Sánchez-Velandia, J. E.; Villa, A. L., Isomerization of α - and β - pinene epoxides over Fe or Cu supported MCM-41 and SBA-15 materials. *Applied Catalysis A: General* **2019**, *580*, 17-27.

Reduced sensitivity RDX and HMX crystallized and spheriodized in propylene carbonate

Radovan Skácel, Jan Šabach, Markéta Zikmundová, Veronika Kožená,
Martin Kubíček, Ondřej Fryš

Explosia a.s., VÚPCH, Pardubice, Czech Republic

radovan.skacel@explosia.cz

Abstract:

Propylene carbonate is eco-friendly solvent usable for high explosive crystallization. This solvent is possible to use in closed loop without distillation necessity, saving energy for solvent recovery. Energetic materials were crystallized from propylene carbonate solutions with the help of fatty acids. From tested additives, stearic acid causes formation of more spherical and less defect crystal materials. Obtained reduced sensitivity RDX was less impact sensitive in comparison with starting material (7.5 J, 15 J resp.) and also less friction sensitive (110 N starting RDX, 160 N crystallized). HMX and RDX crystals were then spheriodized in propylene carbonate suspension at a constant temperature for 2-4 hours. Final spherical or oval-shaped crystal materials were submitted to GAP test and mechanical sensitivity tests.

Keywords: RDX; HMX; propylene carbonate; sensitivity; spherical.

1 Introduction

Propylene carbonate is today low price (approx. 1.4-1.7 Euro / kg in EU in 2020), low volatile solvent. This compound does not form combustible vapors up to a temperature of 130° C. In the US, propylene carbonate is not regulated as a volatile organic compound (VOC) because it does not contribute significantly to the formation of smog and because its vapor is not known or suspected to cause cancer or other toxic effects. In some cases, propylene carbonate can be used as a replacement of acetone, cyclohexanone, DMF, DMSO or N-methylpyrrolidone.

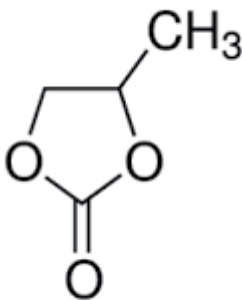


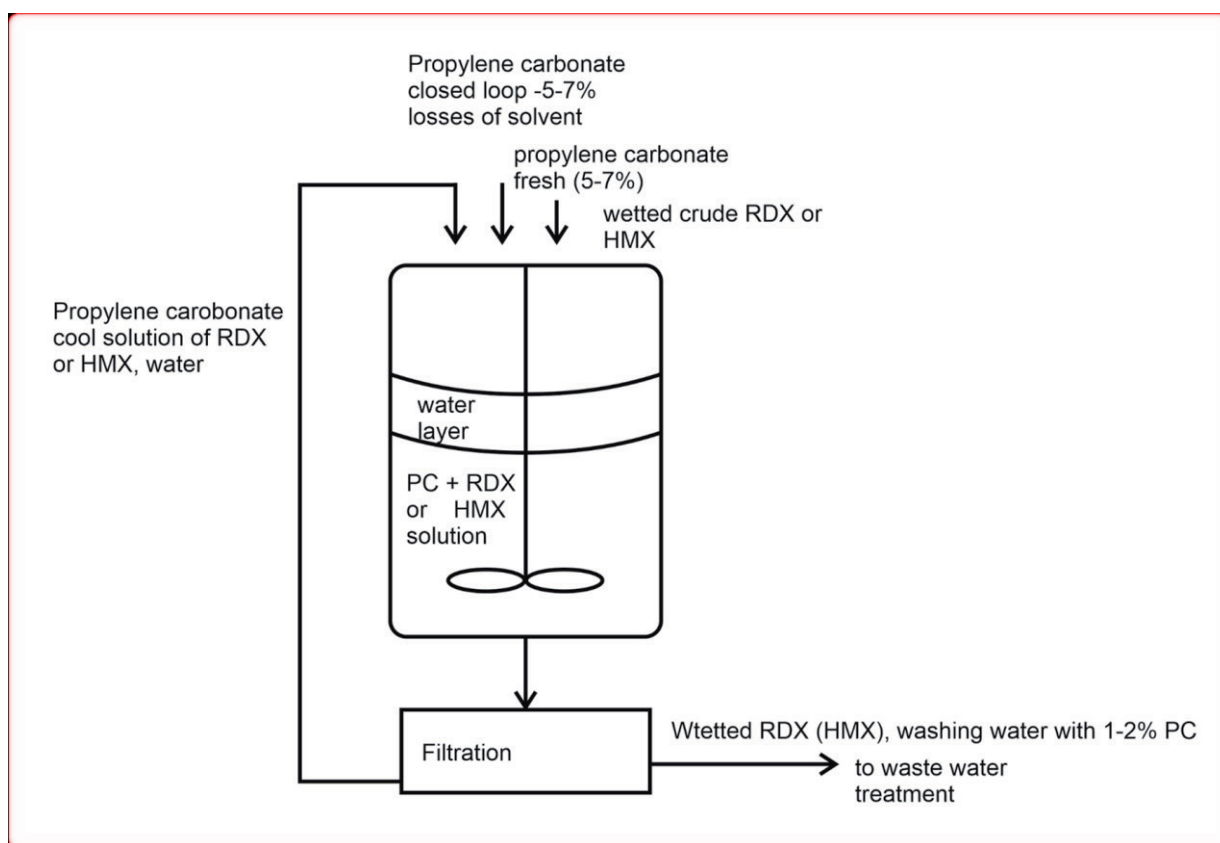
Figure 1: Propylene carbonate molecule

Propylene carbonate is used as a polar, aprotic solvent. It has a high molecular dipole moment (4.9 D), considerably higher than those of acetone (2.91 D) and ethyl acetate (1.78 D). It is possible, for example, to obtain potassium, sodium, and other alkali metals by electrolysis of their chlorides and other salts dissolved in propylene carbonate.

Advantage of this compound for explosive crystallization processes is only partial solubility in water (approx. 20% in water, 7% water in propylene carbonate). When wet material is added to a solution in many cycles, water forms individual layer and can be separated. At the final, solution can be used many times without regeneration of the solvent (more than 30 times). This allows low energy consumption and relatively green nature of the process.

In the previous work was described one step method for preparation of reduced sensitivity RDX by the help of stearic acid. Stearic acid probably decreases nucleation rate of acetone- RDX crystallization system. Produced materials contained lower amount of small and defect crystals. Obtained crystals of RDX are more spherical shaped and contained lower amount of inner defects. Produced material had comparable parameters with classical produced RS-RDX of Eurenco (year 2000). Decrease of nucleation rate is published for improvement of crystal quality of energetic materials [1,2].

Kröber and Teipel [12] described crystallization of HMX from propylene carbonate: In this study HMX was recrystallized from different solvents by a cooling crystallization process to improve the product quality and to produce a more insensitive product. It was found that particles with the best quality were crystallized from propylene carbonate with a nucleation initiation by dosing a small amount of water as drowning-out substance. This leads to particles with a very high density (near to the theoretical value) and thus to particles with a small amount of inclusions. GAP tests with this product show less sensitivity against shock.



2 Experimental

2.1.1. Crystallization of RDX

300 g of crude wet RDX (SH process) was added to 600 ml of propylene carbonate by stirring and heating, in baffled apparatus. After complete dissolution of crystals (99°C), 2.5 grams of

crystallization additive stearic acid) was introduced and solution was cooled to 25°C (cooling rate approx. 2°C/min). In certain cases addition of 50 ml of water was tested during cooling. Obtained crystal product was filtered off, washed with water and dried.

2.1.2. Spheriodization of RDX

300 g of crystalized RDX was added to 300 ml of propylene carbonate and 100 ml of water by stirring and heating, in baffled apparatus. Temperature was maintained ($99^{\circ}\text{C} \pm 1^{\circ}\text{C}$), for 2-4 hours (emulsion with crystals slightly boiled) and solution was cooled to 25°C (cooling rate approx. 2°C/min).

2.1.3. Crystallization of HMX

140 g of HMX was added to 400 ml of propylene carbonate, containing 10% of water by stirring and heating. After complete dissolution of crystals ($99\text{-}102^{\circ}\text{C}$), 1.3-2.6 grams of crystallization additive (mainly stearic acid) was introduced and solution was cooled to 25°C. Obtained crystal product was filtered off, washed with water and dried.

2.1.4. Spheriodization of HMX

300 g of crystalized HMX was added to 400 ml of propylene carbonate by stirring and heating, in baffled apparatus. Temperature was maintained ($120^{\circ}\text{C} \pm 1^{\circ}\text{C}$), for 2-4 hours and solution was cooled to 25°C (cooling rate approx. 2°C/min).

3. Results

For GAP test, RDX and dental wax was melted 70/30 w/w ratio, for small-scale GAP test.

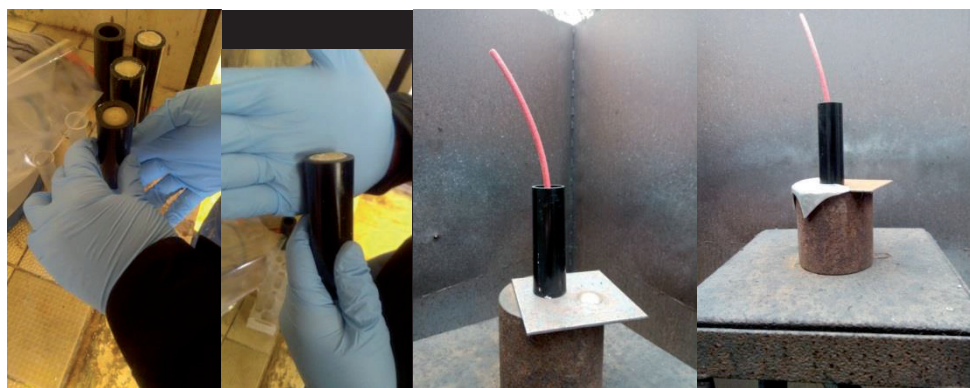


Figure 2: Instalation of „small“ GAP test

Impact and friction sensitivity was measured for clean compounds, GAP test for RDX/wax melt-casted composition:

Sensitivity of RDX (impact, friction, GAP test)				
Sample (solvent)	Impact E 50 [J]	Friction F 50 [N]	residual stearic acid	GAP test [mm]
RDX (acetone)	9.1	94.6	-	7.38
RDX (propylene carbonate)	11.5	108.4	-	-
RDX (propylene carbonate + stearic acid*)	15.2	176.6	0.18 %	5.50
RDX (propylene carbonate + stearic acid, spheriodized*)	12.4	106.6	0.06 %	5.80
RS-RDX (Dyno Nobel)	10.5	110.0	-	5.88
FOX-7	20 (lit.)	>350	-	3.60

Table 1: RDX sensitivity parameters, solution from PC contained 2% of stearic acid/RDX.

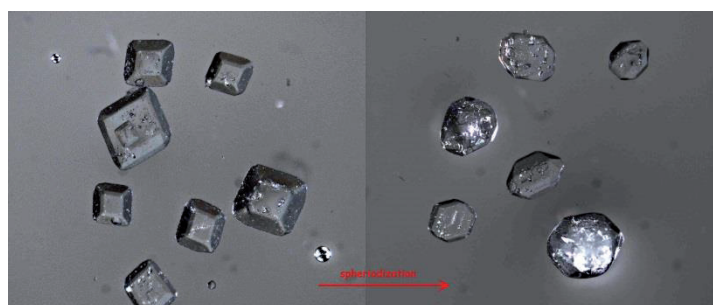


Figure 3: Crystals of RDX after 2 hours of spheriodization in PC/water emulsion, 99°C approx. middle of a process).



Figure 4: Crystals of RDX from PC solvent by cooling crystallization with the help of stearic acid and oleic acid (1+1%/RDX). Crystals were extremely clear.

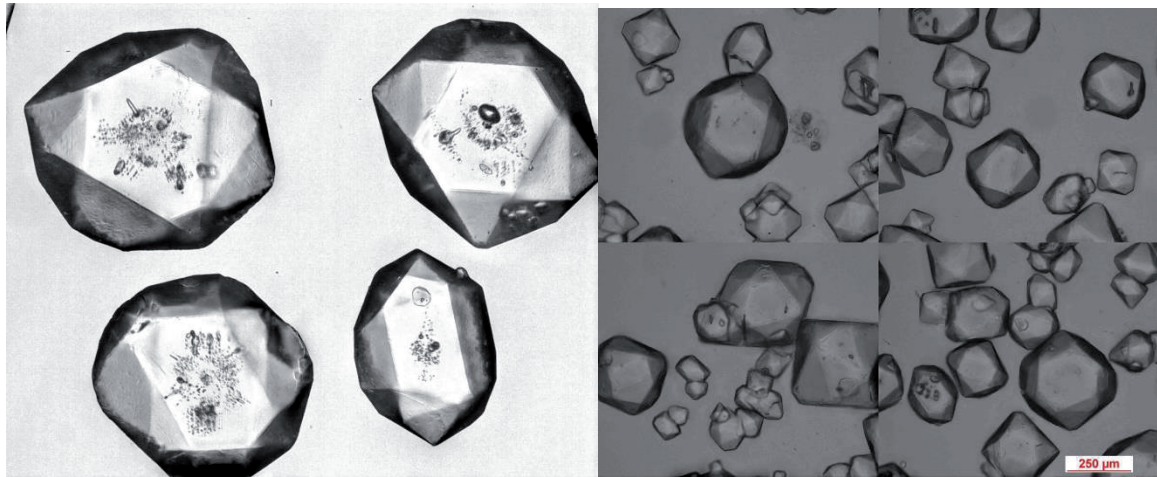


Figure 5: Crystals of RDX from PC solvent by cooling crystallization with the help of surfactant – causing formation of internal defects and without surfactants (right).

Sensitivity of HMX (impact, friction, GAP test)

	Impact E 50 [J]	Friction F 50 [N]	residual stearic acid	GAP test [mm]
HMX (acetone)	8.7	101.1	-	-
HMX (propylene carbonate)	8.7	125.7	-	5.9
HMX (propylene carbonate + stearic acid*)	8.9	164.7	0.11 %	5.6
HMX (propylene carbonate + stearic acid*, spheroidized)	7.9	122.5	0.05 %	5.4

Table 2: HMX crystal materials sensitivity parameters, solution from PC contained 1-2% of stearic-oleic acid/HMX. GAP test corresponds to HMX/wax 70/30.



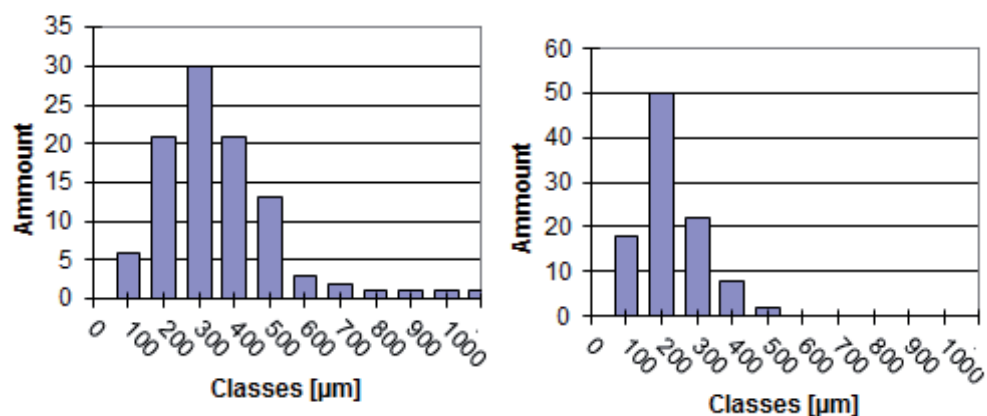


Figure 6: Crystals of HMX from PC solvent by cooling crystallization, with a fatty acid (left) and without (right).

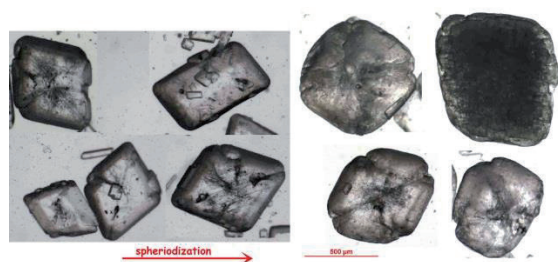


Figure 7: Crystals of HMX from PC before spheriodization (left) and after spheriodization process, 120°C, 150 min. (right). Crystals were spheriodized only partially.

Conclusion

Propylene carbonate was tested as a replacement of acetone and cyclohexanone for spherical RS-RDX and HMX production. It is a promising solvent for big scale applications in explosive industry. It is a low price (1.4-1.7 Euro/kg) and not flammable solvent up to a temperature of 130°C. Solutions can be use more than 50 times (Explosia a.s use this solvent for RDX treatment and isolation energetics from ammunition in pilot plant).

It is also green solvent from the viewpoint of energy saving, because no distillation is necessary and solvent can be use more than a year without purification.

Fatty acids are useful crystallization additives for production of different sizes of crystal fractions, also help to obtain low-sensitive products.

Without fatty acids, obtained HMX crystals ranges between 0.1-0.3 mm, with 1-2% mixture of oleic and stearic acid 0.2-0.5 mm crystals can be obtained. Residual fatty acids in crystals (0.05-0.2%) does not affect stability of RDX or HMX products.

Spheriodization process was most effective when a water-propylencarbonate emulsion is used (1/1-1/3 w/w) at a temperature of $99 \pm 1^\circ\text{C}$, in the case of RDX.

Obtained materials have bulk density $1.195 \text{ g}\cdot\text{cm}^{-3}$ in the case of RDX and $1.085 \text{ g}\cdot\text{cm}^{-3}$ for HMX. HMX shape is necessary to improve by some additives or process leading.

Crystals obtained from propylene carbonate contain low amount of internal defects. Next improvement of safety parameters can bring stearic or oleic acid. Another waxy compound do not have a same effect. Probably is important amphiphilic nature of SA or hydrogen bonding between SA and nitro group of energetic material.

Safer RDX on the level of reduced sensitivity RDX can be easily obtained. Crystals of RDX are uniform and better shaped than from acetone solvent.

References

- [1] R. Skácel, M. Zikmundová, K. Dudek, Influence of polyacrylamide and stearic acid on crystal growth of RDX Part II: Sensitivity testing of RDX in Composition B, *New trends in research of energetic Materials*, Pardubice, Czech republic, **2017**
- [2] J.W. Kim, J.S. Park, H.S. Kim, K.K. Koo., Effect of PVP On Nucleation and Crystal Growth of RDX, *2012 Annual Meeting of AIChE*, **2012**.
- [3] US patent No. 8,747,581 B2, **2014**.
- [4] R. Skácel, L. Říha, K. Dudek, R. Špásová, High bulk density bicyclo-HMX and RDX crystal materials for use in plastic explosives, PBX and propellants, *New trends in research of energetic Materials*, Pardubice, Czech republic, **2013**.
- [5] W. X. Yuan, Study on Recrystallization Process for Spheroidization of PETN, *Master's thesis*, University of North, **2009**.
- [6] J. Nývlt, *Kryštalizácia z roztokov*, (pg.76), Slovenské vydavateľstvo technickej literatúry v Bratislave, 160 pg., **1967**.
- [7] D. McRee, *Practical Protein Crystallography*. San Diego: Academic Press. pp. 1–23. ISBN 978-0-12-486052-0, **1993**.
- [8] "Recommendations on the Transport of Dangerous Goods, Manual of Tests and Criteria", Fifth revised edition, United Nations, New York and Geneva, (ST/SG/AC.10/11/Rev.5) (Test 3(a)(ii): BAM Fallhammer), **2009**.
- [9] D.Y.Kim, K.J.Kim, Semi-quantitative Study on the Inclusion in Cooling Crystallization of RDX Using Various Solvents, *Propellants, explosives and Pyrotechnics*, 35,38-45, **2010**.
- [10] R. Skácel, M. Vontorčíková, K. Dudek, Influence of polyacrylamide and stearic acid on crystal growth of RDX, *New trends in research of energetic Materials*, Pardubice, Czech republic, **2016**.
- [11] ČSN EN 13631-3 "Stanovení citlivosti výbušin ke tření".
- [12] R. Skácel, M. Zikmundová, V. Kožená, O. Fryš, M. Kubíček, Reduced sensitivity RDX, HMX and PETN crystallized from propylene carbonate in a presence of stearic acid, *New trends in research of energetic Materials*, Pardubice, Czech republic, **2019**.
- [13] Kröber H., Tiepel U., Leisinger K., Krause H., Formation of HMX Crystals with High Internal Quality by Cooling Crystallization, *29th International Annual Conference of ICT*, Karlsruhe, 30th June – 2nd July, 66.1- 66.18, **1998**.

STUDY OF SPECIFIC PROPERTIES OF COBALT CATALYST FOR APPLYING IN A NEW LARGE-SCALE CAPACITY UNIT FOR THE CYCLOHEXYLAMINE PRODUCTION

Valeš R., Krupka J.

*University of Chemistry and Technology in Prague, Department of Organic Technology, Technická 5, Prague 6, 166 28, Czech Republic
roman.vales@vscht.cz*

Abstract

In the presented work the properties of Co/CaCO₃-Na₂CO₃ catalyst used for hydrogenation of aniline to cyclohexylamine were studied. The effect of 7 mol. % of ammonia in hydrogenation gas on the activation period of cobalt catalyst, reactivity and selectivity of hydrogenation of aniline with 0.3 wt. % of water was investigated. Results showed that the 7 mol. % of ammonia inhibits the function of water on the origin and progress of activation period and leading to decrease of hydrogenation reactivity by 61 %. Nevertheless, ammonia leading to reversible poisoning of cobalt catalyst. The ammonia improves the selectivity of the hydrogenation of aniline, reducing the formation of undesirable side products. With the presence of 7 mol. % of ammonia there is up to fivefold decrease in concentration of secondary amine dicyclohexylamine.

Introduction

Amines are important intermediates used in chemical industry due to their high reactivity. Amines are applied as agrochemicals, lubricants, detergents, drugs, food-additives and as monomers used in production of polyamides, polyureas and polyepoxydes¹. Cyclohexylamine (**CHA**) is useful in the production of insecticides, plasticizers, artificial sweeteners, corrosion inhibitors, dyes and pharmacological stuffs. In addition, CHA is used for the synthesis of vulcanization accelerators as for example the *N*-cyclohexyl-2-benzothiazole sulphonamide². There is a number of catalytic methods for the synthesis of CHA: hydrogenation of aniline (**AN**) or nitrocyclohexane, amination of cyclohexanone or cyclohexanol and amination of chlorocyclohexane. However, the most simple and efficient among these is the hydrogenation of AN to CHA³. Hydrogenation of AN can be carried out in liquid or gaseous phase over a various metal-supported catalysts as Ni, Co, Pt and Pd⁴. Nevertheless, the cobalt catalysts as Co/Al₂O₃ are more selective for the formation of primary amine, CHA, whilst nickel catalysts as Ni/Al₂O₃ leading hydrogenation of aniline to the main products the secondary amines as dicyclohexylamine and *N*-phenylcyclohexylamine⁵.

This work dealing with the study of specific properties of Co/CaCO₃-Na₂CO₃ catalyst applied for the gas-phase hydrogenation of AN to CHA in chemical plant of BorsodChem MCHZ, s. r. o. which is the one of the largest world producers of CHA⁶. Recently, a phenomenon called activation period (**AP**) of cobalt catalyst, *i.e.* time period during which, under constant reaction conditions the conversion of aniline will increase up 2-3 times, has been presented⁷. According to current knowledge, the AP is conditioned by the reduction of cobalt precursor at temperature higher than a 260 °C and the water dissolved in aniline. The application of AN with 0.3 wt. % of water leading to sevenfold higher value of conversion of AN to CHA compared to use of dry aniline (<0.02 wt. % of water) for the hydrogenation reaction. The highest value of conversion, thus hydrogenation reactivity, was achieved with the use of aniline with 1.5-2.0 wt. % of water⁷. For the application of Co/CaCO₃-Na₂CO₃ catalyst in a new large-scale capacity unit of cyclohexylamine process in BorsodChem MCHZ, s. r. o. it is crucial to know whether the content of ammonia in hydrogenation gas (**HG**) will affect the function of water in aniline on its hydrogenation. During industrial production of CHA, the concentration of ammonia in circulating HG is near to 7 mol. %. For this reason, in this contribution is studied the effect of 7 mol. % of ammonia in HG on the hydrogenation of aniline from the view of activation period of cobalt catalyst and the reactivity and selectivity of catalysed hydrogenation reaction.

Experimental

Chemical and gases

The aniline was acquired from BorsodChem MCHZ, s. r. o. (99.9 %) and the solvent methanol was purchased from Penta, s. r. o. (99.9 %). Both chemicals were used without further purification. The technical gases, electrolytic hydrogen (grade 3.0), nitrogen (grade 4.0) and helium (grade 5.5) were purchased from SIAD Czech spol. and catalytically purified. Ammonia (grade 5.0) was purchased from Linde Gas, a. s.

Experimental apparatus

The experiments of hydrogenation of AN were carried out in apparatus described as follows: The hydrogen (or mixture of hydrogen and nitrogen) **1** was fed into apparatus filled with copper catalyst **2** and subsequently to column with molecular sieve **3** for the purpose of the additional depuration of trace amount of O₂ and H₂O. Refined H₂ (H₂+N₂), the liquid aniline **4** and gaseous ammonia **5** flows into the tubular, flow-through U-shaped reactor **6** (inner diameter 7 mm). The reactor was placed in bath of heat transfer medium **7**, the Rose's metal alloy. For the suppression of premature condensation of outlet reaction mixture, the side arm of the reactor was still heated by the infrared lamp **8**. The outlet reaction mixture was condensed in Liebig condenser **9** cooled by water (*ca.* 15 °C) **10** and absorbed into methanol in freeze trap **11** placed in a cooling bath filled with a water-ice mixture **12**, tempered at 0 °C. Waste gases (H₂, N₂ or NH₃) were disposed **13**.

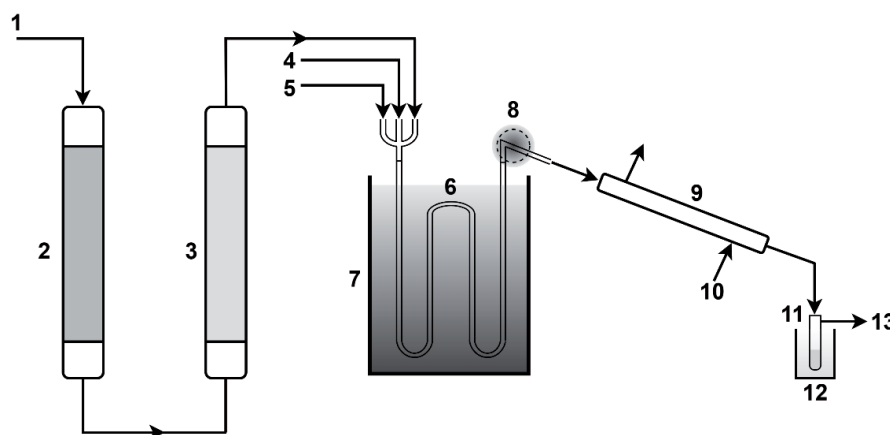


Figure 1. Schematic diagram of the experimental apparatus for the hydrogenation experiments.

Catalyst reduction

The conditions of reduction of cobalt Co/CaCO₃-Na₂CO₃ catalyst were as follows: **1**) 230 °C, 50 l h⁻¹ of H₂+N₂ (30:70 mol. %/mol. %), 2 hours; **2**) 230 °C, 50 l h⁻¹ of H₂, 14 hours; **3**) 330 °C, 50 l h⁻¹ of H₂, 0.5 hour.

Reaction procedure

The experiments of hydrogenation of AN were carried out over a 14.5 g of Co/CaCO₃-Na₂CO₃ catalyst in the form of granulate 0.80-1.25 mm. Hydrogenation reaction was carried out at reaction temperature 165 °C, atmospheric pressure, molar ratio of AN:HG 1:11, 7 mol. % of NH₃ in HG and 0.3 wt. % of H₂O in AN.

Analytical

Quantitative chromatographic analyses were performed using a Shimadzu GC-2010 chromatograph: Rxi®-624Sil MS column (30 m x 0.25 mm x 1.40 μm), flame-ionization detector using helium as a support gas. The column temperature regime was set as follows: Initial temperature 80 °C for 2 min, heating with the temperature ramp of 15 °C per min up to the temperature of 210 °C. The injector and detector temperatures were set to 250 °C. The concentration of water in samples was determined by the coulometric Karl-Fischer titration on Titrator C 30 Mettler Toledo.

Data processing

The obtained gas-chromatographic data (area %) were converted to mass fractions (wt. %) and subsequently to molar fractions (mol. %). The hydrogenation of AN was evaluated in terms of conversion of AN and reaction (percentage) selectivity where:

$$X_{AN} = \left[\frac{x_{AN,in} - x_{AN,out}}{x_{AN,in}} \right] \cdot 100 \quad (1)$$

$$S_i = \left[\frac{x_{i,out}}{x_{AN,in} - x_{AN,out}} \right] \cdot 100 \quad (2)$$

X_{AN} is conversion of aniline, x_{AN} molar fraction of aniline, S_i reaction (percentage) selectivity of species i and x_i molar fraction of species i . The effect of concentration ammonia (and water) on the reactivity of hydrogenation of AN was determined by the comparative, simplified kinetic method at the constant conversion of AN⁷:

$$\text{rel. } r_w = \left[\frac{(W/F_{AN})_{\text{ref}}}{(W/F_{AN})} \right]_{X_{AN}} \cdot \text{rel. } r_{w,\text{ref}} \quad (3)$$

where $\text{rel. } r_w$ is the relative (weight) reactivity, W is the weight of catalyst, F_{AN} is mass flow rate of aniline and the $\text{rel. } r_{w,\text{ref}}$ is reference relative (weight) reactivity ($\text{rel. } r_{w,\text{ref}} = 1$). The reaction system was also described by the relative selectivity defined as:

$$\text{rel. } S = \left[\frac{(x_i)_{\text{ref}}}{x_i} \right]_{X_{AN}} \cdot \text{rel. } S_{\text{ref}} \quad (4)$$

where $\text{rel. } S$ is the relative selectivity of catalyst towards the CHA in preference to by-products and the $\text{rel. } S_{\text{ref}}$ is reference relative selectivity ($\text{rel. } S_{\text{ref}} = 1$).

Results and discussion

The effect of ammonia on the activation period and reactivity of hydrogenation of aniline

First, it was studied the effect of 7 mol. % of ammonia in HG on the activation period of cobalt catalyst. It was hydrogenated aniline with added amount of water (0.3 wt. %) at constant mass flow of $15 \text{ g}_{AN} \text{ h}^{-1}$. It can be seen (Fig. 2a) that hydrogenation of AN with 0.3 wt. % of H_2O without presence of NH_3 in HG (**Exp. A**) leading to progress of AP to steady-state conversion of AN 70-72 %, which is reproducible to same experiment of the work dealing with the effect of water on hydrogenation of AN⁷. However, the feed of 7 mol. % of NH_3 in HG (**Exp. B**) resulted in significant decrease in conversion of AN to 6 %. Subsequent weaning of NH_3 , *i.e.* hydrogenation of AN without NH_3 again (**Exp. C**), leading to rapid arise of conversion of AN to the original value (*ca.* 71-72 %). The comparison of hydrogenation of AN with 0.3 wt. % of H_2O after the reduction of catalyst without (**Exp. A**) and with (**Exp. D**) the 7 mol. % of NH_3 in HG is presented in the Figure 2b. It can be seen that the hydrogenation of AN with added amount of water in the presence of ammonia shows no AP. The results shows that already 7 mol. % of NH_3 in HG greatly inhibits the function of water on the AP. Nevertheless, the ammonia leading to reversible poisoning of $\text{Co}/\text{CaCO}_3\text{-Na}_2\text{CO}_3$ catalyst for hydrogenation of AN to CHA.

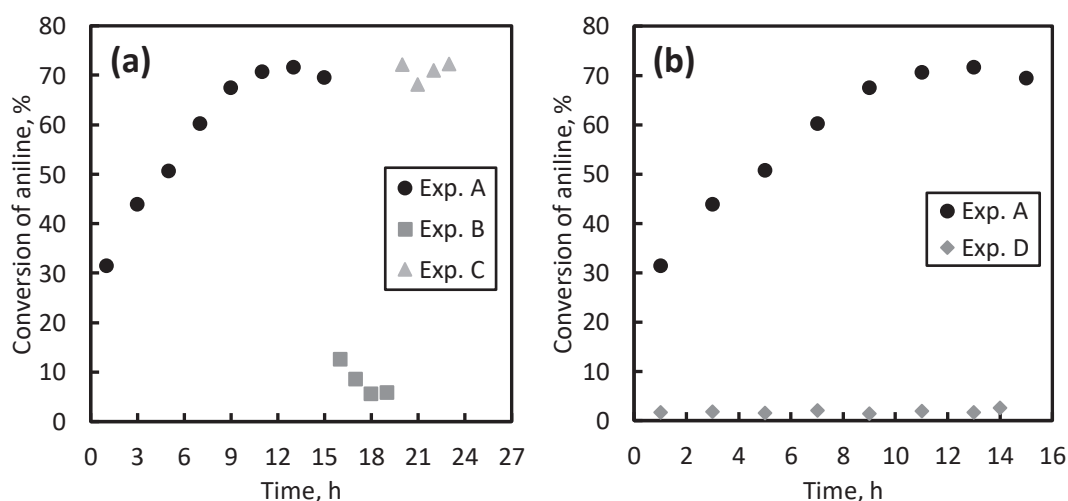


Figure 2. Time dependence of the arise of the conversion of AN during its hydrogenation at the constant reaction conditions. The specific arrangement of hydrogenation of AN to CHA:

- (a) Exp. A) after the reduction of catalyst, AN (0.3 wt. % of H_2O), no NH_3 in hydrogenation gas,
- Exp. B) after the Exp. A, AN (0.3 wt. % of H_2O), 7 mol. % of NH_3 in hydrogenation gas,
- Exp. C) after the Exp. B, AN (0.3 wt. % of H_2O), no NH_3 in hydrogenation gas,
- (b) Exp. A) after the reduction of catalyst, AN (0.3 wt. % of H_2O), no NH_3 in hydrogenation gas,
- Exp. D) after the reduction of catalyst, AN (0.3 wt. % of H_2O), 7 mol. % of NH_3 in hydrogenation gas.

Further, the effect of 7 mol. % of ammonia in HG on the reactivity of hydrogenation of AN was studied. The reactivity of hydrogenation of AN was quantified through the catalytic tests after the achieving steady-state conversion of AN, that's after the end of AP. Catalytic tests (Fig. 3) were performed in the range of mass flow of AN of 6-15 $\text{g}_{\text{AN}} \text{h}^{-1}$, *i.e.* range of parameter W/F_{AN} (catalyst contact time) of 0.97-2.42 $\text{g}_{\text{cat}}/\text{g}_{\text{AN}} \text{h}^{-1}$. Feed of 7 mol. % in HG decreases the reactivity of hydrogenation of aniline by 61 % (Table I). However, as has already been demonstrated, the reduction of concentration of NH_3 in feed of HG from 7 mol. % to 0 mol. % leads again to the original value of the hydrogenation reactivity (catalyst performance). It cannot be ruled out that the reversible poisoning of $\text{Co}/\text{CaCO}_3\text{-Na}_2\text{CO}_3$ catalyst by ammonia is the result of competitive chemisorption of AN, H_2O and NH_3 , while the ammonia bonds stronger on the active sites of the cobalt catalyst.

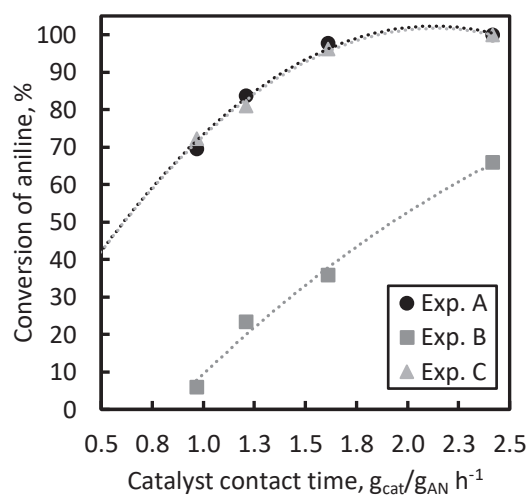


Figure 3. The effect of ammonia on the reactivity of hydrogenation of aniline. The specific arrangement of hydrogenation of AN to CHA:

Exp. A) after the reduction of catalyst, AN (0.3 wt. % of H_2O), no NH_3 in hydrogenation gas,

Exp. B) after the Exp. A, AN (0.3 wt. % of H_2O), 7 mol. % of NH_3 in hydrogenation gas,

Exp. C) after the Exp. B, AN (0.3 wt. % of H_2O), no NH_3 in hydrogenation gas.

Table I

The effect of ammonia on the reactivity of hydrogenation of aniline

experiment	rel. r_w [-]
Exp. A*	1.00
Exp. B	0.39
Exp. C	1.06

*Reference experiment

The effect of ammonia on the selectivity of hydrogenation of aniline

It was studied the effect of 7 mol. % of ammonia in HG on the selectivity of hydrogenation of AN (with 0.3 wt. % of water) to CHA over a $\text{Co}/\text{CaCO}_3\text{-Na}_2\text{CO}_3$ catalyst. It was observed the competitive effect of H_2O and NH_3 on the transformation of CHA (I) to cyclohexanol (**CHOL**, II)⁸ and the effect of NH_3 on the formation of secondary amine dicyclohexylamine (**DCHA**, III)⁵ and imine *N*-cyclohexylidencyclohexylamine (**NCCHA**, IV)⁵.

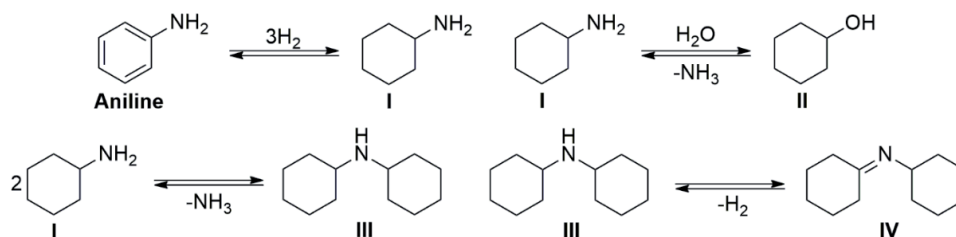


Figure 4. Reaction scheme of the hydrogenation of aniline to CHA (I), alongside with consecutive reactions leading to arise of CHOL (II), DCHA (III) and NCCHA (IV).

It can be seen (Fig. 5a) that the 7 mol. % of ammonia in HG inhibits the formation of CHOL, insomuch as the excess of ammonia in reaction mixture shifts the chemical equilibrium to the side of the CHA. Likewise, the excess of ammonia greatly inhibits the formation of secondary amine DCHA (Fig. 5b), due to the direction of chemical equilibrium of the disproportionation reaction to the side of primary amine CHA. The suppression of formation of DCHA due to the excess of ammonia is also stated in the work dealing with study of hydrogenation of aniline over a Pt catalysts⁹. The decrease in the concentration of NCCHA (Fig. 5c) is connected with the suppressed formation of DCHA, which is starting material for the formation of NCCHA.

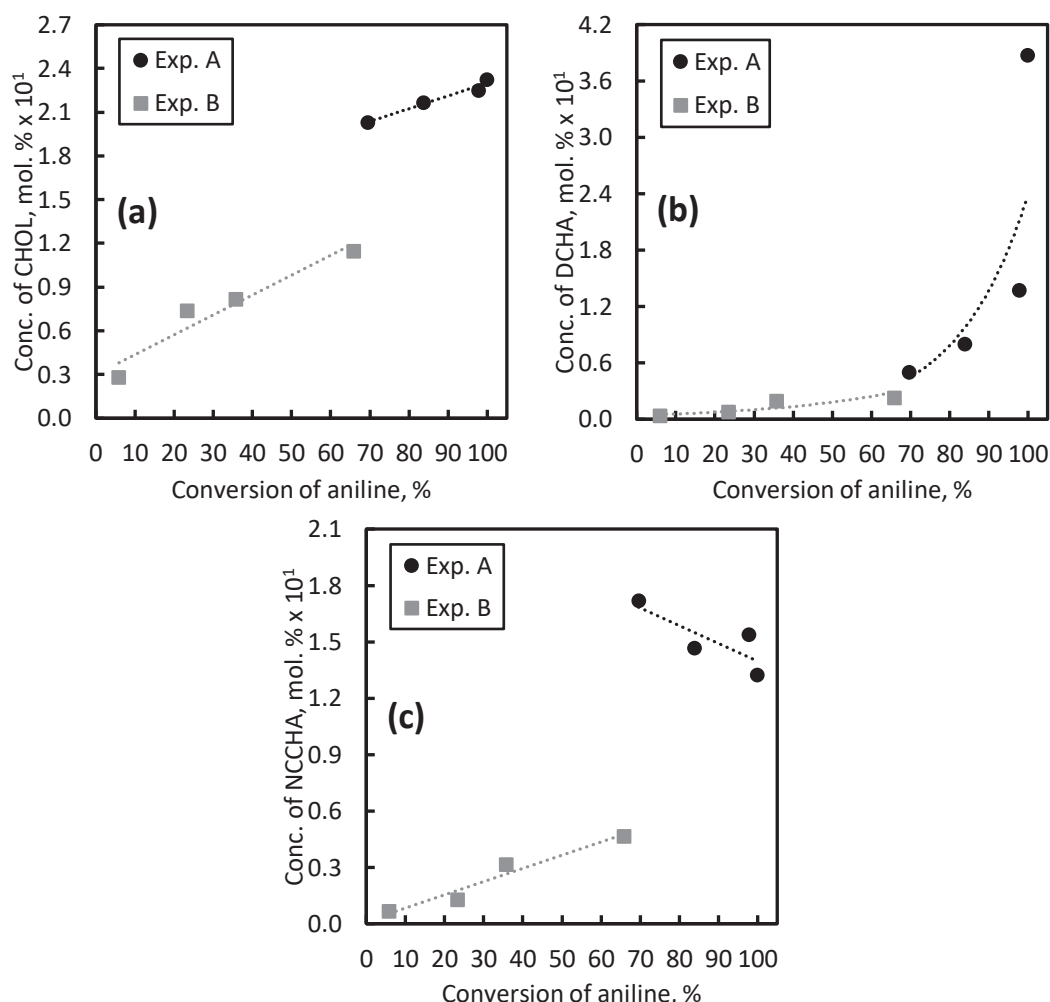


Figure 5. The effect of ammonia on the formation of a) CHOL, b) DCHA, c) NCCHA. The specific arrangement of hydrogenation of AN to CHA:

Exp. A) after the reduction of catalyst, AN (0.3 wt. % of H₂O), no NH₃ in hydrogenation gas,

Exp. B) after the Exp. A, AN (0.3 wt. % of H₂O), 7 mol. % of NH₃ in hydrogenation gas.

The results presented in the above-given pictures are also quantified in the Table II. For the constant conversion of aniline of 99.9 % the reaction (percentage) selectivity and relative selectivity of products CHOL, DCHA and NCCHA were calculated. The concentrations of products of the **Exp. B** at the conversion of AN of 99.9 % were obtained by extrapolation.

Table II

The effect of ammonia on the formation of CHOL, DCHA and NCCHA during hydrogenation of aniline

experiment	CHOL		DCHA		NCCHA	
	S [%]	rel.S [-]	S [%]	rel.S [-]	S [%]	rel.S [-]
Exp. A*	0.23	1.00	0.39	1.00	0.13	1.00
Exp. B	0.17	1.40	0.08	4.98	0.07	1.86

*Reference experiment

Conclusion

This work summarizes and expands the knowledge about properties of Co/CaCO₃-Na₂CO₃ catalyst used for cyclohexylamine process. Through hydrogenation of aniline with 0.3 wt. % of water in stream of hydrogenation gas with 7 mol. % of ammonia it was discovered that already such a concentration of ammonia utterly eliminates the promotional effect of water on the activation period of cobalt catalyst and also decreases the reactivity of aniline hydrogenation to cyclohexylamine by 61 %. However, the ammonia leads to reversible poisoning of cobalt catalyst for hydrogenation reaction, more importantly, interruption injection of ammonia to hydrogenation gas leads in short period to return to the original efficiency of catalyst for aniline hydrogenation. In contrast with poor reactivity of hydrogenation of aniline, the 7 mol. % of ammonia in hydrogenation gas increases the selectivity of the process. The presence of ammonia leading to up to fivefold decrease in concentration of dicyclohexylamine and twofold decrease in concentration of imine *N*-cyclohexylidencyclohexanamine.

In conclusion, this work contributes to the practise of cyclohexylamine production. It is appropriate to work without the content of ammonia in circulating hydrogenation gas and with leastwise 0.3 wt. % of water in aniline for good performance of Co/CaCO₃-Na₂CO₃ catalyst used in hydrogenation of aniline to cyclohexylamine process.

Acknowledgement

This work was supported from the grant of Specific university research – grant No A1_FCHT_2022_010.

List of abbreviations

AN	Aniline
AP	Activation period (of cobalt catalyst)
CHA	Cyclohexylamine
CHOL	Cyclohexanol
DCHA	Dicyclohexylamine
HG	Hydrogenation gas
NCCHA	<i>N</i> -Cyclohexylidencyclohexanamine

References

1. Froidevaux V., Negrell C., Caillol S., Pascault J.-P., Boutevin, B.: Chem. Rev. *116*, 14181 (2016).
2. Ranjbar S., Soltanabadi A., Fakhri Z.: J. Chem. Eng. Data *61*, 3077 (2016).
3. Chaudhari Ch., Sato K., Ikeda Y., Terada K., Abe N., Nagaoka K.: New. J. Chem. *45*, 9743 (2021).
4. Chatterjee M., Sato M., Kawanami H., Ishizaka T. Appl. Catal., A, *396*, 186 (2011).
5. Valeš R., Dvořák B., Krupka J.: Pol. J. Chem. Tech. *23*, 43 (2021).
6. Manufacturers of cyclohexylamine and Suppliers of cyclohexylamine. [Online] 2022. [Cited: 25 May 2022]. <https://panjiva.com/Manufacturers-Of/cyclohexylamine#>.
7. Valeš R., Dvořák B., Krupka J.: The effect of water and substituents of aromatic ring on its hydrogenation over a cobalt catalyst, in: *Proceedings of the 8th International Conference on Chemical Technology*, Czech Society of Industrial Chemistry, Prague 98-103 (2021).
8. Khusnutdinova J. R., Ben-David Y., Milstein D.: Angew. Chem. Int. Ed. *52*, 6269 (2013).
9. Greenfield H.: J. Org. Chem. *29*, 3082 (1964).

ORGANIC TECHNOLOGY

POLYMERS, COMPOSITES

GOALS AND CHALLENGES OF RUBBER SUSTAINABILITY

Brejcha J.^{1,2}, Hrdlička Z.³, Krmela J.², Beneš L.², Hittlová M.³

¹Faculty of Mechanical Engineering, J. E. Purkyně University, Ústí nad Labem, Czech Republic

²Brejcha Rubber Consulting, Prague, Czech Republic

³Department of polymers, University of Chemistry and Technology, Prague, Czech Republic
JiriBrejcha@seznam.cz

Abstract

The rubber industry is facing different challenges at the current time. Sustainability is one of the most used terms in every presentation, document, or communication act. However, what is the factual background and meaning of this expression? What are management, purchasing, marketing, production, or development circumstances? How differently can we look at it? Main trends, potential bottlenecks and challenges for future growth and the role of industry and research actors will be discussed in the paper. Sustainability has become one of the leading trends in the industry, research, and innovation. Reasons are visible in continued increase of interest of society in environment and related tasks. Political and economical changes in current world are also important fuel for this process.

Sustainability – Main trends

Identification of goals is strongly bound to introduction of trends, aspects, stakeholders, and limitations. Complexity of this problematic is also one of the key elements. Main trends are aimed to following:

- Article – features, functionality, footprint
- Recycling – possibility to stay in new flow concepts
- Emissions – elimination of production as well as life-cycle aspect in term of external factors
- Footprint – direct and indirect production and product impacts
- Green materials – use of naturally occurring materials

Sustainability – Main aspects

When we start to discuss sustainability, we cannot avoid describing main aspects and implications of this task.

- Definition? How we effectively define process, material, or product as sustainable?
- Bio based – quite often materials are presented as environmentally friendly, but bio-based materials present specific group of them.
- Circular materials are materials with possibility or potential to be use in more than one cycle and help to limit their own impact and save other sources related to application.
- Green materials are group of materials including also biobased materials, but generally with positive influence on elimination of negative impacts within production process as well life cycle and next phase of cycle – recycling.
- Critical materials. In complex understanding, sustainability is not strictly linked only with green, bio and environmental aspects, but also with supporting of industry and society in everyday life and processes. European Commission defined a list of critical materials which can play essential or vital role in case of any potential problems or issues in supply chains. Natural rubber consumption and production development can be taken as a very good example. European Commission identified natural rubber as 4th most critical material for EU industry.
- Market availability – sustainability of industry is also linked to availability of materials on the market and possibility for industrial actors to achieve them in reasonable economic environment without negative influence on market situation.

- Logistic costs – one of indirect aspect of sustainability and stability of industry. Typical example can be illustrated on situation within recent Covid 19 pandemic situation and logistic struggles mainly on the road from Asia (China) to Europe. Increase of Shanghai index can be taken as great example of figure in that direction.
- Political bans – European rubber industry has been exposed to many political bans within last decade. Examples can be found in today’s situation in Ukraine, impact of Covid as well as other ban between markets and countries.

Production footprint – trend to eliminate negative influence of industry process within Europe plays important role in development and maintenance of production technologies of rubber

Product life cycle – Increasing requirements of final users in hand with global initiatives in field of safety, environment protection, speeded up the pressure to develop new generation of rubber industrial solutions.

Rubber use in cars – Potential of circular rubber materials

Rubber is material we meet every day, and we consider it as part of our life. Typical example of variety is car – we can find three main applications – tire, but also many of smaller volume, but still high importance as breaking membrane, sealings, isolations, engine components etc.

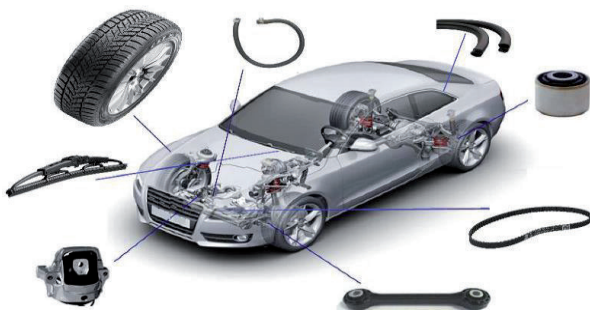


Figure 1 – Rubber part examples in car



Figure 2 – Schematic expression of different MATERIAL AND ENERGY FLOW CONCEPTS

But car is not the only example of rubber; we can find it also in many other applications. That makes this material important, interesting and challenging in term of sustainability.

Within sustainability targets one of the main approaches can be identified changing of MATERIAL AND ENERGY FLOW CONCEPTS from Linear economy to Recycling economy and in the final stage Circular economy. This shift would bring strong quantitative improvement in all related aspects.

Confirmation of importance of this process can be presented on basic figures related to automotive industry and rubber spends.

Global tire production forecasts a sharp continuous increase mainly in markets with strong motivation in improvement of life standards as China and India. Every year these markets are drivers of increase. It is strongly dependent also on vehicle production.

How do main players react on sustainability requirements?

Most of the goals are developing in line with request of new policies in EU and respecting other global pacts and agreements. From original steps almost all big tire companies converting to 2050 as year of 100% sustainable materials in productions and achieving of carbon neutrality as mandatory. Important part of the store can be

also inclusion of recycling goals into general sustainable roadmaps. This goals still should be considered as long term and very sensitive to political and economical influences. Also, long term advance exceeds standard management and political lifetimes and „service life “. But the trends are clearly demonstrated. To achieve them, strong, sustainable, and long-term incorporation of research and innovation are required.

Achieving of sustainability goals for rubber industry is impossible without strong connection and support from raw material producer side as important partners in these activities. Many initiatives in that field are presented in last years. Typical example of complex solution can be found e.g. Synthos development strategy including all important steps and impacts – features of product, focusing on modern and future solutions e.g., EV cars, elimination of CO₂ emissions with own production and involvement of green and bio-based feed stock as important raw materials entering process. Also harmonized activity together with companies like TRS, producer of recycled material form end-of-life tires (ELT), can help to bring reasonable values into chain.



Figure 3 – Company strategies in raw material sector

Aside from rubber compound, we can find also challenging area in reinforcing materials – important and volume providing part of tire and other engineered polymer products. Great example of this direction is RECYCLED POLYESTER YARN - PROJECT 2021-2022 of Continental. A set of standard passenger car tires uses the material from around 40 recycled PET bottles. It brings new trend of use this high volume waste.

Visualization of features in close correlation to sustainability aspects, that is also novelty of NEW TYRE LABELLING SYSTEM, effective since 1 May 2021.

- Enhanced road safety in specific conditions
- Lower environmental impact
- Increase product safety
- Passenger car, 4x4, SUV, van, light truck, truck and bus tires.
- renewed to be similar to other household appliances.
- The empty classes are removed, and the scale is from A to E.
- In addition, the noise class linked to the level of decibels is informed in new way by using letters from A to C

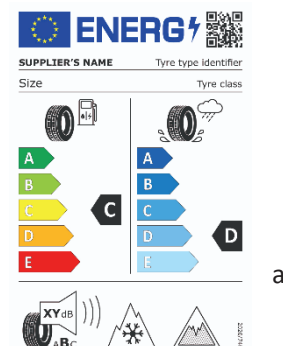


Figure 4 - NEW TYRE LABELLING SYSTEM, effective since 1 May 2021.

Important tool of regulation of negative production impact was the original idea of EU ETS system for CO₂ ALLOWANCES dedicated to energy production. Unfortunately, system under current conditions is questionable if play initially expected role. PRICE DEVELOPMENT chart demonstrated development of impact of allowances to production cost of rubber sector, important feature of future of rubber industry stay in EU.

Circular materials – Best solution



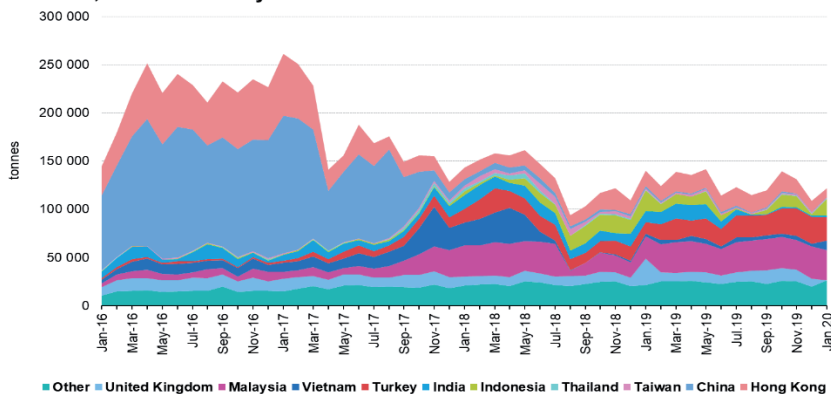
Figure 5 - Waste fields to tire as basic concept

END OF LIFE TYRES – ELT- represented interesting and challenging source for future development

Since the end of last century, big changes in direction of material form landfilling and wasting of material to potential changing of MATERIAL AND ENERGY FLOW CONCEPTS from Linear economy to Recycling economy. Final stage should be Circular economy. Also, part of the story can be a stable development in retreading of used tires.

As a demonstration of not only rubber-related problems, we can mention PLASTIC MATERIAL WASTE STREAM - Export of plastic waste from EU countries

Export of plastic waste for recycling from the EU to receiving countries, 2016 to January 2020



Source: Eurostat COMEXT

eurostat

Figure 6 - Eurostat chart - export of plastic waste development

For ELT we can identify MAIN RECYCLING APPROACHES – 3 ways:

- Material reuse
- Material downcycling
- Energy production

In this order, we can also see level of recycling and sustainability maturity. But all the three represent positive approaches compared to landfilling which was prohibited in EU in previous decades.

Important step and aspects of identification and tuning of technologies for CIRCULAR MATERIALS from ELT.

- Mechanical process
- Thermal chemical process
- Energy production
- Pyrolysis
- Ambient milling
- Sieves and cleaning
- Devulcanization
 - extruders
 - milling

GROUPS of output in sources into CIRCULAR MATERIALS for rubber industry.

- Rubber reclaim
- „Devulc“ materials
- Rubber powder
- Reprocess carbon black
- Pyrolysis – powder, gas, oil

The MAIN TASK within application of recycled materials is a question of surface activation and “devulcanization” of the material. Understanding of chemistry of carbon – sulfur net and changes inside it due to changing of conditions is a crucial barrier for all new applications and processes.

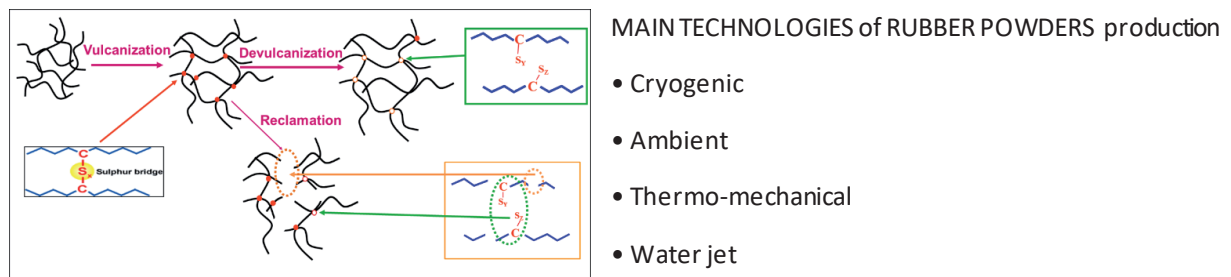


Figure 7 – Basic schematic principles within rubber processing

Important aspects of RUBBER POWDERS production are:

- Size of particles
- Shape of particles
- Feed stock
- Mixing

Main different in output is linked to morphology and size of particles. Different final applications utilize different sets of parameters as preference. Also condition of milling influence surface quality of material and contribute to their affinity to matrix.

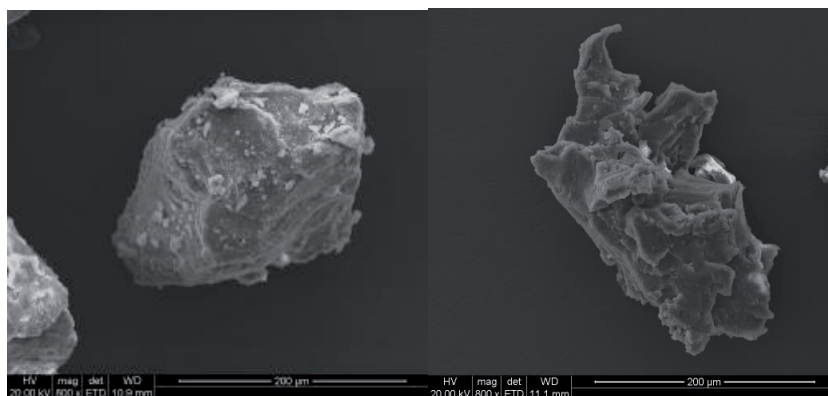


Figure 8 – SEM pictures of waterjet and cryogenic rubber powder

A side of process composition of RUBBER POWDERS can predict characteristics and performance in combination with virgin materials or another type of composite material.

Another direction of recycling of „old“ rubber is a thermal process – PYROLYSIS.

Compared to the other technological approaches, pyrolysis starts with one component and achieves a several components.

- Carbon powder
- Oil
- Gas
- Steel



Figure 9 – Basic scheme of material flow in pyrolysis

- Calorific value table

One reason for interest in thermic process, especially in a time of potential energy crisis, due to e.g. current situation in Ukraine, can be ELT (and other polymer waste). ELT 25 000-32 000 kJ/kg, Black coal (Ostrava origin) 28 200 – 29 400 kJ/kg, Brown coal (Most origin) 10 200-17 200 kJ/kg, dry wood 13 000- 17 000 kJ/kg, liquid organic fuels 40 000- 44 500 kJ/kg etc.

Risk points of circular materials

Not only positive aspects are linked to circular materials. Original material and process, together with market drivers, can bring to the table also some risks whose mitigation or elimination should be part of the story.

- Non-stability of sources
- PAH (polycyclic aromatic hydrocarbons) issue – oil, carbon black
- EU limits - 1 mg/kg benzo(a)pyrene, 10 mg/kg Σ PAH
- 18 PAH are listed in ZEK – GS standard
- REACH and other legislative acts, grey export/import
- registration of chemical substances
- Import of tyres /GRG to EU27 market

Recent news in bans – challenge or support?

Regulatory authorities define goals, ways, and steps, but sometimes, they face challenges like rubber granulates and infills in sports fields. Therefore, a complex and holistic approach must be taken to avoid any risk of fundamental mistakes and wrong decisions.

Contact with public sector and professionals is an important part of exploitation and dissemination of outputs. Leading and respected journals and associations are active in that. An example is the ELASTOMERS FOR SUSTAINABILITY initiative of the European Rubber Journal, which evaluates submitted projects from the industry by an expert panel and presents a chart of the most valuable.



Figure 10 - Logo of E4S initiative

PATRICK RALEIGH – European Rubber Journal

PROF JAMES BUSFIELD - Queen Mary University of London

DR. CHRISTOPH SOKOLOWSKI - WDK (Wirtschaftsverband der deutschen Kautschukindustrie)

MARTYN BENNETT ARTIS consultancy service

JIRÍ BREJCHA Brejcha Rubber Consulting

Conclusion

The rubber industry is facing different challenges at the current time. Sustainability is one of the most recent and current topic for industry.

Understanding sources, processes and methodologies is crucial to make adequate outputs. Also, an interdisciplinary approach is necessary to avoid any single approach ideas and wrong exploitation.

The article discusses most of the related aspects, technologies, and circumstances from research and industrial perspectives. Positive trends of recent activities must speed up application and initiatives to achieve ambitious governmental and industrial policies and regulations goals. Without the strong support of research and innovation, it could bring just partial achievements. All benefits are partial without right and appropriate dissemination and exploitation.

Acknowledgement

This article, presentation, and the research behind would not have been possible without the exceptional support of UJEP-SGS-2022-48-001-2.

INFLUENCE OF PROCESSING METHODS ON THE BEHAVIOR OF WASTE RUBBER POWDER-MODIFIED RUBBER MATRIX

Hittlová M.¹, Hrdlička Z.¹, Brejcha J.^{2,3}, Ustinov O.¹, Pradas A.¹

¹*Department of polymers, University of Chemistry and Technology, Prague, Czech Republic*

²*Faculty of Mechanical Engineering, J. E. Purkyně University, Ústí nad Labem, Czech Republic*

³*Brejcha Rubber Consulting, Prague, Czech Republic*

Abstract

Rubber waste is one of the biggest problems in current industry and society. All problems are also challenges for development. The largest amount of rubber waste comes from tires, the landfilling of which is prohibited in the most developed countries. In our study, ways of tire recycling must be found and further developed. Here, we investigate the possibility of using waste rubber powder (WRP) in a test matrix without sacrificing the mechanical properties of the thus-modified matrix. The WRP (particle size < 0.4 mm) produced by the water jet process, was added to the new rubber matrix by applying different processing parameters (mixing machine, order of mixing, temperature, revolutions of rotors, WRP activation). The properties (tensile test, DMA, SEM etc. of all samples were measured and compared with each other.

Introduction

Natural rubber is an important raw material for the European tire and rubber industry and a key enabler for several industries. Natural rubber must be imported into Europe which makes it dependent on countries with rubber plantations. This is not the only problem with natural rubber but also other components needed for the production of rubber compounds. Therefore, the EU has included it in the list of critical raw materials.

Rubber products must be vulcanized which turns the rubber into an insoluble, infusible form. Vulcanization is the process of chemical crosslinking. The rubber products must be chemically crosslinked to achieve the required properties of the final product. These products are composed of different rubbers and also other various components. Therefore, it is not easily recyclable.

Landfilling, as the earliest waste management technique, causes health and environmental risks of accidental fires and contamination of the underground water resources¹. Regulations for the recovery and disposal of waste tires have been introduced by governments and environmental organizations to adopt more eco-friendly recycling of waste tires. Also, from an economical point of view, discarded tires with low cost can be used in several markets such as tire-derived fuel^{2,3}, asphalt pavements⁴, concrete^{5,6}, plastic composite^{7,8}, and rubber compounds⁹.

Our experiments focus on processing conditions because they could have a considerable influence on the properties of final product. Compound with added waste rubber powder (WRP) will always have worse mechanical properties than virgin materials compound. Therefore, we should avoid unsuitable processing conditions that will affect the mechanical properties of the resulting compound. We compared primary mechanical properties of the compounds prepared under different processing conditions.

Experiment

This work's aim is to compare different process conditions and find a way to prepare a rubber compound with WRP with the least possible loss of mechanical properties. 36 mixtures of the same formulation (Table I) were prepared under different process conditions. The mixtures differed in the procedure (mixing equipment, order of components addition – Table II) and the preparation conditions (temperature, speed of mixing rotors). The rubber compounds were mixed on a laboratory two-roll mill and a laboratory kneader (Brabender, Germany).

Table I
Composition of rubber compounds

Component	[phr]
NR	15
BR	15
SBR 1500	70
Processing additive	0.15
CB N220	65
Zinc oxide	4
Stearic acid	2
Antioxidant 6PPD	2.5
oil	20
Sulfur	1.6
Accelerator CBS	1.3
Accelerator MBT	0.06
PVI	0.1
WRP (7 %)	14

phr – parts per hundred of rubber, NR – natural rubber, BR – butadiene rubber, SBR – styrene-butadiene rubber, CB – carbon black, CBS – N-cyclohexylbenzothiazol sulphenamide, MBT – 2-mercaptobenzothiazol, PVI – pre-vulcanization inhibitor (N-cyclohexylthio phthalimide), WRP – waste rubber powder

Table II
Order of components addition

Compound	Order of components addition
1	masterbatch (rubber + WRP) + other components
2	premix (SBR + WRP) + other components
3	premix 1 (SBR + part of WRP) + premix 2 (BR + part of WRP) + premix 3 (NR + part of WRP) + other components
4	all in one mixing
5	masterbatch (rubber + thermo-mechanical activated WRP) + other components
6	premix (rubber + additives) + WRP

We used waste rubber powder (WRP) made from personal car tire tread by water jet process. WRP particle size should be less than 0.4 mm, but sieve analysis showed real particle/agglomerate size (Figure 1.). We added 7 % (14 phr) of WRP to each compound.

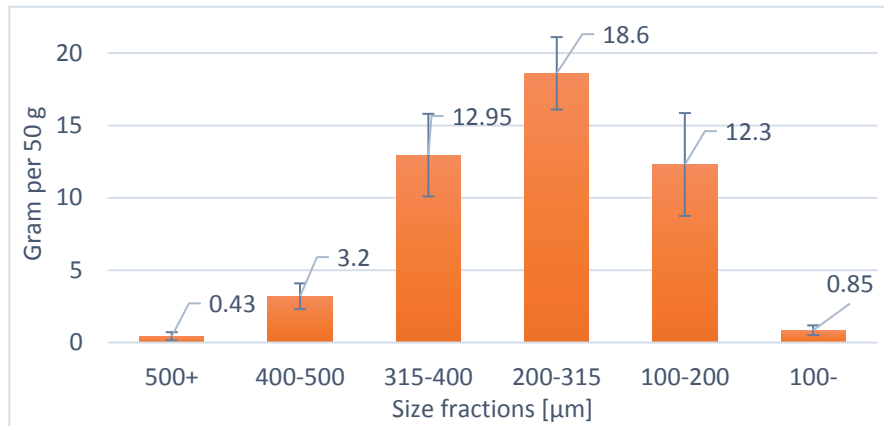


Figure 1. Sieve analysis - particle size distribution

The mixing on the Brabender was as follows: the mixture of the first two ingredients was always mixed for 5 minutes and with each subsequent addition of substances it was mixed for another 2 minutes to form a homogeneous mixture. The viscosity of the compounds was tested on a Mooney viscometer (MonTech, Germany). The course of vulcanization was measured using a moving die rheometer RPA 2000 (Alpha Technologies, USA) under the following conditions: 160 ° C, 30 min, oscillation amplitude 0.50 deg, frequency 100 cpm. For the tensile test we used Instron 3365 (Instron, USA) using dumb-bell specimens of cured rubbers (ISO 37, type 2) to determine the tensile properties at break. The tests of hardness of the vulcanized plates (hand hardness tester, Shore A, Mitutoyo, Japan), tear strength (ISO 34, type B; Instron 3365), dynamic mechanical analysis (DMA DX04T, Czech Republic), and abrasion resistance (DIN / Bussen-Schlobach type, PolymerTest, Czech Republic) were also determined. To reveal the compound's structure and WRP distribution, we took scanning electron microscopy (SEM) images of the cryo-fractured and gold-plated cured rubbers (Tescan VEGA, Czech Republic).

Discussion and result analysis

The SEM images show the structure of the mixtures and the dispersion of the fillers but cannot observe dust particles. Element maps can demonstrate the shape and size of the particle because WRP, having been obtained from passenger tires, contains silicon (Si) which is absent in the matrix. On SEM elemental maps (Figure 2), we can see particles are getting smaller and have somewhat different shapes. It could be some influence of the processing on the WRP particle shape and size, but more experimentation is needed.

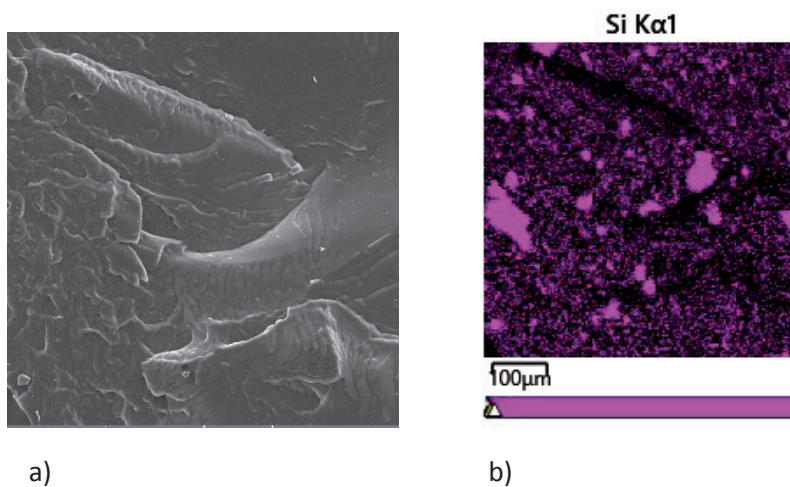


Figure 2. SEM picture – C1, kneader_100 °C/40 rpm a) compound structure, b) Si element map

In compound No. 6, WRP acts as a filler only, resulting in inferior mechanical properties. Therefore, this approach is not appropriate as it will not exploit the potential of WRP. Regarding the mixing processes, numbers 1 and 5 give the best mechanical properties. Mixing process No. 4 gives also quite good results; however, it is more sensitive to changes in temperature and rotors` speed. According to our results, the kneader is better than the two-roll mill. The best mixing condition is the combination of temperature of 120 °C and rotors` speed of 40 rpm. For brevity, we present selected results in Figure 3 (stress at break) and 4 (abrasion).

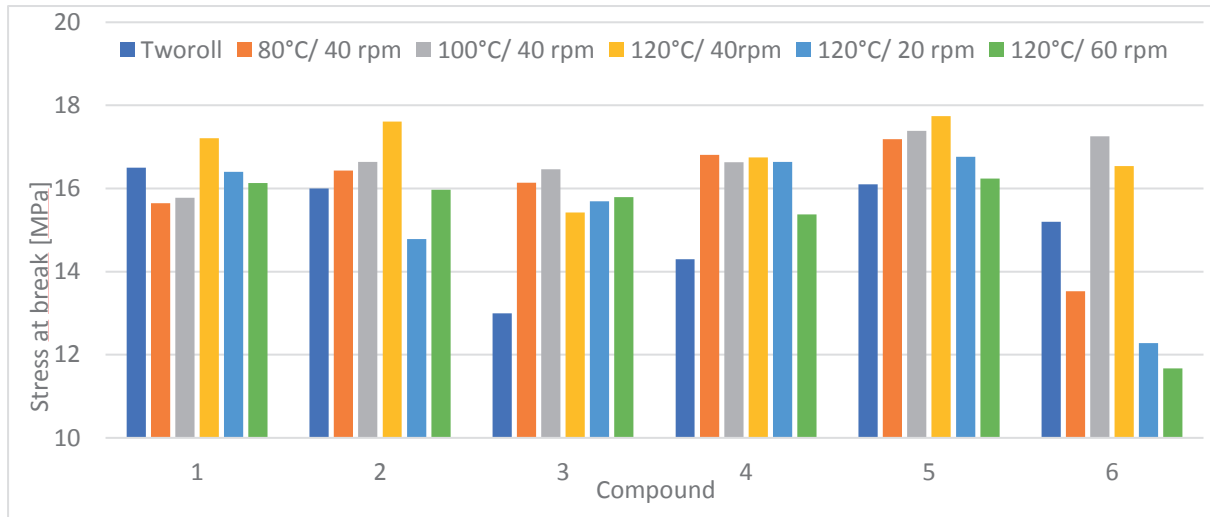


Figure 3. Stress at break of the cured rubbers

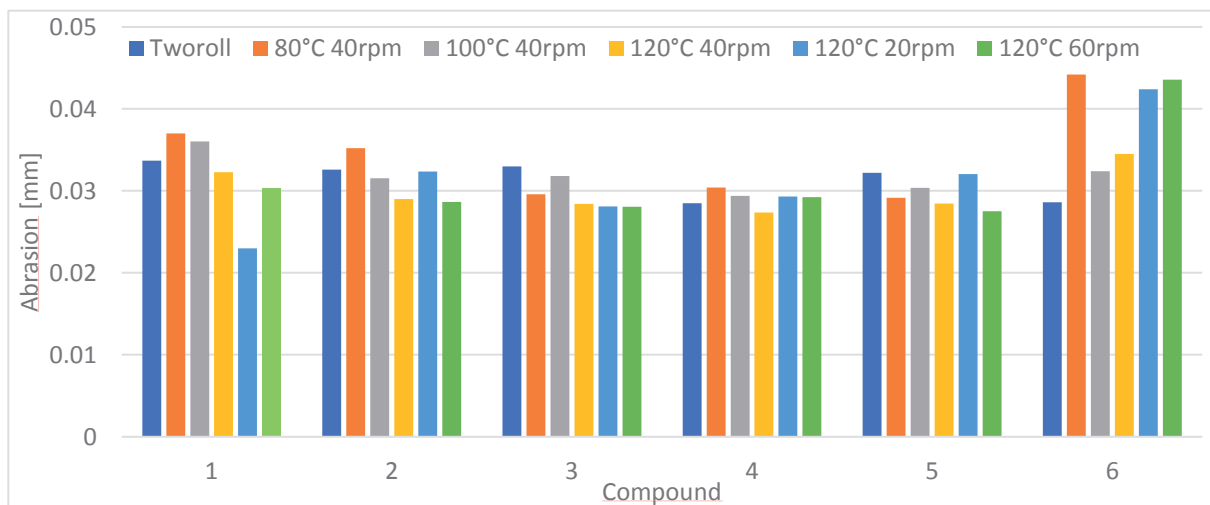


Figure 4. Abrasion of the cured rubbers

Conclusion

We investigated the effect of processing conditions at mixing of waste rubber powder (WRP) with rubber matrix based on fresh rubber. When using recycled rubber, the mechanical properties of the new product usually decrease. Therefore, we should avoid unsuitable processing conditions that will affect the mechanical properties of the resulting compound. Thus, we applied various mixing protocols (order of component addition) and mixing conditions (equipment, temperature and rotors` revolutions) and tested their influence on the properties of the resulting materials.

From all the tests performed, it follows that mixing procedure No. 6 (WRP is added as a filler) gives significantly worse properties of cured rubber; therefore, this procedure of adding WRP does not seem suitable. This means

that the rubber powder which acts as a filler is not well dispersed in the matrix. As a result, compound 6 is more prone to the correct choice of process conditions and equipment.

Compounds 1 and 5 show the best mechanical properties in most cases. From the data obtained, we can conclude that the activation of the WRP by partial devulcanization (compound 5) has a good effect on the results. The resulting properties are less dependent on process conditions. For this reason, the process appears to be procedurally favorable. However, compound 4 also often shows a small variance of values, indicating less influence on process conditions. The assumptions regarding the sticking of particles under more demanding conditions can be confirmed. However, the effect of higher speeds (60 rpm) needs to be further investigated since partial degradation of the polymer chains may occur.

We also compared two mixing devices: a two-roll mill and a Brabender kneader. From the obtained data it can be stated that a greater possibility of regulating the mixing conditions on the kneader can lead to better results. The best results were obtained for compound 5 mixed on the kneader with a temperature of 120 °C and a speed of 40 rpm.

It was shown that the study of technological conditions of mixing WRP into the compound is important. For this reason, it is necessary to further investigate this issue and characterize the influence of other machines and technological parameters. More attention should be also paid to the study of internal mixture morphology, dispersion quality, and WRP behavior during mixing. These steps can then lead to better use of recycled material in the production of new mixtures and products.

References

1. Sienkiewicz M., Kucinska-Lipka J., Janik H., Balas A.: *Waste Manag.* **32**, 1742 (2012).
2. Khan S.R., Zeeshan M., Masood A.: *Waste Manag.* **106**, 21 (2020).
3. Banar M., Akyıldız V., Ozkan A., Cokaygil Z., Onay O.: *Energy Convers. Manag.* **62**, 22 (2012).
4. Ge D., Yan K., You Z., Xu H.: *Constr. Build. Mater.* **126**, 66 (2016).
5. Yung W.H., Yung L.C., Lee H.H.: *Constr. Build. Mater.* **41**, 665 (2013).
6. Aiello M., Leuzzi F.: *Waste Manag.* **30**, 1696 (2010).
7. Kakroodi A.R., Rodrigue D.: *Plast. Rubber Compos.* **42**, 115 (2013).
8. Ramarad S., Khalid M., Ratnam C.T., Abdullah L., Rashmi W.: *Prog. Mater. Sci.* **72**, 100 (2015).
9. Araujo-Morera J., Hernández M., Verdejo R., López-Manchado M.A.: *Polymers* **11**, 2122 (2019).

ALTERNATIVE BIO-BASED PLASTICIZERS FOR RUBBER INDUSTRY

Hrdlička Z.¹, Břejcha J.^{2,3}, Hittlová M.¹, Alexová C.¹,

¹University of Chemistry and Technology, Prague, Technická 5, 166 28 Prague 6

²Jan Evangelista Purkyně University in Ústí nad Labem, Pasteurova 1, 400 96 Ústí nad Labem

³Břejcha Rubber Consulting, Prague

zdenek.hrdlicka@vscht.cz

Abstract

Plasticisers are important components of rubber compounds, facilitating their processing and influencing product properties. So far used plasticisers are mostly oils of petroleum origin, i.e. from a non-renewable source. Within the decarbonisation strategy of today's world and for geopolitical reasons, it is desirable to decrease the dependence of rubber industry on the fossil raw materials. Thus, the alternative bio-based plasticisers have been introduced which, however, have different chemical composition than the petroleum-based ones. We present a basic benchmark of the application of vegetable oils in rubber compounds for production of tyre treads.

Introduction

A rubber compound is a mixture of rubber, either natural or synthetic, with various additives: curing system, lubricants, plasticisers, fillers, antidegradants, factices, pigments etc. Plasticisers are liquid or semi-solid substances soluble in rubber. Their main purpose is to facilitate the processing of rubber compounds, mainly by decreasing its viscosity. They allow for mixing of more fillers into the compound. At the same time, they influence properties of cured rubber, e.g. they decrease modulus and hardness and increase elongation at break.

Currently, the most used plasticisers are mineral oils of petroleum origin, i.e. from non-renewable resource. As the ones most compatible with rubber, aromatic oils has been used for decades; however, some of them may be harmful to human life. DAE type oils (Distillate Aromatic Extract) used to be very popular due to their availability, price-to-performance ratio and excellent compatibility with rubber. However, they contain polycyclic aromatic hydrocarbons (PAH) that are toxic carcinogens. Thus, PAH-rich oils, as DAE, have been prohibited in tyres produced in or imported to EU (Directive 2005/69/EC). Alternative petroleum-based oils with low PAH content are RAE (Residual Aromatic Extract), the viscosity of which may be too high; TRAE (Treated Residual Aromatic Extract) and TDAE (Treated Distillate Aromatic Extracts), which are usually more expensive than DAE; and MES (Mild Extraction Solvates) with higher content of paraffin. Naphthenic oils are produced from rare highly naphthenic crude oils. Paraffinic oils are less polar and thus may be unsuitable for some types of rubber, e.g. for the most common styrene-butadiene rubber (SBR). For these reasons, together with decarbonisation strategy of today's world and for geopolitical reasons, there is a need to look for alternative, harmless and eco-friendly plasticisers for rubber industry¹⁻⁵.

Vegetable oils are abundant, biodegradable, easy available and non-toxic (excepting castor oil). They are isolated from seeds and fruits. The production of 10 major vegetable oils reached 198 million metric tons in 2017/2018¹. About 15% of vegetable and animal oils are used for industrial purposes¹. Vegetable oils are mainly used for production of food and bio-fuels, lubricating oils, soaps, paints and surfactants¹⁻². In Europe, the most common technical application of rapeseed oil is the production of bio-diesel, which increased rapidly after 2000¹. The vegetable oils are isolated by pressing of seed or fruit pulp, extraction and refining. Globally the most important are soybean, palm, sunflower and rapeseed oil. Linseed, palm kernel, peanut, coconut, castor and jatropa oil are also very important depending on the region. For technical applications, less attention is paid to cotton seed, olive, cashew nut shell liquid, rice bran, hazelnut, rubber seed, orange peel, and jojoba oil.^{1-2,4-8}

Compared with mineral oils, vegetable oils have different chemical composition. They are composed mostly of triacylglycerols, i.e. esters of glycerol and fatty acid containing 8 to 24 carbon atoms with 0 to 5 double bonds between them. Other constituents are mono- and diacylglycerols, free fatty acids, phospholipids, pigments, flavours etc. A drawback of vegetable oils may be their (i) low viscosity which may cause limitation at mixing stage, and (ii) double bonds that support undesirable reaction with sulphur, concurrent to vulcanization, which

leads to lower crosslink density and deteriorated properties of cured rubber. The both issues become distinct at higher oil contents. To remove these drawbacks, vegetable oils are modified by polymerization or epoxidation in some cases. The epoxidation also increases the polarity of the oil to become compatible with more polar kinds of rubber (NBR) where it can replace phthalate plasticisers. On the contrary, some vegetable oils contain natural antioxidants that may prevent their oxidation, which is advantageous^{1-4,6-8}.

Compared with standard mineral oils, vegetable oils influence the properties of uncured rubber, course of curing, and properties of cured rubber product. They can improve some properties while deteriorate other properties at the same time. Various papers report different results that depend on the particular type of oil, oil concentration, formulation of rubber compound (type of rubber, type and concentration of filler), way of mixing, etc. Such way, controversial trends are reported that do not allow for making a general conclusion¹⁻⁸. Therefore, we focus particularly on the properties of rapeseed oil and mixed vegetable/mineral oil on the properties of rubber compound based on SBR/NR/BR, filled with combined carbon black and silica, the formulation of which is designed for off-road tyre tread.

Experiment

The aim of our work was to test two types of alternative oil applied as plasticizers of a model rubber compound suitable for off-road tyre tread. The first tested oil (oil 1) was rapeseed oil for technical use, the second one (oil 2) was mixed oil dedicated for use in rubber industry. The trademark and origin of the oils cannot be disclosed, unfortunately. Basic composition of the oils was tested via paper chromatography. We confirmed that the rapeseed oil is composed mostly of triacylglycerols as expected (Figure 1 right). Conversely, the mixed oil, although labelled as “alternative”, is composed mostly of hydrocarbons with very low content of triacylglycerols (Figure 1 left).

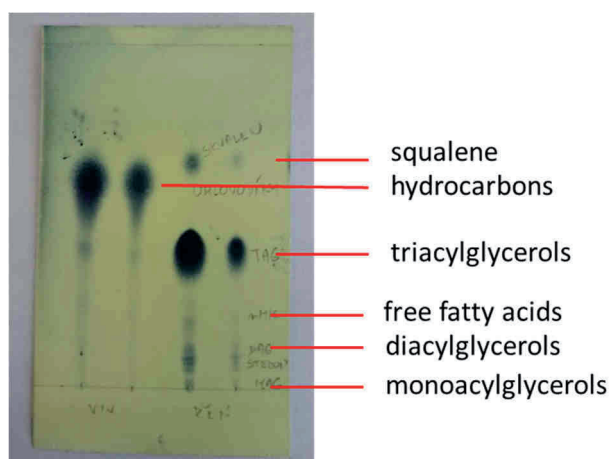


Figure 1. Results of paper chromatography of the rapeseed oil (oil 1, right) and mixed oil (oil 2, left).

The content of fatty acid in oil 1 (rapeseed) was determined by gas chromatography as methyl esters (after saponification and esterification). The results confirm the typical composition of rapeseed oil with a dominance of oleic acid (63%) and minorities of linoleic and linolenic acids (Table I).

The influence of the tested oils on the processing properties of raw rubber, course of vulcanization and properties of cured rubber product was tested on model rubber compounds targeted to production of off-road tyre treads (Table II). The formulation was based on styrene-butadiene rubber (SBR) with two minor rubbers, natural rubber (NR) and butadiene rubber (BR). A double filler system with major carbon black and minor silica was used. A reference compound A contained 21 phr (parts per hundred parts of sum of the rubbers) of standard mineral oil; in compounds B, 7 phr of the standard oil was replaced by an alternative one (oil 1 and oil 2 in B1 and B2, respectively); in compounds C, 14 phr of the standard oil was replaced by an alternative one (oil 1 and oil 2 in C1 and C2, respectively). Thus, the total content of oil was 21 phr in each compound. The compounds contained a sulphur-based curing system. All the raw materials were of standard quality for rubber industry.

Table I
Composition of fatty acid in tested rapeseed oil (oil 1)

Acid name	Acid type	Content in oil, % (w/w)
myristic	14:0	0.05
palmitic	16:0	4.66
palmitoleic	9c-16:1	0.23
heptadecanoic	17:0	0.07
stearic	18:0	1.54
elaidic	9t-18:1	0.05
oleic	9c-18:1	62.81
linelaidic	9t12t-18:2	0.10
linoleic	9c12c-18:2	19.23
linolenic	9c12c15c-18:3	9.83
arachidic	20:0	0.56
eicosenoic	20:1	0.29
behenic	22:0	0.33
erucic	13c-22:1	0.13
lignoceric	24:0	0.12

Table II
Formulation of rubber compounds

Compound denotation	A	B1	B2	C1	C2
SBR	70	70	70	70	70
NR	15	15	15	15	15
BR	15	15	15	15	15
carbon black N220	60	60	60	60	60
silica	6	6	6	6	6
zinc oxide	3.7	3.7	3.7	3.7	3.7
stearic acid	2	2	2	2	2
standard mineral oil	21	14	14	7	7
test oil 1: rapeseed	-	7	-	14	-
test oil 2: mixed	-	-	7	-	14
accelerator CBS	1.33	1.33	1.33	1.33	1.33
sulphur	1.6	1.6	1.6	1.6	1.6

The compounding was conducted on a laboratory two-roll mill (150 mm x 400 mm, friction 11:9). Mooney viscosity of rubber compounds was measured on Variables Mooney viscometer V-MV 3000 (MonTech, Germany) as ML 1+4 at 100 °C and 2 rpm. The course of vulcanization was measured on Rubber Process Analyzer RPA 2000 (Alpha Technologies, USA) at 160 °C, 100 cpm and 0.5 deg amplitude. The samples were compression-moulded in a hydraulic press (Fontijne, Netherlands) at 160 °C for (T90 + 2 min) to obtain plates (150 mm x 150 mm x 2 mm) for tensile testing and for (T90 + 5 min) to obtain cylinders (15 mm x 15 mm) for abrasion test where T90 stands for the optimum cure time derived from the vulcanization tests. The tensile test was conducted according to ISO 37 on Instron 3365 (Instron, USA) with type 2 specimens. The tear strength was measured on the same device according to ISO 34-1 with type B specimens (Graves). The dynamic mechanical analysis was conducted on DMA DX04T (RMI, Czech Republic) in a tensile mode using rectangular specimen with dimensions width, 6 mm; thickness, 2.5 mm; length, 30 mm. These were subjected to tensile

loading with amplitude, 0.033 mm, and frequency, 1 Hz in a heating programme from -20 °C to 160 °C with rate 2 °C.min⁻¹. The hardness Shore A was measured with Mitutoyo manual hardness tester using the offcuts after tensile specimen had been punched from the moulded plates (the total thickness of three layers was 6 mm). The abrasion resistance was measured on a DIN-type (Bussen-Schlobach) tester (Polymertest, Czech Republic) according to ČSN 62 1466. Each specimen was abraded on an emery paper for 40 m travelling distance. The abrasion was evaluated as the change of specimen volume. The rebound resilience was measured on a Schob pendulum (Polymertest, Czech Republic) according to ISO 4662. The resistance to flex cracking and to crack growth was measured according to ČSN 62 1488 on a device by Polymertest (Czech Republic). The dynamic fatigue of the rubber was evaluated by DPGi method. Cylindrical specimens (length, 100 mm; diameter, 25 mm) were fixed in the clamps and subjected to rotation while being bent. The heat build-up was evaluated as the temperature increase after 5 min of loading. The resistance to dynamic fatigue was evaluated as the number of kilocycles till the specimen break. The density of cured rubber was evaluated according to ČSN 62 1405.

Results and Discussion

The results of processing and curing properties are summarized in Table III. The Mooney viscosity of the compounds containing alternative oils is higher than that of the reference compound (A). This may be caused by lower plasticising effect of the alternative oils and may indicate a bit worse processability. Against expectations, the mixed oil (B2 and C2) caused higher viscosity increase than the rapeseed oil (B1, C1). The relaxation behaviour of the uncured rubber compounds were measured by Mooney relaxation, which followed the standard viscosity measurement. The ability of elastic relaxation was assessed as the final decay index (FDI), i.e. the percent decrease of viscosity value after 30 s from rotor stop related to the final viscosity (ML 1+4). All the compound reached almost the same value of FDI and thus they showed the same ability of elastic relaxation.

Table III
Processing and curing properties of the rubber compounds

Compound	A	B1	B2	C1	C2
Mooney viscosity (ML 1+4, 100 °C), MU	38.5	40.7	45.6	40.0	43.2
Mooney relaxation final decay index, %	92.7	92.4	92.1	92.4	92.3
Scorch time TS2, min	4.6	4.0	4.7	4.9	4.2
Optimum cure time T90, min	10.4	8.9	10.5	10.7	10.2
Cure rate index, min ⁻¹	17.3	20.6	17.2	17.4	16.5
Cure minimum torque, dNm	1.7	1.8	2.0	1.8	1.9
Cure maximum torque, dNm	13.3	13.6	12.9	10.9	11.7
Delta torque ΔM , dNm	11.5	11.8	10.9	9.1	9.9

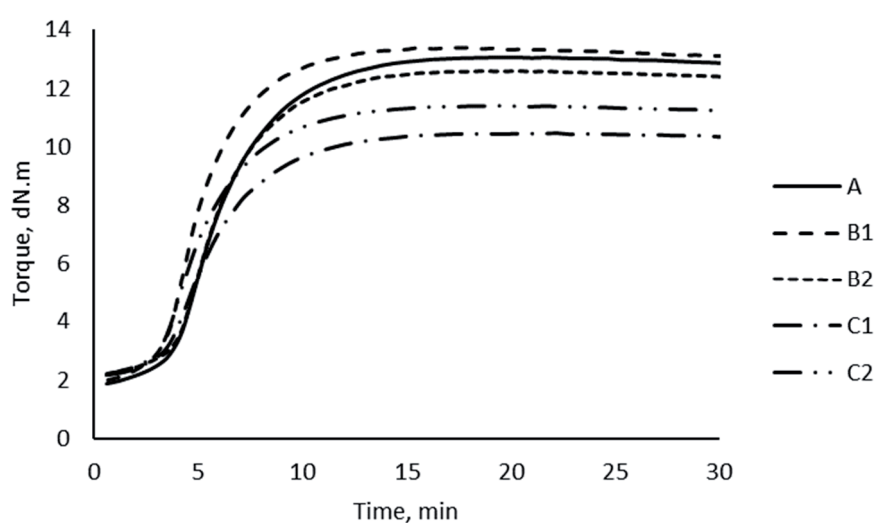


Figure 2. Vulcanization curves of the rubber compounds.

The vulcanization curves are depicted in Figure 2 and the data summarized in Table III. The difference in minimum torque is negligible. The maximum torque and thus the torque difference (ΔM) is lower namely for the compounds containing 14 phr of alternative oils (C1, C2). This is also clearly visible on the vulcanization curve (Figure 2). This may be caused by side reaction of unsaturated fatty acid moiety of oil with sulphur.³ Note that the total concentration of oil is the same in each compound (21 phr). The scorch time TS2, i.e. the time necessary for the torque to rise by 2 dN.m from the minimum point, does show any significant difference among the compounds. The optimum cure time T90, i.e. the time to reach 90% of the torque difference (ΔM), is lower for the compound B1 only. This is connected with the increase of its cure rate index (faster vulcanization).

Table IV
Properties of the cured rubber

Compound	A	B1	B2	C1	C2
Tensile strength, MPa	15.7	17.0	17.7	15.3	15.3
Elongation at break, %	580	515	650	630	770
Modulus at 300% elongation, MPa	6.44	8.36	6.15	5.42	5.98
Tear strength, N.mm ⁻¹	52.8	49.0	50.8	42.1	46.9
Hardness, ShA	59	61	61	57	60
Abrasion, mm ³	127	116	114	118	122
Schob rebound resilience, %	37	40	37	37	35
Cracking resistance, kilocycles	30	40	40	50	50
DPGi heat build up after 5 min, °C	171	155	168	151	172
DPGi, kilocycles to break	7.4	14.1	7.8	9.5	5.9
Density, g.cm ⁻³	1.140	1.140	1.146	1.140	1.149

The properties of cured rubber are summarized in Table IV. The tensile strength is higher for the compounds containing 7 phr of alternative oil (B1, B2) while the compounds containing 14 phr of alternative oil (C1, C2) show the tensile strength comparable with the reference compound (A). For C1 and C2, the modulus at 300% elongation and the tear strength are the lowest and the elongation at break is high. This finding can be explained again by the side reaction of unsaturated vegetable part of oil with sulphur that leads to decreased crosslink density of cured rubber. This is in accordance with the lower delta torque at vulcanization. The abrasion resistance is improved when part of the standard oil is replaced with the alternative one. The crack resistance is improved with distinctive dependence on the concentration of alternative oil regardless the type of oil. The compound with 7 phr of rapeseed oil (B1) shows clearly the highest modulus 300% and number of cycles till specimen break at DPGi test. On contrary, the hardness, rebound resilience and density show only minor variations with type and concentration of alternative oil.

The results of dynamic mechanical analysis of the cured rubbers are depicted in Figure 3. The loss factor at low temperatures is related to adhesion of a tyre to wet, icy or snowy surface while the loss factor at 60 °C is related to rolling resistance. The loss factor of the compounds containing 14 phr of alternative oil (C1, C2) at -17 and 0 °C is slightly higher than the reference, showing these compounds possess better ice/wet grip. The compound with 7 phr of rapeseed oil (B1) shows lower loss factor at 60 °C, indicating lower rolling resistance.

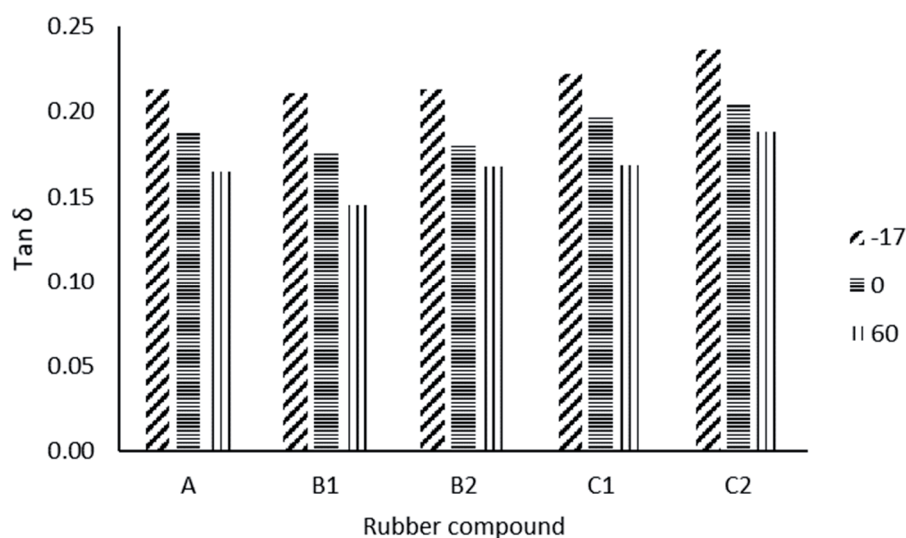


Figure 3. Dynamic mechanical analysis of the cured rubbers, loss factor ($\tan \delta$) at -17, 0 and 60 °C.

Conclusions

We tested possibilities to decrease the amount of traditional petroleum-based plasticisers used in rubber industry. Thus, two types of bio-based alternative oils, 100% rapeseed and partially vegetable, were tested as partial replacements of standard mineral oil in a model rubber compound having formulation suitable for off-road tyre tread, based on SBR/NR/BR and filled with both carbon black and silica. The total concentration of oil (standard and alternative) was constant (21 phr). The rubbers containing alternative oils show higher Mooney viscosity, lower torque difference at the vulcanization and lower tear strength; on contrary, they possess better abrasion resistance, better wet/ice grip of tyres (as indicated from the loss factor) and better resistance to cracking. The tensile strength, elongation at break, modulus at 300% elongation, resistance to dynamic fatigue (DPGi test) depend on the type and concentration of oil while the hardness, rebound resilience and density do not show such dependence. The results confirm that mineral oils can be partially replaced by bio-based oils in plasticisers of rubber; however, attention must be paid to proper choice of type and concentration of oil for each specific application.

Acknowledgement

This work was supported by Ministry of Education, Youth and Sports (specific university research). The authors would also like to thank Dr. Markéta Berčíková and Dr. Jan Kyselka for characterization of the alternative oils and to Mrs. Jana Růžová for some of the analyses of mechanical properties.

References

1. Sovtic N., Predrag K. S., Bera O. J., Pavlicevic J. M., Govedarica O. M., Jovicic M. C., Govedarica D. D.: Polym. Eng. Sci. 60, 1097 (2020).
2. Roy K., Poompiew N., Pongwisuthiruchte A., Potiyaraj P.: ACS Omega 6, 31384 (2021).
3. Fard-Zolfaghari G., Abbasian A., Razzaghi-Kashani M.: Polym. Eng. Sci. 61, 1379 (2021).
4. Intharapat P., Kongnoo A., Maiwat P.: J. Vinyl Addit. Technol. 26, 62 (2020).
5. Li J. X., Isayev A. I.: Rubber Chem. Technol. 91, 719 (2018).
6. Ward A. A., Abd-El-Messieh S. L., Khalaf A. I., El Nashar D. A.: KGK-Kautsch. Gummi Kunstst. 72, 36 (2019).
7. Hayichelaeh C., Reuvekamp L., Dierkes W. K., Blume A., Noordermeer J. W. M., Sahakaro K.: Rubber Chem. Technol. 93, 195 (2020).
8. Hassan A. A., Abbas A., Rasheed T., Bilal M., Iqbal H. M. N., Wang S. F.: Sci. Total Environ. 682, (2019).

MATERIALS RECYCLING IN THE PRODUCTION OF POROUS POLYMERIC MOLDS

Pokorný J.¹, Motyčková J.¹, Riedelová K.¹, Sedlářová I.², Urbánek J.¹, Blažek Z.³

¹University of Chemistry and Technology Prague, Technoparc Kralupy, Kralupy nad Vltavou, Czech Republic

²University of Chemistry and Technology Prague, Department of Inorganic Technology, Prague, Czech Republic

³Dřevojas, v.d., Svitavy, Czech Republic

Abstract

A waste cured polymeric material is generated in the manufacture of porous polymeric molds used for the production of sanitary ceramics ware by the pressure slip casting process. This paper deals with the possibility to recycle these wastes in the production of new molds. Attention is paid to the influence of the particle size of recycled powders, their content in the composition, the particle shape, and some other parameters on the properties of polymeric porous mass. Achieving suitable flow properties of the polymeric compound composition is crucial for the successful application of recyclates on the technical scale. With proper adjustment the content at least 10 % of recycled material can be achieved in the new recipe.

Introduction

Sanitary ware products, such as washbasins, toilet bowls, urinals, and others, are produced by casting ceramic slip into porous molds, followed by a number of other technological operations, such as drying, firing, glazing, and repeated firing. The original gypsum molds are being continuously replaced by molds made of porous polymeric materials. Polymeric molds have better mechanical properties, thus enabling casting / pressing of products at higher pressures, shortening the cycle time and production of 10 – 15 thousands pieces of castings on one mold.

Porous polymeric molds for pressure casting sanitary ware are produced by curing a reactive casting composition in a primary mold¹. The main components of this composition are: a) water, b) powder-like homopolymers or copolymers of methacrylic acid esters as fillers, c) liquid polymerizable monomers, most often methyl methacrylate and styrene, as a curable matrix, d) suitable nonionic wetting agents and emulsifiers for stabilization of the whole dispersion, and e) a two-component hardener composed of initiator of radical polymerization of monomers, usually based on organic peroxide mixtures, e.g. benzoyl peroxide, and an accelerator, usually a tertiary amine, such as N, N-dimethyl-p-toluidine. During the polymerization of the monomers, the mass hardens in the shape of the future mold and at the same time a network of open and interconnected pores filled with water is formed. Typical pore size is in the range of 5-25 μm . The pore size can be regulated, for example, by the addition of sodium tetraborate decahydrate² or by a suitable combination of two emulsifiers based on poloxamer triblock copolymers with different compositions³. Other materials with spherical or spheroidal particles can be used as fillers, such as glass or ceramic, solid and hollow microspheres, or even short glass fibers, the addition of which can significantly reduce mold shrinkage during curing². The application of metal powders, mainly aluminum, has also been described⁴.

In the production of porous polymeric molds, there is generated a waste cured polymeric material. Its sources are mainly residues from cleaning equipment, chips from mechanical processing - milling of hardened molds and occasionally produced non-functional molds, i.e. the whole molds that do not meet the quality requirements for the target application. These wastes belong to the category of hazardous wastes and require special disposal procedures, which further increases the cost of mold production. In our project, we focused on the possibility of reusing these wastes as recycled materials in the production of new porous molds for the same application. At least partial recycling would help to reduce material costs and the environmental impact of the production itself. This paper presents some of the results obtained.

Experiment

Materials

Methyl methacrylate (MMA), styrene (S), ethylene glycol dimethacrylate (EGDMA), dibenzoyl peroxide Luperox A75 (BPO) and N, N-dimethyl-p-toluidine (DMPT) were purchased from Merck. Polymeric powders - PMMA beads - with mean diameter of 40 μm (PMMA-1) and 500 μm (PMMA-2) were obtained from Lucite International and Polycasa, respectively. Poloxamer type EO-PO block copolymer emulsifiers with EO block content 40 % was obtained from BASF. All materials were used without further treatment.

Preparation of recycled powders

Recycled materials, from different commercially available hardened polymeric masses, were supplied by Dřevojas v.d. Recycled powders mostly originated from the shaping of the freshly casted porous mold by milling, thus the particles have a shape of small chips. These were dried at ambient conditions for 3 - 5 days, typical content of water after this treatment was 1 %. Dry powders, after divided into selected fractions on sieves, were used in the formulation of new porous polymer compounds or, alternatively, they were further ground in a laboratory planetary ball mill Retsch PM 100 before sieving.

Preparation of porous polymeric compounds

The casting dispersion of porous polymer mass was prepared from two premixes - aqueous phase (premix No. 1) and organic phase (premix No. 2). The aqueous phase (premix No. 1) typically contained 23 – 25 % demineralized water and 14 - 45 % PMMA powder blends based on the entire dispersion. The blend of powders usually contained the finer of the two commercial PMMA powders (PMMA-1) and the recycled one. A small amount of nonionic emulsifier (typically 0.1 %) was added to facilitate dispersion of the powders. The premix No. 1 was stirred for 20 minutes while cooling to 10 ° C. The organic phase (premix No. 2) initially contained a liquid mixture of monomers MMA, S and EGDMA (17 – 20 %), poloxamer emulsifier (0.2 – 0.3 %) and DMPT (0.05 - 0.2 %). After complete dissolution of the emulsifier, BPO (0.5-1.5%) was added and this was after 1-2 minutes followed by a coarse PMMA-2 powder (15 – 35 %). Thus completed premix No. 2 was stirred for another 1-3 minutes. Immediately afterwards, the entire amount of premix No. 1 was poured into it at once. The whole mixture was stirred vigorously for another 30 - 60 s and immediately afterwards poured into the prepared molds, where it was allowed to harden for 90 minutes. After removal from the molds, the cured samples were stored in water.

Methods of characterization

The mean pore radius, r_{Hg} , and total porosity, P_{Hg} , were determined by mercury porosimetry on an AutoPore IV 9500 instrument from Micromeritics.

Gel content was determined as dried insoluble residue after dissolution of recycled porous mass in toluene gravimetrically.

Fluidity of the casting composition was determined by a modified method of cup with bottom orifice. The amount of a casting dispersion passed through the orifice before it hardens was weighed and expressed as Flow index (FI) in % R680 (means percentage of the weight of the selected well-flowing recipe R680, $FI(R680) = 100 \%$).

The determination of bulk density, BD, and apparent porosity, P_z , of porous masses was carried out in water according to the modified procedure from the standard ČSN EN 993-1. Cylindrical samples with a diameter of 18 mm and a height of 28 mm were used for the determination. The samples were dried at 45 ° C for 48 hours.

Determination of compressive strength characteristics was performed according to ČSN EN ISO 604 on universal testing machine UTS-E50 (LaborMachine) with measuring force up to 50 kN. The dried cylindrical samples after the determination of bulk density and apparent porosity were used. The measurements were performed at a constant strain rate of 2.8 mm/min. The values of compressive stress σ_c at nominal relative compression $\epsilon_c = 5$ and 10 % were evaluated on the compression stress vs. strain curve.

The water permeability of the porous material was measured on a laboratory-assembled device supplied by drinking water pipeline. The principle of the method was to measure the amount of water that flows through a sample of porous material at the prescribed pressure. The sample had the shape of a cylinder with a diameter of 36 mm (active diameter 33 mm) and a height of 15 mm and was placed in the measuring chamber so that water flowed in and out only over the opposite circular surfaces. The water pressure difference in front of and behind the sample was 1.0 ± 0.1 bar. The measurement results are given as the normalized water permeability Q_r in $kg \cdot min^{-1}$ through the porous mass with a surface area of 1 cm^2 and a thickness of 1 cm at a unit pressure difference of 1 bar.

Scanning electron microscopy (SEM) of the fracture surfaces of the samples was performed using an EVO 15 microscope (Zeiss). Prior to analysis, the samples were sprayed with a thin layer of palladium and glued on the microscope plate with double-sided conductive adhesive tape. The samples were scanned using a secondary electron detector at an accelerating voltage of 4.0 kV, magnification in the range of 112 - 560x.

Discussion and result analysis

Control of casting mass fluidity

Viscosity, resp. fluidity, of the mixed casting mass is an important technological parameter. The mixture must fill easily the entire volume of the primary mold without imperfections and bubbles, at the same time it must be sufficiently colloidally stable and harden quickly so that the dispersion does not separate after casting. During

the mixing of the composition and further after its pouring into the mold, the viscosity increases rapidly, which is caused both by the dissolution of PMMA powders in the monomers and by chemical curing due to the polymerization of the monomers present. Preliminary experiments showed that the recycled powder must be added as a part of the water premix No. 1, since in premix No. 2 it immediately swells by monomers and dissolves and the compound cannot be processed at all. However, even under such measures, significant differences in fluidity were observed for blends containing recyclates from various commercial porous polymeric materials. It was found that these recyclates differed mainly in the gel content.

To confirm this observation, an experiment was carried out according to Table 1. Three samples R680, R729 and R730 without any recycled porous material added were prepared that differed in the dosage of EGDMA bi-functional monomer in a monomer mixture. Presence of EGDMA caused crosslinking of the binder matrix during curing. Further, recycled powders were prepared from the thus cured materials and were used in the amount 10% of the whole batch in the manufacture of new samples of porous polymeric materials R728, R736 and R737 with otherwise same formula as R680. The results confirmed a positive effect of crosslinking the binder in the original porous material on the viscosity of the new mixture. The FI of R736 and R737 containing recyclates with high gel content is almost identical to the mixture without recycled material.

Table I

Effect of matrix crosslinking on flow index of compounds with recycled material

Recipe No.	R680	R729	R730	R728	R736	R737		
Crosslinking agent in monomers, %	-	5	10	-	-	-		
Recyclate type [from recipe No.]	-	-	-	R680	R729	R730		
Recyclate content in recipe, %	-	-	-	10	10	10		
Gel content in dry recyclate, %	-	-	-	4	35	38		
Flow index	FI	% R680	100	100	101	38.5	97.1	98.5

The negative effect of the rapidly increasing viscosity of the compositions containing fast dissolving recycled powders with low gel content is shown in SEM images (Figure 1). The porous mass without recyclate has smooth and rounded surface of the inner pores. Due to rapid dissolution of recycled powders with low gel content and fast increase of viscosity of the binder the inner pores surface is rough, covered by protrusions of the cured material, which can impair water flow through the pores and make it easier for dirt to adhere and clog the pores. When the recycled material with a higher gel content is applied, the surface of the inner pores is smooth again.

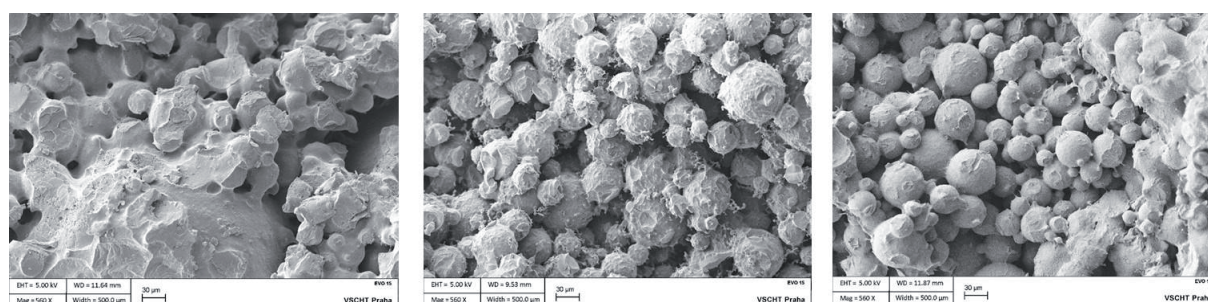


Figure 1. SEM images of porous masses inner structure. Left: R680, middle: R728, right: R737

Effect of recycled material dosage

With increased recyclate dosage there is observed a steady decrease of the fluidity of the mixed composition (Table II). However, at the level of 36 % of gel in the dry recycled powder the flow index is even at the dosage level of 15 % higher than 95 %, which is still well acceptable for technical application. Recycled powder dosage decreases the water permeability and the pore radius and broadens the pores distribution (Figure 2), which is probably due to irregular non-bead-like particle shapes that affect geometrical assembly of the whole composition.

Table II

Effect of recycle dosage and particle shape. Recyclate: commercial, substituted for coarse beads particles, contains 36 % gel, sieved fraction 0.25 – 1.00 mm, shape A – chips from milling and B – powder from grinding.

Recipe No.		R680	R713	R714	R715	R727
Recyclate content in recipe, %		0	5	10	15	10
Recyclate shape		-	A	A	A	B
Flow index	FI, % R680	100	101	98.9	95.4	97.6
Water porosity	BD, g.cm ⁻³	0.843	0.846	0.842	0.835	0.837
	P _z , %vol	29.0	28.4	28.7	29.6	29.3
Hg porosity	P _{Hg} , %vol	26.7	25.7	26.4	27.3	-
	r _{Hg} , μm	8.2	8.3	7.2	6.7	-
Water permeability	Q _r , kg.min ⁻¹	0.077	0.062	0.045	0.036	0.046
Compression stress at defined strain	σ ₅ , MPa	24.6	26.7	25.5	25.5	26.4
	σ ₁₀ , MPa	31.5	33.0	32.0	32.5	33.2

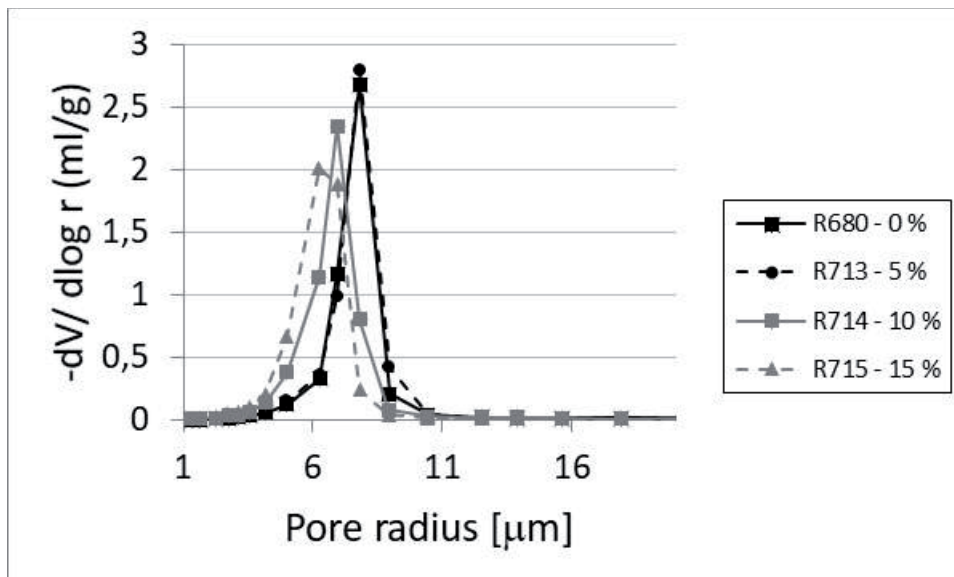


Figure 2. Pores radius distribution of masses with different recyclate content.

Effect of recycled particle shape

The shapes of particles of the recycled materials depend on the way the wastes are processed. Processing on the milling machine leaves the particles in the form of chips having certain aspect ratio while grinding leaves mostly symmetrical shapes, however still very much different from regular bead-like particles of the original commercial PMMAs. No difference in the properties of porous mass was observed due to different particle shapes of recycled powders as is documented in Table II, R714 vs. R727. Worse flow properties of the water premix No. 1 (not documented in Table II) was associated with application of chips-shape particles (R714), therefore grinding step in preparation of recyclates is recommended even for the machine milled wastes.

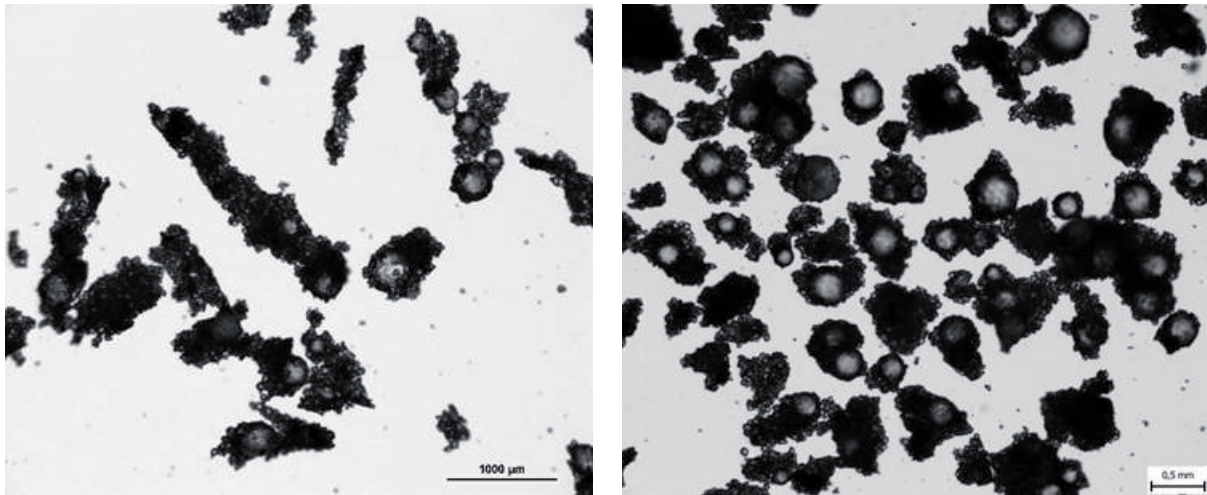


Figure 3. Shapes of recycled material particles from commercial porous mass wastes. Left: chips from milling, right: symmetrical particles from grinding

Effect of recycle particle size

It was expected that as other parameters of the recycled material also the particle size will affect the properties of the casting compound and the hardened porous mass. The most serious effect was observed by the finest particle fraction (Table III) that at the level 10 % in the formulation significantly decreased fluidity, pore size and permeability. It is assumed that the smallest particles have the largest specific surface area and require the largest amount of monomers to wet it, thus more affecting the viscosity of the mixture compared to the fractions with bigger particles. Moreover, decreasing particle size will lead to smaller size of pores between them⁵. On the other hand, with increase of particle size, especially above 1.0 mm, gradual decrease of fluidity of the water premix No. 1 was observed (not documented in Table III). The most suitable range of recycle particle size is expected 0.25 – 0.75 mm.

Table III

Effect of recycle particle size (R680 without recycle). Recycle: commercial, substituted for fine beads particles, contains 36 % gel, content in recipe 10 %, different sieved fractions, shape A – chips from milling.

Recipe No.		R680	R676	R677	R678	R679
Recycle – Particle size fraction, mm		-	<0.25	0.25-1.0	1.0-2.5	>2.5
Flow index	FI, % R680	100	93.9	99.5	99.3	99.4
	BD, g.cm ⁻³	0.843	0.844	0.846	0.843	0.838
Water porosity	P _z , %vol	29.0	28.7	28.3	29.1	29.7
	P _{Hg} , %vol	26.7	26.2	26.0	25.5	25.9
Hg porosity	r _{Hg} , µm	8.2	7.0	8.5	8.3	8.3
	Water permeability	Q _r , kg.min ⁻¹	0.077	0.055	0.064	0.065
Compression stress at defined strain	σ ₅ , MPa	24.6	21.2	20.8	23.4	22.1
	σ ₁₀ , MPa	31.5	28.2	28.3	30.2	29.0

Effect of substitution for fine or coarse beads PMMA

The results presented in Table II and Table III, and especially R714 and R677, were obtained by modifying the same original recipe R680 by the same recycled powder and at the same dosage level. Closer comparison of these results reveals certain differences. In case of the recipe R714 the addition of 10 % recycled material resulted in a very significant reduction in water permeability (by about 40 % relative) and pore radius compared to R680. In case of R677 the influence on permeability for water and pore size was much smaller, and there was a significant deterioration of mechanical properties, especially stress at 5 % strain, σ₅. These differences can be explained by

different way of application of the recycled powder in the new compound. While in case of R714 the recycled material substituted a part of coarse particle PMMA, in case of R677 there was a substitution for a part of the fine bead particles. Fine bead particles with higher specific surface area dissolve readily in monomer, thus increase the volume fraction of the matrix binder, thickness and strength of the connections between PMMA beads in the mass. Therefore, the mechanical properties of R714 having the same amount of fine bead particles as the recipe without recycled powder are unaffected (maybe even slightly increased due to presence of fine particles in recycle), while the same for R677 at which the fine particles were substituted by coarser recycle are lowered. One might also expect decreasing fluidity of R714, but this would probably be more significant only at higher recycle dosage. Coarse bead particles function as the filler. Increasing of the coarse particle size usually increase water permeability and pore radius⁵. Thus, substitution of fine beads PMMA by coarser recycle in R677 has only low effect on water permeability and average pore radius. It is assumed that a partial substitution of recycled powder for combination of both fine and coarse beads PMMAs will allow to achieve good compromise for all important properties of the porous mass.

Conclusions

It was shown, that the recycled powder from polymeric porous molds production and exploitation can be applied in the recipes of a new porous mold up to the level at least 10 %. The most critical parameter when recycled powder is applied is the fluidity of the casting composition. To cope with it, recycled powder must be introduced via water premix and should contain crosslinked original binder to reduce its solubility. Crosslinking of the binder in original mold production is best achieved by an addition of di- or multifunctional monomer.

It was further shown that the size and shape of recycled powder particles affect mainly the fluidity of the whole casting composition and/or the fluidity and processability of the water premix – too fine, too coarse and asymmetric particles should be omitted.

The presence of recycled powder decreases both, water permeability and mechanical properties. The extent of this effect depends on the composition of the whole compound.

Acknowledgement

This work was supported by the Ministry of Industry and Trade of the Czech Republic project FV40392.

References

1. DE 1928026
2. EP 0516224 B1
3. CZ 32336 U1
4. EP 2583995 A1
5. Pokorný J., Motyčková J., Riedelová K., Sedlářová I., Blažek Z., Hisem P.: *Porous polymeric compound with controlled properties*, Proceedings of the 7th International Conference on Chemical Technology (2019) 292-297

PREPARATION OF STRONG CATION EXCHANGE RESIN ON THE BASE OF STYRENE – DIVINYLBENZENE COPOLYMER FOR WATER TREATMENT

Skálová H.¹, Jelínek L.¹, Štěpánková Z.¹

¹University of Chemistry and Technology, Prague, Czech Republic
skalovah@vscht.cz

Abstract

The aim of this work was the preparation of mechanically and chemically resistant polymer sorbent based on the poly(styrene-co-divinylbenzene) that was further functionalized to a strong acid cation exchange resin. The preparation of the resin is divided into two steps - suspension polymerization of the polymeric beads and subsequent chemical functionalization. Suspension polymerization was carried out in a heated reactor where mixture of monomers with initiator were dispersed in a solution of a suspension stabilizing agent. The viscosity of solution of monomers was controlled by addition of linear polystyrene. The polymer droplets were cured into sub-500 µm spherical beads, which are insoluble in water and organic solvents. The functionalization was performed by sulfonation in sulfuric acid or chlorosulfonation in chlorosulfuric acid. The sorption capacity of the prepared strong cation exchange resins was ascertained with the sorption of cadmium and zinc ions from aqueous solution in batch experiments. The sorption capacity of prepared strong cation exchange resin prepared by optimal conditions is comparable to commercial resins (around 2meq/L).

Introduction

Heavy metals, such as cadmium and zinc, are found in greater quantities in the environment due to increased industrial activity. Therefore, it is important to effectively remove them from the environment.

To remove ions from water source we have many options that differ according to many parameters. Water purification is a process with many steps where ion exchange resins are among the final methods. The process differs according to the source of water and the required quality at the end of purification process. Based on these conditions, individual methods or their sequence are selected.

In this work we choose to synthesize and further functionalize polymer sorbent for sorption of zinc and cadmium ions from aqueous solution. Our main reason was the possibility to control the particle size, degree of functionalization and crosslinking percentage. These parameters are among the most important characteristics of used polymer sorbent in a water purification and also determines their price and commercial availability.

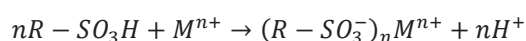
Zinc and cadmium are removed from aqueous solutions using various technologies. The most commonly used technologies include chemical precipitation, coagulation, flotation, extraction, cementation, complexation, electrochemical processes, biological processes, adsorption, membrane processes and ion exchange technologies^[1,2].

However, some of these methods have disadvantages such as reduced efficiency, delicate operating conditions, and high costs. Ion exchange method is one of the most used and effective methods of wastewater treatment worldwide due to its various benefits including regeneration capability of ion exchangers, low pH independence, high selectivity, low cost, etc. The Cation exchange resin has the specific ability to exchange its cations with the metallic cations in the aqueous solutions. Synthetic resins are widely preferred among the other ion-exchange materials on the grounds that they are effective in almost completely removing heavy metals from solution. The main advantages of strong cation exchange resins are uniform properties and chemical stability^[3, 4, 5].

The most used polymer matrices include the styrene-DVB copolymer and polyacrylates [6]. The styrene-DVB copolymer is prepared by suspension polymerization. Based on the amount of crosslinking agent (DVB) and the presence of a porogen agent, it is possible to synthesize macroporous or gel type ion exchangers. When the copolymer matrix is functionalized, it becomes an active ion exchanger^[7, 8].

Functionalization is the process by which the functional groups are bonded onto the polymer beads. To ensure high exchange capacity, functional groups must be bonded not only onto the surface but also inside the beads. This is ensured by the process taking place in a solution. Functionalization can be carried out in various ways based on the chemical properties of the polymer matrix as well as on the required functional group. It can be carried out during the preparation of the polymer matrix or afterwards^[7, 9].

One of the most prevalent cation exchangers is strongly acidic resin with a functional group of sulfonic acid (-SO₃H). Heavy metal cations are exchanged with the hydrogen ions of the sulfonic group on the resin with the following process:



The uptake level of metals by ion-exchange resins is affected by factors as pH, temperature, phase contact time and initial concentration of metal in the solution [10, 11].

Experiment

1. Preparation and functionalization of polymer sorbent

In the first step we prepared the matrix in the form of polymeric beads with particle distribution 10-200 μm . Suspension polymerization method in aqueous medium was used as the selected method of preparation for polymer matrix. Polymerization took place in a heated reactor with an axial shaft stirrer where the monomer blend of styrene and divinylbenzene in molar ratio 9:1 with a dissolved initiator dibenzoyl peroxide (DBP) dispersed in 5 w% aqueous solution of (polyvinyl)alcohol (PVA). We have added DBP in a molar ratio approximately 1:3 000 to the monomer blend. Aqueous solution of PVA is immiscible with the monomer blend and at the same time acts as a suspension stabilizer which prevents agglomeration of monomer droplets and sintering of the resulting polymer particles. The monomer blend was dispersed in the aqueous solution of PVA by stirring and also due to the continuous stirring the monomer droplets and resulting polymer particles were floating in the reaction medium. During the polymerization the monomer droplets have been heat-cured to polymer particles. The optimal temperature for suspension polymerization was set at 90°C for the entire polymerization time of 2,5 h.

To increase the viscosity of monomer blend, we dissolved linear polystyrene (PS) in a monomer blend to increase the size of the resulting particles. We have dissolved approximately 0,6 g of linear PS ($M_w = 35\ 000$) 10 ml of monomer blend. Linear polystyrene was removed from finished polymer beads by Soxhlet extraction with organic solvent (xylene) after the polymerization. Without the increased viscosity of monomer blend we acquired polymer particles of size around 10 μm that was too small for our use.

To obtain strong cation exchange resin with a sulfonic functional group we tested two functionalization method. Firstly, we tested the sulfonation method with excess of hot sulfuric acid. We used silver sulfate as a catalyst which we dissolved in a hot sulphuric acid before adding swollen polymeric beads. Silver sulfate molar ration to a functionalization agent was approximately 1:600. We tested different reaction temperatures and functionalization time between 30 min to 4 h. As a second method of functionalization, we choose chlorosulfonation with a subsequent hydrolysis in water. Chlorosulfonation process was carried out in a chloroform solution where the polymer beads were swollen. We have used a chlorosulfuric acid in a mass ratio 3:1 to polymer beads. It was crucial to add chlorosulfuric acid dropwise due to the exothermic character of the reaction. And it was also necessary to cool down the reaction mixture throughout the reaction. In this process, sulfonyl chloride was firstly bound to a polymer matrix, which is subsequently hydrolysed in water to sulfonic acid functional group.

2. Batch experiments

Model solutions for the batch experiments containing Cd(II) or Zn(II) were prepared. The model solution of Cd(II) was prepared from $\text{CdSO}_4 \cdot 8\text{H}_2\text{O}$ and final concentration of Cd(II) was 140 mg/L on the average. The model solution of Zn(II) was prepared from $\text{ZnSO}_4 \cdot 7\text{H}_2\text{O}$ and contained around 57 mg/L of Zn(II). These solutions were tested at the optimal pH values based on previous experiments with commercially available strongly acidic cation exchange resin Lewatit MonoPlus S 100. The optimum pH value of the initial model solution was found for the sorption of Cd(II) at the value of 8 and for the sorption Zn(II) at the value of 6.

The batch experiments were carried out using overhead stirrers for the sake of better contact ability of the sorbent with the solution. The volume ratio of sorbent to the model solution was 1:1000. Monitoring of the kinetics of ion-exchange reaction during the batch experiments was performed by taking the individual samples at the specific time intervals for 4 h. These individual samples were analysed using AAS spectrophotometer. Results from the analysis were then used to determine the captured amount of metal in sorbent (q) by following formula:

$$q_n = \frac{\left((\rho_0 - \rho_n) \cdot (V_0 - (n - 1) \cdot V_V) + \sum_{i=0}^{n-1} (\rho_0 - \rho_j) \cdot V_V \right)}{V_S}$$

where ρ_0 was input concentration of metal in the solution [mg/L], ρ_n was residual concentration of metal in the n^{th} sample [mg/L], V_0 was initial volume of the sorption solution [L], V_V was volume of the collected sample [L], ρ_j was concentration of metal in the previous samples [mg/L] and V_S was volume of sorbent [mL].

Discussion and results analysis

1. Results of preparation and functionalization of polymer sorbent

For the preparation of polymer matrix, it was necessary to optimize the reaction conditions to obtain polymer beads with particle size 10-200 μm and to select suitable added reagents. Among the most important optimized reaction conditions were reaction stirring speed, steady heating, sufficient polymerization time and the molar ratio of monomers in the monomer blend.

For both functionalization methods we tested various reaction conditions. Both functionalization methods were carried out in excess of functionalization agent. For sulfonation method we optimized the reaction temperature to 72 $^{\circ}\text{C}$, at higher temperatures the polymer beads were destroyed. Different sulfonation times were also tested, ranging from 30 min to 4 h. The highest total exchange capacity was obtained when sulfonation was carried out for 4 h. However, longer sulfonation times resulted in a higher degree of polymer sorbent destruction. For optimization of chlorosulfonation method it was crucial to add the chlorosulfuric acid drop wise and to cool down the reaction mixture to 0 $^{\circ}\text{C}$ due to the exothermic character of the reaction. Different chlorosulfonation times were tested, ranging from 30 min to 4 h. The highest total exchange capacity was obtained when the chlorosulfonation was carried out for 3 h. The longer time of chlorosulfonation could lead to the formation of sulfone bridges, which reduced the overall total exchange capacity of the prepared strong acid cation exchange resin [12, 13]. In the Table 1 we compare the results for individual reaction times of the two functionalization methods. The highest achieved total exchange capacity for both methods is comparable to the total exchange capacity of commercially available strong cation exchange resins (1,8 – 2 meq/mL).

Table 1: Comparison of functionalization time and total capacity for laboratory prepared strong acid cation exchange resins

SULFONATION METHOD		CHLOROSULFONATION METHOD	
reaction time [h]	Total exchange capacity [meq/mL]	reaction time [hod]	Total exchange capacity [meq/mL]
0.5	0.49	0.5	1.53
1	0.73	1	1.37
2	1.23	2	1.39
3	1.32	3	2.04
4	1.62	4	1.84

The prepared sorbents were further tested for the sorption of cadmium and zinc from model aqueous solutions in batch experiment.

2. Results from batch experiments

The batch experiments were carried out with model solution of Cd(II) at the selected optimal pH of 8 and with the model solution of Zn(II) at the selected optimal pH of 6 with laboratory prepared sorbents. These sorbents were used in the Na^+ form.

For the sake of better clarity, in the Figure 1 and Figure 2 were for the comparison selected only those representatives of sorbents prepared by sulfonation and chlorosulfonation, that had the lowest and the highest amounts of captured metal in the sorbent (q values).

• Removal of Cd(II)

The Figure 1 shows the processes of cadmium ions captured over a period of 4 h, when the equilibrium of ion exchange was reached. We compare the sorbents after sulfonation and chlorosulfonation with the highest and lowest values of q and for comparison also shows the sorption history on the commercial strongly acidic cation exchange resin Lewatit MonoPlus S 100 (107 g/L).

The highest maximum value of q (105 g/L) was exhibited by the sorbent after 3 hours of chlorosulfonation, the ion exchange equilibrium was reached after 1.5 h of the experiment. On the other hand, the sorbent achieving the lowest value of q (26 g/L) was prepared by sulfonation for 0.5 h and the ion exchange equilibrium occurred after 2.5 h of reaction. The other prepared sorbents reached ion exchange equilibrium after approximately 1.5 h of the experiment and their values of q ranged from 45 to 103 g/L.

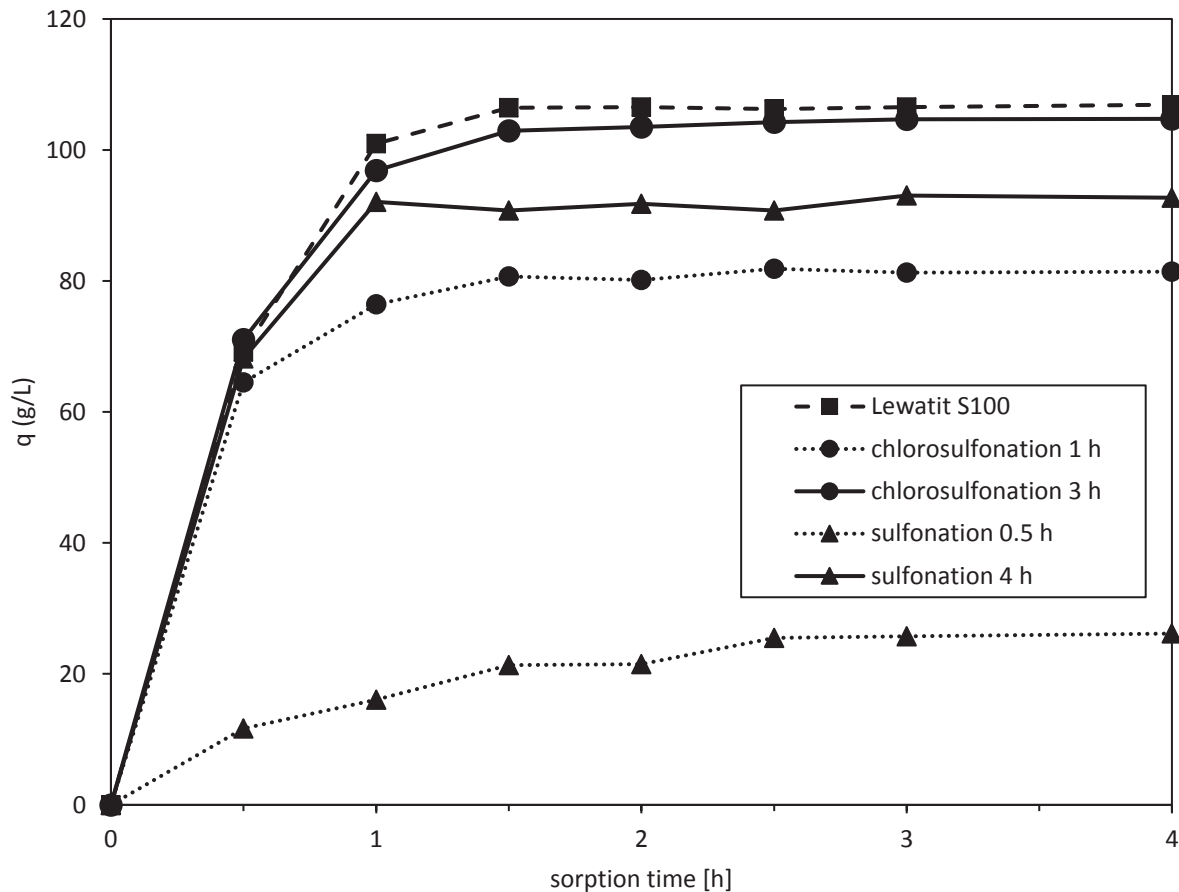


Figure 1: Cadmium - dependence of the q on the sorption time using laboratory prepared sorbents and commercial sorbent Lewatit MonoPlus S 100.

- **Removal of Zn(II)**

The Figure 2 shows the processes of zinc ions capture over a period of 4 h, when the equilibrium of ion exchange was reached. We compare the sorbents after sulfonation and chlorosulfonation with the highest and lowest values of q and for comparison also shows the sorption history on the commercial strongly acidic cation exchange resin Lewatit MonoPlus S 100 (54 g/L).

The best results were achieved by the sorbent after 4 h of chlorosulfonation (q was 47 g/L), when the ion exchange equilibrium was reached after 4 h of experiment. Very similar results were also achieved by the sorbent after 3 h of chlorosulfonation. On the contrary, the sorbent after sulfonation for 0.5 h achieved the lowest maximum value of q (14 g/L). Similar results were also obtained by the sorbent after sulfonation for 1 h and both sorbents reached the ion exchange equilibrium after 1 h of the experiment. The other prepared sorbents reached the ion exchange equilibrium after 1-3 h of the experiment and their sorption efficiencies ranged from 16 to 46 g/L.

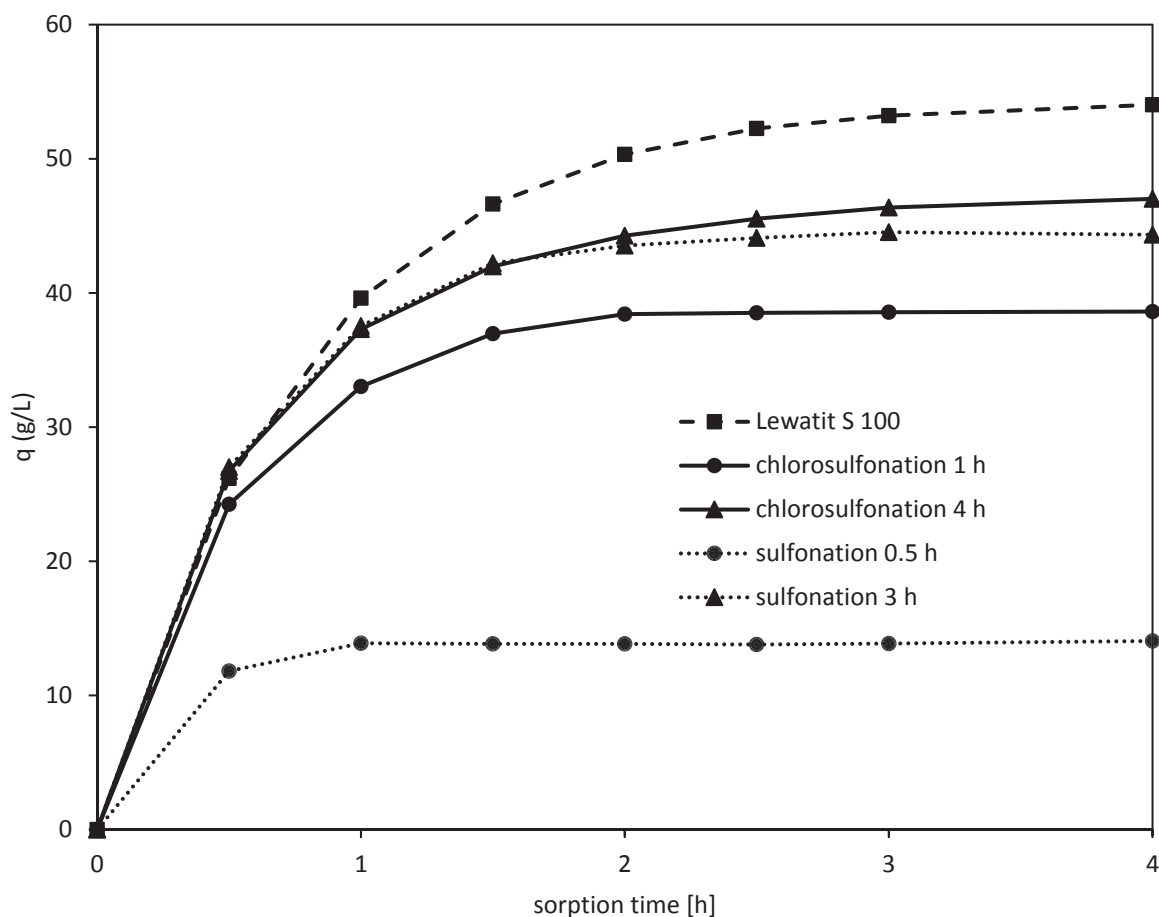


Figure 2: Zinc - dependence of the q on the sorption time using laboratory prepared sorbents and commercial sorbent Lewatit MonoPlus S 100.

Moreover, the q of the sorbents prepared by chlorosulfonation for 3 and 4 h (47 g/L) was not approaching the q of the commercial sorbent Lewatit MonoPlus S100 (54 g/L) as well as it was in the case of Cd(II). The maximum q of these laboratory-prepared sorbents reached only 87 % of the maximum q of Lewatit MonoPlus S 100. The reason is the fact that the general selectivity of the strongly acidic cation exchange resins towards Cd(II) is higher than Zn(II).

Conclusion

By successive modification of the suspension polymerization, we were able to prepare polymer beads with a particle distribution of 10-200 μm with good mechanical and chemical resistance. By subsequent optimization of the functionalization methods of sulfonation and chlorosulfonation we prepared a strong cation exchange resin with a total exchange capacity comparable to commercially available sorbents. By comparing both sulfonation and chlorosulfonation methods, it can be deduced that the sulfonation method is characterized by a higher degree of polymer particle destruction.

From the results of batch experiments it was found that the sorbent chlorosulfonated for 3 h was suitable for the Cd(II) removal. This sorbent had similar results as commercial sorbent Lewatit MonoPlus S100.

Acknowledgement

This work was supported from the grant of Specific university research – grant No A1_FTOP_2022_001 and grant No A2_FTOP_2022_005.

References

1. Kumar, J., Balomajumder, C. & Mondal, P. Application of Agro-Based Biomasses for Zinc Removal from Wastewater - A Review. Clean - Soil, Air, Water 39, 641–652 (2011).

2. Purkayastha, D., Mishra, U. & Biswas, S. A comprehensive review on Cd(II) removal from aqueous solution. *J. Water Process Eng.* 2, 105–128 (2014).
3. Bashir, A. et al. Removal of heavy metal ions from aqueous system by ion-exchange and biosorption methods. *Environ. Chem. Lett.* 17, 729–754 (2019).
4. Naushad, M., Mittal, A., Rathore, M. & Gupta, V. Ion-exchange kinetic studies for Cd(II), Co(II), Cu(II), and Pb(II) metal ions over a composite cation exchanger. *Desalin. Water Treat.* 54, 2883–2890 (2015)
5. W. Rieman and H.F. Walton, *Ion Exchange in Analytical Chemistry*. 1970: Pergamon
6. Adams, R.S., Use of Ion Exchange Resins in Study of Chrome Liqours. *Journal of the American Leather Chemists' Association* 1946. 41(12): p. 552-573.
7. Arshady, R. and A. Ledwith, Suspension polymerization and its application to the preparation of polymer supports. *Reactive Polymers*, 1983. 1: p. 159-174.
8. Hamielec, A.E. and H. Tobita, Polymerization Processes, in *Encyclopedia of Industrial Chemistry*, I. VCH Publishers, New York, Editor. 1992. p. 305-428.
9. Fu, F. & Wang, Q. Removal of heavy metal ions from wastewaters: A review. *J. Environ. Manage.* 92, 407–418 (2011).
10. Hubicki, Z. & Koodynsk, D. Selective Removal of Heavy Metal Ions from Waters and Waste Waters Using Ion Exchange Methods. *Ion Exch. Technol.* (2012) doi:10.5772/51040.
11. Kołodyńska, D., Sofińska-Chmiel, W., Mendyk, E. & Hubicki, Z. DOWEX M 4195 and LEWATIT® MonoPlus TP 220 in Heavy Metal Ions Removal from Acidic Streams. *Sep. Sci. Technol.* 49, 2003–2015 (2014).
12. Valle, Chiara & Zecca, Marco & Rastrelli, Federico & Tubaro, Cristina & Centomo, Paolo. (2020). Effect of the Sulfonation on the Swollen State Morphology of Styrenic Cross-Linked Polymers. *Polymers*. 12. 1-14. 10.3390/polym12030600.
13. Rabia, I.; Zerouk, J.; Kerkouche, M.; Belkhouja, M. Chemical and textural characteristics of porous styrene—divinylbenzene copolymers as a function of chlorosulfonation reaction parameters, *Reactive and Functional Polymers*. *Reactive and Functional Polymers* 1996, 28 (3), 279–285.

PREPARATION AND POTENTIAL APPLICATIONS OF LIGNIN-BASED NANOSYSTEMS

Maršík D.¹, Thoresen P.P.², Kulišová M.¹, Masák J.¹, Rova U.², Christakopoulos P.², Matsakas L.²

¹University of Chemistry and Technology, Prague, Department of Biotechnology, Technická 5, 166 28 Prague 6, Czech Republic

²Biochemical Process Engineering, Division of Chemical Engineering, Department of Civil, Environmental and Natural Resources Engineering, Luleå University of Technology, 971 87 Luleå, Sweden
marsikd@vscht.cz

Abstract

Lignin is a product of the secondary metabolism of plants that arise from phenylalanine through the phenylpropanoid pathway. The resulting structure of lignin is strongly dependent on its origin and the isolation process. In general, it is a complex and biodegradable polymer with antimicrobial properties, antioxidant effects, and low cytotoxicity. As a result of these properties, lignin has high potentials for valorisation, which could also find application in medicine. The application of lignin in the form of nanoparticles, for example, as a drug delivery system, is currently being considered. To enable their use in niche applications, their preparation and characterization ought to be developed and optimized. Here, we discuss the essentials for the successful application of these systems in the production of value-added products.

Introduction

The sustainable development of society should include, among other things, the production of fuels, chemicals, and materials from renewable sources. Lignocellulosic biomass composed mainly of cellulose, hemicellulose, and lignin is a renewable raw material, the successful use of which is conditioned by efficient fractionation into individual components¹. Despite extensive studies on the valorisation of the carbohydrate fraction, especially cellulose, the use of lignin in the production of value-added products has been neglected, and lignin is still predominantly seen as a waste product of industry². This is mainly due to the complex and heterogeneous structure of irregularly crosslinked phenylpropanoid units³. Furthermore, the resulting content and composition of lignin depend on abiotic factors, plant species, tissue type, and except for 3 hydroxycinnamic alcohols coniferyl alcohol, *p*-coumaryl alcohol and sinapyl alcohol, 32 other compounds have been identified in the structure of the lignin⁴. Therefore, the progress in lignin valorisation is conditioned by the constant availability of quality raw material with the required properties. Lignin is known for its biocompatibility, antioxidant and antimicrobial effects that can be potentially used in medicine, cosmetics, or environmental fields. Therefore, many current works focus on the preparation of nanoparticles based on this polymer⁵. Nanomaterials have emerging applications in almost all industries, and new products that take advantage of nanoscale size are constantly being developed⁶. The introduction of new valuable applications and therefore an increase in the market price of lignin would support the lignocellulosic biomass processing industry, such as the production of biofuels by second-generation biorefineries⁷.

Raw material for the preparation of lignin nanoparticles

Lignin is the most abundant renewable source of aromatic compounds⁸ and the second most abundant biopolymer on Earth after cellulose⁹. Lignin can be separated from lignocellulosic materials by several physical, chemical, or biological pre-treatment methods^{10,11}. However, the main industrial sources of lignin are kraft, sulphite, soda, and organosolv lignins, of which we currently use about 2% to produce value-added products, and the rest is usually incinerated for energy purposes^{7,12}.

The traditional source of lignin is the pulp and paper industry, where the kraft process is used primarily for the pre-treatment of lignocellulose¹², during which the lignocellulosic material is heated in a mixture of sodium hydroxide and sodium sulphide and lignin macromolecules are cleaved at the positions β -O-4 and α -O-4¹³. In addition to degradation reactions, condensation also occurs between the released fragments, which give rise to new C-C bonds^{14,15}. Therefore, kraft lignin is largely different from the native lignin structure, and the polymer additionally contains 2 to 3% sulphur, which causes an unpleasant odour of the raw material¹⁶. On the other hand, kraft lignin accounts for approximately 85% of total production¹⁷, which is one of the reasons why many current studies on the preparation of lignin nanosystems choose this source^{18,19}.

Another common industrial method for paper production is the sulphite process. The pulping of wood biomass takes place at a temperature of 120 to 150 °C under the action of sulfuric acid and sulphite salts such as calcium sulphite, sodium sulphite, magnesium sulphite, or ammonium sulphite. The cooking solution is saturated with sulphur dioxide during the process. The main product, cellulose, is gradually separated from the leachate of sulphite that contains dissolved lignin in the form of lignosulfonate²⁰, which is water soluble due to the incorporated sulfonate groups¹⁷. The final composition of the cooking solution depends on the specific process, but sulfonated lignin complexes contain, among others, toxic phenol derivatives²¹. The total sulphur content ranges from 3.5 to 8.0%¹². Commercially, lignosulfonates are the most widely used technical lignins²², but because the sulphite process is gradually being replaced by the kraft process, some companies produce lignosulfonate form kraft lignin²¹.

The traditional delignification method used to pulp non-wood material, usually flax, straw, or bagasse, is the soda process. The production capacities of this process are considerably limited due to the year-on-year variability of raw materials⁷. Methodologically, the soda process is similar to the kraft process; even here the native structure of lignin is fragmented under conditions of elevated temperature and strongly alkaline conditions²³. The main difference is the absence of sodium sulphate, which is reduced to sodium sulphide resulting from the production of the sulphate pulp. Sodium sulphide is further hydrolysed to sodium hydrosulphide and sodium hydroxide. The presence of the hydrogen sulphide anion during the kraft process causes the collapse of the β -O-4' ether bond between the phenolic units of the lignin, and thus significantly improves the selectivity, rate, and overall efficiency of the delignification²⁴. Thus, kraft lignin contains higher amounts of phenolic hydroxyl groups compared to soda lignin¹³. On the contrary, during the soda process, there is no artificial increase in the sulphur content of the lignin. However, the resulting ash content is higher compared to organosolv lignin¹². Similarly to the kraft process, soda lignin can be precipitated by acidifying black liquor²³.

The very promising and ever evolving method of pretreatment of lignocellulose is the organosolv process, in which the material is fractionated in a mixture of organic solvent and water under conditions of high temperature and pressure²⁵. During the fractionation process, lignin macromolecules are preferably cleaved at the α -O-4' position²⁶ and as a result the organosolv lignin may be structurally closer to the native structure of the polymer compared to kraft lignin²⁷. In addition, organosolv lignin does not contain artificially added sulphur in its structure and is characterized by high purity, low molecular weight, good solubility in organic solvents, and high purity, *i.e.*, low in carbohydrates and ash⁷. Despite the higher quality of the raw material¹², organosolv has not received yet such attention in the field of nanoparticle preparation as kraft lignin²⁸. As such, taking into account the positive characteristics of organosolv lignin, it consists a novel and very promising feedstock for the production of nanostructures.

Preparation, application, and significant properties of lignin nanoparticles

Lignin nanoparticles preparation methods are summarized in detail Chauham²⁸. These are usually bottom-up approaches, where the basic components are assembled into larger units and include polymerization, acidic, basic, or antisolvent precipitation, interfacial cross-linking, and emulsification or solvent exchange. Lignin nanoparticles can also be prepared by a top-down approach, which involves the breakdown of the bulk material into nanosized particles. In the preparation of lignin nanoparticles, for example, ultrasonication, homogenization, or biological methods have been used. The resulting structure of nanoparticles and associated properties will depend not only on the input raw material but also on the choice of the method for their preparation. This should be taken into account in the future application of nanoparticles, which could include antimicrobials, reinforcing materials, packaging materials in the food industry, cosmetic components or nanocarriers of other substances or nanoparticles²⁹. Furthermore, lignin nanoparticles show low toxicity to human cell lines and therefore medical applications such as drug delivery systems are also considered³⁰. However, to achieve the desired effect, the nanosystem must meet complex requirements, which are devoted in the following section.

For the use of lignin nanoparticles as drug delivery systems, effective cellular uptake is essential to get the nanoparticles to the target tissue or organ, where they can induce the desired therapeutic effect. Cellular uptake strongly depends on size, shape, and surface properties³¹. Several studies have reported that the optimal nanoparticle size for cellular uptake is 50 nm. Nanoparticles of this size interact effectively with cytoplasmic membrane receptors, leading to internalization through receptor-mediated endocytosis. The increase in size is associated with increased elimination of nanoparticles by reticuloendothelial uptake leading to an increase in

the clearance rate³². This statement should not be generalized because, for example, Win and Feng³³ have found that uptake by Caco-2 cells, an *in vitro* model that mimics intestinal epithelium, is more than twice higher for 100 nm polystyrene nanoparticles compared to 50 nm nanoparticles. Thus, there will always be an optimal size range for a particular application and type of nanoparticles, whose diameter should be greater than the size cut-off of the renal filtration barrier corresponding to approximately 10 nm. The approximate upper limit of the diameter of nanoparticles is set at 200 nm, because nanoparticles of this size activate a complement system that primes quick removal from the bloodstream and nanoparticles accumulate in the liver and spleen³¹. In addition, a pathway for trafficking outside the endolysosomal system has been described for small polymeric nanoparticles below 25 nm. Polymeric particles of this size are rapidly transported to the perinuclear region of cells in nondegradable vesicles. Transported active ingredients encapsulated in a polymer can be delivered without being exposed to low pH and an enzyme-rich degradation environment in the endolysosomal pathway³⁴. Cell uptake also depends on the shape of the nanoparticle. Higher cellular uptake was observed in cylindrical polymer nanoparticles compared to spherical ones, probably due to higher surface contact with cell membranes³⁵. Because of the negative charge of the cytoplasmic membranes, it is necessary to take into account the charge properties of the nanoparticles themselves, which also influence the mechanism of uptake. Membranes prefer the internalization of positively charged nanoparticles to negatively charged ones, but when negatively and neutrally charged nanoparticles are compared, uptake is preferred for negatively charged ones. Furthermore, positively charged nanoparticles can alter the integrity of the cytoplasmic membrane and increase cytotoxicity³².

Another property that should be considered when choosing lignin as the raw material for the preparation of nanoparticles is hydrophobicity, which affects the interaction of nanoparticles with biomolecules. Hydrophobic and hydrophilic nanoparticles interact with cells by different mechanisms, and hydrophobicity is thus a determining factor in the interaction of nanoparticles with the cytoplasmic membrane and affects their uptake, opsonization, and biodistribution³⁶. Simulation studies suggest that hydrophobic nanoparticles can be internalized into the bilayer, whereas semi hydrophilic nanoparticles are adsorbed on the bilayer surface³⁷. For hydrophilic nanoparticles, it has been observed that particles larger than 2 nm are wrapped by membranes while smaller nanoparticles can be embedded in the bilayer surface where they interact with hydrophilic head groups of the lipid molecules³⁸. Due to the presence of an aromatic nucleus, lignin phenylpropanoid units are generally hydrophobic, but also contain hydroxyl groups that interact favourably with water³⁹. Hydrophobicity of the overall nanoparticles can be influenced by the type of lignin and modifications, but also by the preparation process. For example, lignin nanoparticles prepared by the process of exchanging an organic solvent for water contain a core composed of hydrophobic and less polar molecules. The surface of these nanoparticles is formed by the adsorbed most polar molecules forming a low density layer⁴⁰.

The nanoparticles are further evaluated for mechanical properties, namely elasticity, which also affect cell uptake. Quantifying the effect of elasticity is experimentally demanding, and current knowledge in this area is ambiguous. However, it is undoubtedly another property that should not be underestimated in the biological system³⁶.

The described properties can be significantly altered in the biological environment due to the interaction between nanoparticles and biomolecules. Biomolecules (usually proteins) can interact with nanoparticles, adsorb to the surface, and form a corona layer. This modification can be prevented by pegylation, during which the surface of the nanoparticles is coated with a layer of polyethylene glycol, which sterically precludes protein adsorption and reduces the ability of the nanoparticles to be recognized by macrophages³⁶. The formation of corona on the surface of pure lignin nanoparticles with a size of 232 nm was observed by Figueiredo *et al.*³⁰, where the particle size determined by diffraction light scattering almost doubled and ζ -potential increase from -44 mV to -26 mV after incubation in blood plasma for a few minutes. For some biomedical applications, corona formation may be desirable. In colloidal lignin nanoparticles, efficient corona formation was observed using gelatine and poly-L-lysine. Proteins can be adsorbed on the surface of lignin nanoparticles mainly through electrostatic, hydrophobic, and van der Waals interactions and hydrogen bonding. The contribution of a particular interaction strongly depends on the ionic strength of the medium⁴¹.

Conclusion

Currently, lignin nanoparticles of various sizes and shapes can be prepared. For this purpose, several different methods have been developed, for which we can also choose different input raw materials. This variability should be taken into account when nanoparticles are prepared for a particulate application, since the type of lignin and the preparation process itself greatly affect the nanosystem properties. For medical applications, as well as other considered applications, we should focus on the required size, shape, and surface properties of nanoparticles when designing the process. From the point of view of the quality of the raw material, organosolv lignin, which does not have an artificially increased sulphur content and contains a small amount of impurities, appears to be very promising. In addition, the structure of organosolv lignin may be closer to that of the native polymer structure compared to other industrial lignins. However, the industrial availability of the organosolv is still minor compared to, for example, kraft lignin.

Acknowledgement

This work was supported from the grant of Specific university research – grant No. A2_FPBT_2022_057.

References

1. Lorenci Woiciechowski A., Dalmas Neto C. J., Porto de Souza Vandenberghe L., de Carvalho Neto D. P., Novak Sydney A. C., Letti L. A. J., Karp S. G., Zevallos Torres L. A., Soccol C. R.: *Bioresour. Technol.* **304**, 122848 (2020).
2. Luo H., Klein I. M., Jiang Y., Zhu H., Liu B., Kenttämä H. I., Abu-Omar M. M.: *ACS Sustain. Chem. Eng.* **4**, 2316 (2016).
3. Chio C., Sain M., Qin W.: *Renew. Sust. Energ. Rev.* **107**, 232 (2019).
4. Vanholme R., De Meester B., Ralph J., Boerjan W.: *Curr. Opi. Biotechnol.* **56**, 230 (2019).
5. Iravani S., Varma R. S.: *Green Chem.* **22**, 612 (2020).
6. Subhan M. A., Choudhury K. P., Neogi N.: *Nanomanuf.* **1**, 75 (2021).
7. Haq I., Mazumder P., Kalamdhad A. S.: *Bioresour. Technol.* **312**, 123636 (2020).
8. Cao Y., Chen S. S., Zhang S., Ok Y. S., Matsagar B. M., Wu K. C. W., Tsang D. C. W.: *Bioresour. Technol.* **291**, 121878 (2019).
9. Sharma S., Sharma A., Mulla S. I., Pant D., Sharma T., Kumar A.: *Lignin, Biosynthesis and Transformation for Industrial Applications*, Springer Series on Polymer and composite materials. Springer **1** (2020).
10. Eraghi Kazzaz A., Fatehi P.: *Ind. Crops Prod.* **154**, 112732 (2020).
11. Xu N., Liu S., Xin F., Zhou J., Jia H., Xu J., Jiang M., Dong W.: *Front. Bioeng. Biotech.* **7**, 191 (2019).
12. Bajwa D. S., Pourhashem G., Ullah A. H., Bajwa S. G.: *Ind. Crops Prod.* **139**, 111526 (2019).
13. Sameni J., Jaffer S. A., Sain M.: *Composites Part A: Appl. Sci. Manuf.* **115**, 104 (2018).
14. Fodil Cherif M., Trache D., Brosse N., Benaliouche F., Tarchoun A. F.: *Waste Biomass Valori.* **11**, 6541 (2020).
15. Gierer J.: *Wood Sci. Technol.* **14**, 241 (1980).
16. Evdokimov A. N., Kurzin A. V., Fedorova O. V., Lukanin P. V., Kazakov V. G., Trifonova A. D.: *Wood Sci. Technol.* **52**, 1165 (2018).
17. Chen H.: *Lignocellulose Biorefinery Engineering* (Chen H., ed.), pg. 37. Woodhead Publishing, 2015.
18. Lievonon M., Valle-Delgado J. J., Mattinen M.-L., Hult E.-L., Lintinen K., Kostianen M. A., Paananen A., Szilvay G. R., Setälä H., Österberg M.: *Green Chem.* **18**, 1416 (2016).
19. Nair S. S., Sharma S., Pu Y., Sun Q., Pan S., Zhu J. Y., Deng Y., Ragauskas A. J.: *ChemSusChem.* **7**, 3513 (2014).
20. Rajesh Banu J., Kavitha S., Yukesh Kannah R., Poornima Devi T., Gunasekaran M., Kim S.-H., Kumar G.: *Bioresour. Technol.* **290**, 121790 (2019).
21. Tsvetkov M. V., Salganskii E. A.: *Russ. J. Appl. Chem.* **91**, 1129 (2018).
22. Aro T., Fatehi P.: *ChemSusChem.* **10**, 1861 (2017).
23. Windeisen E., Wegener G.: *Polymer Science: A Comprehensive Reference* (Matyjaszewski K., Möller M., ed.), pg. 255. Elsevier, Amsterdam 2012.
24. Augusto Q.: The role of sulfidity during kraft pulping. Retrieved from Pulp & Paper Canada website 20.06.2022: <https://www.pulpandpapercanada.com/the-role-of-sulfidity-during-kraft-pulping/> (2021)
25. Thoresen P. P., Matsakas L., Rova U., Christakopoulos P.: *Bioresour. Technol.* **306**, 123189 (2020).
26. Jasiukaitytė-Grojzdek E., Huš M., Grilc M., Likozar B.: *Sci. Rep.* **10**, 11037 (2020).

27. Constant S., Wienk H. L., Frissen A. E., de Peinder P., Boelens R., Van Es D. S., Grisel R. J., Weckhuysen B. M., Huijgen W. J., Gosselink R. J.: *Green Chem.* **18**, 2651 (2016).
28. Chauhan P. S.: *Bioresour. Technol. Rep.* **9**, 100374 (2020).
29. Zhang Z., Terrasson V., Guénin E.: *Nanomat.* **11**, 1336 (2021).
30. Figueiredo P. a X spoluautorú: *Biomaterials* **121**, 97 (2017).
31. Hoshyar N., Gray S., Han H., Bao G.: *Nanomed. (Lond)* **11**, 673 (2016).
32. Foroozandeh P., Aziz A. A.: *Nanoscale Res. Lett.* **13**, 339 (2018).
33. Yin Win K., Feng S.-S.: *Biomaterials* **26**, 2713 (2005).
34. Lai S. K., Hida K., Man S. T., Chen C., Machamer C., Schroer T. A., Hanes J.: *Biomaterials* **28**, 2876 (2007).
35. Karagoz B., Esser L., Duong H. T., Basuki J. S., Boyer C., Davis T. P.: *Polym. Chem.* **5**, 350 (2014).
36. Sabourian P., Yazdani G., Ashraf S. S., Frounchi M., Mashayekhan S., Kiani S., Kakkar A.: *Int. J. Mol. Sci.* **21**, 8019 (2020).
37. Li Y., Chen X., Gu N.: *J. Phys. Chem. B* **112**, 16647 (2008).
38. Curtis E. M., Bahrami A. H., Weikl T. R., Hall C. K.: *Nanoscale* **7**, 14505 (2015).
39. Petridis L., Smith J. C.: *ChemSusChem* **9**, 289 (2016).
40. Pylypchuk I. V., Lindén P. A., Lindström M. E., Sevastyanova O.: *ACS Sustain. Chem. Eng.* **8**, 13805 (2020).
41. Leskinen T., Witos J., Valle-Delgado J. J., Lintinen K., Kostianen M., Wiedmer S. K., Österberg M., Mattinen M.-L.: *Biomacromolecules* **18**, 2767 (2017).

SINTERING OF PTFE-PEEK POLYMER BLEND IN AIR ATMOSPHERE

Melichar J.¹, Foitlová A.¹, Mészáros M.¹, Steiner V.¹

¹SVÚM a.s., Polymers and Fluoroplastics Technology Department, Čelákovice, Czech republic
melichar@svum.cz

Abstract

The poly(tetrafluoroethylene) (PTFE) holds a unique position in the industry as a base material for tribological components, for example, journal bearings or piston rings. The pure PTFE has very low abrasion resistance. For this reason, it is commonly enhanced by fillers, which can cause problems in specific applications. In recent decades, several scientific papers have dealt with a polymer blend based on PTFE and poly(etheretherketone) (PEEK), which may exhibit better wear resistance than individual pure components while maintaining other important properties^{1,2}. The literature mentions mainly tribological properties but no or minimum information about the sintering in an air atmosphere, which is crucial for the industry, where PTFE-based materials are typically prepared by pressing and sintering in a mentioned atmosphere. In this work, initial steps to find basic principles of "how to design a suitable sintering temperature program" have been done.

Introduction

The poly(tetrafluoroethylene) (PTFE) is a polymer with exceptional self-lubricating properties, a low coefficient of friction (CoF), good chemical resistance, and operating temperature up to 250 °C³. Thanks to these properties, PTFE finds a unique position in the industry as a base material for tribological components, for example, journal bearings or piston rings. The pure PTFE has very low abrasion resistance. For this reason, it is commonly filled - typically by glass fibres, bronze, MoS₂, or graphite. This can cause problems since the potential release of fillers is not allowed in specific applications or can cause abrasion of the counterpart.

In recent decades, several scientific papers have dealt with a polymer blend based on PTFE and poly(etheretherketone) (PEEK). It was found that a suitably prepared mixture may exhibit better wear resistance than individual pure components while maintaining a low CoF, self-lubricating behaviour, and high service temperature. Research topics were focused mainly on tribological properties (CoF and wear rate) across the blend composition or in different environments^{1,2}. Although different methods of preparation and sintering temperature programs were used, the literature mentions no or minimum information about the sintering in an air atmosphere.

For industry, where PTFE-based materials are typically prepared by pressing and sintering in the air atmosphere, this knowledge can be essential since a PTFE sintering temperature program causes significant degradation of PEEK. In this work, initial steps to find basic principles of "how to design a suitable sintering temperature program" have been done. Several programs were designed and used. Changes in thermal properties of sintered PTFE-PEEK samples, which related to the degradation, were evaluated by differential scanning calorimetry. Measurements were made from the surface, in the middle, and across the cross-section. As a result, a sintering program that causes a minimum degree of degradation was chosen for the following research.

Experiment

Used materials

For blend preparation were selected specific PTFE and PEEK powder grades:

- PTFE coagulated dispersion powder with middle molecular weight and average particle size 550 µm
- PEEK fine powder with average particle size 25 µm as a filler

An industrial mixing device specially designed for mixing powder mixtures from Beba Mischtechnik GmbH was used to prepare a homogenous mixture of PTFE and PEEK (wt. 85:15). The homogeneity was controlled by three individual differential scanning calorimetry (DSC) measurements by comparing the enthalpy changes of a thermal transitions.

Design of sintering program

Based on processing guides for pure PTFE powders and our production experiences the main PTFE sintering temperature is about 380 °C for several hours. As already mentioned, the typical PTFE sintering temperature program causes significant degradation of PEEK. The character of degradation is thermo-oxidative and has already been studied, for example at work of Pascual et al. ⁴.

According to the processing guides from Victrex, PEEK can be exposed in the air atmosphere to a temperature of 380 °C for a maximum of 15 minutes, 360 °C for one hour, and 340 °C for several hours. From DSC measurements of the prepared PTFE-PEEK mixture, it was found that the end of the melting peak is around 350 °C and the crystallization starts at about 320 °C.

Based on this information, the main idea of sintering was developed. The main step is to melt the mixture in its entire volume by heating it above 350 °C for a sufficiently long time, and then lower the temperature which is still above the crystallization temperature of 320 °C. This temperature is then maintained for a longer period to allow the material to sinter properly.

According to the main idea and our experiences with the PTFE sintering process, five different sintering programs were designed, see Table 1.

Table I
Sintering programs designed for PTFE-PEEK polymer blend

DESIGNED SINTERING PROGRAMS				
Steps	Type	1s	2s	3s
1.	↑	heat to 340 °C (65 °C/h)	heat to 340 °C (30 °C/h)	heat to 340 °C (65 °C/h)
2.	=	isotherm 2,5 h	isotherm 2,5 h	isotherm 2,5 h
3.	↑	heat to 360 °C (65 °C/h)	heat to 360 °C (30 °C/h)	heat to 380 °C (65 °C/h)
4.	=	isotherm 1 h	isotherm 1 h	isotherm 15 min
5.	↓	cool to 340 °C (65 °C/h)	cool to 340 °C (30 °C/h)	cool to 340 °C (65 °C/h)
6.	=	isotherm 2 h	isotherm 2 h	isotherm 2 h
7.	↓	cool to 40 °C (65 °C/h)	cool to 40 °C (30 °C/h)	cool to 40 °C (65 °C/h)
Steps		4s	5s	Ts (typical PTFE program)
1.	↑	heat to 360 °C (65 °C/h)	heat to 380 °C (65 °C/h)	heat to 380 °C (65 °C/h)
2.	=	isotherm 1 h	isotherm 15 min	isotherm 6 h
3.	↓	cool to 340 °C (65 °C/h)	cool to 340 °C (65 °C/h)	cool to 40 °C (65 °C/h)
4.	=	isotherm 2 h	isotherm 2 h	
5.	↓	cool to 40 °C (65 °C/h)	cool to 40 °C (65 °C/h)	

Sintering of PTFE-PEEK

For sintering tests, samples in form of 50 x 50 x 28 mm blocks were prepared by pressing. To find out how the sample is heated across the cross-section a specific method was designed and tested. The method consists of drilling holes into the block at different distances from the surface so that it is not affected by neighboring sides. Thermocouples with fast response were inserted into these holes. After inputting the sintering program, the block, even with thermocouples connected to the data acquisition device, was placed in a laboratory furnace with precise temperature control.

The temperature records obtained by sintering programs in Table I were plotted in graphs, which show the temperatures across the cross-section of the mixture during the sintering. An example of the graph is in Figure 1, which shows the important part of sintering process. The samples after sintering were cut to see the color changes due to thermo-oxidative degradation, an example can be seen in Figure 2.

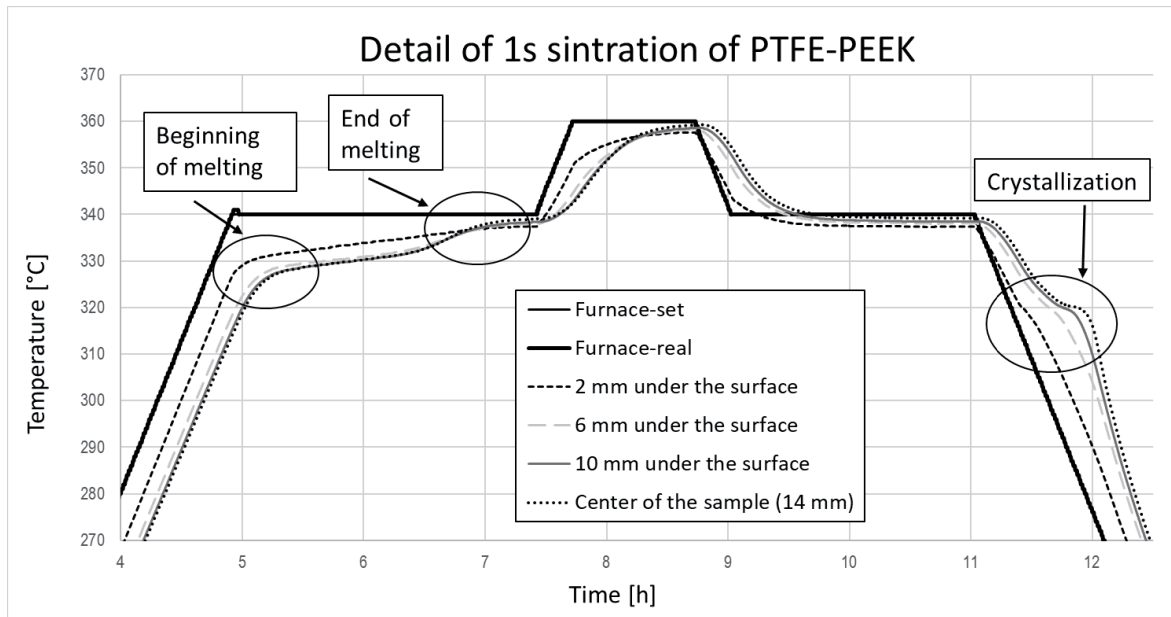


Figure 1: Detail of sintration temperature records of PTFE-PEEK

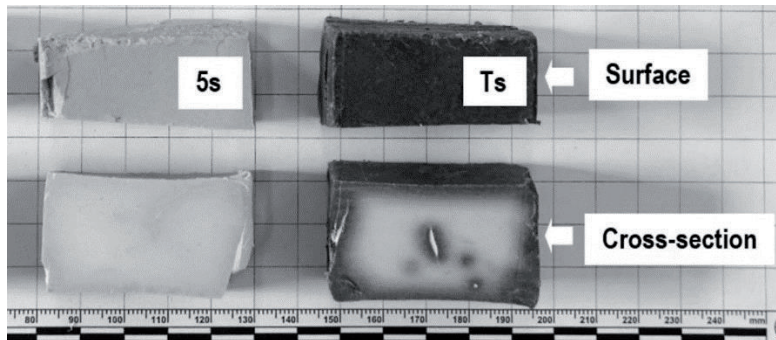


Figure 2: An example of cut samples after sintration programs 5s and Ts

Controlled thermal degradation of PEEK

For evaluation of presence and degree of PEEK degradation in PTFE, samples of the pure PEEK with a different degree of degradation were prepared. The pure PEEK powders in ceramic crucibles were exposed to 380 °C in air atmosphere for various times (30, 60, 90, 120 and 150 min), which led to the thermo-oxidative degradation. The color changes of the surfaces of samples were observed, see Figure 3. With the increasing exposure time the material becomes darker. The changes of thermal properties were measured by DSC by heat-cool-heat method (from -20 to 380°C, 10 °C/h). The changes were observed mainly during the crystallization, see Figure 4 and during the melting. The results were used for evaluation of PEEK degradation in PTFE.

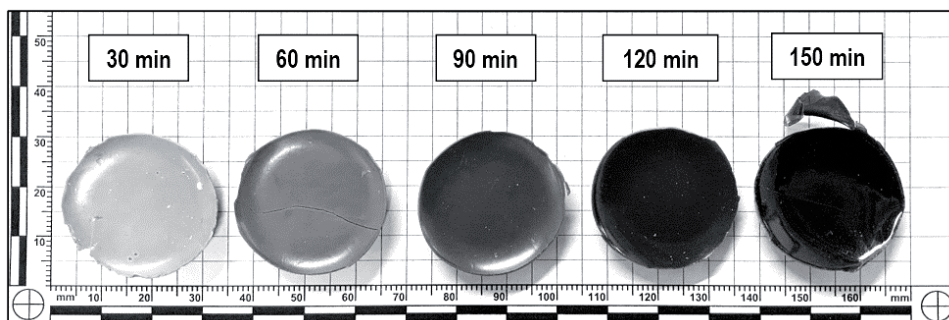


Figure 3: Samples of pure PEEK after controlled degradation by exposition to 380 °C for various times

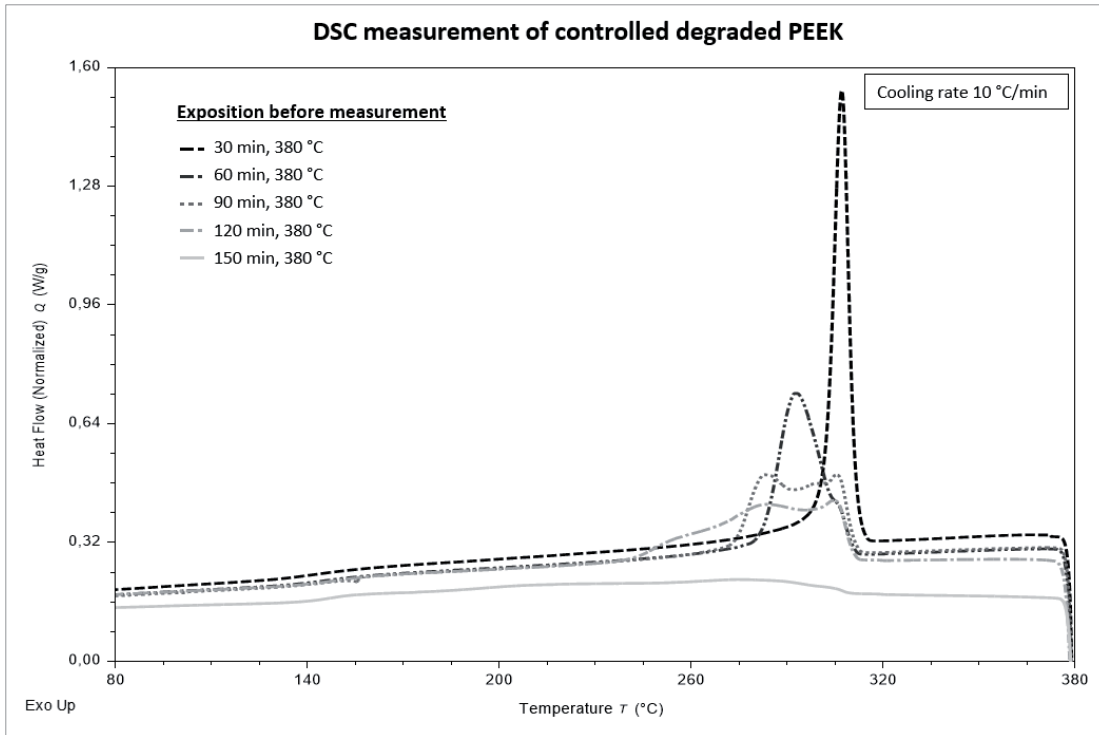


Figure 4: DSC curves with crystallization of controlled degraded PEEK

Differential scanning calorimetry

The thermal properties of the surfaces and centers of sintered PTFE-PEEK blocks by sinteration programs in Table I were measured by DSC by heat-cool-heat method (from -20 to 380°C, 10 °C/h). To find out how the presence and degree of degradation change towards the center, samples from different distances from the surface (1, 2, 3, 4 and 5 mm) of block sintered by 3s program were prepared and measured by DSC, see Figure 5. Unsintered samples were also measured. By comparing these results with controlled degraded PEEK, the presence and degree of degradation of PEEK in PTFE were evaluated.

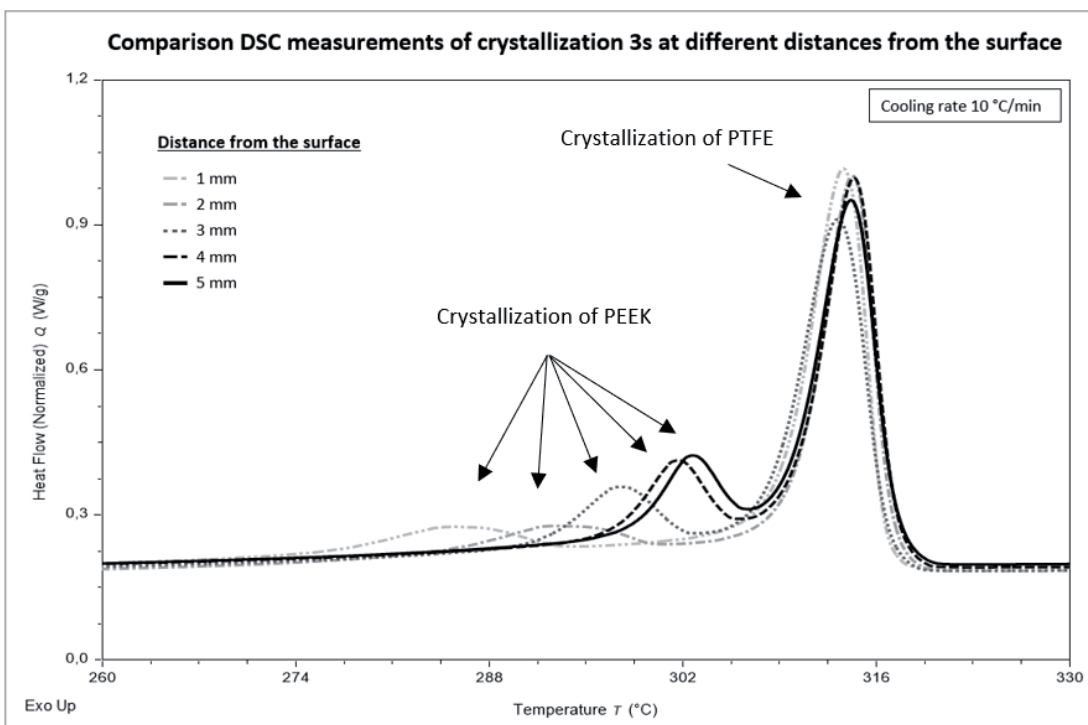


Figure 5: DSC curves with crystallization of PTFE-PEEK polymer blend from different distances from the surface

Discussion

Sinteration programs

The designed sintering temperature programs in Table I were tested. From measurements by inserted thermocouples in PTFE-PEEK blocks across the cross-section (see Figure I) was found, that during all programs, the material was melted in a whole volume. The main idea of sintering mentioned in the experiment part was therefore fulfilled. The blocks after sinteration were cut to see the color changes due to degradation, an example can be seen in Figure 2. Measurement of changes in thermal properties was chosen to verify the degradation.

DSC measurements of controlled degraded PEEK

The changes of thermal properties measured by DSC by the heat-cool-heat method proved to be very suitable for the evaluation of the presence and degree of PEEK degradation in PTFE. Samples of the pure PEEK with a different degree of thermo-oxidative degradation were prepared by exposition to higher temperatures in air atmosphere as a standard for evaluation, see Figure 3. The changes in thermal properties (melting/crystallization temperature and enthalpy) were observed and depended on the degree of degradation, see Figure 4. The changes are in accordance with a scientific work of Pascual et. al⁴.

In our case, we divided the degree of degradation into four characteristic stages. In the first stage is no or minimum degradation, the melting temperature is 345 ± 2 °C, the crystallization temperature is >300 °C and sharp peaks can be observed in a DSC record. In the second stage is a slight degradation, the melting temperature decreases to around 340 °C, crystallization temperature is in a range of 290-300 °C and wider peaks are in a DSC record. In the third stage is a significant degradation, the melting temperature is around 340 °C, and crystallization divides into two peaks, where the first is <290 °C and the second is >300 °C. The fourth stage is extreme degradation, the melting divides into two peaks, where the first is <310 °C and the second is around 340 °C. In this case the crystallization temperature cannot be determined.

Evaluation of degradation of the PTFE-PEEK polymer blend

The presence and degree of degradation of PTFE-PEEK sintered blocks were evaluated by DSC measurement with the acquired DSC data from the controlled degradation of the pure PEEK. The crystallization temperature of PEEK seems to be the most appropriate for degradation evaluation, as it decreases and shifts away from the crystallization peak of PTFE, see Figure 5. The melting peak of PEEK also decreases but it merges with the PTFE melting peak. The following findings were concluded from DSC measurements.:

- degradation occurred at the surface, not in the middle of the sample (block)
- with the increasing degree of degradation of PEEK, the material became darker
- isotherm 2 hours at 340 °C before the main sintering temperature caused a higher degree of degradation than in the case of direct heating to the main sintering temperature
- isotherm 15 min at 380 °C degraded the material more than isotherm 1 h at 360 °C
- heating and cooling rates of 65 °C/h and 30 °C/h did not lead to the different degrees of degradation when 360 °C was the main sintering temperature
- the degradation seemed to be minimal from 2-3 mm from the surface for the sintering program 3s

Based on the results and findings from DSC measurements, it was concluded, that the sintering program 4s shows almost zero degradation at the surface. The program 5s is also suitable for PTFE-PEEK polymer blend sintering since it shows only slightly higher degradation than 4s.

ECONOMICS OF CHEMICAL INDUSTRY

THE ACCOMPLISHMENT OF THE DIGITAL WELL-BEING IN COMPANIES

Botek M.¹, Charvátová D.¹, Dvořáková Z.¹

¹*School of Business, University of Chemistry and Technology Prague, 166 28, Prague 6
botekm@vscht.cz*

Abstract

The COVID-19 pandemic has accelerated the digital transition, leading to a steep rise in online/remote activities. It opens a lot of questions about how to master the burdens of distance working without negative consequences on well-being. It became clear that so many employees have been exposed to grave cases of digital overload with poor or no organizational HR support. The impact of digitally intensive activities on employees' work and personal lives is proving to be very detrimental, especially concerning the stress of having to be online all the time. Many employees have to deal with technostress. Which has a negative influence on both the person itself and his performance. Because of these reasons, the companies lose their competitive advantage in the market. This paper will concern how to reduce these negative consequences in the company and what kind of ways can the company apply for minimizing or reducing these negative factors.

Introduction

The Covid-19 pandemics changed the approach to company management all over the world. The necessity of the social distance accelerated changes realized thanks to the implication of the Technologie 4.0 approach¹. Even though digital transformation started several years ago, it was forced dramatically during the last two years².

To minimize the number of contacts among people, the majority of companies have enabled a flexible working environment³. The previously not very common teleworking has started to be a common tool and changed the name to remote work or hybrid working model³. Also, teleconferences were soon adopted not only in corporations but also by public administration and schools⁴.

Many employees continue to work at least in a hybrid working model, on the other hand, social distancing hurts relationships, and quality of labor and reduces performance and profits. Some jobs cannot be performed at home. Also, some people do not want to work remotely.

A distinction needs to be made between remote working, work from home, and enforced work from home. Remote workers do not solely work from home, instead, they work remotely, anywhere that is not the organization's main physical office⁵. The remote workers can use different coworking centers and do not have to invest in the creation of a workspace at home⁶. But this was not possible during the social distancing⁷. Enforced work from home has been coined to help differentiate between voluntarily working from home by choice and the recent government restrictions which enforced work from home⁸.

Challenges, benefits, and disadvantages of remote work

Remote work is full of challenges for company management, such as managerial, technical, legal, psychological, mental, social, and cultural challenges. The most common challenges of remote management are listed below⁹:

- how to perform managerial functions – remote planning and goal setting, remote organization, remote motivation, remote control, etc.;
- how to shift business processes to remote format;
- how to maintain the involvement of the employees, teams, and departments;
- how to control and delegate;
- how to interact proficiently in a remote format;
- how to maintain remote employees' wellbeing and performance;
- how to organize paperwork;
- how to organize working space (either "in" or "out" the office);
- how to support privacy, etc.

These challenges have to be solved very quickly because the Covid-19 pandemics did not give enough time for a detailed and rational decision-making process¹⁰. Many companies have to change their routine from day to day and if they had no experience with remote work, it was a very energy-consuming period.

Benefits of remote work

The basic benefit during the strongest period of COVID-19 pandemics was minimizing social contacts in the workplace and public transport³. On the other hand, employees have transformed their perceptions of employee benefits during the Crisis. There are some studies that have shown that with the majority of employees working from home due to the Covid situation, it was necessary to support more flexible working benefits^{2,11}. The saving time by reducing the transport and better time management are the other benefits. Many studies found plenty of other benefits for employees and managers, too. The most common ones are “reduced expenses on traveling”, “flexible work schedule and opportunity to achieve work-life balance (spend more time with the family)”, “ability to find or keep a job in difficult situations”, “sense of freedom and responsibility”, “feeling of trust”, “opportunity to mix several jobs or professions”⁹. The managerial benefits found in the same study are eg. “organize high levels of close monitoring and control”, “opportunity to find employees globally”, “transformation of the organizational processes”, “ability to develop flat organization structure based on networks”. The remote working practice provides numerous advantages for the organization, such as “reduced office expenses”, “access to cheap labor”, “low staff turnover”, “automation of organization management processes”, “development of electronic document management”, “equal job rights for people with disabilities”, “opportunity to create organizations of a continuous cycle”, “opportunity going international, creating new markets or branches”⁹. Radonić et al proved, that a hybrid working environment might effectively improve intangible assets, and also have a positive effect on human capital, and also relational, structural, and innovation capital³. The COVID-19 pandemics have accelerated the digitalization of companies and led to big changes in different aspects related to leadership and management¹².

Disadvantages of remote work

There are some studies that have shown the negative impact of remote work on employees, through increased levels of stress and anxiety^{2,13}. The majority of respondents in another study mentioned the following obstacles: limited working conditions (e.g., limited space, software), deterioration of interpersonal relationships (e.g., less engagement, understanding, moral support, development), reduction of work quality, an increase of technical investments, emotional pressures (e.g., uncertainty about the future, limited socialization, fear of a job loss, fear of a freedom loss), technological illiteracy, work-home conflict⁹.

The deterioration of interpersonal relationships can grow from limited communication, stimulation, and leadership. Virtual communication is often problem-oriented, without socialization, and has some nonverbal aspects of communication. Leaders cannot use soft informal control and feedback, employees have to be more independent and tasks are more complex⁹. Such work also produces much more inputs and outputs, thanks to digital technologies, they could be used to manage, but they also increase the number of inputs which is important to work with.

Some problems are often in time management. In this area, there is a different view of time management by the employer and the employee¹⁵. Organizations are trying to manage time more efficiently, but usually do not consider how employees think about time¹⁴. In co-located work environments, social constructions of time become engrained in the daily routine but in remote working, temporal complexity arose as social constructions of time were not applied to the work environment¹⁴. The disruption of the time routine may not occur (to such an extent) if the workers are in permanent contact with their superiors and de facto only changed the place of work, but the structure, especially time, work has been maintained¹⁶.

Technostress

Technostress is created as a result of direct interaction between informational technology and people¹⁷. It was mostly observed in the category of IT employees but digitalization during the COVID-19 remote working increased technostress to the majority of employees¹⁸.

Nisafani et al¹⁷ prepared a review and found that the term technostress comes from Craig Brood, a clinical psychologist who used it first in 1984. It is a modern disease that impacts people they are not able to adapt enough to using informational technologies¹⁷. Technostress affects human behaviors, thoughts, and attitudes. Research realized by Nisafani et al¹⁷ showed that technostress could be a reason for anxiety, exhaustion, decreasing of performance and therefore produces job dissatisfaction. The impact of gender and age are broadly discussed but the results are unclear¹⁷.

It is broadly accepted that they exist some categories of technostress creators¹⁹:

- Techno-overload - the potential of informational technologies (IT) to drive an employee to work faster.

- Techno-invasion - the potential of IT to invade an employee's personal life with possibilities to, for example, perform job tasks.
- Techno-complexity - an inherent quality of IT that makes employees feel incompetent.
- Techno-insecurity - a premise that the nature of IT is to change regularly, and that this may threaten employee job security.
- Techno-uncertainty - constant changes and upgrades of software and hardware may impose stress on employees.

It seems, that they exist some factors minimizing technostress. They could be higher educational level, higher technology self-efficacy, and a lower level of technology dependency¹⁷. The possibility to decrease the technostress is in proactive coping, which can protect employees working with IT. Some researchers also write about technostress inhibitors like technical (organizational) support, eg. helpdesk; literacy facilitation, which means increasing IT knowledge; and involvement facilitation which leads to strengthening employee engagement in new technology²⁰.

Later Tarafdar et al. offered three categories of coping²¹:

- Reducing IT-related emotions and distress
 - Venting: Expressing negative emotions
 - Executive Distancing: Diverting from the IT use situa
- Developing IT capacity
 - Positive IT outlook: Being optimistic about technostress situations
 - IT use skills: Developing competence in IT use
- Developing IT use demarcations
 - IT use autonomy: Having control over IT use
 - Time related demarcations: Setting aside specific times for particular types of IT use
 - Work and non-work IT use separation: Demarcating work and non-work IT use.

Possible solutions

Due to space constraints, this section will be limited to only some remote work challenges, namely:

- how to maintain remote employees' wellbeing and performance;
- how to organize working space (either "in" or "out" the office);
- how to support privacy.

This will be matched by a focus on retention of benefits like flexible work schedule and minimizing of disadvantages like limited working conditions (space, software); deterioration of interpersonal relationships, decreasing of work quality; work-home conflict; and technostress.

The COVID-19 pandemic has certainly contributed to the development of technostress, especially as the staff has been forced to work with IT without training or coaching, and often without support, much more intensively than before. Particularly in the early days of forced remote working, communication tools, the way work was reported and monitored, and the tools and rules of online meetings changed frequently. Gradually, the rules became more stable, companies prepared manuals, expanded support options and codified rules for organizing and controlling work. As a result, the amount of technostress in the categories techno – insecurity, and techno-uncertainty has decreased. Further work is needed to ensure that employees do not perceive IT as a threat, but rather as support. A good IT department that can make the necessary changes on its own will help to reduce techno-uncertainty, and employees can be confident that they have someone to turn to if they run into trouble.

However, the stress in remote working and especially in forced remote working is not only caused by IT, but also by changing schedules. In normal conditions, it is "only" necessary for the organization to decide whether the working hours will be identical to the organization's fixed working hours or whether flexible working hours will be introduced. The advantages and disadvantages of flexible working are well known and are not much affected by the place of work. The only major difference is that employees do not have to commute to work and thus gain a certain amount of extra time. In the COVID-19 pandemic, however, it was not uncommon to have to coordinate an employee's work schedule with that of his or her partner and possibly children who had distance learning. It also led to increasing in techno-invasion.

The ability to work at any time leads to staff working anywhere from 'as little as tolerated' to 'as much as they can stand', i.e. well beyond the set working hours. To control and minimize under-performance, companies have quickly developed tools; they often do not mind excessive work, even if it is harmful to people.

All of this influenced employee well-being and create work-home (or work-life) conflicts. The solution could be an organizational agreement about the necessary interval of work and unbreakable time of rest. This would mean, for example, that on Tuesdays and Thursdays (every working day) the employee must be immediately reachable by email, telephone, or teleconference between 9 am and 3 pm, except for the break between 11:30 am and 12 pm. On other working days, he/she must be immediately reachable between one and three in the afternoon. Naturally, he/she must respond to work emails within a reasonable time interval (within two hours, by the next day, etc.). It must also be stipulated that work calls will not be made between 6 p.m. and 8 a.m. And that emails received during this interval should be viewed as emails received only at the beginning of business hours the next day. Of course, this interval needs to be adjusted according to company practice. This will give the employee a better opportunity to manage his time, reduce the stress given by techno-invasion and limit work-life conflicts. The above rules apply only to the case of flexible working and must be adapted according to their rules. If the employee works from home but has fixed working hours, the situation is simpler. These fixed working hours must be respected, both by being available and by not being tasked outside working hours.

However, work availability is only a framework. Companies must ensure and control the quantity and quality of work output. The simplest way to do this is to produce regular timesheets, linked to specific work tasks or targets. This allows both employer and employee to see whether the amount of work is adequate.

However, remote work always causes a deterioration of interpersonal relationships. Therefore, it is highly advisable to have set days on which work is ordered from the workplace. Optimally at least two days a week and with the participation of at least the whole team. The work output on these days may be lower than during remote work, but it is necessary for maintaining social contacts and during informal conversations often solutions to protracted work problems or new ideas and potential projects will also emerge.

Due to the need to move to remote working suddenly, in many cases a suitable working environment has not been prepared for employees. The time issues have already been mentioned, now it is appropriate to insist on space and security requirements.

While ergonomics are usually taken into account in company headquarters and occupational health and safety are always monitored, this was initially ignored in the home environment. Workers were sitting at unsuitable desks or using laptops in various comfortable but unhealthy positions. Later, OSH rules were introduced to remote working and the working environment in homes had to be modified.

In some places, companies contributed to this, in others they did not. Yet digital wellbeing is also indirectly affected by whether the company has contributed to cover the increased costs of heating, food, internet access, or telephone that would not be incurred when working at the company's headquarters.

It is essential that OSH manuals are developed for working from home and that employees are well trained on what kind of working environment they should create at home and why. This may increase the number of work-home conflicts, but it will contribute to the well-being and health of the employees, even if in the optimal case they will not be aware of it because the goal is that they do not develop health problems. However, health is usually taken for granted and workers would be more likely to notice if it deteriorated.

Conclusion

The COVID-19 pandemic has supported changes in work at most companies. It is logical that these changes initially caused increased stress, but once adapted, it would be advisable to maintain as many of the benefits discovered as possible. The biggest benefit appears to be the fact that remote working can be used extensively in many firms.

It is therefore advisable that, in returning to normal post-pandemic life, working life should not revert to pre-COVID-19 times. However, the preservation of remote working should be conditional on the creation and maintenance of rules that maximise the benefits while reducing the drawbacks of this form of work.

Acknowledgement

This work was supported by DWEL, Erasmus+ Project No 2021-1-SK01-KA220-HED-000032017.

References

1. Strachotová D., Strachota S.: Enhancing Productivity in Plastics Industry through the Concept of Lean Production, In: 29th IBIMA, (2017).

2. Bednarikova M., Kostalova J.: The HR Management Changes Related to the COVID-19 Pandemic in Chemical Industry. In: Hed Economic Days, 9.-10.5.2022, Hradec Králové, Czech Rep., in press.
3. Radonić M., Vukmirović V., Milosavljević, M.: The Impact of Hybrid Workplace Models on Intangible Assets: The Case of an Emerging Country. *Amfiteatru Econ*, 23(58), 770 2021.
4. Teräs M., Suoranta J., Teräs H., Curcher M.: Post-COVID-19 Education and education technology “solutionism”: A seller’s market. *Postdigital Sc Edu*. 2(3), 863 2020.
5. Ralph P., Baltés S., Adisaputri G., Torkar R., Kovalenko V., Kalinowski M., Novielli N., Yoo S., Devroey X., Tan X., Zhou M.: Pandemic Programming: How COVID-19 affects software developers and how their organizations can help. *Emp Soft Eng*. 25, 1 (2020).
6. Bendarikova M., Kostalova J.: Sharing Economy in the Czech Republic. In: Hradec Economic Days, 11(1), 36 (2021).
7. Vrba Z., Strachotová D., Kutnohorská O.: Economic Dimension of Artificial Intelligence in Future Medicine. In: 35th IBIMA, (2020).
8. Waizenegger L., McKenna B., Cai W., Bend, T.: An affordance perspective of team collaboration and enforced working from home during COVID-19. *Eur J Inform Syst*, 29(4), 429 (2020).
9. Mirakyan A., Berezka S.: Management and COVID-19: Digital Shift to Remote Work and Remote Management. *DTGS 2021, CCIS 1503*, 446 2022.
10. Mikkelsen B.E., Strachotová D., Romani A.Q.: Does removal of value added tax on fruit and vegetables increase sale - case of a Danish retailer. *Appl Econ*. 53(24), 2743 (2021).
11. Jílková P.: Sustainable Corporate Strategy: The Role of Human Capital in the Time of COVID-19 Crisis. *Tem J*, 10(2), 699 (2021).
12. Donthu N., Gustafsson A.: Effects of COVID-19 on business and research, *J Bus Res*, 117, 284 (2020).
13. Shaw W.S., Main C.J., Findley P.A., Collie A., Kristman V.L., Gross D.P.: Opening the workplace after COVID-19: what lessons can be learned from return-to-work research? *J Occup Rehabil* 30, 299 (2020).
14. O’Connor M., Conboy K., Dennehy D.: COVID-19 affected remote workers: a temporal analysis of information system development during the pandemic, *J Decis Syst*, 31(3), 207 (2022).
15. Kutnohorská O., Strachotová D.: Consumer behaviour in the bread market, In: 7th ICCT, Mikulov, Czechia (2019).
16. Leonardi P. M.: COVID-19 and the new technologies of organizing: digital exhaust, digital footprints, and artificial intelligence in the wake of remote work. *J Manag Stud* 58, 247 (2021).
17. Nisafani A. Sh., Kiely G., Mahony C.: Workers’ technostress: a review of its causes, strains, inhibitors, and impacts, *J Decis Syst*, 29(sup1), 243 (2020).
18. Spagnoli P., Molino M., Molinaro D., Giancaspro M. L., Manuti A., Ghislieri C.: Workaholism and technostress during the COVID-19 emergency: The crucial role of the leaders on remote working. *Front Psychol*, 11, 3714 (2020).
19. Tarafdar M., Tu Q., Ragu-Nathan B. S., Ragu-Nathan T. S.: The impact of technostress on role stress and productivity. *J Manage Inform Syst*, 24(1), 301 (2007).
20. Ragu-Nathan T. S., Tarafdar M., Ragu-Nathan B. S., Tu Q.: The consequences of technostress for end users in organizations: Conceptual development and empirical validation. *INFORM SYST RES*, 19(4), 417 (2008).
21. Tarafdar M., Pirkkalainen H., Salo M., Makkonen M.: Taking on the “Dark Side” : Coping With Technostress. *It Prof*, 22(6), 82 (2020).

IMPORTANCE OF AN ECO-LABEL FOR THE CUSTOMER

Branská L.¹, Paták M.², Pecinová Z.³, Kocmanova A.⁴

^{1,2,3} *University of Pardubice, Faculty of Chemical Technology, Czech Republic*

⁴ *Brno University of Technology, Faculty of Business and Management, Czech Republic*
lenka.branska@upce.cz

Abstract

Producers increase the sustainability of their products and/or their packaging not only as part of their own contribution to environmental protection, but also as an opportunity to provide greater value to consumers. Increasingly, consumers are moving towards consuming more environmentally friendly products. A way to easily identify these products is through an eco-label usually placed on the packaging of the products. However, the problem is the overwhelming number of these eco-labels and the lack of consumer awareness thereof. This could affect consumers' perception of the importance of the eco-label. This paper addresses this issue in relation to consumer chemical products. It presents the results of primary quantitative research among 200 consumers focus on the importance of environmentally oriented labels on packaging. It specifies the importance of an environmentally oriented label in relation to other selected parameters of the product offer and then analyses the importance of the eco-label for individual customer segments identified both by demographic characteristics and attitudes towards selected environmental issues.

Introduction

As consumer knowledge about the responsibility of consumer goods for the large amount of waste produced on the planet is steadily increasing, changes in consumer behaviour are taking place. Consumers are increasingly assessing the environmental impact of their purchases¹. Their awareness of environmentally friendly products increases and they are more selective in their choice of products for consumption². Eco-labels have been introduced to help them assess the environmental performance of products. They are seen as a good way of informing customers about the environmental performance of selected products³. Over the past few decades, a number of these have emerged, particularly to appeal to customers with eco-friendly tastes⁴.

Eco-labels can be complemented (on the product or on the packaging) by other tools to signal environmental orientation and enhance consumer response, e.g. by colour or image. However, while eco-labels are always used to signal environmental orientation and thus have a clear link to environmental schemes, and e.g. the green colour reinforces this link, the other way around is not the case. The use of the colour green without an eco-label may have a different purpose, e.g. to indicate a scent or flavour in relation to products such as mint or apple⁵.

Eco-labels are logos that express that a product or service meets standardised criteria set by a certification organisation and is considered a sustainable option in its product category¹. Eco-labels aim to communicate verifiable and accurate information about the environmental aspects of products and services in order to encourage demand for products that cause much less environmental impact. The aim is therefore to stimulate the potential for continuous, market-driven environmental improvement⁶. The set of eco-labels consists of voluntary and compulsory eco-labels, eco-labels from different industries (e.g. related to plants, food, appliances) and eco-labels awarded by various accreditation institutions (government, industry associations, private companies, etc.). They often vary according to product category and country⁷. Eco-labels can refer to the product itself (indicating environmentally friendly products or services) or to its packaging. Some can be considered comprehensive (e.g. "The Flower" indicating an eco-friendly product), some can be sub-labels, conveying selected sub-environmental information (e.g. the Möbius strip is a claim about recyclable or recycled content⁶).

Eco-labels are used not only by manufacturers to demonstrate environmental credibility, but also by retailers to differentiate themselves from competitors. With few exceptions, it is a voluntary tool. The standards developed by the International Organisation for Standardisation (ISO) in the ISO 14020 series, Environmental labels and declarations, have become key in the development of eco-labels to ensure credibility with the different links in the chain (producers, retailers and consumers)⁸.

The problem with the use of eco-labels, which threatens to undermine their function, is that there are too many eco-labels. According to the Ecolabel Index⁹, there are 455 eco-labels. This causes a certain degree of confusion as to their precise meaning¹⁰, which in turn impairs or even completely eliminates the ability of customers to know their way about this area. According to the research by Boesen, Bey and Niero¹¹, only 6.1% - 72.4% of respondents were able to correctly identify the meaning of the 7 eco-labels in the research. More than 50% of

respondents were able to correctly identify the meaning of only three eco-labels. If consumers are unable to understand the meaning of an eco-label, their willingness to buy the product or pay a higher price than for products without an eco-label decreases. For example, Belgian consumers were unwilling to pay a higher price for products with a carbon label because they could not associate the environmental characteristics of eco-friendly products with carbon labels¹².

It is therefore clear from the above that the consumer often has a limited ability to make an informed voluntary decision based on the presence of an eco-label and knowledge of what it means¹. However, this knowledge can be at least partially replaced by trust in the organisation that introduced and/or sponsors the label (government, state institutions, reputable NGOs). The consumer may not know the meaning of the eco-label, but if a trusted institution stands behind it, he or she knows that a certain degree of environmental protection is taking place. However, if the consumer has a lack of knowledge of eco-labels and little trust in the institution associated with their marketing, the label has no informational value to them and, as a result, the relevance of the label declines. The paper discusses the importance of the eco-label for consumers in relation to consumer chemical products. In this way, it extends scientific knowledge, as existing research has not yet covered this issue in relation to consumer chemicals. The paper presents the results of a primary quantitative survey among 200 consumers on the importance of the eco-label on packaging. The results of the research can be used for improvement in this area, i.e. in the use of eco-labels in relation to this specific type of products. Improvements could contribute to directing consumers towards more environmentally friendly consumer chemicals, which in turn may represent a rather significant step in environmental protection.

Research methodology

The main objective of the primary quantitative research was to determine the importance of environmentally oriented labels on the packaging of consumer chemical products in relation to other product parameters and selected characteristics of the respondents.

The importance of the environmentally oriented label was examined in relation to the following product parameters:

- the content of environmentally damaging substances,
- the product packaged in environmentally friendly materials,
- the product packaged in returnable packaging,
- the possibility of buying the product unpackaged,
- local origin of the product, and
- the manufacturer's concern for environmental protection.

The characteristics of the respondents examined were both demographic characteristics (gender, age, education and size of the municipality in which the respondent lives) and attitudes towards environmental protection and eco-products. The respondent's attitudes towards environmental protection and eco-products were examined by the following statements:

- I am concerned about the deteriorating quality of the environment.
- I am doing my best to contribute to preserving an acceptable environment for future generations.
- I know more about environmental problems and solutions than the average person.
- I understand the labels used on the packaging of environmental products.
- I can judge whether the products I buy are environmentally friendly.
- I tend to try a new product that is environmentally friendly.
- I repeatedly buy organic products.
- I trust organic products.

The data collection was done through an electronically distributed questionnaire. Respondents expressed their level of agreement with the statements, through which both preferences for individual parameters of the offer and attitudes towards environmental protection and eco-products were examined. A Likert scale was used to express the level of agreement (1 = strongly disagree, 2 = disagree, 3 = neutral, 4 = agree, 5 = strongly agree).

Prior to the start of data collection, piloting was first carried out, focusing mainly on the clarity of the statements and the time commitment from the respondent's perspective.

The data collection was carried out in the period August-October 2021 among the population of the Czech Republic aged 15-64 years. Respondents were included in the survey on the basis of quota sampling with quotas

linked to gender and age according to the CSO data as of 31 December 2020¹³. 200 respondents took part in the research. Their structure by age and gender is shown in Table I.

Table I
Structure of respondents by gender and age

Gender	Age					Total
	15–24	25–34	35–44	45–54	55–64	
Male	15	20	25	24	19	103
Female	14	19	23	22	19	97
Total	29	39	48	46	38	200

Respondents came from municipalities of varying sizes: 17.3% of respondents came from small municipalities with populations under 2,000, 17.8% of respondents came from municipalities with populations between 2001 and 10,000, 47.7% of respondents came from cities with populations between 10,001 and 100,000, and 17.3% of respondents came from cities with populations greater than 100,000. 14% of respondents with primary education (PE) and secondary education (SE) without a secondary school leaving certificate (SSLC), 42.5% of respondents with secondary education with a secondary school leaving certificate and 43.5% of respondents with university education participated in the survey.

Descriptive and inferential statistical methods were used in data analysis. First, label preference was examined in relation to other attributes of the offer through arithmetic mean and median. Friedman's test at 0.05 significance level was used to test the statistical significance of differences in perceived preferences for individual product attributes. Subsequently, differences in respondents' opinions were examined by individual demographic characteristics (gender, age, education, and size of the municipality in which the respondent lives). The Kruskal-Wallis test at 0.05 significance level was used to test the statistical significance of the differences in the attitudes of respondents from different demographic groups. The last part of the analysis examined the dependence of perceived label importance on respondents' attitudes towards environmental protection. Given the type of attitude scale used, the strength of this dependence was measured by Spearman's rank correlation coefficient.

Discussion and result analysis

Somewhat surprisingly, primary research among consumers has shown that an environmentally oriented label is the least preferred product attribute. All the other attributes studied have a higher preference, meaning that consumers care more about the environmental friendliness of the product itself, the environmentally friendly packaging, the local origin of the product and the declared environmental friendliness of the producer than they do about the eco-label. Table II shows the differences in attitudes towards the importance of product attributes. According to the results of the Friedman test, the differences in attitudes are statistically significant ($\chi^2 = 197,504$; $p < 0,001$).

Table II
Attitudes towards the importance of individual product attribute

Product attribute	Mean ^{*)}	Median ^{*)}
The product does not contain environmentally harmful substances.	3.92	4
The product is packaged in environmentally friendly materials.	3.71	4
The product is in returnable packaging.	3.64	4
Local product.	3.52	4
The manufacturer of the product shows concern for the protection of the environment.	3.43	3.5

Product attribute	Mean ^{*)}	Median ^{*)}
The product is unpackaged.	3.28	3
The product is environmentally certified (labelled).	3.01	3

^{*)} Measured on a Likert scale (1 = strongly disagree, 2 = disagree, 3 = neutral, 4 = agree, 5 = strongly agree)

Subsequently, an analysis of the importance of environment-friendly labels in relation to demographic parameters was conducted. The results of the analysis are shown in Table III. It shows the observed differences in eco-label preferences according to the individual demographic characteristics (gender, age, education and size of the municipality in which the respondent lives), including the results of the Kruskal-Wallis test, which verifies the statistical significance of these differences. A statistically significant difference exists only by gender. Eco-label is more important for women than for men (mean 3.27 versus 2.76).

Table III
Differences in attitudes towards the importance of the eco-label by respondent demographic characteristics

Characteristic	Group	Mean importance ^{*)}	Kruskal-Wallis test	
			χ^2	<i>p</i>
Gender	Male	2.76	10.087	0.001
	Female	3.27		
Age	15–24 years	3.10	7.266	0.122
	25–34 years	2.82		
	35–44 years	2.83		
	45–54 years	3.30		
	55–64 years	2.97		
Education	PE and SE without SSLC	3.18	2.342	0.310
	SE with SSLC	3.08		
	University degree	2.87		
Size of the municipality	up to 2.000 inhabitants	3.21	7.391	0.060
	2.001-10.000 inhabitants	3.34		
	10.001-100.000 inhabitants	2.82		
	100.001 and more	2.97		

^{*)} Measured on a Likert scale (1 = strongly disagree, 2 = disagree, 3 = neutral, 4 = agree, 5 = strongly agree)

The influence of other demographic characteristics on attitudes towards the importance of the eco-label is not statistically significant. However, it can be observed that the importance of the eco-label is higher among the youngest respondents, i.e. in the age group 15-24 years (mean 3.10) and in the group of respondents 45-54 years (mean 3.30). For the other age groups the importance of the eco-label was lower and comparable to each other. Interestingly, the importance of the eco-friendly label decreases with the level of education.

The survey results also suggest that an eco-friendly label is more important to respondents from small towns and cities than to respondents from large cities.

The analysis of the importance of the eco-friendly label was also carried out depending on the respondent's attitudes towards the environment, its protection and eco-products. The results of the analysis are shown in Table IV.

Table IV
Attitudes towards the importance of individual product attribute

Product attribute	Spearman's rho
I tend to try a new product that is environmentally friendly.	0.491 ^{*)}
I trust eco-friendly products.	0.465 ^{*)}
I repeatedly buy eco-friendly products.	0.463 ^{*)}
I do everything I can to contribute to preserving an acceptable environment for future generations.	0.461 ^{*)}
I am concerned about the deteriorating quality of the environment.	0.434 ^{*)}
I understand the eco-labels used on the packaging of eco-friendly products.	0.348 ^{*)}
I can judge whether the products I buy are eco-friendly.	0.347 ^{*)}
I know more about eco-friendly products than the average person.	0.340 ^{*)}

^{*)} The value is statistically significant at 0.05 significance level

Table IV shows that the importance of the eco-label correlates with all the examined attitudes towards environmental protection and eco-products in a statistically significant way. This means that the label is more important to those respondents who tended to agree with the statements examining attitudes towards environmental protection and eco-products.

Based on the value of Spearman's rank correlation coefficient, it can be concluded that the greatest influence on the perceived importance of an eco-label is the tendency to try a new product that is environmentally friendly and trust in these products. Knowledge of eco-products has the least influence on perceived eco-label importance.

Conclusion

Eco-labels are a communication tool whose primary objective is to communicate information about the environmental aspects of products. For this reason, they should be important to consumers. Primary research has only partially confirmed this assumption. The inclusion of the eco-label cannot be assessed as unimportant, but the other attributes studied were of higher importance to the respondents. Respondents care more about the environmental friendliness of the product itself, its packaging and the focus of the manufacturer than the eco-label itself.

The eco-label is significantly more important for women than for men. The eco-label seems to be more important for younger, less educated women living in villages and small towns. It can also be concluded that the eco-label is more important for respondents who are more inclined towards environmental protection and eco-products. This is probably because they know at least its function and get some information through it. This conclusion corresponds to a general recommendation concerning the need for increased education on eco-labels, e.g.¹⁴. However, it is particularly relevant for more environmentally engaged and generally more environmentally educated consumers who care more about the eco-label. For less environmentally engaged and educated consumers, it is more about raising their overall environmental awareness. This is a prerequisite for their higher perception of the importance of the eco-label.

Acknowledgement

This study was supported by a grant from the Fund for Bilateral Relations within the framework of the EEA and Norway Grants 2014-2021 (EHP-BFNU-OVNKM-3-134-01-2020).

References

1. Lefébure A., Rosales Muñoz R.: *Communicating to consumers in Sweden with eco-labels: Is the message getting through?* Umeå School of Business, Umeå 2011.
2. Norazah M.S., Norbayah M. S., Nur S. A.: *Procedia Econ. Financ.*, 37, 262 (2016).

3. Xu D., Karray, M.H., Archimède B.: *Comput. Ind.*, 98, 118 (2018).
4. Forlin V.: *Am J Agric Econ*, 103, 682 (2021).
5. Pancer E., McShane L., Noseworthy, T.J.: *J. Bus. Ethics*, 143, 159 (2017).
6. ČSN EN ISO 14021: *Environmentální značky a prohlášení – Vlastní environmentální tvrzení (environmentální značení typu II)*. Úřad pro technickou normalizaci, metrologii a státní zkušebnictví, Praha 2016.
7. Khachatryan H., Rihn A., Wei X.: *J Behav Exp Econ*, 91, 101659 (2021).
8. Grinnall A., Burnett S.: *Sustainability*, 7, 6086 (2015).
9. Ecolabel index: All ecolables. Retrieved April 26, 2021, from <https://www.ecolabelindex.com/ecolabels/>
10. Kavaliauske M., Ulyana V., Seimiene E.: *Economics and Management*, 18, 802 (2014).
11. Boesen S., Bey N., Niero M.: *J. Clean. Prod.*, 210, 1193 (2019).
12. Zhou S.J., Wang H., Li S., Chen Y., Wu J.Y.: *Glob. Ecol. Conserv.*, 18, e00609 (2019).
13. Czech Statistical Office: Distribution of the population by age [Data set]. Retrieved June 26, 2021, from <https://vdb.czso.cz/vdbvo2/faces/cs/index.jsf?page=vystup->
14. Song L., Lim Y.C., Chang P.I., Guo Y.N., Zhang M.Y., Wang X., Yu X.Y., Lehto M.R., Cai H.: *J. Clean. Prod.*, 218, 685 (2019).

DECENT WORK IN THE GREEN ECONOMY

Dvorakova Z.¹, Polents I.²

¹University of Chemistry and Technology, Prague, Technická 5, 166 28 Prague 6, Czech Republic

²University of West Bohemia in Pilsen, Univerzitní 22, 306 14 Plzeň, Czech Republic
zuzan.dvorak@gmail.com

Abstract

Scientific evidence from workers provides an insight into factors determining the workplace in the green economy. Corporations incorporate the green economy principle into human resource management. Some declare their responsibility to implement Sustainable Development Goals in managing people. The paper aims to identify future changes in decent work influenced by the green economy. Methodology insists on literature review, mainly from the Web of Science, and data provided by the Czech Social Security Administration. The topic is fragmented and interdisciplinary, which causes difficulties in providing insight into the opportunities and threats. Green HRM has emerged in the past decade within and separate from the broader topic of sustainable HRM. Employers intend to influence employee green behavior. It assumes that the individual green values will influence the psychological green climate at work, and HRM can help lead to a green work-life balance as employees act in their twofold role as producers and consumers.

Introduction

Human resource management (HRM) trends reflect changes emerging in demography, the economy, and society. Jetha et al.¹ describe nine categories influencing the future work, i.e., the digital transformation of the economy, artificial intelligence/machine learning-enhanced automation, AI-enabled human resource management systems, skill requirements for the future of work, globalization 4.0, climate change, and the green economy, Gen Zs and the work environment; based on them they believe that populism together with the future of work and external shocks will accelerate the changing nature of work. Some employers declare their responsibility to implement Sustainable Development Goals in managing human resources and personnel practices. Furthermore, the current study links the subject matter of Decent Work and Economic Growth with the topics of Green Economy. Multinational corporations are already addressing sustainable development and incorporating the green economy principle into HRM. However, the supportive role will play social dialogue and industrial relations as they support the transition to the green economy. An illustration gives an analysis of the Czech renewable energy sources where green job creation depends on financial incentives in the context of social dialogue, even though biomass and waste energy processing offer the highest employment per MWh².

The paper aims to identify the future of work influenced by the green economy and the environment. The accent is put on the Czech reality in the labor market of the older workforce aged 50-64, who can become prospective human resources for emerging green jobs. The topic is currently fragmented and interdisciplinary, which causes difficulties in providing thoroughness and rigor insight into the opportunities and threats to the quality of work life. The research methods use literature review because it enables an overview of the state-of-the-art. Furthermore, it can provide a systematic way of collecting and synthesizing knowledge in each field of business research, including academic literature and resources shared over social media. The literature review focuses on the Web of Science in the first part and the second part analyses data published by the Czech Social Security Administration (CSSA) about the early retirement of workers aged 50 – 64 in the years 2010 – 2020.

Literature review

Green human resource management has emerged in the past decade within and separate from the broader topic of sustainable HRM³. Future HR practices must consider either green jobs or motives. The workplace will influence green employee behavior. Employers will develop how to measure green HRM and utilize a mediation of psychological green climate. Individual green values can moderate the effect of psychological green climate as employees act in their twofold role as producers and consumers⁴ and solve issues stemming from their reciprocal interactions between working life and private life in the greening economy.

Literature reveals a debate about a green jobs' definition based on a belief that green jobs, being in line with the Sustainable Development Goals, encourage "smart, sustainable and inclusive growth," ensure healthy functioning of Earth's ecosystems, and guarantee decent work for all workers and high levels of workers' health. The concept of green jobs has yet to be clearly defined. The current stage confirms findings by Kouri and Clarke⁵,

who analyzed print media and policy documents from 1999 to 2009 and discovered that coverage of green jobs discourse has sharply increased since 2008. They identify five predominant frames in green jobs discourse, i.e., environment-economy bridge, green entrepreneurship, nascent industry creation, internal industry transformation, and structural adjustment. Another piece of evidence about the situation shows the US O*NET database, and its definition of green jobs - 19.4 % of US workers could currently be part of the green economy in a broad sense. Non-green jobs generally appear to differ from their green counterparts in only a few skill-specific aspects⁶. In general, green jobs give the impression that the term is predominantly used as a strategic link between the recession and climate change policy. They are a critical strategy to overcome the economic and ecological crises. Even though aspects of occupational health and safety (OHS) issues connected with green jobs have been limited, a need is emerging to assess traditional and new OHS risks within them. Analyses in the area are scarce; however, at least two cases can provide insight. Moreira, Vasconcelos, and Santos⁷ explore occupational health indicators of 281,124 establishments and 2,780,686 workers in Portugal and conclude that a green job is not necessarily translated into safe, healthy, and decent work because the incidence and severity of accidents at work are, firstly, higher. Secondly, these jobs are occupied chiefly by workers with a lower level of professional qualification. Another case presents Brandl and Zielinska⁸, who analyze the Smart City Vienna Framework Strategy (SCWR) and identify that the Strategy is not perceived as an eco-social policy and no connection is made between environmental issues and the quality of work.

In cooperation with stakeholders, the government must strengthen the development of a green labor market. The European Directive 89/391 / EEC-OSH is already implemented in the Czech legal system⁹, but it is only the starting point. In this process, a specific role plays the tripartite and social dialogue at macro-and mezzo levels. Constructive industrial relations can support the transition to the greening economy and positively affect employment. Ge and Zhi¹⁰ find out that the green economy positively affects employment in developing and developed countries. An example is an area analyzing renewable energy production in European countries from 1991 to 2019. It illustrates that this kind of production significantly reduced unemployment in European countries in the long run¹¹. However, an obstacle represents a political will to invest in new green education programs¹² as educators and practitioners must deliver effective green education and certification programs targeting "green" skills. The evidence provides the EU alone, where green education policy and practice get no systemic feature yet, despite constantly growing public initiatives¹³. Moreover, due to the population aging in the EU¹⁴, it is unlikely that young newcomers to businesses will bring green skills when they replace the retired ones.

HR policies and practices will support designing green jobs. Based on empirical analysis of United States labor force characteristics, Consoli, Marin, Marzucchi, and Vona¹⁵ reveal that green jobs use more intensively high-level cognitive and interpersonal skills compared to non-green jobs. They argue that green occupations need formal education, work experience, and on-the-job training and retraining. According to the International Labour Organization¹⁶ the need for 'green' skills is valuable and urgent, mainly for women to support their employment and the quality of life.

Discussion and result analysis

At the EU level, a positive relationship exists between environmental protection expenditure and green jobs; however, significant differences happen between countries on green markets and resource efficiency. CEDEFOP¹⁷ believes that implementing the European Green Deal will positively affect employment. Benefits will concentrate in sectors directly targeted, like extraction industries, construction, and waste management, and indirectly in service sectors, such as engineering and administration. Employment transition towards green jobs can forecast in other sectors. Policy priority for greening the economy must focus on extensive accelerating of up- and reskilling and support workers willing to change occupation, sector, or geographic location.

In mid-2022, OECD¹⁸ reflects the war in Ukraine in Preliminary Economic Outlook. It argues that the need for economy-wide income support has disappeared and should be replaced by better-targeted measures as public debts are and remain high. The barriers in the supply of energy sources require re-thinking public investment in defense and greener energy. Other investments, like health, digitalization, aging, and education, are becoming less important. In the case of the CR, OECD imagines that investment into greener energy and electro mobility would decrease reliance on the gas and oil markets and help the recovery. Finally, policy should unleash labor supply, and greening the economy would support the country's growth. It involves boosting domestic labor supply (through increased employment of mothers and older workers), better matching skills provision with skills needs, and using immigration policy more effectively to attract and retain a productive and skilled labor force.

Based on those mentioned above, an administration policy can motivate Czech working populations to stay in the labor market until the ordinary retirement age. A long-term tendency shows that workers aged 50 and older

belong to job seekers who tend to have low self-esteem and have a negative experience from selection procedures when encountering prejudices about their competencies. Employees with specific qualifications and working for decades with a dominant employer in a small town or micro-region experience the stress of finding a new job and losing motivation. Their failures to get a new job to provoke fear, lose confidence as they are frustrated, have low self-esteem, and generally consider it their failure. Moreover, their strong connection to home, surroundings, and social relationships in their place of residence plays another role in their decision-making on dealing with it. For this group, involuntary unemployment, and the idea of commuting to work or moving to work represent the most significant stressors of life. Influenced by such stressors, they consider early retirement as a way out of this mentally very demanding situation. Data provided openly by the CSSA show from 2010 to 2020 that, there has been an increase in many older workers retiring before reaching their full retirement age (see Table I). Currently, Czech employers often provide no incentive to retain this workforce, although they could benefit from their knowledge and experience until they are legally entitled to a pension. The situation can be a part of a macroeconomic discussion when a reformed pension system will implement.

Table I
Number of paid early retirement pensions

Parameter	Year										
	2010	2011	2012	2013	2014	2015	2016	2017	2018	2019	2020
Number	425168	498803	521090	540711	563424	583666	601277	616744	628920	640802	651139
Basic Index	.	1,173	1,226	1,271	1,325	1,373	1,414	1,451	1,479	1,507	1,531
Chain index	.	1,173	1,045	1,038	1,042	1,036	1,030	1,026	1,020	1,019	1,016

Source: Author. Based on CSSA data. <https://data.cssz.cz/web/otevrena-data/katalog-otevrenych-dat>. Accessed 2022-06-19.

Early retirement characterizes the number of paid pensions and the number of newly granted pensions, both for the group 50 - 64 for 2010 - 2020. The numbers of paid ordinary old-age pensions and early retirement pensions give Table II. In 2010, 362 035 recipients of ordinary pensions; in 2019, they count 188 149, and in 2020, showing 160 320. In 2010, 232 132 recipients received early pensions; in 2019, they are 130 895, and in 2020 early pensions represent 118 293. Over the decade, the share of early retirement changes to compare to ordinary pensions. The most significant shares were reached 0.951 in 2013 and 0.956 in 2014. In 2020, it was 0.738 and signified an increase related to 0.696 in 2019.

Table II
Number of paid pensions in the group aged 50 – 64 by age category

Parameter	Year										
	2010	2011	2012	2013	2014	2015	2016	2017	2018	2019	2020
S											
50-54	655	426	210	85	19	0	0	0	0	0	0
55-59	44011	37748	22725	14167	9526	9044	6217	3548	1530	1317	916
60-64	317369	306982	275822	245469	233565	230259	220955	208734	200754	186832	159404
Total	362035	345156	298757	259721	243110	239303	227172	212282	202284	188149	160320
ST											
50-54	539	757	635	542	451	354	289	213	113	6	4
55-59	61924	74751	59489	42293	30834	23104	16427	10824	7085	5263	3738

Parameter	Year										
	2010	2011	2012	2013	2014	2015	2016	2017	2018	2019	2020
60-64	169669	193893	198883	204329	201057	190145	175828	160933	141385	125626	114551
Total	232132	269401	259007	247164	232342	213603	192544	171970	148583	130895	118293
ST _{Total} :T _{Total}	0,641	0,781	0,867	0,951	0,956	0,893	0,848	0,810	0,735	0,696	0,738

Source: Author. Based on CSSA data. <https://data.cssz.cz/web/otevrena-data/katalog-otevrenych-dat>. Accessed on 2022-06-19.

S - Ordinary old-age pension granted upon reaching retirement age.

ST - Old-age pension granted before retirement age (early retirement) permanently reduced for premature.

Note: Data of paid pensions in 2021 are not available yet.

The numbers of newly granted pensions cover Table III showing the structure of ordinary old-age and early retirement. In 2010, the number of newly granted ordinary pensions for the 50-64 group was 68 279, 60 873 in 2019, and 44 695 pensions in 2020. The number of newly granted early retirement pensions is 30 087 in 2010, 27 867 in 2019, and 30 448 in 2020. An extraordinary year-on-year increase in early retirement is in 2011 compared to 2010, namely 2.5 times when newly granted early retirement pensions exceeded the number of old-age pensions newly granted by 26.5%. From 2015 to 2019, the share of early retirement pensions to ordinary old age ranges from 0.428 to 0.482. A significant increase to 0.681 in 2020 exists compared to 0.458 in 2019. The numbers of newly granted early retirement pensions for the group aged 50-64 boost substantially in unfavorable economic developments as shown by their numbers in 2011 and 2020.

Table III
Number of newly granted pensions for the group aged 54-64

Parameter	Year										
	2010	2011	2012	2013	2014	2015	2016	2017	2018	2019	2020
T _{Total}	68279	60504	39173	45026	52724	68797	61132	55654	56245	60873	44695
ST _{Total}	30087	76563	20815	27917	30366	29443	27682	26849	24702	27867	30448
ST : S	0,441	1,265	0,531	0,620	0,576	0,428	0,453	0,482	0,439	0,458	0,681
ST _n : ST _{n-1}	X	2,54	0,27	1,34	1,09	0,97	0,94	0,97	0,92	1,13	1,09

Source: Author. Based on CSSA data. <https://data.cssz.cz/web/otevrena-data/katalog-otevrenych-dat>. Accessed 2022-06-19.

S - Ordinary old-age pension granted upon reaching retirement age.

ST - Old-age pension granted before retirement age (early retirement) permanently reduced for premature.

Note: Data of newly granted pensions for the group aged 50-64 in 2021 are not available yet.

The newly granted early retirements vary according to gender - see Table IV. For example, women aged 50-54 do not retire early in 2012-2020. Instead, their departures show enormous numbers in 55-59, especially in 2010-2016. In general, this age group always has significantly higher numbers of women than men who intend to early retirement in 60-64. However, at the current date, the open CSSA data show the average age of newly granted pensions by gender (early retirement), which does not clarify the differences between men and women by age group.

Table IV
Number of newly granted pensions (early retirement) by gender in the group aged 50-64

ST	Year										
	2010	2011	2012	2013	2014	2015	2016	2017	2018	2019	2020
Total											

ST	Year										
	2010	2011	2012	2013	2014	2015	2016	2017	2018	2019	2020
50-54	361	513	211	239	197	145	188	211	229	223	2
55-59	17136	42054	12943	12704	13484	12592	10900	8211	5309	4805	3115
60-64	12590	33996	7661	14974	16685	16706	16594	18427	19164	22839	27331
Man											
50-54	328	451	211	239	197	145	188	211	229	223	2
55-59	2997	5393	2912	197	185	220	307	205	130	162	389
60-64	12371	33425	7436	14306	15353	15308	13958	14324	13418	15686	16395
Woman											
50-54	33	62	0	0	0	0	0	0	0	0	0
55-59	14139	36661	10031	12507	13299	12372	10593	8006	5179	4643	2726
60-64	219	571	225	668	1332	1398	2636	4103	5746	7153	10936

Source: Author. Based on CSSA data. <https://data.cssz.cz/web/otevrena-data/katalog-otevrenych-dat>. Accessed on 2021-10-23.

ST - Old-age pension granted before retirement age (early retirement) permanently reduced for premature.

Conclusion

Based on the literature review, we find several practices supporting green jobs. They stem from knowing that green jobs use more intensively high-level cognitive and interpersonal skills than non-green jobs. Green occupations need formal education, work experience, and on-the-job training and retraining. In the Czech Republic, the HRM aimed at the greening economy remains on the edge of employers' strategies due to unclear macroeconomic trends and austerity measures.

The employees are threatened by unemployment, inflation, and worsening labor relations, which negatively impact their job motivation. Moreover, a slightly generous social security system is outdated and determines that the economically active population aged 50-64 gradually intends to retire early. Therefore, supporting green jobs will need to identify the factors that can motivate older workers to remain in the labor market until the period of their regular retirement. However, it is a matter of investing in green jobs ergonomics, promoting the massive application of individualized and flexible working time, providing lifelong education, and achieving a reasonable relation between pensions and lifetime wages.

Acknowledgement

This work was supported by DWEL, Erasmus+ Project No 2021-1-SK01-KA220-HED-000032017.

References

1. Jetha A., Shamaee A., Bonaccio S., Gignac M.A.M., Tucker L.B., Tompa E., Bultmann U., Norman C.D.: Fragmentation in the future of work: A horizon scan examining the impact of the changing nature of work on workers experiencing vulnerability. *American Journal of Industrial Medicine*, 64, 649 (2021).
2. Dvorak P., Martinat S., Van der Horst D., Frantal B., Tureckova K.: (2017). Renewable energy investment and job creation; a cross-sectoral assessment for the Czech Republic with reference to EU benchmarks. *Renewable & Sustainable Energy Reviews*, 69, 360 (2017).
3. Paulet R., Holland P., Morgan D.: A meta-review of 10 years of green human resource management: is Green HRM headed towards a roadblock or a revitalization? *Asia Pacific Journal of Human Resources*. 59, 159 (2021).
4. Kutnohorská O., Strachotová D.: Consumer behaviour in the bread market, *Proceedings of the 7th International conference on chemical technology*, (2019).

5. Kouri R., Clarke, A.: Framing "Green Jobs" Discourse: Analysis of Popular Usage. *Sustainable Development*. 22, 217 (2014).
6. Bowen A., Kuralbayeva K., Tipoe, E.: Characterizing green employment: The impacts of 'greening' on workforce composition. *Energy Economics*, 72, 263 (2018).
7. Moreira S., Vasconcelos L., Santos C.S.: Occupational health indicators: Exploring the social and decent work dimensions of green jobs in Portugal. *Work: A Journal of Prevention, Assessment & Rehabilitation*. 61, 189 (2018).
8. Brandl J., Zielinska I.: Reviewing the Smart City Vienna Framework Strategy's Potential as an Eco-Social Policy in the Context of Quality of Work and Socio-Ecological Transformation. *Sustainability*. 12, 859 (2020).
9. Botek M., Strachotová D.: Impact of Maintenance on Health and safety management at work. In ICCT Mikulov, 138-143 (2018).
10. Ge Y., Zhi Q.: Literature Review: The Green Economy, Clean Energy Policy and Employment. *Applied Energy Symposium and Summit 2015: Low Carbon Cities and Urban Energy Systems*, 88, 257 (2016).
11. Naqvi S., Wang J.C., Ali, R.: Towards a green economy in Europe: does renewable energy production has asymmetric effects on unemployment? *Environmental Science and Pollution Research*, 29, 18832 (2022).
12. Scully-Russ E.: Are Green Jobs Career Pathways a Path to a 21st-Century Workforce Development System? *Adult Learning*, 24, 6 (2013).
13. Green education initiatives. [cit. 2022-06-08]. <https://education.ec.europa.eu/focus-topics/green-education/about>.
14. Botek M.: Economical aspects of population aging. In ICCT Mikulov, 114-117 (2017).
15. Consoli D., Marin G., Marzucchi A., Vona F.: Do green jobs differ from non-green jobs in terms of skills and human capital? *Research Policy*. 45, 1046 (2016).
16. International Labour Organization: Gender Equality and Green Jobs. *Green Jobs Programme*. (2015). https://www.ilo.org/wcmsp5/groups/public/---ed_emp/---emp_ent/documents/publication/wcms_360572.pdf.
17. CEDEFOP: The green employment and skills transformation. Insights from a European Green Deal skills forecast scenario. Luxembourg: Publications Office of the European Union (2021). <http://data.europa.eu/doi/10.2801/112540>
18. OECD Economic Outlook, Volume 2022 Issue 1: Preliminary version. https://www.oecd-ilibrary.org/sites/62d0ca31-en/1/3/1/index.html?itemId=/content/publication/62d0ca31-en&_csp_=0cf9a35c204747c5f82f56787b31b42b&itemIGO=oecd&itemContentType=book
19. Czech Social Security Administration (CSSA). <https://data.cssz.cz/web/otevrena-data/katalog-otevrenych-dat>.

MODELLING STEAM METHANE REFORMER OPERATION WITH HYDROGEN-ENRICHED FEEDSTOCK

Hoppej D.¹, Variny M.¹, Kondáš R.¹

¹ Faculty of Chemical and Food Technology, Slovak University of Technology in Bratislava, Radlinského 9, 812 37 Bratislava, Slovakia
dominik.hoppej@gmail.com

Abstract

Natural gas enrichment by renewable hydrogen belongs to key tools in reaching the ambitious decarbonization goals set by the European Union. Problems related to the renewable hydrogen production, its co-transport with natural gas and combustion properties of hydrogen-natural gas mixtures are researched intensely. Less attention is paid to the consequences of consumption of such gas mixtures in steam reformers – important natural gas consumers for industrial hydrogen production. Available studies recommend and assess hydrogen pre-separation. While possible, it is quite costly, especially regarding the inevitable presence of a large pressure gradient, whether in membrane or adsorption-desorption separations, coupled with large power requirements for the recompression of the low-pressure effluent. This stimulated the presented study devoted to assessing the operation of an industrial steam methane reformer with hydrogen-enriched feed and comparing the energy and carbon footprint of hydrogen production from conventional and enriched feed. Key findings are obtained, indicating which way of hydrogen recovery is more cost-effective and more environmentally friendly: whether hydrogen pre-separation or routing the hydrogen-enriched feed to the steam reformer.

Introduction

Blending green hydrogen in the natural gas pipelines is one of key tools in reaching ambitious decarbonization goals set by European Union^{1,2}. While most of scientific work dedicated to blending natural gas with hydrogen is focused on possible associated risks, as its leakage³, or steel pipeline integrity⁴, the aim of this work is to examine consequences of feedstock composition change, considering feasible hydrogen content of up to 15 vol. %⁵ for steam methane reforming process. This process is the most common technology of hydrogen production⁶. In this work, 2 scenarios are compared, among them the hydrogen separation from the natural gas before its usage in the process, and direct usage of hydrogen enriched feedstock in the steam methane reforming process. In addition, third, theoretical scenario of delivering hydrogen equivalent to hydrogen blended in the natural gas to the natural gas pipelines was analysed.

Modelling of hydrogen plant

As the aim of developed model was to evaluate the impact of blending hydrogen to the natural gas on steam methane reforming process, existing hydrogen plant was used as the template for mathematical model, using the available documentation of this plant. Scheme of developed model can be found in Figure 1. To avoid unnecessary robustness of model, several assumptions were considered, which we believe will not serve as serious bottlenecks for the interpretation of obtained results. Among these assumptions, or simplifications, was the perfect combustion at the furnace of reforming reactor. Also, due to the low content of odorization substances in natural gas and low impact on the plant energy balance, the process of desulphurization was neglected in terms of reactor simulation and instead was simulated by addition of heat exchanger, with the same temperature (15 °C) and pressure loss (50 kPa), as was projected for this process.

Preparation of reaction mixture in this plant consists of the addition of recycled stream of hydrogen to natural gas in device M_ZP-H, and subsequent compression (K-100), and desulphurization of natural gas (DSU) after preheating in the heat exchangers (CONV_D1 and CONV_D2) of convective section of the furnace of reforming reactor. After desulphurization, natural gas is blended with high pressure steam and heated in CONV_A before entering the reforming reactor REF at projected temperature. Molar ratio of natural gas and stream was set to 3, in accordance with projected ratio. Reforming reactor, filled with Ni-containing catalyst, which operates in temperature 850 °C favours reactions (1) and (2).



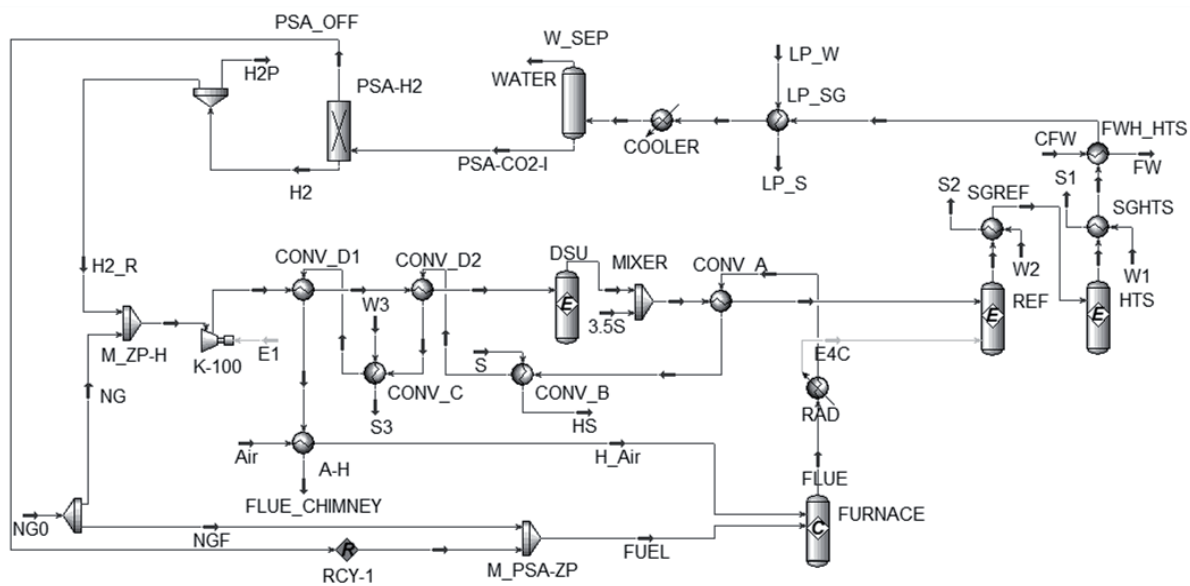
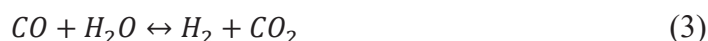


Figure 1. Scheme of mathematical model in Aspen Hysys V11.

Before the reaction mixture enters high temperature shift reactor (HTS) it is cooled down in steam generator, SGREF, below 400 °C. HTS reactor is filled with Fe-based catalyst, selective towards reaction (3).



Reforming reactor and high temperature shift (HTS) reactor were modelled with the use of ATE. This parameter allows us to assess the influence of uneven heat and mass transfer, uneven velocity profile and mixing intensity, distribution of catalyst, etc., on the final composition of reaction mixture. Comparison of calculated and projected composition on the outlet of reforming reactor and HTS reactor can be observed in Table I. Reaction mixture at the outlet of HTS is then cooled down in high pressure steam generator (SGHTS), feed water heater (FWH_HTS) and low-pressure steam generator (LP_SG). Low pressure steam is utilized in consequent process, where the steam present in reaction mixture is condensed at COOLER and separated in W_SEP. Condensed steam is then stripped using low pressure steam, which was, however, not our object of interest, due to negligible impact on process energy consumption.

After separation of condensed water the reaction mixture is processed in pressure swing adsorption process (PSA-H2), where the hydrogen is separated and the process tailgas (PSA-OFF) is combusted in the FURNACE, together with natural gas. Flue gas delivers heat in radiation section of the reforming reactor (RAD) and then is cooled down at the convective section of the furnace, consisting of heat exchangers preheating reaction mixture (CONV_A, CONV_D2, CONV_D1) and air (A-H) and steam generator (CONV_C), as well as steam heater (CONV_B). Heat exchangers and steam generators present in hydrogen plant, were modelled assuming constant value of heat transfer coefficient, nondependent on the flowrate changes.

Methodology

To achieve main goals, simulations with natural gas containing 0, 5, 10 and 15 volume % of hydrogen were performed. For hydrogen content higher than 5 vol. % a stream of recycled hydrogen used for desulfurization of natural gas stopped and the amount of process steam was changed, to limit steam to carbohydrates ratio equal to 3.0. Due to the rise of volume flow of natural gas and consequent increase of pressure losses, calculated using Darcy law, the outlet pressure of produced hydrogen decreased. However, as the designed pressure of hydrogen is higher, than the pressure of hydrogen pipelines network, it was not necessary to increase the outlet pressure of feed compressor. Still, as the volume flow is increased, electricity consumption of feed compressor rises, which was taken into account when calculating the price of produced hydrogen. Changes of natural gas consumption and steam production were also considered. To sustain constant steam production, compensation mechanism of central power plant was considered, which increases its steam output to compensate decrease of steam production in plants of refinery. The consumption of natural gas in the central power plant was also considered, as well as its carbon dioxide emissions - the impact of hydrogen presence in the natural gas on total

carbon dioxide emissions was also observed. The price of produced hydrogen was calculated for maximum capacity of hydrogen plant.

For the economy analysis, price of long-term contracts for the natural gas were taken⁷. Due to observed correlation between the natural gas and electricity prices of long-term contracts, price of electricity was assumed to be 2.5 times higher in comparison with natural gas price. For the emission allowances, current price was taken⁸, as of 14.4.2022. Necessary for the analysis was to determine the price of natural gas blended with hydrogen. Our assumption was to use the same price per heating value of blended natural gas, as current prices of long-term contracts suggest and add the costs to produce hydrogen. As hydrogen used for blending should be made off renewable energy sources, energy consumption of electrolysis was considered, at 48 MWh/t of hydrogen⁹. Prior to the economic analysis, hydrogen content was considered as the equivalent of the natural gas used up for the electricity production for water electrolysis process, with 40% thermic efficiency, in accordance with the assumption of electricity price correlation.

Price of produced hydrogen was thus calculated as the sum of costs of natural gas, emission allowances for the emitted carbon dioxide and electricity consumed in the feed compressor. From this sum, the equivalent costs for natural gas consumption at the central power plant were deducted. For the scenario with the separation unit, energy consumption for the separation was added and the price of separated green hydrogen was deducted from the hydrogen price, as it could be transferred to the market for the price of green hydrogen, in accordance with the assumptions in previous section. This was also the case for the last scenario, which assumed delivery of green hydrogen directly from the stream of produced hydrogen. Price of the green hydrogen present in the natural gas used as the process feed was thus deducted from the price of produced hydrogen.

Analysis of hydrogen separation from the natural gas before its usage in the process was based on the results of study aiming at the optimization of this separation process¹⁰. This study develops separation process for the 80% yield of hydrogen and 99.97% purity of separated hydrogen, high enough to be used in fuel cells. with the energy consumption dependant on hydrogen content, as can be seen in the Table I.

Table I
Separation process electricity consumption¹⁰

Hydrogen content of natural gas [vol. %]	Energy consumption [kWh of electricity/m ³ of H ₂]
1	2.2
4	0.6
10	0.4

Results

As can be observed in the Table II, despite the decrease in the natural gas consumption, hydrogen presence in the natural gas has a significant impact on total energy consumption if the hydrogen production costs are included. As reaction rate of reforming reactions decreases due to higher hydrogen content of natural gas, less heat is consumed in the reforming reactor. Consequently, less natural gas is combusted in the furnace of the reforming reactor, which results in the decrease of steam production. This decrease is compensated by the increase of central power plant emissions, which were also considered, when calculating total carbon dioxide emissions – as we can see in Table II, total carbon dioxide emissions decrease, as lower natural gas consumption and lower emission factor of natural gas blended with hydrogen has incomparably higher impact on the process emissions. Power consumption of feed compressor increases, but as can be seen, this effect has very little impact on final price of produced hydrogen. Still, the price of produced hydrogen rises significantly.

The second scenario was based on separation of green hydrogen from the natural gas before its usage in the steam reforming process. Results of this analysis can be observed in the Table III.

Due to high yield of proposed separation process, residue hydrogen content of natural gas after the separation was reduced to the amount smaller than the amount used for desulphurization. Thus, changes of steam production, CO₂ emissions and compressor power consumption were not observable. Separated hydrogen was then, in accordance with the proposed usage in the article, sold for the price of green hydrogen, to compensate for higher price of purchased natural gas blended with hydrogen.

Following the results obtained by simulations with natural gas blended with hydrogen, economic analysis was performed, results of which can be observed in Table II.

Table II
Results of direct usage scenario

Natural gas H ₂ content (vol. %)	Natural gas consumption / H ₂ as natural gas eq. (kWh/kg)	Steam production (kWh/kg)	CO ₂ emissions (kg/kg)	Separated H ₂ as NG eq. (kWh/kg)	Price of produced H ₂ (€/kg)
0	55.856 / 0.000	5.729	10.099	-	5.345
5	+ 0.869 / 2.878	+ 0.027	- 0.051	2.566	+ 0.103
10	+ 2.023 / 6.080	+ 0.110	- 0.046	5.468	+ 0.232
15	+ 3.258 / 9.662	+ 0.189	- 0.045	8.780	+ 0.365

Table III
Results of hydrogen separation scenario

Natural gas H ₂ content (vol. %)	Natural gas consumption / H ₂ as natural gas equiv. (kWh/kg)	Steam production (kWh/kg)	CO ₂ emissions (kg/kg)	Compressor power consumption (kWh/kg)	Price of produced H ₂ (€/kg)
0	55.856 / 0.000	5.729	10.099	0.116	5.345
5	- 0.319 / + 2.818	- 0.093	- 0.226	+ 0.001	+ 0.216
10	- 0.500 / + 5.815	- 0.145	- 0.418	+ 0.006	+ 0.459
15	- 0.773 / + 9.003	- 0.214	- 0.630	+ 0.011	+ 0.712

As hydrogen present in the natural gas is not changed in the process, the third scenario was considered, to deliver part of produced hydrogen back to the natural gas grid. Still, the hydrogen from the natural gas combusted in the furnace of reforming reactor was not delivered back to the natural gas grid. This approach allows us to compensate higher prices, similarly as in the previous scenario. Despite lack of legislative backup, the simulations of this scenario were performed, and results can be seen in the Table IV.

Table IV
Results of hydrogen delivery back to the natural gas grid scenario

Natural gas H ₂ content (vol. %)	Natural gas consumption / H ₂ as natural gas eq. (kWh/kg)	Separation power consumption (kWh/kg)	Separated H ₂ as natural gas eq. (kWh/kg)	Price of produced H ₂ (€/kg)
0	55.856 / 0.000	-	-	5.345
5	+ 0.934 / 2.881	0.140	2.305	+ 0.167
10	+ 1.970 / 6.075	0.197	4.860	+ 0.331
15	+ 3.239 / 9.641	0.312	7.713	+ 0.525

Table V
Comparison of hydrogen prices according to analysed scenarios

Natural gas H ₂ content (vol. %)	Direct usage (€/kg)	Hydrogen separation (€/kg)	Hydrogen delivery back to the natural gas grid (€/kg)
0	5.345	5.345	5.345
5	5.561 / + 4.03 %	5.513 / + 3.13 %	5.449 / + 1.94 %
10	5.805 / + 8.59 %	5.676 / + 6.19 %	5.577 / + 4.34 %
15	6.058 / + 13.32 %	5.871 / + 9.83 %	5.711 / + 6.83 %

Main setback of this scenario is reduction in productivity of hydrogen, as part of produced hydrogen is delivered to the natural gas grid. That is the reason, why the results in Table IV are different from the results in Table II. This influences natural gas consumption, as well as steam production and CO₂ emissions. Still, due to significant reduction of non-compensated consumption of green hydrogen, price of produced hydrogen is lower in comparison with previous scenarios.

Comparison of obtained prices of hydrogen produced in accordance with each scenario can be observed in Table V. As results from this table, delivery of hydrogen back to the natural gas grid is the most feasible way of mitigation of negative economic effects of hydrogen presence in the natural gas from the economic point of view. By this approach it is possible to compensate higher prices of natural gas, without consuming surplus electricity for separation of hydrogen.

Conclusion

Despite hydrogen delivery back to the natural gas grid scenario being the most economically feasible way of usage of natural gas blended with hydrogen for hydrogen production, it has setbacks. At first, lack of legislation enabling this option makes it purely hypothetical. It also results in the decrease of hydrogen production, as part of produced/processed hydrogen is taken back to the natural gas grid. Scenario with hydrogen separation before its usage in the process is slightly less economically feasible, but it has drawbacks of its own. The biggest issue could be connected to the market size – due to low number of fuel-cells powered vehicles currently on the road, demand for green hydrogen could be the most serious problem for this scenario. Considering direct usage of natural gas blended with hydrogen, hazard analysis is necessary, as this was not among the aims of this study. Also, as higher flowing velocities impact reaction time, ATE parameter, which was calculated for conventional natural gas, would have had different value. Due to this, another work is needed to be performed, using rigorous model for reforming reactor, which is being prepared.

Acknowledgement

The authors would like to express gratitude to Slovak Research and Development Agency, Grant No. APVV-19-0170 and APVV-18-0134 and to Faculty of Chemical and Food Technology of Slovak University of Technology.

References

1. HYDROGEN EUROPE, Vision on the Role of Hydrogen and Gas Infrastructure on the Road Toward a Climate Neutral Economy, 2019. In [online]. [cit. 13-06-2022]. <https://ec.europa.eu/info/sites/info/files/hydrogen_europe_-_vision_on_the_role_of_hydrogen_and_gas_infrastructure.pdf>
2. Mahajan D., Tan K., Venkatesh T., Kileti P. Clayton C. R.: *Energies* 15, 3582 (2022).
3. Hormaza Mejia A., Brouwer J., Mac Kinnon M.: *Int. J. Hydrogen Energy* 45(15), 8810 (2020).
4. Bouledroua O., Hafsi Z., Djukic M. B., Elaoud S.: *Int. J. Hydrogen Energy* 45(35), 18010 (2020).
5. Fraunhofer Institute for Energy Economics and Energy System Technology, The limitations of hydrogen blending in the European gas grid, 2022, ECF, Berlin
6. Kafková V., Karas D., Cyprichová V. *Vodík*. Centrum Výskumu a Vývoja, Leopoldov 2021.
7. PXE - Zemní plyn - ceny a grafy PXE zemního plynu, vývoj ceny PXE zemního plynu 1 MWh - 1 rok - měna EUR | Kurzy.cz
8. EU Carbon Permits - 2022 Data - 2005-2021 Historical - 2023 Forecast - Price - Quote (tradingeconomics.com)
9. Machhammer O., Bode A., Hormuth W.: *Chem. Eng. Technol.* 39(6), 1185 (2016).
10. Liemberger W., Halmschlager D., Miltner M., Harasek M.: *Appl. Energy* 233-234, 747 (2019).

CHANGES IN MANAGING HUMAN RESOURCES IN THE POST COVID ERA IN THE CZECH REPUBLIC

Charvatova D.¹, Botek M.¹

¹University of Chemistry and Technology, Prague, Technická 5, 166 28 Prague 6, Czech Republic
dagmarch@seznam.cz

Abstract

The last two years have brought a significant change to the HR field all over the world. A global pandemic has transformed the reality of millions of employees and redefined where and how employees will work. Employees started to work from home during the global pandemic. Research has shown that even though nowadays employees can work from their office, they are more likely to choose to work from home. This is easier to apply in the services but the industry will have to adapt to some of these trends. In order to apply these new trends, companies will have to expend further time and costs, but with correct changes, high profits can be also achieved. Nowadays, HR managers across the world are facing the same problems and these are how employers attract, retain and engage the talent they need to remain successful.

This paper will look ahead to what kind of HR trends are currently in the Czech Republic in the context of EU legislation and which changes in HR practices will continue to drive transformation as well as the consequences of the flow of refugees from Ukraine on HR adaptation.

Introduction

COVID-19 had a big impact on human resources. The impacts that have affected human resources are permanent. HR leaders had to consider these changes and adapt to them in order to remain competitive in the labour market.

“Chief human resource officers (CHROs) are facing historic challenges from an exhausted workforce and a highly competitive labor market,” says Brian Kropp, Distinguished Vice President at Gartner. “At the same time, this environment creates an exciting opportunity for CHROs to lead talent into the future and differentiate their organizations as employers of choice.”¹

Based on the literature review, the paper aims to identify how the employer behaves toward the employees after the COVID-19 and in which areas the employer supports the employees and how many employers started to support the employees. The methodology insists on literature review and quantitative research. The questionnaire was sent to 8469 managers and employees. Of the respondents, 202 respondents answered, which is 2.39% return. Of these respondents were 62% of women and 43% of these respondents were working as managers. The answers of these respondents were examined and subsequently evaluated. Percentage results were rounded to whole numbers.

Literature review

*“HR leaders now face the difficult task of managing the interests of workers and their corporations. The outbreak of COVID-19 has proved that this is not just a difficult time but rather a testing time for companies across the globe to check and ensure how swiftly they adapt themselves by thinking and planning differently. An enterprise evolves with nature, and change is unavoidable if performance and productivity are to improve. Changes in structure, technology, and priorities are overgrowing, posing big obstacles to leaders. Corporations worldwide have looked to technology to pursue creative solutions to some of the world’s most pressing problems.”*²

Carnevale J.B. and Hatak I. wrote, that: *“The COVID-19 pandemic has created a particularly challenging environment for human resource management (HRM) – with managers having to quickly venture into the “unknown unknowns” as they strive to help their workforce adapt to and cope with radical changes occurring in the work and social environment. For example, employees who formerly spent all or most of their time working inside their organization’s physical boundaries now have to quickly adjust to remote work environments. Due to shelter in place orders and the closure of non-essential businesses, even those who might be well adjusted to remote working conditions are now faced with their own unique challenges due to an inability to seek alternative workspaces (e.g., cafés, libraries, coworking-spaces) outside of the home itself.”*³

*“Manpower is one of the basic and vital resources of the organization, and organizations need an efficient workforce to achieve their goals. But, in the COVID-19 era, human resources’ productivity can be reduced due to stress, high labor force, reduced organizational performance and profits, unfavorable organizational conditions, inability to manage and lack of training.”*⁴

Discussion and result analysis

Based on the literature review, we can identify that one of HR's primary roles is managing rewards and benefits for an organization's staff and making sure of satisfied employees. Proper management of compensation, time off, and dealing with employees is what keeps employee satisfaction high. For example, some of the authors state, that: *“Technological advance and its influence on organisations, their performance and their responses to the stakeholders has been the subject of continuous research. It entirely affects such organisations' human capital, which will require being innovative and proactive. This can be achieved through happy human resources at work. Happiness and more efficient results constitute a well-argued binomial throughout the literature. Efficiency in organisations has been addressed, among other diverse approaches, by establishing specific standards that have ensured the overall quality of their production/performance system.”*⁵

Many of the authors believe that is necessary to get a sustainable competitive advantage. They believe, that HR play an important role in getting this sustainable competitive advantage. Some of them wrote, that: *“A foundational concern of Strategic HR is identifying firm-level HR systems and practices that allow organizations to secure sustainable competitive advantage. Therefore, identifying HR practices that enable organizations to be sustainable in the face of disruptive environments is a critical endeavor. Two concepts are especially significant in this regard: organizational resilience and high-reliability organization.”*⁶

In the research, we focused on areas, which influence the satisfaction of employees and minimize the occupational risks.

The first area, which we researched, was connected with the minimization of psychological and physical occupational risks. As is possible to see below most employers are aware that sustainable performance is necessary to minimize these risks.

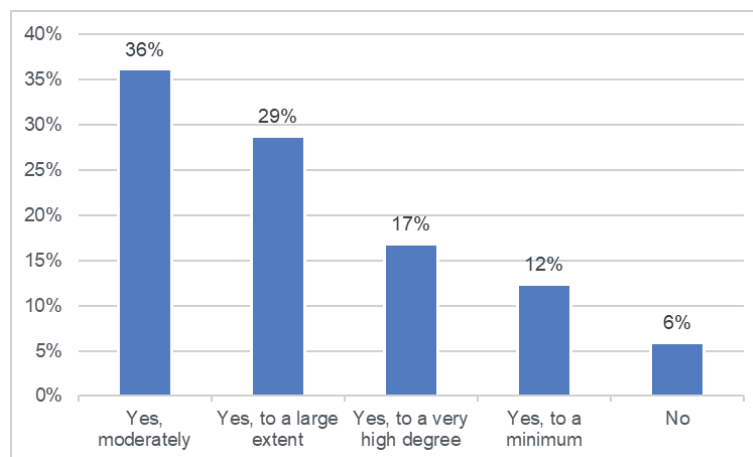


Figure 1. Minimization of psychological and physical occupational risks (Self-plotted graph, data from research, 2022).

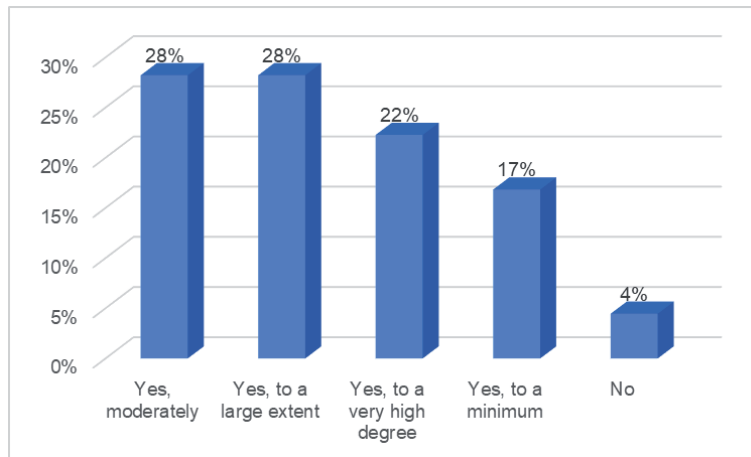


Figure 2. The effort of companies to ensure the development of employee potential and relationships so that people have a sense of meaning and success at all levels of the organization (Self-plotted graph, data research, 2022).

Employers also realised that is necessary to take care of the health of their employees. Employers have also recognized the importance of fitness not only to keep employees healthy but also for their well-being. As a result, some employers have begun to promote sport more in the form of benefits for their employees, but still, around 35 % of employers do not promote the sport and a healthy lifestyle at work as it is possible to see in figure 3.

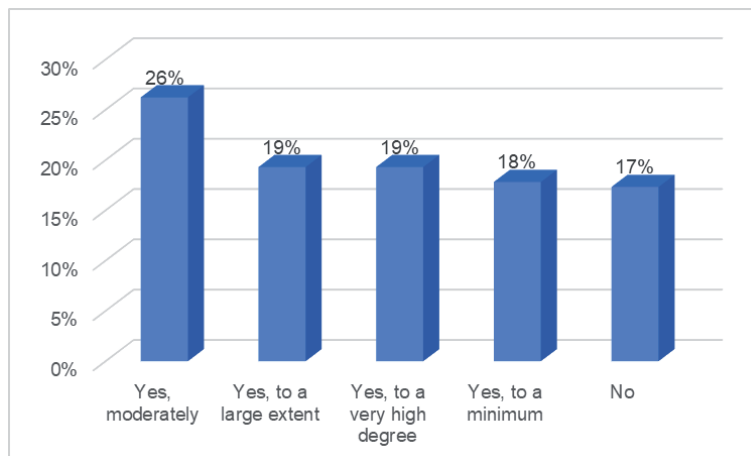


Figure 3. Promoting sport and a healthy lifestyle at work and beyond; for example, the development of sports activities, raising awareness of the benefits of a healthy lifestyle, etc. (Self-plotted graph, data from research, 2022).

Before the COVID-19 employers did not want to allow the employees to work remotely. The vast majority of employees had to work from an office. But with the onset of a pandemic employers had to let employees work remotely. After the end of the pandemic measures, many employees did not want to give up working remotely and HR had to deal with this situation. As it is possible to see in figure 4 most employers support remote work.

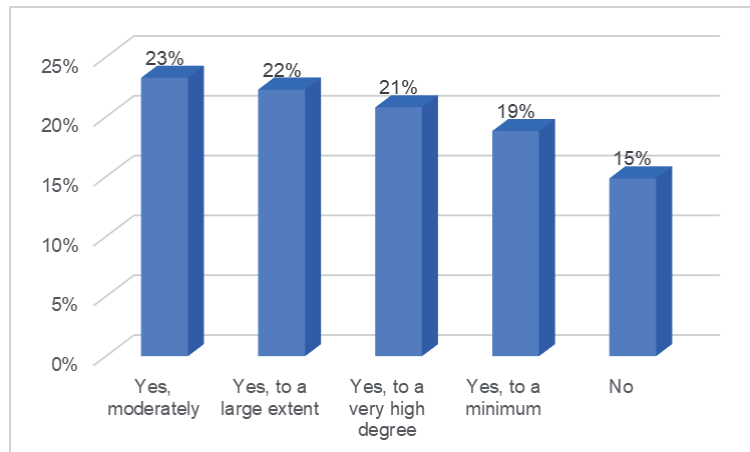


Figure 4 Support of employees to work remotely (Self-plotted graph, data from research, 2022)

Employers also realised the importance of the relationship between the employee and the company. They are aware that sustainable performance is necessary to develop the relationship between the employee and employer.

Some of the authors realised that HR can be helped to reduce the stress of their employees. For example, Chen wrote, that: *“COVID-19 can put a lot of stress in the workplace. Because some employees are facing stressful challenges that are different from those of the past, they will need HR managers to support them in handling the challenges under the crisis. HR personnel should assume that employees working during COVID-19 are feeling the stress of the pandemic, rather than trying to determine if they are showing signs of stress. This stress comes from either the fear of the pandemic itself, the impact of social isolation, or the impact of losing control of what is happening in the world. It is important for HR professionals to understand these stressors and try to help ease the burden on employees.”*⁷

As it is possible to see in figure 5, many employers try to support this development of the relationship, so they can form a bond with the employee and thus keep him in the company.

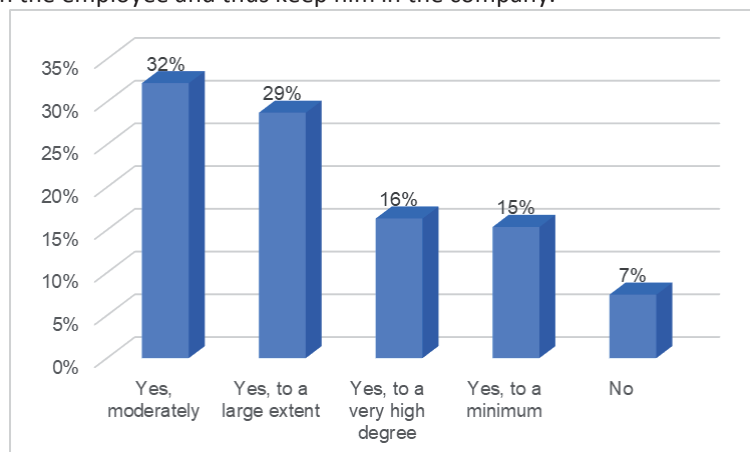


Figure 5 Support the development of the relationship between the employee and company to improve sustainable performance (Self-plotted graph, data from research, 2022).

Because of the pandemic, many employees had to stay in the isolation and quarantine and employers realised that is crucial and necessary to train and educated employees to support their employability. As it is possible to see in figure number 6, only 13% of employers do not support training and education programs that help the employability of workers.

Many authors deal with the importance of training and education programs. Some of these authors believe, that: *“Human capital is determined by the quality of the company’s human potential, which includes knowledge, skills, talents, information, and experience. Their rate of use is determined by individuals’ willingness to use this potential as well as their ability to use it. The essence of creating and increasing the value of human capital is the current expenditure of non-monetary funds to achieve future monetary or non-monetary returns.”*⁸

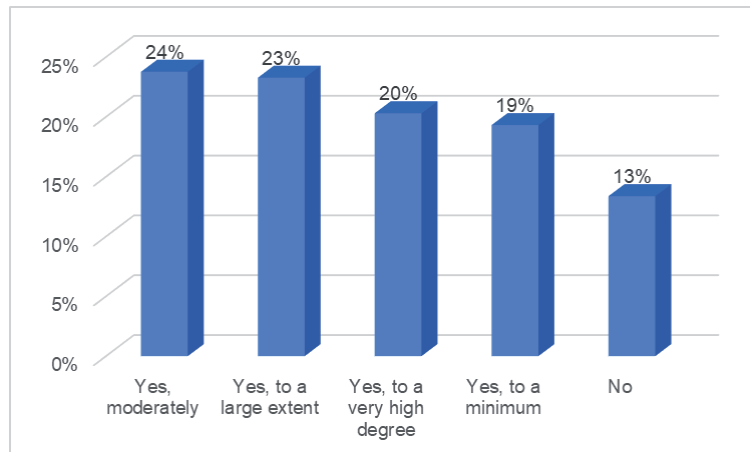


Figure 6 Percentage of employers who have skills training and further education programs that support the employability of workers (Self-plotted graph, data from research, 2022).

Many HR realised that if the training should be successful, it is necessary to take into account the preferences of employees. After a pandemic, most HR takes more into account staff preferences in training. Only 10 % of employees stated, that their preferences in the area of training HR do not consider, as is possible to see in the figure number 7.

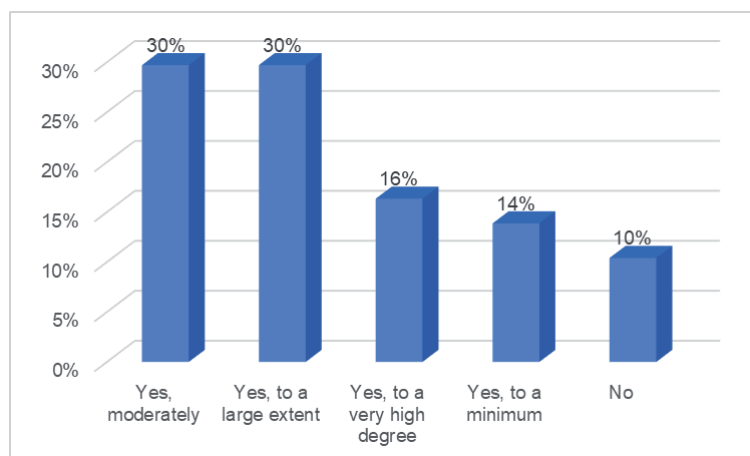


Figure 7 Percentage of HR who take into account employee preferences when determining training (Self-plotted graph, data from research, 2022).

Conclusion

In general, our research showed that most HR people there realized the importance of employee satisfaction and made many changes to the proper management of employees in the workplace. Nevertheless, there are differences in the work of HR professionals, for example, not all HR professionals were aware of the importance of sports and a healthy lifestyle at work, but most HR realized the need to support the development of the relationship between employees and company for improving sustainable performance.

Most HR realised that it is important to put a high impact on minimization of psychological and physical occupational risks.

Research also showed that companies have an effort to ensure the development of employee potential and relationships with them so that people have a sense of meaning and success at all levels of the organization. COVID-19 presented many challenges and opportunities for HRM practice, as well as related pathways for future HR research. Although the implications for HR that COVID-19 has brought are undoubtedly severe, HR will continue to face not only the challenges but also the threats that COVID-19 has brought.

Acknowledgement

This work was supported by DWEL, Erasmus+ Project No 2021-1-SK01-KA220-HED-000032017.

References

1. Turner J., Baker M.: 9 Future of Work Trends Post Covid-19. Garner, www.gartner.com, (2022).
2. Sahar V.: The role of IT-based technologies on the management of human resources in the COVID-19 era. *Kybernetes* 51(6), 2065 (2022).
3. Carnevale J.B., Hatak I.: Employee adjustment and well-being in the era of COVID-19: Implications for human resource management. *J BUS RES* 116, 183 (2020).
4. Xiaojun Y., Masoumeh A.: Do cloud-based enterprise resource planning systems affect the productivity of human resources in the COVID-19 era? *Kybernetes*, 1967 (2021).
5. Ravina-Ripoll R., Foncubierta-Rodriguez M.J., Lopez-Sanchez J.A.: Certification Happiness Management: an integral instrument for human resources management in post-COVID-19 era. *INT J BUS ENV* 12(3), 287 (2021).
6. Kim S., Vaiman V., Sanders, K.: Strategic human resource management in the era of environmental disruptions. *HUM RESOUR MANAGE* 61(3), 283 (2022).
7. Chen Z.: Home Working Stress in the COVID-19 Crisis Era. *J OCCUP ENVIRON MED*, 64(5), 273 (2022).
8. Sebestova J.D., Popescu C.R.G.: Factors Influencing Investments into Human Resources to Support Company Performance. *J RISK FIN MANAG* 15(1), 19 (2022).

CAPACITY CALCULATIONS USING QUANTITATIVE METHODS IN CHEMICAL OPERATIONAL MANAGEMENT

Kostalek J.¹, Kotatkova Stranska P.²

UCT Prague – Department of Economics and Management, Jankovcova 23, 17 000, Prague 7

¹josef.kostalek@vscht.cz, ²pavla.kotatkova.stranska@vscht.cz

Abstract

In industrial plants, especially in chemical plants, the amount of production is not constant over time. This is influenced by a number of factors, such as the gradual process of running in production facilities, where the volume of production increases rapidly at the beginning of the time interval, but then there is digressive growth, where the amount of production gradually converges to a certain value that cannot be exceeded. The production facility reaches the top of its production, where it is not possible to generate further production growth. A new impetus for production growth can come from a quantitative or qualitative change (deployment of more machines, deployment of more workers, deployment of more productive machines, change of production technology, etc.). Even these changes do not necessarily imply an increase in the production of the production plant, because there will be a problem of bottlenecks in production. When production approaches its maximum values, the amount of production is almost constant. This phase lasts a relatively long time, but then the amount of production and thus the use of production capacity begins to decrease. The decrease in production is due to wear and tear of the production equipment. This phase is characterized by an increasing frequency of downtime caused by failures and an increasing percentage of scrap in the production.

For production organization and capacity planning, it is useful to obtain information on how the amount of production will evolve over time. Using appropriate calculations, we can determine future values from past values. The aim of this article is to present computational tools using quantitative methods that will be able to model the amount of production over time. If we can describe the development of production over time using a mathematical model, then we can use the model inversely and determine the time intervals in which the stages of the life of the production equipment take place. The output will serve the production management as a basis for decision-making in the field of management of available production capacities, production planning, planning of preventive maintenance and replacement of production equipment.

Introduction

The article is a guide that describes the use of mathematical methods and statistical software to create mathematical models that are able to describe the development trend of the amount of production over time. The object of interest is when the amount of production changes significantly over time¹. A typical example is the start-up phase of a production facility, where the amount of production is low but growing rapidly². The phase of rapid growth is replaced by a phase of very slow growth, where the amount of production is almost constant. Using a mathematical model describing the situation, we are able to make forecasts of production over time. Each model is a purposeful simplification of reality and therefore works with some precision. The aim of the following text will be to describe a model that models the amount of production over time and to calculate the accuracy of such a model.

Simulation and experiment

We are considering a situation where a new production line starts operating and our experiment will be a prediction of production development over time. Today's production facilities are characterized by complexity and sophistication³, which brings high demands on maintenance staff and complexity during the adjustment and start-up of production^{4, 10}. It is also necessary to train production workers⁵. In our model situation, we will consider that we monitor the number of pieces produced per one day and we have data for 10 days, see Table I, where "x" indicates the time [days] and "y" the number of pieces produced.

Table I

Data on the number of pieces produced per day

x_i	1	2	3	4	5	6	7	8	9	10
y_i	390	450	550	690	760	770	778	810	812	815

The values show that the number of pieces produced is increasing, but the growth is digressive. Our goal is to describe the behaviour of this phenomenon as accurately as possible using quantitative methods, specifically regression analysis. The task is to replace the values from Table I with a mathematical model. In other words, the values from Table I are the points that we replace as accurately as possible with the curve, and the equation of this curve is the mathematical model, which we are looking for. Using a mathematical model, we can predict future developments. For modelling this situation is well suited e.g. the first Törnquist's function or the second Törnquist's function^{6,7}. Both functions will be used, the first Törnquist's function (see formula 1. and figure 1.) we will use for the model A and the second Törnquist's function we will use for the model B (in the next chapter).

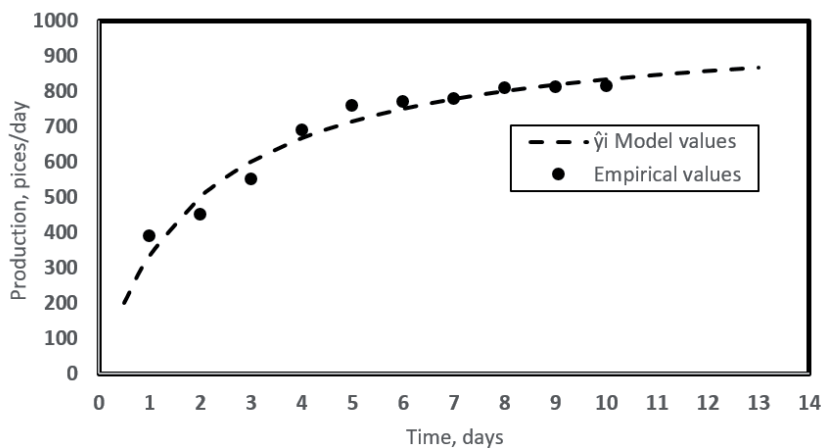


Figure 1. Production over time (data from Table I) and mathematical model A.

$$\hat{y}_i = \frac{ax_i}{b+x_i} \quad (1.)$$

Where a, b are regression parameters that we calculate using formulas 2. and 3., where we substitute the values from the Table I.

$$a = \frac{n \sum_{i=1}^n \frac{1}{x_i^2} - \left(\sum_{i=1}^n \frac{1}{x_i} \right)^2}{\sum_{i=1}^n \frac{1}{x_i^2} \sum_{i=1}^n \frac{1}{y_i} - \sum_{i=1}^n \frac{1}{x_i} \sum_{i=1}^n \frac{1}{x_i y_i}} = \frac{10 \cdot 1.5497 - 8.5789}{1.5498 \cdot 0.0156 - 2.9290 \cdot 0.0057} \doteq 923.362 \quad (2.)$$

$$b = \frac{n \sum_{i=1}^n \frac{1}{x_i y_i} - \sum_{i=1}^n \frac{1}{x_i} \sum_{i=1}^n \frac{1}{y_i}}{\sum_{i=1}^n \frac{1}{x_i^2} \sum_{i=1}^n \frac{1}{y_i} - \sum_{i=1}^n \frac{1}{x_i} \sum_{i=1}^n \frac{1}{x_i y_i}} = \frac{10 \cdot 0.0057 - 2.9290 \cdot 0.0156}{1.5498 \cdot 0.0156 - 2.9290 \cdot 0.0057} \doteq 1.518 \quad (3.)$$

Then we get the resulting form of the mathematical model A, see formula 4.

$$\hat{y}_i = \frac{923.362x_i}{1.518+x_i} \quad (4.)$$

Formulas 2. and 3. were derived using the least squares method. But because function (see formula 1.) is nonlinear, a linear transformation was performed, which is described by formulas 5. and 6.

$$\hat{y}_i = \frac{ax_i}{b+x_i} \Leftrightarrow \frac{1}{\hat{y}_i} = \frac{b+x_i}{ax_i} = \frac{b}{ax_i} + \frac{x_i}{ax_i} = \frac{b}{a} \cdot \frac{1}{x_i} + \frac{1}{a} \quad (5.)$$

$$\hat{z}_i = Bw_i + A, \quad \text{where: } \hat{z}_i = \frac{1}{\hat{y}_i} \Rightarrow z_i = \frac{1}{y_i}, B = \frac{b}{a}, w_i = \frac{1}{x_i}, A = \frac{1}{a} \quad (6.)$$

We will use the linear transformation (described by formulas 5. and 6.) also in the case of calculating the regression parameters by SW for example Statistica or the tool Solver in MS Excel.

Now we need to determine the accuracy of this model A. We will verify the accuracy of the model using the tools of diagnostics of regression models. One of the tools is the correlation index I_{2w} ⁸. To do this, we will again use formula 6., which describes a linear transformation. Then the calculation of the correlation index will be modified to the form see formula 7.

$$I_{ZW} = \sqrt{1 - \frac{S_{ZW}^2}{S_z^2}} = \sqrt{1 - \frac{1.824 \cdot 10^{-8}}{2.054 \cdot 10^{-7}}} \doteq 0.955 \quad (7.)$$

where: $S_{ZW}^2 = \frac{1}{n} \sum_{i=1}^n (z_i - \hat{z}_i)^2$ and $S_z^2 = \frac{1}{n} \sum_{i=1}^n (z_i - \bar{z}_i)^2$

If we substitute the values from Table I into the formula 7., we get the value of the correlation index 0.955 and this means a relatively high accuracy of model A.

Discussion and result analysis

The previous chapter described the principle of quantitative forecasting methods. Using calculations from formulas, a mathematical model, denoted A, was created (see formula 4.) This model can also be obtained using SW, which will be shown here. If the results obtained from the SW will be identical with the calculations from the formulas from the previous chapter, it will also verify the correctness of model A. The values of the regression parameters of the model were determined using the numerical method and the statistical SW Statistica version 12.1. The results are shown in Table II.

Table II

Output of regression analysis - SW Statistica for selected regression model A

Regression parameters	Value	p-value
a	923.3619	0.000000
b	1.5185	0.000018
Regression model		0.00002

The values of the regression parameters (a, b) obtained by SW are identical to the values that were calculated, see Table II. Since we want to use model A for prediction, it is necessary to diagnose the model with residual analysis, see Figure 2. Table II shows also that the model is statistically significant, p-value is less than the 0.05 (significance level). Also the regression parameters are statistically significant, again the p-value is less than the (significance level) 0.05. Because the value of the correlation index of the model is 0.955, index of determination is 0.912 (0.955^2) then the reliability of the model results will be 91.2%.

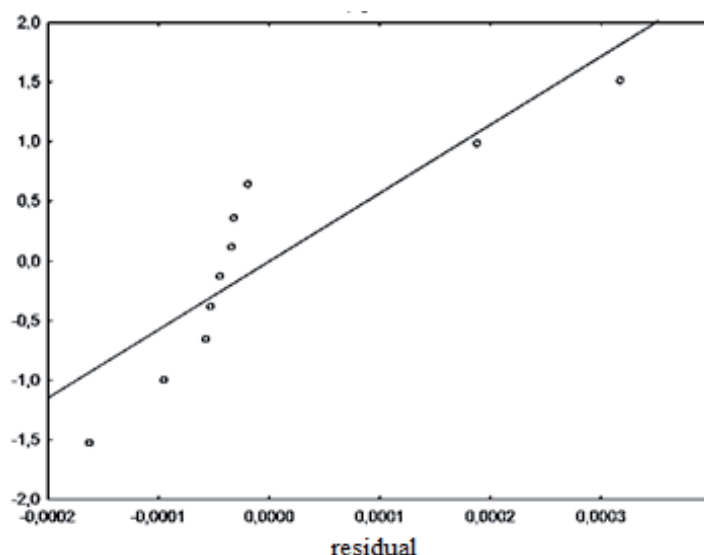


Figure 2. Normal probability graph of residues – model A.

Based on the results (created model A) we can model the development of production growth over time and this is our main goal. The production prediction over time is obtained by substituting the times into the model A (formula 4.) and the results are recorded in Table III.

Table III

Production growth prediction - model A

Selected time value [days]	12	14	28	100
Production capacity prediction [pieces/day]	833	843	876	910

The first Törnquist’s function has the important property that its values converge to the value of the regression parameter "a" ⁷. This fact is confirmed by the values in Table III. And it can be proved mathematically by calculating the limit of the function. In practice, this means that by calculating the correlation parameters, we also obtained information about what production can be maximally achieved (923 pieces per day). All connections are described in figure 1 at the top of the article.

In the next part of this article, we will look for a solution to the situation if the model A used does not reach the required accuracy. For our reasoning, we will use the input values from Table I. We would have to use a different curve (different function) and a different model. The second Törnquist’s function (see formula 8.) would be well suited for such a situation.

$$\hat{y}_i = \frac{a(x_i+b)}{c+x_i}, \text{ where: } a, b \text{ are regression parameters, } \hat{y}_i \text{ is model values, } x_i \text{ is time} \quad (8.)$$

We will create a new model, which we will call the model B. This model contains three regression parameters, which will be estimated using statistical SW, the Levenberg-Marquardt’s method. The values of regression parameters were calculated using SW Statistica 12.0. SW outputs, including regression model diagnostics, are included in Table IV.

Table IV

Output of regression analysis for the selected regression model B

Regression parameters	Value	p-value
a	1062.283	0.000021
b	0.390	0.491704
c	3.076	0.105889
Regression model		0.000251
Index of determination	0.95564	

When we substitute the calculated values of regression parameters into formula 8. we get the resulting regression model B, see formula 9.

$$\hat{y}_i = \frac{1062.283(x_i+0.390)}{3.076+x_i} \quad (9.)$$

The Figure 3. describes the situation graphically, where the dots are empirical values from Table I and the curve is model B.

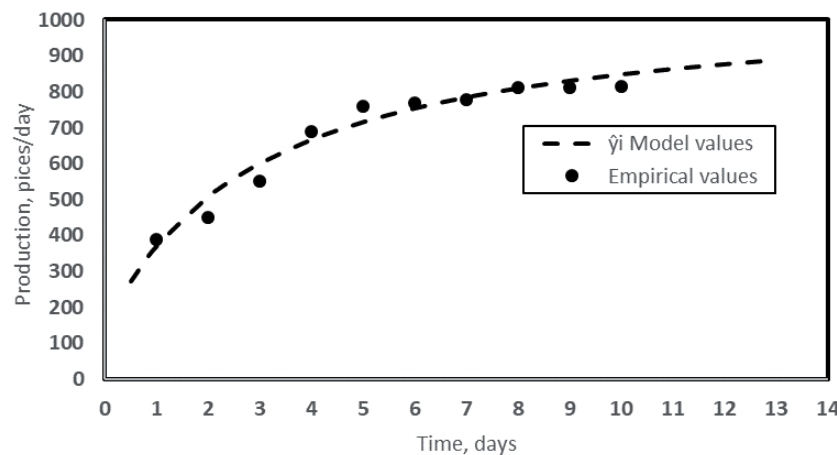


Figure 3. Production over time - model B.

The output from the statistical SW (Table IV) provides other important information: Index of determination is 0.95564 then the reliability of the model results will be 95.56%. This implies that the model B is more accurate

than the model A. The p-values show that the regression model as well as the regression parameters are statistically significant. The significance of model B was also confirmed by the residual analysis, see Figure 4.

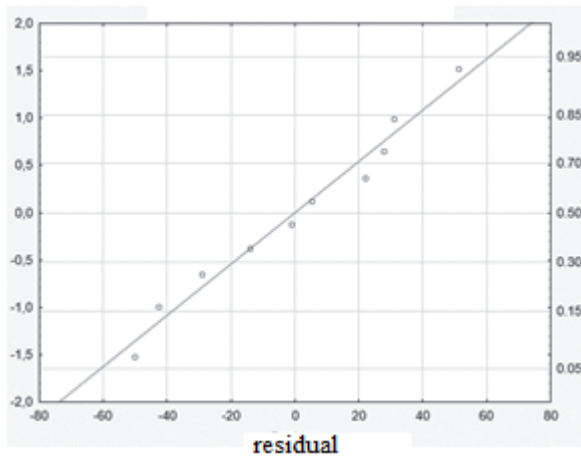


Figure 4. Normal probability graph of residues – model B.

Based on the results (formula 9), it is again possible to extrapolate the trend of the development of the amount of production and thus predict the time when production will reach a specified level, see Table IV. At the same time, we are able to predict to what extent production will increase, because the second Törnquist's function has also the important property that its values converge to the value of the regression parameter "a"^{9,10}.

Table V
Production growth prediction - model B

Selected time value [days]	12	14	28	100
Production capacity prediction [pieces/day]	873	895	970	1035

The production values from Table IV calculated using model B confirm this fact and converge to the value of 1062 pcs/day.

Conclusion

One of the situations when the production capacity changes sharply over time is in the start-up operation. The article describes the tools that production management can use in a situation where a new production facility starts operating, which produces a fraction of its maximum production capacity, but its production is higher and higher every day. Over time, production has stabilized and production capacity utilization is not constant, but depends on factors other than time. The next phase follows, when the utilization of production capacity decreases over time. This is mainly due to the increased failure rate of the production equipment. The models for this phase did not fit into the article, but would work on the same principle as the described growth phase. The difference would be that a suitable declining curve would be selected for the regression analysis.

The article describes two models and their use in a situation of rapid production growth and subsequent digressive growth. Where we can extrapolate future values from past values using quantitative methods and create a mathematical model capable of describing the situation. Model A uses the first Törnquist's function and model B uses the second Törnquist's function. Model B has higher accuracy, but is more complex and requires statistical software to determine its parameters. Model A is less accurate, but its parameters can be easily calculated in MS Excel by substituting into formulas without special software. Both models also give information where the maximum value of production lies, because it is the value to which the model functions converge.

References

1. Fiala P.: *Modely produkčních systémů*. VŠE, Praha 2005.
2. Kavan M.: *Výrobní a provozní management*. Grada, Praha 2002.
3. Nenadál J.: *Management kvality pro 21. století*. Management Press, Praha 2018.

4. Švecová L., Veber J.: *Produkční a provozní management*. Grada, Praha, 2021.
5. Kuchařová A., Tokarčíková E., Ďurišová, M., Jacková, A.: *Efektivní výroba. Využijte výrobní faktory a připravte se na změny na trzích*. Computer Press, Brno 2011.
6. Kavan M.: *Výrobní management*. ČVUT, Praha 2006.
7. Kavan M.: *Projektový management inovací*. ČVUT, Praha 2007.
8. Kožíšek J., Stieberová B.: *Statistická a rozhodovací analýza*. ČVUT, Praha 2014.
9. Taeho Kim a Way Kuo, "Modeling production yield and reliability", v *IEEE Transactions on Semiconductor Manufacturing*, 12 (4), 485 (1999).
10. Tao Yuan, Suk Joo Bae, Yue Kuo, *Statistical Quality Technologies*, 375 (2019).

MATHEMATICAL MODELING OF HEAT AND MASS TRANSFER IN A ROTARY KILN

Kozakovic M.^{1,2}, Cada J.², Kokavcova A.², Havlica J.^{2,3}, Huchet F.⁴

¹ Jan Evangelista Purkyně University in Ústí nad Labem, Faculty of Mechanical Engineering, Pasteurova 1, 400 96 Ústí nad Labem Czech Republic

² Jan Evangelista Purkyně University in Ústí nad Labem, Faculty of Science, Pasteurova 3632/15, 400 96 Ústí nad Labem, Czech Republic

³ Czech Academy of Sciences, Institute of Chemical Process Fundamentals, Rozvojova 2/135, 165 02 Prague, Czech Republic

⁴ Université Gustave Eiffel, MAST/GPEM, Campus de Nantes, Allée des Ponts et Chaussées CS5004 44344 Bouguenais cedex France
martin.kozakovic@gmail.com

Abstract

The main objective of this research was to compare the results of the proposed 1D transport model with numerical simulations of mass transport in a direct-heat rotary kiln at laboratory scale. Another objective was to investigate the effect of the number of flights on the formation of an active particle surface in the airborne phase, which enables efficient heat transport.

The studied rotary kiln is a low-angle cylinder with a length of 0.5 meter and a diameter of 0.108 meter with regularly arranged flights on the inside. The heat is transported into the rotary kiln by hot air at the inlet. The load in the rotary kiln consists of spherical particles with 1 millimeter diameter. The rotary kiln rotation speed is 21.5 rpm. For each simulation, 20 rotations were performed. The Discrete Element Method implemented in an open-source code LIGGGHTS was used for simulations.

Efficient heat transfer is made possible primarily by the large number of particles in the airborne phase, which are heated by the warm air blowing in. To begin with, the number of flights and their geometry were found to be a key parameter controlling the amount of particles in the gaseous regime. It was also found that an area in the right part of the base of the cylinder is formed which is not reached by particles from the flights. This phenomenon is due to the dynamics of particle transport, as the particles are not maintained in the active phase and move rapidly towards the load due to gravity. In conclusion, the effect of this zone is negative, as hot air flows through it without resistance, preventing the system from heating effectively.

Introduction

The climatic context highlights the needs to carefully manage the energetic resources. Thus, the industrial activity must be sized with respect to the new energy strategy. The energy-intensive process steps used in the industrial plant are particularly targeted. For one of them, they appeal to the rotary kiln. This device is widely used in the field of civil, metallurgical and chemical industries as a unit operation in chemical engineering especially for drying, reacting, mixing, granulating and heating of granular materials.

Figure 1 shows the dependence of the amount of extracted materials (left) and stock traded materials (right) as a function of time. Here we can observe an exponential increase in the extraction and stock trading of materials over the past hundred years. Note that cement and asphalt are mainly processed in rotary kilns. It is obvious that the current management of materials is unsustainable. In the near future we will have to move towards a circular economy in order to increase the efficiency of processing these materials. Therefore, examining the heat transfer phenomena in order to improve modelling tools and understand the dynamics of mass transport in rotary kilns is of fundamental importance.

A simplified scheme of a direct heated rotary kiln is shown in Figure 2. A rotary kiln is usually a longer steel tube with a drive gear that provides the rotation. There are flights on the inside of the tube that lift the material out of the bed. For the preparation of the asphalt, direct heating with a hot flame is mainly used, as shown in the figure. In the case of direct heating, all mechanisms contribute to heat transport. It is essential to lift particles from the bed to the so-called active phase.

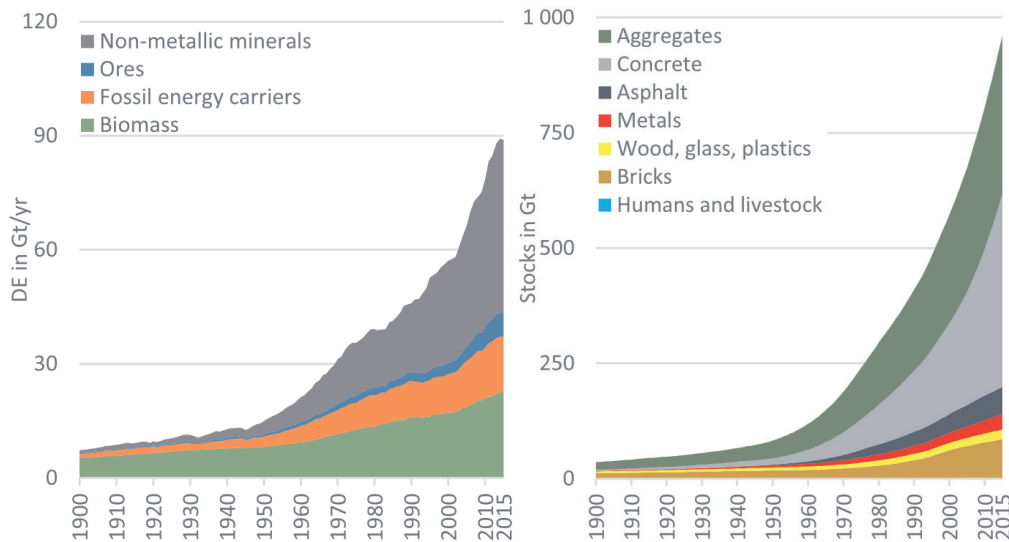


Figure 1. Extraction of different materials and traded stocks of materials in the past 100 years ¹.

A 1D heat and mass transport model was introduced by Sunkara et al. ³. Piton et al. ⁴ extended this model with additional flight's geometry and used it to investigate a particle's discharge in an industrial device. Nascimento et al. ⁵ studied solids holdup in flighted rotating drums by using the euler-euler approach. Karali et al. ⁶ found an optimal loading volume ratio of about 12.5 % in an operated flighted rotary drum. Zhang et al. ⁷ studied the influence of the number of flights on the phase ratio in rotary kilns by using the Discrete Element Method (DEM). They found out that eight flights in a kiln are optimal for their geometry. The design and arrangement of flights in a rotary drum by using DEM were recently studied by Silveira ⁸. In their research, they determined the ideal kiln arrangement leading to the highest active phase.

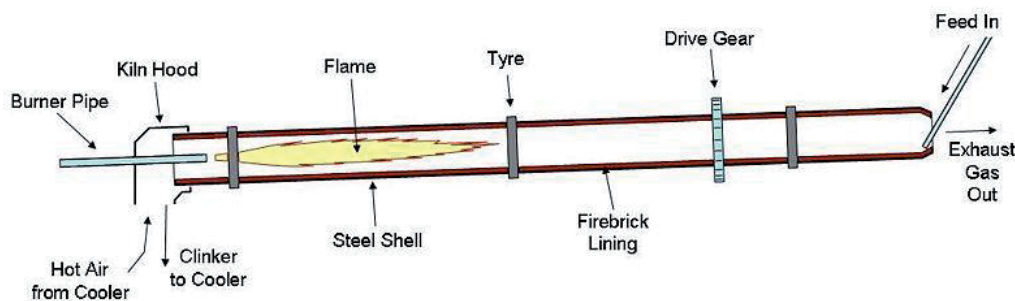


Figure 2. The scheme of a direct-heated rotary kiln ².

The main objective of this research is to compare the results of the 1D transport model with Discrete Element Method (DEM) numerical simulations of mass transport in a direct-heat rotary kiln at a laboratory scale. Another objective is to investigate the effect of the number of flights on the formation of particles in the active phase, which enables efficient heat transport.

Method

In this work, the effect of the number of flights on the active phase formation in a rotary kiln was studied by using a 1D axial model and DEM. The scheme of the studied rotary kiln including the flight geometry is shown in Figure 3. The geometrical parameters of the rotary kiln are given in Table I. The rotary kiln rotation speed was 21.3 rpm corresponding to a Froude number of 0.0274. DEM parameters i.e. Young's modulus Y , coefficient of restitution e , timestep Δt , coefficient of friction μ , rolling friction μ_r and Poisson's ratio ν were set according to Silveira ⁸, see Table I, Parameters section.

The 1D model derived by Sunkara consists of integral equations that can be solved by simple implementation of advanced integration methods and obtain results quickly. The 1D model generally works only for over-loaded systems. A sufficient condition is that the height of the bed exceeds the length of the flight. The chosen volume

ratio $V_f = 15\%$ satisfies this condition. DEM is basically a molecular dynamics method for repulsive force interaction. The system of second-order ordinary differential equations is solved by using Verlet's algorithm. The DEM used in this paper is implemented in the open-source code LIGGGHTS. The obtained results are detailed information on particle positions, velocities, forces and rotational velocities. DEM, on the other hand, is a more time consuming method. In this case, according to Silveira, only 10% of the rotary kiln length, i.e. 5 cm, is modelled with the application of periodic boundary conditions. The number of particles at the same volume ratio corresponds to $N = 63.837$. This method significantly reduces the computation time. Data post-processing was performed in Matlab.

Table I
Geometrical parameters and DEM simulation conditions of the rotary kiln

Geometry				Parameter s			
L [m]	0.5	L_{oart} [m]	0.05	N [-]	63,837	μ_r [-]	0.04
D [m]	0.108	V_f [-]	0.15	Fr [-]	0.0274	e_{pp} [-]	0.8
l_1 [m]	0.01	d_p [m]	0.00109	γ [Pa]	$5 \cdot 10^6$	e_{ww} [-]	0.9
l_2 [m]	0.005	ρ [$\text{kg} \cdot \text{m}^{-3}$]	2445	μ_{pp} [-]	0.7	Δt [s]	$2.10 \cdot 10^{-5}$
l_3 [m]	0.005	ω [s^{-1}]	21.3	μ_{ww} [-]	0.4	v [-]	0.3



Figure 3. Geometry of the rotary kiln according to Silveira.

Results

Figure 4 on the left shows a visualisation of the DEM results for 20 flights in the 80th revolution. Particles in the kiln are coloured by the magnitude of the velocity. Based on this simple visualisation, we can distinguish between particles in the active phase and in the bed. Particles in the active phase (gaseous regime) have a higher magnitude of velocity. It can be observed that the active zone of the particles forms mainly in the centre of the cylinder with a diameter of about 7 cm. In this active zone, however, there are two main areas, or bands, where particles cannot reach. These bands are located in the left and right sections of the cylinder base. In the left particle section of the cylinder base the particles don't fall out of the flight because of lower inclination. In the right section of the cylinder base, the particles fall back into the bed very quickly due to free fall. It can also be seen that particles from the bed are evenly distributed in all flights. It is obvious that for this case the height of the bed is less than the length of the flight.

For an objective evaluation of the active phase, it is necessary to proceed to more detailed characteristics. It is useful to evaluate the volume ratio of particles in a single flight as a function of its angular position. The first flight located at the highest point of the cylindrical base is displaced 90 degrees counterclockwise at each full revolution. The shifted position is equal to $\delta = 0$ degree. The scheme is shown in the upper right part in figure 4. This characteristic is usually manifested by a steeply declining curve.

In the figure 4 on the right there can be seen the volume ratio of the particles in the flight relativized to the mass of the bed depending on its angular position for different number of flights. The graph shows that about 12 % of

the total particle mass is in the flight. This volume ratio of the flight is almost the same for the number of flights from one to fifteen on the other hand it decreases for higher numbers of flights. This decrease in the volume ratio can be explained by the spreading of the particles in a larger number of flights, which in total have a larger volume than the particles in the bed.

The graph in the figure 4 on the right also shows that within about fifteen flights the particles fall out of the flight at a smaller angle of inclination. For a higher number of flights than fifteen, however, the particles tend to stick in the flight even for larger inclination of the kiln. The particles then discharge the flight more steeply at kiln's inclination about 50°. In the case of twenty-five flights particles falling out of the kiln are an exception. In this case the flights are already very close and there is not enough space for the particles to fall out of the flight. However, a higher number than twenty five flights leads to an undesirable steric effect. The particles neither enter the flight nor fall out of it. In this way a higher number of flights don't support the formation of the active phase.

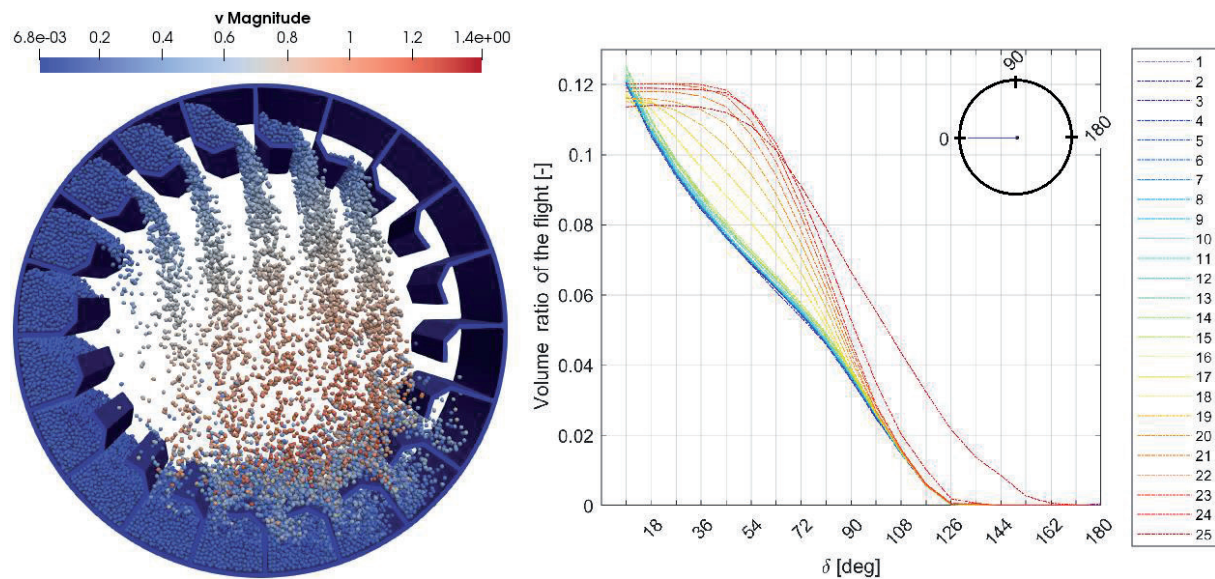


Figure 4. Visualisation of particles in the rotary kiln for 20 flights in the 80th revolution (left), the volume ratio of particles within the flight depending on its angular position for different numbers of flights (right).

To analyse the results, it is most important to track the formation of the particles' in the active phase. In the 1D model, the volume ratio of particles' in the active phase is determined by the calculation in the model. In the case of DEM, it is necessary to trace these particles by using physical quantities. The magnitude of the velocity was chosen as a suitable quantity. In this case, the particle in the active phase was set to have a magnitude of the velocity superior to 0.4 m/s.

Figure 5 on the left shows the dependence of the volume ratio of the particles' active phase relative to the total volume of the bed on the angular position of the flight. We can observe three zones on the graph. For a smaller number of flights, a zone with periodic dependence of the active phase on the position of the flight is evident. In this case the active phase occurs only in peaks and then completely disappears during the rotation. From about five flights onwards, the value of the volume ratio of the active phase stabilises at an average. The active phase does not cease in this second zone. For about fifteen flights, it can be seen that the volume ratio of the active phase reaches its highest value. In the case of this third zone we can talk about reaching a certain optimal value of the active phase volume ratio. After reaching this zone a higher number of lifters no longer contributes to an increase in the active phase.

In order to easily detect the value of the active phase, the mean value of the function given by the curve in Figure 5 on the left was calculated. The resulting mean values of the volume ratio of the active phase as a function of the number of flights in the kiln are shown in Figure 5 on the right for both 1D model and DEM.

The graph in Figure 5 on the right corresponds to the three zones presented in the left graph. For the first zone up to 5 flights a small active phase can be observed. In the second zone we can see that the active phase increases linearly. An optimal number of flights at which the value of the active phase reaches its highest point and does not grow further corresponds to the third zone. Furthermore, the 1D model seems to give bad results for a higher number of flights than the reached optimum by the DEM results. This phenomenon corresponds to the visualisation, see Figure 4 on the left, that the bed volume spreads out in the flights. In this case the total sum of

the volume of particles in the flights appears to exceed the volume of the bed. Obviously, the over-loaded condition of the system is violated. As a result, the 1D model does not work correctly in this case.

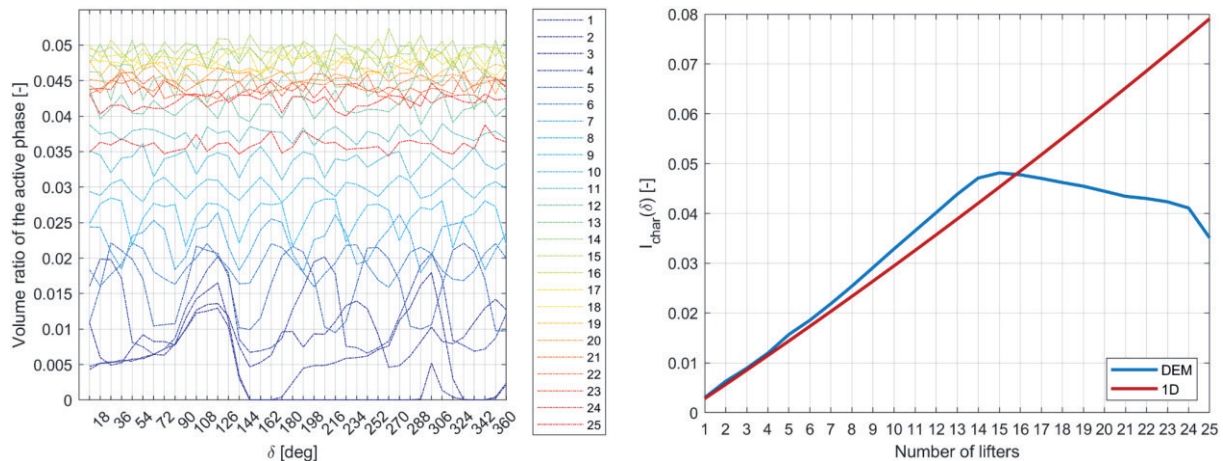


Figure 5. The volume ratio of the active phase depending on the angular position of the flight in the rotary kiln (left), the mean of a volume ratio of the active phase depending on the number of flights in the rotary kiln (right).

Conclusion

In this work, the effect of the number of flights on the active phase formation in a rotary kiln was studied by using a 1D axial model and DEM.

It was found out that the active zone of the particles forms mainly in the centre of the cylinder with a diameter of about 7 cm. In this active zone, however, there are two main areas, or bands, where particles cannot reach. It was also observed that particles from the bed are evenly distributed in all flights for a higher number of flights and as a consequence the height of the bed is less than the length of the flight in this case. Furthermore it was found out that a higher number than twenty five flights leads to an undesirable steric effect. The particles neither enter the flight nor fall out of it. In this way a higher number of flights don't support the formation of the active phase.

Moreover three zones of the active phase were observed. For a smaller number of flights, the active phase occurs only in peaks and then completely disappears during the rotation. From about five flights onwards, the value of the volume ratio of the active phase stabilised at an average. The active phase didn't cease in this second zone. For about fifteen flights the volume ratio of the active phase reached its highest value. After reaching this optimum a higher number of lifters no longer contributed to an increase in the active phase.

To conclude an optimal number of flights at which the value of the active phase reaches its highest point and does not grow further was found out. The 1D model seemed to give bad results for a higher number of flights. However, this phenomenon was explained by the violation of the over-loaded condition of the system. As a result it was found out, the 1D model does not work correctly for a higher number of lifters. The operating range of the 1D model can be approximately determined by the equality of the flights' volume summation and the bed volume.

Acknowledgement

This research was supported by the project U21-Kvalitní lidské zdroje pro posílení mezinárodního prostředí II CZ.02.2.69/0.0/0.0/18_053/0017815, by the internal grant UJEP-SGS-2020-53-003-3 and by the Strategy AV21 of the Czech Academy of Sciences, VP20 - Water for life for valuable support.



EVROPSKÁ UNIE
Evropské strukturální a investiční fondy
Operační program Výzkum, vývoj a vzdělávání



UJEP

U21REPROREG

References

1. KRAUSMANN, Fridolin, Christian LAUK, Willi HAAS and Dominik WIEDENHOFER. From resource extraction

- to outflows of wastes and emissions: The socioeconomic metabolism of the global economy, 1900–2015. *Global Environmental Change* [online]. 2018, 52, 131-140 [cit. 2022-05-10]. ISSN 09593780. Available from: doi:10.1016/j.gloenvcha.2018.07.003
2. CemKilnKiln. In: *Wikipedia commons: Wikimedia* [online]. San Francisco (CA): Wikimedia Foundation, 2001-, 9. 10. 2006 [cit. 2022-05-10]. Available from: <https://commons.wikimedia.org/>
 3. SUNKARA, Koteswara Rao, Fabian HERZ, Eckehard SPECHT, Jochen MELLMANN and Richard ERPELDING. Modeling the discharge characteristics of rectangular flights in a flighted rotary drum. *Powder Technology* [online]. 2013, 234, 107-116 [cit. 2022-05-10]. ISSN 00325910. Available: doi:10.1016/j.powtec.2012.09.007
 4. PITON, Maxime, Florian HUCHET, Olivier LE CORRE, Laurédan LE GUEN a Bogdan CAZACLIU. A coupled thermal-granular model in flights rotary kiln: Industrial validation and process design. *Applied Thermal Engineering* [online]. 2015, 75, 1011-1021 [cit. 2022-05-10]. ISSN 13594311. Available from: doi:10.1016/j.applthermaleng.2014.10.052
 5. NASCIMENTO, Suellen M., Rondinelli M. LIMA, Rodolfo J. BRANDÃO, Claudio R. DUARTE a Marcos A. S. BARROZO. Eulerian study of flights discharge in a rotating drum. *The Canadian Journal of Chemical Engineering* [online]. 2019, 97(2), 477-484 [cit. 2022-05-10]. ISSN 00084034. Available from: doi:10.1002/cjce.23291
 6. KARALI, Mohamed A., Koteswara Rao SUNKARA, Fabian HERZ and Eckehard SPECHT. Experimental analysis of a flighted rotary drum to assess the optimum loading. *Chemical Engineering Science* [online]. 2015, 138, 772-779 [cit. 2022-05-10]. ISSN 00092509. Available from: doi:10.1016/j.ces.2015.09.004
 7. ZHANG, Lanyue, Zhaochen JIANG, Jochen MELLMANN, Fabian WEIGLER, Fabian HERZ, Andreas BÜCK and Evangelos TSOTSAS. Influence of the number of flights on the dilute phase ratio in flighted rotating drums by PTV measurements and DEM simulations. *Particuology* [online]. 2021, 56, 171-182 [cit. 2022-05-10]. ISSN 16742001. Available from: doi:10.1016/j.partic.2020.09.010
 8. Silveira, Jeniffer C., Rondinelli M. Lima, Rodolfo J. Brandao, Claudio R. Duarte, and Marcos A.S. Barrozo. 2022. *Powder Technol.* 395: 195–206. <https://doi.org/10.1016/j.powtec.2021.09.043>.

CONSUMER BEHAVIOUR IN THE GERMAN BREAD MARKET

Kutnohorská O.¹, Strachotová D.¹

¹*School of Business, University of Chemistry and Technology Prague, Prague, Czech Republic, kutnohoo@vscht.cz*

Abstract

Consumer behavior of customers has long been the focus of manufacturers and retailers. Knowledge of the significant factors that influence consumer behavior and decisions can represent a significant competitive advantage. The paper shows seven main criteria that German consumers consider when buying bread. The set of criteria was evaluated by 553 respondents of different age categories on a five-point scale. The taste proved to be the most important, followed by the quality and type of bread. On the contrary, the size of the loaf and the producer play the least important role in the purchase decision. The significance of these criteria varies slightly between older and younger consumers.

Introduction

Bread is one of the basic pillars of human diet. Its original composition was given by plants that naturally occurred in the place of settlement, later supplemented by those that were more productive and for which there were favorable conditions for cultivation in the locality, especially cereals. Although it is not possible to prove when and where exactly this method of cereal processing occurred, the first unconfirmed evidence of bread history can be found about 30,000 years ago¹, unleavened dough bread tortillas were common during various prehistoric periods². In today's households around the world, bread has a wide range of uses - it is used as a food alone, greased with sweet or salted spread, but also as a side dish or starting material for further processing (eg for thickening, wrapping, etc.). The assortment of breads is currently very diverse, in the offer of bakeries and shops you can choose from many types, sizes, flavors and shapes. The importance of bread for humans is demonstrated by the fact that when its availability in the sales network was limited in the last two years due to a pandemic, the trend of home baking of bread spread around in the society.

Bread has remained a fixture in the human diet for millennia, but in different cultures its recipes changed over time, and with them their favorite taste, shape, color or size. In order for a manufacturer to optimize its offer, gain and maintain a competitive advantage, it is important to understand the trends that are taking place in the market and at the same time to understand the consumer behavior of its customers, i.e. consumer purchasing decisions, wishes, needs and criteria, that guide their purchasing decisions. When evaluating the options, consumers search for information and process it, the course of such processes and methods applied may differ³. There are many models that can be used for a general description of consumer behavior, they vary according to the type of purchase, or the type of goods purchased. For food, it seems appropriate to use the Steenkamp model, which focuses on consumer decision-making accompanied by environmental factors (economic, cultural, marketing), human personal factors (biological, psychological, socio-demographic) and food properties (sensory perception, physiological effects)⁴. The general properties of food rated by consumers include taste / flavor, freshness, quality, price, easiness of preparation, availability in the normal supermarket, natural ingredients, brand, long storage time and durability, organic, seasonal product, calories, environmentally friendly packaging and production process, animal welfare, regional products, fair-trade⁵. Some of the most important factors of choosing bread are freshness, appearance, habit and price⁶. Factors are not stable, their significance and importance evolves over time. For example Czech consumers preferences when choosing bread according to NMS 2012 study are freshness, taste, appearance and roasting, durability, composition, nutritional value and according to KPMG 2016 study are quality, price, composition and country of origin⁷.

Overview of the German bread market

The following text provides a brief overview of the basic characteristics of the German bread market. German bread market is one of the most developed bread markets in Europe. German consumer spends approximately 10 % of his salary on food, this number has decreased during decades as the standard of living has been growing. There are four very strong retail groups (Edeka, Rewe, Schwarz, Aldi) in Germany, which control approximately two thirds of the food market. This position allows them to control suppliers in a very strong extent which leads to significantly lower prices on this kind of market, but at the same time it reduces competitiveness or liquidation of smaller bakeries⁸. The total consumption of bakery products is 5.5 million tons per year, the average

consumption of bread is 60.2 kg per person and bread products 13.6 kg per person. It turns out that consumers are more willing to pay for bread products (6.91 Eur per kg) than for conventional bread (2.43 Eur per kg). The most popular place of purchase is bakery, where 58 % of purchases of bread and bread products take place⁹. Consumer trends that are more pronounced on the German market include a shift towards healthier alternatives, the associated demand for less preservatives and the growing popularity of gluten-free pastries and spelt flour products¹⁰. Functional foods are gaining popularity¹¹, there is a growing tendency towards ethical consumption - organic packaging or the possibility to buy unwrapped pastries in customers' own packaging play an important role in purchasing decisions, but this trend is associated with an increased risk of biological contamination of the product. Consumers are also generally more open to news, the popularity of frozen pre-baked bread is constantly growing (currently pre-baked bread accounts for about 15 % of total consumption)¹⁰. There are some volatile trends on the market connected to younger consumers, such as circling around healthier lifestyle, enjoyment of taste, originality, regionality and freshness. People are also willing to pay more for higher quality products and performance food – healthy food that also increases performance of people¹². To illustrate the situation, individual types of bread are listed according to the popularity among German consumers in Figure 1.

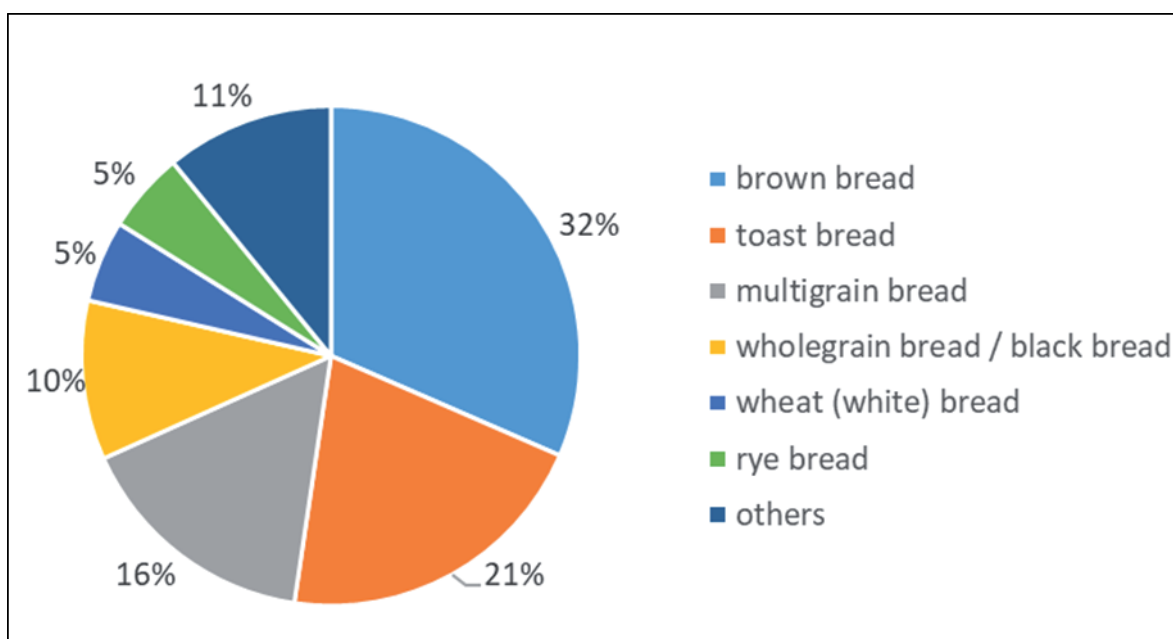


Figure 1. Popularity of types of bread in 2016¹³.

Materials and methods

The paper is based on a survey using a questionnaire. In order to analyze buying behavior for bread in Germany, a questionnaire was elaborated for collecting the necessary data about consumption and preferences of customers / respondents when buying bread and bread products. Quantitative research was conducted through personal interviewing (PAPI) in the German state of Bayern in April and May 2018. The questionnaire was piloted before the actual survey, respondents included in the pilot were not included in the research. The question of preferential criteria underwent a major adjustment during the piloting, it was proved to be too difficult for respondents to decide on a seven-point scale of importance, so the scale was reduced to only five levels (very important - important - neither important nor unimportant - unimportant - completely unimportant). There were 553 properly filled questionnaires used for the analysis and the data were processed using SPSS software.

Discussion and result analysis

The structure of respondents in terms of gender was relatively balanced, 56 % were women and 44 % were men. The age structure was recorded by groups ranging in age from 19 years or younger (19 %), 20 - 29 years (29 %), 30 – 39 years (24 %), 40 - 49 years (11 %), 50 - 59 years (7 %), 60 – 69 years (6 %) and 70 years or more (4 %). For further evaluation, age categories were also regrouped into three groups (less than 30 years, 30 – 50 years, more than 50 years).

In terms of the usual place of purchase, the strong tendency of consumers to buy bread directly at the place of production itself was confirmed - bakery (60 %), second place are supermarkets (39 %), mini-market representation (1 %) and online (0 %) is completely negligible, these outlets play virtually no role in bread purchases.

The reasons for preference for buying bread in a given distribution channel vary, customers in bakeries prefer to buy bread because of the quality (73 %), in supermarkets this reason is stated by only 8 % of customers. Convenience is especially important for supermarket customers, the main reasons given for the purchase are that their store is close to the place of residence (42 %) and they can buy other products here at the same time (43 %). Price sensitivity was not significantly reflected in any group of customers, which is in line with current trends in the German market. An overview of preferences by individual distribution channels is given in Figure 2.

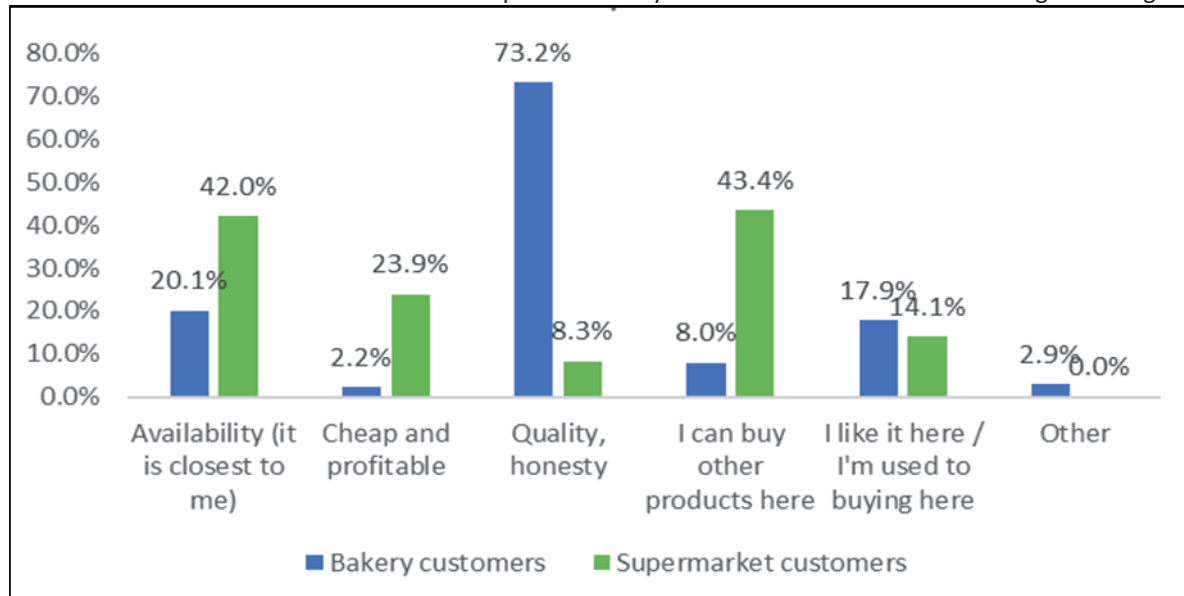


Figure 2. Preferences according to the place of purchase¹⁴.

The main part of the survey was devoted to the criteria on the basis of which consumers choose bread and according to which they decide on the purchase. Based on the theoretical background and pre-test of the questionnaire, the criteria size, type, quality, price, taste, availability and producer were included in the selection. The importance of individual items was measured using a five-point scale, where 1 means “most important” and 5 “completely unimportant.” Researchers assumed that differences between preferences may be manifested mainly by gender and age of respondents.

For all respondents, the most important aspect was taste, followed by the quality and type of bread. On the contrary, the size of the bread and the producer (origin) of the bread proved to be the least important criteria for the decision. If we look at preferences in the context of gender, it turns out that women pay more attention to the importance and assessment of the criteria than men, on a given scale, most of them move one degree more to the side of importance. The results are shown in Figure 3.

Differences in the importance of the criteria are also apparent according to the age of the respondents. It turns out that the group of the youngest respondents moves more at the margins of the scale for most criteria. The size of the bread proved to be the least important for all age groups. Price does not play a big role in all categories. The main difference between age groups is the criterion of producer, where for young people (under 30) he plays no role at all (least important), while the oldest age category (over 50) considers the producer important. The results are shown in Figure 3.

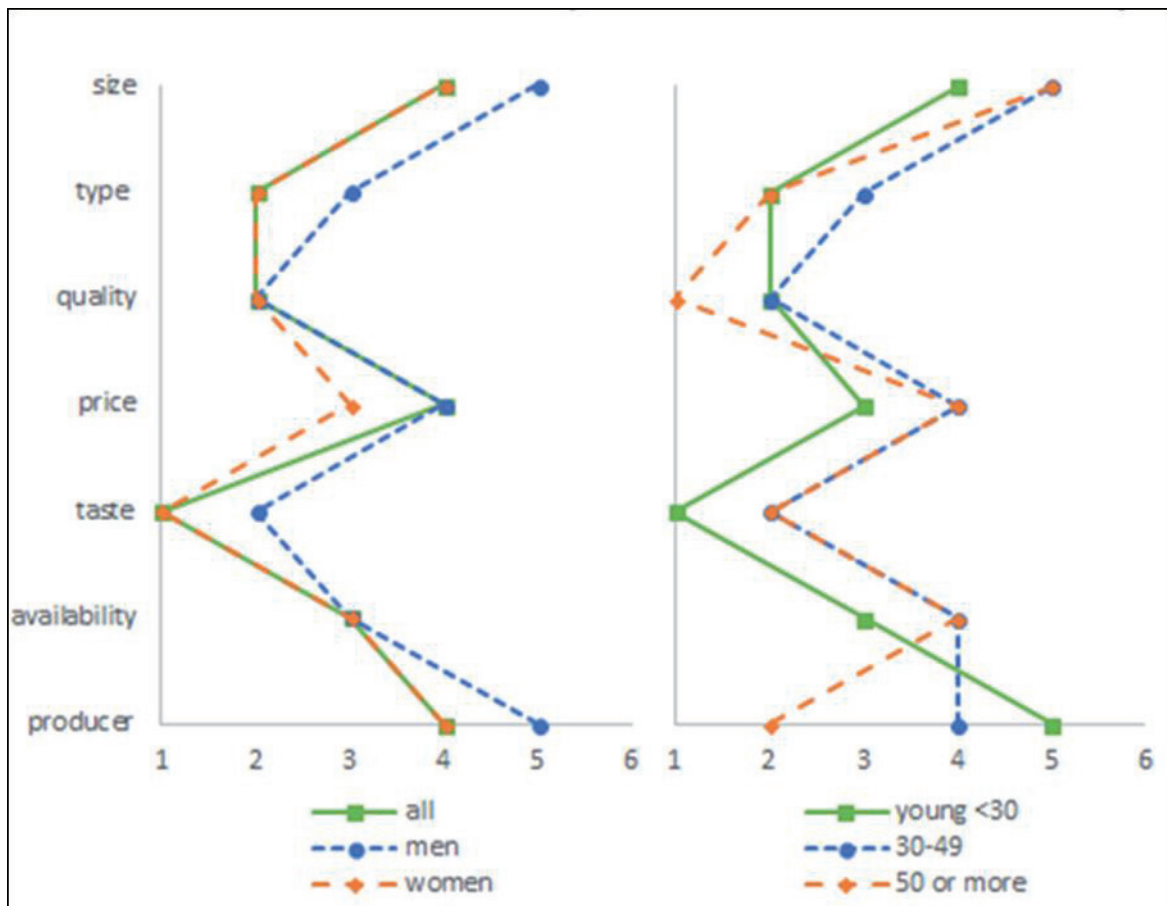


Figure 3. Criteria for buying bread by age and sex¹⁴.

Conclusion

Bread has accompanied man since the dawn of our civilization and is a permanent part of human diet, people's requirements and preferences for what the "right" bread should look like are different for different cultures and change in time and space. The research objective of this paper is to determine what are the factors that influenced German consumers when purchase bread. The research results show that the most important criteria of bread selection include attributes linked with sensory qualities of bread such as taste and quality. By contrast, the least important criteria are size of loaf and producer. However, the low importance of the producer does not apply to the age group over 50, who, on the contrary, consider this criterion to be important. It was further confirmed that German consumers are not very price sensitive across all age groups. The optimal levels of the tested criteria can be specified for practical use by manufacturers, for example by conjoint analysis.

References

1. Lohman S.: A Brief History of Bread [online]. [cited 2022-03-11].
2. Beranová M.: *Jídlo a pití v pravěku a středověku*. Academia, Praha 2005.
3. Kotler P., Keller K. L.: *Marketing Management*. 14th ed. Grada, Praha 2013.
4. Steenkamp J.B.E.M.: *Agricultural Marketing and Consumer Behavior in a Changing World*. Springer, Boston 1997.
5. Statista: Purchase criteria for food in the U.S. 2022 [online]. [cited 2022-06-15].
6. Skořepa L., Pícha K.: *Acta Univ. Agric. et Silv. Mendelianae Brun.*, 64, 1067 (2016).
7. KPMG: *Nákupní zvyklosti 2017* [online]. [cited 2019-04-10].
8. Brotexpert: *Überraschung beim Brotpreis: Brot vom Bäcker kostengünstiger als vom Discounter* [online]. [cited 2018-07-19].
9. Statista: *Brot & Getreideprodukte* [online]. [cited 2018-07-09].
10. Stumpf H.: *Die Bäckerei als Kompetenzzentrum für das Besondere* [online]. [cited 2022-03-11].
11. Meyerding S. G.H., Kürzdörfer A., Gassler B.: *Sustainability*, 10, 4667 (2018).

12. Wolf R.: Bei Trends ist Authentizität der entscheidende Faktor [online]. [cited 2022-03-11].
13. Statista: Most popular types of bread In Germany 2016 [online]. [cited 2022-03-11].
14. Getta I.: *Consumption Analysis of the Bakery Product of Developed European Market*. VŠCHT, Praha 2018.

PRODUCTIVE ECONOMIC VIEW OF THE BAKERY INDUSTRY

Strachotová D.¹, Kutnohorská O.¹

¹*School of Business, University of Chemistry and Technology Prague, Prague, Czech Republic
strachod@vscht.cz*

Abstract

The presented research was caused by the fact that food production is still growing, but trends in the bakery industry do not correspond to this growth, especially recently. The authors therefore asked a number of partial questions. Is the demand for bakery products really declining? How do customers react to pastries with different proportions of rye flour? What is the profitability of bakers, do prices react to price carousels? How does the situation on the labor market, the development of minimum wages, affect the profitability of bakeries? The aim of this paper was to analyze selected production and economic indicators of the bakery industry at present. At the same time, using the methodology of sensitivity analysis, it tests the sensitivity of the profitability of selected bakery products to the development of input prices.

Introduction

What effect does the current situation have on the bakery? On the one hand in connection with food self-sufficiency and on the other hand in connection with inflation. These are topics that are more discussed due to the threat of some form of covid epidemic (still still ¹), but mainly due to the current war. Ukraine has rightly always been a world grain. At the moment, the war not only threatens future harvests, but also de facto threatens last year's harvest. Because you can't reach your customers. Related to this are issues of food self-sufficiency.

Self-sufficiency can be measured on various products and their consumption. The Czech Republic is one of the twelve European countries that can meet the needs of their population with their own production². This applies to a certain food mix. How is it in terms of individual sub-food sources? Longer-term developments show a decrease in almost all commodities of plant origin (wheat flour, onions, tomatoes, apples, etc.)³. Only self-sufficiency in beer production shows an upward trend. What affects food self-sufficiency? On the one hand, there is domestic production of commodities, on the other hand, their consumption. The impact of supply arising from food imports from abroad cannot be overlooked. Changes in Czech agricultural production also have an impact on this. Decreases in sown areas, increased profitability, but recently also a decrease in manpower⁴. Demand, supply from abroad, the situation on the labor market and price fluctuations in the basic commodity (wheat flour) - these are factors that the downstream industry is struggling with – bakery⁵.

It is also necessary to look in more detail at the effect of inflation. Year-on-year price growth exceeded 11%. Consumer price indices were mainly affected by higher prices in the housing section, but also in the food and non-alcoholic beverages section⁶. Table I shows the selected values (valid at the time of preparation of the paper).

Table I
Inflation development - Czech Republic (own processing from⁶)

		Consumer price indices	
section	item	I/22-II/22	II/21 – II/22 (january)
housing	electricity	3.2 %	22.6 % (18.8 %)
	natural gas	5.6 %	28.3 % (21.5 %)
	solid fuels	2.2 %	
food and beverages	bakery products and cereals	1.6 %	11.3 % (9.4 %)
	milk, cheese, eggs, cottage cheese	1.9 %	8.8 % (7.2 %)
	vegetables	5.9 %	8.0 % (7.3 %)
	nonalcoholic drinks	2.1 %	7.0 % (3.9 %)
	poultry meat	2.2 %	
	pork	decrease 2 %	1.8 %

The year-on-year growth in food and non-alcoholic beverages was most affected by the year-on-year growth in prices of flour (+ 25.3%), semi-skimmed milk powder (+18.1%), butter (+30.0%), potatoes (+14.7%). % and sugar (+24.2%)⁶.

The price of flour (the main entrance for the bakery industry) has always been a problem. The current situation has long surpassed even the blackest scenarios from previous years. The price of food wheat on the Paris Stock

Exchange is decisive for the prices of wheat and flour in the Czech Republic. And it is constantly rising to new historical records. At the beginning of March 2022, it was up to 11580 crowns per tunu⁷. And it's not just about wheat. The price of corn or soybean oil is also close to the ten-year high. This year, bread or oilseedsxx will become more expensive by tens of percent in the Czech Republic³. According to Lukáš Kovanda¹, the world's stocks of basic wheat-type foods will be depleted next year. The reason is the ongoing war in Ukraine. This means that the dramatic rise in food prices will continue.

Analysis of selected economic indicators of the bakery industry

The results of various analyzes show that the performance of an industry strongly depends on many microeconomic factors as well as on the overall economic situation⁸. An important factor is the trend in pricing policy⁹. This places the Czech Republic among the countries that have prices at a completely different level than countries with comparable purchasing power². Another problem is the margins on the Czech market (Figure 1).

From an economic point of view, the trend in consumption is also a problem. According to the Czech Statistical Office, in 1950 almost 90 kilograms of bread per year per capita were consumed. By 2019, this volume had fallen by more than half (approximately 40 kg)¹⁰. On the other hand, consumption of wheat flour products increased (Figure 2). This group also includes pastries such as baguettes, croissants, toasted bread. Thus, there is an interesting trend that is not fully in line with general nutritional trends. In any case, total consumption is still falling.

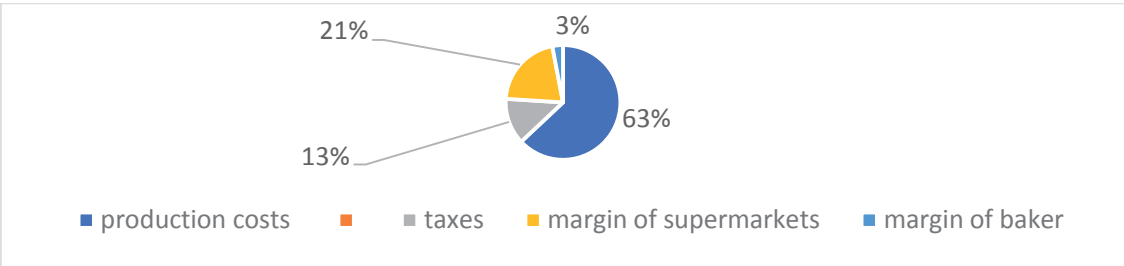


Figure 1. Price structure – Czech republic (own processing from⁵).

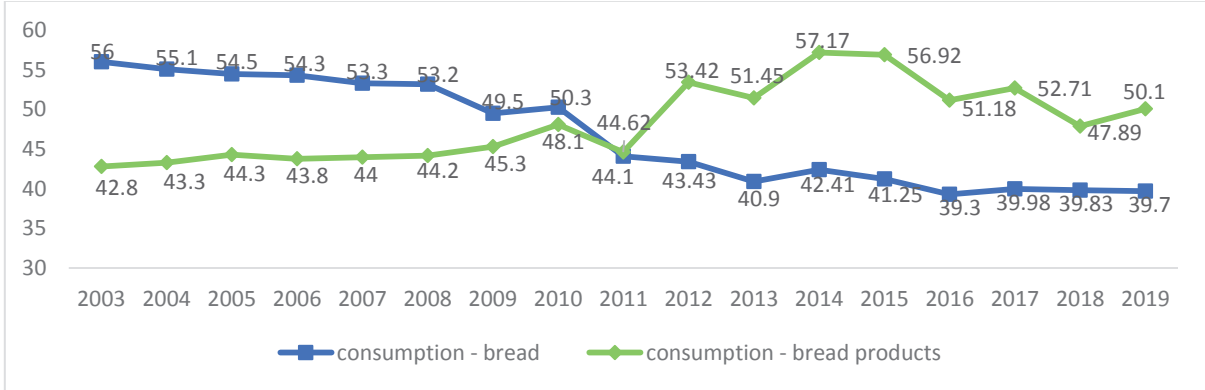


Figure 2. Consumption development of baking products on Czech market (kg) (own processing from¹⁰).

The same study¹⁰ also published the development of bakery product prices. Until the end of 2019, prices on the Czech market were relatively stable, strong turbulence in prices was only around 2010/2011. Wheat prices are approximately 1.9 times higher than the price of bread (Figure 3).

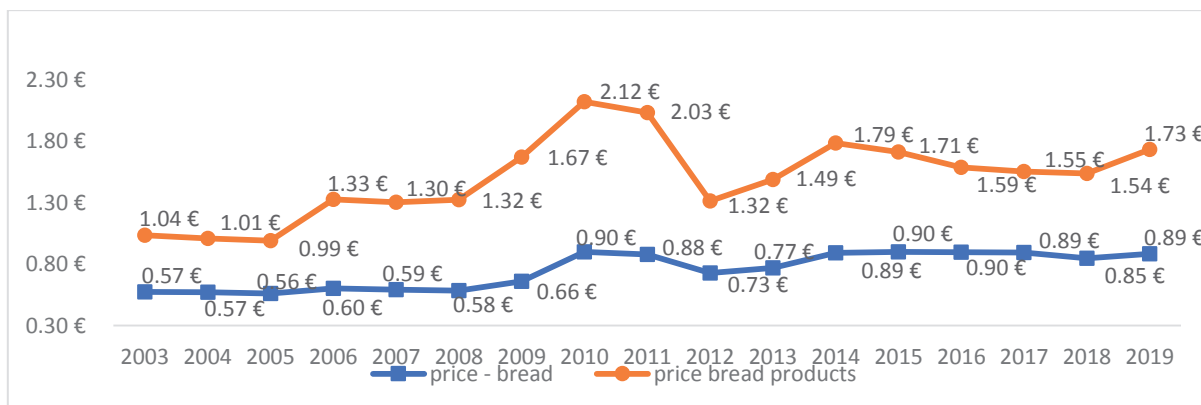


Figure 3. Price development of baking products on Czech market per kg (own processing from¹⁰).

Other characteristics of the Czech bakery industry

There are a number of surveys focusing on the preferences of Czech consumers. The results are similar to, showing the order in terms of preferences (Figure 4). Research also shows that most Czech consumers shop in a bakery or a store with a large assortment, and a significant number of people do not mind buying frozen semi-finished products¹¹, but still the point of freshness still wins.

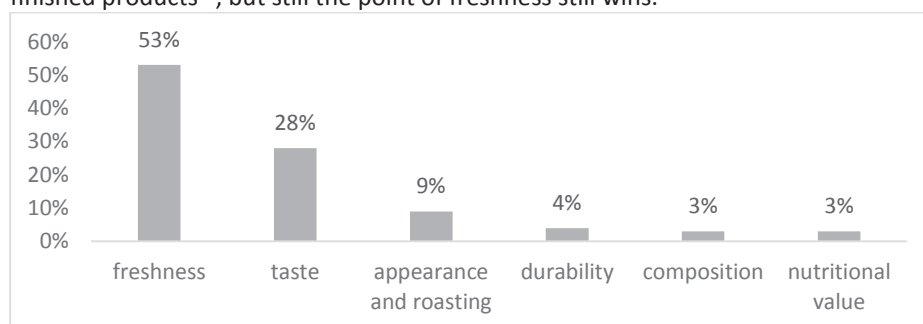


Figure 4. Czech preferences when choosing bread¹¹.

Further research brings conclusions that only illustrate the overall development of consumption of bakery products on the Czech market. Only 27% of customers (Figure 5) direct their expenses to bread, most of the expenses are white or sweet pastries.

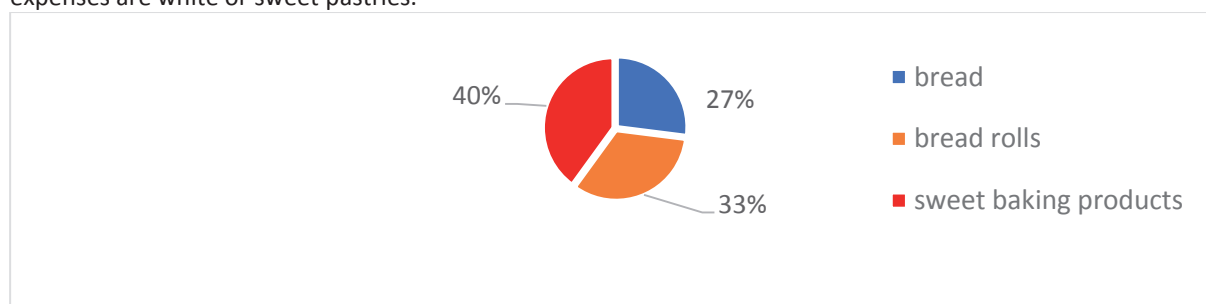


Figure 5. Spending on baking products by Czech consumers (own processing from¹⁰).

These research results have not changed much in the long run. On the other hand, shopping habits are changing - in 2019 it was true that more than half of Czech consumers (56%) are used to buying bread daily. Earlier (2012) it was less (Figure 6). But unfortunately, the place of purchase is also changing - in favor of large chains - which is logical, as they have the most comprehensive offer (Figure 7). Further research has shown factors influencing consumer behavior (Figure 8). A comparative study (2019) shows a greater propensity for quality. Many results regarding consumer behavior look stable. Nevertheless, the revenues of the bakery industry are going through a number of reversals. Figure 9 shows the turbulent development in the period 2008/2016. These were the effects of the 2008/2009 crisis. After 2016, a certain stabilization is evident. Data are in EUR, the average exchange rate of 2019 was used, when the time series ended (25.75 CZK / EUR).

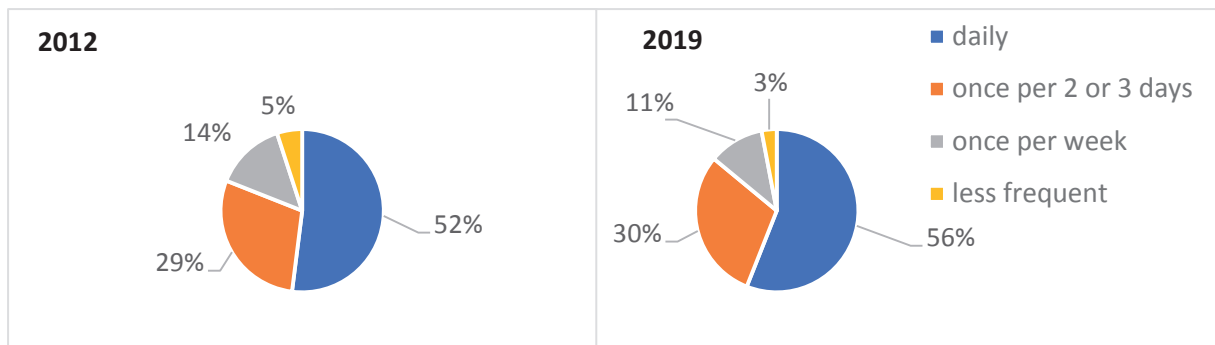


Figure 6. Frequency of Czech buying baking products (own processing from^{10,12}).

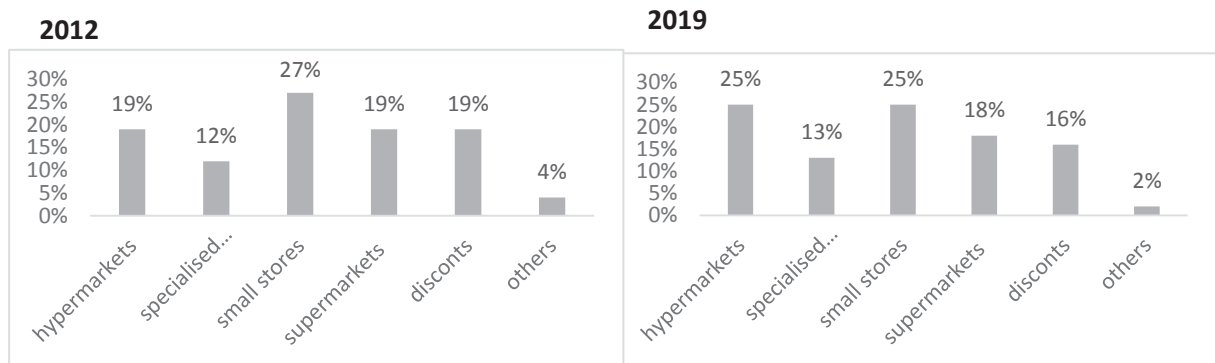


Figure 7. Where Czech prefer to buy baking products (own processing from^{10,12}).

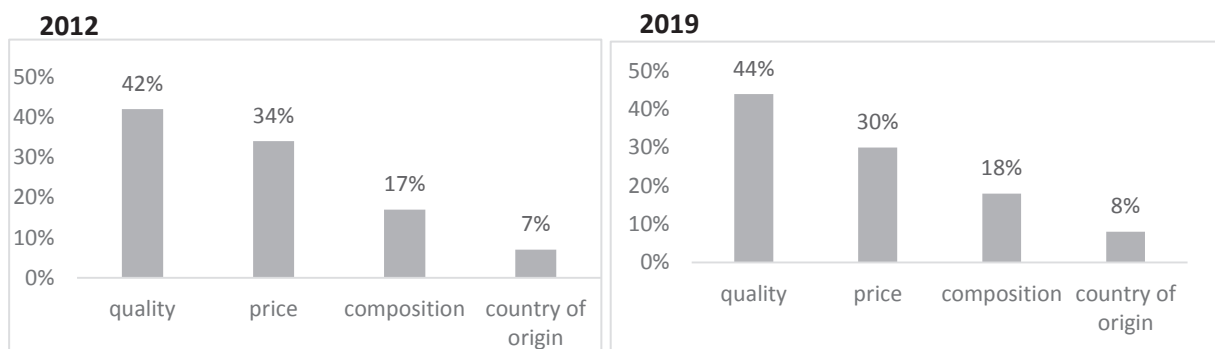


Figure 8. Czech preferences when choosing bread (own processing from^{10,12}).

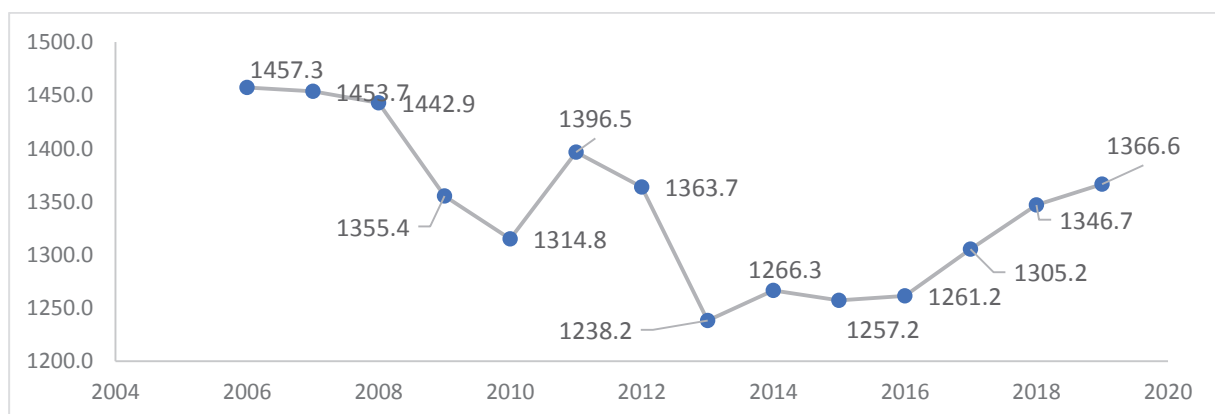


Figure 9. Revenues of baking companies on Czech market in billion euros (own processing from¹⁰).

Profitability of bakery products

The development of these factors affects the profitability of bakery products. We have previously examined the impact of the turbulent development of minimum wages after the 2008/2009 crisis. This idea is now relevant again. Social dialogue is becoming a sharp conflict of interest among tripartite partners, mainly regarding wages in public services as it was during the global financial crisis, since 2008, when Czech public administration was under severe cuts, and the wage gap between public administration and the national economy became narrower year by year¹³. The reason is not only the pressure on wage growth, but above all the development of prices of raw materials, energy and fuels for distribution. Sensitivity analysis (SA) was chosen as the methodology of this research. It is a method suitable for managerial decisions¹⁴. The data for analysis represent a medium-sized bakery. The selection of products was made by the ABC method. The object of analysis was three products (bread 1200g, croissant and bun). The monitored factory SA was determined by a general calculation formula. To determine the SA scenario, the deviations of the monitored factors in the costs of ten bakeries were evaluated.

Table II

SA results (source: own processing)

Item (factor)	Bread 1200g				Roll				Bun			
	SA 2016		SA 2022		SA 2016		SA 2022		SA 2016		SA 2022	
	S (%)	R (%)	S (%)	R (%)	S (%)	R (%)	S (%)	R (%)	S (%)	R (%)	S (%)	R (%)
Selling price	5	91	10	182	5	30	10	59	5	98	10	98
Wheat plain flour	25	77	45	138	25	23	45	42	25	90	45	90
Rye bread flour	20	39	40	77								
Direct wages	10	15	20	31	10	5	20	10	10	19	5	19
Price of electricity	10	2	25	5	10	1	30	2	10	3	20	3
Price of gas	15	11	30	21	15	4	30	7	15	13	30	13
Price of diesel	5	4	25	18	5	1	25	6	5	4	25	4
Price of benzine	20	3	25	4	20	1	25	1	20	4	25	4

*S ... scenario; R ... results

Conclusion

The bakery market in the Czech Republic is competitive and most bakeries are financed from domestic capital. Foreign investment is slowly declining or may be considered stable if we do not count the companies that are returning from tax havens. The market is relatively fragmented and does not have one strong leader. Penam and Unit ed Bacery can be described as leaders. La Lorraine is a strong leader in frozen semi-finished products.

Basic characteristics:

- In recent years, the trend in customer demand for frozen semi-finished products has increased.
- There is clear pressure from supermarket chains, which are ruthlessly forcing smaller bakers to make concessions.
- The overall offer of the bakery assortment is very rich and growth is also recorded in regional specialties and organic products.
- History shows that the volume of bread consumption is slowly decreasing. At the same time, the trend with wheat bread is going against this.

The price at which bakeries supplied products to stores until last year stagnated or fell and, according to bakers, did not correspond to its true value. The low price of bread does not allow:

- invest in development,
- properly reward their employees,
- the craft loses its attractiveness for young people.

We can currently count on about 700 hundred bakers (companies) on the market, in recent years supermarket chains have confirmed their position in baking their own baking products or semi-finished products from frozen products. In this difficult situation, bakeries are trying to change their competitive strategies, so they are trying to be closer to the customer with quality fresh goods. Research in the area of preferences - freshness preferences - also states that most Czech consumers shop in a bakery or a store with a large assortment, these are practically daily purchases - but mainly in supermarkets.

It is obvious that the situation is also different for large bakery companies, forming certain chains - the situation in small craft bakeries will be completely different. Both types of entities can use certain factors of their stakeholders to secure their position in the market. The biggest problem is that of medium-sized bakery operations (ie with 200-250-300 employees), of which there is still a large number in the Czech Republic and they supply more than 60% of bakery products on the Czech market.

And it was such entities during the last crisis that struggled the most with the shrinking workforce. In general - The number of bakers has a declining trend. For example, in 2008 the industry employed approximately 34.5 thousand bakers, while in 2019 it was only less than 30 thousand bakers. One of the reasons could be the high workload of bakers, unattractive working hours and low pay.

Average salaries are well below the average or modal population. In 2016, the average salary of a baker was approximately CZK 16.400, while the average wage in the economy was at the level of CZK 25.570, so the salaries are approximately 64% of the average. The situation in 2019 worsened: the average salary of a baker was approximately CZK 21.100, while the average wage in the economy was at the level of CZK 34.100, so the salaries are approximately 62% of the average. This situation is likely to put pressure on rising wages and, consequently, on rising bread product prices.

References

1. Kovanda L. Cena pšenice a válka na Ukrajině. Kurzy CZ <https://www.kurzy.cz/zpravy/638528-cena-psenice-je-rekordni-v-dejinach-dramaticky-zdrazi-pecivo-valka-na-ukrajine-muze-vyvolat/> [Access 15.03.2022].
2. Potravinová soběstačnost. Evropa v datech. <https://www.evropavdatech.cz/clanek/72-potravinova-sobestacnost/> [Access 18.03.2022].
3. Soukup J. Válka ukazuje, jak důležitá je půda a potravinová soběstačnost. <https://www.denik.cz/udrzitelnost-ve-state/valka-puda-potravinova-sobestacnost-20220304.html> [Access 15.03.2022].
4. Mikkelsen B. E., Sudzina F., Botek M., Romani A. Q., Larsen K. Are Perceptions of Health Dependant on Social Class? Studying Soft Power and Symbolic Violence in a Health Promotion Program among Young Men at Vocational Schools, *International journal of environmental research and public health*, 18 (14), 7517 (2021).
5. Botek M., Vrba Z., Rančák J. Comparing German And Czech Bakery Products Markets, In IBIMA 2020, p. 15837-15851 (2020).
6. ČSÚ Statistika https://www.czso.cz/csu/czso/inflace_spotrebitelske_ceny [Access 15.03.2022]
7. Makroekonomika Meziroční růst cen - Indexy spotřebitelských cen <https://www.kurzy.cz/zpravy/> [Access 25.03.2022].
8. Čamská D., Klečka J. Comparison of Prediction Models Applied in Economic Recession and Expansion. *Journal of Risk and Financial Management*, 13/3 (2020).
9. Švecová L., Scholleová H., Fotr J. Selected aspects of investment decision making (empirical research evidence) *Journal Ekonomie a Management*, 3, 125 (2012).
10. Kozelský T., Novák R. Pekárenský trh v ČR. Česká spořitelna. <https://www.investicniweb.cz/Files/pdf-pekarensky-trh-v-cr/> [Access 20.02.2022].
11. Kutnohorská O., Strachotová D. Consumer behaviour in the bread market. In 7th International conference on chemical technology, pp. 79-81 (2019).
12. Dřížal J. Trh pekařských výrobků v ČR. *Potravinářská revue* 1/2013. <http://www.chlebnasvezdejsi.cz/Frontend/Webroot/uploads/files/2015/11/trh-pekarskych-vyrobku-v-cr.pdf> [Access 03.07.2018].
13. Dvořáková Z. Social dialogue and Czech local and regional government in an era of austerity. In: The 6th International Days of Statistics and Economics. Melandrium, 350 (2012).
14. Fotr J., Švecová L. Riziko a nejistota ve strategickém rozhodování. *Journal Politická ekonomie*, University of Economics and Business, 1 /87, (2006).

USE OF DIGITIZATION IN CHEMICAL ENTERPRISES

Vávra J., Spáčil P., Bakeš O.

*University of Pardubice, Studentská 95, 532 10, Pardubice
Jan.vavra@upce.cz*

Abstract

Industrial transformation and especially the digitization of business processes is a prerequisite for maintaining competitiveness, across industries. However, the use of digitization Key Enabling Technologies (KETs) differs in the mechanical, process, and hybrid industries. The chemical industry, as a typical representative of process production, differs significantly, especially in the possibilities of product monitoring or in the operation of production equipment. No significant impact of digitization on raw material purchasing, logistics, research, and development processes is expected. Perceived benefits, on the other hand, are expected in production, sales & marketing, and administration processes. To confirm these starting points and verify the state and perception of the importance of digitization in the Czech Republic among chemical production companies, research was carried out in selected chemical companies. Areas and processes in which digitization is already developing have been identified, as well as obstacles and barriers to a faster transformation of the chemical industry according to the Industry 4.0 concept.

Introduction

With the mass development of Industry 4.0 technologies, there has been a revolutionary transformation of industrial production in the last decade. Many mechanical industries adopt technologies of individualized production according to customer requirements, while maintaining a production speed comparable to mass production [1]. Digitally monitored and controlled production technologies are the basis for maintaining the speed of individualized production while increasing quality and minimizing losses and poor-quality production. [2] The list of technologies that form the basis of a digitally controlled production system is based on the digitized form (cyber layer) of the real production process (physical layer) and thus creates a Cyber-Physical System (CPS or Digital Twin) [3], which collects data using sensors, connects via the Internet of Things creates Big Data files, which are used to analyze and adjust the optimal production process. For large amounts of data, companies use Big Data Analysis, Artificial Intelligence (AI) and Cloud Computing (CC) [4]. Other Key Enabling Technologies (KETs) are used in production (3D print, autonomous and collaborative robots, Machine Learning (ML), machine-as-a-service, RFID Tags, RTLS Systems, and other) [5], in research and development (simulations, modelling) [6] and in service processes (augmented and virtual reality, wearables, predictive maintenance, etc.) [7, 8]. The use of these KETs is growing rapidly, but not at the same pace in all industrial areas. Especially for mechanical production, it is not difficult to use Artificial Intelligence elements to adapt production according to customer requirements for almost every individual product [1, 9]. The product is clearly traceable during the production process and the production equipment can be modified quickly and relatively easily. The production process is based mainly on modifiable processes of pressing, machining, welding, assembling, or surface treatment, in which there is no conversion of substances, but in principle to mechanical modifications and component addition [10]. Using sensors, data collection during production, connection of the production system via the Internet of Things and remote control with elements of Artificial Intelligence, it is relatively easy to control production processes in real time [11].

However, in chemical and other process productions, the production process is more complex, usually based on chemical transformation [12]. During production, materials change their nature, input substances disappear, the resulting product has different physical and chemical properties, and production must respect specific chemical balance conditions with a number of reaction conditions related to temperature, pressure, density, humidity, viscosity, chemical reaction speed or concentration [13]. The equipment and reactors built are usually adapted to a single production process and their service life and payback period are extremely long [14, 15]. Despite these limitations, it is desirable that process productions should be digitally monitored and Cyber-Physical Systems should be created for them to achieve production efficiency, product quality, or its differentiation, if technologically possible [16].

Although the digitization of business processes in mechanical production (especially for the automotive industry, electronics, consumer goods) is currently a common practice not only for production itself, but also for logistics, sales & marketing, purchasing, R&D, and administration, in chemical and other process production we identify obvious implementation delays [17]. Nevertheless, the leading companies in the chemical industry in the EU, as

well as consulting companies Deloitte, KPMG, Ernst & Young, PwC give maximum support to the implementation of KETs and promote digitization as a key tool for maintaining competitiveness and sustainability [15, 18, 19, 20, 21]. And while it may not be possible to achieve a higher degree of product diversification for the production process itself, its digitization will allow higher productivity, efficiency and quality [22]. According to Deloitte, there is great potential to significantly improve R&D, logistics, sales & marketing, and administration processes [18].

Although large chemical corporations show a strong interest in introducing KET and digitizing, implementation is not easy and fast for them either [17]. All the more, digital transformation is more difficult for other medium and smaller manufacturers (SMEs) [23]. High financial and personnel demands for implementation, adoption, maintenance and cyber security can significantly hinder digitization and there is a risk of significant lags in the digital transformation for process productions.

As a result of our theoretical study and assumptions we formulate three research goals to confirm:

Goal 1: To verify the state and perception of the importance of digitization in the Czech Republic in chemical production companies with regard to the competitiveness and sustainability of the company.

Goal 2: To identify the benefits, limits, and barriers related with individual KETs in chemical production.

Goal 3: To confirm the specifics of KETs implementation and digitization in chemical companies and process productions.

Research methodology

Academic researches and studies from relevant fields of research, Industry 4.0 technologies and digitization KETs are used to address the validity of theoretical problems and assumptions concerning expected benefits and limits of digitization and KETs implementation. Previously realized analysis suggests that the chemical industry shows significant specifics in monitoring the product during the production process and specific production conditions do not allow to diversify production - the equipment used is designed to meet the requirements of individual productions.

A form of qualitative research with representatives of large chemical production companies was chosen for the research itself. The intention was to address representatives of multinational corporations with demonstrable experience with Industry 4.0 technologies and more advanced implementation of digitization. The pre-selection was made on the basis of press releases and awards received in the field of digitization and innovation, on the assumption that large multinational companies have sufficient resources for digitization solutions and are among the early adopters of KETs.

Based on theoretical basis qualitative research was carried out as structured one-to-one interviews with managers of three chemical companies producing basic chemicals. All surveyed companies can be considered leaders in national markets in the Czech Republic in terms of both market share and sales volume. Each of the surveyed companies has sufficient support from the group's management and the digitization process is thus not limited by a lack of resources or the will to change current processes.

The respondents were business managers, IT managers, production managers, and production technologist of the companies. The research was carried out in the period September 2021 - April 2022. Information obtained was processed using content analysis. The first set of questions inquired into the importance of digitization, perceived benefits for the company and other stakeholders and finding out the current state and degree of digitization in the company. The second set of questions investigated individual KETs, the degree of their implementation, benefits and limits in their use, as well as the reasons for their rejection or restriction. The third set of questions focused on the specifics of chemical production in relation to digitization.

Prior to the research, business representatives confirmed that digitalisation is considered an undeniable pillar of competitive advantage and therefore the anonymity of individual companies, including a more detailed specification of products and customers, had to be ensured. Despite the different assortment and form of individual production processes, mostly common perceived benefits and limits were identified and there was also a strong agreement on attitudes to the importance of digitization, as well as on procedures for implementing KETs.

Research findings

The first set of questions first confirmed that the assumption of more advanced digitization in large multinational companies was fully justified. Each of the companies has shown significant progress in digitizing its processes and implementing individual KETs. However, for none of the companies is the goal to achieve a completely digitized factory in the sense of an almost autonomous "Smart Factory" and therefore they do not consider digitization as a goal, but a means to achieve business goals.

All respondents, without exception, stated in the evaluation of the importance of digitization that in the first place it is considered as a necessary requirement to maintain competitiveness. In principle, it was important for each of the companies to primarily digitize the production process, create the most reliable “Digital Twin” and monitor the state and changes in the production process. Thanks to real-time process monitoring, the key benefit of increasing efficiency was mentioned in the second place, based on three perceived partial benefits: first mapping of processes, their control and immediate optimization; second saving materials and other resources; and finally increasing product quality.

Perceived benefits for employees are also considered important, as technologies not only reduce the need for insufficient workforce (benefits for employers), but also reduce the need for risky and demanding work (benefits for employees). Furthermore, the benefits for customers and consumers were mentioned to a lesser extent, for other stakeholders the benefits are considered to be minor.

However, the digitization process is not progressing smoothly. The need to consider and defend the meaningfulness of digitization is considered by all respondents to be the most important limits and barriers. The need for the owner of each solution and the reasonable rate of return on each investment decision based on the processed business case are mentioned. Only solutions with a demonstrable payback period within three years can be implemented usually, and it has once again been confirmed that digitization is not the ultimate goal, but a tool for improvement.

The historical context of each of the companies is problematic - for each of them, the production facilities were built in the last century and therefore the process of digitization is more difficult than in building a completely new facility. In addition, each production is unique and completely specific, all digitized solutions must be customized and adapted to the specifics of production. This also increases the financial complexity of each change adopted.

Problems related to IT security and the reluctance of people (management and employees) to accept change were considered to be limits and obstacles of lesser importance. Although the organization always shows some resistance and rigidity to change, these barriers can be overcome by proper communication and motivation. Last but not least, there were interesting restrictions on the sustainability of already digitized processes. The need to maintain digitized elements for years (sensors, software, hardware) is growing significantly, which places new demands on the structure of job positions, and in one of the companies the lack of competent staff has become a limiting factor that has slowed down the digitization process.

The second set of questions targeting individual KETs, examining the experience with the use of individual KETs, resulted in the classification of individual KETs into groups: the most frequently used (implemented by each of the surveyed companies), the second group included less used KETs (used by 1-2 companies) and the third groups of technologies that companies did not implement or did not evaluate as promising and viable after initial testing. Table I shows an overview of individual KETs according to the categories of their use.

Table I
KETs implementation and utilization

The most important KETs	Less used KETs	Not used or rejected KETs
Big Data/Analysis	3D print (prototypes)	Machine Learning/AI
Sensors	Virtual and Augmented Reality	Autonomous robots
Internet of Things	Digital Twin	Wearables
Cloud computing	Collaborative robots	Edge computing
Automatic robots	Predictive Maintenance	Cognitive computing
Cybersecurity	Machine as-a-service	Digital modelling

It follows from the individual groups that each of the companies used basic KETs to digitize their production process. The production lines are equipped with sensors, data is collected in real time using the Internet of Things and processed for other analytical purposes using Cloud Computing. Digitized system is secured on the basis of security protocols and firewalls, as disruption of production due to cyber threats or attacks would have a fatal impact on financial results and increases the risk of accidents and failures.

Two of the three companies use Digital Twin, 3D print technology, especially for prototyping and spare parts production. Sensor data is also used for predictive maintenance in two companies. To a lesser extent, the elements of Virtual and Augmented Reality are used, and if so, mostly for training or simple remote instructions for repairing equipment. Collaborative robots are also used to a lesser extent (as opposed to automatic ones, which are usually considered a common part of production equipment when handling a product or material). Machine as-a-service is used by only one of the companies and only for a small segment of the production line. Machine Learning and Artificial Intelligence, digital modeling and autonomous robots have already been tested in some companies, but were no longer considered viable - a meaningful business case was not created and companies decided to step down from early adopters in these technologies.

The third set of questions focus on the specifics of process production in relation to digitization. Each of the respondents confirmed that chemical production has such strong specifics compared to mechanical production that every production process is completely unique. Due to the need to meet the technological criteria, it is not possible to achieve a higher degree of modularity / variability of production, and at the same time the high expertise and experience of the operating personnel is absolutely essential.

The risks associated with the failure of the human factor and the ability / necessity to avoid working in a hazardous environment are also significant.

In terms of the use of digitization in R&D of new products, differences in prototyping were mentioned, because in the chemical industry the prototype is not a physical product, but a laboratory sample that cannot be printed on a 3D printer but can be modeled using appropriate software, which none of the companies does not use.

All respondents agreed that with high demands on the consumption of materials and energy in chemical processes, digitization helps them to save these resources as much as possible and thus increase cost savings even in the conditions of unfavorable developments in the markets for materials and energy.

Discussion and result analysis

Despite the expected opportunity in logistics, R&D, sales & marketing, and administration processes, companies promote and implement digitization primarily in production processes. So far, they use various platforms for communication with customers and suppliers, from emails, telephones, personal meetings to e-shops. Significant digitized communication platforms are not used yet, which is not a surprise in B2B markets, however, for B2C markets these platforms should already be at least on the rise.

Due to the focus of process production, it is difficult to use many KETs that would be easy to use in mechanical production, such as 3D printing. The reason is the different nature of the chemical product, which is created not by shaping but by chemical transformation. Machine-as-a-service technology is not used; the primary reason is the robustness of production lines, which are traditionally investment-intensive and long-term. It is not customary in the industry to operate them in service mode.

Artificial Intelligence systems and Machine Learning are also poorly promoted due to the low standardization of the developed solutions. The principles of AI and Machine Learning must be tailored to the specific process, which prevents subsequent commercialization when selling to other entities. The design of the solution is thus too investment-intensive. Due to the relatively low need to move materials, intermediates and final products by hand, autonomous robots, wearables (exoskeletons) are not widely used either. The technology of the production process usually works with the flows of liquids, gases, bulk materials and transport must be solved in large volumes using conveyors, pipes, or gravity.

The research revealed that the reason for not introducing technologies is not inexperience or ambiguity in their application. All respondents showed a high level of familiarity with the possibilities of digitization and individual KETs. It was confirmed that the specifics of the built process production cause low variability of the resulting products. The proposed equipment with the used construction material does not allow to fundamentally change the production technology, to achieve individualized production is difficult or almost impossible for most chemical productions.

Conclusion

During the qualitative research, it was found that the digitization of production processes in particular is not underestimated in the chemical industry in the Czech Republic. However, one of the most fundamental findings is the relatively slow pace of transformation. Although the research was conducted in companies with sufficient resources, background and support, none of them proceeded to implement digitization with radical innovations. On the contrary, the pace of digitization is chosen gradually, in partial steps and only on the basis of meaningful business cases that are viable and financially advantageous with short payback period. The reason may be the historical context, where many productions have been in operation for decades and digitization would be

disproportionately demanding, but not impossible. Nevertheless, even at a slow pace, digitization is considered highly investment-intensive for these companies.

Related to this is the finding that none of the companies aims to transform into a so-called "smart factory", which would create a comprehensive view of all business processes from marketing and market development, customer contact, order confirmation, purchasing, production, expedition and administration. Again, the changes adopted are rather local and gradual.

Many advanced digitization technologies were identified in the surveyed companies and it was also confirmed that their implementation could not be carried out without the information and financial support of the corporate management. It is therefore worth considering whether it is possible to make the same progress for other companies in the Czech Republic that do not have a similar background, face current problems due to rising costs and therefore cannot consider launching large-scale renovations at high capital expenditures. Unfortunately, this has and will have a direct impact on future competitiveness, especially for SMEs. The direct threat will be the inability to achieve high efficiency, while maintaining the required quality and minimizing waste of resources.

In conclusion, it can be stated that the research confirmed both the limits in the introduction of digitization in process production, as well as certain delays that Czech chemical companies show in comparison with world and European leaders in the chemical industry. However, these companies have achieved especially in the production very advanced forms of digitization and implementation of KETs, which proves that digitization is feasible in the conditions of process production.

Acknowledgement

This work was supported project "Research in key areas of environmental chemistry and engineering and sustainable business process management" No. SGS_2022_001.

References

1. Zakoldaev D. A., Shukalov A. V., Zharinov I. O., Zharinov A. O. O.: *J. Phys. Conf. Ser.*, 1015(5), 52033 (2018).
2. Ejsmont K., Gladysz B., Corti D., Castaño F., Mohammed W. M., Martinez Lastra L. J.: *Cogent Bus. Manag.*, 7(1), 1781995 (2020).
3. Lee J., Jin C., Bagheri B.: *Cyber physical systems for predictive production systems. Prod. Eng.*, 11(2), 155 (2017).
4. Fracapane G., Ivanov D., Peron M., Sgarbossa F., Strandhagen O. J.: *Ann. Oper. Res.*, 308.1-2, 125 (2020).
5. O'Donovan P., Gallagher C., Bruton K., O'Sullivan D. T. J.: *Manuf. Lett.*, 15, 139 (2018).
6. Molinaro M., Orzes G., Pedrini G.: *J. Manuf. Technol. Manag.*, 32(9), 369 (2021).
7. Drakaki M., Linardos V., Tzionas P.: *J. Ind. Eng. Manag.*, 15(1), 31 (2022).
8. Dalzochio J., Kunst R., Pignaton E., Binotto A., Sanyal S., Favilla J., Barbosa J.: *Comput. Ind.*, 123, 103298 (2020).
9. Ghobakhloo M., Fathi M.: *J. Manuf. Technol. Manag.*, 31(1), 1 (2020).
10. Rossini M., Costa F., Tortorella L. G., Portioli-Staudacher A.: *Int. J. Adv. Manuf. Technol.*, 102(9-12), 3963 (2019).
11. Tao F., Qi Q., Wang L., Nee A. Y. C.: *Engineering (Beijing, China)*, 5(4), 653, (2019).
12. Thonemann N., Pizzol M.: *Energy Environ. Sci.*, 12(7), 2253, (2019).
13. Wernet G., Papadokonstantakis S., Hellweg S., Hungerbühler K.: *Green Chem.*, 11.11, 1826 (2009).
14. Prado V., Glaspie R., Waymire R., Laurin L.: *J. Clean. Prod.*, 257, 120550 (2020).
15. Santos A. P. H., Zattar C. I., Seleme R.: *Int. J. Sci. Res.*, 9(07), 2293 (2021).
16. Qian F., Zhong W., Du W.: *Engineering*, 3(2), 154 (2017).
17. Mohan S. V., Katakajwala R.: *Curr. Opin. Green Sustain. Chem.*, 28, 100434 (2021).
18. Deloitte, *Chemistry 4.0 Growth through innovation in a transforming world*. [available online: <https://www2.deloitte.com/global/en/pages/consumer-industrial-products/articles/cip-chemistry.html>] - [cit. 2022-03-21] 2017.
19. KPMG, *Chemistry 4.0: Reinventing the chemical company with digital transformation*. [available online: <https://home.kpmg/xx/en/home/insights/2017/06/reaction-chemistry-4-0-reinventing-the-chemical-company-with-digital-transformation.html>] [cit. 2022-03-15] 2017.
20. Ernst&Young *How long before the digital disruption reaches the chemical industry?* [available online: https://www.ey.com/en_gl/advanced-manufacturing/how-long-before-the-digital-disruption-reaches-the-chemicals-industry] [cit. 2022-03-16] 2021.

21. PwC, Industry 4.0: Building the Digital Enterprise Chemicals [available online: <https://www.pwc.nl/nl/assets/documents/industry-4-0-building-the-digital-enterprise-chemicals.pdf> [cit. 2022-04-02] 2016.
22. Ghobakhloo M.: *J. Clean. Prod.*, 252, 119869 (2020).
23. Saad M. S., Bahadori R., Hafarnejad H.: *J. Manuf. Technol. Manag.*, 32(5), 1037 (2021).

LOWERING THE ENERGY AND WATER FOOTPRINT OF A LAUNDRY FACILITY

Čižmár M.¹, [Variny M.](#)¹

¹ *Institute of Chemical and Environmental Engineering, Faculty of Chemical and Food Technology, Slovak University of Technology in Bratislava, Radlinského 9, 812 37, Bratislava, Slovak Republic*
miroslav.variny@stuba.sk

Abstract

Rapidly increasing prices of fuels, electricity and, subsequently, of all utilities, force industrial enterprises to reduce their energy footprint. Following this need, small and medium enterprises face additional barriers compared to large industries. Shorter annual working time and unfavourable economy of scale typically allow for simple low-cost solutions to be implemented only. This indicates that an untapped potential for becoming more energy efficient still exists in small and medium enterprises. A case study performed in an industrial laundry company aimed at identifying economically feasible energy saving measures confirmed this assumption. A discrepancy between actual and benchmarked water and energy consumption in the washing process was revealed with the help of dedicated on-site measurements. Further analyses will follow, focused on the drying process as well as on the steam production efficiency.

Introduction

Energy efficiency and sustainable operation of small and medium enterprises (SMEs) belongs to key pillars of reducing industrial energy consumption and related greenhouse gases (GHG) emissions^{1,2}. Compared to large industrial entities, SMEs face additional challenges in following this goal^{3,4}. Firstly, their annual working time is usually shorter, and several operations are performed batch-wise, on the contrary to continuous production processes in most large industries. As a result, simple and easily implemented projects constitute the majority of the actions undertaken to reduce energy consumption, waste creation and GHG emissions^{5,6}. Secondly, various technical, economic and other barriers⁷⁻⁹ must be usually overcome in SMEs to implement, monitor and target any such energy saving-related measure.

Internal or external benchmarking programmes¹⁰ and energy audits^{11,12} represent well-known and reliable tools in facilitating the needed changes in energy management of any energy consumer. Experiences from various countries¹³⁻¹⁵ confirm that energy consumption and the related expenses can be cut down by several percent just by screening for standard measures and their adoption. These include but are not limited to: improving the utilities consumption recording systems, implementing more efficient equipment, paying more attention to preventive maintenance, utilizing renewable energy sources, upgrading process control, and facilitating changes in habits of energy consumers¹⁶⁻¹⁸. Besides cutting down the operational expenses, further benefits of making the production more sustainable include environmental load reduction^{19,20}, new jobs opportunities and increased market competitiveness^{21,22}.

Laundry services are characteristic by high energy and water consumption associated with textiles' washing and drying²³. Recommended actions to be undertaken in such industrial branch comprise partial water reuse²⁴, heat recovery^{25,26}, heat source operation optimization, and water heating by solar energy²⁷. Additional savings can result from optimized operation management²⁸.

Lindström is a small enterprise in the laundry industry, focused on renting and laundry of industrial workwear and floor mats²⁹. The goal of our study was the assessment of energies and media utilization, and the analysis of media consumption trends. The results were used to propose energy efficiency measures.

Materials and methods

The enterprise operates eight laundry washing modules divided into two sections. The first section is specialized in washing workwear (WW), the other in washing mats. Each module contains two large capacity washing machines and a large capacity drying machine, with modules in the WW section additionally containing one smaller washing and drying machine. The module WW1 is powered entirely by electricity as well as all the aforementioned smaller devices in the entire WW section. Electricity also powers all the motors, displays, lights and some regulation elements in all of the modules. In the remaining modules the main energy demand, which is used for heating of process water or air, is supplied by steam. This steam is generated in two ways. In modules WW2, MAT1 and MAT2 the steam is generated in a compact steam boiler, which is incorporated into the

structure of the module itself. In the case of modules WW3, WW4, MAT3 and MAT4, the steam is generated in the nearby boiler room. The layout of the enterprise is shown in Figure 1.

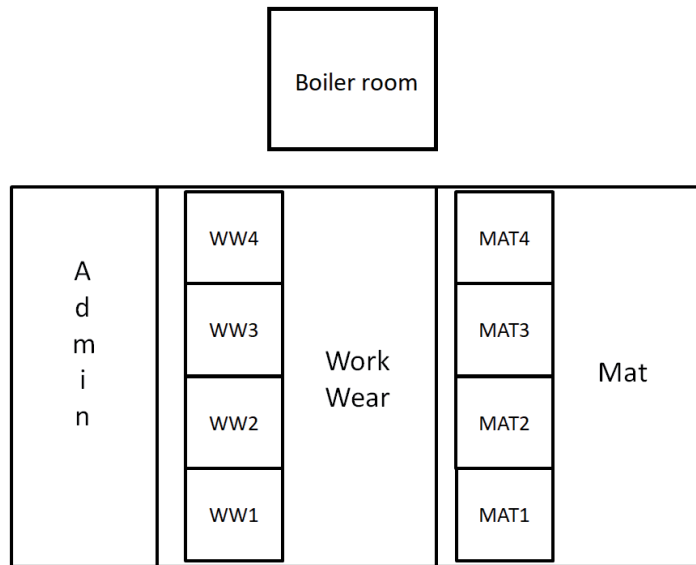


Figure 2. Layout of the enterprise

A measurement of the washing and drying programs was carried out at the enterprise in order to obtain the amount of steam used in these programs at the module MAT4. The washing program is divided into two washes, with the first one using recycled water from the last program, which is discarded after the wash. The second wash uses chemically treated water (CHTW). After the second wash it is lead through a filter into the recycled water reservoir, where it is stored for the next washing program. The piping of the machines as well as related devices was adjusted for the measurement, as shown in Figure 2. The amount of moisture present in mats was determined by differential mass measurement. The mats were weighed before and after the washing program, and the amount of moisture was determined as the difference of these two values. This information was then also used in the calculation of the drying program. The amount of drain water in both of the washes was determined volumetrically. The drain water was collected in 200 l cylindrical barrels; the water level was measured in each of the barrels and the volume of water in each barrel was calculated. Then, assuming the density of this water to be that of pure water at the same temperature, the mass of drain water was determined.

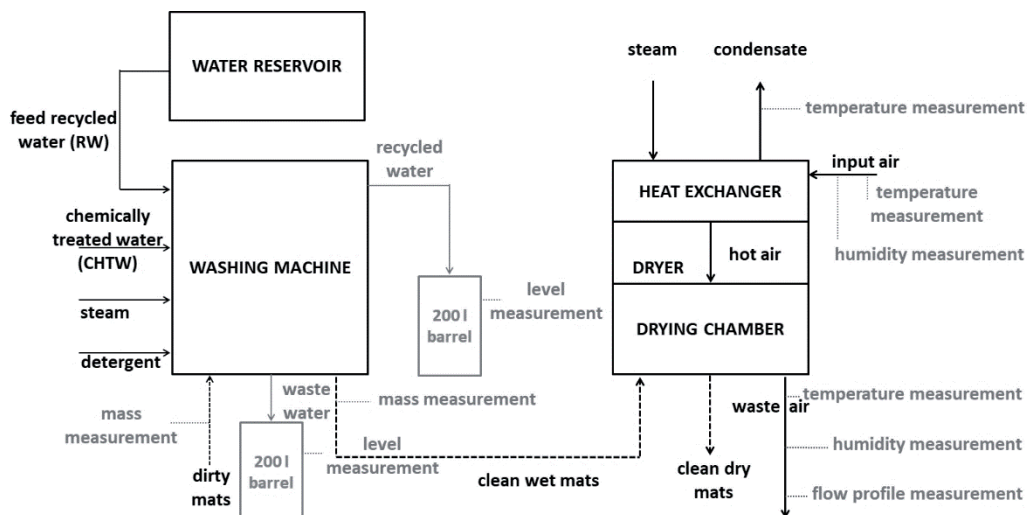


Figure 3. Flow diagram of the measurement of the washing and drying programs (adjustments and measurements shown in grey).

The results of the measurement were processed using a mass and enthalpy balance equation system to show theoretical and real steam and water consumption values. Further details of the calculation can be found in³⁰.

The theoretical steam consumption of the drying machine was determined using its nominal power output. Real drying air consumption was determined by numerical integration of the flow profile data using equation (1),

$$\dot{V} = \frac{\pi}{4} \int_0^r v_r r dr \quad (1)$$

where \dot{V} is the volumetric flow of air, r is the distance of the point of measurement from the axis of the pipe and v_r is the velocity of the air at the point of measurement.

Real steam consumption was then determined using the enthalpy balance of the heat exchanger in the drying machine.

Consumption data, which was provided by the enterprise, was processed to show a relationship between media consumption and production volume by combining data relevant to the studied device, groups of devices with the same powering method or entire WW or MAT sections into graphs. These were then assessed to identify energy efficiency shortcomings. The assumption was that batch processes would provide linear relationships with minimal scatter or intercept value due to the fact that batch production is the iteration of the same process, therefore consumption should be solely a function of processed batches. Any deviation from this state would signify energy inefficiency. For example, an increased intercept value (increased constant consumption) could indicate a leak from an inaccessible piping, which could be otherwise impossible to identify. Further information on the methods of analysis of consumption data relationships can be found in³¹.

Results

The measurement of the washing program yielded results shown in Table I.

Table I
Measurement of the washing program results

	1 st measurement		2 nd measurement		3 rd measurement
$m_{\text{mats;dirty}}$ [kg]	80.9	$m_{\text{mats;dirty}}$ [kg]	76.8	$m_{\text{mats;dirty}}$ [kg]	81.4
$m_{\text{mats;wet}}$ [kg]	96.1	$m_{\text{mats;wet}}$ [kg]	94.2	$m_{\text{mats;wet}}$ [kg]	91.8
m_{moisture} [kg]	15.2	m_{moisture} [kg]	17.4	m_{moisture} [kg]	10.4
$m_{\text{drain;1st wash}}$ [kg]	258.5	$m_{\text{drain;1st wash}}$ [kg]	220.6	$m_{\text{drain;1st wash}}$ [kg]	227.8
$m_{\text{drain;2nd wash}}$ [kg]	343.0	$m_{\text{drain;2nd wash}}$ [kg]	323.8	$m_{\text{drain;2nd wash}}$ [kg]	286.7
m_{drain} [kg]	601.5	m_{drain} [kg]	544.4	m_{drain} [kg]	514.5

The air flow velocity profile measured in the drying machine is visualized in Figure 3.

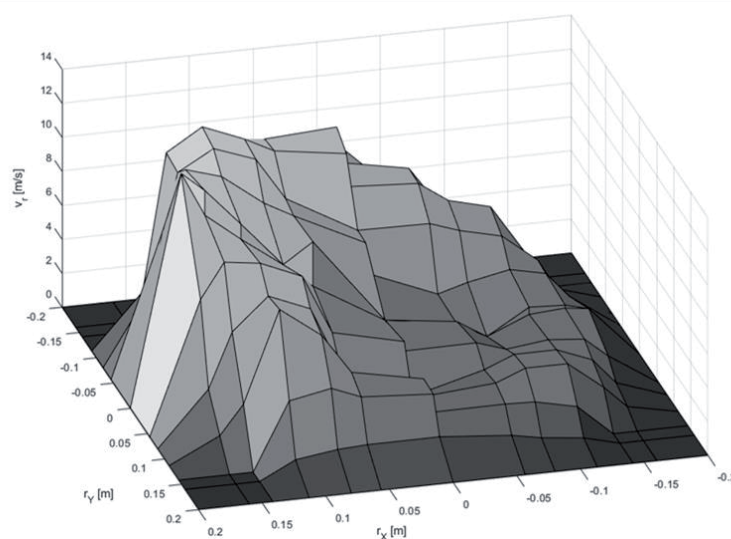


Figure 4. Visualization of the flow profile in the drying machine outlet pipe.

The outputs of calculations of the washing and drying programs are shown in Tables II-IV.

Table II
Results of the calculation of the washing program

Measurement [kg/batch]	Theoretical	1 st	2 nd	3 rd	Average
m _{RW}	158	267.1	229.9	232.1	243.0
m _{CHTW}	182	322.0	303.9	269.1	298.3
m _{steam}	15.3	27.4	25.5	23.4	25.4

Table III
Results of the calculation of the drying program

m _{steam; theoretical} [kg/batch]	27
m _{steam} [kg/batch]	26.1

Table IV
Comparison of the results with monthly production data

Lindström washing machine data	Average CHTW per batch [kg]		
Batches per year	19 664	Lindström data	314.4
Water per year [m ³]	6 182	Measurement	298.3

The graphs, which were used to identify an energy inefficiency and propose a mitigating measure are shown in Figures 4 and 5.

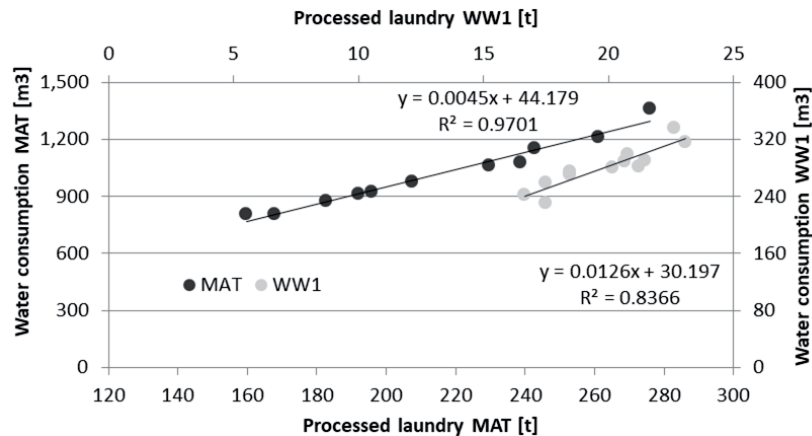


Figure 5. Water consumption relationship.

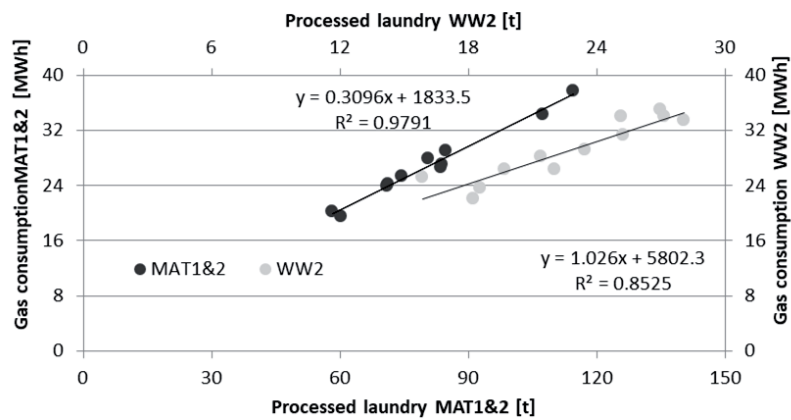


Figure 6. Gas consumption relationship.

Discussion

The direct results of the measurements, shown in Table I and Figure 3 were first processed using the described calculation methods. At first, in the measurement of the washing program, only steam consumption was desired, however, a considerable discrepancy between theoretical and real amount of used water in the washing program was discovered based on data in Table II. The presence of this discrepancy was further confirmed by comparison of output data with monthly production data provided by the enterprise, as shown in Table IV. Upon further examination of the machines and consultation with the enterprise, we identified, that upon rotation of the drum, the textile mats absorb some of the washing water, reducing the water level in the machine, which prompts the inlet pump to add more water into the mix. The amount of additional water corresponds with the amount of water that the mats can hold, which further confirms this effect. We recommended that the enterprise consult this discrepancy with the company responsible for washing program management in order to change the settings of the inlet pump, so that only the amount of water described in the washing program definition is pumped. Potential annual savings of 12% of total water and gas expenditure of the enterprise were anticipated upon mitigating this inefficiency on all relevant modules. The enterprise has implemented this measure on modules MAT3 and MAT4, and is already reporting savings of 5 m³ of water per day.

No discrepancy was found with the measurement and calculation of the drying program, as can be seen in Table III, and the resulting values were considered correct, therefore, they were used for further energy assessment at the enterprise.

The consumption and production trends, which can be observed in Figures 4 and 5, indicate that the relationship in the MAT section displays expected qualities with minimal scatter, as shown by the R² value and proportionally low intercept value. However, we can also observe, that the relationships in the WW section display greater scatter from a linear relationship as well as proportionally greater intercept. Based on this information and upon consultation with the enterprise, we identified a possible cause. Metal and plastic bits (bolts, coins, screws, pens, screwdrivers), are often forgotten in the rented WW by the customers of the enterprise. These then fall out of the WW during the washing program and jam the outlet valve. This leads to high water and energy losses due to pumping of heated water into the machine, which then immediately goes down the drain. This continues until the operator of the machine notices that the first step of the wash is taking too long. At first, installation of a filter with magnetic separator was proposed to mitigate this inefficiency, this was however deemed impossible to implement by the staff of the enterprise due to the geometry of the washing machine. The bits fall into the valve through a gap between the drum and the door of the washing machine. Therefore, installation of a rubber or nylon brush “gasket” at this spot, which would allow the rotation of the drum and allow water to pass through, but would stop any larger pieces of material, was proposed.

Conclusions

A case study confirmed that SMEs indeed exhibit unutilized energy efficiency potential. Due to this fact, energy auditing can often lead to the proposal of low investment, short payback time measures; therefore, it is cost effective for SMEs to be subjected to such auditing³². Mitigation measures were proposed, which would increase energy efficiency at the enterprise. The implementation of one of the mitigation measures led to significant water and subsequently energy savings.

Acknowledgement

This work was financially supported by the Slovak Research and Development Agency, Grant No. APVV-15-0148 and APVV-18-0134 as well as by the Faculty of Chemical and Food Technology, Slovak University of Technology in Bratislava.

References

1. Malinauskaitė J., Jouhara H., Ahmad. L., Milani M., Montorsi L., Venturelli M.: *Energy* 172, 255 (2019).
2. Rehfeldt M., Worrell E., Eichhammer W., Fleiter T.: *Renewable Sustainable Energy Rev.* 120, 109672 (2020).
3. Cagno E., Neri A., Trianni A.: *Energy Effic.* 11, 1193 (2018).
4. Fleiter T., Worrell E., Eichhammer W.: *Renewable Sustainable Energy Rev.* 15, 3099 (2011).
5. Hrovatin N., Cagno E., Dolšák J., Zorić J.: *J. Cleaner Prod.* 323, 129123 (2021).
6. Máša V., Stehlík P., Touš M., Vondra M.: *Energy* 158, 293 (2018).
7. Palm J., Backman F.: *Energy Effic.* 13, 809 (2020).
8. Therkelsen P., McKane A.: *Energy Policy* 57, 318 (2013).

9. Mahapatra K., Alm R., Hallgren R., Bischoff L., Tuglu N., Kuai L., Yang Y., Umoru I.: *Energy Effic.* *11*, 1103 (2018).
10. Locmelis K., Blumberga D., Blumberga A., Kubule A.: *Energies* *13*, 2210 (2020).
11. Kalantzis F., Revoltella D.: *Energy Econ.* *83*, 229 (2019).
12. Fresner J., Morea F., Krenn Ch., Aranda Uson J., Tomasi F.: *J. Cleaner Prod.* *142*, 1650 (2017).
13. Patel J. D., Shah R., Trivedi R. H.: *J. Cleaner Prod.* *333*, 130170 (2022).
14. Redmond J., Walker B.: *Energy Effic.* *9*, 1053 (2015).
15. Cunha P., Neves S. A., Marques A. C., Serrasqueiro Z.: *Energy Policy* *146*, 111776 (2020).
16. Errigo A., Choi J.-K., Kissock K.: *Sustainable Energy Tech. Assess.* *49*, 101694 (2022).
17. Andersson E., Karlsson M., Thollander P., Paramonova S.: *Renewable Sustainable Energy Rev.* *93*, 165 (2018).
18. Birat J.-P., Declich A., Quinti G., Signore P., Fick G., Chiappini M., Millet D., Alix T.: *Mater. Tech.* *108*, 505 (2021).
19. Fadly, D.: *Sustainability* *12*, 7455 (2020).
20. Viesi D., Pozzar F., Federici A., Crema L., Mahbub M. S.: *Energy Policy* *105*, 363 (2017).
21. Maciková L., Smorada M., Dorčák P., Beug B., Markovič P.: *Sustainability* *10*, 2274 (2018).
22. Malega P., Majerník M., Rudy V., Daneshjo N.: *Pol. J. Environ. Stud.* *30*, 3753 (2021).
23. Bobák P., Pavlas M., Kšenzuliak V., Stehlík P.: *Chem. Eng. Trans.* *21*, 109 (2010).
24. Nicolaidis Ch., Vyrides I.: *Resour., Conserv. Recycl.* *92*, 128 (2014).
25. Conde M. R.: *Appl. Therm. Eng.* *17*, 1163 (1997).
26. Valenti G., Bonacina C. N., Bamoshmoosh A.: *Case Stud. Therm. Eng.* *22*, 100734 (2020).
27. Lima T. P., Dutra J. C. C., Primo A. R. M., Rohatgi J., Ochoa A. A. V.: *Sol. Energy* *122*, 737 (2015).
28. Nunes J. R. R., da Silva J. E. A. R., da Silva Moris V. A., Giannetti B. F.: *J. Cleaner Prod.* *218*, 357 (2019).
29. <https://lindstromgroup.com/>
30. Čižmár M., Variny M., Vráblik P.: *Proceedings of the 16th Biannual CER Comparative European Research Conference*, 114 (2021).
31. Hasanbeigi A., Price L.: *Ernest Orlando Lawrence Berkeley National Laboratory* (2010).
32. Thollander P., Kimura O., Wakabayashi M., Rohdin P.: *Renewable Sustainable Energy Rev.* *50*, 504 (2015).

SELECTED OPTIONS TO INCREASE THE EFFICIENCY OF A STEAM METHANE REFORMER

Hoppej D.¹, Variny M.¹, Kondáš R.¹

¹ Faculty of Chemical and Food Technology, Slovak University of Technology in Bratislava, Radlinského 9, 812 37 Bratislava, Slovakia
dominik.hoppej@gmail.com

Abstract

Industrial hydrogen production via Steam Methane Reforming (SMR) is characteristic by a two-step production mechanism: a high-temperature catalytic reforming of hydrocarbons is followed by water gas shift reaction performed at lower temperatures. SMR units may employ one or two shift reactors. In this study we examined the possible means of increasing the efficiency and lowering the energy intensity of an industrial SMR unit: Addition of the low-temperature shift reactor and CO₂ removal from syngas via pressure swing adsorption. Both options were assessed by their impact on auxiliary fuel consumption, electricity consumption and maximal production capacity of the plant. The impact of changed high pressure steam export was included as well. Shift reactor addition reduced specific feed (natural gas) consumption but led to increased specific auxiliary fuel consumption with the overall change in the natural gas balance being close to zero. Carbon dioxide removal, even without its sequestration, reduced the energy intensity of the plant.

Introduction

The aim of this work is to analyze the impact of addition of low temperature shift (LTS) reactor and utilization of hydrogen separation process tailgas by reduction of CO₂ content. To fulfil the aims of proper evaluation of proposed alternatives, mathematical model of industrial hydrogen plant was constructed in Aspen Hysys V11 software. Scheme of this plant is visualised in Figure 1.

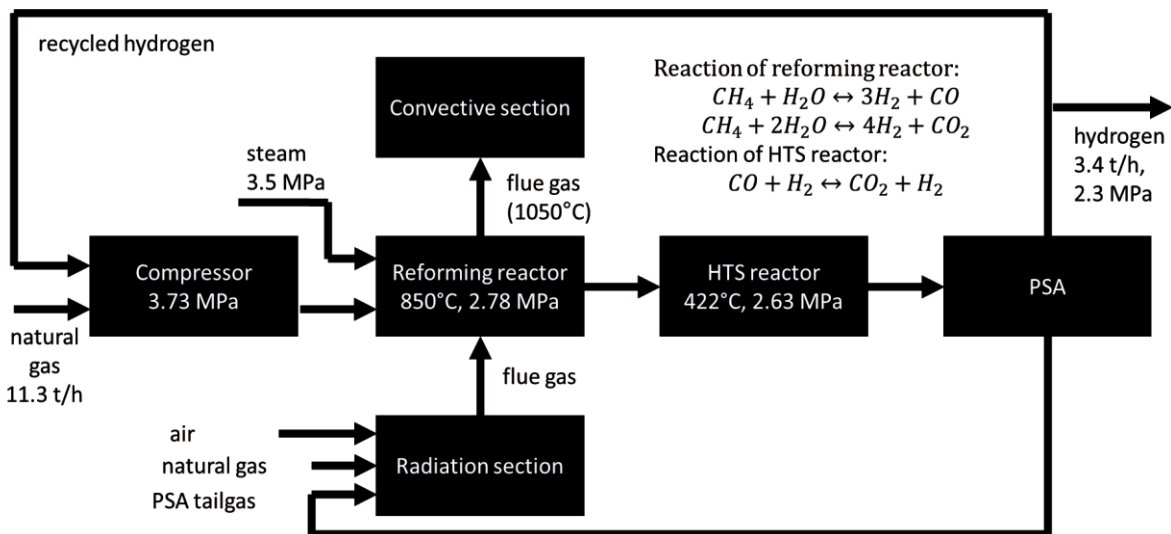


Figure 1. Scheme of modelled hydrogen plant.

Natural gas entering the hydrogen plant is blended with small amount of recycled hydrogen for desulphurization of natural gas. After the compression and desulphurization, high pressure steam is added in projected ratio and this reaction mixture enters the reforming reactor, where steam reforming reactions take place. The amount of carbon monoxide present in the syngas produced in reforming reactor is greatly reduced at high temperature shift (HTS) reactor by water gas shift reaction. After the HTS reactor, reaction mixture is cooled down and hydrogen is separated at pressure swing adsorption (PSA) unit. Offgas from the PSA unit is combusted at the furnace of reforming reactor with enough natural gas to deliver the heat necessary for the endothermic steam reforming reactions. Flue gas, still at the high temperature, is then cooled down at convective section of reforming reactor furnace, while the steam is produced, and reaction mixture is preheated.

Modelling of hydrogen plant

The aim of modelling of hydrogen plant was to develop mathematical model able to evaluate the impact of proposed alternatives addition to the hydrogen plant. Model was based on the available documentation of an existing hydrogen plant. Scheme of developed model can be found in Figure 2. To avoid unnecessary robustness of model, several assumptions were considered, mainly quantitative reaction of all hydrocarbons higher than methane (C2+) and perfect combustion at the furnace of reforming reactor. Due to low content of odorization substances in natural gas and low impact on the plant energy balance, this process was neglected in terms of reactor simulation and instead was simulated by addition of heat exchanger, with the same temperature (15 °C) and pressure loss (50 kPa), as was projected for this process. Fluid package was chosen in accordance with the literature¹. Peng-Robinson fluid package was used, confirming the results obtained at the previous study².

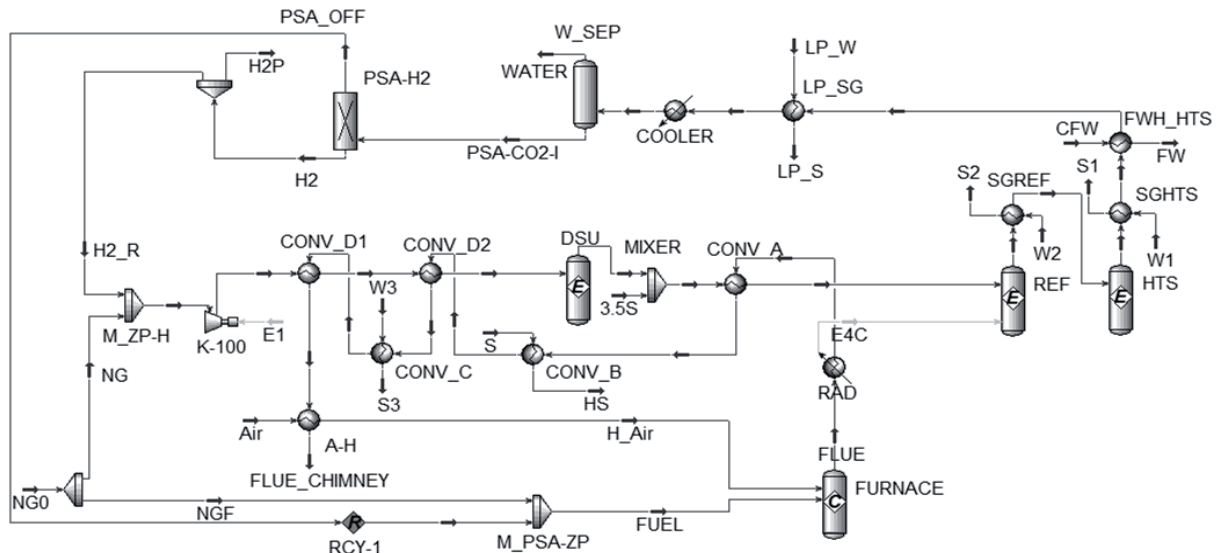


Figure 2. Scheme of developed mathematical model in Aspen Hysys.

To simulate reforming reactor, equilibrium model was used with ATE, Approach to equilibrium, parameter. Usage of ATE parameter allows taking into account basically all of the effects on final composition of reaction mixture and sufficient compliance with operational data was obtained in MATLAB software². HTS (high temperature shift), was modelled in the same manner as reforming reactor – with the use of equilibrium model, at design pressure and inlet temperature, while equilibrium composition at the outlet of reactor was modified by ATE parameter. Comparison of design and modelled data is provided in Table I.

Water steam is produced in 3 steam generators, CONV_C, SGREF and SGHTS from 151°C feed water, preheated before entrance to steam generators in FWH heat exchanger. Calculations were made with the assumption of constant value of UA parameter [kW/K].

Table I
Comparison of design and calculated data

Mole %	Reforming reactor outlet		HTS reactor outlet	
	Design data	Aspen data	Design data	Aspen data
H ₂	71.57	71.51	73.93	73.95
CO	12.39	12.79	3.05	3.13
CO ₂	8.54	8.22	16.14	16.09
N ₂	0.23	0.23	0.21	0.21
CH ₄	7.27	7.24	6.67	6.62

Equipment addition

Consequently, the model was developed with proposed equipment for the analysis of LTS reactor addition and CO₂ content reduction at the PSA tailgas. Two equipment items were proposed, PSA unit for CO₂ separation and LTS reactor.

A. PSA unit for CO₂ separation from the reaction mixture (PSA-CO₂). Assumption for this PSA unit was the capture of solely carbon dioxide, which is the process first described in 1951³ unlike PSA unit for hydrogen separation (PSA-H₂), where every gas except hydrogen is captured. This way is change of hydrogen gas pressure reduced to unit pressure loss and there is no need to desorb the gas off the adsorbent. Efficiency of carbon dioxide separation was, in accordance with PSA-H₂ efficiency, assumed as 85.6%, with 99.9% purity of separated carbon dioxide – high purity was assumed to be reached by consequent liquefaction of captured carbon dioxide. Important for this alternative is the positioning of PSA-CO₂ unit in the hydrogen plant⁴. As the most favourable, position immediately before the PSA-H₂ unit was chosen. Main advantage of this position is avoidance of need for the compressor. Another big advantage is lowering of carbon dioxide content of gas entering the PSA-H₂ unit. This results in the increase of PSA-H₂-offgas heating value, which can possibly reduce consumption of natural gas in the reforming reactor furnace and further reduce carbon emissions. Scheme of this equipment is in Figure 3.

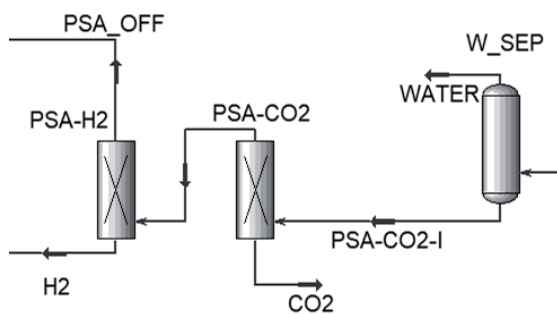


Figure 3. Scheme of PSA-CO₂ unit addition to the plant.

B. To support the conversion of carbon monoxide, which is produced in reforming reactor by reaction (2), addition of low temperature shift reactor was considered. Like the HTS reactor, this reactor was also modelled as equilibrium reactor, while ATE parameter value was assumed to be the same as in HTS reactor. LTS reactor size was chosen to be equal to HTS reactor size⁵ and temperature at the inlet of this reactor was 200°C, to minimise the risk of thermal degradation of catalyst at temperature higher than 260°C⁶. Proposed position of this reactor in the scheme is after the FWH heat exchanger, as can be seen in Figure 3. To achieve desired temperature of LTS reactor inlet, operating conditions of FWH heat exchanger were changed, so the temperature of reaction mixture at the outlet of FWH remains at 200 °C. To utilize heat of reaction mixture at the outlet of LTS reactor, another heat exchanger, FWPH was proposed, to preheat feed water before entering FWH heat exchanger. Reaction mixture in this proposed heat exchanger is cooled down to 168 °C, to avoid condensation of unreacted water steam. Scheme of this proposed equipment is visualised in Figure 4.

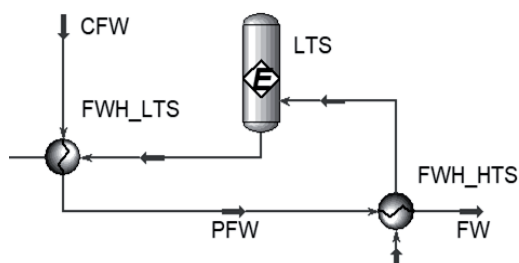


Figure 4. Scheme of LTS reactor addition to the plant.

Methodology

Four production rates of hydrogen were simulated: 3.4 t/h, that is maximum production capacity of modelled industrial plant, 3.0 t/h, 2.7 t/h and 2.4 t/h, which are standard production rates throughout the year. Each of proposed alternatives was used, while the process-side pressure loss during maximum capacity was calculated. Results of simulations were compared with the reference H₂ plant with the emphasis on CO₂ emissions and energy consumption. Economic evaluation was calculated for annual average hydrogen production of 2.7 t/h. Natural gas energy savings (NGES) were calculated by equation (1), from the difference in reference natural gas consumption (NG_{ref}) and actual natural gas consumption (NG_{mod}). To obtain results in kJ/h, high heat value (q_{NG}) was added to equation. Compensation mechanism of refinery steam network was also taken into account, so the reduction of steam production resulted in rise of fuel consumption at refinery power plant. Thus, steam energy savings (SES), equation (2), were calculated from the difference in reference (SP_{ref}) and actual (SP_{mod}) production of steam, which was multiplied by steam condensing heat value (h_s) and divided by refinery power plant efficiency (η_{PP}).

$$NGES = (NG_{ref} - NG_{mod})q_{NG} \quad (4)$$

$$SES = \frac{(SP_{ref} - SP_{mod})h_s}{\eta_{PP}} \quad (5)$$

Every change of steam production in hydrogen plant is manifested in power plant fuel consumption, which is also linked with the change of total carbon emissions of refinery – this was included in equation (3) for calculation of carbon dioxide emissions savings.

$$CES = (CE_{ref} - CE_{mod}) + \frac{(SP_{ref} - SP_{mod})h_s}{q_{PP}\eta_{PP}} EF_{PP} \quad (6)$$

Electricity consumption of liquefaction process was assumed to be 98 kWh/t of CO₂⁷. Capital costs needed for the liquefaction unit was taken from the same source, as 67.15 mil. USD for the liquefaction of 316 t/h of carbon dioxide, in 2012. Emissions from the electricity grid were not taken into account. All of equipment prices were adapted to current prices using CECPI parameter and indirect costs of 160% of equipment price were assumed when calculating total capital costs.

Results

Table II provides an overview of proposed alternatives, pressure loss at maximum capacity of hydrogen plant and total capital cost, as well as operating costs. Each alternative was able to fulfil pressure limits of refinery hydrogen network of 2.0 MPa.

Table II
Overview of proposed alternatives for hydrogen plant modification

Alternative	Equipment addition	Pressure. loss / H ₂ press. [kPa]	Total capital cost [thousand €]	Operating costs [thousand €]
PSA	PSA-CO ₂ unit	150 / 2150	8 680	41.8
PSA+LTS	PSA-CO ₂ unit + LTS reactor	280 / 2100	9 280	81.7
LTS	LTS reactor	130 / 2250	588	39.9

Savings in comparison with reference hydrogen plant can be observed in Figure 5. These savings already take into account reduction of steam production and simultaneous increase of fuel consumption in refinery power plant. These savings represent 2-3% of total energy consumption of H₂ production process, including natural gas consumption as feed in the H₂ production.

This decrease is enabled by higher heating value of PSA tailgas from the hydrogen separation – as the amount of CO₂ present in the tailgas is significantly reduced, fuel consumed for heating this part of the tailgas is no longer needed, which results in lower consumption of natural gas as the fuel of reforming reactor furnace. Despite the reduction of steam production, which was considered to be compensated by refinery power plant with the energy efficiency of 85%, total natural gas consumption is decreased.

Alternative PSA+LTS results in similar results. However, as more hydrogen can be produced from the natural gas used as the process feed, energy savings are higher in comparison with PSA alternative. Still, lower carbon

monoxide content in PSA-H2 offgas slightly increases consumption of natural gas in the furnace, to the point it outweighs reduction of natural gas consumption as the feed in the process. However, higher consumption of natural gas in the furnace could be balanced out by rise in the steam production, which can reduce fuel consumption in refinery power plant. This effect can be observed in the LTS alternative – despite the decrease of natural gas consumption as the process feed, no significant change of total energy consumption is visible, due to higher fuel consumption. The decrease of power plant fuel consumption is not able to compensate for higher fuel consumption in the furnace of reforming reactor.

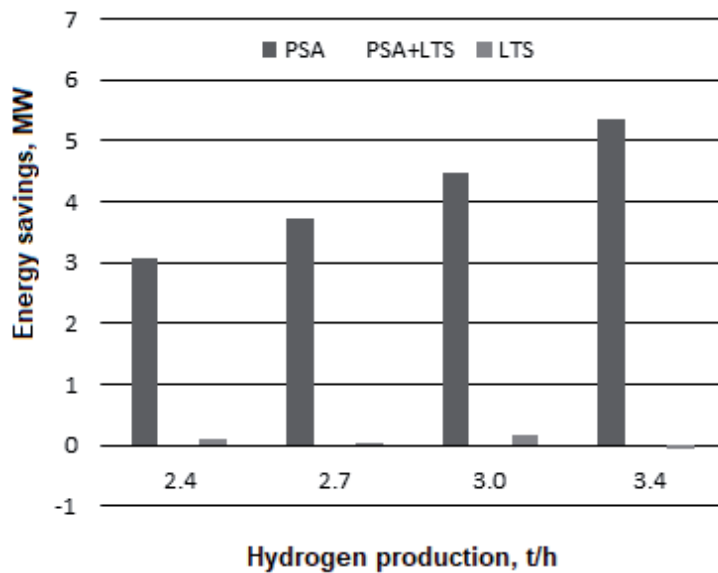


Figure 5. Energy savings of proposed alternatives in comparison with reference plant

As the decrease of natural gas consumption is also connected to the decrease of the carbon dioxide emissions, naturally, the next step is to analyze the impact of proposed alternatives on savings of carbon dioxide emissions. Due to the rise of carbon emission allowances price, decrease of carbon dioxide emissions significantly contributes to the total economic impact. Savings of carbon dioxide emissions can be observed in Figure 6.

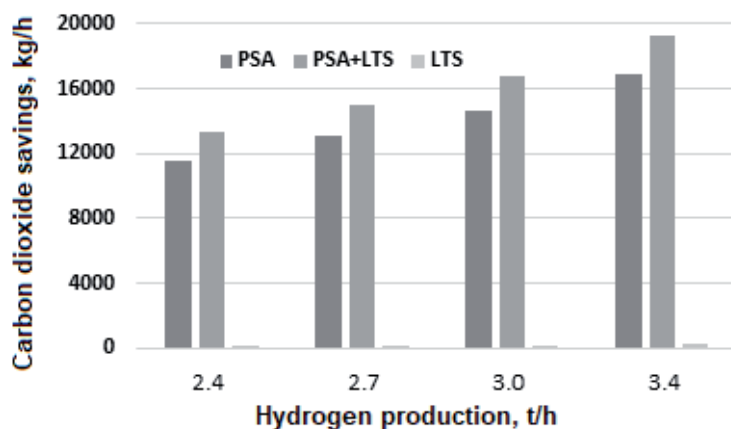


Figure 6. Carbon dioxide savings of proposed alternatives in comparison with reference plant.

As results in Figure 6 suggests, PSA and PSA+LTS alternatives bring in significant decrease of carbon dioxide emissions, which are not outweighed by carbon dioxide emitted from the fuel combusted in central power plant. In accordance with the results observable in Figure 5, addition of sole LTS reactor does not bring in sufficient savings of natural gas and neither carbon dioxide emissions. However, it should be mentioned that the savings in PSA and PSA+LTS alternative are achieved by capturing and liquefaction of carbon dioxide. Because of this, subsequent economic evaluation is necessary.

Considering long-term course of futures contract for natural gas and electricity on Prague Stock Exchange⁸, assumption was made, that electricity price can be considered as 2.5 times higher than that of natural gas. Then payback period was calculated, results can be seen in Table III. Using the assumption of price relation of natural gas and electricity, low sensitivity of payback period on changes in prices of natural gas means, that energy savings obtained by CO₂ elimination from the tailgas covers most of costs for CO₂ liquefaction.

Table III
Overview of payback periods (in years) for various prices of natural gas and carbon dioxide emissions allowances

CO ₂ allowances price [€/t]	30				60	80
NG price [€/MWh]	20	50	80	110	80	80
PSA	2.68	2.57	2.47	2.38	1.30	0.99
PSA+LTS	2.49	2.37	2.27	2.17	1.20	0.92
LTS	16.47	12.13	9.61	7.95	6.65	5.52

Conclusion

As energy savings achieved by PSA-CO₂ addition are able to cover expenses for CO₂ liquefaction, with the current prices of emission allowances, short payback period is good promise for the next scientific works. Addition of LTS reactor alone has quite long age of return and reduction of CO₂ emission is almost negligible. However, PSA-CO₂ unit fairly enhances achieved savings, if used in the combination. Next work should be aimed at the development of rigorous mathematical model, mainly to include dependence of heat transfer coefficients on the flowrates, which could provide us with more detailed results on the decrease of steam production. Also, more detailed research of current advances in carbon dioxide separation by adsorption should be performed, to evaluate accepted assumptions for PSA-CO₂, like 87 % recovery of CO₂ and purity above 99.9%.

Acknowledgement

The authors would like to express gratitude to Slovak Research and Development Agency, Grant No. APVV-19-0170 and APVV-18-0134 and to Faculty of Chemical and Food Technology of Slovak University of Technology.

References

1. Aspen Tech, Aspen physical property system: physical property methods, 2010, Burlington, USA.
2. Hoppej, D., Variny M.: ATPET J. 4, 9 (2021).
3. Colburn, A. P., Dodge, B. F. Adsorption process for removal of carbon dioxide from the atmosphere of a submarine, US2545194, 1951.
4. Luberti M., Brown A., Balsamo M., Capocelli M.: *Energies* 15, 1091 (2022).
5. Pearce B. B., Twigg M. V., Woodward C.: *Methanation*. Catalyst Handbook. 2nd ed. Wolfe Publishing Ltd., London 1989.
6. Bell D. A., Towler B. F., Fan, M.: *Hydrogen Production and Integrated Gasification Combined Cycle (IGCC)*. Coal Gasification and Its Applications. Elsevier, Amsterdam 2011.
7. Lee U., Yang S., Jeong Y. S., Lim Y., Lee Ch. S., Han Ch.: *Ind. Eng. Chem. Res.* 51, 15122 (2012).
8. Prague Stock Exchange, In [online] cit. 7.4.2022 (pse.cz).

INDUSTRIAL PACKAGING MANAGEMENT IN THE CIRCULAR ECONOMY MODEL

Paták M.¹, Hromadníková K.², Branská L.³, Kocmanová A.⁴

^{1,2,3}University of Pardubice, Faculty of Chemical Technology, Studentská 95, 53210 Pardubice, Czech Republic

⁴Brno University of Technology, Faculty of Business and Management, Czech Republic
michal.patak@upce.cz

Abstract

Introducing circular economy principles into a company's packaging management is one possible way to reduce the environmental impact of excessive use of packaging materials in industry, but also an opportunity to reduce the costs associated with packaging logistics. The aim of this paper is to identify the main opportunities and barriers for the management of industrial packaging according to the circular economy model based on qualitative research in a selected company in the chemical industry. The research was conducted through in-depth interviews with four managers of the company who are involved in the packaging management of the selected company. The research results provide examples of good practice while highlighting the main issues related to industrial packaging management in the areas of: sustainable material design, material savings, packaging reuse and packaging waste recycling.

Introduction

Circular packaging is a relatively new concept that has attracted a lot of attention in the literature in recent years¹. The use of excessive amounts of packaging from non-renewable raw materials for single-use purposes further damages and disrupts the environmental balance². To avoid this, businesses' approach to packaging must change³. Packaging must meet specific environmental protection requirements throughout its entire life cycle, from production to consumption. Introducing circular economy principles into packaging management is one of the keyways to meet these objectives.

The circular economy and its principles raise concerns about environmental impacts right from product design. They lead to the design of environmentally friendly supply chains, enabling both the production of environmentally friendly products and, above all, their reuse¹. The circular economy model is applied in the packaging management environment to create reusable packaging and close material flows through packaging return flows and material recycling. Desirable activities in industrial packaging supply chains include⁴:

- sustainable material design,
- material savings,
- packaging reuse and
- packaging waste recycling.

The first activity mentioned above is related to the search for suitable packaging material. Currently, the most used material in packaging is plastic. This is considered to be a negative phenomenon, especially in view of the consumption of oil and natural gas in its production⁵. But according to Callari⁶, plastic is a versatile and efficient material. However, its benefits can only be fully exploited if its environmental disposal at the end of its life cycle is properly handled. The combination of different materials in the production of packaging (so-called composite packaging) also creates problems due to complications in recycling processes. Moving towards sustainable packaging materials, which are usually considered to be materials derived from renewable sources (e.g. wood, paper, textiles, biodegradable materials)⁴, seems to be an appropriate solution to both problems. According to the companies, barriers to switching to sustainable packaging materials include higher acquisition costs, lack of certified packaging materials on the market and poorer conditions for processing them in production⁷.

Another way towards sustainable packaging is to reduce the amount of packaging material used. Businesses are trying to reduce material, in particular by designing thinner and lighter packaging or reducing the number of primary and secondary packaging. However, according to Hellström and Olsson⁸, too much reduction in the material used leads to compromising the correct performance of packaging functions and product losses. Larger packaging sizes, on the other hand, can help optimise transport and storage in the supply chain⁹. Davis and Song¹⁰ recommend reducing the number of levels of packaging due to contamination and mixing of different types of materials, which makes subsequent recycling of the packaging impossible. Beitzel-Heineke et al.¹¹ also see the packaging-free selling phenomenon as another route to material savings. In industrial markets, this could take

the form of pumping liquid or gaseous products into the customer's own vessels or equipment or transporting the products directly to the customer's plant via pipelines.

Circular economy principles can also be implemented through reusable packaging, either immediately or after simple treatment¹². According to Mahmoudi and Parviziomran¹³, this approach brings a number of benefits in the packaging industry. It reduces the demand for primary raw materials, saves costs for production and disposal of packaging, due to the smaller quantities of packaging. Returnable packaging is also generally stronger and of higher quality, so there is less likelihood of packaging failure, for example by rupture. However, the introduction of reusable packaging is associated with higher capital expenditure, higher costs for the implementation of return flows and higher business process management requirements¹⁴. However, research by Skerlic and Muha¹⁵, which compared the life cycle costs of disposable and reusable packaging, shows that reusable packaging tends to be a more cost-effective option overall from the business economics perspective.

When packaging is at the end of its life cycle and can no longer be used, it is recycled. This can be done with material or energy recovery of the waste¹⁶. Mechanical recycling is the transformation of a recycled material into a new product without changing the chemical structure of the material. Chemical recycling is based on the breaking down of recycled material into starting materials or the extraction of chemical and petrochemical feedstock that can then be reused to produce new products. Energy recovery is understood as the environmentally acceptable incineration of waste using the heat generated in the process. However, incineration should not be the primary method of recycling and only packaging that can no longer be used as secondary raw materials should be incinerated.

Introducing circular economy principles into the packaging economy is a key tool for innovation towards sustainable packaging¹. Circular packaging innovations and their barriers largely depend on the type of the industry. Since these innovations for chemical industry are not sufficiently reflected in the literature, the aim of the paper is to identify main opportunities and barriers for the management of industrial packaging according to the circular economy model, based on primary research.

Research methods

The research was organized as a qualitative study in a selected company in the chemical industry. The data collection was based on personal interviews of five respondents from among the employees of the company according to a semi-structured questionnaire in order to identify:

- the types of packaging and packaging materials used in the enterprise,
- the packaging and packaging waste streams in the enterprise,
- opportunities and barriers to the introduction of packaging eco-innovation in the areas: sustainable material design, material savings, packaging reuse and packaging waste recycling.

Respondents were interviewed through individual interviews lasting 1-2 hours. In case of any ambiguities and the need for additional information, follow-up interviews with respondents were carried out. The interviewees were: the company's production manager, the head of the company's waste and pallet management department, a representative of the company's purchasing department and two representatives of the sales department. The data was processed by content analysis of the interviews and subsequent synthesis of the findings.

Selected for the research was a company in the chemical industry with a tradition in plastics processing of more than 80 years. The company is part of a larger concern and is one of the world's major processors of plastics such as PVC, PE and PET. The company offers high-end products and specialised customer solutions that include not only production but also development activities and consulting services. It sells its products to 49 countries worldwide and in 2021 generated revenues of CZK 4.3 billion for its products and services. It is thus an integral part of the global plastics industry.

The company has implemented an integrated quality, environmental and safety management system through ČSN EN ISO 9001, ČSN EN ISO 14001 standards and the "Safe Enterprise" programme. As part of its environmental care, the company has invested over CZK 160 million in direct environmental protection over the last ten years. It has reduced emissions of volatile organic compounds by 90% compared to the early 1990s. The company's strategy is also to focus on purchasing environmentally friendly technologies, focusing on new materials and finding new ways to use plastics. Thanks to new technologies and production optimisation, the company is continuously reducing its consumption of water and all types of energy. The environmental impact indicators in relation to the quantity of production are also on a downward trend.

Results and Discussion

Packaging used, packaging materials and their flows in the company

The company uses primary packaging, secondary packaging, tertiary packaging and other auxiliary packaging materials for packaging products. Primary and secondary packaging consists of cardboard boxes, paper tubes, plastic bags, big bags and plastic bags. This is packaging made from a single material. However, in order to increase the quality protection of the product, it was necessary to introduce a new composite packaging, namely a paper tube with a foamed PE coating. The tertiary packaging used are octabins (large paper boxes), EURO pallets, paper and wooden atypical pallets, KTP packaging (metal pallet containers), metal cages, carriages and ASP pallets. The company uses two sizes of cages depending on whether they are used for packing smaller or larger rolls of coiled product. The cages can also be further adjusted to the dimensions of the product in order to maximise the use of the packaging space and at the same time achieve maximum stabilisation of the product in the packaging. The auxiliary packaging material consists of cardboard cuttings, honeycomb boards and pressed cardboard edges. They provide additional protection against product crushing during storage and transport. The inserts and labels serve an informative function. Binding tapes, stretch films and clips are used to stabilise products on the pallet.

Primary and secondary packaging and octabins are disposable, however, clean LDPE and PP packaging waste is collected for recycling through a system of collection depots. The EURO pallets are not returned to the company, but the customer has the option to continue using the pallet thanks to its standardised dimensions. Packaging of atypical dimensions, KTP packaging and metal cages are returnable packaging. Carriages and ASP pallets are packaging used for internal purposes only. Auxiliary packaging material is used on a one-off basis within the company.

Most of the packaging in which purchased raw materials are packaged can be reused in the packaging management of the company in accordance with the principles of the circular economy. These are mainly pallets (tertiary packaging of products) and big bags (handling and transport of products within the company). The contaminated packaging waste is sold to a recycling organisation, which then decides on further processing.

Pure LDPE and PP packaging waste (both purchased and recovered) is recycled on the company's own recycling line. In order to make greater use of the recycling line, the company also buys clean LDPE and PP packaging waste from other companies. The regranulate obtained from recycling is then sold or processed in the production of injection moulded products from the recycled material.

A detailed diagram of the flows of packaging, packaging materials and packaging waste through the company is shown in Figure 1.

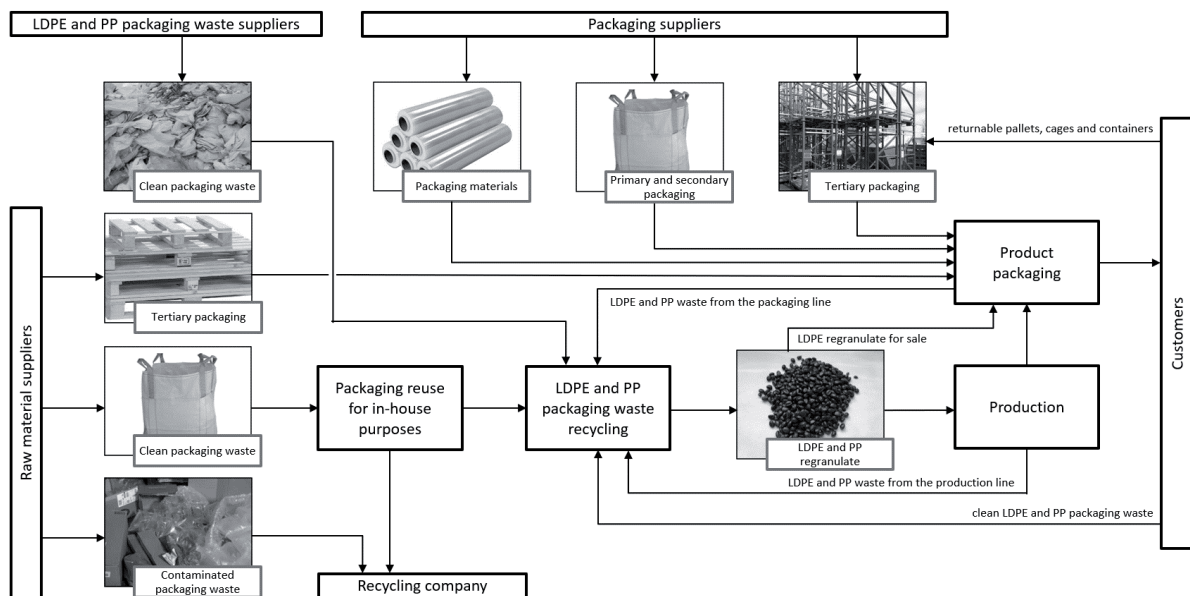


Figure 1. Diagram of packaging flows in the company.

Opportunities and barriers for eco-innovative packaging in sustainable material design

The choice of specific packaging and packaging materials is mainly influenced by customer requirements. Some customers require the use of FSC-certified paper packaging. Special paper pallets are required for the transport of some products, which the company must assemble from components purchased from certified suppliers (recommended by the customer). Customers also often require the use of packaging made from recycled materials (with at least 70 % recycled content).

As part of the introduction of circular economy principles, a company could in the future introduce the use of recycled or sustainably certified packaging for all its products. However, for industrial products, the introduction of sustainable packaging is difficult according to respondents. The main reason is the obligation for the packaging supplier to certify the proportion of recycled material contained in the packaging, which constitutes a significant increase in administrative costs. If only a negligible percentage of customers demand recycled packaging, such investments are usually not economically worthwhile for the supplier. In contrast to similar findings from research in Swedish manufacturing companies⁷, a further barrier to the introduction of sustainable packaging materials was identified, namely the lack of certified suppliers in the market, which also results in longer transport distances between the company and packaging suppliers, and thus a greater environmental burden of transporting empty packaging to the company.

Opportunities and barriers to the introduction of eco-innovative packaging in material savings

In 2001, the company upgraded most of its packaging to meet the requirements of the new legislation¹⁷. They therefore choose packaging for their products in such a way that the packaging is not unnecessarily large and bulky and does not contain unnecessarily large amounts of packaging material.

To this end, the company often tests the possibilities of using thinner films and paper materials. However, it often encounters the increasing risk of packaging damage during packaging, storage, handling or transport described by Hellström and Olsson⁸, which results in an increase in material consumption due to the need to repackage the product. The same problem arises when welding bags. When using bags made of higher quality materials, there is less scrap in the welding and packaging of the products, therefore the consumption of higher quality material is again lower than the consumption of lower quality material.

Attitudes towards changes in the packaging system of products that are first packed in bags and then in boxes vary among the respondents. Some respondents agree with Davis and Song¹⁰, who recommend reducing the number of packaging levels as an appropriate way to save the amount of packaging material used. However, this is contradicted by another respondent who believes that there will be frequent product destruction through scratching if the primary packaging layer (bags) is dropped. However, the risk of scratching has not yet been tested or confirmed in the company.

As part of the reduction of packaging material, the company innovated the packaging of the protective non-slip film used for kitchen units. Previously, these were wrapped in several layers of stretch film to hold the shape and attach the product information insert. Since 2008, the product has been packaged automatically in only one layer of film, under which the insert is loosely inserted and held by the end of the product.

The company is planning another change for the packaging of another product. The idea is to optimise the size of the handling unit when using paper pallets, which are more variable in their dimensions. Thanks to the more efficient use of the truck, the company will then transport 528 more items in one vehicle than before, thus saving on transport costs and the carbon footprint of the product when it is transported to the customer. A comparison of the original and new packaging methods is shown in Table I.

Table I
Comparison of original and new packaging

Characteristics	Original packing method	New packaging method
Pallet area	0.672 m ²	0.757 m ²
Number of products per pallet area	44 pcs/m ²	47 pcs/m ²
Number of products per column	60 pcs	108 pcs
Total number of products in the truck	2280 pcs	2808 pcs
Percentage of truck utilisation	56.00 %	64.75 %

Barriers to the introduction of similar packaging innovations for other products lie primarily in the weight limitations of the truck load, the shape and stability of the products when stacked, and the small number of products purchased by the customer.

Packaging-free selling is another way to reduce packaging. The company transports selected raw materials (PVC and CaCO₃) to the plant in tankers or RAJ wagons but excludes the use of this distribution method for its own products. The company sees the risk of non-compliance with the required product quality (deformation, scratching, soiling or contamination of the product) as a barrier. It would also make it more difficult to handle the product in the supply chain.

Opportunities and barriers to eco-innovation in packaging reuse

The company operates several take-back systems for reusable tertiary packaging, depending on the type of packaging and the customer. No third party is involved in these systems, so the packaging take-back system is not outsourced, and the returnable packaging is either owned by the company at all times or sold together with the products to customers. The company encourages customers to reuse tertiary packaging, in particular by ensuring that the packaging is taken back at the company's expense (using the empty means of transport used to deliver the products to customers).

The most common barrier to the reuse of tertiary packaging is the long transport distance between the company and the customer, and thus the greater environmental burden of reverse packaging logistics. For this reason, it seems more appropriate to use standardised packaging (e.g. EURO pallets) which do not need to be returned to the companies, as they continue to be used for the same purpose by customers all over Europe.

Opportunities and barriers to eco-innovation in packaging waste recycling

The final area of industrial packaging management in the circular economy concept is the recycling of packaging waste. For the enterprise under study, it proved beneficial to acquire its own recycling line for processing plastic waste. The company can produce regranulate from clean LDPE and PP waste, which it sells on or uses in the production of injection moulded products. At the same time, it buys disposable LDPE and PP packaging from its customers and from other companies in the area, thus contributing to the development of the circular economy not only in the management of its own packaging but also in the management of packaging in other manufacturing companies.

In order to maximise the use of the recycling line, the company also offers a recycling service where the customer brings their own waste materials from which the company produces regranulate. The customer then pays the company for the recycling and then processes the regranulate himself on his own injection moulding line. These services are mainly used by companies in the immediate vicinity of the plant, as the service would not be economically or environmentally viable if the waste material were brought in from further afield.

The processing of packaging waste in the company is limited by its cleanliness, as the company does not own a washing line for this waste. The introduction of an on-site waste washing plant is particularly hampered by legislative barriers (the plant is located in a groundwater protection zone). Using the services of an external line would increase the costs and environmental impacts associated with transporting the packaging waste material to and from the external company.

The possibility to use the services of recycling organisations is also important for the company. They can recycle packaging waste that the company cannot recycle itself (other single-sort and composite packaging). However, respondents agree with the literature⁴ that packaging recycling is only undertaken when the packaging is at the end of its life cycle and cannot be reused (even for internal purposes).

Conclusion

Based on the results of the primary research and their comparison with the literature, opportunities and barriers to the introduction of circular economy principles into the packaging management of manufacturing companies in the chemical industry were identified (see Table II).

Table II

Opportunities and barriers for the management of industrial packaging according to the circular economy model

Opportunities	Barriers
Discarding composite packaging	Lower product protection

Greater use of local packaging suppliers	Limited (or non-existent) supply of packaging
Use of sustainably certified packaging	Lack of certified suppliers Long transport distance from certified suppliers Higher cost of packaging
Automation of packaging to save packaging material	High capital expenditure
Optimising the amount of packaging material used	Ensuring sufficient product protection Customer requirements for packaging design Costly change in packaging process
Optimising the size of handling units and filling of transport vehicles	Use of non-standardised packaging Permissible total weight of means of transport Costly change in packaging process
Using fewer packaging levels	Risk of product damage Costly change in packaging process
Packaging-free selling	Physical and mechanical properties of products Risk of product contamination Difficulty in handling the product across the supply chain
Use of standardised pallets	Limited pallet dimensions
Use of returnable tertiary packaging	Transport distance between the company and its customers Organisation of transport operations
Reuse of disposable packaging	Risk of packaging failure
Acquisition of a recycling line	High capital expenditure Possibilities of processing recyclate in production Limited possibility to sell recyclate to external customer

The above opportunities for increasing the sustainability of packaging can represent significant benefits, from the perspective of a single company. Further improvements can be made if the company starts to work closely with its supply chain partners in this regard. A coordinated effort based on circular economy and supply chain management principles can represent a truly radical shift towards sustainable packaging as well as other logistics activities.

Acknowledgement

This study was supported by a grant from the Fund for Bilateral Relations within the framework of the EEA and Norway Grants 2014-2021 (EHP-BFNU-OVNKM-3-134-01-2020).

References

1. Meherishi L., Narayana A., Ranjani K. S.: J. Clean. Prod. 237, 117582 (2019).
2. Wang R. L., Hsu Z. F., Hu C. Z.: Sustainability 13, 5384 (2021).

3. Guillard V., Gaucel S., Fornaciari C., Angellier-Coussy H., Buche P., Gontard, N.: *Front. Nutr.* 5, 121 (2018).
4. Escursell S., Llorach-Massana P., Roncero M. B.: *J. Clean. Prod.* 280, 124314 (2021).
5. Selke S. E. M.: *Packaging and the Environment: Alternatives, Trends and Solutions*. Technomic Publishing, Lancaster 1990.
6. Callari J.: *Plastics Technology* 64, 6 (2018).
7. Molina-Besch K., Pålsson H.: *Packag. Technol. Sci.* 29, 45 (2016).
8. Hellström D., Olsson A.: *Managing packaging design for sustainable development: A Compass for Strategic Directions*. Wiley, Hoboken 2016.
9. Gustavo J. U. Jr., Pereira G. M., Bond A. J., Viegas C. V., Borchardt M.: *J. Clean. Prod.* 187, 18 (2018).
10. Davis G., Song J. H.: *Ind. Crop. Prod.* 23, 147 (2006).
11. Beitzel-Heineke E. F., Balta-Ozkan N., Reefke H.: *J. Clean. Prod.* 140, 14 (2016).
12. Zhang G., Zhao, Z.: *Green Packaging Management of Logistics Enterprises*. In *International Conference on Applied Physics and Industrial Engineering 2012, PT B*. Elsevier, Amsterdam 2012.
13. Mahmoudi M., Parviziomran I.: *Int. J. Prod. Econ.* 228, 107730 (2020).
14. Pålsson H.: *Packaging Logistics: Understanding and managing the economic and environmental impacts of packaging in supply chains*. Kogan Page, London 2018.
15. Skerlic S., Muha R.: *Sustainability* 12, 9431 (2020).
16. Voštová V., Fries J.: *Zpracování pevných odpadů*. ČVUT, Praha 2003.
17. Zákon č. 477/2001 Sb., Zákon o obalech a o změně některých zákonů (zákon o obalech).

ASSESSING VARIANTS OF LOW-GRADE HEAT VALORIZATION IN THE REFINING INDUSTRY

Rybár P.¹, Variny M.¹

¹ *Institute of Chemical and Environmental Engineering, Faculty of Chemical and Food Technology, Slovak University of Technology in Bratislava, Radlinského 9, 812 37, Bratislava, Slovak Republic*
miroslav.variny@stuba.sk

Abstract

Industrial heat recovery is one of the key features of an economical and efficient production process. Clustering of production units allows for enhanced heat and mass exchange, utilizing heat cascading efficiently, while the options to do so are limited in remote production units. If a stable and sufficiently large waste heat source is available, it can be used either to produce water steam for export (provided a demand for it exists), or to produce power with the help of either a condensing steam turbine or an Organic Rankine Cycle. The presented study investigates waste heat valorization options in a polymer production unit located within a refinery. Key factors impacting the optimal solution are highlighted, including the steam export constraints related both to variable heat demand in the refinery and the operation of marginal steam source. Basic energy and economic indicators are calculated.

Introduction

Industrial production belongs to major primary energy consumers and is, likewise, one of the major sources of atmospheric pollution worldwide¹. Substantial effort is thus directed to reducing the energy intensity by means of both implementing new, more efficient technologies, and improving the energy management of industrial enterprises^{2,3}. One of the factors that, despite numerous actions already undertaken^{4,5}, still offers remarkable potential to contribute to industrial production sustainability is industrial waste heat and its utilization⁶. Solely in Germany, a study by Brueckner et al.⁷ estimated the industrial waste heat availability as 127 PJ/a, or 13 % of total industrial fuel consumption. Likewise, its availability in the UK was 144 PJ/a, according to Jouhara et al.⁸. Industrial waste heat results from heat cascading as well as from exotherm processes. Its internal recovery and recuperation are one of the key pillars of economic feasibility of any industrial production. In case of industrial clusters, recuperation and heat sharing options are widened by the possibilities and synergies resulting from material and energy exchange between production units forming the cluster^{9,10}. Means of waste heat valorization are enriched by the options to convert it either to cold by absorption cooling¹¹, or to electricity¹² by Steam or Organic Rankine Cycle, or to increase its value by utilizing a heat pump¹³. Factors affecting the right waste heat valorization route include but are not limited to: heat source abundance and its mean temperature, heat availability character (continuous/periodic/irregular), annual heat availability, type and character of production process and available infrastructure for heat transport^{14,15}. The hierarchy of priorities starts with local heat recovery and recuperation, being the cheapest and most effective option¹⁶. Rest of available waste heat can be transported to adjacent units to replace heat utilities there, or, alternatively, to the nearby municipality to cover seasonal district heating demand^{17,18}. Usually, option with the lowest priority is transforming the waste heat to electricity^{2,19}. Multiple options have to be considered in parallel, though, as the optimal solution^{20,21}, identified by techno-economic analysis, might be a combination of several options²². This study focuses on waste heat formed in a polymerization process, with the production unit being incorporated in a refining and petrochemical complex. Heat export in form of low-pressure steam, or in form of middle-pressure steam are considered with respect to real plant's production features and the operation regimes of the combined heat and power plant, serving as the steam source for the industrial complex. Alternatives including power production via a steam or Organic Rankine Cycle are evaluated as well.

Methodology

Waste heat from polymerization process is considered, released at a temperature of 180 °C. Annual polymer production rate of 250 thousand tons is supposed. Polymerization reactor is cooled by hot-water loop. This energy in hot-water stream is then available for wide variety of uses. In this work, the production of power by steam is compared to that by Organic Rankine Cycle (ORC).

Figure 1 shows the components of the power production either by steam (a) or by ORC (b). The hot-water stream delivers the thermal energy to water/ORC medium in heat exchanger, where it is evaporated. Saturated steam passes to turbine and performs work. This work is converted to electric energy by a generator. On the turbine

exit, it condenses in condenser and transmits heat to cooling water circuit. Cooling water is cooled in a cooling tower by air with variable temperature, differing according to the season of the year. Water condensate passes to deaerator, where it is deaerated by steam. ORC condensates are pumped directly to the heat exchanger.

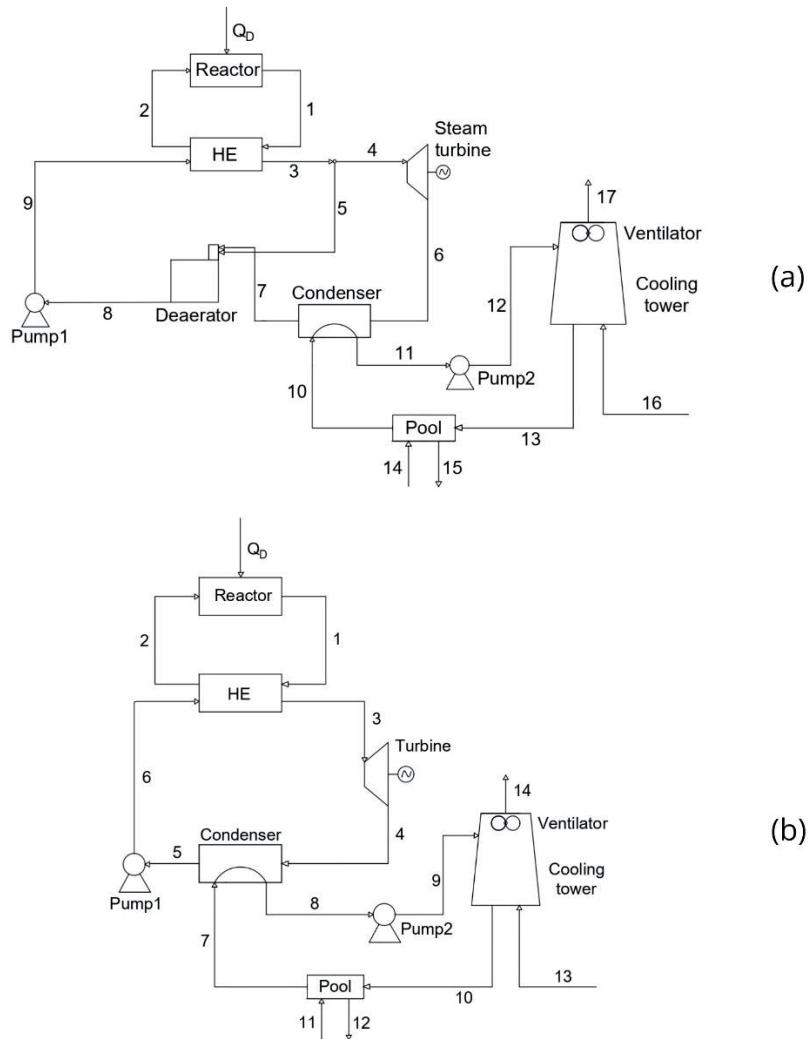


Figure 1. Scheme of the power production by steam (a) and by ORC (b), HE – heat exchanger.

Table I
Summary of critical parameters of the chosen working fluids.

Working fluid	IUPAC name	T _c [°C]	P _c [MPa]
R245fa	1,1,1,3,3-pentafluoropropane	154.01	3.651
R123	2,2-dichloro-1,1,1-trifluoroethane	183.68	3.662
R1233zd(E)	trans-1-chloro-3,3,3-trifluoropropene	166.45	3.624
R600	butane	151.98	3.796
R601	pentane	196.55	3.370
R601a	isopentane	187.20	3.378
R365mfc	1,1,1,3,3-pentafluorobutane	186.85	3.266
R245ca	1,1,2,2,3-pentafluoropropane	174.42	3.925
R21	dichlorofluoromethane	178.33	5.181
R141b	1,1-dichloro-1-fluoroethane	204.35	4.212

Preliminary selection of working fluids was done based on the critical parameters of the fluids. Operation parameters were chosen to be lower than the corresponding critical parameters, in order to ensure subcritical operation, see Table I.

The basic mass flows and energy indicators of the power production by either SRC or ORC were calculated by the material and energy balances of the main components, Table II and Table III. Electric energy consumption in compressor, pumps, and ventilators was calculated, as well as the net power produced by steam and by ORC.

Table II
Summary of equations for SRC.

Name of equation	Equation
Heat flow in reactor	$\dot{Q}_D = \dot{m} \cdot \Delta_r h$
EB of reactor	$\dot{m}_1(h_1 - h_2) = \dot{Q}_D$
EB of heat exchanger	$\dot{m}_1 \cdot (h_1 - h_2) = \dot{m}_3 \cdot (h_3 - h_9)$
MB of heat exchanger and pump1	$\dot{m}_3 = \dot{m}_8 = \dot{m}_9$
MB of deaerator	$\dot{m}_5 + \dot{m}_7 = \dot{m}_8$
EB of deaerator	$\dot{m}_5 \cdot h_5 + \dot{m}_7 \cdot h_7 = \dot{m}_8 \cdot h_8$
Mass flow of steam to turbine	$\dot{m}_4 = \dot{m}_3 - \dot{m}_5$
MB of steam turbine and condenser	$\dot{m}_4 = \dot{m}_6 = \dot{m}_7$
MB of condenser	$\dot{m}_{10} = \dot{m}_{11}$
EB of condenser	$\dot{m}_6 \cdot (h_6 - h_7) = \dot{m}_{10} \cdot (h_{11} - h_{10})$
MB of cooling tower	$\dot{m}_G \cdot (\bar{Y}_{17} - \bar{Y}_{16}) = \dot{m}_{12} - \dot{m}_{13}$
EB of cooling tower	$\dot{m}_{12} \cdot h_{12} + \dot{m}_G \cdot h_{\bar{Y}_{16}} = \dot{m}_{13} \cdot h_{13} + \dot{m}_G \cdot h_{\bar{Y}_{17}}$
Relative mass fraction	$\bar{Y} = \frac{M_w \cdot \varphi \cdot p_w^\circ}{M_G \cdot (p - \varphi \cdot p_w^\circ)}$
Mass flow of blowdown from cooling tower pool	$\dot{m}_{15} = 1/3 \cdot \dot{m}_{14}$
MB of cooling tower pool	$\dot{m}_{13} + \dot{m}_{14} = \dot{m}_{10} + \dot{m}_{15}$
Power production	$P_{el} = \eta_{mech} \cdot \dot{m}_4 \cdot (h_4 - h_6)$
Power consumption by pump1	$P_{pump1} = \frac{\dot{V}_8 \cdot (p_9 - p_8)}{\eta_{pump}}$
Power consumption by pump2	$P_{pump2} = \frac{\dot{V}_{11} \cdot \Delta p_{pump2}}{\eta_{pump}}$
Power consumption by ventilator	$P_{vent} = \frac{\dot{V}_{16} \cdot \Delta p_{vent}}{\eta_{vent}}$

Table III
Summary of equations for ORC.

Name of equation	Equation
Heat flow	$\dot{Q}_D = \dot{m} \cdot \Delta_r h$
EB of reactor	$\dot{m}_1(h_1 - h_2) = \dot{Q}_D$
EB of heat exchanger	$\dot{m}_1 \cdot (h_1 - h_2) = \dot{G} \cdot (h_3 - h_6)$
Power production	$P_{el} = \eta_{mech} \cdot \dot{G} \cdot (h_4 - h_6)$
MB of condenser	$\dot{m}_{CW} = \dot{m}_8 = \dot{m}_7$
EB of condenser	$\dot{m}_{CW} \cdot (h_8 - h_7) = \dot{G} \cdot (h_4 - h_5)$
MB of cooling tower	$\dot{m}_G \cdot (\bar{Y}_{14} - \bar{Y}_{13}) = \dot{m}_9 - \dot{m}_{10}$
EB of cooling tower	$\dot{m}_9 \cdot h_9 + \dot{m}_G \cdot h_{\bar{Y}_{13}} = \dot{m}_{10} \cdot h_{10} + \dot{m}_G \cdot h_{\bar{Y}_{14}}$
Mass flow of blowdown from cooling tower pool	$\dot{m}_{12} = 1/3 \cdot \dot{m}_{11}$
MB of cooling tower pool	$\dot{m}_{10} + \dot{m}_{11} = \dot{m}_7 + \dot{m}_{12}$
Power consumption by pump1	$P_{pump1} = \frac{\dot{V}_8 \cdot (p_9 - p_8)}{\eta_{pump}}$
Power consumption by pump2	$P_{pump2} = \frac{\dot{V}_{11} \cdot \Delta p_{pump2}}{\eta_{pump}}$
Power consumption by ventilator	$P_{vent} = \frac{\dot{V}_{13} \cdot \Delta p_{vent}}{\eta_{vent}}$

Table II and Table III: MB – mass balance, EB – energy balance, \dot{Q}_D - heat flow in reactor, \dot{m} - mass flow of polyethylene, $\Delta_r h$ - standard enthalpy of reaction ($\Delta_r h = -3500 \text{ kJ/kg}$)²³, h - specific enthalpy, \dot{m}_G - mass flow of dry air in cooling tower, $h_{\bar{Y}}$ - specific enthalpy of moist air, \bar{Y} - relative mass fraction, M_w and M_G - molar mass of water and dry air, φ - relative humidity (φ on the entry is supposed equal to 0.4 and on the exit it equals to

0.9), p_w° - saturated vapour pressure, p - pressure, P_{el} - power produced by turbine, η_{mech} - mechanical efficiency of turbine ($\eta_{mech}=0.95$), P_i (i = pump1, pump2, ventilator) - power consumption, \dot{V} - volumetric flow, η_i (i = pump1, pump2, ventilator) – total efficiency ($\eta_i = 0.85$), Δp_{pump2} – pressure difference in pump2 ($\Delta p_{pump2} = 200 \text{ kPa}$), Δp_{vent} – pressure difference in ventilator ($\Delta p_{vent} = 0.2 \text{ kPa}$), \dot{G} – mass flow of working fluid, \dot{m}_{CW} – mass flow of cooling water.

Results

The amount of produced electric energy depends on ambient temperature, varying seasonally. Cooling water temperature affects the condensation temperature, as well as the condensation pressure of the working fluid. In winter, it is possible to expand the working fluid to lower pressure, and, therefore, to produce more electricity, as is documented by power production for individual ORC working fluids in Figure 2.

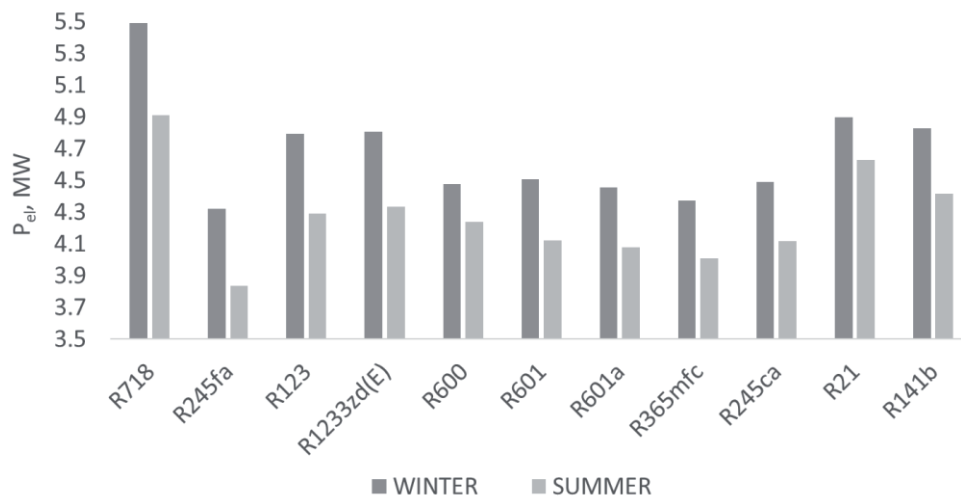


Figure 2. Power production based on the working fluid in winter and summer conditions.

The difference in the working fluids sensitivity to cooling water temperature is caused by their different thermodynamic features (different p-h diagrams), as documented in Figure 3. The power output differences vary significantly and unique features of individual working fluids impact thus the ORC design and its operation as well.

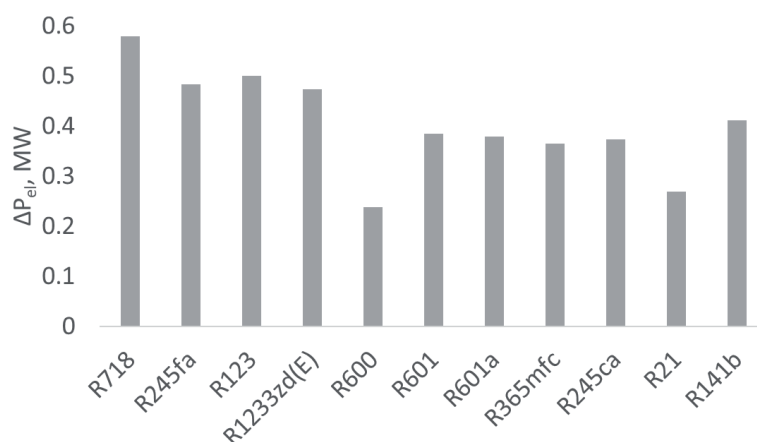


Figure 3. The difference in power production, comparing winter and summer conditions.

According to Table IV, ten ORC media were considered, from which the most perspective was chosen. They were considered according to three main criteria (environmental, safety and technical).

Environmental effect of the working fluid was judged according to two parameters, ODP (Ozone depletion potential) and GWP (Global warming potential). Based on the Regulation (EU) No 517/2014 of the European

Parliament and of the Council of 16 April 2014 on fluorinated greenhouse gases and repealing Regulation (EC) No 842/2006²⁴, working fluids with ODP higher than 0 and GWP higher than 2500 were eliminated (R123, R21, R141b).

Considering safety criteria, working fluids were classified into 6 safety groups (A1, A2, A3, B1, B2, B3). Letter A symbolizes low toxic fluids and B are high toxic fluids. Working media with number 1 are non-flammable, 2 are flammable and 3 are explosive. Working fluids belonging to groups A3 and B1 were eliminated from further consideration (R245fa, R123, R600, R601, R601a, R21).

Remaining fluids were considered according to the technical criteria, following produced net power.

Based on the environmental, safety and technical criteria, R1233zd(E) was determined as the medium with the most suitable features for power production from low potential heat from polymer production process.

Table IV

Comparison of the organic working fluids, a²⁵, b²⁶, c²⁷, d²⁸, e²⁹, f³⁰, g³¹, h³², i³³, j³⁴.

Working fluid	ODP	GWP	Safety	P _{el,net} [MW]
R245fa	0 ^a	950 ^a	B1 ^b	3.777
R123	0.022 ^a	76 ^a	B1 ^b	4.366
R1233zd(E)	0 ^c	1 ^c	A1 ^d	4.313
R600	0 ^a	20 ^a	A3 ^b	3.843
R601	0 ^e	11 ^e	A3 ^e	4.124
R601a	0 ^f	5 ^f	A3 ^b	4.039
R365mfc	0 ^g	782 ^g	A2 ^h	3.993
R245ca	0 ⁱ	693 ⁱ	-	4.055
R21	0.01 ^a	210 ^a	B1 ^b	4.388
R141b	0.12 ^a	713 ^a	A2 ^j	4.444

Steam, on the contrary to ORC media, leaves the turbine as wet steam, which requires the turbine to be manufactured from more durable, and, thus, more expensive materials. However, Table V shows that comparing water as a working fluid and R1233zd(E), water has superior features as it is environmentally friendly, non-toxic, non-flammable, cheap and even more technically suitable working medium for power production.

Table V

Results of the system using R1233zd(E) and water steam as the working fluid.

Name	T _c [°C]	P _c [MPa]	\dot{G} [t/h]	P _{el} [MW]	P _{self} [kW]	P _{el,net} [MW]	η _{el} [%]
trans-1-chloro-3,3,3-trifluoropropene	166.45	3.624	455.3	4.8	493.0	4.3	14.1
			479.7	4.3	504.5	3.8	12.5
water	374.15	22.129	48.2	5.5	235.7	5.3	17.1
			48.2	4.9	242.6	4.7	15.2

Conclusions

The aim of this work was to create a model and calculate the main parameters of power production from waste heat in refinery by ORC and SRC, as well as to choose the most perspective working fluid.

To conclude, the most perspective working fluid in this case is water. It is environmentally friendly, safe, accessible, cheap, and even the most technically effective. Efficiency of the electric energy production by steam is more than 17 %. Using water as a working fluid, 5.3 MW of net power can be produced in winter conditions and 4.7 MW in summer conditions. The most feasible ORC working medium, R1233zd(E), delivers net power output lower by around 0.5 MW, compared to net power production by water steam.

Acknowledgement

This work was financially supported by the Slovak Research and Development Agency, Grant No. APVV-15-0148 and APVV-18-0134 as well as by the Faculty of Chemical and Food Technology, Slovak University of Technology in Bratislava.

References

1. Bonilla-Campos I., Nieto N., del Portillo-Valdez L., Egilegor B., Manzanedo J., Gaztañaga H.: *Energy Convers. Manage.* 196, 1180 (2019).
2. Wooley E., Luo Y., Simeone A.: *Sustainable Energy Technol. Assess.* 29, 50 (2018).
3. Locmelis K., Blumberga A., Bariss U., Blumberga D., Balode L.: *Environ. Clim. Technol.* 25, 42 (2021).
4. Oluleye G., Jobson M., Smith R., Perry S. J.: *Appl. Energy* 161, 627 (2016).
5. Vance D., Nimbalkar S., Thekdi A., Armstrong K., Wenning T., Cresko J., Mingzhou J.: *J. Cleaner Prod.* 222, 539 (2019).
6. Tian Y., Li S.: *Energy* 243, 123047 (2022).
7. Brueckner S., Arbter R., Pehnt M., Laevermann E.: *Energy Effic.* 10, 513 (2017).
8. Jouhara H., Khordehghah N., Almahmoud S., Delpech B., Chauhan A., Tassou S. A.: *Therm. Sci. Eng. Prog.* 6, 268 (2018).
9. Bungener S., Hackl R., Van Eetvelde G., Harvey S., Marechal F.: *Energy* 93, 220 (2015).
10. Ramanaiah V., Khanam S.: *Chem. Eng. Res. Des.* 133, 142 (2018).
11. Jamalludin K., Wan Alwi S. R., Abdul Manan Z., Hamzah K., Klemeš J. J.: *Energies* 12, 1030 (2019).
12. Chen Q., Hammond G. P., Norman J. B.: *Appl. Energy* 164, 984 (2016).
13. Gangar N., Macchietto S., Markides Ch. N.: *Energies* 13, 2560 (2020).
14. van de Bor D. M., Infante Ferreira C. A., Kiss A. A.: *Energy* 89, 864 (2015).
15. Miah J. H., Griffiths A., McNeill R., Poonaji I., Martin R., Leiser A., Morse S., Yang A., Sadhukhan J.: *Appl. Energy* 160, 172 (2015).
16. Marton S., Svensson E., Harvey S.: *Energies* 13, 3478 (2020).
17. Morandin M., Hackl R., Harvey S.: *Energy* 65, 209 (2014).
18. Guo F., Zhu X., Li P., Yang X.: *Energy* 239(E), 122345 (2022).
19. Cruz I., Wallén M., Svensson E., Harvey S.: *Energies* 14, 8499 (2021).
20. Simeoni P., Ciotti G., Cottés M., Meneghetti A.: *Energy* 175, 941 (2019).
21. Laouid Y. A. A., Kezrane Ch., Lasbet Y., Pesyridis A.: *Int. J. Thermofluids* 11, 100100 (2021).
22. Law R., Harvey S., Reay D.: *Appl. Therm. Eng.* 94, 590 (2016).
23. Veselý V., Mostecký J.: *Petrochémiá. Vydavateľstvo technickej a ekonomickej literatúry*, Bratislava 1989.
24. EUR-Lex: Regulation (EU) No 517/2014 of the European Parliament and of the Council of 16 April 2014 on fluorinated greenhouse gases and repealing Regulation (EC) No 842/2006.
25. Restrepo G., Weckert M., Brüggemann R., Gerstmann S., Frank H.: *Environmental Science and Technology*, 42(8), 2925 (2008).
26. Ashrae: Designation and Safety Classification of Refrigerants (2008). [online]. [cited 2022-02-20].
27. Honeywell: Solstice® zd (R-1233zd). [online]. [cited 2022-02-01].
28. A-GAS: R1233ZD(E). [online]. [cited 2022-02-01].
29. Zhang T., Mohamed S.: *Journal of Solar Energy Engineering*, 137(2), 021001-1 (2015).
30. Javanshir A., Sarunac N.: *ASME 2017 11th International Conference on Energy Sustainability*, 3174 (2017).
31. Abdalla M. E., Pannir S.: *16th International Refrigeration and Air-Conditioning Conference at West Lafayette*, 1564 (2016).
32. HVAC Buddy: R-365MFC Refrigerant. [online]. [cited 2022-02-02].
33. Latrash F. A., Agnew B., Al-Weshahi M. A., Eshoul N. M.: *5th International Conference on Environment Science and Engineering*, 83 (2015).
34. Whacool: R141B. [online]. [cited 2022-02-02].

THE DYNAMICS OF THE PRODUCTION OF THERMAL INSULATION MATERIALS USED IN THE CONSTRUCTION INDUSTRY

Vytlačil D.¹

¹University of Chemistry and Technology, Department of Economics and Management, Prague
vytlacid@vscht.cz

Abstract

The important field for energy savings arrangements is the construction industry. About 40% of the energy in the Europe is used in buildings. The strategy of energy consumption decreasing is usually based on the improvements of thermal characteristics of the buildings. It means, the implementation of this strategy is connected with the production of thermal insulation materials as EPS. The manufacturing companies face with the dynamics of the material production but also with the dynamics connected with the production capacity changes. The paper is focused on the description of the dynamic changes which are evoked by changes in the demand and which are very often the step changes. The model was built for the description of the behavior of this system. The model is based on system dynamics methodology and makes possible to calculate the acquisition rate according to the demand and therefore to design the capacity of the production facilities.

Introduction

We have to deal with many problems concerning energy consumption. Especially consumption of fossil fuels is important problem because of CO₂ production. The important part of consumed energy has a relationship to the operating conditions in the existing buildings. The life time of buildings can be more than 70 years. During this time building are not only built but they are refurbished several times. The energy consumption decreasing is based usually on the improvement of technical parameters of the building shell as well as heat sources. This changes require using thermal insulations.

Production of EPS in the Czech Republic in 2020 was 60200 tons (it is about 3% less than in the middle of the second decade) and about 85% is used in the construction industry for the construction of new buildings but important part is used for the refurbishment. This is the reason why to deal with the capacity of the production lines. Very important feature of the investigated system are step changes in the demand. These changes are evoked by the subsidy programs focused on the energy savings projects connected with the stock of existing buildings. The program usually takes 3 – 4 years and it means that in the end all stakeholders have to deal with fast decreasing in the demand. It means they are faced with two fast changes in the system. To solve the problems based on this feature is important task for the management of all companies included in the supply chain. Another problem nowadays can be growing interest rates which influence the investors but also construction companies (operating loans) and thermal insulation producers.

The system is described in Figure 1.

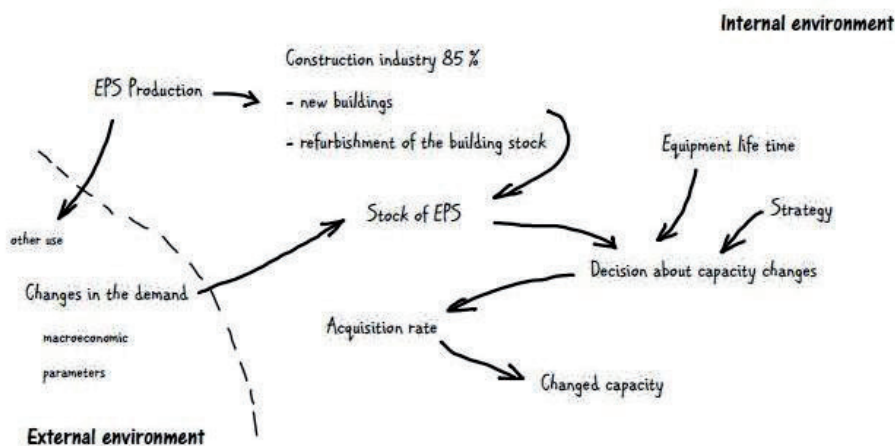


Figure 1. Problem situation – investigated system.

Method

To solve this problem, it is necessary to describe the dynamics of the distribution chains¹. The system dynamics method was used for the design of the system model². The model uses stock and flow elements as key parts of the model. Together with information links the causal loops are designed³. The calculation of the stock value changes is determined on the basis of the set off equations derived from the model structure.

Dynamic model

The dynamic model describes the changes in the supply chain¹. For this topic it is possible to find many supply chains, e.g. production and distribution of various construction materials (not only thermal insulations), the stock of future projects in the construction companies, chains related to the human resources including hiring, training. Depicted model in Figure 2 deals with the supply chain related to the capacity planning. This means that the model is able to calculate the *acquisition rate* and the amplification ratio is also evaluated according to this model. This parameter is the ratio between the increased acquisition rate and the desired change of the stock. Both input values are expressed in percentage.

The model includes as the main stock the parameter *Stock of equipment*. The equipment is used for the production of the material. This stock is decreasing by using, therefore *loss rate* is added. The main input for calculating *loss rate* is *life time* parameter of the machines (in general terms equipment). Another flow influencing this stock is *acquisition rate*. The flow depends on the structure depicted in Figure 2 and is based on the management decisions. The input for the requested changes is the converter *desired stock initial* based on the market evaluation in the future and *adjustment SE – time*.

Initial simulation was performed for the investigation of the dynamic behaviour of the system. Life time is expected 6 years and initial *stock of equipment SE* is 100 production units. According to the description of the problem situation the step change of the desired stock of the equipment is considered. The desired change of the stock is 10 % increasing, *adjustment SE - time* is 1 year. The second simulation was done for two step changes. The time interval of the higher demand was 2 years. This time corresponds to the duration of the subsidy programs which support the energy saving projects in the stock of existing buildings.

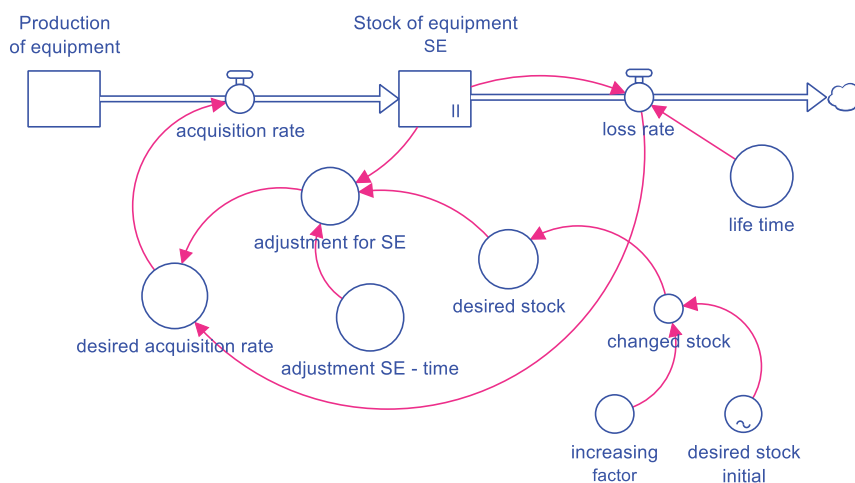


Figure 2. System model for output parameters calculation.

Results

Resultant values are depicted in Figure 3 and in Figure 4. It is possible to observe the difference between the desired stock and current value of the stock. The acquisition rate has to ensure the stock increasing but also the replacement of existing equipment. In case of two changes in the demand, the stock of equipment did not reach the desired value before the end of the time period of higher value demand.

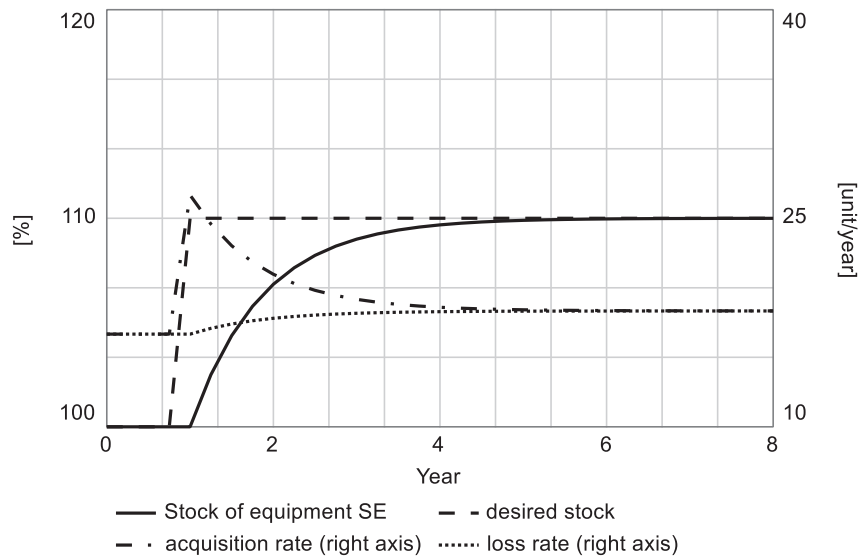


Figure 3. Changes of parameter values for one step change in the demand.

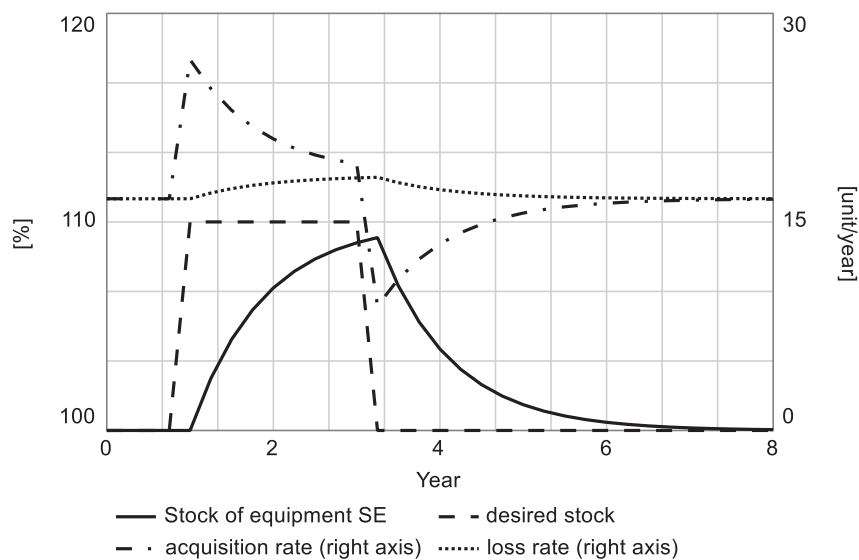


Figure 4. Changes of parameter values for two step changes in the demand.

Two parameters were investigated for finding the sensitivity to changes of *adjustment SE – time* parameter - *Stock of equipment SE* and *acquisition rate*. The parameter values are in Figure 5 and Figure 6. The adjustment time was considered from 0.5 to 2.0 years. The graphs demonstrate the high sensitivity to this parameter. The peak value of the acquisition rate is higher by 70 % when the time is decreased from 2.0 to 0.5 year. The final evaluation of the dynamic behaviour of the system was the calculation of acquisition and amplification rate for three values of demand change and three values of adjustment time. The results are depicted in Figure 7 and Figure 8.

Table I

Input values for acquisition rate and amplification rate calculations

Parameter	Values
Desired stock change (increasing) [%]	5 10 15

Parameter	Values			
Adjustment time	[year]	0.5	1.0	1.5

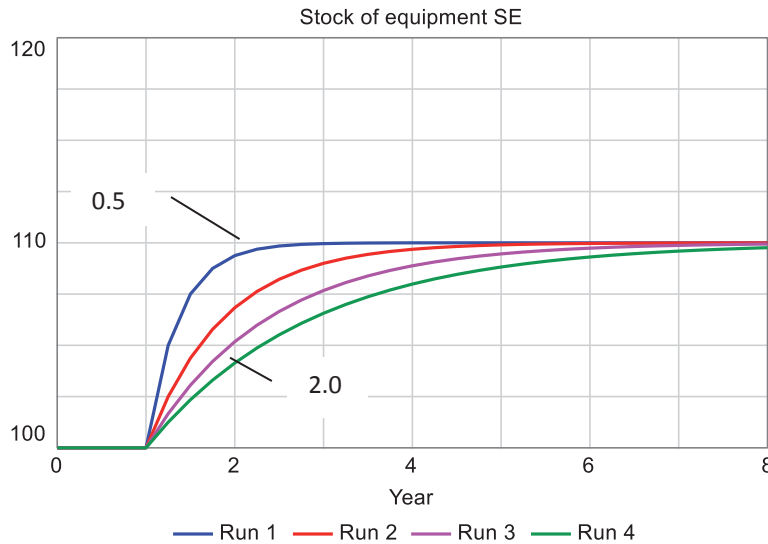


Figure 5. Sensitivity analysis – *Stock of equipment SE* - adjustment time is changed from 0.5 to 2.0 years.

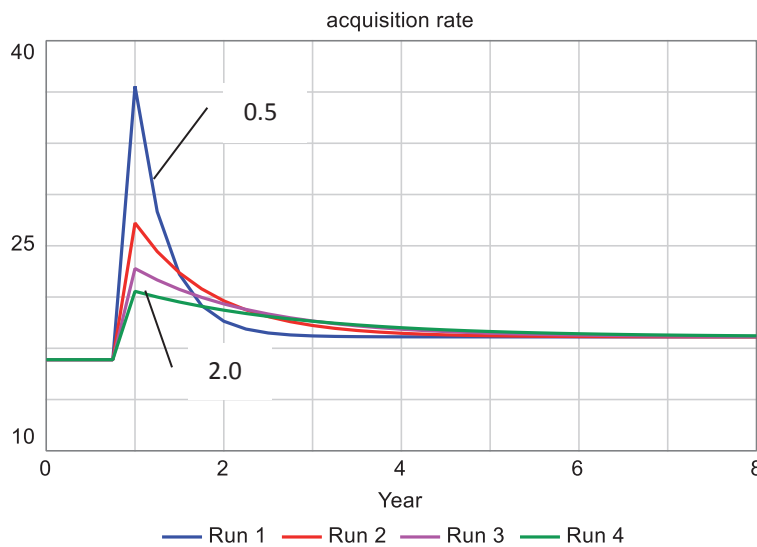


Figure 6. Sensitivity analysis – *acquisition rate* - adjustment time is changed from 0.5 to 2.0 years.

Conclusions and discussion

The dynamic model for the investigation of changes in the capital investments has been developed. The model makes possible to find out influences in the demand on the stock of equipment and production lines. In this case the model was used in EPS production sector influenced by the step changes.

The proposed model is the contribution to the sustainability in the field of the construction sector but also it solves the problem of the profitability for the EPS production company investment activities. The paper is focused mainly on the assessment of the reaction to the step change in the demand in the investigated system that is

typical for this problem situation. The changes are evoked by the external environment and very often are based on political decisions that are unpredictable.

Future work will be focused on the development of the model with the description of the *Production line* stock. This part will include also acquisition lag. Introducing this element will ensure better output from simulations concerning *amplification rate*.



Figure 7. Acquisition rate for adjustment time 0.5 – 1.5 year and desired stock change 5 – 15 %.

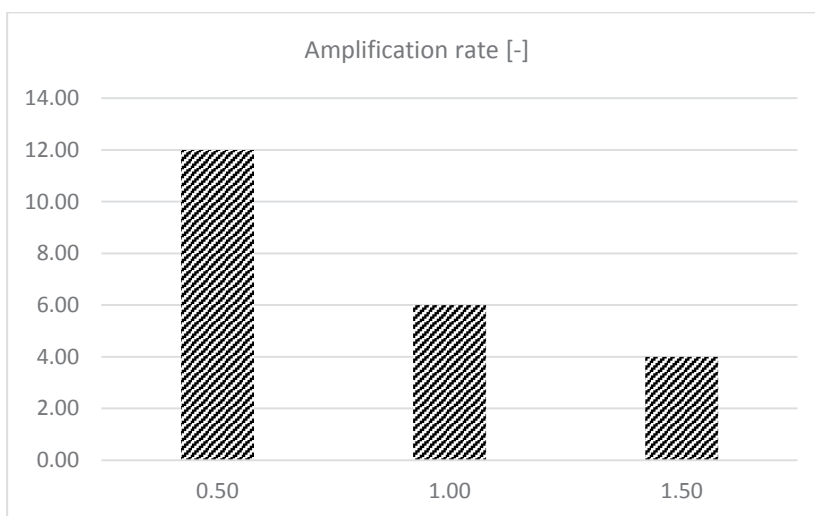


Figure 8. Amplification rate for adjustment time 0.5 – 1.5 year and desired stock change 5 – 15 %.

References

1. Sterman J.D.: *Business Dynamics – System Thinking and Modeling for a Complex World*. McGraw-Hill, Boston 2000.
2. Pidd M.: *Tools for Thinking – Modelling in Management Science*. Wiley, Chichester 2000.
3. Morecroft J.: *Strategic Modelling and Business Dynamics – A Feedback Systems Approach*. Wiley, Chichester 2008.

SYNTHESIS AND PRODUCTION OF DRUGS

TECHNOLOGY TRANSFER FOR THE DRY GRANULATION PROCESS AIMING AT KEEPING IDENTICAL RIBBON PROPERTIES

Jan Petr,^{1,2} Petr Zamostný¹, Pawel Stasiak²

¹Faculty of Chemical Technology, University of Chemistry and Technology Prague, Technická 5, 166 28 Prague 6 - Dejvice, the Czech Republic

²Pharma Development, Zentiva, k.s., U Kabelovny 130, 102 00 Prague 10 - Dolni Mecholupy, the Czech Republic
jan.petr@vscht.cz

Abstract

Dry granulation (DG) process is common technique, where a bulk solid (feed powder, FP) is subjected to a consolidation stress to get the ribbons. Granulation by roll compaction is a process in which powder particles are compressed to adhere to each other, resulting in larger, multi-particle entities (granules) with better flow properties. The FP is deformed plastically by compression, whereby its volume is reduced, and its bulk density is being increased. Different designs of the roller compactors and interactions between process parameters and raw material properties affect the ribbon texture.

The objective of this work is to predict the ribbon stiffness parameter of model drug formulation manufactured using different types of roller compactors and scale sizes, respectively.

Introduction

The existence of different roll-compactor designs and diversity of operational parameters and material properties render the interpretation of the intrinsic properties of the intermediate products (ribbons and granules) and the resulting properties of the tablet difficult. Therefore, quality of intermediate products should be maintained across the different unit operations of the process²⁻⁴. The ribbon properties are identified by peak pressure [MPa], Figure 1. Highest level of the bulk solid strain is expressed as solid density of the ribbon¹, and its value is not measured by roller compactor type of Alexanderwerk AG, and Gerteis AG. Extent of the compaction process is being measured by indirect indicators such as being a specific compaction force, SCF [kN/cm] (Gerteis AG), and a hydraulic pressure, pHYD [bar] (Alexanderwerk AG).

The stiffness parameter k [N/mm] for compressed material using the consolidation stress¹, thus the ribbon stiffness from a roller compaction process⁶, has been selected to find the technology transfer for this type of DG process and it might compare different scale size. The approach of indirectly measured the peak pressure, where the various setups of the roller compactor might be predicted by uniaxial compression test on the powder compaction analysis system (Gamlen Instruments, UK). It will be further attached for improving precision of technology transfer and scale up studies. We have tested one API as model formulation in this report.

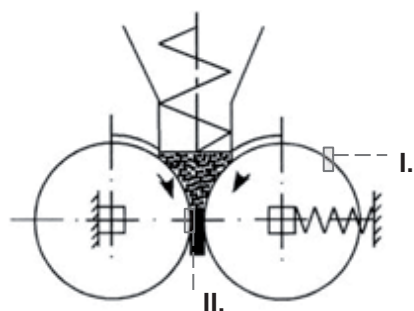


Figure 1. Design of a roller compactor and FP loading⁵ (loose powder is compressed in a ribbon texture and thereby undergoes plastic deformation¹).

- I. SCF, specific compaction force⁶ (Gerteis AG), or pHYD, hydraulic pressure (Alexanderwerk AG);
- II. region with a peak pressure – the FP is densified to the ribbons.

Experiment – materials and methods

In this work, several batches comprising different ribbons of model API were prepared. Differences were in the compressive stress exerted on the FP and the roll speed parameter according to selected size of the scale (Alexanderwerk AG, Gerteis AG).

Materials

Atorvastatin calcium trihydrate in crystalline form (MSN Pharmachem Pvt.Ltd., Telangana, India) was selected as model API. Microcrystalline cellulose (Avicel PH-102, Mingtai Chemical Co.Ltd., Bah-Der District, Taiwan) as a filler/binder, and calcium carbonate precipitated (Scora, Caffiers, France) as diluent (dissolution aid in dispersion process), buffering agent, and opacifier⁷ were main pharmaceutical excipients in this model formulation, Table I. Three batches were created at production scale (Alexandewerk AG), and six batches at laboratory scale (Gerteis AG).

Table I Feed powder (input material) for DG process by roller compaction process

Model API	Excipient
	- major excipients for DG process
atorvastatin 12.92 % (mass fraction, w/w [%])	calcium carbonate 36.64 %
	cellulose microcrystalline 33.27 %

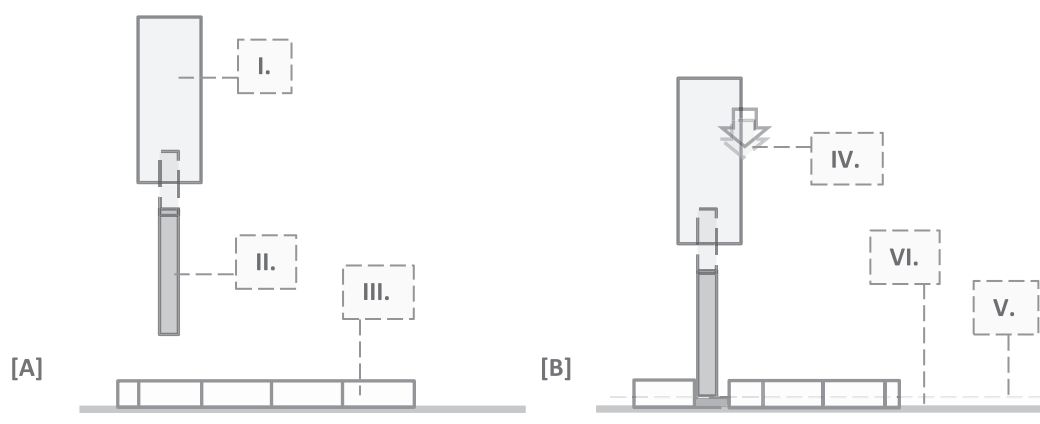
Methods

Texture analysis of densified FP – ribbon texture analysis

The texture analysis technique (TA) evaluates effectiveness of each compaction mode on the equipment (Alexanderwerk AG, and Gerteis AG) and strength uniformity of the ribbon texture respectively.

The ribbons are exposed the compression testing with needle (probe), Figures 2-[A], [B]. In the vertical direction, positive normal stress (compressive stress) is exerted¹ on the ribbon texture surface in the specific length intervals from the ribbon edge for model API. In result, ribbon texture was indented up to the end condition of the test; the final distance is set up to the value of 1 mm from the surface of area of CTX texture analyzer (AMETEK Brookfield, USA). From the correlation between a ribbon loading (force) and a ribbon depth (set length of the track for probe to achieve the end condition of test), the slope at the point of maximum force gradient was recorded and labelled as ribbon stiffness, k [N/mm], Figure 3.

The ribbon uniformity was recorded by ribbon stiffness profile in its traverse direction (ribbon width, Figure 4); calculated individual ribbon stiffness points from the measurements by compression test (needle indentation to the ribbon texture) at specific interval length from the ribbon edge. From the ribbon stiffness profiles measured by TA, the mean integral ribbon stiffness value, k -MEAN [N/mm], was further calculated. The k -MEAN parameter is output evaluated parameter at the ribbon level, and it represents ribbon stiffness, k , as a whole.



Figures 2-[A], 2-[B]. The test type compression on the CTX texture analyzer; graphical scheme of one measurement.

NOTE: I. CTX Texture Analyzer, II. needle (probe), III. ribbon (model API), IV. test type compression, V. final distance (test end condition), VI. surface of the area of the CTX TA.

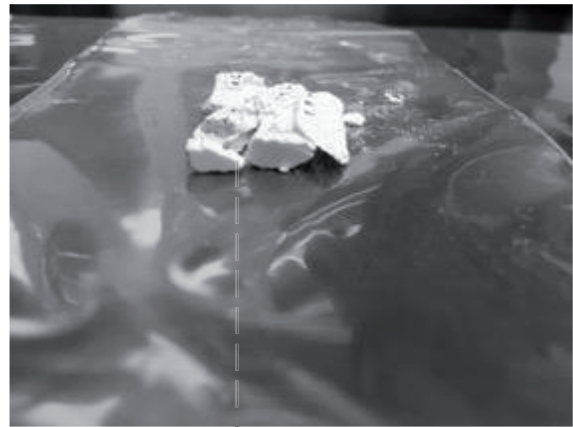


Figure 4. The ribbon specimens after the compression tests on the CTX TA. SCF 9.6 kN/cm; Gerteis AG.

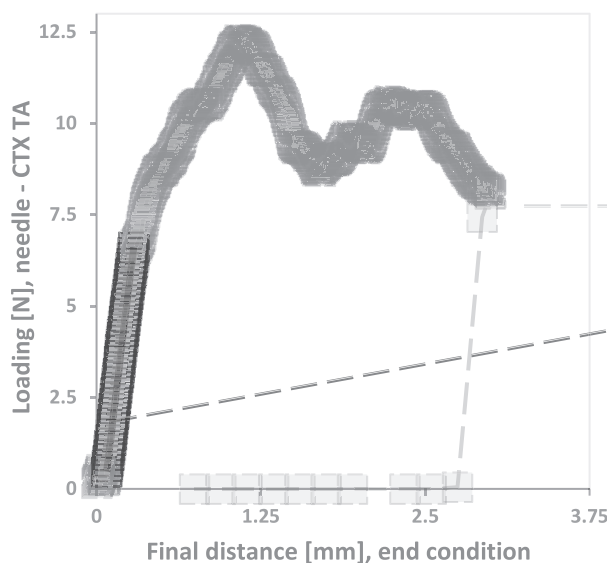


Figure 3. Track of needle (probe on the CTX TA) to the end condition of compression test (black length interval); the result: one measured point of the local stiffness k [N/mm].

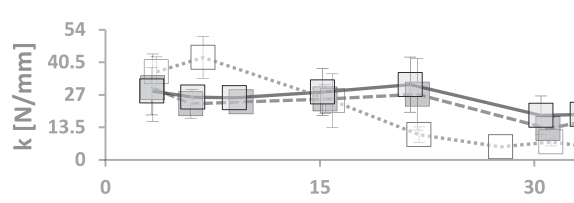
Individual ribbons were tested by TA technique along the measured points on the ribbon texture. Following ribbon the ribbon width, regardless of applied type of scale size, the stiffness profile was extensive, Figures 5 and 6. Therefore k [N/mm] has been selected as output property at the compactors (Alexanderwerk AG, Gerteis AG).

Alexanderwerk AG

The ribbon width was up to 50 mm of length. It was not roller (75 mm), Figure 5. Model API was tested with the compacted material had not been exposed to uniform profile. The cause is unequal filling of the gap in compression type (high with curves) using hydraulic pressure, the local hydraulic pressure (compaction pressure, particles are compacted in the peripheral part of the ribbon of the ribbon. The particles are not enough compacted hydraulic pressure, the particles were produced using firm-rolled as the side thickness, regular shape and better ribbon uniformity measurement of the ribbon stiffness profile. The ribbon instances. Exception was the lowest value of SCF that width; the size of ribbon width was up to length about SCF (11.2, 12.5), the ribbon texture will be laminated between compacted model API and roll surface. This is grided roll surface after finishing these operation process ribbon. This is consequence of the particle over-compaction.

Roll compaction

The preparation of ribbons was performed using two types of roller compactor Gerteis, Mini-Pactor [250/25] (Gerteis Maschinen+Processengineering AG, Switzerland; laboratory scale) and Alexanderwerk WP 200 [200/75] (Alexanderwerk AG, Germany; production scale).
 Gerteis, Mini-Pactor [250/25]: The six batches with variability of specific compaction pressure (12.5 kN/cm) were compacted. The roll gap size (3.5 mm) and roll speed (3 L setting of this equipment type).
 Alexanderwerk, WP 200 [200/75]: The three batches with hydraulic pressure size (3.5 mm) and roll speed (14 UPM) were manufactured. The ribbons width was achieved for each set of conditions³.



Discussion and result analysis

The ribbon stiffness profile in its traverse direction, calculation of the k -M-Law values

The roll gap size, roll speed and compressive stress on the FP described using SCF and/or PHD were controlled by the fully automatic operation modes on the equipment (Alexanderwerk AG, Gerteis AG). Obvious differences have been found in the ribbon texture by TA technique. The ribbon stiffness parameter k , [N/mm] has these advantages. It should correspond to the ribbon apparent density [g/L]. And this measured ribbon feature furnish possibility to transfer technology with scale-up.

Figure 5. The ribbon stiffness profile from Alexanderwerk compaction pressure, PHD (120-140-160 bar).

Gerteis AG
 The ribbons were produced using firm-rolled as the side thickness, regular shape and better ribbon uniformity measurement of the ribbon stiffness profile. The ribbon instances. Exception was the lowest value of SCF that width; the size of ribbon width was up to length about SCF (11.2, 12.5), the ribbon texture will be laminated between compacted model API and roll surface. This is grided roll surface after finishing these operation process ribbon. This is consequence of the particle over-compaction.



[A]



[B]

Figure 7. Comparison of the ribbons from Gerteis, Mini-Pactor [250/25] ([A], SCF 9.6 kN/cm) and Alexanderwerk, WP 200 [200/75] ([B], pHYD 160 bar).

Technology transfer with keeping equal ribbon stiffness as process parameter

The relationship between mean integral value of ribbon stiffness, *k-MEAN*, and material loading on the roller compactor (SCF/pHYD) by using range of operating parameters from two scales (Alexanderwerk AG, Gerteis AG) has been obtained. The load applied on the bulk solid consolidation is expressed differently in accordance with type of dry compaction equipment (scale size). Gerteis AG company operates with SCF parameter. On other hand the hydraulic pressure (pHYD) being typical process parameter for Alexanderwerk AG as manufacturer. Dry compaction equipment manufacturers provide a conversion relationship between SCF and pHYD parameters, and its use respectively. It was not possible to use these mathematical equations for the conversion SCF to pHYD and conversely. Derived SCF value for Alexanderwerk, WP 200 is not identical with SCF for Gerteis, Mini-Pactor, and this leads to the ribbons with different values of *k-MEAN*.

Therefore, we acceded to new solution of technology transfer, where the design of new regression model have been based on the conversion of compressive parameters mentioned above (SCF, pHYD) to satisfy the matching condition of the target intermediate product property (*k-MEAN* for purpose this report here). The general principle of this procedure is to find a compressive parameter that generates ribbon with the same properties; *k-MEAN* as parameter represents material resistance and material apparent density in model API respectively. Particular ribbon stiffness, its *k-MEAN* value, is the main attribute for comparing different modes of compressive stresses¹ (SCF, pHYD) at two types of compaction equipment, Figures 8-[A], [B]. The pHYD and SCF values for both devices, taken off for the same *k-MEAN* value, are a prediction of the conditions that lead to identical intermediate product (ribbon) on these different compaction devices (scale size), Figure 9. It is elementary knowledge for understanding of successful and perspective technology transfer. This relationship is described by regression equation [A], which might be modified to equation [B] to turn the technology transfer backwards.

$$\text{pHYD}_{\text{AW}} = e^{(1.955 + 1.6776 \cdot \ln \text{SCF}_{\text{GER}})} - 177.39 \quad \text{Equation [A]}$$

$$\text{SCF}_{\text{GER}} = e^{[0.5961 \cdot \ln(\text{pHYD}_{\text{AW}} + 177.39)]} - 1.1654 \quad \text{Equation [B]}$$

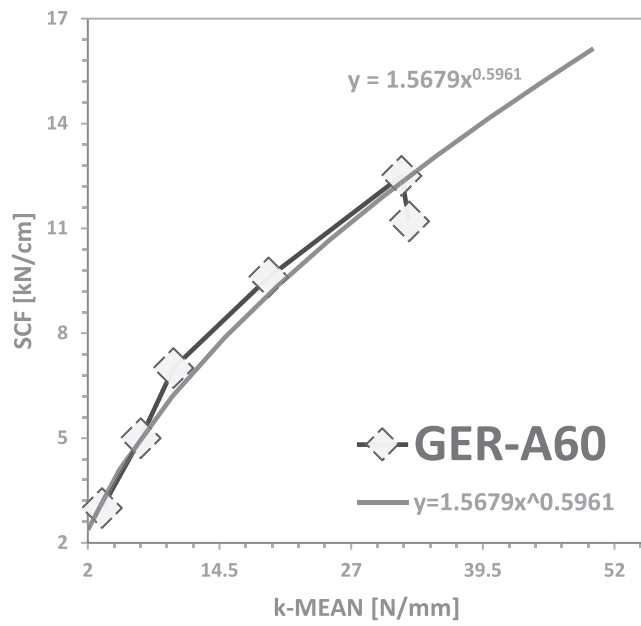


Figure 8-[A]. Gerteis, Mini-Pactor [250/25], k-MEAN parameter for A-60 as model API.

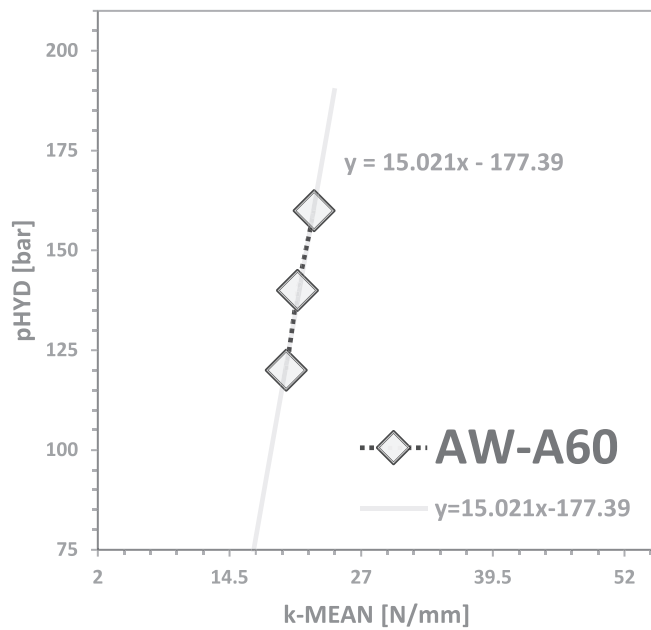


Figure 8-[B]. Alexanderwerk, WP 200 [200/75], k-MEAN parameter for A-60 as model API.

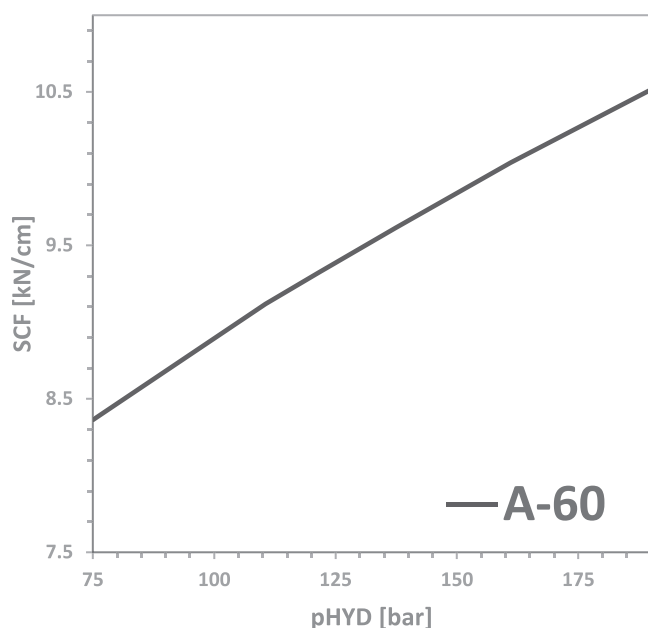


Figure 9. The correlation between two roller compactors Gerteis, Mini-Pactor [250/25] and Alexanderwerk, WP 200 [200/75]. The k-MEAN parameter for A-60 as model API has the same values for these conditions of compressive stress¹ on both compaction devices.

Conclusion

Regression models based on conversion of the compression parameters such as hydraulic pressure, and specific compaction force were developed. The combination of those models for different compactors yielded a conversion equation, which could facilitate the technology transfer maintaining constant ribbon stiffness on studied formulation. Further work is needed to validate, whether the conversion can be generalized also for different materials to further help with the technology transfer process.

Acknowledgement

This work was supported from the grant of Specific university research – grant No.: A1 FCHT 2022 006.

References

1. Schulze D.: Powders and Bulk Solids. Springer-Verlag, Berlin, Heidelberg 2008.
2. Kuntz T., Schubert M. A., Kleinebudde P.: Eur. J. of Pharm. and Biopharm., Elsevier, 77, 164 (2011).
3. Perez-Gandarillas L., Perez-Gago A., Mazar A., Kleinebudde P., Lecoq O., Michrafy A.: Eur. J. of Pharm. and Biopharm., Elsevier, 106, 38 (2016).
4. Sun W.-J., Rantanen J., Sun C. C.: Pow. Tech., Elsevier, 338, 162 (2018).
5. Bröckel U., Meier W., Wagner G.: Product Design and Engineering. 1, Wiley-vch, Weinheim 2007.
6. Toson P., Lopes D. G., Paus R., Kumar A., Geens J., Stibale S., Quodbach J., Kleinebudde P., Hsiao W.-K., Khinast J.: Inter. J. of Pharm.: X, Elsevier, 1, 1 (2019).
7. Rowe R. C., Sheskey P. J., Quinn M. E.: Handbook of Pharmaceutical Excipients. Pharmaceutical Press and American Pharmacists Association, 6th edition, Washington, DC 2009.

EFFECT OF THE MIXING STRATEGY ON THE UNIFORMITY OF POWDER MIXTURES FOR DIRECT COMPRESSION

Römerová S., Novák D., Zámotný P.

University of Chemistry and Technology Prague, Department of Organic Technology, Technická 5, 166 28, Prague 6 - Dejvice, Czech Republic

Simona.Romerova@vscht.cz, Petr.Zamotny@vscht.cz

Abstract

In the direct compression of tablets, it is crucial to have the input tableting mixture well homogenized. Widely used tumbling blenders are usually not very effective in the disintegration of aggregates of cohesive powders, which can be vital in such mixtures. Therefore, specific strategies, such as subdividing the mixing process into multiple steps and introducing sieving before each one of them, are being adopted in industrial practice.

Presented work deals with an active substance (API) incorporated into the placebo mix intended for direct compression, where some specific mixing strategy is necessary. For each of the evaluated mixing processes for its preparation the final mixture homogeneity (variation coefficient, CV) and complexity (process complexity index, PCI) were evaluated. Based on these process properties, the most promising for the manufacturing of the tested API proved a process consisting of two mixing steps with one sieving, which represents simplification compared to the process currently utilized in the industry.

Introduction

Tablets persist as the most common pharmaceutical dosage form nowadays. The preferred process of their preparation is direct compression (DC). Technically, it is a quite simple process of tablet production consisting only of material mixing (frequently with gradual addition of the processed material) and subsequent compression of prepared mixture into tablets. Moreover, it is usually the easier and cheaper variant than other frequently used operations for tablet preparation, wet granulation or roller compaction. However, the DC process is still very complex in terms of resulting mixture homogeneity, which is not secured like in the granulation processes, and its stability during manipulation.¹

The blend for direct compression does not undergo extensive process steps (like the creation of interactive mixtures during wet granulation), so high levels of homogeneity are necessary. Ideally, a homogenous mixture exhibits the same composition and properties in all of the samples taken from different positions in the bulk powder mixture. In practice, the samples are never exactly the same, crucial is the level of variance between them. The variance is closely connected to the sample size, which needs to be chosen correctly to give representative results.²

The crucial step in the DC is therefore mixing, which can be described as a transfer of particles relative to each other until the maximum level of disorder is achieved.³ Widely used tumbling blenders are well suitable for larger amounts of mixed material and they are easy to maintain and clean.⁴ They are designed as closed containers of various shapes rotating around an axis and the most dominant mixing mechanism is diffusive mixing.⁵ However, this mechanism is not very effective in the disintegration of clusters/aggregates of particulate materials.⁴ Adding baffles inside the mixing container or incorporating more complicated mixing strategies can overcome the disintegration issue to some extent.⁵

The specific strategies, such as subdividing the mixing into multiple steps and introducing sieving before each one of them, are routinely being adopted in industrial practice. The topic of assessing the appropriate mixing strategy to achieve the desired level of homogeneity in the resulting mixture is not widely explored. However, Some studies have been published on the topic of the influence of mixing technique and excipient characteristics on the low dose tableting mixture development.⁶ The presented work deals with a mixture intended for direct compression, where some specific mixing strategy is necessary. The main objective is to examine and describe different mixing strategies consisting of different steps, compare them according to resulting homogeneity and process complexity and recommend the ideal process for industrial use.

Materials and methods

Experiments were performed on a model mixture having 5.6 wt.% drug loading. It consisted of a placebo (excipient mixture) and a specific drug batch with a specific particle morphology, which is quite problematic in direct tablet compression. The tested mixing processes consisted of a different number of mixing steps, some with preceding sieving.

Materials

As mentioned above, model active substance (API) was a specific batch of API commonly used in direct compression processes, having small, needle-like crystals (Figure 1). The complementary placebo mixture consisted of microcrystalline cellulose (Avicel PH102), pregelatinized corn starch, crospovidone (Polyplasdone XL), colloidal silica (Aerosil 200) and yellow iron oxide. All of the materials were kindly provided by Zentiva, k.s.

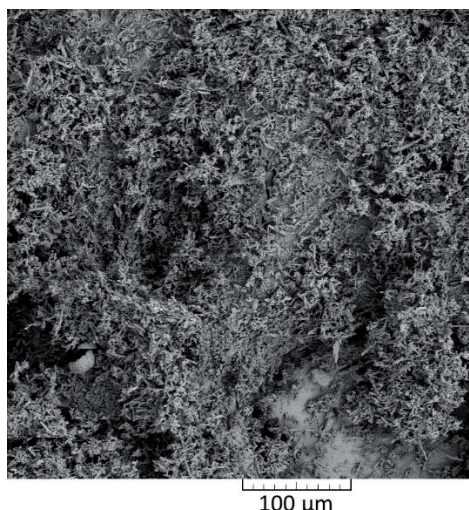


Figure 1. SEM picture of model API batch used in the presented work. 500x mag.

Model mixtures preparation

Model mixture composition for each of the tested mixing processes weighs 10 g in total. The placebo was divided into 1 – 3 doses which were added gradually according to the number of mixing steps in the respective tested mixing processes (Table I).

Table I. Model mixture and placebo mixture compositions.

Material	w, %	m, g
API		0.58
placebo mixture (3 doses)		3 × 3.22
- microcrystalline cellulose	78.4	
- pregelatinized corn starch	15.3	
- crospovidone	3.4	
- colloidal silica	2.8	
- yellow iron oxide	0.1	
Total		10.24

Mixing was performed on Turbula T2F 3D-mixer (Willi A. Bachhofen AG, CH), total mixing time for all processes was 60 minutes at 55 rpm, where each dose of placebo mix, which was added in a certain process step, corresponds to 20 minutes of mixing. Individual tested mixing strategies are summarized in Figure 2. They can be generally distinguished by the number of mixing steps involved (one, two or three), while before each one of the mixing steps there can be sieving involved.

For a better orientation in the scheme presented in Figure 2, there is an example of the workflow while preparing the model mixture according to the process P9. In the first step, the API and one dose of placebo mixture were weighed, transferred to the sieve shaker AS 200 (Retsch GmbH, DE) equipped with a test sieve having a mesh size of 710 µm and sieved. Then the sieved mixture was transferred to a homogenization vessel and mixed for 20 minutes. To the obtained premix, additional two doses of placebo were added and all materials were directly mixed for 40 minutes.

Another process from Figure 2 worth mentioning is the one marked as P11 since it is mimicking preparation of such low dosed direct compression mixtures mostly utilized in the pharmaceutical industry.

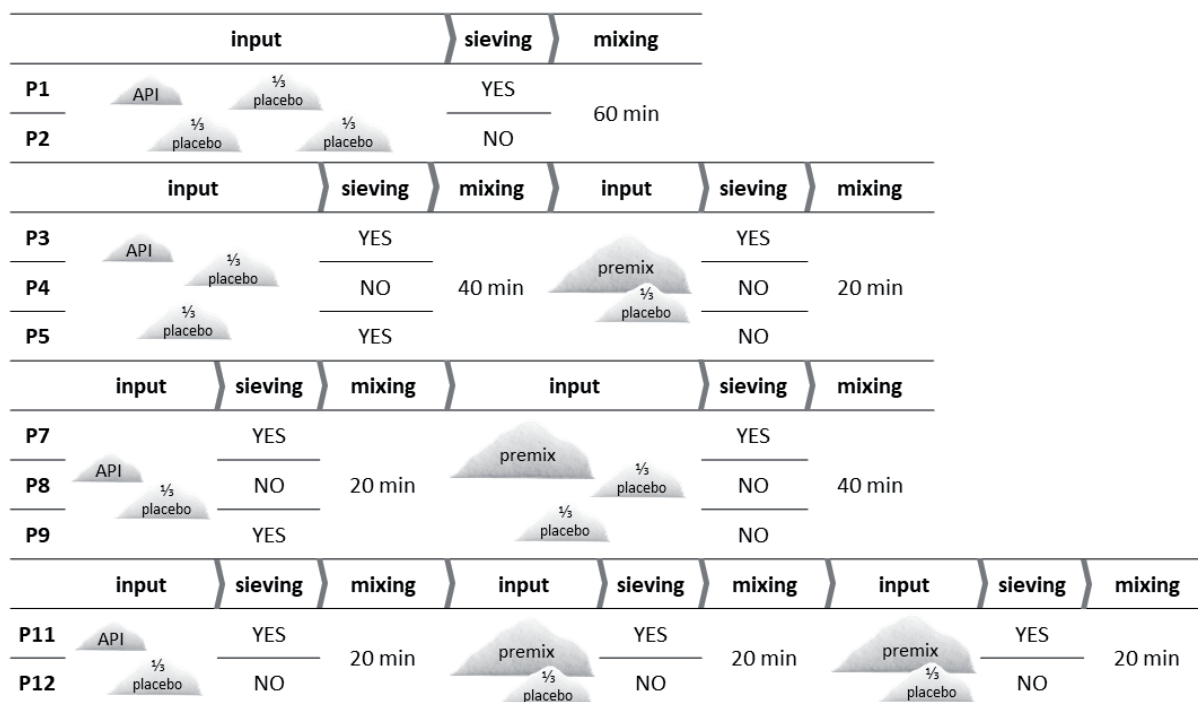


Figure 2. Schematic representation of mixing processes for model API direct compression mixture preparation evaluated in the presented work.

Homogeneity of model mixtures

After each of the mixing processes is completed, six samples (approximately 1 g) are taken straight out of the homogenization vessel from different positions (see Figure 3). These samples were then prepared for HPLC analysis (Prominence LC 20 with PDA detector, Shimadzu, JPN), in order to assess the model active substance concentration in them. It was subsequently used to calculate an amount of the API that would be present in a hypothetical tablet prepared from this particular sample. These values were compared between every six samples belonging to each of the mixing processes and their coefficient of variance (CV, %) was used for describing the mixtures' homogeneity.

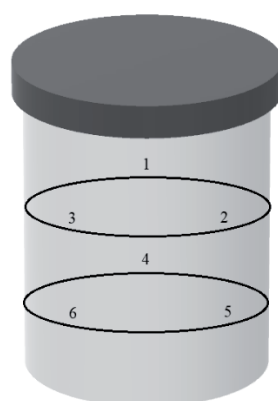


Figure 3. Positions for sampling from the homogenization vessel.

Process complexity

Each one of the tested mixing processes, if performed at an industrial scale, would have different time, personnel and equipment demands. All of these requirements were quantified in a form of a process complexity index (PCI, -). It combines the contributions of all the individual steps required for mixture preparation using a given mixing process (Equation 1).

$$PCI = S + C + M + T \quad (1)$$

The process steps taken into consideration are mixture sieving (S), equipment cleaning (C), mixing (M) and material handling (T). Furthermore, each of the steps has its own level of significance, as explained in Table II.

The *PCI* is a relative quantity and its values are in the range of 0 - 1, where 1 indicates the most demanding process (specifically in the model case, it is an industrially used process P11).

Table II. Process steps included in the process complexity index (*PCI*) calculation and their respective significance.

Process step		% of <i>PCI</i>	Value based on
sieving	(S)	50	amount of mixture sieved
cleaning	(C)	25	type of cleaned equipment
mixing	(M)	15	number of mixing steps
manipulation	(T)	10	number of mixture transfers between the equipment

To clarify the calculation, Equation 2 presents an example for process P9.

$$\begin{aligned}
 PCI &= S + C + M + T = 0.5 \cdot \frac{n_S}{n_{S,max}} + 0.25 \cdot n_C + 0.15 \cdot n_M + 0.1 \cdot \frac{n_T}{n_{T,max}} \\
 &= 0.5 \cdot \frac{0.33}{2} + 0.25 \cdot 1 + 0.15 \cdot 0.66 + 0.1 \cdot \frac{6}{12} = 0.482, \quad (2)
 \end{aligned}$$

where n_S stands for the amount of sieved placebo mixture (for process P9 it is only one dose, 1/3 of the placebo) and $n_{S,max}$ is the respective value for process P11 (where the amount of placebo is eventually sieved twice – 1/3, 2/3 and 3/3 in the three respective mixing steps), the values of n_C were set up as a qualified estimation (for the sieve the value is 0.75, for a tumbling container 0.25, if both of the equipment is used, n_C equals to 1), n_M reflects the number of mixing steps in each process (one step has a value of 1/3) and finally n_T and $n_{T,max}$ stand for the number of manipulation steps for the evaluated process and process P11, respectively.

Discussion and result analysis

The resulting homogeneity obtained after each one of the tested mixing processes was evaluated while taking pharmacopoeial limits into account. Thus, only the processes producing mixtures with variation coefficient values lower than 5 % were considered suitable for possible model mixture production. All of the *CV* values are summarized in Table III.

From these results, it can be observed, that the sieving step before any mixing of this particular model blend is crucial for obtaining a suitable homogeneity. However, it turned out that it is not necessary to perform it before each step. It has a significant role mostly in the first step (out of 1 – 3), where the drug is added.

Table III. Resulting homogeneity of the model mixture prepared using each one of the tested process variants and their respective process complexity indices.

Mixing process	P1	P2	P3	P4	P5	P7	P8	P9	P11	P12
<i>CV</i> , %	2.28	24.94	6.49	11.29	4.86	3.34	9.27	2.81	2.36	16.64
<i>PCI</i> , -	0.58	0.13	0.83	0.20	0.57	0.75	0.20	0.48	1.00	0.26

Then, the information about mixture homogeneity (*CV*) was correlated with the complexity of the individual processes (*PCI*) as also presented in Table III. In general, an ideal mixing process would be the one with values as low as possible for both of the studied parameters.

From Table III, it can be also confirmed, that processes without any sieving included are not suitable for model mixture preparation, since they present poor homogeneity (too high values of variance between obtained samples). Namely, these are processes marked as P2, P4, P8 and P12. There is also one process, where sieving was included, however, the homogeneity is not suitable for possible utilization in the industrial practice, process P3.

On the other hand, there are processes, between the evaluated ones, that are less demanding while having suitable levels of variation coefficient. These can be divided into two separate groups. The first group would be comprised of processes P1 and P7, which are in the range of 60 – 80 % of the reference, industrially used, process P11 complexity. The second group would then be occupied by the two least demanding processes (marked as P5 and P9). Especially, process P9 consisting of only two steps and one sieving showed very promising results (final

mixtures' coefficient of variation $CV = 2.81\%$ comparable to the original process P11 ($CV = 2.36\%$). In general, these two processes represent a certain simplification in comparison with the industrially used process P11.

Conclusion

During the experimental part of the presented work, 10 different mixing approaches were tested on a model mixture intended for DC production of tablets. As the sieving step is usually quite time-consuming in the industry, its necessity and the number of mixing steps where it needs to be incorporated were examined closely. Alternatively to the commonly used approach of placing the sieving before each one of the mixing steps, quality by design approach was demonstrated to identify the necessary critical steps and adjust the mixing process strategy. Out of the 10 tested mixing strategies, two consisting of two mixing steps and one sieving at the beginning showed suitable homogeneity, comparable with mostly used process strategy (three mixing steps, all with preceding sieving) in the industry, while having a lower time, equipment and personnel demands. Incorporation of one of them into the industrial practice could significantly streamline the model mixture preparation. The proposed system of experiments can be, after some further validation, adopted as a profiling approach to prevent overdesigning in the newly developed direct compression processes or to re-evaluate the complexity of already established ones.

Acknowledgement

This work was supported from the grant of Specific university research – grant No.: A2_FCCHT_2022_009.

References

1. Thoorens G., Krier F., Leclercq B., Carlin B., Evrard, B.: *Int. J. Pharm.*, 473, 64 (2014).
2. Lamotte T.: *Chem. Process.* (2018).
3. Hickey A. J.: *Pharmaceutical Process Engineering*. Taylor & Francis, Abingdon 2001.
4. Perry R. H., Green D. W., Maloney J. O.: *Perry's chemical engineers' handbook. 7th ed.* McGraw-Hill, New York 1997.
5. Rhodes M. J.: *Introduction to particle technology*. John Wiley & Sons, Hoboken 2008.
6. Alyami H., Dahmash E., Bowen J., Mohammed A. R.: *PLoS One*, 12 (2017).

MECHANISMS OF TABLET DISINTEGRATION AND DRUG RELEASE – TOWARDS THE DEEPER UNDERSTANDING OF THE DISSOLUTION PROCESS

Zámotný P., Bittner R., Dufková K., Römerová S.

*University of Chemistry and Technology Prague, Department of Organic Technology, Technická 5, 166 28, Prague 6 - Dejvice, Czech Republic
petr.zamostny@vscht.cz*

Abstract

This paper describes a technique of in vitro monitoring of fragment population generated from a tablet during the dissolution test using static light scattering and optical microscope combined approach. A mathematical model is suggested for processing the experimental data by regression analysis to obtain the rate constant of critical processes involved in the disintegration. A case study is present to demonstrate the possible application of the method for comparing alternative formulations using two different marketed formulations of ibuprofen. In those formulations, the primary erosion of the tablet was successfully identified as the rate-controlling parameter for the dissolution. The proposed technique can be used to streamline the formulation efforts on a developed dosage form and for troubleshooting the development of drug generics. Also, it can be used as a tool for studying the microstructure effects in compressed solid dosage forms on dissolution kinetics.

Introduction

The dissolution performance of a solid dosage form is pre-determined by its disintegration process. The disintegration is a complex process of tablet break up, which occurs in body after liquid penetration into the porous matrix of the tablet and is dependent on the tablet microstructure (Figure 1).

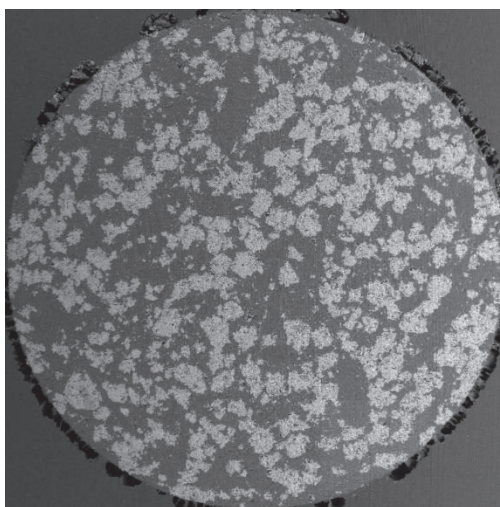


Figure 1. SEM picture of a tablet cross-section illustrating the tablet micro-structure.

The pharmacopoeial method for testing disintegration is very simple and it is not suitable for studying detailed disintegration kinetics. New techniques to measure fragmentation during disintegration could help to understand the process better and establish the relationships between the tablet structure and the disintegration process kinetics¹. Methods based on monitoring water uptake² are used for determining the disintegrating force of disintegrant and tablet mechanical properties in wet state. Imaging techniques (light microscopy, scanning probe microscopy, high-speed video imaging or real-time magnetic resonance imaging)³ are best suited for understanding the mechanisms of particle release. Techniques based on particle size distribution (PSD) can be utilized to provide information on particle population development. Those techniques involve light scattering⁴, micro CT⁵, or focused beam reflectance measurement⁶ and they provide data for mathematical modeling of the disintegration process.

The present work is focused on using combined in vitro monitoring of fragment distribution and fragment generation kinetics of different formulations and using a regression model to identify controlling steps of the disintegration process.

Materials and methods

Commercially available tablets containing 400 mg of ibuprofen per tablet, Ibalgin 400 (Zentiva) and APO-Ibuprofen 400 (Apotex), were used for the study. Disintegration experiments on all tablets were performed using laser diffraction particle size analyzer Mastersizer 3000E, Malvern, UK using Hydro EV unit filled with 500 ml of distilled water at laboratory temperature. Tablets were placed in tablet holder, magnetically mounted to a fixed position on the beaker wall. The agitator speed was set to 1000 rpm or 1300 rpm to ensure sufficient fluid flow and prevent sedimentation of particles. PSD were recorded each minute using a 10 s measurement period followed by a 50 s pause.

Dissolution test was performed using dissolution apparatus Sotax AT7 Smart, Sotax AG, CH at 37 °C using paddles at 50 rpm. 900 ml of pH 7.2 phosphate buffer was used as a dissolution medium. Samples were taken after 2, 5, 10, 15, 30, 45 and 60 minutes of measurement using a dissolution sampler with a polypropylene filter and syringes.

The data obtained from the disintegration experiments were processed using a regression model. The model was based on the fragment population balance according to the Figure 2. The model involves balance equation (1) for mass of the i -th fragment and equation (2) for soluble part thereof. These parameters are dependent on erosion rate $r_{e,i}$, secondary disintegration rate of fragments $r_{d,i}$ and the dissolution rate r_{dis} . Parameter φ_i characterizes the amount of soluble part in mixture.

$$\frac{dm_i}{dt} = r_{e,i} \cdot S_{6i} - r_{d,i} + \sum_{j=i+1}^5 r_{d,j} S_{ji} - r_{dis,i} \quad (1)$$

$$\frac{dm_{s,i}}{dt} = r_{e,i} \cdot S_{6i} \cdot \varphi_i - r_{d,i} \cdot \varphi_i + \sum_{j=i+1}^5 r_{d,j} S_{ji} \cdot \varphi_j - r_{dis,i} \quad (2)$$

Erosion and disintegration rate could be described by erosion and disintegration constants multiplied by appropriate selectivities $k_e \cdot S_{6i}$ and $k_{d,i} \cdot S_{ji}$. Constant k_{dis} is dependent on surface, volume and weight of particles m_p (5)

$$r_e = k_e \cdot m_6^n \quad (3)$$

$$r_{d,i} = k_{d,i} \sqrt{m_i} \cdot (m_{sublim,i} - m_{sub,i}) \quad (4)$$

$$r_{dis,i} = k_{dis} \cdot \frac{1}{d_i} \cdot m_{s,i} \quad (5)$$

Primary fragment is formed by the erosion of tablet, which depends on the amount of mixture inside tablet m_6 (mg). Disintegration of that fragment is dependent on its weight m_i and also on the difference between $m_{sublim,i}$ (weight of all fragments with an index lower than i in equilibrium) and $m_{sub,i}$ (actual weight of all fragments with an index lower than i , in real time). Selectivity S_{ji} of disintegration is also important and d_i was used in the model to define mean particle size in each fragment class.

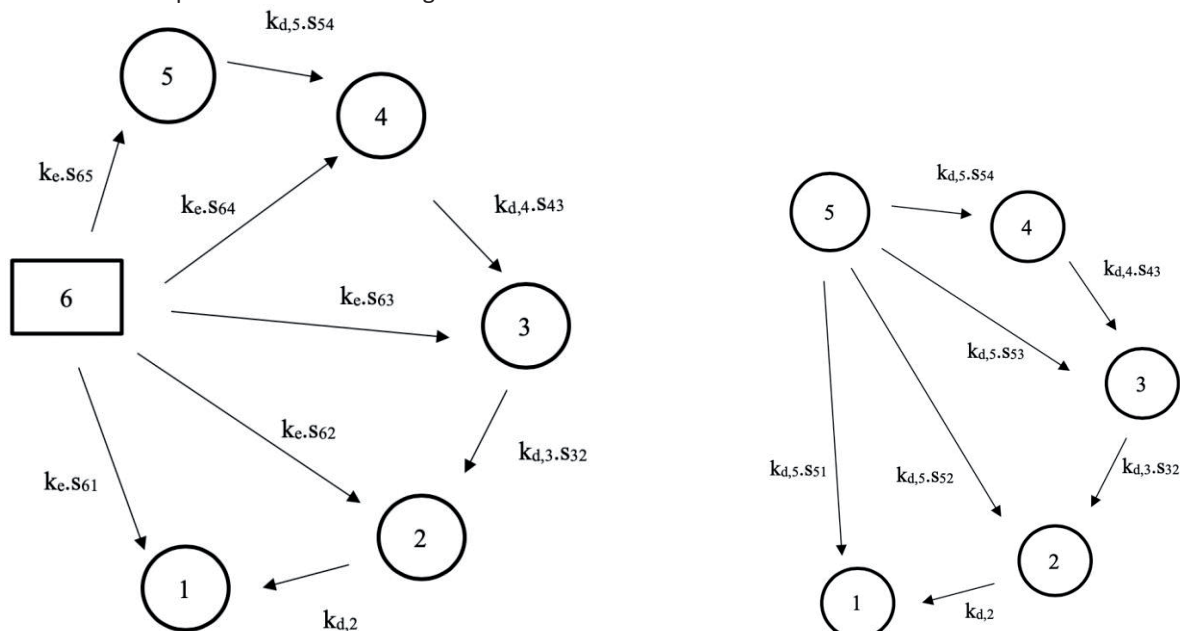


Figure 2. Simplified scheme of tablet (size class 6) break-up into primary fragments (1-5) (left) and detailed scheme of disintegration of primary fragment 5 into smaller fragments (right).

Results and Discussion

The dissolution experiments in pH 7.2 phosphate buffer produced dissolution profiles shown in Fig. 3. The APO ibuprofen exhibited a faster onset of the release and it also released the drug in a shorter time.

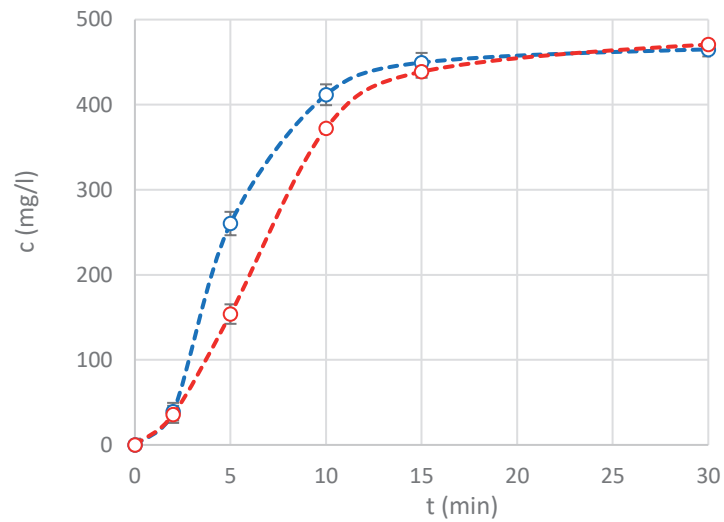


Figure 3. Dissolution profile of ibuprofen tablets (Ibalgin – red, APO-Ibuprofen – blue).

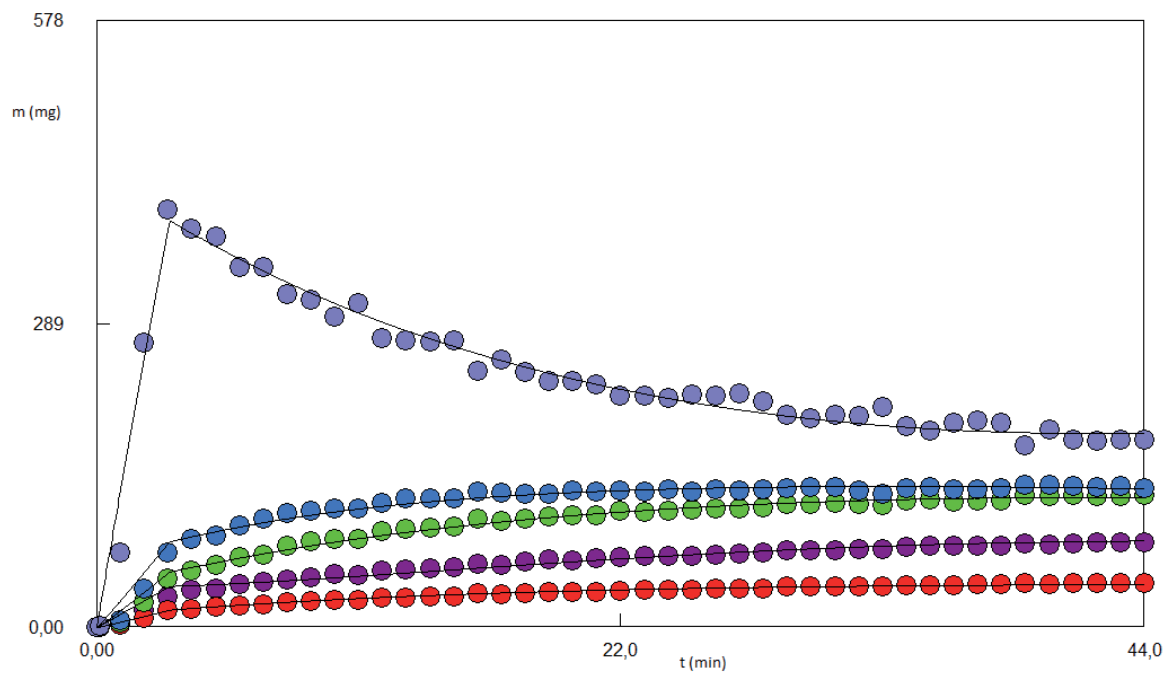


Figure 4. Fitting the APO-ibuprofen disintegration data using mathematical model (size classes in μm : 0-98.1 (purple), 98.1-127 (red), 127-186 (green), 186-272 (blue), 272+ (gray))

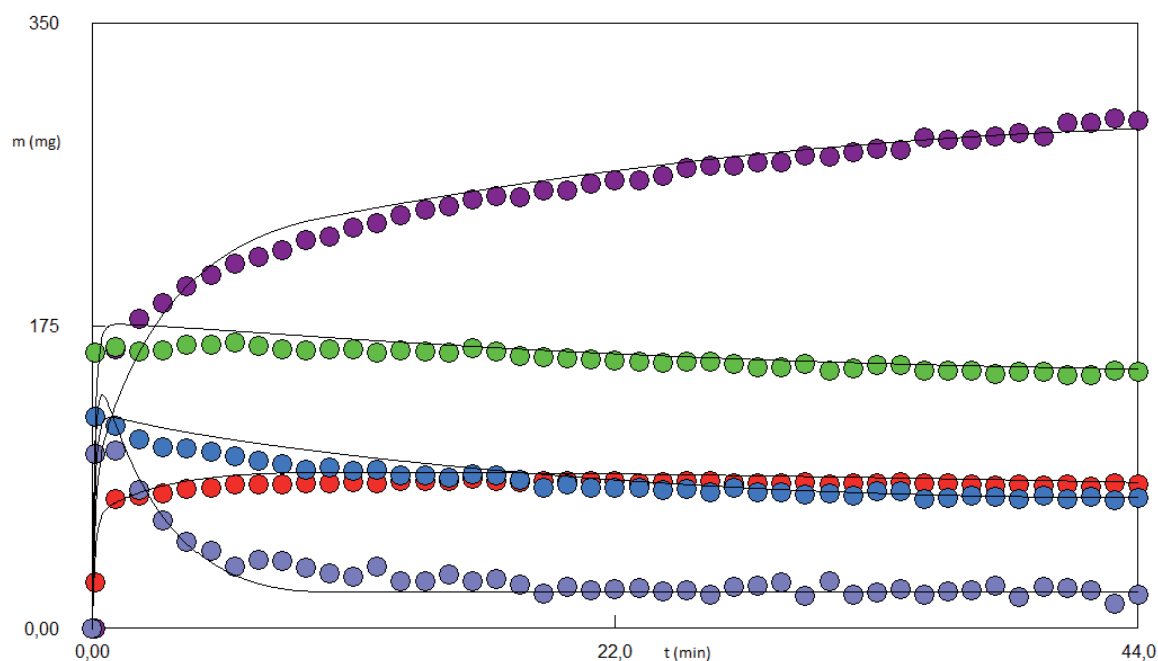


Figure 5. Fitting the Ibalgin disintegration data using mathematical model (size classes in μm : 0-98.1 (purple), 98.1-127 (red), 127-186 (green), 186-272 (blue), 272 + (gray))

The disintegration data are provided in Figures 4 and 5. Ibalgin tablet released a high number of small particles. Particles of size above 272 μm were released and disaggregated to smaller particles within the first minutes. The amount of the smallest particles rose with a slow decline in all other clusters after 5 minutes of measurement. On the other hand, APO-ibuprofen tablets quickly disintegrated into big particles, which then slowly disaggregated into smaller particles within 4 remaining fragment classes.

Estimated parameters from the mathematic model are displayed in Table I. Erosion of APO-ibuprofen tablet is faster and disintegration of largest fragments into smaller fragments is faster as well. Ibalgin tablet disintegrates into smaller particles more quickly (from 5th class into 1st and 2nd class or from 2nd class to 1st class) and the dissolution constant is higher compared to APO-ibuprofen tablet. Total erosion constant in the case of Ibalgin was 0.3 min^{-1} , but all disintegration constants and dissolution constant were higher. The erosion constant of APO-ibuprofen was 171 min^{-1} , but the disintegration of particular fragment class and dissolution had a lower impact.

Table I. Estimated parameters of the disintegration model

Parameter [min^{-1}]	APO-IBU	Ibalgin
$k_e \cdot S_{65}$	124.7	9.5×10^{-2}
$k_e \cdot S_{64}$	20.2	7.2×10^{-2}
$k_e \cdot S_{63}$	12	3.6×10^{-2}
$k_e \cdot S_{62}$	3.4	10.4×10^{-2}
$k_e \cdot S_{61}$	10.7	5.2×10^{-2}
$k_{d,5} \cdot S_{54}$	32×10^{-3}	7.5×10^{-3}
$k_{d,5} \cdot S_{53}$	19.2×10^{-3}	4.1×10^{-3}
$k_{d,5} \cdot S_{52}$	6.8×10^{-3}	62.7×10^{-3}
$k_{d,5} \cdot S_{51}$	0	2.6×10^{-1}
$k_{d,4} \cdot S_{43}$	4.4×10^{-3}	3.2×10^{-1}
$k_{d,4} \cdot S_{42}$	3.4×10^{-3}	6.5×10^{-3}
$k_{d,4} \cdot S_{41}$	2.3×10^{-2}	0
$k_{d,3} \cdot S_{32}$	1.5×10^{-4}	1.7×10^{-2}
$k_{d,3} \cdot S_{31}$	9×10^{-3}	0
$k_{d,2}$	9.4×10^{-3}	20.1×10^{-3}
k_{dis}	2×10^{-2}	3.8×10^{-2}

Conclusion

Method for measurement of tablet disintegration and particle size distribution was established and interconnected with UV spectroscopy and dissolution. Dissolution could be partially predicted according to disintegration profile, final particle size distribution and measured specific surface area thanks to those measurements. Mathematical model is useful for the comparison of disintegration mechanisms of different formulations. It can identify the key differences in the disintegration processes and show the bottlenecks in the drug release process. The case study exemplified, that in comparison of the two model drugs, the different rate of erosion had a more severe impact than the release rate from particles. Quicker tablet erosion in the case of APO-ibuprofen then caused faster dissolution even though the mean particle size was higher.

Acknowledgement

This work was supported from the grant of Specific university research – grant No.: A1_FCHT_2022_006.

References

1. Mesnier, X.; Althaus, T. O.; Forny, L.; Niederreiter, G.; Palzer, S.; Hounslow, M. J. and Salman, A. D., A novel method to quantify tablet disintegration. *Powder Technol.* 2013, 238, 27-34.
2. Caramella, C.; Ferrari, F.; Bonferoni, M.C. and Ronchi, M., Disintegrants in solid dosage forms. *Drug. Dev. Ind. Pharm.* 1990, 16 (17), 2561-2577.
3. Desai, P. M.; Liew, C. V. and Heng, P. W. S., Review of disintegrants and the disintegration phenomena. *J. Pharm. Sci.* 2016, 105 (9), 2545-2555.
4. Quodbach, J. and Kleinebudde, P., A New Apparatus for Real-Time Assessment of the Particle Size Distribution of Disintegrating Tablets. *J. Pharm. Sci.* 2014, 103 (11), 3657-3665.
5. Smrcka, D.; Dohnal, J. and Stepanek, F., Dissolution and disintegration kinetics of high-active pharmaceutical granules produced at laboratory and manufacturing scale. *Eur. J. Pharm. Biopharm.* 2016, 106, 107-116.
6. Coutant, C.A.; Skibic, M.J.; Doddridge, G.D.; Kemp, C.A. and Sperry, D.C., In vitro monitoring of dissolution of an immediate release tablet by focused beam reflectance measurement. *Mol. Pharm.* 2010, 7 (5), 1508-15.

PREDICTING BULK DENSITY OF BINARY POWDER MIXTURES FROM PURE COMPONENT PROPERTIES

Komínová P.¹, Smrčka D.², Gajdošová M.², Zámostný P.¹

¹Department of Organic Technology, University of Chemistry and Technology Prague, Technická 5, 166 28, Prague, Czech Republic

²Zentiva, k.s., U Kabelovny 130, 102 37, Prague, Czech Republic
pavlina.kominova@vscht.cz

Abstract

The bulk density of pharmaceutical powders (ρ_b) is an essential parameter for solid dosage forms. Its knowledge is valuable in both manufacturing processes and product research and development. Unfortunately, ρ_b is not an additive characteristic in the case of mixtures and must be determined experimentally for each mixture. Therefore, the possibility of predicting mixture ρ_b using properties of pure components would make the development of new formulations faster and cheaper and eliminate the risk of process failure. Given this knowledge, the aim of this study is the development of a simple model and evaluation of its ability to predict binary mixture bulk density ($\rho_{b,mix}$) based on the properties of starting materials. This model arises from a hypothesis based on a presumption that one component serves as a matrix and particles of the second component are incorporated into voids of that matrix.

Introduction

Pharmaceutical solid dosage forms can be described by several parameters. One of these parameters is a bulk density (ρ_b). The packing of the particles is a characteristic feature of each powder system. The way the particles are arranged in a powder bed has a significant effect on handling it. ρ_b may define during manufacture the amount of powder that can be poured into a hopper, tablet press die or capsule filling machine. In addition, ρ_b can indicate the degree of densification of the powder during storage, under the application of external stresses, or reflect the sensitivity of powder to external influences such as shaking or vibrations. Knowledge of ρ_b is also helpful in the research and development of solid drug formulations. If the studied mixture is targeted at the production of pharmaceutical tablets and has a poor ρ_b , it is likely that the direct compression process is not suitable for the preparation of tablets due to non-compliance with the required filling weight and API content. So, the granulation step leading to an increase of ρ_b at desired values is needed to be included.

The possibility of predicting ρ_b of the mixture using properties of pure components could therefore speed up the process and reduce the costs of new formulation development and eliminate the possibility of process failures. Among others, ρ_b is closely related to the ability of the powder to flow by gravity, which makes it a key parameter for mixtures intended for tablet direct compression.

Materials and Methods

Materials

Binary mixtures consisting of excipient and API in several ratios (30, 50, and 70 % by weight) were used in this study. Three types of lactose (spray-dried Supertab[®] 14SD, granulated Tablettose[®] 80 and anhydrous lactose) and two types of microcrystalline cellulose (Avicel[®] PH200 and Avicel[®] PH102) were chosen as representatives of excipients. Ibuprofen powders from two producers (Shandong Xinhua Pharmaceutical Co., Ltd. and Hubei Biocause Pharmaceutical Co., Ltd.) served as a model API in this study. To make the evaluation more feasible, abbreviations IBU Shandong and IBU Hubei are used in the document respectively.

Bulk Density Measurement

To verify the validity of the created model, the ρ_b of all mixtures was obtained using FT4 powder rheometer that offers to measure so-called conditioned bulk density (CBD). CBD is the powder sample's density that is free of localized stress and any excess air.

Theoretical Background of Mathematical Model

The applied approach uses a simple model arising from the hypothesis that particulate systems are porous systems. If two substances are mixed together, one component of the mixture (A) can be assumed to form a matrix having a certain volume of voids. The particles of the second component (B) can fill those voids to some extent as long as the B particles fit into the A void size. It follows that the volume of the binary mixture cannot be determined as a simple sum of the volumes of these components but must be reduced by the volume of component B particles that fill up voids of component A. In the equation (1) below for obtaining the theoretically calculated bulk density ($\rho_{b,mix}^T$), this volume is expressed as ΔV

$$\rho_{b,mix}^T = \frac{m_{mix}}{V_{b,mix}} = \frac{m_A + m_B}{\frac{m_A}{\rho_{b,A}} + \frac{m_B}{\rho_{b,B}} - \Delta V} \quad (1)$$

where m_{mix} indicates the weight of the mixture (kg), $V_{b,mix}$ indicates the bulk volume of the mixture (m^3), m_A indicates the weight of the component A (kg), m_B indicates the weight of the component B (kg), $\rho_{b,A}$ indicates the bulk density of the component A (kg/m^3), $\rho_{b,B}$ indicates the bulk density of the component B (kg/m^3), ΔV indicates the volume of component B particles that fill up voids of component A (m^3).

Two approaches were applied to obtain the numerical value of the parameter ΔV . The first one is based on the porosity of the matrix and the volume filled with the particles of component B corresponds to the volume of these pores. ΔV can then be expressed using the equation (2)

$$\Delta V = \varepsilon_A \cdot V_{b,A} \quad (2)$$

where ε_A indicates the porosity of matrix, component A (-), $V_{b,A}$ indicates the bulk volume of component A (m^3).

However, these pores can also be characterized by an equivalent diameter (d_{ekv}) and are therefore accessible only to particles of component B with a size equal to or lower than the value of d_{ekv} . Then, ΔV corresponds to the volume of these particles and can be calculated using the equation (3) below

$$\Delta V = (1 - \varepsilon_B) \cdot V_{b,B} \cdot F_B(d_{ekv}) \quad (3)$$

where ε_B indicates the porosity of component B (-), $V_{b,B}$ indicates the bulk volume of component B (m^3), $F_B(d_{ekv})$ indicates the ratio of volume particle size distribution of component B corresponding to the particles with $d < d_{ekv}$ (-).

The theory of fluid flow through a porous medium was used to obtain the d_{ekv} of matrix and the so-called surface density (a) was calculated. This parameter can be obtained either from a matrix specific surface area (A_{sp}) using equation (4) or selected particle characteristic (d_p) for the matrix particles using equation (5)

$$a = \frac{A_{sp}}{V_{b,A}} \quad (4)$$

$$a = \frac{6 \cdot (1 - \varepsilon_A)}{\psi \cdot d_p} \quad (5)$$

where A_{sp} indicates the specific surface area of matrix (m^2), $V_{b,A}$ indicates the bulk volume of matrix (m^3), ε_A indicates the porosity of the matrix (-), ψ indicates the sphericity of matrix particles (-), and d_p indicates the particle size characteristic (m). In this study, d_{10} , d_{50} , $d(3,2)$ or $d(4,3)$ were evaluated as d_p .

The d_{ekv} is afterwards obtained by substituting the surface density a into the following equation (6).

$$d_{ekv} = \frac{4 \cdot \varepsilon_A}{a} \quad (6)$$

As the matrix, the compound with a larger particle size was chosen. For all mixtures, it was the used excipient. Component B was then API, i.e., IBU Shandong or IBU Hubei.

$\rho_{b,mix}^T$ was calculated for each mixture applying equation (1). To obtain ΔV , both above mentioned approaches were utilized. However, the lower value was used in the equation.

Results and Discussion

Validation of the model prediction quality was performed graphically for each studied system (API - excipient) based on the dependence of the $\rho_{b,mix}^T$ marked in the graphs as ρ_T on experimentally obtained values of CBD marked as ρ_M .

Based on the result, it was found that the quality of the ρ_b prediction using the developed model is given by the nature of the used components. As the results in the graphs in Figure 1 for the Supertab® 14SD - API system indicate, the model can determine the ρ_b value quite satisfactorily for systems where both starting components have similar porosity, see Table I. Similar outputs were also obtained for the lactose Tablettose® 80 - API system plotted in Figure 2. For these two systems, the best model prediction quality was reached using d_{10} or d_{50} for the calculation of the d_{ekv} and surface density a . Moreover, it is also possible to observe from the values in Table II that the mixture CBD values are in the range given by the values of the pure components.

Table I
Porosity values of pure components

	$\epsilon, -$
Lactose Supertab® 14SD	0.58
Lactose Tablettose® 80	0.60
Anhydrous lactose	0.68
MCC Avicel® PH200	0.76
MCC Avicel® PH102	0.79
IBU Shandong	0.62
IBU Hubei	0.65

Table II
CBD values of pure components and mixtures for systems containing lactose Supertab® 14SD and Tablettose® 80

Amount of IBU in mixture, w/w %		CBD, g/cm ³				
		0	30	50	70	100
Lactose Supertab® 14SD	IBU Shandong	0.620	0.591	0.535	0.483	0.412
	IBU Hubei	0.620	0.601	0.544	0.478	0.382
Lactose Tablettose® 80	IBU Shandong	0.594	0.604	0.566	0.514	0.412
	IBU Hubei	0.594	0.591	0.540	0.462	0.382

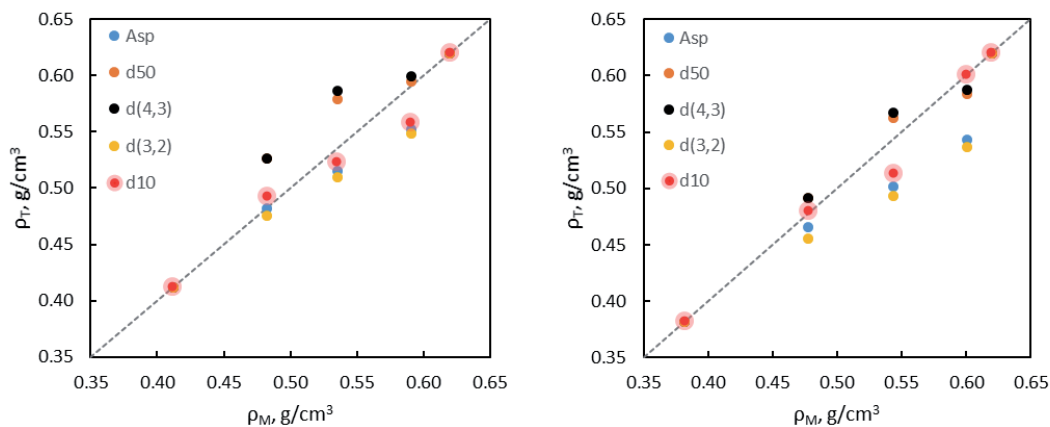


Figure 1. Correlation between ρ_T and ρ_M for lactose Supertab® 14SD systems with IBU Shandong (left) and IBU Hubei (right).

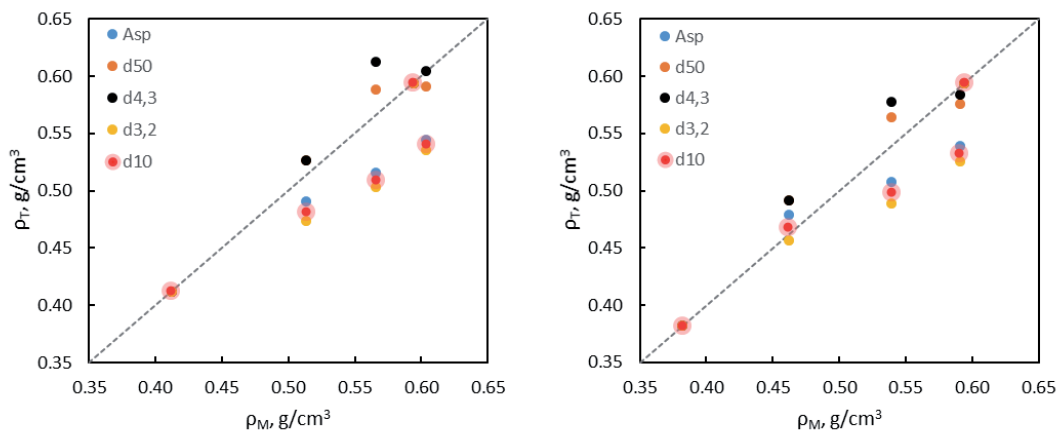


Figure 2. Correlation between ρ_T and ρ_M for lactose Tablettose® 80 systems with IBU Shandong (left) and IBU Hubei (right).

The best prediction of mixture ρ_b using the lower decile d_{10} was also achieved in the case of systems consisting of components with different porosities. However, the graphs in Figure 3 for the Avicel® PH102 - API system show the limited applicability of the model and its potentially possible application only to a certain composition range. The same trends can be seen for systems of MCC Avicel® PH200 and anhydrous lactose, see Figures 4 and 5. The values in Table III show the mixture CBD values of these systems are in some cases higher than the value of the starting component having a higher density.

Table III

CBD values of pure components and mixtures for systems containing MCC Avicel® PH102, MCC Avicel® PH200 and anhydrous lactose

Amount of IBU in mixture, w/w %		CBD, g/cm ³				
		0	30	50	70	100
MCC Avicel® PH102	IBU Shandong	0.333	0.386	0.404	0.418	0.412
	IBU Hubei	0.333	0.384	0.386	0.386	0.382
MCC Avicel® PH200	IBU Shandong	0.358	0.426	0.442	0.436	0.412
	IBU Hubei	0.358	0.407	0.399	0.398	0.382
Anhydrous lactose	IBU Shandong	0.503	0.528	0.530	0.507	0.412
	IBU Hubei	0.503	0.622	0.591	0.554	0.382

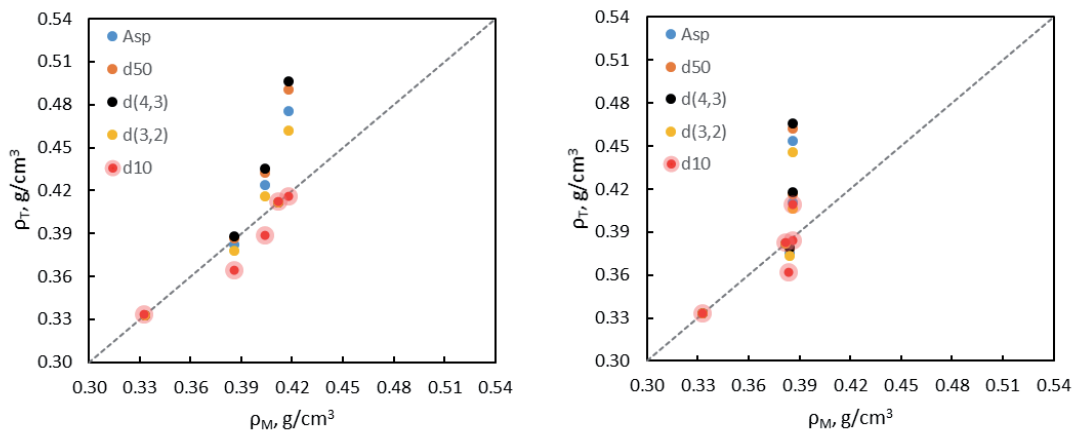


Figure 3. Correlation between ρ_T and ρ_M for MCC Avicel® PH102 systems with IBU Shandong (left) and IBU Hubei (right).

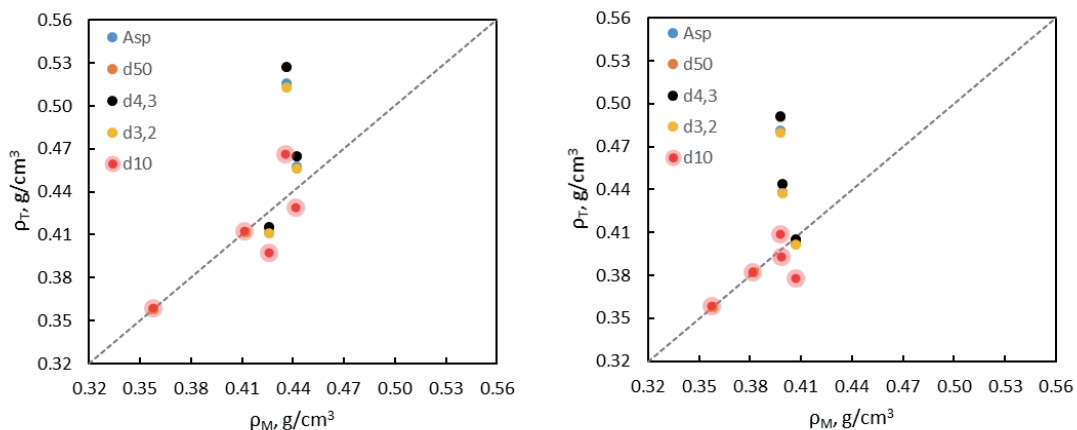


Figure 4. Correlation between ρ_T and ρ_M for MCC Avicel® PH200 systems with IBU Shandong (left) and IBU Hubei (right).

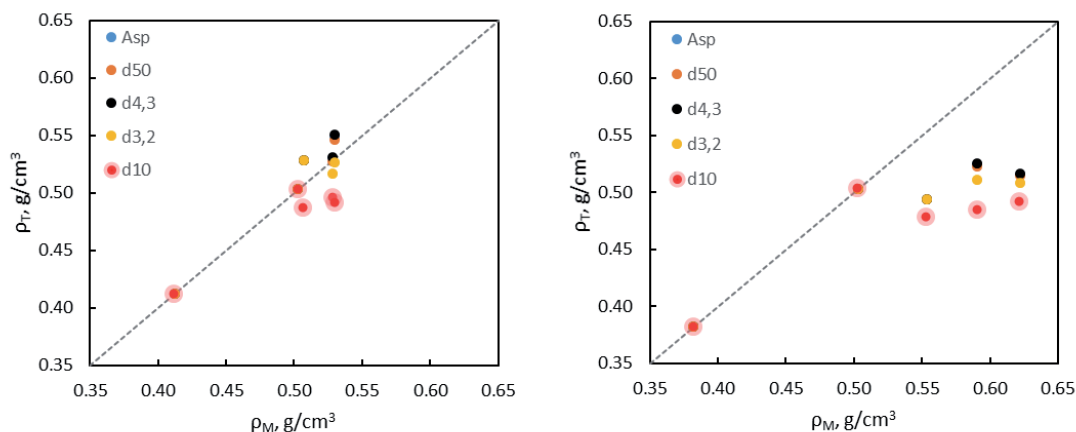


Figure 5. Correlation between ρ_T and ρ_M for anhydrous lactose systems with IBU Shandong (left) and IBU Hubei (right).

In general, ρ_b is a very complex parameter, and its value depends not only on the porosity, but also, for example, on the true density of the solid fraction or the interparticle interaction. Thus, it is possible that in the case of these systems, where the matrix exhibits higher porosity, the influence of factors such as cohesion, particle repulsion, electrostatic charge is more pronounced. However, these factors are not taken into account in the model and so its predictive ability loses potential. On the other hand, the results can be analysed from a perspective that the model is suitable for predicting the bulk density of any well designed pharmaceutical particulate system. Poor prediction would mean the model is pointing out certain incompatibility between the components in the system considered. The $\rho_{b,mix}^T$ values follow the same trend in terms of increasing API content in the mixture as the measured ones with the FT4 powder rheometer. However, for mixtures, especially with a higher API content, the values of the $\rho_{b,mix}^T$ deviate significantly. So, it could indicate from this point of view that the components contained in the mixture cannot be arranged together in such rearrangement to give the highest possible density on the condition that the theoretically calculated value is the highest bulk density of the mixture that components are able to reach in a given representation.

However, the main reason for the unsuitability of this model is probably the fact that the assumption of one component as the matrix into which the particles of the other component incorporating is far away from reality, where both components alternate each other in the role of the matrix. For this reason, the next step of this work will use a more advanced approach to calculate ρ_b . This will be based on the theoretical calculation of the particle size distribution of the mixture from the distributions of the pure components and division of this distribution into several fractions. For each size fraction of the mixture, *CBD* will be obtained in a similar manner using profiles of the *CBD* dependence on the particle size of the starting materials. The principle of this advanced approach is the sequential filling of the voids of each mixture fraction with particles of smaller fractions to obtain the final volume, weight, and desired ρ_b of the mixture.

Conclusion

In this study, the model for the prediction of binary mixture ρ_b was developed. Based on its verification using experimentally measured ρ_b values, it was found out the quality of the ρ_b prediction is given by the nature of the used components. This model exhibits good prediction ability for mixtures consisting of compounds having similar porosities. However, it is not suitable for systems that comprise compounds having different porosities. In such case, the model validity is limited to a certain composition range.

Acknowledgements

This research was financially supported by the university research A1_FCHT_2022_006 and by the pharmaceutical research platform The Parc.

SOLID DISPLACEMENT METHOD TO DETERMINE ENVELOPE DENSITY OF ROLLER COMPACTED RIBBONS

Marinko N.¹, Zámostný P.¹, Gajdošová M.²

¹University of Chemistry and Technology, Prague, Department of Organic Technology, Technická 5, Prague 6, 16628, Czech Republic

²Zentiva k.s., U Kabelovny 130, 10237, Prague 102

marinkon@vscht.cz

Abstract

Achieving the same quality of intermediate product on a different roller compaction scale is crucial in a scale-up project for production of a pharmaceutical formulation. The widely accepted notion for transferability of roller compaction processes lies in the physical property of the intermediate which is ribbon envelope density. Through a pilot study on a small-scale roller compactor, it is possible to prepare multiple batches of granulate under different process parameters to select the most preferable batch for further processing. The ribbon densities of intermediate compacts for each batch differ due to process parameters set during compaction. The method presented in this work allows to determine envelope density of roller compacted ribbons by an accurate measurement of their envelope volume. This is done by utilizing volume displacement of solid glass microspheres. The data acquired by the application of this method are additionally demonstrated for utilization in mathematical modelling to predict process parameters of a pharmaceutical mixture based on samples from pilot studies.

Introduction

Roller compaction (RC) is a method utilized in pharmaceutical industry for dry granulation of powders with poor flow properties. The prepared granulates are more suitable in further processing such as tableting or encapsulation¹. The method was commonly used with pharmaceutical mixtures that contain active pharmaceutical ingredients (APIs) that are sensitive to heat and moisture, and therefore incompatible for wet and fluid-bed granulation processes. However, the utilization of RC for granulation of pharmaceutical mixtures is becoming even more widespread due to its advantages in terms of scalability and manufacture cost that are of concern in other significantly more complex granulation processes²⁻⁵.

The widely recognized tactic that is applied to control the RC process is to maintain identical quality of the intermediate product of RC which is the ribbon (roller compacted compact). Therefore, preliminary experiments have to be performed to identify the optimal batch. Such pilot studies are aimed to produce many granulate batches that differ in their specific ribbon physical properties due to the process parameters that are set on the roller compactors. The three most important process parameters that affect ribbon properties and are usually subjected to monitoring of their influence are compaction pressure, gap size (between rolls) and roll speed. Optimal granulate batch is often selected based on the ease of granulation, feasibility in following manufacturing processes or end-product in-vitro and in-vivo performance^{6,7}.

To characterize the physical properties of ribbons, the ribbons are sampled in-process of compaction at the chosen process parameters during steady-state. Most important quality of the intermediate that is monitored to maintain process reproducibility is the ribbon envelope density. In order to determine envelope density of a sampled ribbon batch, the individual samples of ribbons are subjected to measurement of envelope volume (volume that includes pore spaces) for which the most reliable method is mercury porosimetry. That is because it is possible to determine envelope density and total porosity from the intrusion data. The effort to utilize this measurement less routinely bears significance due to the health and environmental hazards of mercury and also due to the difficult execution of the measurement^{8,9}. The aim of this work was to develop a method that utilizes displacement of glass microspheres to determine envelope density and confirm its accuracy by comparison to mercury porosimetry. Additionally, the use case of the acquired envelope density data is shown to be utilized in validation of a mathematical model and its potential use case is demonstrated.

Materials and Methods

Ribbon batches

Roller compaction experiments to obtain ribbon batches were done on WP200 (Alexanderwerk GmbH, Germany) with one real pharmaceutical mixture Z1 (provided by Zentiva k.s., Czech Republic) and on RCC 100x20 (POWTEC Maschinen und Engineering GmbH, Germany) with one model mixture M1 containing Ibuprofen API (provided by Zentiva k.s., Czech Republic) and microcrystalline cellulose Avicel® PH 101 (Dupont, USA) in ratio 30:70 respectively. The process parameters used to produce ribbon batches utilized a specific fixed gap size and roll speed (RPM) setting and were optimized in preliminary experiments so that each experiment allowed formation of uniform ribbon structure. The Z1 mixture was compacted with the gap size of 3.5 mm and roll speed of 10 RPM and the M1 mixture was compacted with the gap size of 2 mm and roll speed of 3 RPM. The individual ribbon batches for both mixtures were obtained in experiments with different setting of hydraulic pressure (which was increased for each batch). The hydraulic pressure parameters used in every experiment are listed in results and discussion part to identify each batch.

Solid displacement method

The solid displacement method utilizes glass microspheres (Glass Sphere s.r.o, Czech Republic) with sphere diameter distribution of 100 – 200 µm. The experiments are done in a glass cylinder on a tap density analyzer JV1000 (Pharmatron AG, Switzerland). Firstly, a sample of glass microspheres (large enough to cover the ribbons) is weighed and then calibrated to measure their exact volume without samples. The volume is calculated from geometric measurements of dimensions using a digital caliper after the vibrational consolidation. Afterwards, the glass microspheres with approximately 2 g of ribbon samples is vibrated to determine the extent of the microsphere column displacement. The displaced volume of the glass microspheres (from the calibrated value) corresponds to the envelope volume of the tested ribbon samples which is then used to calculate their envelope density. The envelope density for each ribbon batch is then calculated as an average from individual measurements (which included reproducibility tests) of a sample set of randomly selected ribbon samples for each batch.

Mercury porosimetry

Mercury porosimetry was used to determine the accuracy of the solid displacement method. Structural and bulk characteristics of the samples were acquired with mercury porosimetry using the AutoPore IV 9500 (Micromeritics GmbH, Germany). Each analysis was performed with approximately 1.5 g of ribbon samples tightly packed in the measurement cell. The macropore and mesopore distribution of the samples was assessed in pressure range of 0,005 – 400 MPa (i.e., for pore radius of $1 \cdot 10^{-4}$ – $1,5 \cdot 10^{-9}$).

Results and discussion

Batches of Z1 pharmaceutical mixtures were prepared at three settings of hydraulic pressure and batches of M1 model mixture were prepared at five settings of hydraulic pressure and the results of determined envelope density for every batch by both solid displacement and mercury porosimetry methods are listed in Table 1 and 2 respectively. From the results, it is evident that the solid displacement method is as accurate as the mercury porosimetry method and the evaluated standard deviations of the measurements indicate acceptable reproducibility of the method.

Z1 batch h. pressure (bar)	Solid displacement ρ_{ribbon} (g/cm ³)	Mercury porosimetry ρ_{ribbon} (g/cm ³)
70	1.069 ± 0.046	1.074
90	1.150 ± 0.018	1.138
110	1.183 ± 0.028	1.178

Table 1: Results of ribbon envelope density batches determination of Z1 mixture by solid displacement and mercury porosimetry of three ribbon batches compacted under different hydraulic pressure settings

M1 batch h. pressure (bar)	Solid displacement ρ_{ribbon} (g/cm ³)	Mercury porosimetry ρ_{ribbon} (g/cm ³)
25	0.972 ± 0.005	0.971
50	0.990 ± 0.013	0.966
100	1.023 ± 0.048	1.007
150	1.063 ± 0.015	1.026
200	1.124 ± 0.029	1.031

Table 2: Results of ribbon envelope density batches determination of M1 mixture by solid displacement and mercury porosimetry of five ribbon batches compacted under different hydraulic pressure settings

Only the M1-200 bar batch showed a larger difference in comparison of the methods. Therefore, robustness of the solid displacement method was further investigated. Three batches of M1 model mixture were tested again with a different batch of glass microspheres (from the same supplier) after one month from the initial testing and the results are shown in Table 3. The outcome of the solid displacement verification experiments (Table 2) is very close to the previous measurements (Table 3). Therefore, the reproducibility of the measurement for the same ribbon samples to determine their envelope volume is accurate even after storage. This presents another benefit over mercury porosimetry experiments which are destructive to the tested samples. The discrepancy between mercury porosimetry and solid displacement method for the M1-200 bar batch is believed to be caused by overpacking the porosimetry cell and breakage of the ribbon samples before the intrusion of mercury.

M1 batch h. pressure (bar)	Solid displacement ρ_{ribbon} (g/cm ³)	Mercury porosimetry ρ_{ribbon} (g/cm ³)
50	0.987 ± 0.020	0.966
150	1.041 ± 0.018	1.026
200	1.146 ± 0.021	1.031

Table 3: Results of solid displacement method after 1 month on three ribbon batches samples of M1 mixture with a new batch of glass microspheres compared to their respective densities determined by mercury porosimetry

The acquired data can be then used to determine compressibility (K)¹⁰ of the powder mixture for use in mathematical modelling of roller compaction scale-up operations. Such use case is demonstrated with Z1 pharmaceutical mixture. The compressibility parameter for the Z1 pharmaceutical mixture was obtained by model validation in accordance to the Reynolds RC mathematical model¹⁰ with the software gProms Formulated Products (Process Systems Enterprise, United Kingdom). The software requires to specify the geometry of the roller compaction equipment that was utilized to prepare the ribbon batches. The envelope density data of the ribbon batch is then paired with the process parameters at which the powder mixture underwent compaction. The compressibility value of the Z1 mixture was determined in the software by regression analysis from the experimental batch data to the initial bulk density of the powder which was measured in preliminary characterization of the bulk mixture with FT4 powder rheometer (Freeman Technology, Switzerland). The software evaluated compressibility of Z1 mixture was $K = 9.3$.

Once the mathematical model for the powder mixture is validated it can be used to predict compaction behavior under different circumstances. The use case of mathematical modelling is beneficial when considering optimization on the same roller compaction equipment: to increase production throughput or to find process parameters that provide a different desired batch ribbon density. The other important use case applies when scale-up operations are targeted for different roller compaction equipment so that the same ribbon quality can be achieved as in small scale equipment. Therefore, it is possible to predict design space for a different system of process parameters or equipment. Using the validated model for Z1 mixture we generated a design space for the same RC equipment which was WP200 but under different process parameters (Fig. 1). The fixed gap size was changed to 3.3 mm and roll speed to 12 RPM, while the hydraulic pressure parameter was set to uniformly distribute over 20 – 220 bar. This way a sensitivity analysis of ribbon envelope density (Fig. 1) was obtained for the described system of process parameters. If batch Z1-70 bar ($\rho_{\text{ribbon}} = 1069 \text{ kg/m}^3$) was chosen as optimal, the sensitivity analysis reveals that with the new fixed settings the required pressure to compact this batch would be approximately 30 bar (mainly due to smaller gap size).

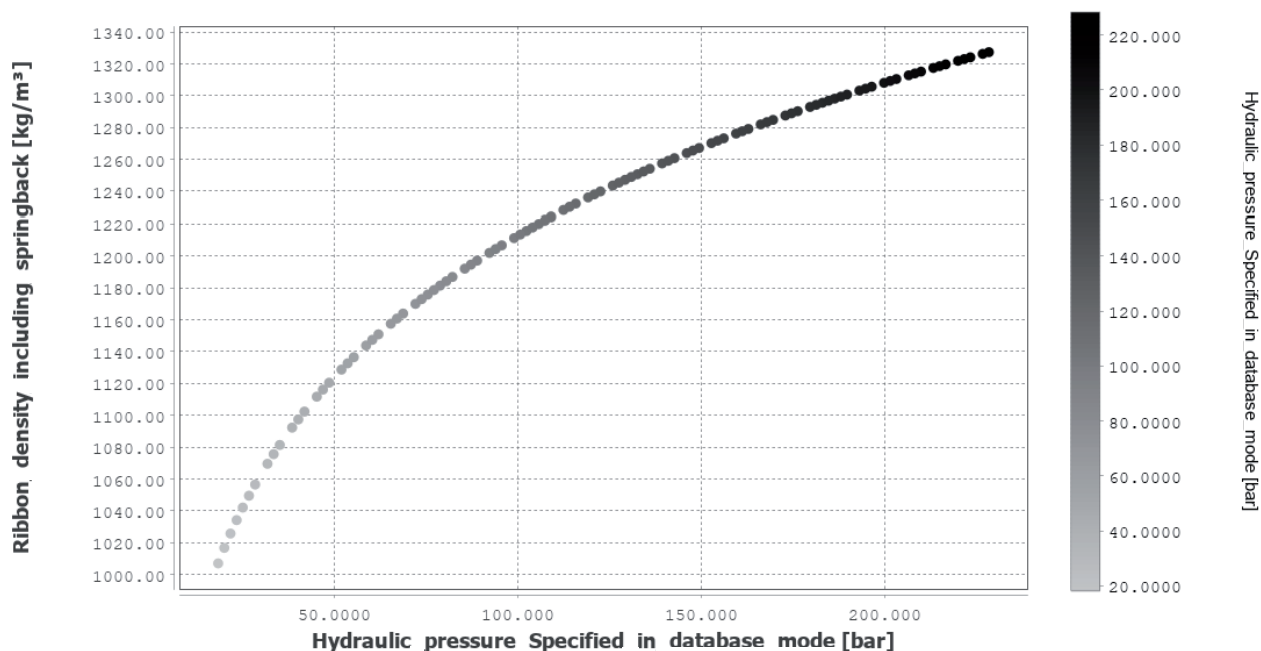


Figure 1: Prediction of design space for ribbon envelope density against hydraulic pressure setting (20-220 bar; grey to black) with fixed gap size of 3.3 mm and roll speed of 12 RPM

Conclusion

The developed method that utilizes displacement of solid media was shown to be as accurate as mercury porosimetry when determining the envelope density of several ribbon batches prepared from two pharmaceutical mixtures (each compacted on different RC equipment). The novel method presents a simple, fast and inexpensive solution. The data provided by this method are feasible to use in mathematical modelling and future efforts of the authors are focused on transfer of technology to different RC equipment in production scale-up operations assisted by mathematical modelling.

Acknowledgement

This work was supported from the grant of Specific university research – grant no. A2_FCHT_2022_027 (University of Chemistry and Technology, Prague).

References

1. Shanmugam, S., Granulation techniques and technologies: recent progresses. *Bioimpacts* **2015**, *5* (1), 55-63. DOI: <https://doi.org/10.15171%2Fbi.2015.04>
2. Wilms, A.; Kleinebudde, P., Towards better understanding of the influence of process parameters in roll compaction/dry granulation on throughput, ribbon microhardness and granule failure load. *Int J Pharm X* **2020**, *2*, 100059. DOI: <https://doi.org/10.1016/j.ijpx.2020.100059>
3. Kalaria, D. R.; Parker, K.; Reynolds, G. K.; Laru, J., An industrial approach towards solid dosage development for first-in-human studies: Application of predictive science and lean principles. *Drug Discovery Today* **2020**, *25* (3), 505-518. DOI: <https://doi.org/10.1016/j.drudis.2019.12.012>
4. Muliadi, A. R.; Banda, A.; Mao, C., Recent Progress in Roll Compaction Process Development for Pharmaceutical Solid Dosage Form Manufacture. In *Continuous Pharmaceutical Processing*, Nagy, Z. K.; El Hagrasy, A.; Litster, J., Eds. Springer International Publishing: Cham, 2020; pp 227-267. DOI: https://doi.org/10.1007/978-3-030-41524-2_7
5. Leane, M.; Pitt, K.; Reynolds, G., A proposal for a drug product Manufacturing Classification System (MCS) for oral solid dosage forms. *Pharmaceutical Development and Technology* **2015**, *20* (1), 12-21. DOI: <https://doi.org/10.3109/10837450.2014.954728>

6. Reynolds, G., MODEL-BASED DEVELOPMENT OF ROLLER COMPACTION PROCESSES. 2019; pp 119-145. DOI: <http://dx.doi.org/10.1002/9781119600800.ch55>
7. Amini, H.; Akseli, I., A first principle model for simulating the ribbon solid fraction during pharmaceutical roller compaction process. *Powder Technology* **2020**, *368*, 32-44. DOI: <https://doi.org/10.1016/j.powtec.2020.04.022>
8. Riepma, K. A.; Vromans, H.; Zuurman, K.; Lerk, C. F., The effect of dry granulation on the consolidation and compaction of crystalline lactose. *International Journal of Pharmaceutics* **1993**, *97* (1), 29-38. DOI: [https://doi.org/10.1016/0378-5173\(93\)90123-W](https://doi.org/10.1016/0378-5173(93)90123-W)
9. Matji, A.; Donato, N.; Gagol, A.; Morales, E.; Carvajal, L.; Serrano, D. R.; Worku, Z. A.; Healy, A. M.; Torrado, J. J., Predicting the critical quality attributes of ibuprofen tablets via modelling of process parameters for roller compaction and tableting. *International Journal of Pharmaceutics* **2019**, *565*, 209-218. DOI: <https://doi.org/10.1016/j.ijpharm.2019.05.011>
10. Reynolds, G.; Ingale, R.; Roberts, R.; Kothari, S.; Gururajan, B., Practical application of roller compaction process modeling. *Computers & Chemical Engineering* **2010**, *34* (7), 1049-1057. DOI: <https://doi.org/10.1016/j.compchemeng.2010.03.004>

DRUGS PRODUCTION BY UNIAXIAL COMPACTION OF POWDER MATERIAL

Peciar P.¹, Gušťačík A.¹, Jezsó K.¹, Fekete R.¹, Peciar M.¹

¹*Slovak University of Technology in Bratislava, Faculty of Mechanical Engineering, Institute of Process Engineering. Námetstie Slobody 17, 812 31 Bratislava, Slovakia
peter.peciar@stuba.sk*

Abstract

One of the most common unit operations in the pharmaceutical industry in the production of drugs is the process of high-pressure compression - tableting. During tableting, the particles are rearranged, which causes friction between the particles and between the particles and the compression tool, until a uniform compact tablet is formed. In the process of tablet production, it is necessary to examine the physical and mechanical properties of tablets, and currently, the thermal aspect is also coming to the fore. For this purpose, a unique device was designed at the Institute of Process Engineering of the Faculty of Mechanical Engineering STU in Bratislava, which allows measuring the compression pressure in the axial and radial direction, as well as measuring the temperature in the tablet during pressing. The material to be analysed was AVICEL PH102 microcrystalline cellulose, which is the most commonly used in the pharmaceutical industry for direct tablet compression. The investigated physical quantity presented in this work was the maximum compression pressure and its influence on the compression process using the Heckel equation, and on the strength of the tablet.

Experimental material

The main component of the experimental material was AVICEL PH102 microcrystalline cellulose, as it is one of the most commonly used excipients in the manufacture of tablets. In addition to API, other additives are added to the powder, such as magnesium stearate, which serves as a lubricating additive. Prior to the compression process itself, the experimental material must be analysed for which the following equipment has been used.

Particle size distribution

The particle size distribution of the pharmaceutical powder was measured using the Malver Mastersizer 3000 particle size analyzer⁴. Figure 1 and Figure 2 show the particle size distribution as a function of volume density.

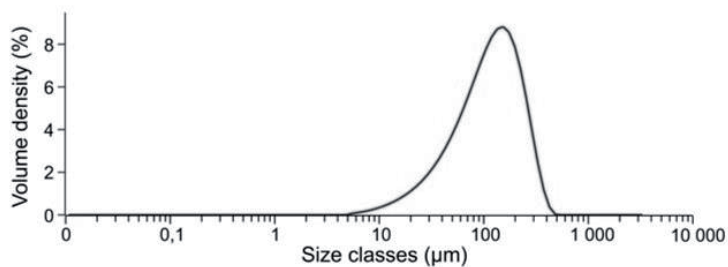


Figure 1. Particle size distribution of MCC Avicel PH102^{1,2,4}

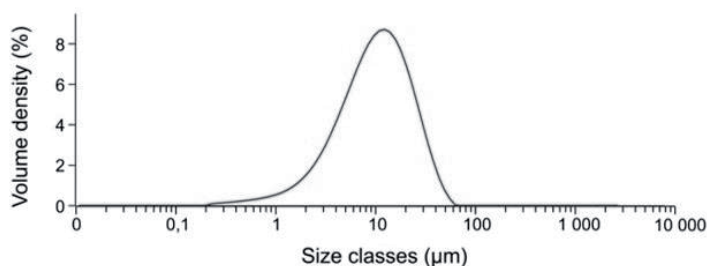


Figure 2. Particle size distribution of Magnesium Stearate¹

Bulk density and true density

Because the powder material was used, it was necessary to determine the bulk density of the powder as well as the true density of the material. Bulk density was determined using a SOTAX Tapped Density Tester TD1, which allows the measurement of poured bulk density and tapped bulk density. A Quantachrome Ultrapyc 1200e automatic gas pycnometer was used to measure true density³.

Further material analysis

The structure of the material was examined using a JEOL JSM IT300LV electron microscope and the images from this device can be seen in Figures 3 and 4. The rheological properties of the material used were investigated on a FREEMAN FT4 Powder Rheometer. One of the most important properties of the powder is its moisture, which was determined on the VWR Moisture Analyser MB 60⁵.

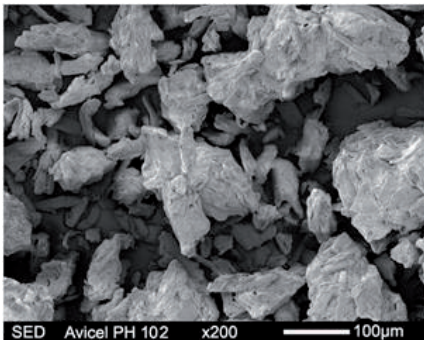


Figure 3. Avicel PH102^{1,2}

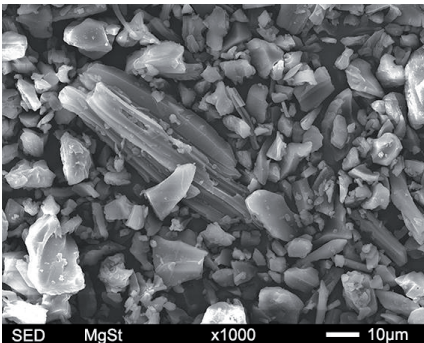


Figure 4. Magnesium Stearate¹

Experimental station

The base of the station is a KISTLER NCFN 2153A electromechanical press (Fig. 5) with integrated punch position and pressing force sensors. The compression itself took place in a special measuring system (Fig. 6), which allows the addition of additional force sensors and a thermocouple.



Figure 5. KISTLER NCFN 2153A electromechanical press⁶

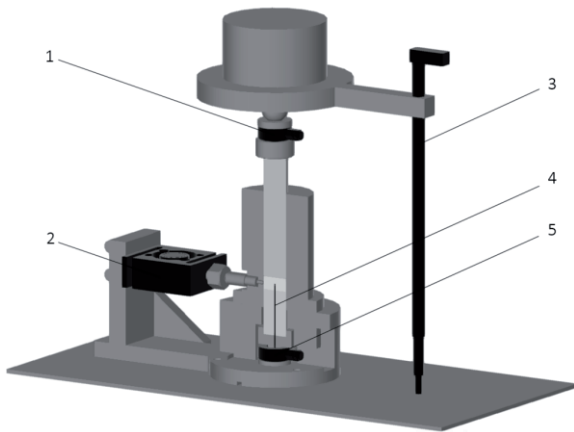


Figure 6. Measuring system^{1,6}: 1 - upper punch force sensor; 2 - radial pressure sensor; 3 - upper punch position sensor; 4 - thermocouple; 5 - lower punch force sensor

Data evaluation method

The Heckel equation was used to evaluate the compression process, as it is one of the most widely used equations and gives a clear comparison of the effect of compression pressure. Heckel hypothesized that the compression process is analogous to a first-order chemical reaction, where pores are reactants and compacted material is final product. The final form of the equation is expressed by the Equation 1 and its graphical representation in Figure 7.

$$\ln \left[\frac{1}{1 - \rho_r} \right] = kP + A \quad (\text{Eq. 1})$$

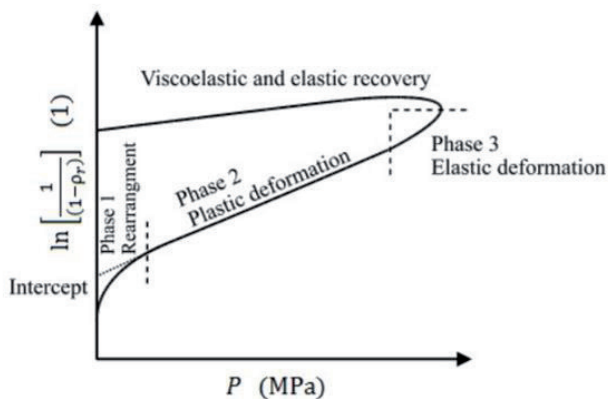


Figure 7. Typical course of Heckel graph²

The strength of the tablet was evaluated by a radial pressure test, during which a force was applied to the tablet in the radial direction until a fracture occurred, and numerically expressed in the form of stress using Equation 2.

$$\sigma_T = \frac{2 F_{max}}{\pi D H} \quad (\text{Eq. 2})$$

Results

The influence of the maximum compression pressure on the behaviour of the powder during compression can be observed in Figure 8. The graph shows that the maximum compression pressure has a significant effect on the compression process. The curves representing the higher maximum compression pressures have a larger area of plastic deformation and this phase occurs later in the compression process. The effect of maximum compression pressure on tablet strength is shown in Figure 9. The strength of the tablets increases significantly at higher maximum compression pressures.

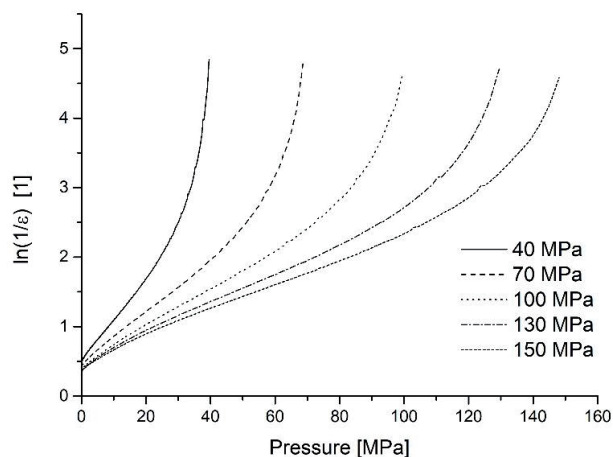


Figure 8. Heckel graphs for tablets made at different maximum compression pressures.

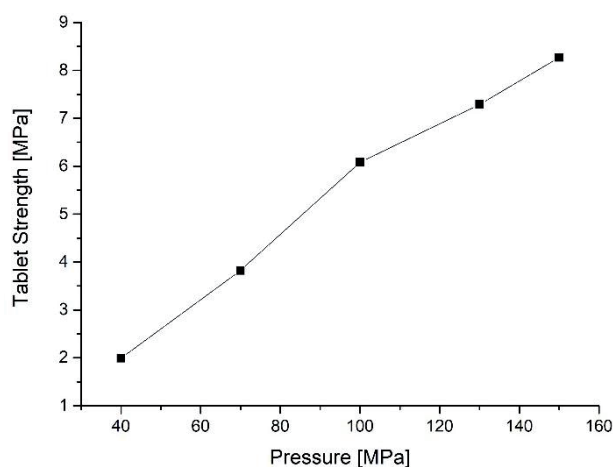


Figure 9. Dependence of tablet strength on maximum compression pressure.

Conclusion

The process of uniaxial high-pressure pressing in which the raw material is compacted represents one of the most important unit operations in the pharmaceutical industry. Physical and mechanical properties of the tablets, such as density and mechanical strength, are often significantly affected by this process. During compression, the particles are rearranged, which causes friction between them but also between the particles and the compression tool. Due to this friction, the heat is usually generated, which can cause degradation of the active pharmaceutical ingredient.

For this reason, it is necessary to systematically examine the powder compaction process not only from a mechanical point of view but also from a thermal perspective. For this purpose, a unique device was designed at Institute of Process Engineering which allows the measurement of the compression pressure in the axial and radial direction but also the measurement of the temperature in the tablet during compaction. The powder examined in this paper was microcrystalline cellulose AVICEL PH102, as it is the most widely used pharmaceutical excipient for direct compression of tablets. The process of compression is influenced by several factors that affect the quality of the final product such as the material moisture or maximum compression pressure.

Acknowledgement

The authors wish to acknowledge the Ministry of Education, Science, Research and Sport of the Slovak Republic for the financial support of this research by grant KEGA 036STU-4/2020.

List of symbols

ρ_r	- relative density	(1)
k	- slope of linear section (Phase 2 – Plastic deformation)	(Pa ⁻¹)
P	- applied pressure	(Pa)
A	- intercept of linear section (Phase 2 – Plastic deformation)	(1)
σ_T	- tensile strength	(Pa)
F_{max}	- fracture force	(N)
D	- tablet diameter	(m)
H	- tablet height	(m)

References

1. Peciar P.: Research of the selected processes of particulate materials processing. Habilitation thesis. STU, Faculty of Mechanical Engineering, Bratislava (2018). ISBN 978-80-227-4801-8. (In Slovak)
2. Peciar P., Eckert M., Fekete R., Hrnčiar V.: Analysis of pharmaceutical excipient MCC Avicel PH102 using compaction equations. *Strojnícky časopis = Journal of Mechanical Engineering*. 66, 1 (2016). ISSN 0039-2472.
3. Peciar P., Juriga M., Gušťačík A., Kohútová M., Jezsó K.: *Procesné strojnictvo: Príklady*. Bratislava: Spektrum STU (2021). ISBN 978-80-227-5081-3. (In Slovak)
4. Jezsó K., Peciar P.: Influence of the Selected Sieving Parameters on the Sieving Efficiency of Material MCC Avicel PH102. *Strojnícky časopis = Journal of Mechanical Engineering*. 72, 1 (2022). ISSN 0039-2472.
5. Gušťačík A., Jezsó K., Vaľková K., Macho O., Peciar P.: Effect of Moisture of Pharmaceutical Material MCC Avicel PH102 and Tablet Diameter on the Compression Process and Tablet Strength. *Strojnícky časopis = Journal of Mechanical Engineering*. 72, 1 (2022). ISSN 0039-2472.
6. Gušťačík A., Peciar P., Krok A., Jezsó K., Macho O., Fekete R.: Thermomechanical analysis of pharmaceutical powder during uniaxial compaction. CHISA 2021. (2021). Czech Society of Chemical Engineering.

DETERMINATION OF HANSEN SOLUBILITY PARAMETERS OF BINARY MIXTURES OF POLYMERS

Petríková E.¹, Čerňová M.², Adamska K.³, Voelkel A.³, Dammer O.², Krejčík L.², Patera J.¹

¹University of Chemistry and Technology Prague, Faculty of Chemical Technology, Department of Organic Technology, Technická 5, Prague 6, 166 28, Czech Republic

eva.petrkova@vscht.cz

²Zentiva, k.s., Prague, U Kabelovny 130, 102 37 Prague 10, Czech Republic

³Institute of Chemical Technology and Engineering, Poznań University of Technology, Berdychowo 4, 60 965 Poznań, Poland

Abstract

Nowadays, with the increasing number of registered drugs on the market, the importance to simplify the preformulation and formulation processes is increasing. To obey the possible patent collision, it is advantageous for generic pharmaceutical companies to have an API in amorphous form. However, the physical and chemical stability of an amorphous API is often poor, and the API needs to be stabilized by a proper excipient(s). Thus, the formulation into amorphous solid dispersions became more popular. Excipient selection is often based on experience and knowledge with similar API. However, unexpected and unwanted interactions between API and excipients may cause API recrystallization or even degradation, and other formulation problems. With a proper selection model and proper excipient characterization, many unwanted reactions and product degradations can be prevented. For the selection of a suitable excipient(s), the Hansen solubility parameters can be used as a prediction model. The pure materials manifest different behaviour compared with binary mixtures of excipients. Thus, this work aimed to examine the bulk properties represented by their Hansen solubility parameters of selected binary mixtures of polymers often used in the pharmaceutical industry. Moreover, the influence of common processes to form amorphous solid dispersions on bulk properties of binary mixtures was examined. Hansen solubility parameters have proven their sensitivity not only to the chemical nature of used excipients but also to the various processes used.

Introduction

The selection of appropriate excipient(s) for API for further drug formulation is a crucial step in the pharmaceutical industry. Preformulation chemists often rely on their experience, when selecting a proper formulation, however, several issues may occur. For instance, the inappropriate API-excipient interaction can start with API recrystallization and lead to API degradation¹. It is necessary to characterize not only the API but also the excipients properly and appropriately select the excipient(s) choice for the API at hand. Especially in the case where the API is formulated into amorphous solid dispersion. It is a convenient way to produce a new drug in stabilized form without patent obstacles and other patent issues, moreover, the dissolution profile of poorly soluble or almost insoluble API in water can be improved.

The Hansen solubility parameters (HSPs) are based on the work of Hildebrand, Scott, and Scatchard², who first came up with a definition of the solubility parameter, which was later called the Hildebrand solubility parameter. However, the Hildebrand solubility parameter cannot be used for materials other than alkanes because it neglects other specific interactions between molecules, i.e. polar and hydrogen bonding interactions³. Charles M. Hansen⁴ in his dissertation thesis expanded Hildebrand solubility parameter to three individual elements, which included the small non-binding interactions between molecules: dispersive (δ_D), polar (δ_P) and hydrogen bonding (δ_H). The total solubility parameter (δ_T) can be obtained according to Equation 1⁵.

$$\delta_T^2 = \delta_D^2 + \delta_P^2 + \delta_H^2 \quad (1)$$

Hansen solubility parameters can be determined using inverse gas chromatography (IGC). The IGC schema can be found in Figure 1.

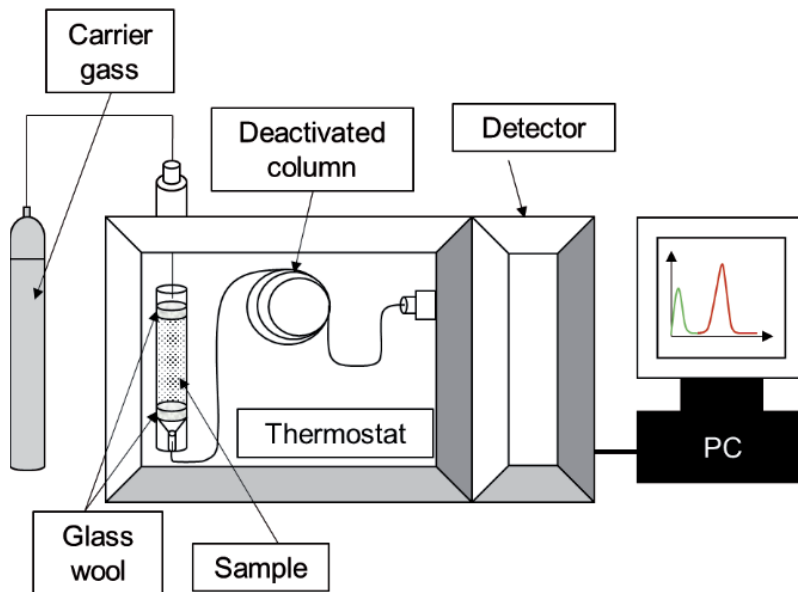


Figure 1: Schema of the IGC instrument

In this case, the stationary phase is the examined material and the mobile phase is inert gas (commonly nitrogen or helium). The molecular probes are injected into a continuously flowing mobile phase to characterize the examined sample. Molecular probes are well-defined gaseous molecules with determined Hansen solubility parameters and other thermodynamic properties⁶. From the IGC measurements, the main retention parameter for the characterization of the examined sample is the specific retention volume. Hansen solubility parameters were determined using the Voelkel and Adamska⁶ approach based on the Snyder and Karger⁷ adsorption model. In this model, the adsorption energy can be obtained from the energy balance between the dissolved tested substance i , which is adsorbed on the surface of the solid adsorbent j (examined material). The derivation from the energy balance can be seen in the following equations (2-4).

$$-\Delta E_A = V_i \cdot CED_{ij} \quad (2)$$

$$-\Delta E_A = V_i \cdot \sqrt{CED_{ii}} \cdot \sqrt{CED_{jj}} \quad (3)$$

$$-\Delta E_A = V_i \cdot \delta_i \cdot \delta_j \quad (4)$$

Where V_i is the molar volume of the tested solute and CED_{ij} represents the cohesive energy density of the interaction between the sample and the molecular probe, δ_i stand for the solubility parameter of a dissolved tested substance and δ_j is solubility parameter of the solid adsorbent.

Equation 2 can also be expressed by Equation 5.

$$-\Delta E_A = V_i \cdot \left[(E_{ij})_D + (E_{ij})_P + (E_{ij})_H \right] \quad (5)$$

When implementing the partial HSPs, Equation 6 is obtained.

$$-\Delta E_A = V_i \cdot (\delta_D^i \cdot \delta_D^j + \delta_P^i \cdot \delta_P^j + \delta_H^i \cdot \delta_H^j) \quad (6)$$

The adsorption energy is related to the specific retention volume according to Equation 7.

$$\ln V_g = -\left(\frac{\Delta E_A}{R \cdot T}\right) + constant \quad (7)$$

It is common to use more molecular probes in IGC experiment. The number of molecular probes can be expressed by N , then the system of N equations can be obtained, simply described by the following matrix form (Equation 8).

$$\begin{pmatrix} -\Delta E_{A1} \\ -\Delta E_{A2} \\ -\Delta E_{A3} \\ \vdots \\ -\Delta E_{AN} \end{pmatrix} = \begin{pmatrix} V_{i1} \cdot \delta_{i1D} & V_{i1} \cdot \delta_{i1P} & V_{i1} \cdot \delta_{i1H} \\ V_{i2} \cdot \delta_{i2D} & V_{i2} \cdot \delta_{i2P} & V_{i2} \cdot \delta_{i2H} \\ V_{i3} \cdot \delta_{i3D} & V_{i3} \cdot \delta_{i3P} & V_{i3} \cdot \delta_{i3H} \\ \vdots & \vdots & \vdots \\ V_{iN} \cdot \delta_{iND} & V_{iN} \cdot \delta_{iNP} & V_{iN} \cdot \delta_{iNH} \end{pmatrix} \cdot \begin{pmatrix} \delta_{jD} \\ \delta_{jP} \\ \delta_{jH} \end{pmatrix} + \begin{pmatrix} \varepsilon_1 \\ \varepsilon_2 \\ \varepsilon_3 \\ \vdots \\ \varepsilon_N \end{pmatrix} \quad (8)$$

The left side of Equation 8 represents the measured experimental energy, V_{iN} stands for the molar volume of the molecular probe, and $\delta_{iND}, \delta_{iNP}, \delta_{iNH}$ represents partial HSPs of the molecular probe and δ_{jD}, δ_{jP} and δ_{jH} are the actual HSPs of the examined material. The last component of Equation 8 is residual scattering, ε_n ^{3,5,6}.

The Hansen solubility parameters appear to be a promising prediction model for proper excipient selection. Based on the generally well-known basic principle “like dissolves like”, the determination of a suitable excipient(s) for API can make the preformulation process more effective. The majority of the pure polymers are well characterized. However, the properties and behaviour of mixtures cannot be predicted from data for individually characterized excipients⁸.

This work aimed to study and properly characterize polymers and their binary mixtures, commonly used as excipients in the pharmaceutical industry. The Hansen solubility parameters of all samples were determined using inverse gas chromatography. The influence of various sample preparations conditions on Hansen solubility parameters was studied i.e., binary physical mixtures and mixtures from the hot-melt extrusion and spray dry processes were compared.

Materials and methods

In this study, several binary mixtures were prepared to discover differences between physical mixtures, binary mixtures subjected to hot-melt extrusion (HME), and binary spray dried (SD) mixtures.

Materials

Materials for IGC, HME and SD experiments were Soluplus[®] and Kollidon[®] 30, kindly provided by Zentiva k.s. Molecular probes in IGC experiments and solvents used in SD process: heptane, octane, nonane, dichloromethane, 1,4-dioxane, ethyl acetate, ethanol, acetonitrile, 2-propanol, 1-butanol, toluene, acetone and methanol were kindly provided by Zentiva k.s. and Poznań University of Technology.

Physical mixtures

Both selected polymers in ratio 1:1 (w/w) were blended for 10 minutes at 49 rpm using a Turbula T2F (WAB, Switzerland) in order to achieve a sufficiently homogeneous blend.

HME experiments

The prepared physical mixtures were further processed by twin screw-type extrusion using a ZE5 Twin Screw Extruder ZE5 (Three-Tec, Switzerland) using different temperature settings with a feeder to achieve continuous supply of material. Table 1 lists the process parameters of the HME experiments.

Table 1: HME process parameters (K30:Sol 1:1 - Kollidon[®] 30 : Soluplus[®] 1:1)

Mixture	Heating block 1 [°C]	Heating block 2 [°C]	Heating block 3 [°C]	Heating block 4 [°C]	Screw speed [rpm]	Feed rate [%]
K30:Sol 1:1	90	120	120	110	40	4
K30:Sol 1:1	120	140	140	135	40	4

The extruded materials were milled using a Mini Mill Pulverisette 23 (Fritsch, Germany) at 35 rps for 2 minutes. Extrudates were then analyzed using X-ray powder diffraction (XRPD) and differential scanning calorimetry (DSC) analyses to discover, whether amorphous solid solution or dispersion was obtained.

SD process

The prepared physical mixture was dissolved in methanol and sprayed as a 13.7% (w/v) solution. For this process, the Mini spray dryer B-290 (Büchi, Switzerland) was used. Before spray drying, dissolved sample was filtrated. The process parameters are summarized in Table 2.

Table 2: SD process parameters (K30:Sol 1:1 - Kollidon® 30 : Soluplus® 1:1)

Mixture	T _{inlet} [°C]	T _{outlet} [°C]	Aspirator [%]	Pump rate [%]
K30:Sol 1:1	80	39	90	30

IGC measurements

Pure polymers, physical mixture, HME, and SD samples were measured on IGC using the iGC-SEA instrument (SMS, UK).

Results and discussion

Samples prepared by HME and SD processes were first subjected to XRPD and DSC analyzes before IGC measurements. On the basis of XRPD analyses, two amorphous haloes were clearly observed in the patterns. DSC analyses showed that the samples are amorphous solid dispersions, and the temperatures of glass transitions of both polymers were clearly visible on DSC thermograms (around 70 °C for Soluplus® and 168 °C for Kollidon® 30). Physically mixed and pure polymers samples were directly measured on IGC to determine their HSPs.

In Table 3 you can see HSPs of individual polymers (Kollidon® 30 and Soluplus®), their physical mixture, milled extrudate, and spray dried mixture.

Table 3: Hansen solubility parameters of measured substances (K30:Sol 1:1 - Kollidon® 30 : Soluplus® 1:1, PHM – physical mixture, HME hot-melt extruded, SD – spray dried)

Measured substance	δ_D [MPa ^{1/2}]	δ_P [MPa ^{1/2}]	δ_H [MPa ^{1/2}]	δ_T [MPa ^{1/2}]
Kollidon® 30	9.83	21.76	55.76	60.66
Soluplus®	4.84	17.48	0.13	18.14
K30:Sol 1:1 PHM	10.36	12.39	3.66	16.56
K30:Sol 1:1 (120 °C) HME	6.70	13.12	3.16	15.06
K30:Sol 1:1 (140 °C) HME	6.21	10.97	4.25	13.30
K30:Sol 1:1 SD	13.27	35.15	5.82	38.02

As can be seen in Table 3, the Hansen solubility parameters are sensitive to the chemical nature of the materials examined. Differences between Soluplus® and Kollidon 30® are clearly manifested in all partial solubility parameters. The greatest difference can be seen at the partial solubility parameter, where Kollidon® 30 clearly favors hydrogen bonding interactions, in contrast to Soluplus®. The measured values for Kollidon® 30 appear a bit overestimated, however, the character and favorable hydrogen bonding interactions remain the same. Soluplus® would rather prefer polar interactions instead of hydrogen or dispersive interactions. When both polymers are blended, chemical nature of this binary mixtures change its character. The presence of Kollidon® 30 in mixture slightly increase the hydrogen bond partial solubility parameter, but decrease the polar element. This phenomenon is a prove, that simple blending into a homogeneous mixture change completely the surface character of used materials.

When extruded samples with those physically mixed are compared, the influence of the used process can be seen. During HME process, certain specific groups can reach the surface and thus change completely the mixture character. In this case it seems, that dispersive groups were slightly overshadowed by polar and hydrogen interactions. With respect to the smaller value of the dispersive element, it could be assumed that the Soluplus® character may prevail over Kollidon® 30, because its glass transition temperature is lower. Thus, Kollidon® 30 could be surrounded by a Soluplus® melt but did not dissolve in the melt to form an amorphous solid solution. The difference between the temperatures used during the HME process is not that remarkable; however, HSPs are sufficiently sensitive to discover even minority differences between the values of individual partial solubility parameters.

The sprayed sample manifests with noticeable differences compared to the physical mixture. It seems that during the SD process the polar interactions were more exposed to the surfaces; thus, a spray-dried sample will

favor these kinds of interactions. From SD process, fine particles were obtained, which could be a reason for higher values of dispersive and hydrogen bonding elements.

From mentioned above, Hansen solubility parameters are sensitive not only to the chemical nature of the examined material, but also to the processes used in this experiment. Simply blending completely changed the surface character of the mixture, and further processing exposes different structural groups for molecular nonbinding interactions.

Conclusion

Hansen solubility parameters of a pure polymers and their binary mixtures (physically mixed, HME and SD processed) often used in pharmaceutical industry were determined using IGC. Samples subjected to HME and SD processes were analyzed by XRPD and DSC techniques to investigate whether the amorphous solid dispersions were obtained. It was discovered that pure polymers have values of HSPs different from those of their binary physical mixture. Moreover, the influence of used processes on their HSPs was observed in comparison with their physical mixture. The sensitivity of the Hansen solubility parameters to the chemical nature of the examined materials proves that it is important to characterize not only the API but also the excipients because the behaviour of the binary mixture cannot be predicted only from the measured pure polymers.

Acknowledgement

This project has received funding from the European Union's Horizon 2020 research and innovation programme under the Marie Skłodowska-Curie grant agreement No 778051. This work was supported by the grant of Specific university research – grant No. A2_FCHT_2021_026 and from the Zentiva k.s.. The authors would like to thank to The Parc for all the support during the research.

References

1. Wu, Y.; Levons, J.; Narang, A.S.; Raghavan, K.; Rao, V.M.; PharmSciTech. 12, 1248-63 (2011)
2. Hildebrand, J. H.; Scott, R.L.; Reinhold Pub. Corp.: New York (1950)
3. Petříková, E.; Patera, J.; Gorlová, O.; EurJPharmSci, 167 (2021)
4. Hansen, C. M.; The three dimensional solubility parameter and solvent diffusion coefficient, CopenHagen Danish technical press (1967)Hansen, C. M.;
5. Hansen Solubility Parameters: A User's Handbook. CRC Press (2007).
6. Adamska, K.; Voelkel, A.; IntBullPharmSci 1, 30-35 (2012)
7. Karger, B. L.; Snyder, L. R.; Eon, C.; AnalChem, 50, 2126-36 (1978).
8. Punčochová, K.; Ewing, A. V.; Gajdošová, M.; PharmRes, 34 (2017)

EFFECT OF POWDER PROPERTIES AND COMPACTION PRESSURE ON PARTICLE SIZE OF ROLL-COMPACTED GRANULATE

Švehla O., Zámostný P.

*University of Chemistry and Technology Prague, Department of Organic Technology, Prague, Czech Republic
ondrej.svehla@vscht.cz*

Abstract

This work deals with the compaction of raw powder materials and crushing produced compacts as factors, that influence properties of produced granules. The study is aimed at transferring the process of making granulates via roller compaction to laboratory-scale uniaxial compaction, therefore affording to test the granulation process in smaller scale before being used in industrial production. This would enable the prediction of the dry granulation product properties using a laboratory test.

The experimental study involved two model feed powders - Avicel PH 102 microcrystalline cellulose and calcium hydrogen phosphate dihydrate. Tablets were prepared using mixtures of these model substances to measure the influence of powder composition on the particle size of granulate. These tablets were then crushed through sieves with various mesh densities to evaluate the effect of mesh density and compaction pressure on the final particle size of the prepared granulate.

Two parameters were introduced to describe the efficiency of the process: the granulation yield expressing the portion of material which were successfully converted into granules and the aggregation number expressing the particle enlargement in the process. The parameters were used in a case study to evaluate the granulation efficiency of industrial drug formulation and compare it to the plastic and brittle excipient benchmarks.

Introduction

Crushing or milling compacted pharmaceutical products of dry granulation is a very important operation that determines the properties of the final granulate used for making tablets or hard gelatine capsules. These properties are influenced by the composition of input material, parameters of the compaction process, and parameters of crushing processes.

The issue of compaction at low temperatures is relevant for numerous industrial branches such as powder metallurgy, ceramics production, pharmaceutical industry, agriculture, briquette production, and the mining industry. Currently, the emphasis is mainly on the research of models, thanks to which it would be possible to predict the degree of compaction and density of the final product. Although this information is important in the design and optimization of production processes, current models are not sufficient in providing accurate information about the mechanical properties of the compacted substance. Current models are considering the strength of the compact only as a function of density. In the first studies focusing on the strength of the powder compact, it was shown that the strength of that compact highly depends on the method of compression. For example, powder compressed by high shear triaxial compaction may have more than twice the flexural strength as the same isostatic compaction product. Therefore, the strength of the compact depends on the method and the force the powder is subjected to.¹

Many such studies are not yet available in the field of pharmacy, and therefore this work aimed to develop a method that would simulate the process of dry granulation in a laboratory environment. Thanks to this, it will be possible to create criteria evaluating the effectiveness of the process and make it easier to predict the properties of the resulting granulate. Then it will be possible to select the optimal granulation conditions for the individual substances or their mixtures.

Materials and methods

Materials used in this study were, Microcrystalline cellulose Avicel® PH 102 (FMC Biopolymers), calcium hydrogen phosphate dihydrate ($\text{CaHPO}_4 \cdot 2\text{H}_2\text{O}$, hereinafter referred to as CAP), and a drug formulation sample for roller compaction provided by an industrial partner (composition known but not specified due to data protection).

The product of roller compaction – ribbon was substituted by preparing tablets using pure Avicel® PH 102, CAP, their two mixtures, and the sample provided by the industrial partner. Tablets were prepared using a hydraulic press with compaction force ranging from 0,2 to 2,0 tons in compression die of 10 mm diameter using flat-faced punches. The target weight of the tablets was 250 mg. To simulate the crushing of ribbon, tablets were crushed through sieves with various mesh densities to compare its effect on the particle size of the final granulate with

the effect of compaction force. Particle size distributions of granulates were measured on Mastersizer 3000 using water as a medium. Based on these results, two parameters were introduced. First being the yield of granulation calculated as follows:

$$\text{the yield of granulation} = \frac{\sum \text{volume of particles} > 250 \mu\text{m}}{\sum \text{volume of all particles}} \quad (1)$$

and the aggregation number calculated as:

$$\text{the aggregation number} = \frac{d_{50} \text{ of compacted material}}{d_{50} \text{ of raw powder}} \quad (2)$$

where d_{50} is median of particle size distribution.

Result analysis and discussion

Figure 1 shows, how different compaction forces and different types of sieves affect the particle size of the final granulate. Evaluation is based on comparing means of particle size distribution because it best describes the characteristic particle size of the granulate.

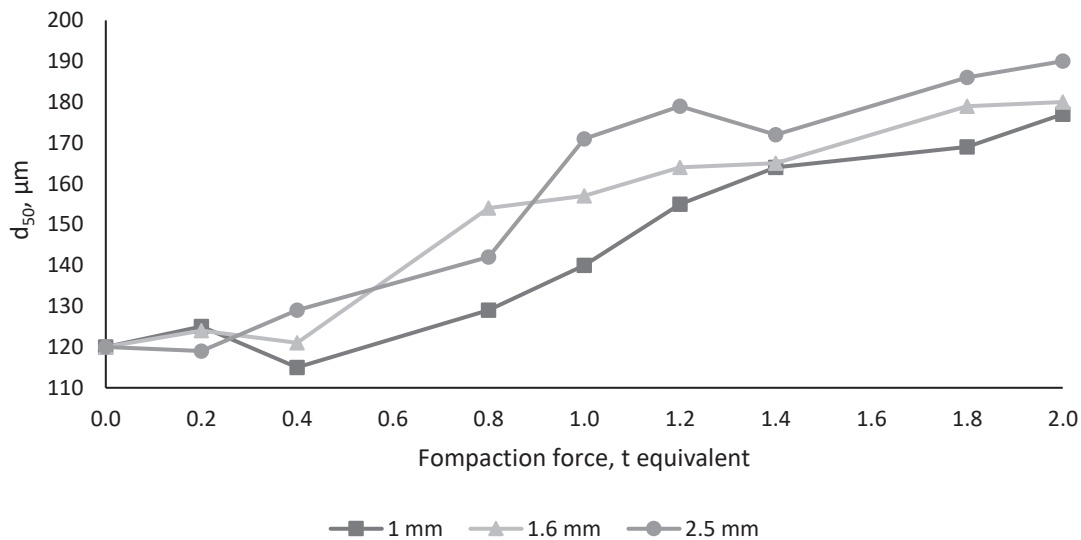


Figure 1. Comparison of the effect of sieve mesh size and compaction force on the particle size of granulate.

After this set of measurements, we can say with certainty, that the effect of the compaction force on the resulting particle size was much greater than the effect of the sieve's mesh density. In addition, the change in mesh size only manifested at higher compaction forces for obvious reasons. If the particles were compressed less, the resulting fragments were not as firm and disintegrated immediately after passing through the sieve. In contrast, at higher compaction forces, the fragments were stronger, and therefore the sieve effect was particularly pronounced. Changing the mesh size of the sieve has a certain effect on the resulting particle size, but for this work, it was possible to describe this effect as negligible compared to the compaction force. Next samples were therefore crushed only through the sieve with a mesh density of 1 mm.

Figure 2 compares the particle size of granulates based on different powder compositions. All samples were prepared by crushing tablets through the sieve with a mesh size of 1 mm.

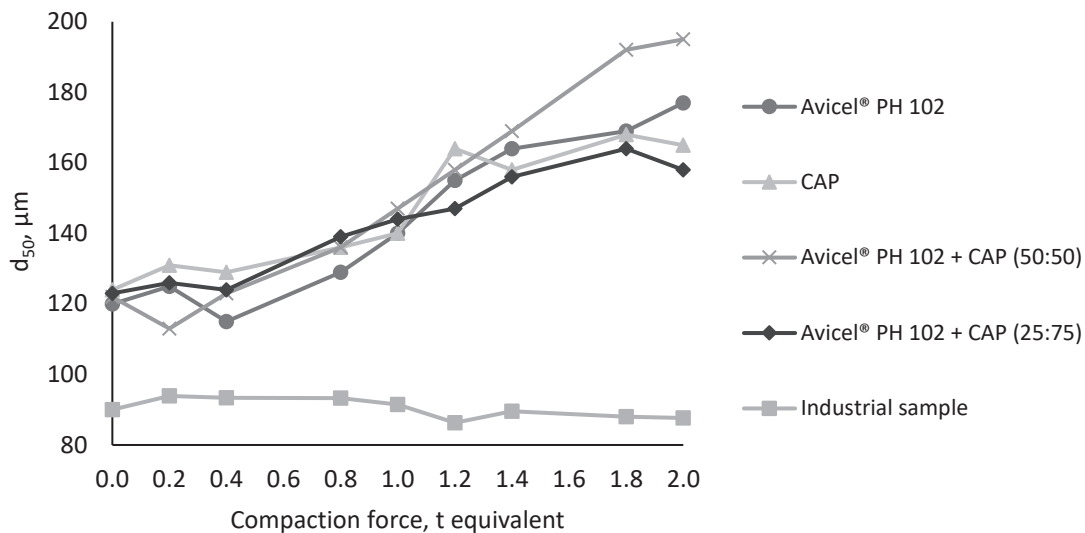


Figure 2. Comparison of the effect of powder composition on the particle size of granulate.

In the case of pure CAP granules, there is a well observable effect of the compaction force on the particle size increase. The maximum particle size, in this case, was about 10 μm smaller than in the case of the granulate formed by crushing Avicel® PH 102 tablets. Given that CAP was chosen as a substance with brittle particles, this difference is not very surprising. The largest particle size was achieved using a mixture of Avicel® PH 102 and CAP in a weight ratio of 50:50 at a compaction force of 2 tons which is a better result even when compared to pure Avicel® PH 102. This can be explained by the fact that at higher compaction forces, the fragments formed by the joining of Avicel® PH 102 were stronger and held CAP particles together. These results also suggest that the industrial sample formulation does not have suitable properties for dry granulation. As shown in the preparation of the tablets, the mixture was well compressible, but the resulting tablets were very brittle. The problem is therefore the low strength of the compacts of this mixture.

The first parameter was the yield of particle size above 250 μm. This was calculated according to equation (1). The limit value of 250 μm is since the raw materials contain practically no particle exceeding this size, therefore the proportion of obtained particles above this size can be considered as an indicator of the yield of compacted fraction, which does not decompose into the original particles. These values are shown in figure 3 as a function of the compaction force.

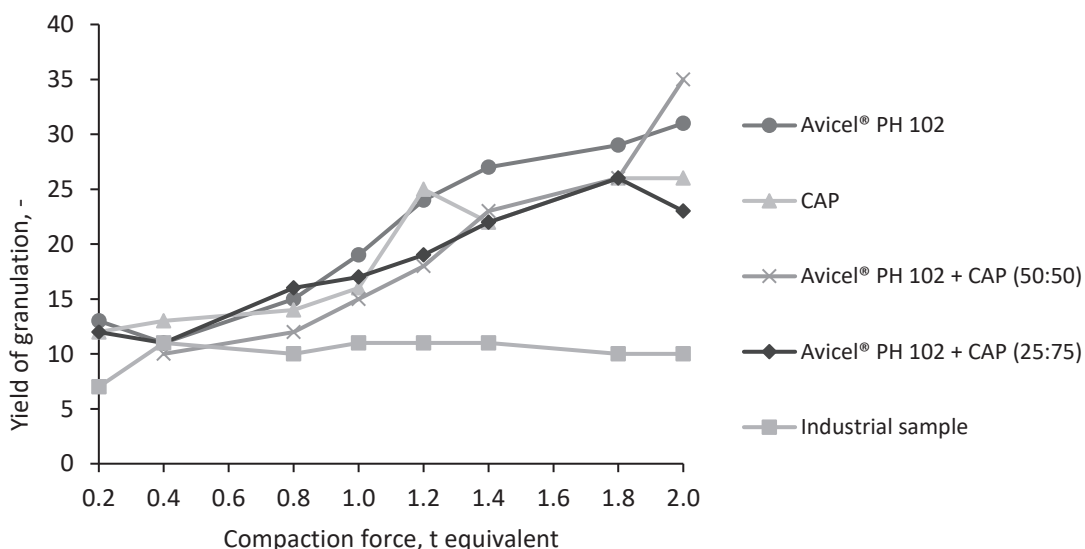


Figure 3. The yield of granulation of tested granulates.

In general, the granulation yield can be defined as the proportion of particles of the granulate which have a size exceeding the maximum particle size in the source material (or exceeding a suitably selected high percentile of this size). The dependence of the yield on the compression pressure obtained using this methodology developed

here then shows the quality of the formulation from the point of view of dry granulation. The formulation suitable for dry granulation should increase its yield as strongly as possible with the compaction force and should lose dynamics as slowly as possible (ideally a linear increasing dependence). Here, the formulation of the industrial sample is not very suitable for dry granulation and its design was probably governed by other requirements. The yield dependence of suitable formulations can also be used to design the optimal compaction pressure.

The aggregation number was introduced as the second evaluation parameter. This represents the ratio of the median particle size distribution after granulation to the median particle size distribution of uncompacted material. The aggregation number was calculated according to equation (2) and these values are summarized in the following figure 4.

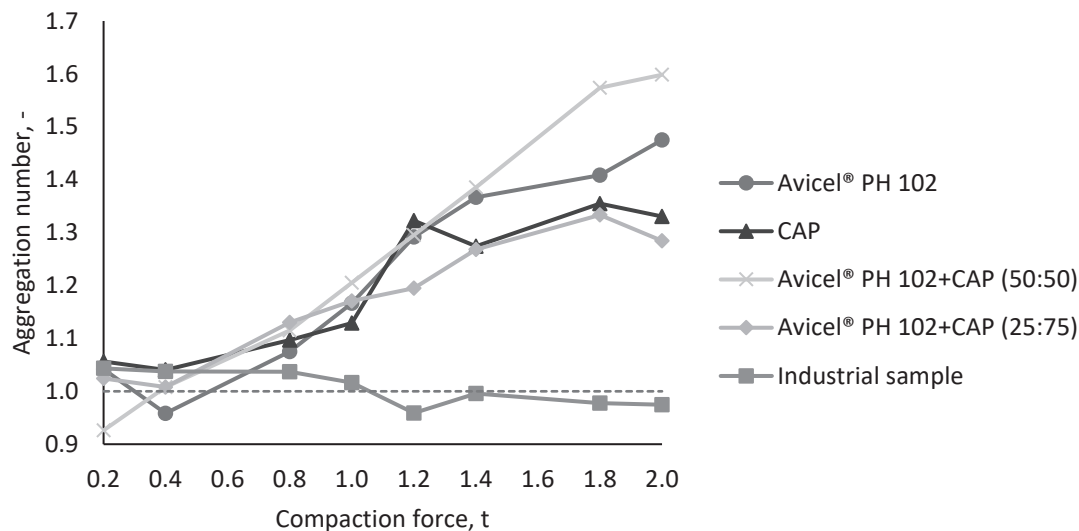


Figure 4. The aggregation number of tested granulates.

Thanks to this value, it is possible to evaluate the benefit of granulation compared to the use of raw powder, not only in large particles but across the entire distribution. All parameters influencing the granulation process are reflected in this issue. If the value of the aggregation number is greater than 1, we can say that there has been an effective enlargement of the granulate particles. This can be observed for all samples except the industrial sample. As mentioned earlier, this formulation has proven unsuitable for use in dry granulation, and for better results it would be appropriate to adjust the composition of this formulation or use another processing method.

Conclusion

This work focused on creating a suitable method for simulating roller compaction in a laboratory environment and determining the parameters that affect the resulting particle size of the prepared granules. First, the compacting of powder material and its subsequent crushing into the granules was proposed. The method of preparing tablets using a hydraulic press and their crushing through sieves was chosen as a suitable approximation. In this method two parameters were examined, the compaction force and the mesh size, which affect the resulting particle size. The analysis of granules prepared from Avicel® PH 102 and calcium hydrogen phosphate dihydrate showed that both examined parameters affect the properties of the resulting granulate. With increasing compaction force, the particle size of the granulate also increased and the effect was manifested even at low compaction forces. The effect of compaction pressure was more significant compared to the effect of sieve roughness. The effect of the sieve, therefore, depends very much on the strength of the compact. Based on previous knowledge, the particle size distribution of the granulate obtained by the industrial partner was measured. In this case, it turned out that the effect of the compaction force was small. There was no particle enlargement and therefore this sample does not have good dry granulation properties. The reason is the low strength of the compacts. Based on the defined criteria, it was evaluated that Avicel® PH 102, calcium hydrogen phosphate dihydrate and their mixtures are suitable for the roller compaction process because there is a significant increase in particles compared to the starting material. In the end, two methods of comparing granular substances were proposed. The first evaluation criterion was the granulation yield. In the case of this work, the limit size was determined to be 250 µm. Based on the yield, it is possible to determine the granulation parameters

to achieve optimal granulate properties. The second criterion for evaluating the prepared granules was the aggregation number. Thanks to this parameter, it was possible to evaluate what effect the granulation had on the resulting particle size and then consider whether the granulation was worth performing for a given material or not.

Acknowledgement

This work was supported from the grant of Specific university research – grant NO.: A2_FCHT_2022_011.

References

1. Galen S., Zavaliangos A.: Acta Mater., 53, 18 (2005).

SYNTHESIS AND PRODUCTION OF DRUGS

WASTE TREATMENT, WATER PROTECTION

ONE-STEP DIRECT CATALYTIC SEWAGE SLUDGE LIQUEFACTION OVER A SULFIDED METAL CATALYST

Hidalgo Herrador J.M., Babor M., Brablíková M., Moghaddam M.A., Vráblík A.

*ORLEN UniCRE a.s., Revoluční 1521/84, 400 01 Ústí nad Labem, Czech Republic
jose.hidalgo@orlenunicre.cz*

Abstract

Sewage sludge residue from wastewater treatment could be transformed to more valuable products. Direct one-step catalytic liquefaction tests were performed to produce synthetic crude and other compounds such as ethylene or propylene from the organic part of the industrial sewage sludge. The catalyst was a commercial metal sulfided hydrocracking NiW/SiO₂-Al₂O₃ material. The reaction was performed with 20 g of dried sewage sludge, 50 g of tetralin and 2 g of catalyst in a batch reactor at 420 °C for 1 h (P_{H₂}=5 MPa at room temperature). The feedstock and products were analysed (GC/FID-TCD, elemental H, C, N, S% analysis, TGA (O₂ and N₂) and ATR-FTIR). For the gases, the main products were ethane, methane, CO₂ and CO. Liquid products in the boiling range of 50-390 °C were obtained. Tetralin was not an inert solvent implying a lower yield to liquids compared to the standard direct coal liquefaction.

Main body

- Introduction

Sewage sludge is a mud-like residue from the wastewater treatment. It is a waste generated by urban and industrial wastewater treatment plants. The sludge containing inorganic and organic compounds which could be then transformed to fuels and other valuable compounds. Sewage sludge can be burned to produce energy or treated by pyrolysis, hydro-treatment, and/or liquefaction reactions to produce more valuable products¹. Furthermore, the sewage sludge can be used as fertilizer but only in cases in which it would not be toxic or environmentally dangerous^{1, 2}.

Because of the industrialization and the continuous growth of the overall population, the number of wastewater treatment plants and the resulting sludge have raised in recent decades. This leads to important environmental and social impacts^{3, 4}. Thus, many practices have been employed to handle sewage sludge⁵. It is a heterogeneous biomass which includes a mixture of inorganic and organic carbon compounds containing nitrogen and phosphorus, heavy metals and pathogens. Nowadays, sludge with high organic matter derived from urban or industrial treatment plants are being used as new renewable energy sources⁶.

Thermochemical technologies for sewage sludge disposal and energy recovery include incineration, torrefaction, gasification and pyrolysis⁷. Among the mentioned thermochemical routes, pyrolysis has gained a significant attention for its ability to optimize the conversion process and to maximize the product yields through novel reactor designs^{8, 9}. In general, pyrolysis includes conventional heating including sometimes microwave irradiation heating processes^{10, 11} because it could increase the energy efficiency of the process¹²⁻¹⁶.

Concretely, the liquefaction of sewage sludge using a hydrogen donor (isopropanol, formic acid, hydrogen gas) has been studied obtaining interesting results¹⁷. Especially, if the use of noble metals would be avoided because of their high costs or to the sulphur content which normally deactivates the active sites of noble metal catalysts. The traditional direct coal liquefaction procedure could be taken as a model reaction for the liquefaction of sewage sludge¹⁸.

In this work, a sewage sludge feedstock was (i) treated using a commercial sulfided metal catalyst in tetralin (similar method than for direct coal liquefaction) and (ii) treated using oxalic acid and isopropanol regarding to the previous experience and literature¹⁸⁻²². The aim was to convert the organic part of the sewage sludge into more useful organic compounds such as syncrude.

- Simulation and/or experiment
 - a) Materials

Sewage sludge were sampled from the wastewater treatment plant treating industrial wastewater and dried at 110 °C for 48 h. Then, the solid obtained was ground to the powder form to be finally homogenised and used for reactions.

Tetralin (Honeywell, ≥97%), oxalic acid dihydrate G.R./1000 g (Lach-ner s.r.o. Company, Czech Republic) and 2-propanol G.R. (Lach-ner s.r.o. Company, Czech Republic) were used. A previously tested commercial NiW/SiO₂-Al₂O₃ catalyst was used²³.

b) Tests

The autoclave 4575/76 with a “4848B” controller delivered by Parr Instruments Company was used for the tests. The sewage sludge (20 g), 2 g of commercial catalyst and tetralin or 2-propanol (50 g) were introduced into the autoclave. The mixture was stirred at 500 rpm during the heating-up stage as well as during the remained reaction time. The reactor was previously tested at high pressures using N₂ (pressure safety tests) and then flushed and pressurized to 50 bar (H₂) at room temperature. When no H₂ gas was used, the autoclave was also previously filled with oxalic acid (30 g) and closed with 0 bar (N₂) at room temperature. Then, the reactor was heated up to 420 °C with a heating rate of 8.3 °C/min. The reaction time of 1 h was used, measured since the required temperature was obtained. After each reaction, the autoclave was cooled down to room temperature by external air flow and then a gas sample was taken. The mass balance was calculated by the weight of the total sediment and liquids filtrated (cold filtration).

Table I

Tests performed (feedstock mixture and pressure conditions).

Test name	Sewage sludge, g	Catalyst, g	Pressure, bar	Oxalic acid, g	Tetralin, g	2-propanol, g
Test Iso-ox	20	2	0 (N ₂)	30	0	50
Test Tetralin	20	2	50 (H ₂)	0	50	0

c) Analyses

Thermal analysis (TGA) was carried out by performing a waters “LLC TA Instruments” with a heating rate of 10 °C/min under nitrogen or air, from 50 to 900 °C and a gas flow rate of 50 mL/min. Composition of metals was analysed by using an ICP-OES instrument Agilent 725 (ICP). The gases composition was analysed by a GC/FID-TCD (Agilent’s “Refinery Gas Analysis” method). Simulated distillation (SIMDIS) performed by gas chromatography following the ASTM D7169. The sample was injected onto a gas chromatographic column separating the hydrocarbons according to their boiling point. An Agilent 7890 HT/SIMDIS system was used. The column installed was DBHT-SIMD, 5 m, 0.53 mm, 0.15 µm. Elemental analysis (C/H) was done by an elemental analyzer FLASH 2000 (Thermo Scientific) by norm ASTM D5291. Nitrogen and sulfur content was measured by a Trace SN Cube Instrument-Abacus Analytical Systems (ASTDM D5453, ASTDM D4629).

Attenuated total reflectance technique (ATR) was used for the FT-IR analyses. The samples were analysed using a Nicolet iS10 spectrophotometer (Thermo Scientific), provided with a crystal diamond (number of scans=64; resolution 4 cm⁻¹).

The feedstock (sewage sludge dried, in powder form and homogenised) was analysed by TGA, ATR and ICP. Liquid products were analysed by SIMDIS, ICP, ATR and elemental C, H, N, S% analyses. Gases products were analysed by GC-FID/TCD.

- Discussion and result analysis

C, H, N, S% and metal% contents were analysed (Table III) for the feedstock. In addition, TGA measurements were performed (Figure 1). No high weight losses were found around 100 °C because the feedstock was previously dried at 110 °C. The weight loss at 200–250 °C (in TGA-O₂, measurement repeated three times) can be due to the combustion of some light organic compound which could be favoured by the metal contents which could catalyse this combustion (Fe, V content values written in Table III). Next weight losses can be due to the decomposition and combustion of the organic matter. Because the final total weight loss for TGA-O₂ is lower compared to TGA-N₂, metal oxidation is expected. The metal oxidation could led to a weight increment of the inorganic part of the feedstock. For TGA-N₂, the weight loss is a progressive loss (200–500 °C) due to the pyrolysis of organic matter¹⁷. The weight loss at 700–900 °C is due to the decomposition of macromolecular refractory substances such as cellulose and humus¹⁷.

For the mass balance results (Table II), the test using oxalic acid (Test Iso-ox) led to a higher amount of products insoluble in *n*-heptane and only to a product with 14.9 wt% of maltenes. Test using tetralin as solvent led to a net production of maltenes. However, the tetralin was not only actuating as a hydrogen donor but also reacting to other molecules as shown in SIMDIS results (Figure 3). In addition, the product from Test Tetralin presented a H/C of 0.11 wt/wt (Table III) which is similar than the H/C of the tetralin (H/C = 0.1 wt/wt) indicating that the tetralin reacted could be reduced partially.

For Test Tetralin, the conversion to maltenes was 51 wt% (*n*-heptane insolubles to *n*-heptane solubles). This conversion was calculated including the inorganic part content of sewage sludge.

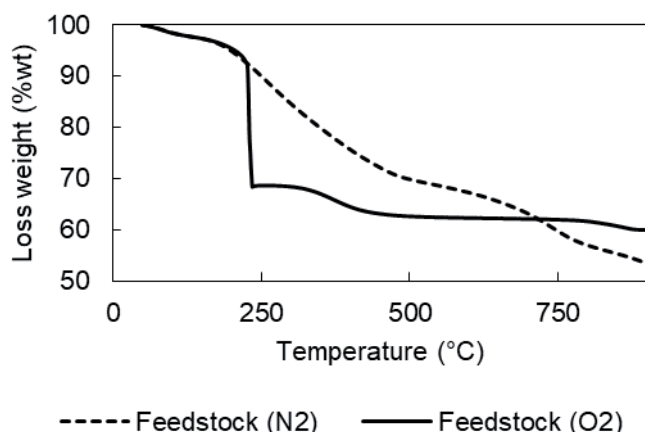


Figure 1. TGA analyses for the feedstock in nitrogen and oxygen atmospheres.

For test Iso-ox, the use of 2-propanol led to the production of a low amount of liquids with a high H/C (0.18 wt/wt). However, this test led to high production of aqueous compounds because of the oxalic acid decomposition (used to produce H₂). This test resulted in an increment of the amount of solid residues being the amount two times higher compared to the test using the direct liquefaction with tetralin. The use of 2-propanol led to the production of propylene (Table IV) with 7.3 wt% content from the total amount of product (gases + solids + liquids) which could be produced mainly from the 2-propanol. Some propane was also produced during the process due to the 2-propanol content in the feedstock.

Table II
Mass balance

	Test Iso-ox	Test tetralin
Gases, wt%	40.4	4.1
Liquids, wt%	23.1	54.1
Solids, wt%	36.5	41.8
Solid residues (<i>n</i> -heptane insolubles), wt%	22.2	10.9
<i>n</i> -heptane solubles in the product, wt%	14.9	85.0
Aqueous product, wt%	8.2	0.0

69.4 wt% of maltenes (tetralin), 30.6 wt% of solid (sewage sludge) in the feedstock-mixture.

The elemental content results of the feedstock and products (Table III) differed. The H/C weight ratio increased in the case of liquid products from Test Iso-ox and decreased for products from the direct liquefaction test. The sulfur content decreased in the two cases and the As content was under the level of detection of the instruments for the liquid products indicating that the As remained in the solid. Sulfur and nitrogen contents were much lower in the liquid products compared to the solid feedstock. The deoxygenation process resulted in low amounts of oxygen in the liquid products as also shown for the ATR-FTIR results (Figure 2).

Table III
Elemental C, H, N, and S% and metal analyses of the feedstock and oil products.

Element	Units	Feedstock	Test Iso-ox	Test Tetralin
C	wt%	20.9±0.4	84.5±1.7	90.2±1.8
H	wt%	3.1±0.1	15.6±0.5	9.54±0.3
H/C	wt/wt	0.15	0.18	0.11
S	wt%	2.11±0.17	0.0115±0.0009	0.0822±0.0066

N	wt%	2.66±0.13	0.00794±0.0004	0.0975±0.0049
Al	wt%	1.19	<0.00002	<0.00002
As	wt%	0.26	<0.000005	<0.000005
Ba	wt%	<0.000001	<0.000001	<0.000001
Ca	wt%	1.19	0.000032	0.000037
Co	wt%	<0.00001	<0.00001	<0.1
Cr	wt%	<0.0125	<0.00001	<0.1
Cu	wt%	<0.00001	<0.00001	<0.1
Fe	wt%	27.7	0.00032	0.00017
K	wt%	0.18	<0.00005	<0.00005
Mg	wt%	0.16	<0.00001	<0.00001
Mn	wt%	0.04	<0.00001	<0.00001
Na	wt%	0.16	0.00004	0.00002
Ni	wt%	0.02	0.00002	0.00002
P	wt%	<0.00005	<0.00005	0.000034
Sr	wt%	<0.000001	<0.000001	<0.000001
Ti	wt%	0.24	<0.00001	0.000004
V	wt%	5.35	0.00008	0.00003
W	wt%	0.00006	<0.00005	<0.00005
Zn	wt%	<0.00001	<0.00001	0.00002
Si	wt%	10.51	<0.00002	<0.00002
Oxygen (by difference) + other compounds	wt%	24.25	--	0.06

The gases content was influenced by the use of 2-propanol (Test Iso-ox) or tetralin as reactants (Table IV). No sulfur compounds were detected in the gases. So, the sulfur compounds remained mainly in the solid. The CO₂ content was the higher for the test using the oxalic acid as feedstock because of its decomposition to H₂, CO, H₂O and CO₂. In addition, more CO₂ could be produced by the Water-Gas-Shift reaction. For both tests, CO₂ was also produced from the deoxygenation reaction.

Table IV
Gases composition

Reactions/ Compound	Test Iso-ox Mole%	Test Tetralin Mole%
Hydrogen	14.69	93.89
Methane	2.42	1.71
Ethane	0.95	1.14
Ethylene	0.13	0
Propane	7.94	0.54
Propylene	18.05 (7.3)	0.01
C ₅ -C ₆	0.34	0.30
CO ₂	50.70	1.65
CO	4.78	0.75

For ATR-FTIR results (Figure 2), FTIR characterization can perform qualitative analysis of functional groups on the surface of the sewage sludge. A strong absorption peak between 3000 cm⁻¹ and 3750 cm⁻¹, which is due to the characteristic peak of -OH stretching vibration (feedstock). At 2650–3000 cm⁻¹, the signals are due to C-H groups for non-aromatic compounds and at 3000–3150 cm⁻¹ to C-H in aromatic compounds. The signals at 1600 and 1100 cm⁻¹ are due to the oxygen content in the feedstock (Figure 2)^{17, 24}.

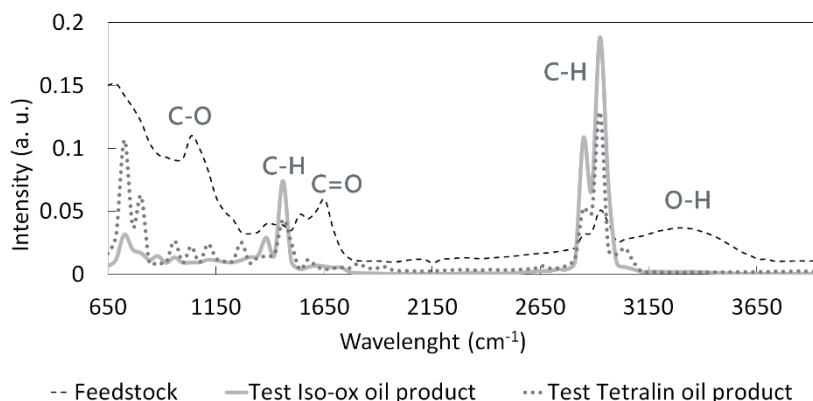


Figure 2. ATR-FTIR spectra for the feedstock and oil products.

The simulated distillation results of the direct oil products are shown in Figure 3 and Table V. Oil products from the test using tetralin were mainly in the boiling range of 200–350 °C (91 wt%) being this boiling point between the values of the tetralin (207 °C b. p.), naphthalene (218 °C b. p.) and, anthracene (340 °C b. p.).

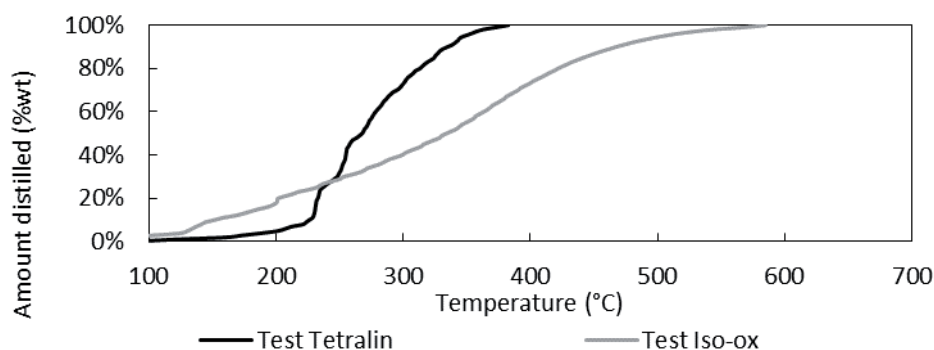


Figure 3. Simulated distillation of the oil products.

Table V. Boiling ranges (SIMDIS results) of the products.

Boiling range, °C	Test Iso-ox, wt%	Test Tetralin, wt%
<200	4	17
200-250	28	11
250-300	40	12
300-350	23	15
350-450	5	31
>450	0	14

- Conclusion

Two tests were carried out to study the sewage sludge hydrotreatment. A higher sewage sludge conversion was found for direct liquefaction test using tetralin. The test using oxalic acid as hydrogen donor and 2-propanol as solvent implied the production of propane and propylene from 2-propanol and a lower sewage sludge total conversion to maltenes. Deoxygenation and cracking reactions were performed. The products contents of sulfur, nitrogen and metals was much lower compared to the feedstock.

Acknowledgement

The work is a result of the project which was carried out within the financial support of the Ministry of Industry and Trade of the Czech Republic with institutional support for long-term conceptual development of research organisation. The result was achieved using the infrastructure included in the project Efficient Use of Energy Resources Using Catalytic Processes (LM2018119) which has been financially supported by MEYS within the targeted support of large infrastructures.

References

1. Topic Sewage Sludge (Waste and recycling), European Commission, https://ec.europa.eu/environment/topics/waste-and-recycling/sewage-sludge_en web accessed on June 6th 2022.
2. Council Directive 86/278/EEC of 12 June 1986 on the protection of the environment, and in particular of the soil, when sewage sludge is used in agriculture
3. Zaker A., Chen Z., Wang X., Zhang Q.: Fuel processing technology 187, 84 (2019).
4. Kwon E. E., Kim S., Jeon Y. J., Yi H.: Environmental science & technology 46, 10222 (2012).
5. Samolada M., Zabaniotou A.: Waste management 34, 411 (2014).
6. Zhang H., Gao Z., Ao W., Li J., Liu G., Fu J., Ran C., Mao X., Kang Q., Liu Y.: Journal of hazardous materials 334, 112 (2017).
7. Aziz S. M. A., Wahi R., Ngaini Z., Hamdan S.: Fuel Processing Technology 106, 744 (2013).
8. Arazo R. O., Genuino D. A. D., de Luna M. D. G., Capareda S. C.: Sustainable Environment Research 27, 7 (2017).
9. Atienza-Martínez M., Fonts I., Lázaro L., Ceamanos J., Gea G.: Chemical Engineering Journal 259, 467 (2015).
10. Xu Q., Liu X., Fu Y., Li Y., Wang D., Wang Q., Liu Y., An H., Zhao J., Wu Y.: Bioresource technology 267, 141 (2018).
11. Li S., Li C., Shao Z.: Sustainable Environment Research 32, 1 (2022).
12. Domínguez A., Menéndez J., Inguanzo M., Pis J.: Bioresource technology 97, 1185 (2006).
13. Xie Q., Peng P., Liu S., Min M., Cheng Y., Wan Y., Li Y., Lin X., Liu Y., Chen P.: Bioresource technology 172, 162 (2014).
14. Dai Q., Wen J., Jiang X., Dai L., Jin Y., Wang F., Chi Y., Yan J.: Journal of Analytical and Applied Pyrolysis 133, 169 (2018).
15. Mokhtar N., Ethaib S., Omar R.: Journal of Engineering Science and Technology 13, 3313 (2018).
16. Domínguez A., Menéndez J., Inguanzo M., Pis J.: Fuel Processing Technology 86, 1007 (2005).
17. Wang Y., Tian F., Guo P., Fu D., Heeres H. J., Tang T., Yuan H., Wang B., Li J.: Sci Rep 10, 18929 (2020).
18. Frątczak J., Hidalgo Herrador J. M., Lederer J., Stevens L., Uguna C., Snape C., Gómez de la Fuente J. L., Anděl L., Svoboda P., Pinto F.: Fuel 234, 364 (2018).
19. Wang Y., Tian F., Guo P., Fu D., Heeres H. J., Tang T., Yuan H., Wang B., Li J.: Sci Rep 10, 18929 (2020).
20. Chen N., Tao S., Xiao K., Liang S., Yang J., Zhang L.: Chemosphere 238, 124598 (2020).
21. Hidalgo Herrador J. M., Frątczak J., Tišler Z., de Paz Carmona H., Velvarská R.: Molecules 25, (2020).
22. Hidalgo Herrador J. M., Frątczak J., Velvarská R., de Paz Carmona H.: Molecular Catalysis 491, (2020).
23. Hidalgo Herrador J.M., Psenička M., Horaček J., Tišler Z., Vráblík A., Černý R., Murat M.: Chemical Engineering and Technology 42, 512 (2019).
24. Chan, W. P., Wang, J.-Y.: Journal of Analytical and Applied Pyrolysis 133, 97 (2018).

CHEMICAL PRETREATMENT OF INDUSTRIAL LIGNIN BY DISSOLVING IN ORGANIC SOLVENTS

Kafková V.¹, Ondrejčíková P.², Hruška M.²

¹Združenie "Energy 21", Trnavská cesta 1033/7, Leopoldov, Slovak republic

²Centrum výskumu a vývoja, s.r.o., Trnavská cesta 1033/7, Leopoldov, Slovak republic
kafkova@enviengroup.eu

Abstract

In the industrial paper production and also second-generation ethanol production processing the straw or wood waste as a feedstock, lignin is produced as a waste stream. To meet the request of a circular economy, there is an aim to further utilize lignin for the production of value-added products or energy. Most of lignin valorization processes strive for efficient lignin pretreatment. Pretreatment of lignin can be performed by biological, physical, chemical or physico-chemical pretreatment processes. This work aims to evaluate chemical treatment of lignin by dissolving in organic solvents. The research is based on the observation that the amount of lignin ash in the filter cake is increased when dissolving the organic part of lignin in organic solvents. The assumption is that the part of the organic matter is passing into the filtrate after filtration. The influence of different solvents on the lignin solubility is compared in the presented work.

Introduction

Lignocellulosic biomass (LCB) contains 10 – 30 % of lignin depending on the type of LCB. Chemically, lignin is a phenolic biopolymer with amorphous structure consisting of three phenylpropanoid monomers, p-hydroxyphenyl, guaiacyl and syringyl units, derived from p-coumaryl, coniferyl and sinapyl alcoholic precursors¹. Lignin is considered to be a barrier to biomass valorization, therefore biomass pretreatment is necessary for the efficient processing of the biomass. In biomass pretreatment processes lignin is thus separated from biomass remaining as a waste material². In 2018, an annual lignin production of approximately 70 Mt was recorded³, mainly recovered from kraft pulping process (kraft lignin) and the minority being produced by sulfite pulping process (lignosulfonates). Furthermore, there are also known the organosolv or soda lignins and hydrolyzed lignin as a by-product from bioethanol production⁴. Especially hydrolyzed lignin obtained by biomass hydrolysis using cellulolytic enzymes possesses a high value with potential applications such as sorbent development (even despite of the high content of impurities including carbohydrates and protein residues). In addition, hydrolyzed lignin can be used for development of new polymers e. g. by combining lignin with a synthetic polymer. The valorization of lignin separated from biomass is critically important for the biorefinery economic viability, as it contributes to significant improvement in biofuel production economics⁵.

Only 1 – 2 % of the lignin is used commercially for chemical conversion to produce lignosulfonates⁶. The rest is used as a low-value combustion fuel in biorefineries². Thus, there is a great potential for lignin valorization and production of the bio-based chemicals or alternative materials to petroleum-based products, which can lead to emission reduction, greener economy and sustainable environment development⁷. Valorization of lignin into the specialty chemicals and value-added products is a major concern in processing of lignocellulosic materials⁴. The current possibilities for lignin valorization can be divided into 2 categories: lignin depolymerization for production of chemicals (phenolic or other aromatic compounds) and lignin modification for the development of new biobased materials⁷. To obtain more uniform structure of lignin, also fractionation has been proposed as a promising method to obtain specific lignin polymer properties for further valorization. Methods for lignin fractionation can be grouped into 4 categories: precipitation with an acidic solution, multiple solvent extraction, solvent/water extraction, and membrane technology, with examples showed in Table I⁸.

Table I

Methods for lignin fractionation⁸

Fractionation methods	Example
pH control (changing pH)	<ul style="list-style-type: none">• Sequential precipitation using H₂SO₄ or HCl at room temperature;• Precipitation with acid and separation of insoluble part;• Separation at high temperature and pressure;
Solvent/water extraction	<ul style="list-style-type: none">• Ethanol/Water, Acetone/Water, THF/Water;• AcOH/Water, room temperature/high temperature/pressure;
Solvent extraction	<ul style="list-style-type: none">• Alcohols, chloroform, ether, DMSO, DCM, THF, hexane, ketones;
Ultrafiltration/membrane	<ul style="list-style-type: none">• Ceramic filters/Polymeric filters.

Discoveries in fractionation of lignin into homogeneous fraction with organic solvents has recently attracted the attention⁴. By using the solvent for dissolving a portion of lignin and by subsequent separation of soluble and insoluble bulk of lignin, it is more likely that the uniform lignin fractions could be obtained⁹. Solvent fractionation could be utilized as the first step in lignin refining to adjust some of its properties before further processing. However, lignin solubility in different solvents is a varying property, dependent mainly on the type of lignin and its origin. Lignin solubility also differs due to the highly heterogeneous nature of lignin. Solubility may be affected by polarity, degree of polymerization and cross-linking, as well as by pH of the solvent⁹. Sameni et al. stated that the lower the molecular weight is the higher the solubility in organic solvents exist, and with the increasing aliphatic hydroxyl number the solubility in organic solvents decreases¹⁰.

Despite of increasing number of publications dealing with the lignin solubility no specific agreement in findings about solubility of lignin in organic solvent was achieved. Rahman et al. (2013) reported that kraft softwood lignin was completely soluble in DMSO and partially soluble in THF and chloroform. Sameni et al. (2017) reported that kraft softwood lignin was almost soluble in DMSO but only slightly soluble in THF and almost insoluble in chloroform. Horvath (2005) stated that the ability of a solvent to dissolve lignin has increased with the increasing hydrogen-bonding capacity of solvent¹⁰. By experimenting with an alcohol and ketone solvents for kraft softwood lignin dissolving process, Sadeghifar and Ragauskas (2020) detected the highest solubility of lignin in acetone with the yield of soluble fraction of 66.5 %, followed by methanol with yield 61.2 %⁸.

This work aims to evaluate chemical treatment of specific lignin by-product known as hydrolyzed lignin by dissolving the lignin in organic solvents (ethanol, methanol, acetone) and to assess the lignin solubility in solvents.

Materials and methods

Solvents used: acetone (Centralchem, s.r.o.), ethanol and methanol (99 % purity) provided by Envien Group.

Lignin characterization

Dried and grinded hydrolyzed wheat lignin from the production of second-generation ethanol was tested. Lignin was characterized in accordance with standardized methods. Total carbon, total hydrogen, total sulfur and total nitrogen contents were determined by elemental analysis on a device with four different detectors in an inert gas. Total oxygen content was calculated by subtraction.

Determination of ash

The ash content was determined by the weight method after incineration of the sample under the established conditions. The crucible was annealed in a muffle furnace at 650 °C for 30 minutes, then cooled in a desiccator to constant weight, and weighed (m_0). Approximately 1 g of sample was weighed and put into the crucible (m_1). The crucible was placed into the muffle furnace and annealed for 3 hours at 650 °C. After incineration, the crucible was cooled in a desiccator and weighed (m_2). The ash content was calculated according to the formula:

$$\% \text{ wt.} = \frac{m_2 - m_0}{m_1 - m_0} * 100$$

Dissolution of lignin in organic solvents

Acetone, methanol and ethanol with/without addition of H₂SO₄ (5 mL, concentrated) were used for dissolving process. The 50 g of lignin was weighed into a flask, then 500 ml of solvent (with/without acid addition) was added and stirred under the following conditions: laboratory temperature (20 °C), or alternative boiling temperature (56 - 78 °C), mixing time and intensity - 12 hours, 300 rpm. Then the sample was vacuum filtered and labelled (see Table II). The liquid part of mixture was saved for further analysis, the solid part was dried in the oven (2 hours, 105 °C) and weighed. The yield was calculated with 2 % deviation. The soluble fraction was calculated based on the weight of the insoluble fraction. The amount of ash was determined according to the method above.

Qualitative analysis of samples M65 and M65K

As a first step, tube-based thermal desorption of volatile compounds was performed under the followed conditions:

- Sorption: nitrogen as a carrier gas with a flow rate 14-18 ml/min, temperature 140 °C, duration 10-15 min, sorbents Tenax[®] and Carbograph[®].
- Desorption: temperature 250 °C, duration 2 min, flow rate of helium 20 ml/min, splitless mode, device Markes Unity 2

Captured compounds were analyzed using gas chromatograph GC 7890A with mass spectrometer detector 5975C and column HP-5MS. Helium was used as a carrier gas. The measured mass spectra were compared with the mass spectra of the compounds using the NIST and Wiley electronic databases.

Table II
Labelling of lignin samples and specification of experiment conditions.

Sample	Conditions		Sample	Conditions	
	Solvent	Temperature, °C		Solvent	Temperature, °C
A56K	acetone + H ₂ SO ₄	56	M65K	methanol + H ₂ SO ₄	65
A56	acetone	56	M65	methanol	65
A20K	acetone + H ₂ SO ₄	20	M20K	methanol + H ₂ SO ₄	20
A20	acetone	20	M20	methanol	20
E78K	ethanol + H ₂ SO ₄	78	E20K	ethanol + H ₂ SO ₄	20
E78	ethanol	78	E20	ethanol	20

Results and discussion

Elemental analysis showed the similar values of the analyzed elements reported in the literature, except increased nitrogen values in all samples. Higher values of sulfur content in selected samples were expected as H₂SO₄ was added. The most important parameter is carbon content. Analyses showed decrease in carbon content after lignin dissolving in almost all samples by 0.3 – 4.4 % (excluding sulfur content in samples with H₂SO₄ addition). By lignin dissolving in used solvents (with or without acid addition), the ash content was increased by 12 – 40 %. This means that the organic part of lignin is partially soluble in selected solvents (with/without acid addition). The highest ash content was observed in sample M65K, the lowest in sample E20. Increasing temperature and addition of acid into the solvent had positive effect on increasing of ash content.

The calculated yield is related to the solid part of lignin after dissolving. Regarding to yield of solid part after dissolving, the lower the yield is, the more organic part of lignin is expected to dissolve in solvent (passes into the filtrate) or the higher solubility of lignin is in the selected solvent. Based on results, the most effective lignin dissolving was carried out under the following conditions - methanol used as a solvent, boiling temperature and H₂SO₄ addition. In this case the yield of solid part after lignin dissolving was almost 70 %, which counts for 30 % of lignin being solubilized in pure methanol. The lowest solubility was observed with ethanol used as solvent at room temperature with reached value accounting for 15 % of soluble part of lignin. All results are shown in Table III.

Table III
Analysis of lignin samples before and after dissolving in organic solvent with/without H₂SO₄ addition

Sample	Ash content, %	Yield, %	Elemental analysis, %				
			N	C	H	S	O
Lignin	9.77	-	1.61	48.76	5.86	0.10	43.67
Lignin (lit.)^{11,12}	< 36	-	0-0.2	42-66	3.4-6.0	0.1-6.3	28-48
A56K	12.73	81.2	1.70	44.00	5.19	3.39	45.72
A56	11.7	83.6	1.74	47.44	5.62	0.16	45.05
A20K	13.05	82.0	1.72	44.95	5.30	3.38	44.65
A20	12.02	82.8	1.76	48.27	5.70	0.16	44.12
E78K	13.67	77.6	1.51	44.45	5.58	2.28	46.19
E78	12.74	80.6	1.71	48.27	5.67	0.15	44.20
E20K	12.37	82.4	1.59	46.41	5.45	1.82	44.72
E20	11.02	85.8	1.62	48.43	5.69	0.12	44.14
M65K	13.68	69.6	1.56	45.58	5.47	2.31	45.08
M65	12.03	76.0	1.73	48.33	5.66	0.15	44.14
M20K	12.66	77.4	1.52	46.72	5.67	1.99	44.10
M20	11.82	79.6	1.67	48.88	5.86	0.13	43.45

Our previous study with the same hydrolyzed lignin¹³ showed that when water solution of solvent was used, the most effective dissolving of lignin took place with acetone-water solution (60 vol. % of acetone) as a solvent. Based on these studies we can conclude that the water as a co-solvent affects lignin solubility in dissolving process. Goldmann et al. (2019) has reported comparable conclusion that kraft lignin solubility in pure ethanol is lower than in ethanol-water solution (60 % of ethanol). Considering lignin:solvent ratio similar to our work, the achieved solubility of lignin in pure ethanol was 27 wt. % while in the ethanol-water solution (60 % of ethanol) the solubility of 90 wt. % was achieved⁹. Solubility of hydrolyzed lignin was also tested by Sameni et al. (2017). To compare our results, Sameni et al. stated the higher solubility in all three solvents observed, while the highest solubility of lignin was achieved in acetone (approximately 45 %), followed by methanol (up to 40 %) and the lowest solubility was detected in ethanol (approximately 25 %). Sameni et al. also stated that lignin was almost completely soluble in pyridine and DMSO, while good solubility was observed also in dioxane used as solvent¹⁰.

The sample with highest yield of soluble part of lignin (M65K) was analyzed for determination of compounds present in liquid part after dissolving. The comparison with liquid part of sample M65 (without acid addition) was performed. A total of 38 compounds and 56 compounds were detected in samples M65K and M65, respectively. The eleven compounds with the largest peak area for each sample are shown in Table IV. Methylated compounds were predominantly present in sample M65K with the largest area of peak corresponding to dimethyl ester sulfuric acid (due to sulfuric acid and methanol reaction not related to lignin dissolving). Compounds present in the sample M65K are mainly used as a flavoring or fragrance components. Levoglucosenone present in sample M65K is reported as a promising bio-renewable platform for the production of polyesters and polyurethanes¹⁴, also with high potential to be used as a template for the synthesis of key intermediates of biologically active products and suitable for the preparation of chiral auxiliaries, catalysts, and organocatalysts applied in asymmetric synthesis¹⁵. Compounds present in M65 sample were significantly different in comparison with compounds present in sample M65K. Three fatty acids and two flavoring and fragrance components (2-methoxy-4-vinylphenol, 2,6-dimethoxy phenol) were present in sample M65. Detected coumaran (2,3-dihydro-benzofuran) compound is used as a potent biofumigant¹⁶. Phytosterols and vanillin presence was also observed.

Table IV

Compounds present in samples M65 and M65K after lignin dissolving in methanol

Sample	RT [min]	Area [Ab*s]	Compounds	Quality	Mol. weight [amu]
M65K	2.858	1293265469	Sulfuric acid, dimethyl ester	87	125.999
	4.904	188478462	Levoglucosenone	46	126.032
	9.664	160139219	Citric acid, trimethyl ester	64	234.074
	10.459	65017033	Dodecanoic acid, methyl ester	98	214.193
	10.565	50984916	Benzoic acid, 4-hydroxy-3-methoxy-, methyl ester	97	182.058
	10.809	48034969	Nonanedioic acid, dimethyl ester	93	216.136
	12.898	45162401	2-Pentadecanone	96	226.230
	12.961	44069450	Methyl myristoleate	91	240.209
	13.023	43734729	Methyl myristoleate	89	240.209
	13.236	39327055	Methyl tetradecanoate	98	242.225
	14.012	37342299	Benzoic acid, 4-hydroxy-3,5-dimethoxy-, hydrazide	98	212.080
M65	18.387	199478577	Octadecanoic acid	99	284.272
	16.354	195555905	n-Hexadecanoic acid	99	256.240
	7.453	186365003	2-Methoxy-4-vinylphenol	94	150.068
	6.114	108422006	Benzofuran, 2,3-dihydro-	74	120.058
	27.945	80652145	Gamma-Sitosterol	99	414.386
	16.023	70780562	Pentyl tetradecyl ether	46	284.308
	17.655	55198696	9-Octadecenoic acid, methyl ester, (E)-	99	296.272
	13.833	33797385	Tetradecanoic acid	99	228.209
	8.01	32529827	Phenol, 2,6-dimethoxy-	97	154.063
	26.97	31998019	Campesterol	96	400.371
	8.823	31902110	Vanillin	96	152.047

Conclusion

Lignin is often considered as a waste stream produced in biomass valorization, being processed mainly as a low-value combustion fuel in biorefineries. Generally, lignin obtained by biomass processing has a great potential for production of higher value-added products. Therefore, an effort is made for finding suitable pretreatment process for lignin valorization. To obtain a more uniform lignin structure, it is possible to choose from wide range of methods based on biological, physical, chemical or physico-chemical pretreatment processes. Lignin dissolving in specific solvents represents the chemical treatment step which is a promising first step for lignin valorization. Taking into account the above-mentioned fact, the aim of our work was to focus on dissolving of industrial lignin in acetone, methanol and ethanol (with or without acid addition) as solvents available for industrial application. The findings of this research are following:

- Elemental analysis did not show any significant changes in composition of samples after the extraction (excluding increased sulfur content due to H₂SO₄ addition);
- The lignin of interest comprises of higher nitrogen content compared to values from literature;
- The temperature rise and addition of acid has a positive effect on increasing of ash content;
- Used solvents are suitable for lignin dissolving, ash concentration, respectively;
- Ash content increased by 12 – 40 % after lignin dissolving;
- The lowest yield of solid parts and the highest lignin solubility was observed under the following conditions – methanol used as a solvent, boiling temperature and H₂SO₄ addition; the soluble part of lignin accounted for 30 % of lignin sample under these conditions;
- The lowest solubility was observed with ethanol used as solvent at room temperature; the soluble part of lignin accounted for 15 % of lignin sample;
- Interesting compounds were found in liquid part of dissolved lignin, but further quantification of compounds has to be done and potential separation process should be discussed.

Acknowledgement

This work was supported by the Slovak Research and Development Agency under the contract No. APVV-18-0255.

Nomenclature

AcOH	Acetic acid
Amu	Atomic mass unit
DCM	Dichloromethane
DMSO	Dimethyl sulfoxide
LCB	Lignocellulosic biomass
RT	Retention time
THF	Tetrahydrofuran

References

1. Lu Y., Lu Y.C., Hu H.-Q., Xie F.-J., Wei X.-Y., Fan X.: *Journal of Spectroscopy* 2017 (2017).
2. Wang Y., Meng X., Jeong K., Li S., Leem G., Kim K. H., Pu Y., Ragauskas A. J., Yoo C. G.: *ACS Sustainable Chem. Eng.* 8, 12542 (2020).
3. Bajwa D. S., Pourhashem G., Ullah A. H., Bajwa S. G.: *Ind. Crops Prod.* 139, 111526 (2019).
4. Li M.-F., Sun S.-N., Xu F., Sun R.-C.: *Sep. Purif. Technol.* 101, 18 (2012).
5. Asin FNU, Brzonova I., Kozliak E., Kubátová A., Ji Y.: *Renewable Sustainable Energy Rev.* 77, 1179 (2017).
6. Demuner I. F., Colodette J. L., Demuner A. J., Jardim C. M.: *BioRes.* 14, 7543 (2019).
7. Sun R.-C., Samec J. S. M., Ragauskas A. J.: *ChemSusChem* 13, 1 (2020).
8. Sadeghifar H., Ragauskas A.: *ACS Sustainable Chem. Eng.* 8, 8086 (2020).
9. Goldmann W. M., Ahola J., Mikola M., Tanskanen J.: *Sep. Purif. Technol.* 209, 826 (2019).
10. Sameni J., Krigstin S., Sain M.: *BioRes.* 12, 1548 (2017).
11. The University of Tennessee, Knoxville, Chemical and Biomolecular Engineering, Elemental analysis of lignin (http://biorefinery.utk.edu/technical_reviews/Lignin%20to%20biofuels-97.pdf) [cited on 10.06.2022].
12. Sameni J., Krigstin S., Rosa D., Leao A., Sain M.: *Bioresources* 9, 725 (2014).
13. Kafková V., Holíčková M., Ondřejíčková P.: *Waste Forum* 1, 17 (2021).
14. Floriand D.-N., Louis M., Sami F., Stephen M., Florent A.: *ChemSusChem* 13, 2613 (2020).

15. Comba M. B., Tsai Y., Sarotti A. M., Mangione M. I., Suárez A. G., Spanevello R. A.: *Eur. J. Org. Chem.* *5*, 590 (2018).
16. Rajashekar Y., Raghavendra A., Bakthavatsalam N.: *BioMed Res. Int.* *2014*, 187019 (2014).

POSSIBILITIES OF HYDRODEBROMINATION OF BROMINATED AROMATIC COMPOUNDS USING Cu-BASED CATALYSTS

Kamenická B.¹, Weidlich T.¹

¹University of Pardubice, Faculty of Chemical Technology, Chemical Technology Group, Studentska 95, 532 10 Pardubice,
barbora.kamenicka@student.upce.cz

Abstract

Polybrominated aromatic compounds are widely used as pesticides, flame retardants and as a part of chemical structures of other organic fine chemicals. Due to their high chemical resistance, they are common non-biodegradable aqueous contaminants. One of the available method applicable for simple degradation of these mentioned polybrominated aromatic compounds is based on hydrodebromination reaction. The hydrodebromination represents robust technique for conversion of polybrominated contaminants to non-brominated ones, which are biodegradable in environment. Our research was focused on the effect of different sources of copper-based hydrodebromination catalysts on the reduction of two industrially important chemicals such as herbicide Bromoxynil and brominated flame retardant Tetrabromobisphenol A.

Introduction

Residues of non-biodegradable specialty fine chemicals such as brominated organic derivatives used as flame retardants (TBBPA) or pesticides (BRX) are found in plastic waste, soil and surface water, even in groundwater¹. In water, it is likely to pose health hazards to non-target aquatic organisms²⁻⁵. Following toxicity of mentioned substances represented by Tetrabromobisphenol A (TBBPA, Fig. 1)⁶ or Bromoxynil (BRX, Fig. 1)⁷, their effective degradation to the readily biodegradable products was studied⁸. The reductive treatment based on hydrodebromination (HDB) plays important role in detoxification of polybrominated aromatic contaminants⁹⁻¹¹. HDB is an effective way for destruction of brominated organic compounds under mild reaction conditions¹⁰. HDB method enables substitution of bromine atoms bound in aromatic ring by hydrogen and formation of non-brominated biodegradable products⁹⁻¹². We proved that some copper-based metallic alloys (e.g. Devarda's Al-Cu-Zn alloy) or other Cu-based materials can be used for HDB of studied BRX or TBBPA in diluted alkali metal hydroxide solution¹²⁻¹⁵. This work deals with searching for the reaction conditions enabling the complete HDB of BRX or TBBPA and with comparing of effect of copper-based materials proved as the effective HDB agents.

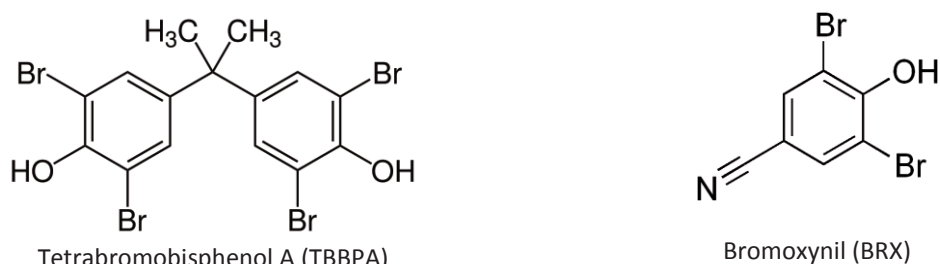


Figure 1. Chemical structures of widely used polybrominated aromatic compounds occurring in environment as contaminants.

Experiment

Materials and Methods

The starting model brominated contaminants Bromoxynil (ABCR Chemicals GmbH., Germany) and Tetrabromobisphenol A (Alfa-Aesar Co., UK) were purchased from commercial sources in a defined purity higher than 95%. The tested aluminium-based alloys (Devarda's Al-Cu-Zn, 45–50–5%, p.a.; Arnd's Mg-Cu, 40–60%; brass, Cu-Zn powder—60 mesh; bronze, Cu-Sn spherical powder—200 mesh) and copper-based compounds (CuO (CuO nanopowder < 50 nm and CuO powder < 10 μm, 98%), metallic Cu (Cu nanopowder 60–80 nm and Cu powder < 425 μm, 99.5%), Cu₂O (powder < 99.99%, anhydrous), CuBr₂ (99%)) and NaBH₄ (95%) and deuterated chloroform (CDCl₃) were purchased from Sigma-Aldrich Co. (Czech Republic). The Fe₃Al (97.5%) and silver brazing alloy (1.6 mm dia, Ag:Cu:Zn 30:38:32) was purchased from Alfa-Aesar Co. (Thermo Fisher Sci., UK). Additional chemicals and solvents in a p.a. quality were obtained from a local supplier (Lach-Ner Co., Neratovice, Czech Republic). The

comparative experiments were performed in 250 mL round-bottomed flasks equipped with magnetic stirring on Starfish equipment (Radleys Discovery Tech., UK) installed on a magnetic stirrer Heidolph Heistandard for parallel reactions. The reaction flasks were fitted by a tube filled with granulated charcoal.

Chemical Analysis

The ^1H NMR spectra were recorded from solutions in CDCl_3 on a Bruker Avance 500 spectrometer (equipped with a Z-gradient 5mm Prodigy TM cryoprobe) at a frequency of 500.14 MHz or on a Bruker Ultra Shield TM 400 spectrometer at frequency of 400.13 MHz at 295 K. The solutions were obtained by dissolving of evaporated residue (resulting from the work-up of reaction mixtures) in 1 mL of CDCl_3 . The values of ^1H chemical shifts were calibrated to the residual signals of CDCl_3 ($\delta(^1\text{H}) = 7.27$ ppm). The mutual content of particular constituents in obtained mixtures was established via the integration of the corresponding area resonances.

HDB of Brominated Phenols Using Studied Al Alloys or Cu-compounds and NaBH_4

Al-based alloy, electropositive metal or Cu-based catalyst (appropriate quantities are specified in Figures 4-6) was mixed with the aqueous solution (5 mM, 100 mL) of Bromoxynil dissolved in aq. NaOH solution and eventually other tested chemical was added slowly under vigorous stirring to the obtained suspension. The reaction mixture was stirred at 500 rpm at 25 °C for the appropriate time period, decanted, aqueous phase was filtered, and the filtrate was acidified to $\text{pH} \sim 2.5-3$ using 16 wt.% H_2SO_4 and extracted with one portion of CH_2Cl_2 (1 x 100 mL) overnight under vigorous stirring. Collected CH_2Cl_2 extract was evaporated to dryness and approximately 30 mg of nonvolatile residue was dissolved in CDCl_3 . ^1H NMR spectrum of obtained CDCl_3 solution (and eventually GC-MS) indicates the conversion of the BRX to HDB products.

HDB of Brominated Phenols Using In Situ Generated Cu

An appropriate quantity of NaBH_4 was dissolved in the solution (5 mM, 100 mL) of BRX dissolved in aqueous NaOH solution, and to this solution, appropriate quantity of additive and subsequently aqueous CuSO_4 solution (40 mM, 50 mL) was added dropwise under vigorous stirring (exact quantities are specified in Figures 5 and 8). The reaction mixture was stirred at 500 rpm at 25 °C overnight, filtered, acidified to $\text{pH} \sim 2.5-3$ using 16 wt.% H_2SO_4 and extracted with one portion of CH_2Cl_2 (1 x 100 mL) overnight using vigorous stirring. The collected CH_2Cl_2 extract evaporated to dryness and approximately 30 mg of nonvolatile residue was dissolved in CDCl_3 . ^1H NMR spectrum of obtained CDCl_3 solution (and eventually GC-MS) indicates the conversion of the BRX to HDB products. For analyses of brominated compounds and products of their reduction in sample of aqueous solutions extraction with CH_2Cl_2 was performed (50 mL of aqueous phase acidified to $\text{pH} = 2-3$ was extracted by 50 mL of CH_2Cl_2 by overnight vigorous stirring) with subsequent evaporation of obtained dichloromethane phase to dryness.

Results and Discussion

A set of experiments, involving different reductants within the HDB of BRX or TBBPA, and dissolved in alkaline aqueous solution, were performed. Electropositive metals, various copper alloys containing electropositive metals and Cu-based compounds in co-action of NaBH_4 were employed as potential HDB agents in mentioned experiments. The total HDB of TBBPA via tribromobisphenol A (triBBPA), dibromobisphenol A (DBBPA) and bromobisphenol A (BBPA), to bisphenol A (BPA) is described in Figure 2.

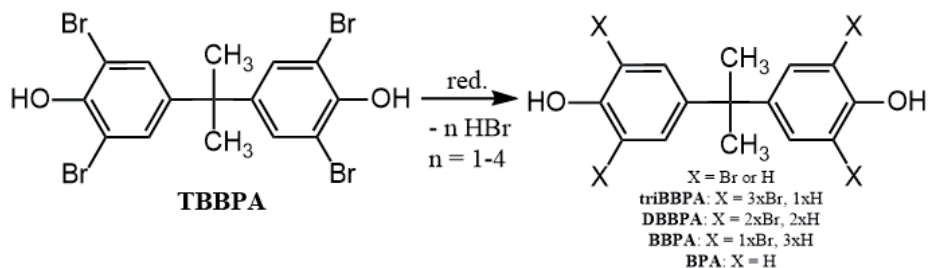


Figure 2. Reaction schemes of hydrodebromination of TBBPA

The total HDB of BRX via the 3-bromo-4-hydroxybenzoxynil (3-Br-4-HBN) to 4-hydroxybenzoxynil (4-HBN) is described in reaction scheme on Figure 3-A. Except the HDB reaction, subsequent formation of 4-hydroxybenzaldehyde (4-HBA) generated by a reduction of the cyano group was observed in some cases (e.g. prolonged reaction times or use of a higher excess of the Devarda's alloy), see Figure 3-B.

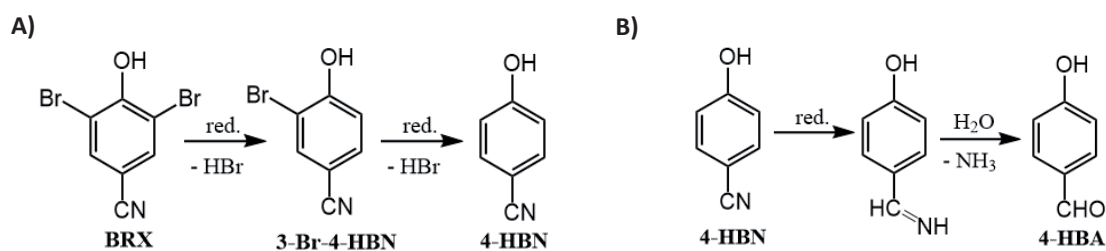


Figure 3. Reaction schemes of hydrodebromination of BRX (A) and subsequent reduction of nitrile (B) observed as the side reaction.

A set of experiments, involving chemically diverse reductants within the HDB of 3,5-dibromo-4-hydroxybenzonitrile (BRX), and dissolved in alkaline aqueous solution, were performed. Various copper alloys containing electropositive metals and elemental copper were employed as potential HDB agents in these experiments. The results summarized in Figure 4 show that only the Devarda's alloy exhibits high HDB activity at room temperature over one hundred minutes of vigorous stirring of the respective reaction mixture.

Testing different copper compounds with co-action of NaBH_4 as the potential sources of Cu-catalyst and HDB agent, CuSO_4 and Cu_2O were found as the very effective sources of HDB catalysts in co-action of NaBH_4 (Figure 5).

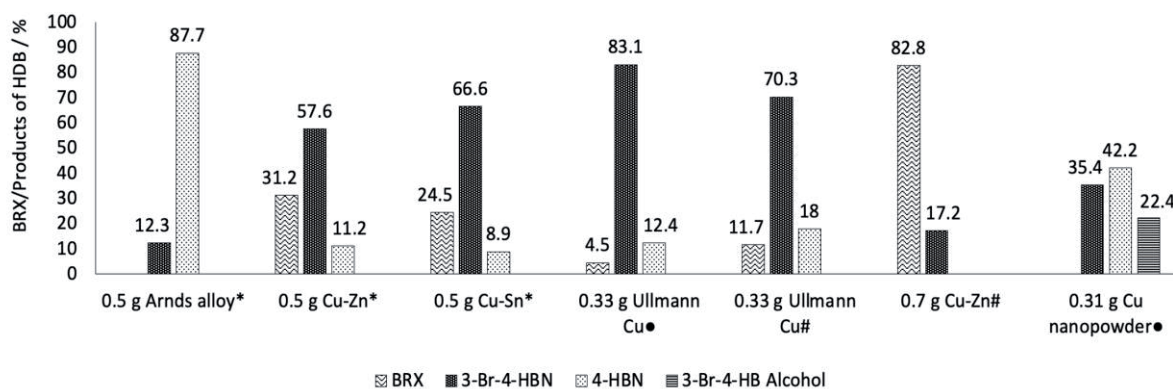


Figure 4. The effect of different sources of Cu-catalysts on HDB of BRX (After 18 h of stirring. Quantity of HDB agents added to the solution of *0.5 mmol BRX + 2 mmol NaOH dissolved in 100 mL H_2O , #0.5 mmol BRX dissolved in 100 mL CH_3OH).

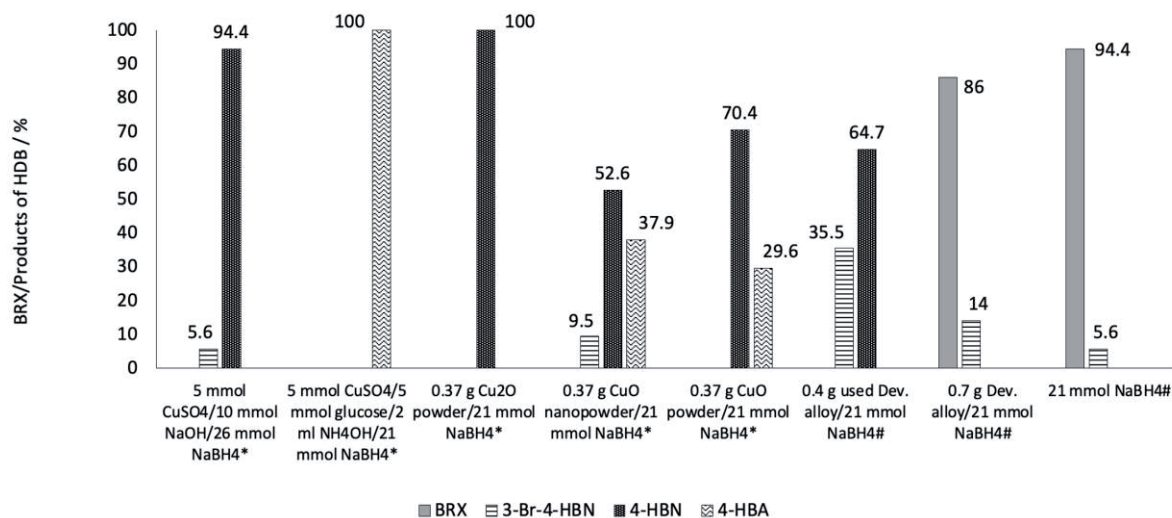


Figure 5. The effect of different sources of Cu-catalyst on HDB of BRX using NaBH₄ as reductant (After 18 h. stirring. The quantity of HDB agents added to the solution of *0.5 mmol BRX + 10 mmol NaOH dissolved in 100 mL H₂O + addition of 5 mmol NaBH₄, ●0.5 mmol BRX + 2 mmol NaOH dissolved in 100 mL H₂O + addition of 21 mmol NaBH₄, #0.5 mmol BRX dissolved in 100 ml CH₃OH + addition of 21 mmol NaBH₄)

The optimal quantity of Devarda's alloy was tested in the range of experiments indicating the minimal quantity 0.6 g of Devarda's alloy for complete hydrodebromination of 1 mmol BRX (Figure 6). The higher quantities of Devarda's alloy cause subsequent reduction of cyano group producing 4-hydroxybenzaldehyde (4-HBA).

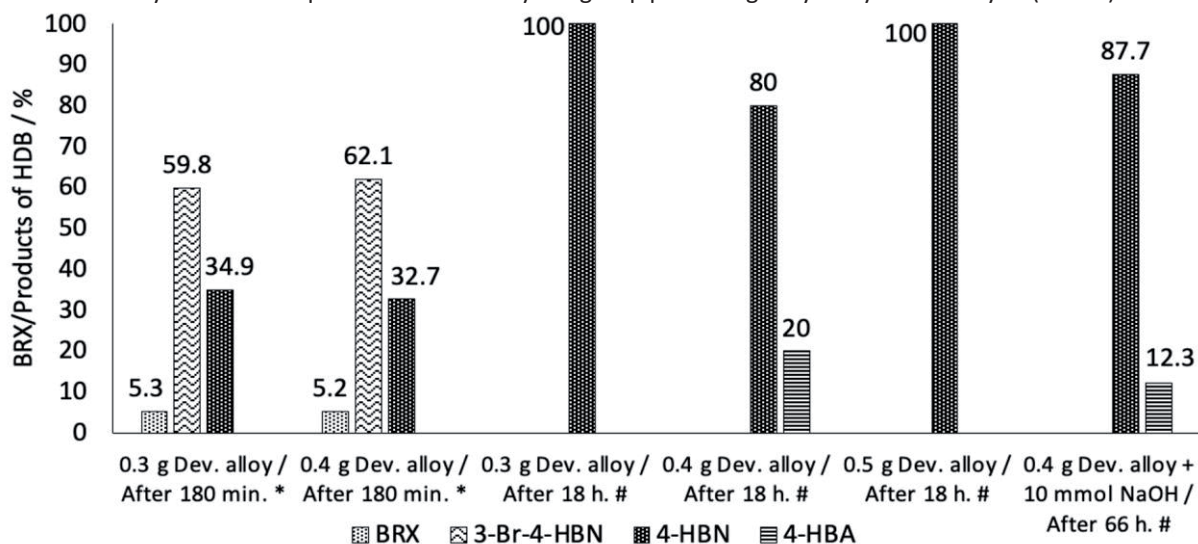


Figure 6. HDB of BRX using Dev. alloy and NaOH (After 18 h of stirring. Quantity of Dev. alloy added to the solution of: *0.5 mmol BRX + 2 mmol NaOH dissolved in 100 mL H₂O, #0.5 mmol BRX + 10 mmol NaOH dissolved in 100 mL H₂O)

For comparison of HDB activity, most effective Cu-based HDB reagents were tested for HDB of TBBPA (Figure 8). As is illustrated in Figure 8, the most active HDB agents are Devarda's alloy or copper sulfate in co-action of excess of NaBH₄.

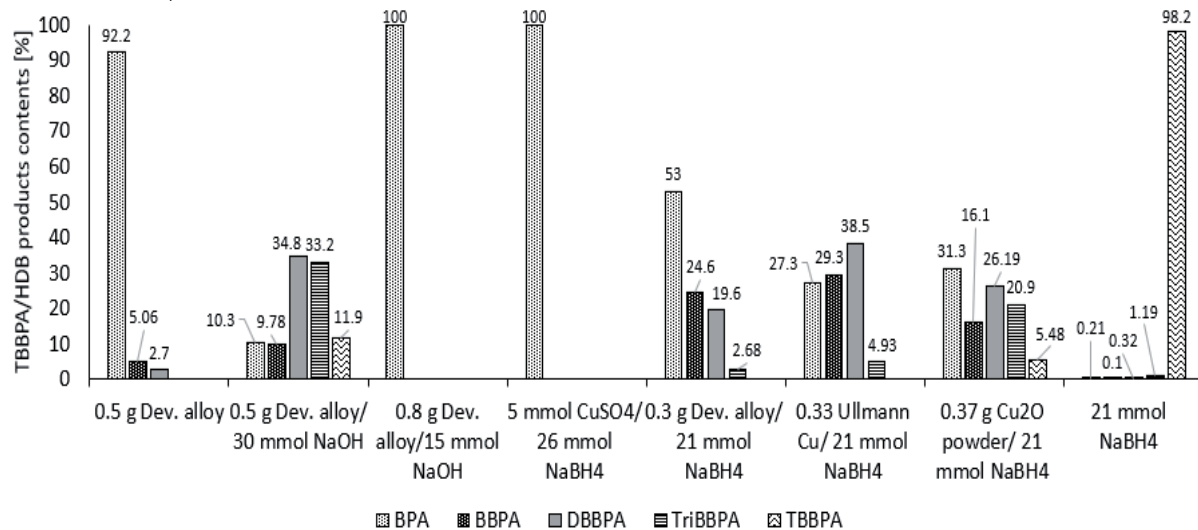


Figure 8. HDB of TBBPA using Dev. alloy and NaOH or different sources of Cu-catalyst (After 18 h of stirring. Quantity of HDB agents added to the solution of 0.5 mmol TBBPA + 2 mmol NaOH dissolved in 100 mL H₂O).

Conclusions

The above results of experiments proved that the some of the tested Cu-based agents (Devarda's alloy, Cu₂O, in-situ generated Cu by CuSO₄ and NaBH₄) for the HDB of studied BRX achieved interesting results (Fig. 5-8). The application of mentioned Devarda's alloy in alkali solution seems to be a promising method of HDB of BRX (Fig. 7). It was also found that some Cu-based materials (Arnd's alloy, Cu-Zn, Cu-Sn, Ullmann Cu or Cu nanopowder) are not as effective for HDB of BRX as mentioned Devarda's alloy (see Fig. 5 and 6). Nevertheless, we have verified

WASTE TREATMENT, WATER PROTECTION

BIOTECHNOLOGY AND BIOREFINERY

OPTIMIZATION OF CULTIVATIONS OF CAROTENOGENIC YEASTS ON POULTRY WASTE SUBSTRATES

Holub J.¹, Chujanov O.¹, Szotkowski M.¹, Šimanský S.¹, Schildová V.¹, Dzurická L.¹, Márová I.¹

¹Brno University of Technology Faculty of Chemistry, Brno, Czech Republic
Jiri.Holub2@vut.cz

Abstract

Carotenogenic yeast, which are also called oleaginous, are microorganisms capable of accumulating significant amounts of carotenoids, lipids, and glucans into their biomass. Their ability of processing waste materials and different carbon sources from various industries, such as agricultural industry, provides the possibility to use them for waste material treatment. This waste treatment process then could be used as a part of circular economy cycle. This research is focused on optimization of cultivation process in Erlenmeyer flasks by changing cultivation conditions and media composition as well. Research is focused on carotenogenic yeasts, especially the genus *Rhodotorula*, *Cystofilobasidium* and *Rhodospiridium* which have achieved significant results with interesting biomass growth (above 20 g/l). The optimization process is focused predominantly on mineral media with addition of animal by-products, namely poultry waste feathers and fat. Hydrolysed feathers play a major role as nitrogen source and waste fat serves as carbon source.

Introduction

Ensuring food security for the growing human population requires a continuous increase in the volume and efficiency of agricultural production and in the processing of food raw materials. One of the ways to make the food production process more efficient is to seek new methods of processing waste materials from food and agriculture industries via processes of circular economy¹. The concept of circular economy within the food industry and agriculture includes more efficient handling of biomass and its reuse, for example in the form of nutritional substrates for animal and microorganisms in order to valorise food waste into valuable products.

Carotenogenic yeasts are heterotrophic, mainly aerobic ubiquitous microorganisms that contain many biologically active compounds within their cells, and they possess extracellular lipase activity, which allows them to process various sources of waste greasy substrates³. The concept of circular economy is applied to reuse waste substrates such as waste poultry fat or poultry feathers in pure or pre-treated form by cultivation of carotenogenic yeasts. Yeasts are capable of incorporating macroelements and microelements from complex waste substrates into biomass and through the biotransformation processes are capable of production of valuable metabolites such as carotenoids, ergosterol, ubiquinone, glucans, and lipids^{4,5}.

Study objectives

Study objectives were aiming on obtainment of information from cultivation of three carotenogenic yeasts strains *Rhodotoridium torulooides*, *Rhodotorula kratochvilovae* and *Cystofilobasidium macerans* on media with content of model and waste substrates with various ratios between them.

Those substrates were:

- Waste poultry fat
- Waste poultry feathers
- Purified glycerol (model for waste glycerol)

Materials and methods

Waste poultry feathers were pre-treated by organic solvent where the lipid content was extracted into nonpolar dissolvent. Feathers stripped of lipid content were dried and then hydrolysed by alkaline hydrolysis using 1% sodium hydroxide solution at the temperature 100 °C. Feather hydrolysate (FE) was added into cultivation media in crude form. Waste poultry fat did not require special pre-treatment due to the fact that carotenogenic yeasts possess natural lipase activity.

Carotenogenic yeasts were cultivated from stock cultures via solid YPD agar on Petri dishes and then via double inoculation in submerge YPD media in Erlenmeyer flasks. Main test cultivations were performed in Erlenmeyer flasks filled with artificial mineral media with addition of waste substrates to adjust to required value of C/N ratio. Glycerol added in media served as control carbon source and as model for usage of waste glycerol for cultivation purposes. Inoculation ratio from inoculation media into production media was 1:5. Production media

were designed to contain the same mineral base but differed in types of carbon and nitrogen substrates while maintaining the same C/N ratio at the start of cultivation. All combinations of used media are described in Table I. Production cultivations persisted 96 hours and then were terminated. Biomass obtained from cultivations was subjected to gravimetric analysis to acquire information about its growth.

Table I
Distribution of experiments described by contain of carbon and nitrogen source

1 st series					
shortcut	GLY	FAT	0,1 GLY	0,25 GLY	GLY+FE
carbon source	100 % glycerol	100 % fat	90 % fat + 10 % glycerol	75 % fat + 25 % glycerol	100 % glycerol + FE
2 nd series					
shortcut	GLY (FE)	FAT+FE	0,1 GLY+FE	0,25 GLY+FE	GLY+FE
carbon source	100 % glycerol	100 % fat + F.H	90 % fat + 10 % glycerol + F.H	75 % fat + 25 % glycerol + F.H	100 % glycerol + F.H

Results and discussion

Rhodospiridium toruloides

The first of cultivated strain was yeast *Rhodospiridium toruloides* which, as it is showed on Figure 1., has significant growth of biomass on glycerol media in the first (20.0 g/l) and in the second series (17.8 g/l). This phenomenon could be used in cultivations with carbon source based on waste glycerol. In the second series of experiments (with FE) an increasing trend can be observed in the biomass growth based on increasing concentration of glycerol and on decreasing amount of added poultry fat.

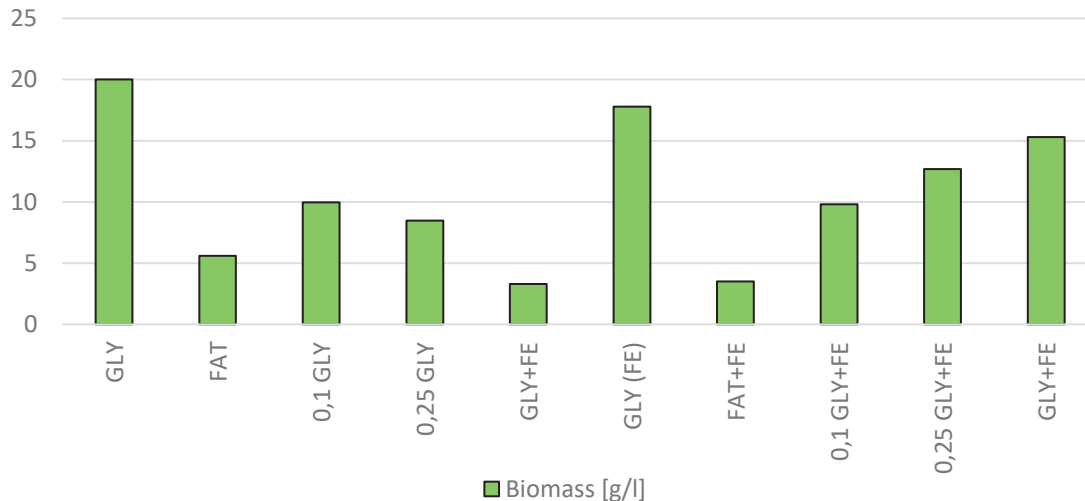


Figure 1. Biomass growth of strain *Rhodospiridium toruloides*

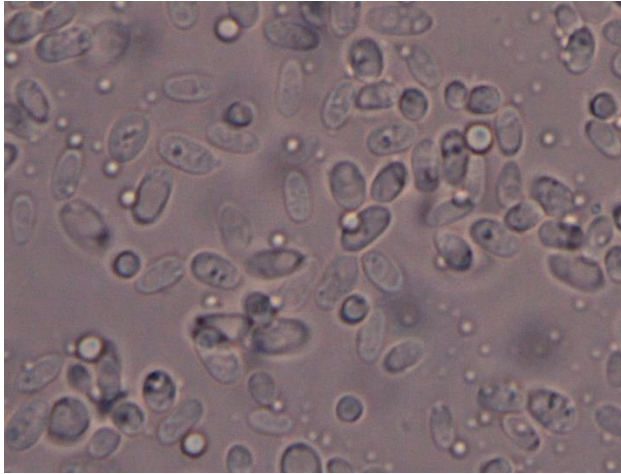


Figure 2. Microscopic image of yeast *Rhodosporidium toruloides* cultivated on waste fat

Rhodotorula kratochvilovae

The second cultivated strain was yeast *Rhodotorula kratochvilovae*. Growth and production parameters of the strain are showed in Figure 2. The largest biomass growth was observed on the medium with 25 % glycerol content and 75 % poultry fat content, with a value of 19.2 g/l followed the medium with 90 % poultry fat content where the biomass growth reached 17.7 g/l.

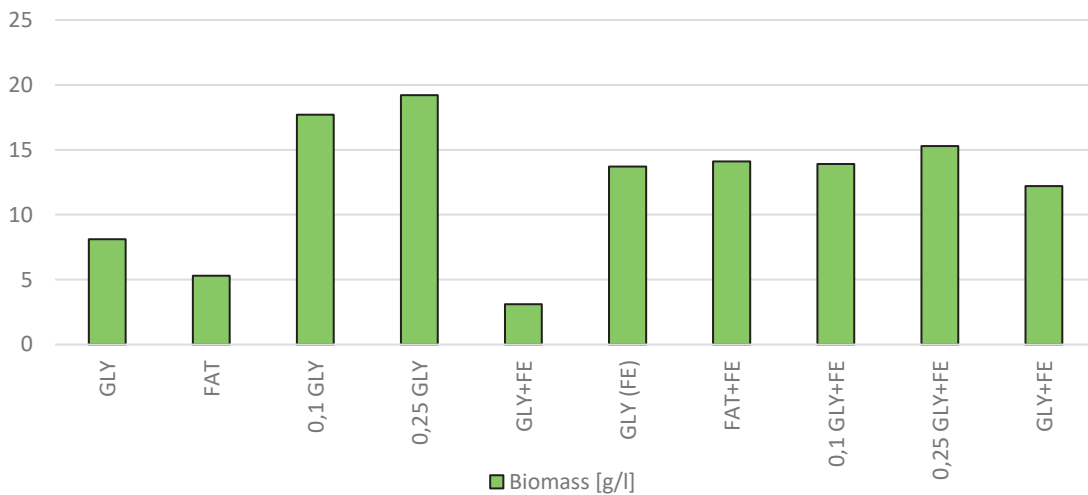


Figure 3. Biomass growth of strain *Rhodotorula kratochvilovae*

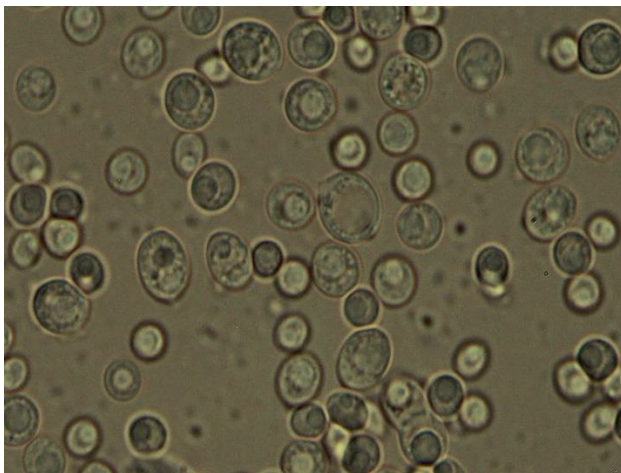


Figure 4: Microscopic image of yeast *Rhodotorula kratochvilovae* cultivated on waste fat

Cystofilobasidium macerans

The third cultivated strain was yeast *Cystofilobasidium macerans*, the results of which are presented in Figure 3. An increasing trend in biomass production can be observed in fat-based media of both series, depending on the decreasing concentration of waste fat in media. The highest biomass yields were achieved in glycerol media with the addition of feather hydrolysate in both series, in the 1st series 14.6 g/l, in the 2nd series 16.6 g/l.

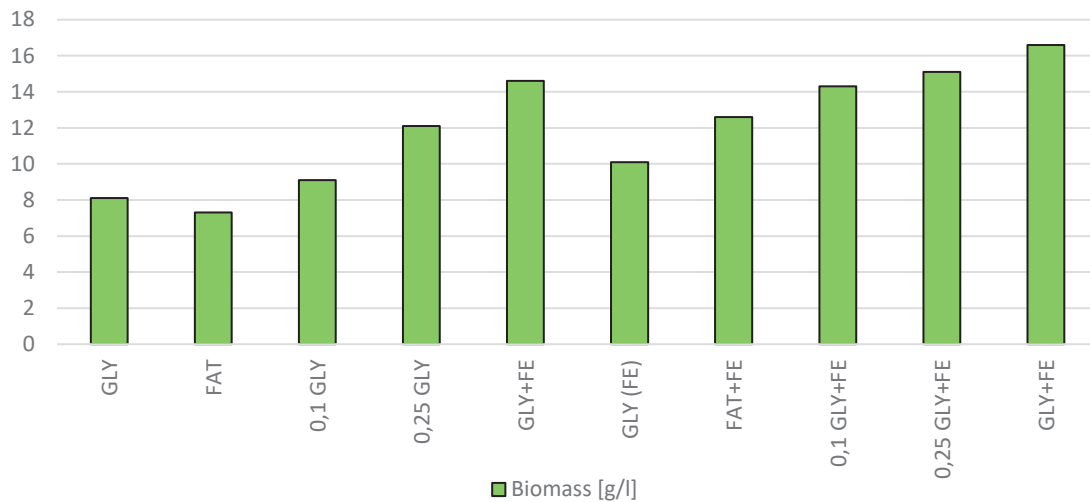


Figure 5. Biomass growth of strain *Cystofilobasidium macerans*

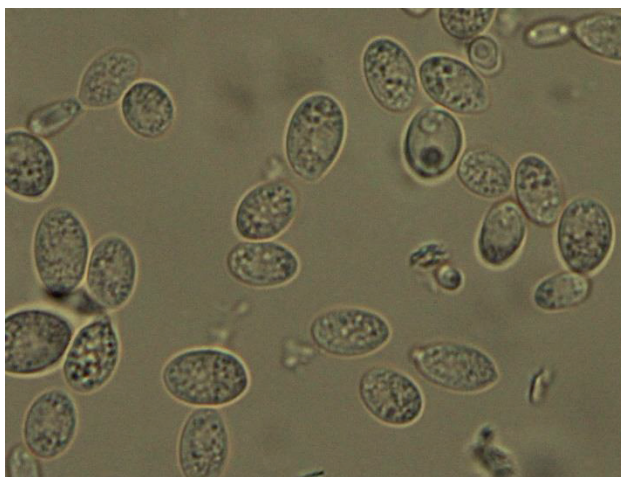


Figure 6. Microscopic image of yeast *Cystofilobasidium macerans* cultivated on waste fat

Conclusion

Cultivations of carotenogenic yeasts on media with added poultry waste materials showed interesting result with significant biomass growths (19.2 or 17.7 g/l). Cultivations on glycerol control media also indicated good results in biomass growth (up to 20.0 g/l) which could serve as a model for cultivations on waste glycerol from biofuels production.

In fat-based media, a favourable effect of reducing the ratio of fat:glycerol on biomass production was observed in almost all strains. This trend was mainly observed in cultivations with the addition of feather hydrolysate. In cultivation of strain *Cystofilobasidium macerans*, the addition of hydrolysate to the media had a significant beneficial effect on biomass production.

In summary, waste poultry fat and feathers can be valorised by carotenogenic yeasts to obtain valuable biomass. By using these waste materials for cultivation purposes, new possibility arises of using these materials for industrial optimization and production valuable biomass and metabolites.

According to results that were obtained from methods used in previous studies, further study is required for optimization of biomass growth and advanced methods implementation^{3,5}. In the process of implementation of new methods, such as HPLC-PDA for carotenoid, ergosterol and ubiquinone detection and GC-FID for lipid

detection, the preliminary data showed good results in carotenoid production (up to 10 mg/g of biomass) and significant lipid accumulation (up to 40 % of dry biomass).

Acknowledgements

The study was supported by the Internal grant competition, which is implemented as part of the OP VVV project entitled Quality internal grants BUT (KInG BUT); reg. number: CZ.02.2.69/0.0/0.0/19_073/0016948 specifically by KInG No. 7746

References

1. Jurgilevich A., T. B. Birge T., Kentala-Lehtonen J., Korhonen-Kurki K., Pietikäinen J., Saikku L., Schösler H.: Sustainability. 8 (2016)
2. Gottardi D., Siroli L., Vannini L., PATRIGNANI F., LANCIOTTI R.: Recovery and valorization of agri-food wastes and by-products using the non-conventional yeast *Yarrowia lipolytica*. 115, 74-86 (2021)
3. Szotkowski M., Holub J., Šimanský S., Hubáčová K., Hladká D., Němcová A., Márová I.: Microorganisms. 9 (2021)
4. Márova I., Carnecka M., Haličková A., Certik M., Dvorakova T., Hronikova A.: Journal of Environmental Management. 95, 338 (2012)
5. Byrtusová D., Szotkowski M., Kurowska K., Shapaval V., Márová I.: Microorganisms. 9 (2021)

STABILITY AND ANTIOXIDANT ACTIVITY OF *MONASCUS* PIGMENTS IN COMPLEX RED YEAST RICE EXTRACTS

Husakova M.¹, Patakova P.¹

¹University of Chemistry and Technology, Prague, Czech republic

husakovm@vscht.cz

Abstract

The representatives of the genus *Monascus* are ascomycetes, traditionally used in Southeast Asia for food dyeing and preservation. These fungi produce a wide range of secondary metabolites. Apart from statins – monacolins, and mycotoxin citrinin, the most important metabolites are azaphilone pigments.

This study was focused on the content and properties of the pigments found in red yeast rice (RYR) extracts. The stability of natural pigments is the key property for their suitability for use in the food or pharmaceutical industry. The complex extracts were prepared by ethanol extraction from RYR fermented by strains *Monascus purpureus* DBM 4630 and *Monascus* sp. DBM 4631. The pigment content of each extract was determined by UHPLC analysis and the stability assays in the temperature range of 30-80 °C, pH 2.5-8, and antioxidant assay were performed. Most stable are yellow pigments, most unstable are orange pigments which react and form the red ones.

Introduction

The *Monascus* fungi belong to the phylum Ascomycota¹, they are used for food dyeing and preservation. The fungus *Monascus* is traditional and very popular in Southeast Asia². Like other representatives of the ascomycetes, also the fungus *Monascus* produce a wide range of secondary metabolites. Apart from pharmaceutically used statins – monacolins, and mycotoxin citrinin, the most important metabolites are azaphilone pigments. *Monascus* pigments are usually divided into three groups, according to their absorbance maxima: yellow (390 nm), orange (470nm) and red (500 nm). *Monascus* pigments are widely used as food colourants in Asian countries³. In European Union, the use of the fungus *Monascus* is only permitted as a dietary supplement with a health claim: “Monacolin K from red yeast rice contributes to the maintenance of normal blood cholesterol concentrations”, if the daily intake of monacolin K from RYR based dietary supplement is 10 mg⁴.

Stability and other properties, e.g. antioxidant capacity, are the key factors for industrial use of RYR or *Monascus* pigments. In previous research made by other groups, effects of temperature, pH or light were studied^{5,6}. But the evaluation of effects was done only spectrophotometrically. This method is very useful for colour characteristics, but it does not give us whole information about changes in the content of each pigment group or particular pigments. Therefore, we performed UHPLC analysis, where this detailed information can be obtained.

Materials and methods

Cultivation

Monascus purpureus DBM 4360 and *Monascus* sp. DBM 4361 strains were maintained on Sabourad agar at 4 °C. Basmati rice (GOLD MENU) was washed with hot water and boiled for 5 minutes. After cooling, the rice was divided into plastic autoclavable bags, bags were closed with cotton plugs and after 24 hours sterilized by autoclaving (20 min, 121 °C). Sterile rice was inoculated by spore suspension (1%) prepared with phosphate buffer saline containing Tween 80 (0.01%). Rice was cultivated for 8 and 14 days at 30 °C.

Extraction and analysis

The RYR was extracted with 85% acidified ethanol (pH 4) for 40 minutes at 30 °C with shaking. The extraction ratio was 0.1 g of RYR sample:1 ml of extraction solution.

Pigments, citrinin and monacolin K content was determined by UHPLC (Agilent Technologies 1260 Infinity II) using Kinetex Polar C18, 100A, 150 × 4.6 mm column, the mobile phase 0.025% H₃PO₄ in water: acetonitrile at a ratio 40:60, isocratic elution at a flow rate 1.2 ml/min. The concentration of monacolin K was determined by diode-array detector at 237.4 nm, yellow pigments at 390 nm, orange at 470 nm, red at 500 nm according to their specific absorbance spectra and citrinin was determined by fluorescence detector set to 331 nm for excitation and 500 nm for emission. As standard compounds lovastatin (Sigma-Aldrich) for monacolin K, monascin (Sigma-Aldrich) for yellow pigments, rubropunctatin (1717 CheMall Corporation) for orange pigments and citrinin (Sigma-Aldrich) were used. As a standard compound for red pigments rubropunctamine, prepared by reaction of rubropunctatin with NH₄OH, was used.

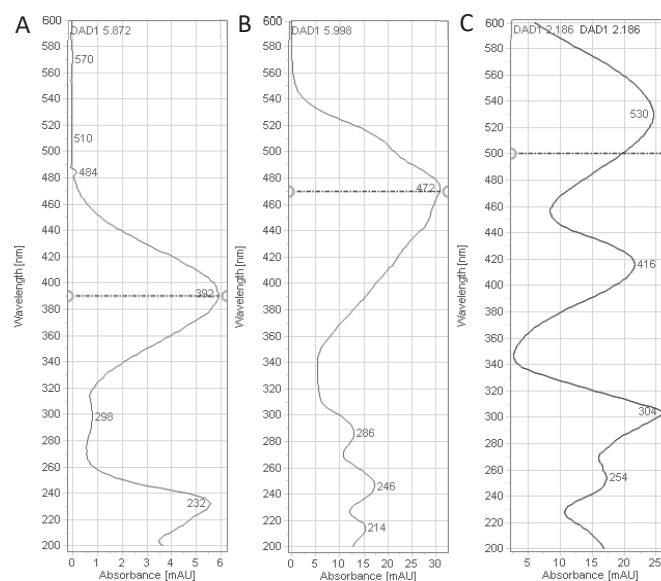


Figure 1. Specific absorbance spectra of pigment group; A: yellow; B: orange; C: red pigment

Stability assays

The effects of temperature and pH on pigment stability were tested. RYR extracts were incubated over a temperature range of 30–80 °C with exposure times of 5, 10 and 60 minutes. The effect of different pH values on pigment extracts was studied at pH 5–8 using a citrate-phosphate buffer with exposure time 1 hour. In all these tests, pigments were analysed by UHPLC as described in the previous section.

ABTS decolorization assay

Stock solutions of 2,2'-azino-bis(3-ethylbenzothiazoline-6-sulfonic acid) (ABTS) (7mM) and potassium persulfate (PP) (140 mM) were prepared by dissolving in distilled water, both stored at 4 °C. ABTS^{•+} solution was prepared by reacting 5 ml of ABTS stock solution and 88 µl of PP stock solution in dark at room temperature for 14 hours. 1 ml of ABTS^{•+} solution was diluted with 60 ml of ethanol to gain the absorbance (734 nm) (Tecan infinite M200Pro Spectrophotometer) 0,0706±0,01. 190 µl of diluted solution was mixed with 10 µl of sample, and absorbance (734 nm) was measured after 10 minutes of incubation in dark at room temperature. Trolox (vitamin E analogue), dissolved in ethanol, was used as standard. The results are expressed as TEAC (Trolox equivalent antioxidant capacity).

Results and discussion

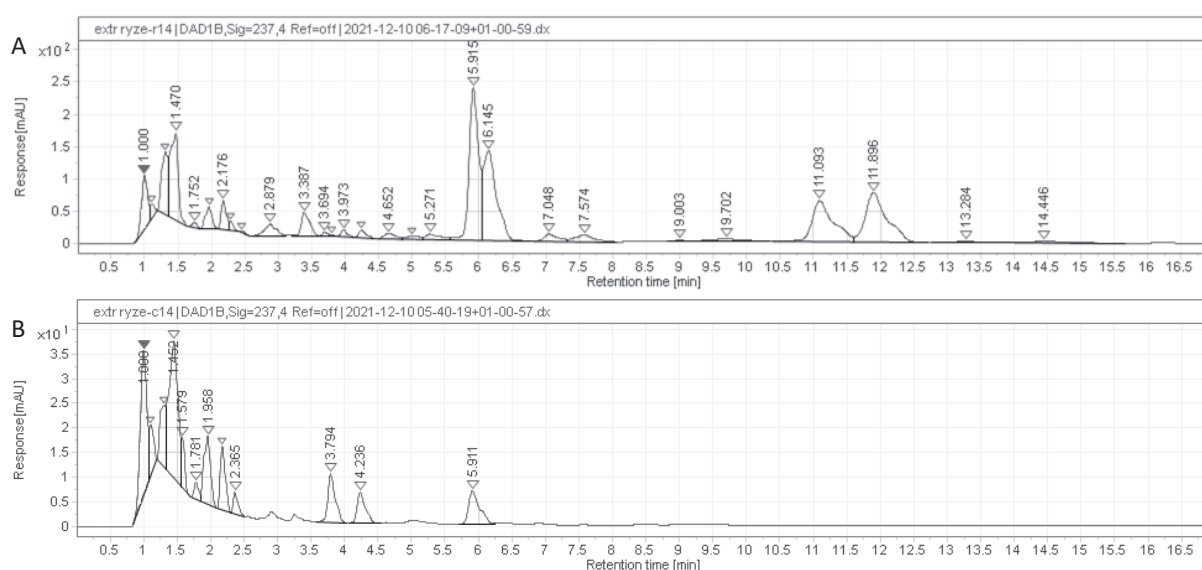
RYR extracts analysis

RYR was extracted with 85% acidified ethanol, extracts were then analyzed by UHPLC. The content of detected pigments and citrinin is shown in Table I. The differences between used strains and cultivation period were observed, content of pigments in extracts from RYR fermented by *Monascus purpureus* DBM 4360 is considerably higher in comparison to RYR fermented by *Monascus* sp. DBM 4361. These differences could be explained by origin of used strains, *Monascus purpureus* DBM 4360 was originally used for industrial production of food dyeing. *Monascus* sp. DBM 4361 was originally used for production of monacolin K in pharmaceutical industry. In Figure 2, the difference between the production of pigments by used strains is shown. The major pigments produced by *Monascus purpureus* DBM 4360 cultivated for 14 days were yellow – monascin (Rt 5.915 min) and ankaflavin (Rt 11.093), orange – rubropunctatin (Rt 6.145) and monascorubrin (Rt 11.896), red – rubropunctamine (Rt 2.176) and monacorubramine (3.387). In comparison the major pigments produced by *Monascus* sp. DBM 4361 were yellow – monascuspiloin⁷ (Rt 3.794) and monascin (Rt 5.911 min) and red – rubropunctamine (Rt 2.176). Orange pigments were not detected. *Monascus* sp. DBM 4361 probably does not produce pigments with longer side chain (ankaflavin, monascorubrin, monacorubramine).

Table I

Content of pigments and citrinin in ethanol extracts (in mg/l)

Used strain	<i>Monascus</i> sp. DBM 4361		<i>Monascus purpureus</i> DBM 4360	
	8	14	8	14
Days of cultivation	8	14	8	14
Yellow pigments (Monascin equivalents)	7.42	50.04	246.47	1041.32
Orange pigments (Rubropunctatin equivalents)	0.63	0.93	135.45	1006.00
Red pigments (Rubropunctamine equivalents)	9.99	13.98	143.17	202.56
Citrinin	-	-	3.80	10.06

Figure 2. RYR extracts chromatograms, 273.4 nm; A: *Monascus* sp. DBM 4361 (14 days); B: *Monascus purpureus* DBM 4360 (14 days).

Stability assays

Effects of temperature and pH on RYR extracts were studied. Stability is the key property of the compounds used in food or pharmaceutical industry. In Figure 3, changes observed in particular pigment groups are shown, extract of RYR fermented by *Monascus purpureus* DBM 4360 for 8 days was chosen as an example. In all cases, regardless of the exposure time or whether the extract is heated or exposed to increasing pH values, decrease of orange pigment content and increase of red pigment content was observed, other metabolites were stable. This observation is in agreement with the previous research⁵ and can be explained by higher reactivity of orange pigments at pH above 4 with compounds containing primary amino groups by forming red pigments (the reaction is shown in Figure 4).

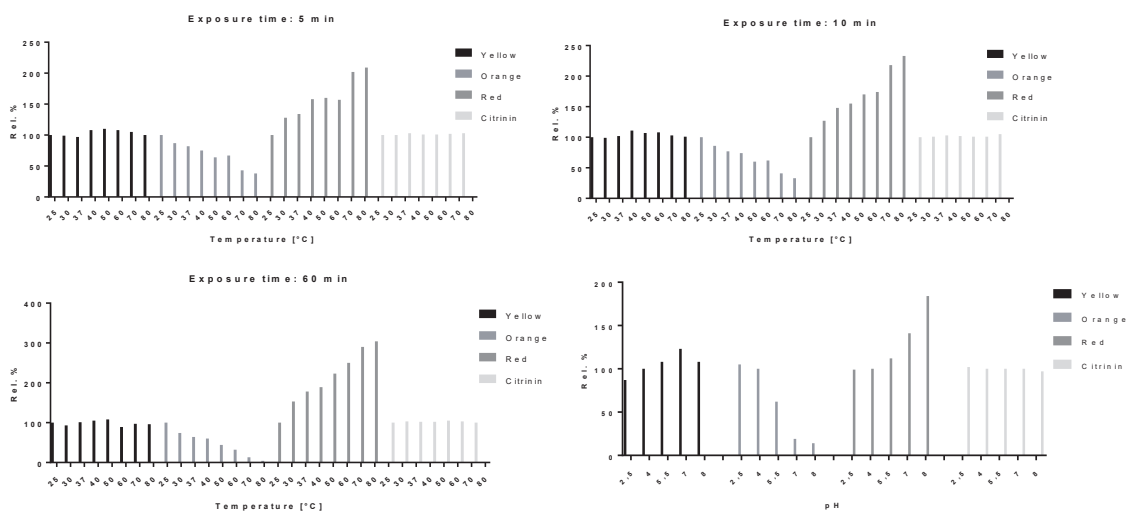


Figure 3. Effects of temperature, with different exposure times, and pH on pigment content. Extract of RYR fermented by *Monascus purpureus* DBM 4360 (8 days).

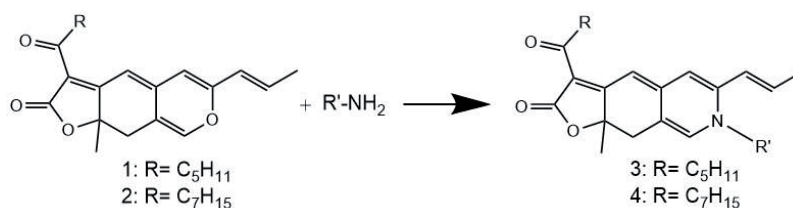


Figure 4. Reaction of orange pigment with compounds containing primary aminogroup

ABTS decolorization assay

The antioxidant capacity of RYR extracts was also tested. Antioxidant activity is beneficial attribute for additives in the food industry, as it may help with food colour stability preservation. For the testing of antioxidant activity, the ABTS decolorization assay was performed. This assay has a huge advantage because it is evaluated at 734 nm, which is outside of the absorbance spectra of RYR extracts. The obtained antioxidant capacity is shown in Table 2 and is evaluated as TEAC, Trolox equivalent antioxidant capacity. Obtained TEAC values correlate with pigment content of extracts.

Table 2

Trolox equivalent antioxidant capacity (TEAC) of RYR ethanol extracts (in mM)

Used strain	<i>Monascus</i> sp. DBM 4361		<i>Monascus purpureus</i> DBM 4360	
	8	14	8	14
Days of cultivation	8	14	8	14
TEAC	0.245	0.324	0.941	1.179

Conclusion

The RYR complex extracts were characterized by UHPL analysis. Used strains differ in production of secondary metabolites, main pigments produced by *Monascus purpureus* DBM 4360 are two major pigments in each pigment group (monascin and ankaflavin, rubropunctatin and monascorubrin, runbropunctamine and monacorubramine). In comparison, the major pigments produced by *Monascus* sp. DBM 4361 are monascuspiloin, monascin, and runbropunctamine. In all cases of temperature and pH stability assays, decrease in orange pigment content and increase in red pigment content were observed. The antioxidant capacity – TEAC values, correlate with pigment content of extracts.

Acknowledgement

This work was supported from the grant of Specific university research – grant A2_FPBT_2022_016.

References

1. Houbraeken, J.; Kocsube, S.; Visagie, C. M.; Yilmaz, N.; Wang, X. C.; Meijer, M.; Kraak, B.; Hubka, V.; Bensch, K.; Samson, R. A.; Frisvad, J. C.: *Stud Mycol*, 95, 5 (2020).
2. Lin Y.-L., Wang T.-H., Lee M.-H., Su N.-W.: *Appl Microbiol Biotechnol* 77, 965 (2008).
3. Chen, W.; Chen, R.; Liu, Q.; He, Y.; He, K.; Ding, X.; Kang, L.; Guo, X.; Xie, N.; Zhou, Y.; Lu, Y.; Cox, R. J.; Molnár, I.; Li, M.; Shao, Y.; Chen, F.: *Chem Sci*, 8, 4917 (2017).
4. EFSA Panel on Food Additives and Nutrient Sources added to Food (ANS): *EFSA J*, 9, 2304 (2011).
5. Shi K., Chen G., Pistolozzi M., Xia F., Wu Z.: *Food Addit Contam* 33, 1396 (2016).
6. Jung H., Kim C., Shin C. S.: *J Agri Food Chem* 53, 7108 (2005).
7. Husakova M., Plechata M., Branska B., Patakova P.: *Front Microbiol* 12, 1254 (2021).

GENOMIC AND FUNCTIONAL ANALYSIS OF POLYHYDROXYALKANOATES PRODUCER *RHODOSPIRILLUM RUBRUM* DSM 467

Jureckova K.¹, Nykrynova M.¹, Slaninova E.², Bezdicek M.^{3,4}, Obruca S.², Skutkova H.¹, Sedlar K.^{1,5}

¹Department of Biomedical Engineering, Brno University of Technology, Brno, Czechia

²Department of Food Chemistry and Biotechnology, Brno University of Technology, Brno, Czechia

³Department of Internal Medicine – Hematology and Oncology, University Hospital Brno, Brno, Czechia

⁴Department of Internal Medicine – Hematology and Oncology, Masaryk University, Brno, Czechia

⁵Institute of Bioinformatics, Department of Informatics, Ludwig-Maximilians-Universität München, Munich, Germany

jureckova@vut.cz

Abstract

Rhodospirillum rubrum is a bacterium capable of the production of polyhydroxyalkanoates (PHA). PHA are polyesters that bacteria primarily use as a storage of energy and carbon in a form of cytoplasmic granules. Nevertheless, PHA are also promising renewable and biodegradable alternatives to petrochemical polymers, which nowadays leads to extensive research of *R. rubrum*. In this study, we focused on the analysis of a genome sequence of *Rhodospirillum rubrum* DSM 467. We sequenced and assembled genome of *R. rubrum* DSM 467 by a hybrid approach using long (Oxford Nanopore) and short (Illumina) reads. Chromosome sequence is available under accession number CP077803.1 and plasmid sequence under CP077804.1 in the GenBank database. Chromosome sequence was 4 352 570 bp long, CG content was 65.4%, and 3 919 open reading frames (ORF) belonged to protein-coding sequences. Plasmid sequence was 53 835 bp long, CG content was 59.8%, and a number of ORF was 49. Functional annotation revealed that protein-coding sequences can be assigned a clusters of orthologous genes group in 90% cases for chromosome sequence and 80% cases for plasmid sequence, respectively. From available genome sequences of *R. rubrum* species, we created its pangenome with 4 572 genes, where we identified the core genome with 1 765 genes, accessory genome with 2 808 genes and 890 genes were unique. Genome annotation was also used for the construction of the genome-scale model of *R. rubrum* DSM 467 in Pathways tool. Our results will be used in further research of metabolic processes behind PHA biosynthesis in *Rhodospirillum rubrum* DSM 467.

Introduction

Polyhydroxyalkanoates (PHA) are polyesters naturally formed by microbial fermentation. Bacteria use PHA primarily as carbon and energy storage in the form of cytoplasmic granules¹. Besides their vital biological role, PHA can also be isolated from biomass and later used in production of renewable and biodegradable plastics. Many bacteria are capable of PHA production, but in our study, we focused on a very promising PHA producing strain *Rhodospirillum rubrum* DSM 467.

R. rubrum DSM 467 (= ATCC 11170) is non-sulfur, purple, Gram-negative bacterium, which is able to grow both under aerobic and anaerobic conditions and is a facultative phototroph². *R. rubrum* DSM 467 is a neotype strain for *R. rubrum* species. Genome sequence of *R. rubrum* ATCC 11170 strain deposited in the American Type Culture Collection is known and published in GenBank database under accession number CP000230 and CP000231 for chromosome and plasmid sequence, respectively³. Available assembly is more than ten years old and might suffer from misassemblies, so we decided to re-sequence the genome of the strain by combination of short and accurate reads from Illumina MiSeq and long but less accurate reads from Oxford Nanopore MiniON. Here we present a high-quality complete genome sequence of *Rhodospirillum rubrum* DSM 467 together with genomic and functional analyses.

Methods

Growth conditions of culture

A lyophilized bacterial culture of *Rhodospirillum rubrum* DSM 467 was obtained from the Leibnitz Institute DSMZ – German Collection of Microorganism and Cell Culture, Braunschweig, Germany. Firstly, the cultivation was performed in 100 mL Erlenmeyer flasks containing 50 mL of LB Broth medium (tryptone 10.0 g/L, yeast extract 5.0 g/L, NaCl 5.0 g/L) under shaking 160 rpm at 30°C for 3 days.

Isolation and sequencing of DNA

Genomic DNA for long-read sequencing was extracted using MagAttract HMW DNA kit (Qiagen, NL). The DNA purity was checked using NanoDrop (Thermo Fisher Scientific, USA), the concentration was measured using Qubit 4.0 Fluorometer (Thermo Fisher Scientific, USA), and the length was measured using Agilent 4200 TapeStation (Agilent Technologies, USA). The sequencing was prepared using Ligation Sequencing 1D Kit (Oxford Nanopore Technologies, UK) and the sequencing was performed using R9.4.1 Flow Cell and the MinION platform (Oxford Nanopore Technologies, UK). Genomic DNA for the short-read sequencing was extracted using GenElut Bacterial Genomic DNA Kit (Sigma-Aldrich, USA) and sequencing library was prepared using KAPA HyperPlus kit and was carried out using MiSeq Reagent kit v2 500 cycles and MiSeq platform (Illumina, USA).

Genome assembly

The nanopore sequencing data were basecalled using Guppy software (3.4.4+a296acb), and the quality of data was checked using PycoQC⁴ (v2.2.3) and MinIONQC⁵. Flye (2.8.1-b1676) software was used to assemble the reads, and then the obtained contigs were polished using Minimap2⁶ (2.17-r941) combined with Racon⁷ (v1.4.13) and final polishing was performed with Medaka (1.1.2).

The hybrid assembly was performed using the reads from Illumina MiSeq, which were firstly checked for quality using FastQC (v0.11.5) combined with MultiQC⁸ (v1.7) and secondly, the low-quality ends of reads and adapters were removed using Trimmomatic⁹ (0.36). Then using BWA¹⁰ (0.7.17-r1188) the reads were mapped to the nanopore contigs. Final polishing of the assembly was made with Pilon¹¹ (1.24). In the last step, the assembled genome was rearranged so that the *dnaA* gene was the first gene in the chromosome and *repB* was the first gene in the plasmid.

Genome annotation and analysis

NCBI Prokaryotic Genome Annotation Pipeline¹² (PGAP) was used for the genome annotation. Operon prediction was performed with Operon-mapper¹³. Functional annotation of protein coding genes was performed by classifying them into clusters of orthologous groups (COG) categories from the eggNOG database via the eggNOG-mapper¹⁴ (v2.1.6). The circular map of chromosome and plasmid was created using DNAPlotter¹⁵, which is integrated into Artemis¹⁶ (v18.1.0). The interspaced short palindromic repeats (CRISPR) arrays were searched by the CRISPDetect tool¹⁷ (v2.4), and *cas* genes were manually searched in the annotated genome. PhiSpy¹⁸ (4.2.6), Prophage Hunter¹⁹ and PHASTER²⁰ were used for prophage DNA identification. The restriction-modification systems were located using REBASE²¹ database. The core and pan genome and the number of unique genes were determined using Roary²² (v3.12) with the minimum percentage identity for sequence comparisons set to 95%. Genome-scale model was created in Pathway Tools²³ software.

Results and discussion

Genome assembly and properties

The Oxford Nanopore Technologies MinION produced 135 804 reads in total. Only 104 955 reads had Q > 7 and were used for further assembly. The mean read's length was approximately 3.5 kbp. The Illumina MiSeq provided 2.5 million of 250 bp-long paired reads with an average Phred score of 35. The assembly process resulted in the final assembly of one circular chromosome and one circular plasmid with coverage of 370x. The sequences were deposited in DDBJ/EMBL/GenBank databases under accession numbers CP077803.1 for the chromosome and CP077804.1 for the plasmid.

The length of obtained chromosome sequence was 4 352 570 bp with GC content 65.4%, and plasmid was 53 835 bp long with GC content 59.8%. In total, 3 968 open reading frames (ORFs) divided into 2 175 operons were identified for both sequences. Most of the genes were protein coding; however, also 49 pseudogenes were found. See Table I for complete statistics for chromosome and plasmid.

The length and GC content corresponded with available genome of *R. rubrum* ATCC 11170, the number of protein coding genes was the same, yet the number of pseudogenes was higher in our genome (9 versus 49 pseudogenes)³. The difference between annotations was rather a result of different annotation workflows. While the genome of *R. rubrum* ATCC 11170 was annotated by custom made annotation pipeline and later manually curated, the strain DSM 467 was annotated by the PGAP.

Table I. Genomics features of *Rhodospirillum rubrum* DSM 467

	Chromosome (CP077803.1)	Plasmid (CP077804.1)
Length [bp]	4 352 570	53 835
GC content [%]	65.4	59.8
Number of ORFs	3 919	49
Number of operons	2 143	32
Protein coding genes	3 807	43
Pseudogenes	43	6
rRNA genes (5S, 16S, 23S)	4, 4, 4	-
tRNA	54	-
ncRNA	3	-

Functional annotation

Protein coding genes and pseudogenes were classified according to COG into 20 categories. For chromosome, 413 CDS (out of all 3 807 protein coding genes and 43 pseudogenes) were not assigned any COG category and class S with unknown function was assigned to 665 CDS. From the remaining CDS classified into COG class, the most abundant was class E (amino acid transport) with 374 CDS (9.71%). For plasmid with 43 protein coding genes and 6 pseudogenes, 10 CDS were not assigned to any COG class, 8 CDS were assigned to S class (function unknown) and 9 CDS classified to L category (replication, recombination and repair). Detailed results can be seen in Table II. The circular map for chromosome and plasmid sequence together with their assigned COG classes can be seen in Figure 1.

Table II. Clusters of orthologous groups (COG) of *Rhodospirillum rubrum* DSM 467

COG class	Description	Chromosome		Plasmid	
		Gene count	% from all CDS	Gene count	% from all CDS
B	Chromatin structure and dynamics	2	0.05	-	-
C	Energy production and conversion	257	6.68	-	-
D	Cell cycle control, cell division, chromosome partitioning	44	1.14	1	2.04
E	Amino acid transport and metabolism	374	9.71	1	2.04
F	Nucleotide transport and metabolism	82	2.13	-	-
G	Carbohydrate transport and metabolism	130	3.38	5	10.20
H	Coenzyme transport and metabolism	161	4.18	2	4.08
I	Lipid transport and metabolism	141	3.66	-	-
J	Translation, ribosomal structure and biogenesis	173	4.49	-	-
K	Transcription	276	7.17	3	6.12
L	Replication, recombination and repair	162	4.21	9	18.37
M	Cell wall/membrane/envelope biogenesis	187	4.86	7	14.29
N	Cell motility	119	3.09	-	-
O	Post-translational modification, protein turnover, and chaperones	114	2.96	-	-
P	Inorganic ion transport and metabolism	204	5.30	-	-
Q	Secondary metabolites biosynthesis, transport, and catabolism	49	1.27	2	4.08
S	Function unknown	665	17.27	8	16.33
T	Signal transduction mechanisms	196	5.09	-	-
U	Intracellular trafficking, secretion, and vesicular transport	44	1.14	-	-
V	Defense mechanisms	57	1.48	1	2.04
-	COG unknown	413	10.73	10	20.41
sum		3850	100.00	49	100.00

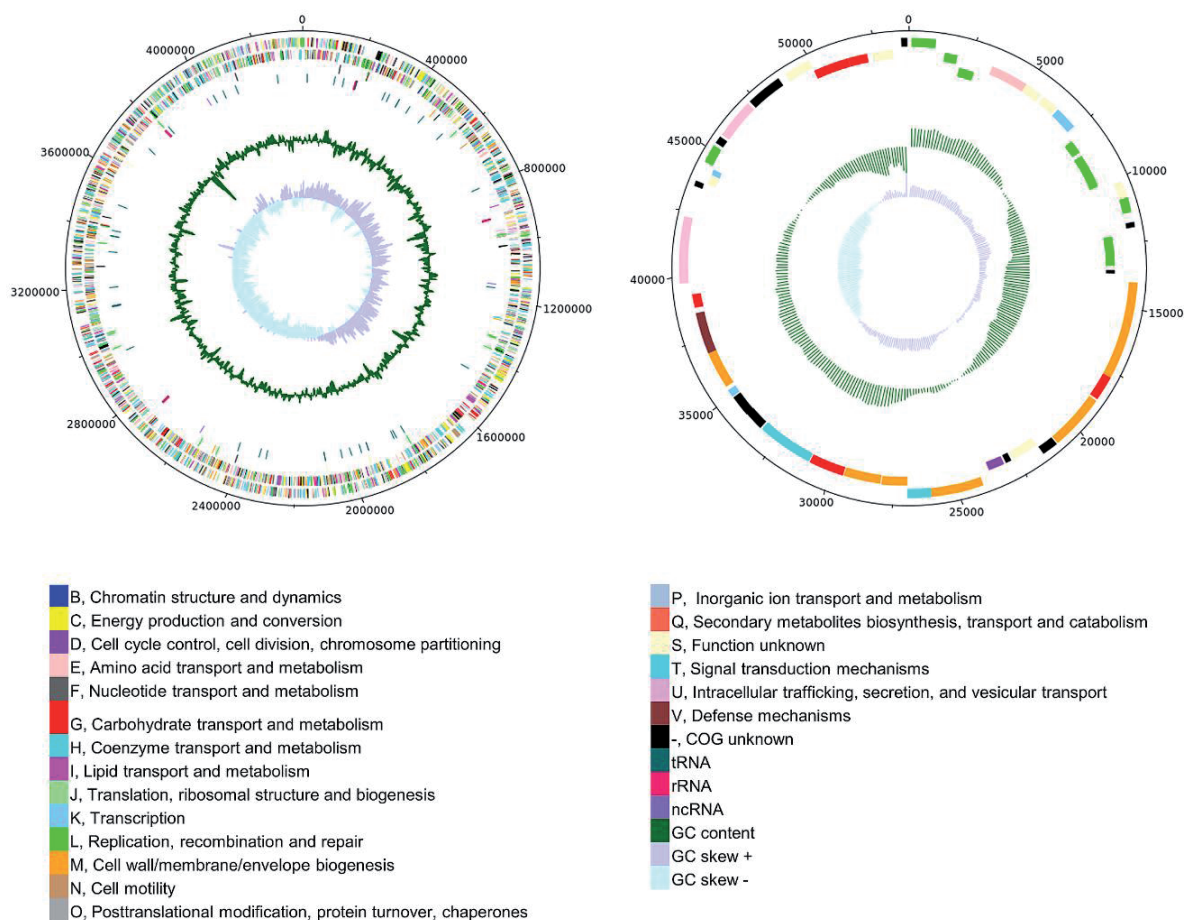


Figure 1. A circular map of a chromosome (on the left) and a plasmid (on the right) sequence of *Rhodospirillum rubrum* DSM 467. From outside to centre: CDS on forward strand (color-coded by COG classes), CDS on reverse strand (color-coded by COG classes), pseudogenes (color-coded by COG classes), RNA genes (tRNA, rRNA, ncRNA), GC content and GC skew.

The CRISPR arrays were searched in the genome and we found 11 arrays with lengths from 337 to 2 467 bp and a number of spacers ranging from 4 to 40, see Table III. We searched genome manually for *cas* genes and we found 34 genes, but no Cas9 protein. All genes were found in the neighbourhood of CRISPR arrays except for arrays number 7, 8, 9 and 11.

Table III. CRISPR arrays of *Rhodospirillum rubrum* DSM 467

No.	Start	End	Length [bp]	Strand	Direct repeats (DR) consensus	DR length [bp]	Number of spacers
1	200 139	198 949	1 191	-	CTGTTCCCCGCATGCGCGGGGATGAACCG	29	19
2	214 446	213 870	577	-	GTCTCCCAGGCAGTAATGCCTCGGCCCTATTGAAAC	37	7
3	420 499	422 970	2 472	+	GGTTCCCCCGACTCGTGGGGATAGACCC	29	40
4	530 220	530 836	617	+	ACTCTACCATGGCGGTGTGGGACGGGCCATGGAAC	36	8
5	989 445	991 911	2 467	+	GTCGCCCCCTTACGGGGGCGTGGATCGAAAC	32	37
6	1 364 501	1 363 926	576	-	CTCGACCCTATGCCCGCCATCGAGGGGACTGAAAC	37	7
7	1 582 023	1 580 652	1 372	-	CTGTTCCCCGCACACGCGGGGATGAACCG	29	22
8	1 696 029	1 694 114	1 916	-	GTCGCTCCCTCACGGGGGCGTGGATTGAAAC	31	29
9	2 668 169	2 669 714	1 546	+	CTCGCAGCCTATGCCCGCCACCGAGGGGACTGAAAC	37	20
10	2 716 021	2 716 357	337	+	GTCTCCCAGGCAGTAATGCCTCGGCCCTATTGAAAC	37	4
11	3 524 515	3 525 391	877	+	CTCGCAGCCCTTGCCCGCTATCGAGGGGACTGAAAC	37	11

The prophages were searched for in assembled sequences. PhiSpy did not identify any viral DNA, Prophage Hunter found one ambiguous prophage candidate, and PHASTER localized four incomplete prophages where all of them had a low score.

The restriction-modification systems were identified. Two systems that contained both restriction endonuclease and methylase were found, and one belonged to type II and one to type III. In addition, another gene coding for methylase type II was also found. The results are in Table IV.

Table IV. Restriction-modification systems of *Rhodospirillum rubrum* DSM 467

Type	Name	Locus tag	Gene
II	Rru467ORF12845P	KUL73_12840	restriction endonuclease
II	M.Rru467ORF12845P	KUL73_12845	methylase
II	M.Rru467ORF16545P	KUL73_16545	methylase
III	M.Rru467ORF1275P	KUL73_01275	methylase
III	Rru467ORF1275P	KUL73_01280	restriction endonuclease

R. rubrum genomes were searched in the GenBank database. In total, eight genome assemblies were obtained, and from them, three contained complete genomes. See Table V for further information. The pan genome, the set of genes from all strains, was formed by 4 572 genes. The core genome consisted of 1 765 genes which were identified in all genomes, accessory genome was formed by 2 808 genes which were present in at least two genomes. 890 genes were labelled as unique as they were found only in the one of the analyzed *R. rubrum* genomes. Further we constructed core genome-based and pan genome-based phylogenetic trees, see Figure 2. According to the core genome-based tree, the core genome is conserved. In the tree constructed according to the pan genome, we can distinguish individual strains and strains DSM 467 and ATCC 11170 are placed in the same cluster with quite small distance between them. We further compared strains ATCC 11170 and DSM 467 and we found that core genome of those two strains contained 3 874 genes, DSM 467 had 2 unique genes and ATCC 1170 had 14 unique genes.

Table V. A list of available GenBank assemblies of *Rhodospirillum rubrum* strains

GenBank assembly accession	Strain	Assembly level
GCA_000225955.1	F11	complete genome
GCA_019134555.1	DSM 467	complete genome
GCA_000013085.1	ATCC 11170	complete genome
GCA_016583945.1	DSM 1068	contig
GCA_016583925.1	DSM 107	contig
GCA_016653395.1	FR1-mutantIV	scaffold
GCA_003530895.1	UBA12186	scaffold
GCA_003457435.1	UBA10083	scaffold

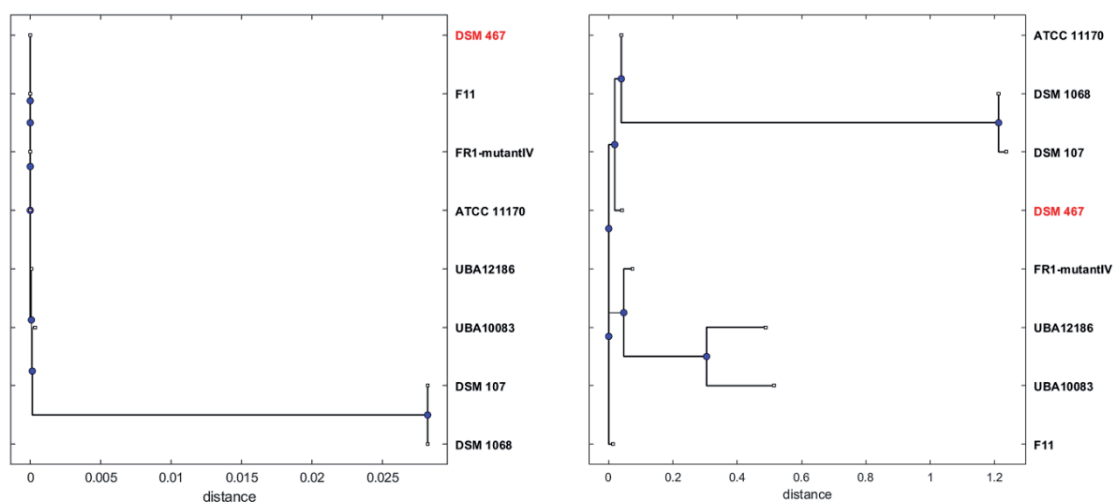


Figure 2. The core genome-based tree (on the left) and the pan genome-based tree (on the right) of *Rhodospirillum rubrum* strains

Last but not least, we created a genome-scale model of *R. rubrum* DSM 467 in Pathway tools software based on the genome annotation. Our model consisted of 260 pathways, 1 491 enzymatic reactions, 23 transport reactions, 3 856 polypeptides, 3 protein complexes, 939 enzymes, 28 transporters, 1 083 compounds, 2 614 transcription units, and 54 tRNAs. The model will be used for further research of metabolic processes behind PHA biosynthesis in *Rhodospirillum rubrum* DSM 467.

Conclusion

In this study, we performed sequencing and assembly of *Rhodospirillum rubrum* DSM 467 genome by hybrid approach. Thanks to combination of long and short reads we were able to provide high quality assembly of *R. rubrum* DSM 467 genome. The genome consists of one circular chromosome and one circular plasmid. We provided genomic and functional annotation, which will be used in further research of *R. rubrum* DSM 467 ability to synthesize PHA.

Acknowledgement

This work has been supported by grant project GACR 21-15958L.

References

1. Rehm B. H. A.: *Biochem J.*, **376**, 15 (2003).
2. Revelles O., Tarazona N., Garcia J. L., Prieto M. A.: *Environ Microbiol.*, **18**, 708 (2016).
3. Munk C. A., Copeland A., Lucas S., Lapidus A., Glavina Del Rio T., Barry K., Detter J. C., Hammon N., Israni S., Pitluck S., Brettin T., Bruce D., Han C., Tapia R., Gilna P., Schmutz J., Larimer F., Land M., Kyrpides N. C., Mavromatis K., Richardson P., Rohde M., Goker M., Klenk H., Zhang Y., Roberts G. P., Reslewic S., Schwartz D. C.: *Stand Genomic Sci.*, **4**, 293 (2011).
4. Leger A., Leomardi T.: *J. Open Source Softw.*, **4**, 1236 (2019).
5. Lanfear R., Schalamun M., Kainer D., Wang W., Schwessinger B.: *Bioinformatics*, **35**, 523 (2019).
6. Li H.: *Bioinformatics*, **34**, 3094 (2018).
7. Vaser R., Sovic I., Nagarajan N., Sikic M.: *Genome Res.*, **27**, 737 (2017).
8. Ewels P., Magnusson M., Lundin S., Kaller M.: *Bioinformatics*, **32**, 3047 (2016).
9. Bolger A. M., Lohse M., Usadel B.: *Bioinformatics*, **30**, 2114 (2014).
10. Li H.: arXiv: 1303.3997v2 [q-bio.GN] (2013).
11. Walker B. J., Abeel T., Shea T., Priest M., Abouelliel A., Sakthikumar S., Cuomo C. A., Zeng Q., Wortman J., Young S. K., Earl A. M.: *PLoS One.*, **9**, e112963 (2014).
12. Tatusova T., DiCuccio M., Badretdin A., Chetvernin V., Nawrocki E. P., Zaslavsky L., Lomsadze A., Pruitt K. D., Borodovsky M., Ostell J.: *Nuclei Acids Res.*, **44**, 6614 (2016).
13. Taboada B., Estrada K., Ciria R., Merino E.: *Bioinformatics*, **34**, 4118 (2018).
14. Cantalapiedra C. P., Hernandez-Plaza A., Letunic I., Bork P., Huerta-Cepas J.: *Mol. Biol. Evol.*, **38**, 5825 (2021).
15. Carver T., Thomson N., Bleasby A., Berriman M., Parkhill J.: *Bioinformatics*, **25**, 119 (2009).
16. Carver T., Harris S. R., Berriman M., Parkhill J., McQuillan J. A.: *Bioinformatics*, **28**, 464 (2012).
17. Biswas A., Staals R. H. J., Morales S. E., Fineran P. C., Brown C. M.: *BMC Genom.*, **17**, 356 (2016).
18. Akhter S., Aziz R. K., Edwards R. A.: *Nuclei Acids Res.*, **40**, e126 (2012).
19. Song W., Sun H., Zhang C., Cheng L., Peng Y., Deng Z., Wang D., Wang Y., Hu M., Liu W., Yang H., Shen Y., Li J., You L., Xiao M.: *Nuclei Acids Res.*, **47**, W74 (2019).
20. Arndt D., Grant J. R., Marcu A., Sajed T., Pon A., Liang Y., Wishart D. S.: *Nuclei Acids Res.*, **44**, W16 (2016).
21. Roberts R. J., Vincze T., Posfai J., Macelis D.: *Nuclei Acid Res.*, **43**, D298 (2015).
22. Page A. J., Cummins C. A., Hunt M., Wong V. K., Reuter S., Holden M. T. G., Fookes M., Falush D., Keane J. A., Parkhill J.: *Bioinformatics*, **31**, 3691 (2015).
23. Karp P. D., Midford P.E., Billington R., Kothari A., Krummenacker M., Latendresse M., Ong W. K., Subhraveti P., Caspi R., Fulcher C., Keseler I. M., Paley S. M.: *Brief. Bioinform.*, **22**, 109 (2021).

DIVERSITY OF *SCHLEGELELLA THERMODEPOLYMERANS* REVEALED WITH NANOPORE SEQUENCING

Sedlar K.¹, Musilova J.¹, Kourilova X.², Bezdicek M.³, Obruca S.²

¹Department of Biomedical Engineering, Faculty of Electrical Engineering and Communication, Brno University of Technology, Technicka 12, 616 00, Brno, Czechia

²Department of Food Chemistry and Biotechnology, Faculty of Chemistry, Brno University of Technology, Purkynova 118, 612 00, Brno, Czechia

³Department of Internal Medicine—Hematology and Oncology, University Hospital Brno, Cernopolni 212, 613 00, Brno, Czechia

sedlar@vut.cz

Abstract

Schlegelella thermodepolymerans is a thermophilic bacterium known for more than two decades thanks to its ability to decompose polyhydroxyalkanoates (PHA), environment-friendly, biodegradable and renewable alternatives to petrochemical polymers. Recently, we proved that the type strain *S. thermodepolymerans* DSM 15344^T is also a potent PHA producer, which suggests its utilization for industrial production of bioplastics. Moreover, the strain prefers xylose over other sugars, including glucose. This is caused by unique *xyl* operon containing genes for xylose transport together with genes for its utilization as we found out from the complete genome assembly we had published previously. Here, we present genome comparisons of the type strain with additional strains *S. thermodepolymerans* DSM 15264, LMG 21645, and CCUG 50061 using nanopore sequencing. While genomes of all strains possessed gene machinery required for PHA metabolism, only strains DSM 15264 and LMG 21645 showed very high genome similarities, 97.9% and 96.1%, to the type strain, calculated as digital DNA-DNA hybridization (dDDH) values. On the contrary, the genome of the strain CCUG 50061 differed from the others not only in overall genome length but its dDDH value to the type strain was only 23.1%. Since the value is below the 70 % threshold for species delineation, the strain *S. thermodepolymerans* CCUG 50061 is probably misidentified. Nevertheless, resequencing with short reads is needed to polish inaccurate nanopore-based draft assemblies.

Introduction

Polyhydroxyalkanoates (PHA) are microbial polyesters produced by numerous prokaryotes as they serve as a reservoir of carbon and energy that is stored in a form of intracellular granules. These granules, or so-called carbonosomes, help organisms overcome stress conditions¹. More importantly, they can be used industrially as polyesters of hydroxyalkanoic acids present renewable and biodegradable alternatives to petrochemical polymers. Thus, they demonstrate suitable materials for current trends of a circular economy where materials need to be biodegradable². Nevertheless, not all prokaryotes producing PHA are suitable for industrial production. The promising producers can be found among extremophilic bacteria, thermophiles and halophiles³. The reason lies in the reduced risk of microbial contamination allowing to perform a fermentation under unsterile conditions, a concept known as “Next Generation Industrial Biotechnology” (NGIB)⁴.

S. thermodepolymerans is a thermophilic, Gram-negative bacterium that is known for almost two decades for its ability to degrade extracellular PHA materials such as copolymers of 3-hydroxybutyrate and 3-mercaptopropionate⁵. Besides the type strain *S. thermodepolymerans* DSM 15344^T, three additional strains, DSM 15264 from the DSZM culture collection, LMG 21645 from the BCCM/LMG culture collection, and CCUG 50061 from the CCUG culture collection, are known. Nevertheless, only the genome of the type strain has been completely assembled so far⁶. The ability of the type strain *S. thermodepolymerans* DSM 15344^T not only to degrade extracellular PHA but also to produce PHA was proved only recently⁷. Its optimal growth temperature is 55°C which highly reduces the risk of contamination and corresponds to the NGIB concept. Moreover, the strain prefers xylose over glucose due to the possession of unique *xyl* operon containing genes for xylose transport to the cell together with genes responsible for its utilization in the non-oxidative branch of pentose phosphate pathway⁷.

In this paper, we sequenced genomes of additional three strains of *S. thermodepolymerans* using the Oxford Nanopore minION platform. We assembled particular genomes, performed their structural and functional annotation, and compared them to the genome of the type strain. While strains DSM 15264, LMG 21645 showed low diversity and were very similar to the type strain, the genome of the strain CCUG 50061 showed substantial differences and probably does not belong to the *S. thermodepolymerans* species.

Materials and methods

Bacterial strains

Schlegelella thermodepolymerans DSM 15264 was obtained from the Leibniz Institute DSMZ-German Collection of Microorganisms and Cell Cultures, Braunschweig, Germany. *Schlegelella thermodepolymerans* LMG 21645 was obtained from the BCCM/LMG collection of microorganisms, Ghent, Belgium. *Schlegelella thermodepolymerans* CCUG 50061 was obtained from the Culture Collection University of Gothenburg, Gothenburg, Sweden.

Cultivation

Optimal temperature for growth of bacterial strains DSM 15264 and LMG 21645 growth was 50°C. In the case of the strain CCUG 50061, the cultivation temperature was 42°C. The inoculum was developed in nutrient-rich medium Nutrient Broth (HiMedia, India) containing peptone 10.0 g/L, beef extract 10.0 g/L and sodium chloride 5.0 g/L. After 24 hours, 5% of the bacterial suspension was inoculated into a mineral salt medium composed of Na₂HPO₄ · 12 H₂O (9.0 g/L), KH₂PO₄ (1.5 g/L), NH₄Cl (1.0 g/L), MgSO₄ · 7 H₂O (0.2 g/L), CaCl₂ · 2 H₂O (0.02 g/L), Fe^(III)NH₄citrate (0.0012 g/L), yeast extract (0.5 g/L), 1 mL/L of microelements solution (EDTA (50.0 g/L), FeCl₃ · 6 H₂O (13.8 g/L), ZnCl₂ (0.84 g/L), CuCl₂ · 2 H₂O (0.13 g/L), CoCl₂ · 6 H₂O (0.1 g/L), MnCl₂ · 6 H₂O (0.016 g/L), H₃BO₃ (0.1 g/L), dissolved in distilled water) and a xylose (20.0 g/L) as a carbon substrate.

DNA extraction and sequencing

Genomic DNA was extracted using MagAttract HMW DNA kit (Qiagen, NL). The DNA purity was checked using NanoDrop (Thermo Fisher Scientific, USA), the concentration was measured using Qubit 2.0 Fluorometer (Thermo Fisher Scientific, USA) and the proper length of the isolated DNA was confirmed using Agilent 4200 TapeStation (Agilent technologies, USA). The sequencing library for Oxford Nanopore sequencing was prepared using Ligation sequencing 1D Kit (Oxford Nanopore Technologies, UK). The sequencing was performed using the R9.4.1 flowcell and the MinION platform (Oxford Nanopore Technologies, UK).

Genome assembly, annotation, and analysis

The Nanopore reads were basecalled using Guppy v3.4.4 (<https://community.nanoporetech.com>) and quality was checked using MiniONQC⁸. Subsequently, the reads were assembled with Flye v2.8.1 (<https://github.com/fenderglass/Flye>). Polishing was done using Racon v1.4.13⁹ and Medaka (<https://github.com/nanoporetech/medaka>); auxiliary PAF files were generated using minimap2¹⁰. Structural genome annotation was done through the NCBI Prokaryotic Genome Annotation Pipeline (PGAP)¹¹. Functional annotation of the protein-coding genes was performed by classifying them into clusters of orthologous groups (COG) from the eggNOG database using the eggNOG-mapper v2.1.7¹². A circular graph showing whole-genome alignments to the reference was produced with BRIG v0.95¹³. Digital DNA to DNA hybridization (dDDH) values were calculated using TYGS server¹⁴. The core and accessory genomes and unique genes were identified with BPGA v1.3.0¹⁵ using amino acid sequences and 90% sequence similarity. Localization and visualization of *xyl* operon were done with CLC Genomics Workbench v22 (QIAGEN Aarhus A/S).

Results and discussion

We assembled genomes of three strains and compared them to the genome assembly of the type strain *S. thermodepolymerans* DSM 15344^T, see Table I.

Table I

Comparison of genome assemblies and structural annotations

Feature	DSM 15344 ^T	DSM 15264	LMG 21645	CCUG 50061
Length (bp)	3,858,501	4,027,621	3,935,359	6,015,883*
GC content (%)	70.28	70.21	70.16	70.41
Total number of ORFs	3,650	4,113	4,188	7,219
Protein coding genes	3,589	4,053	4,128	7,109
Pseudogenes	33	974	1,320	2,280
rRNA genes (5S, 16S, 23S)	2, 2, 2	2, 2, 2	2, 2, 2	4, 4, 4
tRNA	51	50	50	91
ncRNA	4	4	4	7

*draft assembly containing five contigs

Genome assemblies of strains *S. thermodepolymerans* DSM 15264 and LMG 21645 resulted in single circular contigs that probably corresponded to complete genomes formed by circular chromosomes as the type strain possesses no plasmid⁶. Lengths of these circular contigs corresponded roughly to the length of the circular chromosome of the type strain. On the contrary, the predicted genome length of the strain *S. thermodepolymerans* CCUG 50061 was more than 50% longer compared to the type strain and the number of predicted genes was doubled. While total numbers of genes were higher also for the other two strains, the reason can be found in the low quality of nanopore assembly confirmed by numerous predicted pseudogenes suffering mainly from shifts in open reading frames. GC content of all genomes was comparable and genomes possessed two copies of rRNA genes except for *S. thermodepolymerans* CCUG 50061 which contained four copies. Such results suggested that the strain *S. thermodepolymerans* CCUG 50061 does not belong to the *S. thermodepolymerans* species.

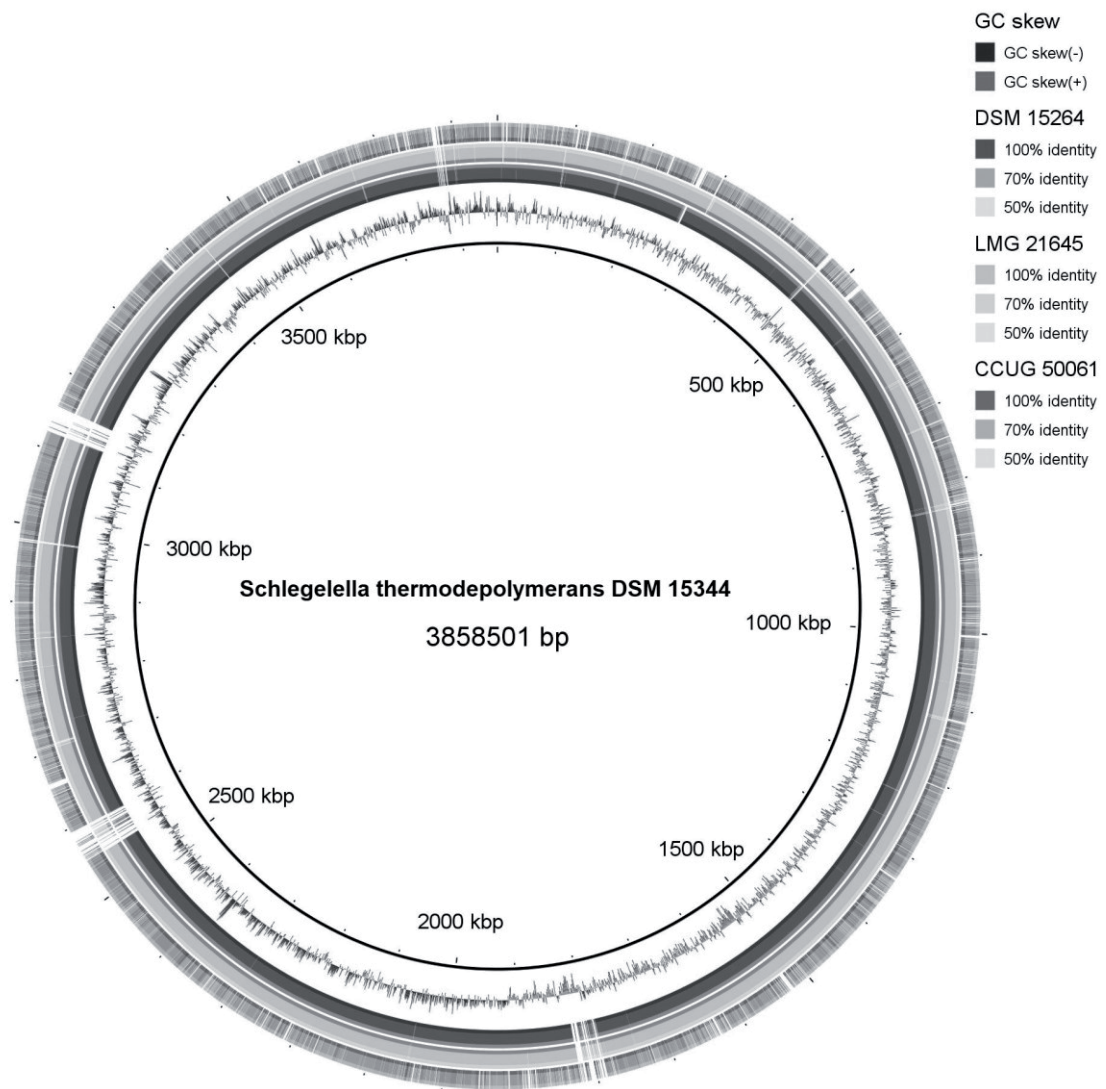


Figure 1. Genome alignments to the type strain *S. thermodepolymerans* DSM 15344^T

Due to differences in genome assemblies, we decided to do genome alignments to the type strain, see Figure 1. While genomes of strains DSM 15264 and LMG 21645 aligned to the type strain with almost 100% similarity across the whole genome as two inner rings showed, the outer ring representing the strain CCUG 50061 showed that its genome differed substantially from that of the type strain. No longer alignment was detected, only many small parts of genomes showed similarity from 50 to 70%. Therefore, we decided to calculate dDDH values of the three analyzed strains in comparison to the type strain, see Table II. While strains DSM 15264 and LMG 21645 reached very high genome similarities, exceeding 70% threshold for species delineation, dDDH value between the type strain and the strain CCUG 50061 was only 23.1% suggesting that the strain does not belong to the *S.*

thermodepolymerans species. Unfortunately, the correct species could not be assigned as the Type Strain Genome Server database did not contain any similar type strain.

Table II
Digital DNA-DNA hybridization to the type strain

Query strain	dDDH (%)	Confidence interval (%)	GC content diff. (%)
DSM 15264	97.9	[97.0 - 98.6]	0.07
LMG 21645	96.1	[94.8 - 97.2]	0.12
CCUG 50061	23.1	[20.8 - 25.5]	0.13

Since we were not able to classify the strain CCUG 50061, we decided to analyze the potential functional capacities of particular genomes by dividing particular genes into COG. Probably due to the lower quality of nanopore assemblies, numbers of genes unassigned any COG were higher for newly analyzed strains. While only 10.7% of genes were not assigned any COG in the high-quality hybrid assembly of the type strain⁶, 37.0%, 45.6%, and 50.8% of genes were not assigned any COG in DSM 15264, LMG 21645, and CCUG 50061, respectively. When only genes divided into particular orthologous groups were counted, the overall potential functional capacity of particular genomes was very similar. This is clearly visible when genes are divided into functional categories assigned to COG, see Table III. Relative abundances of genes in particular functional categories across all analyzed genomes were very similar. This means that despite different genotypes, phenotypic manifestations of particular strains might be very similar. Since no genomic data were available for strain CCUG 50061 so far, this might be a reason for its erroneous classification that was done using only phenotypic manifestation.

Table III
Relative abundance of genes in functional COG categories

COG functional category	DSM 15344 ^T	DSM 15264	LMG 21645	CCUG 50061
A, RNA processing and modification	0.03	0.04	0.09	0.00
B, Chromatin structure and dynamics	0.06	0.08	0.04	0.09
C, Energy production and conversion	8.42	7.45	7.13	5.35
D, Cell cycle control, cell division, chromosome partitioning	1.22	1.29	1.16	1.63
E, Amino acid transport and metabolism	8.64	7.84	7.66	8.30
F, Nucleotide transport and metabolism	2.96	2.63	2.18	2.69
G, Carbohydrate transport and metabolism	3.96	3.92	3.30	3.98
H, Coenzyme transport and metabolism	4.37	3.49	3.52	3.23
I, Lipid transport and metabolism	4.96	4.43	4.90	4.38
J, Translation, ribosomal structure and biogenesis	5.59	5.53	5.21	6.70
K, Transcription	7.83	8.46	8.78	7.41
L, Replication, recombination and repair	4.52	4.15	3.96	8.76
M, Cell wall/membrane/envelope biogenesis	5.77	6.35	6.15	5.78
N, Cell motility	2.93	3.21	3.39	1.80
O, Posttranslational modification, protein turnover, chaperones	3.71	3.49	3.39	3.66
P, Inorganic ion transport and metabolism	5.21	4.98	5.43	4.95
Q, Secondary metabolites biosynthesis, transport and catabolism	2.28	2.66	3.03	1.52
S, Function unknown	20.59	22.57	22.36	21.80
T, Signal transduction mechanisms	3.96	4.66	5.26	4.75
U, Intracellular trafficking, secretion, and vesicular transport	2.06	2.00	2.09	1.46
V, Defense mechanisms	0.90	0.78	0.98	1.77

Although the overall functional capacity of particular bacteria might be very similar, various species usually demonstrate unique phenotypic traits. Such a unique feature for *S. thermodepolymerans* can be found in its preference to utilize xylose over glucose⁷. The reason lies in the structure of *xyl* operon that possesses genes for both, the transport of xylose into a cell as well as for its utilization in the pentose phosphate pathway. In total, *xyl* operon in the genome of the type strain *S. thermodepolymerans* DSM 15344 consists of seven genes, see Figure 2. Besides xylose isomerase *xylA* and two xylulokinases, *xylB* and other unnamed gene (locus IS481_06520), also four genes coding sugar transporters are present. These are probably *xylF*, *xylG* (here as IS481_06500), *xylH* (here as IS481_06505), and *galM* (here as IS481_06490). The same operons were found in

genomes of strains DSM 15264 and LMG 21645. On the contrary, the genome of the strain CCUG 50061 possessed no similar operon.

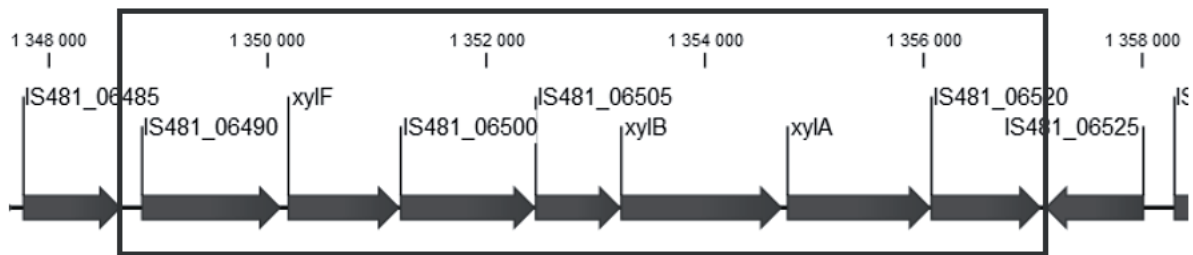


Figure 2. Structure of *xyl* operon in the *S. thermodepolymerans* genome

Finally, we decided to compare sequences of particular genes among analysed strains on a genome-wide scale and performed a pan-genome analysis. The analysis of strains strain *S. thermodepolymerans* DSM 15344^T, DSM 15264, and LMG 21645 resulted in the core genome of 1,925 genes. These genes are shared by all analyzed strains and are supplemented by an accessory genome of 886 genes that are shared by two strains. The number of unique genes for particular strains varied from 221 to 753. These results suggested that strains are closely related. On the contrary, when the strain CCUG 50061 was added to the analysis, the size of the core genome shrunk to only 586 genes since the strain contained 3,688 unique genes. Therefore, it is evident that the strain CCUG 50061 does not belong to the *S. thermodepolymerans* species.

Conclusion

In this study, we compared genomes of three strains DSM 15264, LMG 21645, and CCUG 50061 to the genome of the type strain *S. thermodepolymerans* DSM 15344^T. We showed that strains DSM 15344^T, DSM 15264, and LMG 21645 are closely related and their diversity is low. On the other hand, genome assemblies based on nanopore sequencing suffered from low quality of sequencing reads and re-sequencing using high-quality short reads is needed before final conclusions are drawn. Although experimental evidence is still needed, both non-type strains, DSM 15264 and LMG 21645, will likely prefer xylose over other substrates thanks to a unique *xyl* operon that has the same structure as in the type strain.

Moreover, we showed that the strain CCUG 50061 does not belong to the *S. thermodepolymerans* species. While its potential functional capacity was very similar to remaining strains and similar phenotypic manifestation could be therefore expected, the genome showed essential differences. Unfortunately, no similar type strain could be found. Thus, the classification of the strain is currently not possible. Moreover, its draft genome assembly is of poor quality and re-sequencing will be needed to classify the strain.

Acknowledgement

This work was supported by the grant project GACR 22-10845S.

References

- Obruca S., Sedlacek P., Koller M., Kucera D., Pernicova I.: *Biotechnol Adv.*, 36, 856 (2018).
- Koller M., Marsalek L., de Sousa Dias M., Braunegg G.: *New Biotechnol.*, 37, 24 (2017).
- Obruca S., Dvorak P., Sedlacek P., Koller M., Sedlar K., Pernicova I., Safranek D.: *Biotechnol Adv.*, 58, 107906 (2022).
- Chen GQ., Jiang XR.: *Curr Opin Biotechnol.*, 50, 94 (2018).
- Elbanna K., Lutke-Eversloh T., Van Trappen S., Mergaert J., Swings J., Steinbuchel A.: *Int J Syst Evol Microbiol.*, 53, 1165 (2003).
- Musilova J., Kourilova X., Bezdicek M., Lengerova M., Obruca S., Skutkova H., Sedlar K.: *Genome Biol. Evol.*, 13, evab007 (2021).
- Kourilova X., Pernicova I., Sedlar K., Musilova J., Sedlacek P., Kalina M., Koller M., Obruca S.: *Bioresour. Technol.*, 315, 123885 (2020).
- Lanfeer R., Schalamun M., Kainer D., Wang W., Schwessinger B.: *Bioinformatics*, 35, 523 (2019).
- Vaser R., Sovic I., Nagarajan N., Sikic M.: *Genome Res.*, 27, 737 (2017).

10. Li H.: *Bioinformatics*, *34*, 3094 (2018).
11. Tatusova T., DiCuccio M., Badretdin A., Chetvernin V., Nawrocki E. P., Zaslavsky L., Lomsadze A., Pruitt K. D., Borodovsky M., Ostell, J.: *Nucleic Acids Res.*, *44*, 6614 (2016).
12. Carlos P. C., Hernandez-Plaza A., Letunic I., Bork P., Huerta-Cepas J.: *Mol. Biol. Evol.*, *38*, 5825 (2021).
13. Alikhan N. F., Petty N. K., Ben Zakour N. L., Beatson S. A.: *BMC Genomics*, *12*, 402 (2011).
14. Meier-Kolthoff J. P., Goker M.: *Nat. Commun.*, *10*, 2182 (2019).
15. Chaudhari N. M., Gupta V. K., Dutta C.: *Sci. Rep.*, *6*, 24373 (2016).

OPTIMIZATION OF EXTRACTION, PURIFICATION AND STABILIZATION OF BIOLOGICALLY ACTIVE COMPOUNDS FROM YEAST AND MICROALGAE BIOMASS

Šimanský S., Szotkowski M., Holub J., Obračaj H., Dzurická L., Schildová V., Márová I.

Brno University of Technology, Faculty of Chemistry, Brno, Czech Republic

xcsimansky@vutbr.cz

Abstract

The rapid growth of biotechnological industry is caused by the flexible capabilities of microorganisms, such as their ability to turn waste materials into valuable compounds. Some of these compounds can be used as vitamin precursors or biofuel sources. The topic of this research is focused on the optimisation of extraction of valuable lipophilic compounds from red yeast biomass and microalgae biomass. Solvents used should be suitable for food or pharmaceutical industry, in particular ethanol and hexane. The stability of prepared extracts, while stored at various ambient temperatures, is also tested. Cultivation of these microorganisms includes small-scale fermenter cultivations and cultivations in Pyrex Glass Bottles with profound aeration. Generally, ethanol proved to be better extraction solvent, when it comes to extraction of pigments than hexane. However, hexane seems to be more suitable for extraction of lipids. Also, it is worth noting, there have been observed some specific biomass samples, for which both solvents proved to be comparably efficient. The prepared extracts exhibited good stability while stored in the freezer and only some of them proved to be stable in the fridge. Compounds in almost all extracts quickly deteriorated, while stored at laboratory temperatures.

Introduction

Red yeasts are heterotrophic single-cell eukaryotic microorganisms characteristic by their ability to produce red pigments - carotenoids. These yeasts are belonging to a division of basidiomycetous fungi, and they are unable to ferment sugars. Microalgae are phototrophic eukaryotic single-cell organisms. Cyanobacteria are often practically included to microalgae, because of their phototropic metabolism and similar biomass content. However, cyanobacteria are prokaryotic microorganisms with much smaller and simpler cells [1,2].

Biomass of red yeast contains board spectrum of carotenoids including β -carotene, torulene, torularhodin and γ -carotene. Red yeast can, under specific conditions, accumulate large amounts of lipids (up to 70 %), composed mostly by SFA, MUFA and rarely ω 6-PUFA. Other compounds produced by red yeast, which are attractive for pharmaceutical industry include exopolysaccharides, more specifically β -glucans. Lastly, ergosterol (with provitamin-D function) and Coenzyme Q are present in red yeast biomass. Microalgal and cyanobacterial biomass typically contains large amounts of proteins, broad spectrum of carotenoids, chlorophylls, vitamins, some polysaccharides and lipids, including valuable MUFA and PUFA [1,2].

Experiments

Cultivation

Firstly, for extraction experiments was needed a large amount (in laboratory scale) of biomass. For cultivation of red yeast, a laboratory-scale fermenter with working volume of 3 l was used. Fermenter cultivation allows to precisely monitor amount of dissolved oxygen, pH and temperature. All these aspects were monitored during all yeast cultivations. Cultivations of microalgae and cyanobacteria were performed in Pyrex glass bottles with constant aeration by sterile air and with proper exposure to light.

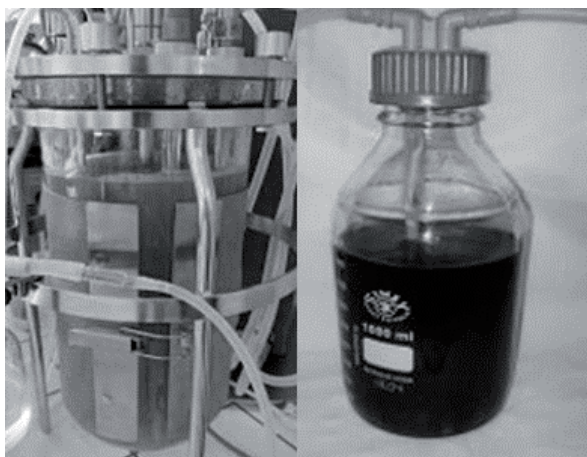


Figure 1: Fermenter cultivation of red yeast (left) and Pyrex glass bottle cultivation of microalgae (right)

Extraction

Extract preparation was carried out in 50 ml plastic centrifuge tubes. Into those tubes was placed approximately 500 mg of lyophilised yeast biomass (or 100 mg of microalgal biomass) or approximately the same amount of fresh biomass. In the next step, glass pearls (used for general laboratory methods like Folch extraction) in amount of 3 volumes of utilised biomass were placed into these tubes. Lastly, organic solvent was added, and tubes were placed on laboratory vortex for about 20 minutes, to assure thorough extraction of all bio-active compounds from biomass. The separation of solvents and biomass remains was achieved by centrifugation. Solvents used for extractions were chosen by their possible application in pharmaceutical and food industries, thus ethanol and hexanes.

Stability

Prepared extracts were stored in small Pyrex glass bottles, or volumetric flasks. Firstly, extraction efficiency was determined by comparing the amount of investigated bio-active compounds in the extracts with the amount obtained by conventional means of extraction, such as Folch extraction. The extracts were then stored in various ambient temperatures including laboratory temperature of around 22 °C, fridge (4 °C), freezer (-32 °C) and physiological temperature (37 °C) and stability of investigated bio-active compounds was observed over the course of one month by performing periodic measurements.

Analysis

Content of carotenoids, chlorophyll, ergosterol and ubiquinone was determined by using reverse phase HPLC. Extracted samples were subjugated to HPLC analysis of brand Thermo Fisher Scientific on column EVO C18 with dimensions 150x4.6x2.6 mm with gradient elution. A PDA detector was used for the detection of analytes.

Content of lipids was determined by analysis of fatty acid spectrum by using GC method. Lipids present in samples were subjugated to trans-esterification and their methyl-esters were then analysed on Thermo Fisher TRACETM Gas Chromatograph with Thermo autosampler Scientific A1 1310, with automatic dosing and flow separator. For the analysis was used a Zebtron-FAME column with dimensions of 30 m x 0.25 mm x 0.25 µm. For detection of analytes was used flame ionization detector (FID).

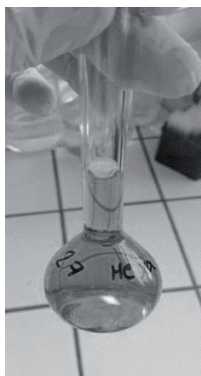


Figure 2: Hexane yeast extract in volumetric flask

Results

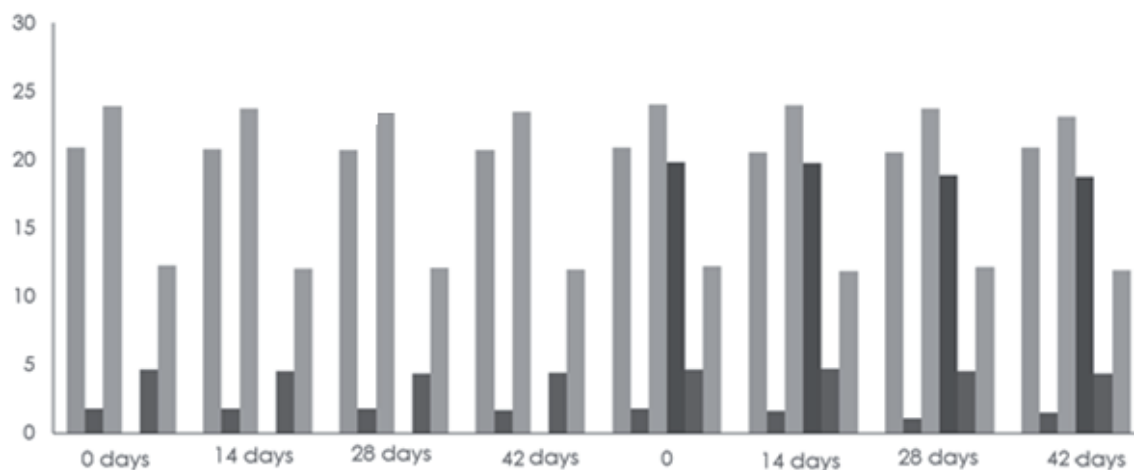


Figure 3: Hexanes extract, *Rhodosporidium toruloides*, -32 °C

In Figure 3 there can be observed changes in the composition of bio-active compounds of hexane extract of yeast strain *Rhodosporidium toruloides* in time (days). For specific samples, first column represents torularhodin, second column represents torulene, third total carotenoids, fourth tocopherol, fifth ubiquinone, sixth ergosterol.

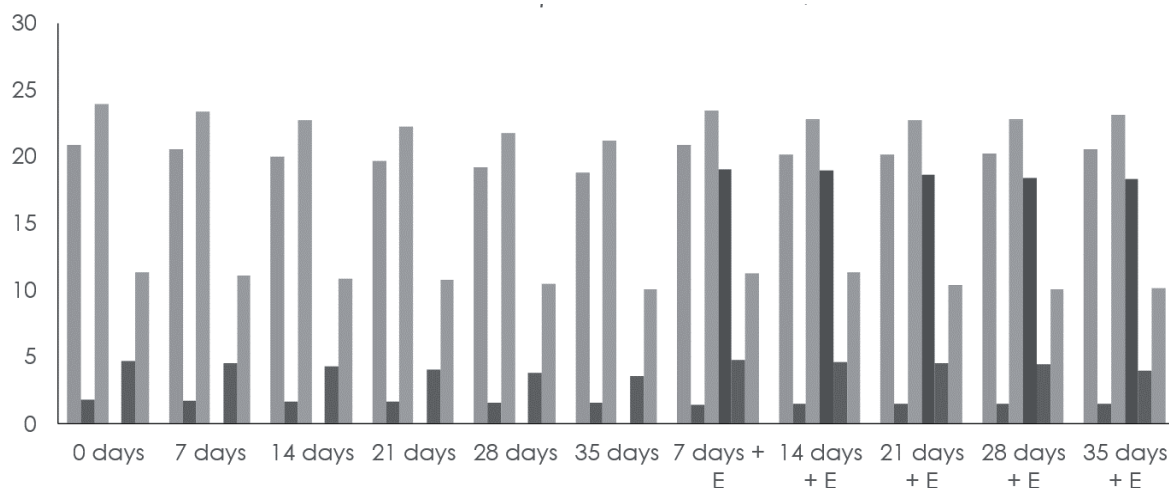


Figure 4: Hexanes extract, *Rhodosporidium toruloides*, 4 °C.

In Figure 4 there can be observed changes in the composition of bio-active compounds of hexane extract of yeast strain *Rhodosporidium toruloides* in time (days). For specific samples, first column represents torularhodin, second column represents torulene, third total carotenoids, fourth tocopherol, fifth ubiquinone, sixth ergosterol. The samples containing added tocopherol are marked with “+ E”.

Discussion

From the results showed in Figure 3 and Figure 4, it seems that that content of lipophilic compounds in hexane extract of *Rhodosporidium toruloides* is generally stable when stored at -32 °C and even if stored at 4 °C. Thus, this extract can be considered as one of the most suitable, as storage in cooler is considerably more affordable, than storage at freezing temperatures. It is also possible to observe, that addition of tocopherol to this extract had little to no effect on stability of other lipophilic compounds (samples marked as n days + E).

Conclusion

Lipophilic compounds isolated from biomass are relatively stable, while stored at lower temperatures. Addition of tocopherol to prepared extracts can improve their stability. Nevertheless, while each cultivation means provided different set of results, it is safe to assume that extraction should be specific for each cultivation method and each strain. Results are most probably related to the primary differences in cell construction and composition of produced pigments in specific biomass samples.

Acknowledgements

The study was supported by projects King (Project Nr. 7746) and ByProValue (Project Nr. 301834 of the Research Council of Norway)

References

- 1 SZOTKOWSKI, Martin, Jiří HOLUB, Samuel ŠIMANSKÝ, Klára HUBAČOVÁ, Pavlína SIKOROVÁ, Veronika MARINIČOVÁ, Andrea NĚMCOVÁ a Ivana MÁROVÁ. Bioreactor Co-Cultivation of High Lipid and Carotenoid Producing Yeast *Rhodotorula kratochvilovae* and Several Microalgae under Stress. *Microorganisms* [online]. MDPI, **9**(6), 1-23 [cit. 2022-09-16]. ISSN 2076-2607.
- 2 BYRTUSOVÁ, Dana, Martin SZOTKOWSKI, Klára KUROWSKA, Volha SHAPAVAL a Ivana MÁROVÁ. *Rhodotorula kratochvilovae* CCY 20-2-26-The Source of Multifunctional Metabolites. *Microorganisms* [online]. MDPI, **9**(6), 1-18 [cit. 2022-09-16]. ISSN 2076-2607.

DETERMINATION OF METHODOLOGY FOR MONITORING BIOFILM FORMATION OF FILAMENTOUS MICROSCOPIC FUNGI

Kulišová M.¹, Kolouchová I.¹

¹Department of Biotechnology, University of Chemistry and Technology Prague, 166 28, Prague 6
marketa.kulisova@vscht.cz

Abstract

Biofilm is a widespread survival strategy for microorganisms. In this form, they are protected from a wide range of adverse conditions (UV radiation, antimicrobials, drying out). For humans, biofilms may be desirable in industrial processes (biofiltration, bioremediation, wastewater treatment plants) or, conversely, cause significant problems (food contamination, deterioration of materials, reduced heat conduction efficiency). Unlike bacterial and yeast biofilms, filamentous microscopic fungal biofilms are neglected. This work focuses on the determination of a methodology suitable for the quantification of filamentous fungal biofilms. Three methods were selected, which are used for quantification of bacterial biofilms, and subsequently tested on single species biofilms of filamentous fungi *Alternaria alternata* DBM 4004, *Aspergillus niger* DBM 4054, *Fusarium culmorum* DBM 4044 and *Fusarium graminearum* DBM 4344. Crystal violet staining for the determination of total biofilm biomass and the MTT assay for the determination of metabolic activity of fungal biofilm were found to be appropriate for the quantification of filamentous fungal biofilm.

Introduction

Biofilm is a set of cells that are coated with extracellular polymeric substances (EPS) that keep cells together and adhere to the surface and provide protection against external conditions and the host's immune system¹ by reducing the concentrations of harmful substances that can penetrate the structure of the biofilm². Biofilms are formed on both natural and clinical material and are difficult to treat due to their increased resistance to antibiotics and biocides compared to planktonic cells³. Biofilms are known to occur in many different natural environments. Due to their unique properties, they better tolerate various environmental influences, such as UV radiation, anaerobic environment, pH change, drying, or higher salinity, they are able to grow in hydrothermal hot springs, on stones, in clean water, etc.⁴ Biofilms form layers on tissues and implanted devices and cause various diseases such as cystic fibrosis, pneumonia and osteomyelitis³.

Bacterial and yeast biofilms have been very well studied, including methods for their quantification. There are only a few studies on the topic concerning filamentous microscopic fungal biofilms. The microscopic filamentous fungal biofilm formation process can be divided into three phases: 1) cell adhesion to the surface, processed by conidia, hyphae; 2) conidia germination and so-called monolayer formation; 3) biofilm maturation (increase of the amount of biomass, creation of water channels and interstitial cavities). In general, in fungi, the adhesion of spores to the biotic or abiotic surface occurs on the basis of many complex physicochemical and biological mechanisms. The physicochemical properties of the surface support the adhesion process and these properties determine the success of adhesion. These are mainly hydrophobicity, electrostatic charge and roughness. The importance of these properties has been described in the past in the formation of bacterial and yeast biofilms⁵.

Strains of the genera *Aspergillus*, *Alternaria* and *Fusarium* were chosen for the study of microscopic filamentous fungal biofilms. The genus *Aspergillus* is one of the most widespread organisms, currently including over 335 known species⁶. It is one of the most economically important fungal genera due to the production of a number of different metabolites. Several antibiotics, antitumor and antifungal agents have been derived from these metabolites. Species *Aspergillus* spp. are used in the industrial production of soy sauce, miso, sake, organic acids and enzymes. On the other hand, the occurrence of the *Aspergillus* genus is one of the main causes of food and feed contamination. In addition, the species *A. niger*, *A. flavus* and *A. fumigatus* are producers of mycotoxins which can lead to mycotoxicosis in animals and the human population. *Fusarium* is a genus of plant pathogenic fungi, of which about one-seventh produce important mycotoxins⁷. The greatest economic impact is related to deoxynivalenol (DON) and its derivatives. Only aflatoxins produced by *Aspergillus* spp. have a greater impact on the food commodity market and animal health than DON⁸. DON belongs to the group of trichothecenes, which are with fumonisins and zearalenone the most important mycotoxins produced by this genus. The most common occurrence of *Fusarium* mycotoxins is in wheat and corn, but can occur in all cereals, asparagus, figs, legumes, spices and nuts (pistachios)^{9,10}. *Fusarium* mycotoxin contamination is also significant during the beer production process¹¹. Microscopic fungi of the genus *Alternaria* are ubiquitous pathogens and saprophytes characterized by the production of brown compartmental macroconidia. Most

species in this genus have a high proportion of melanin in their cell walls and spores. Melanin protects the microorganism from the effects of UV radiation and increases overall resistance to environmental factors¹². Due to their cosmopolitan occurrence and ability to grow and produce toxins even under adverse conditions (low temperatures), *Alternaria* species are a common cause of crop contamination during cold transport and storage¹³.

In vitro yeast and bacterial biofilm cultivation methods are divided into static and dynamic. Both types of methods can be used to monitor adhesion, cell release, or to test resistance to antimicrobials and disinfectants. Biofilm maturation cannot be monitored using static methods. Dynamic methods mimic the conditions of continuous flow that occur naturally in the environment, industry, or the human body. *In vivo* models are not used very often due to difficult condition control during experiments and possible ethical issues¹⁴⁻¹⁶. One of the most widely used methods is the use of microtiter plates to monitor biofilm growth. Other methods include the Christensen test tube method, the Calgary device, the Robinson device, or the use of biofilm reactors¹⁷⁻²¹.

Methods for microscopic fungal biofilm quantification

The following methods were used for the quantification of the filamentous fungal biofilm of *Alternaria alternata* DBM 4004, *Aspergillus niger* DBM 4054, *Fusarium culmorum* DBM 4044 and *Fusarium graminearum* DBM 4344. These microorganisms were stored on Petri dishes containing PDA agar at 4 °C. The inoculation of microtiter plates for all of the methods listed below was performed with 10⁵ spores/ml in saline. In each well of the 24-well microtiter plate (TPP, Switzerland) was added 1 ml of spore solution and 1 ml of PDB was added. The biofilm was grown statically at 26 °C for 24 h, 48 h or 72 h (depending on the experiment).

Crystal violet staining

The amount of biomass of adherent cells at the bottom of the plate was quantified by crystal violet staining. Crystal violet is a purple substance which, due to its structure, binds to negatively charged molecules. Crystal violet stains both living and dead cells and other extracellular structures, so it is used to determine the total amount of biomass. The crystal violet staining procedure was taken over and adapted according to Sabaeifard et al. (2014)²². The suspension was aspirated from the wells of the microtiter plate. The wells were washed three times with saline and then 2000 µl of crystal violet (0.1% (w/v)) was pipetted into each well. After 20 minutes of treatment, the crystal violet was aspirated and the wells were thoroughly washed three times with saline. Then 2000 µl of pure ethanol (96%) was added to the wells and the plate was left to stand for 10 minutes. Finally, 100 µl was removed from each well in a new polystyrene plate and the absorbance at 580 nm was measured on a spectrophotometric reader (Tecan, Switzerland).

MTT assay

MTT (3-(4,5-dimethyl-thiazol-2-yl)-2,5-diphenyltetrazolium bromide) is used to determine the metabolic activity of microorganism cells. In its natural state, MTT is a yellow substance that is transformed into blue crystals of formazan by metabolically active cells. The procedure was taken over and subsequently modified according to Riss et al. (2013)²³. The suspension was aspirated from the wells of the microtiter plate. The wells were then washed twice with 2000 µl of sterile PBS. After washing the wells, 600 µl of glucose solution (57.4 g/l in PBS), 500 µl of MTT solution (1 g/l in PBS) and 150 µl of menadione (0.11 g/l in PBS) were added to each well. The plate was incubated for 3 hours on an orbital shaker (75 rpm) at 26 °C in dark. After incubation, 1000 µl of washing solution was added to each well to dissolve the formed formazan crystals. The plate was placed for 30 minutes on an orbital shaker at 26 °C (150 rpm). At the end of the reaction, 100 µl of the solution from each well was transferred to a new plate intended for the reader, and then the absorbance at 570 nm was measured.

Resazurin assay

Resazurin is a blue dye that is used as an indicator of cell viability. The metabolically active cells reduce it to pink resorufin and further reversibly to colorless hydroresorufin. The procedure was modified according to Mariscal et al. (2009). After culturing the biofilm, non-adherent cells above the biofilm were thoroughly aspirated from the microtiter plate. The biofilm formed was washed twice with 2000 µl of sterile saline. Subsequently, 250 µl of glucose solution (180 g/l in PBS), 250 µl of resazurin solution (0.15 g/l in PBS) and 1000 µl of saline were pipetted into the wells. The microtiter plate was wrapped in aluminum foil (due to the sensitivity of resazurin to light) and the biofilm was statically incubated at 26 °C for a certain time depending on the microorganism (until visible color conversion of the control wells to blank wells). The fluorescence intensity of the resorufin formed in the wells was measured after transferring 100 µl of the solution from each well to the new plate at an excitation wavelength of 545 nm and an emission wavelength of 575 nm.

Results

For selected filamentous microscopic fungi, their biofilm formation was quantified after time periods of 24 h, 48 h and 72 h of culture. 24- and 48-hour cultures were found to be suitable for monitoring the growth of fungal biofilms. In the case of the longest cultivation, 72 hours, the biofilm was separated from the bottom of the wells during the washing steps, which are very important in the selected methods. This phenomenon greatly affected the results of the experiments.

The results of the determination of total biomass by crystal violet staining (Figure 1.) showed an increasing trend in all strains with an increasing cultivation time from 24 to 48 hours. In both *Fusarium* strains, biofilm growth was higher compared to *Alternaria alternata* and *Aspergillus niger*.

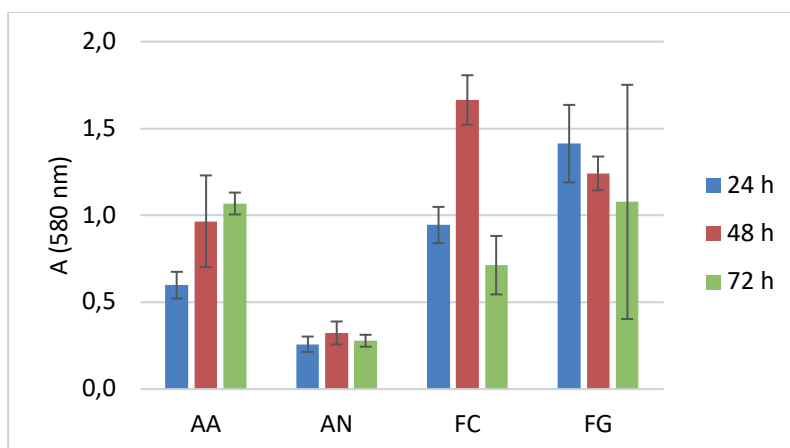


Figure 1. Crystal violet staining results after different cultivation lengths (24 h, 48 h, 72 h) of the microscopic fungal biofilm of *Alternaria alternata* DBM 4004 (AA), *Aspergillus niger* DBM 4054 (AN), *Fusarium culmorum* DBM 4044 (FC) and *Fusarium graminearum* DBM 4344 (FG)

The MTT assay, which determines the metabolic activity of biofilm cells, gave very similar absorbance results for all fungi tested in a 24-hour culture (Figure 2.). *Aspergillus niger* showed similar metabolic activity at all lengths of culture. As with the crystal violet method, the highest metabolic activity was observed in both strains of the genus *Fusarium*.

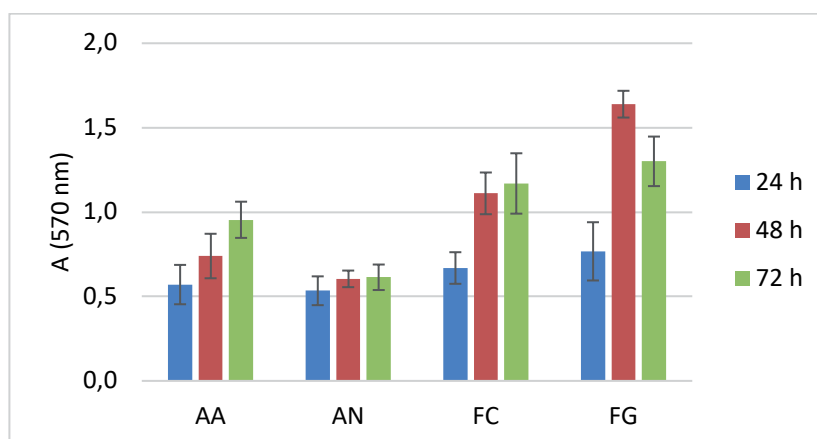


Figure 2. MTT assay results after different cultivation lengths (24 h, 48 h, 72 h) of microscopic fungal biofilm of *Alternaria alternata* DBM 4004 (AA), *Aspergillus niger* DBM 4054 (AN), *Fusarium culmorum* DBM 4044 (FC) and *Fusarium graminearum* DBM 4344 (FG)

The resazurin assay, based on the formation of fluorescent resorufin, was found to be unsuitable for quantifying the metabolic activity of the filamentous fungal biofilm. The color change from purple resazurin to pink resorufin was not observed even after 16 hours of reaction. Due to this finding, this method was excluded from further experiments.

Conclusion

Fungal biofilms are a relatively unexplored area of microbiology. This study is one of the first dealing with the development of the methodology for the quantification of fungal biofilms. From our results, we could conclude that crystal violet staining is suitable for the determination of the total biomass of filamentous fungal biofilm, and the MTT method for the determination of the metabolic activity of these biofilms. The resazurin assay was found to be unsuitable for the quantification of filamentous fungal biofilms. The next steps of the research will be to apply the given methodologies for testing the suppression of biofilm growth using biological reagents and physical effects.

Acknowledgement

This research was supported by The Czech Science Foundation (GACR), grant number 22-13745S and by the Specific university research – grant No. A2_FPBT_2022_036

References

1. Wesseling W.: *AIMS Bioengineering* 2, 104 (2015).
2. Segev-Zarko L.-a., Saar-Dover R., Brumfeld V., Mangoni M. L., Shai Y.: *Biochemical Journal* 468, 259 (2015).
3. Pletzer D., Hancock R. E.: *Journal of bacteriology* 198, 2572 (2016).
4. De La Fuente-Núñez C., Cardoso M. H., de Souza Cândido E., Franco O. L., Hancock R. E.: *Biochimica et Biophysica Acta (BBA)-Biomembranes* 1858, 1061 (2016).
5. Ramage G., Rajendran R., Gutierrez-Correa M., Jones B., Williams C.: *FEMS Microbiology Letters* 324, 89 (2011).
6. Gautier M., Normand A.-C., Ranque S.: *Clinical Microbiology and Infection* 22, 662 (2016).
7. Moss M. O., Thrane U.: *Toxicology letters* 153, 23 (2004).
8. Desjardins A. E.: *Fusarium mycotoxins: chemistry, genetics, and biology*. APS press St. Paul, MN, 2006.
9. Authority E. F. S.: *EFSA Journal* 11, 3379 (2013).
10. Waśkiewicz A., Beszterda M., Goliński P.: *Food Control* 26, 491 (2012).
11. Wolf-Hall C. E., Schwarz P. B.: *Mycotoxins and food safety* 217 (2002).
12. Thomma B. P.: *Molecular plant pathology* 4, 225 (2003).
13. Ostry V.: *World Mycotoxin Journal* 1, 175 (2008).
14. Cattò C., Cappitelli F.: *International journal of molecular sciences* 20, 3794 (2019).
15. Franklin M. J., Chang C., Akiyama T., Bothner B.: *Microbial Biofilms* 1 (2015).
16. Gomes I. B., Meireles A., Gonçalves A. L., Goeres D. M., Sjollema J., Simões L. C., Simões M.: *Critical reviews in biotechnology* 38, 657 (2018).
17. Hassan A., Usman J., Kaleem F., Omair M., Khalid A., Iqbal M.: *Brazilian journal of infectious diseases* 15, 305 (2011).
18. Gomes L. C., Moreira J. M., Simões M., Melo L. F., Mergulhão F. J.: *Scientifica* 2014, (2014).
19. Pesciaroli L., Petruccioli M., Fedi S., Firrincieli A., Federici F., D'Annibale A.: *Applied and environmental microbiology* 79, 6083 (2013).
20. Azeredo J., Azevedo N. F., Briandet R., Cerca N., Coenye T., Costa A. R., Desvaux M., Di Bonaventura G., Hébraud M., Jaglic Z.: *Critical reviews in microbiology* 43, 313 (2017).
21. Xiros C., Studer M. H.: *Frontiers in Microbiology* 8, 1930 (2017).
22. Sabaeifard P., Abdi-Ali A., Soudi M. R., Dinarvand R.: *Journal of microbiological methods* 105, 134 (2014).
23. Assays V., Riss T., Moravec R., Niles A., Duellman S., Benink H., Worzella T., Minor L.: *Activity Assay of Clove Mistletoe (Dendrophthoe pentandra (L.) Miq.) Leaves Extracts Advances in Pharmacological Sciences* 2016, 1 (2013).

SIDEROPHORES – THE ACTIVE COMPONENT OF THE BIOPESTICIDE PREPARATION

Mach J.¹, Halecký M.¹

¹*University of Chemistry and Technology, Technická 5, 166 28, Prague 6
machi@vscht.cz*

Abstract

The environment has recently experienced a challenging period in terms of increasing pollution caused by human activities. The development of biopesticides that are degradable in nature could help reduce the amount of chemicals sprays applied to crops. In this study, non-ribosomally synthesized molecules called siderophores were studied in detail. Their function is to form a complex with the iron ions, which is subsequently transported into the cell interior. The consequence of this process is a reduction in the local amount of iron ions in the soil. This deficiency negatively affects the viability of some soil bacteria, often phytopathogenic, and therefore their presence in the biopesticide preparation would be desirable. The aim of this study was to confirm siderophore production in the studied microorganism with its subsequent identification. To complete the knowledge of these metabolites, it was necessary to determine the dependence of siderophore production on cultivation time and medium composition. Siderophore production in microorganism under study was confirmed. It was pyoverdine. The production of pyoverdine was directly proportional to the cultivation time and the medium composition had a significant effect on its production.

Introduction

The ever-increasing growth of the human population brings complications associated with increasing demands on the quantity of produced crops. The quality and quantity of the harvested crop from a given farmed area is highly dependent on the ability of the plants to resist attack by ubiquitous pests. Humans deliberately promote plant defenses by using chemical products, which can have a negative impact on the environment by disrupting the food chains in the habitat¹. In order to replace or reduce the amount of these substances, biopesticides, which include certain microorganisms or a mixture of microbial producers and their biologically active metabolites, have become the center of attention in recent years².

An essential characteristic of the plant pathogen antagonists under study must be that the preparation has zero toxicity to other organisms inhabiting the environment in which it would be applied³. This environmentally friendly product should be designed as a mixture of biologically active molecules which would give it the unique properties and complex effect mentioned above. The active components of the preparation would consist mainly of antibiotics, enzymes, pigments or biosurfactants (the more preparation wettability to hydrophobic surface of the insect or mould the more effective pest inactivation). Glycerol could also be an important component of the biopreparation, serving mainly as a source of carbon and energy during cultivation. This additive would also have a positive effect on the stability of the enzymes and generally on the durability of the biopreparation⁴.

Pigments, specifically siderophores, were studied in detail in this study. These secondary metabolites belong to a heterogeneous group of organic molecules with a size of 500–1500 Da. Their function is to form a complex with iron ions, resulting in a reduction of the local amount of this nutrient in the soil (or medium). This deficiency negatively affects the viability and growth of soil, often phytopathogenic, bacteria⁵. Due to this property, their presence in the preparation would be desirable. The production of these metabolites is dependent on the composition of the surrounding medium. The rate of siderophore production increases with decreasing iron ion concentration⁶.

The success of the deployment of biopesticides will be very important to satisfy the increasing demand for sustenance by an unstoppably growing human population, but not at the cost of increasing environmental contamination.

Materials and methods

Microorganism

Pseudomonas sp. – a gram-negative, non-sporulating, motile bacterium belonging to the group of fluorescent pseudomonads

Bioprocess

Bioprocess had been carried out for 5 days at 22 °C in a 1 l glass bioreactor (Duran®, Germany). Standard BSM and modified BSM were used as culture media in this work. During the bioprocess, glycerol was added to the culture medium as a carbon and energy source. Feeding rate was 2.5 g·l⁻¹ per day. The medium was aerated (air flow rate was set at 1 VVM) and mechanically agitated (150 rpm) by a printed impeller with flat blades (3D printer – Prusa Research, Czech Republic).

Downstream process

First of all, a sample was taken from culture medium and subsequently centrifuged (10 000 rpm, 5 min) and filtered (0.8 µm pore size). The partially treated sample was loaded onto an activated SPE column with specific stationary phase. Sorbed analytes were released with methanol. Next steps were evaporation of methanol and distilled water addition. Finally, the processed sample was subjected to spectrophotometric, fluorometric or HPLC analysis. The whole procedure is shown schematically in Figure 1.

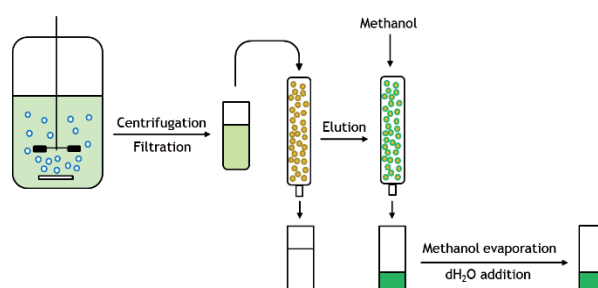


Figure 1. Basic scheme of the downstream process with a description of each important steps

Sorption efficiency of SPE columns

The bacterium under study probably produces several biologically active molecules such as siderophores, antibiotics (2,4-diacetylfluoroglucinol (2,4-DAPG)), rhamnolipids or pyocyanin. This hypothesis is based on knowledge of the genetic material. Two SPE columns (LiChrolut® EN (40–120 µm) 200 mg 3 ml standard glass tube – stationary phase: ethyl vinyl benzene divinyl benzene polymer and Strata® C18-E (55 µm, 70 Å) 200 mg / 6 ml – stationary phase: silica-based end-capped C18) were studied in order to find a more suitable column in terms of sorption efficiency towards the mentioned metabolites represented here by the standards: pyoverdine (Sigma-Aldrich), 2,4-DAPG (Apollo Scientific), pyocyanin (Sigma-Aldrich) and rhamnolipids (Sigma-Aldrich). Two HPLC systems (HPLC with UV detection and two different columns: Watrex Nucleosil 100, C18 and Watrex Polymer IEX H) were used for preliminary testing of the sorption efficiency of SPE columns towards standards presented in the mixed sample. Three fractions were analyzed, specifically the sample before and after passing through the columns and the sample containing desorbed analytes. This step was necessary to select a more suitable HPLC system (chromatographic column) for study of sorption efficiency of the both SPE columns towards individual standard. Samples representing solutions of the standards (except pyoverdine (high molecular weight)) before and after passage through both columns were analyzed by more appropriate HPLC system. Solution with pyoverdine was analyzed spectrophotometrically (microplate reader INFINITE F200 – Tecan, Germany). This experiment was followed by the selection of a more suitable SPE column for subsequent studies (mainly siderophores).

Confirmation of siderophore production in the microorganism under study

Solid CAS agar was used for confirmation of siderophore production. This agar contained a blue pigment called Chrom azurol S. Iron ions are bonded in its structure⁷. A positive response was represented by a colour change from blue to orange. The produced siderophores interacted with iron ions and caused their release from the pigment structure. The consequence of this reaction was the aforementioned colour change. The orange zones in surrounding of colonies are called “Halo zones”, especially in Anglo-Saxon literature⁸.

Identification of an unknown siderophore

The processed sample containing unknown siderophore was analyzed spectrophotometrically and fluorometrically using a microplate reader INFINITE F200. The absorption and emission spectra of the unknown siderophore were compared with spectra of standard (pyoverdine).

Study of the influence of cultivation time on pyoverdine production

Samples were taken the 1st, 4th and 5th day of cultivation. The processed samples were subjected to spectrophotometric analysis and visual analysis. The concentration of pyoverdine was calculated from the relationship between absorbance and concentration of standard (pyoverdine).

Study of the influence of medium composition on pyoverdine production

For this experiment, modified media were used. Specifically, the medium without trace elements and enriched with iron ions, copper ions and a combination of these ions. After a five-day cultivation process, the samples were processed according to the aforementioned downstream procedure. The processed samples were analyzed spectrophotometrically. Alternatively, the pyoverdine content was measured indirectly with CAS solution⁹. The more pyoverdine was present in the sample the more noticeable the colour change was (more iron ions were released from CAS). The data were evaluated according to the following equation: percentage of released iron ions = $[(A_{\text{ref. sample}} - A_{\text{sample}}) / A_{\text{ref. sample}}] \cdot 100$. The reference sample was represented by fresh, original modified BSM with CAS solution¹⁰.

Results and discussion

Sorption efficiency of SPE columns

Preliminary testing of the sorption efficiency of both HPLC systems showed that the HPLC system with UV detection and with the column Watrex Nucleosil 100, C 18 was a better system for the detection of standards (demonstrable interaction between standards and the stationary phase of the HPLC column). Confirmation of this statement is included in Figure 2.

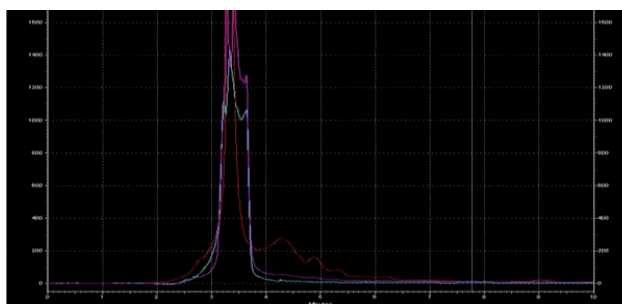


Figure 2. Comparison of chromatograms of three fractions analyzed by HPLC system with UV detection and with the column Watrex Nucleosil 100, C 18: purple one – mixed sample of standards (before loading), green one – sample passed through the column and red one – sample containing desorbed standards (the ability to detect desorbed analytes – a more suitable HPLC system for subsequent analyses)

The sorption efficiency of both SPE columns towards individual standard was determined using only the HPLC system with UV detection and the column Watrex Nucleosil 100, C 18. The resulting graph is included in Figure 3. The LiChrolut® column had a higher sorption efficiency towards pyoverdine and rhamnolipids against the Strata® column. On the other hand, both SPE columns had very similar affinity for 2,4-DAPG and pyocyanin. In view of this result, the LiChrolut® column was used for the samples processing in subsequent studies.

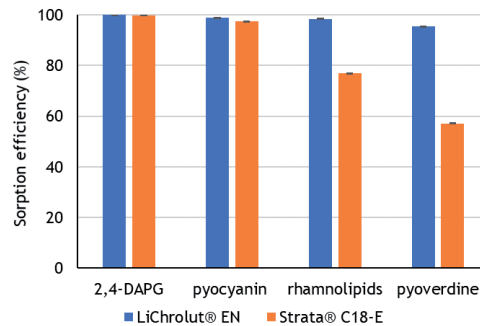


Figure 3. Comparison of sorption efficiencies of LiChrolut® and Strata® columns against individual standards

Confirmation of siderophore production in the microorganism under study

The siderophore production was confirmed in the microorganism under study. This conclusion was based on the observation of orange zones in surrounding of colonies (see Fig. 4).

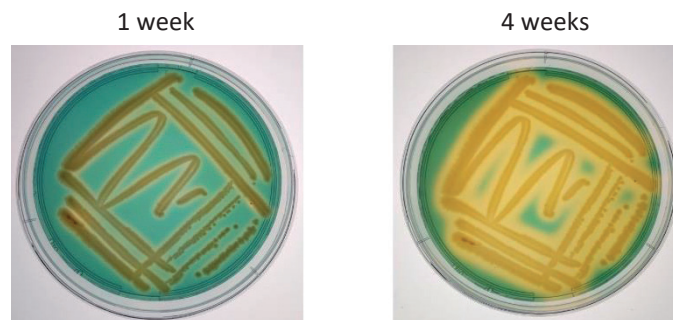


Figure 4. Confirmation of siderophore production using CAS agar based on the observation of orange “Halo zones” in the surrounding of the colonies – time-dependent production of siderophores

Identification of the unknown siderophore

The overlap of absorption and emission spectra allowed the identification of the unknown siderophore. It was pyoverdine. The absorption maximum of identified siderophore (pyoverdine) was measured at $\lambda_{max} = 406$ nm and the maximum intensity of emitted radiation at 460 nm (see Fig. 5).

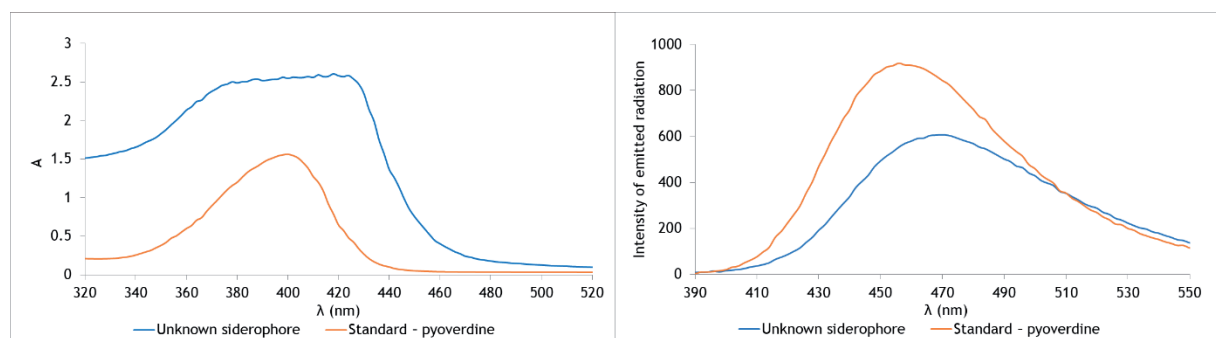


Figure 5. Identification of the unknown siderophore based on the overlap of absorption and emission spectra of the siderophore and the standard

Study of the influence of cultivation time on pyoverdine production

Pyoverdine production was found to be directly proportional to cultivation time (see Fig. 6). This statement resulted from visual analysis of the colour of the processed samples and from the measured absorption spectra of these samples. The concentration of pyoverdine in the processed samples was $0 \text{ mg}\cdot\text{l}^{-1}$ (the 1st day), $138 \text{ mg}\cdot\text{l}^{-1}$ (the 2nd day) and $294 \text{ mg}\cdot\text{l}^{-1}$ (the 3rd day).

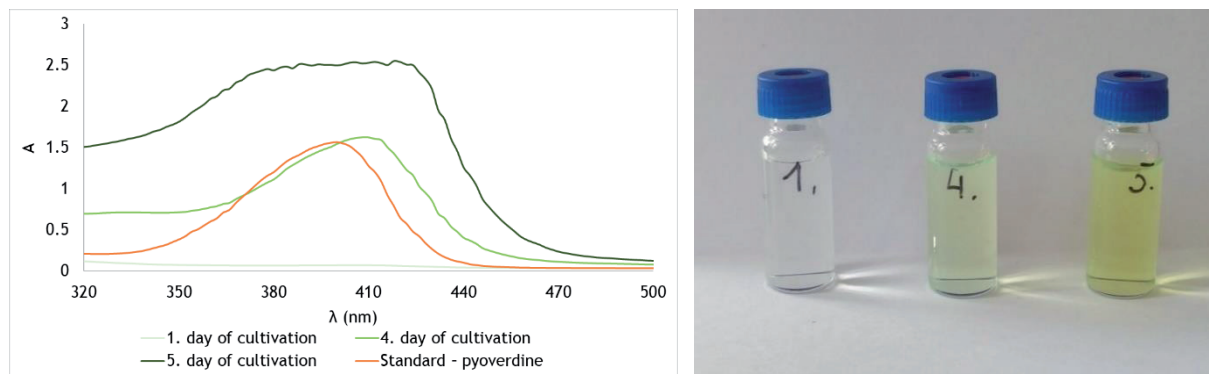


Figure 6. Time-dependent production of pyoverdine

Study of the influence of medium composition on pyoverdine production

The composition of the medium significantly influenced the production of pyoverdine. The absence of trace elements and the presence of copper ions had a positive effect on production. In the medium without trace elements, the value $75 \pm 1 \%$ of released iron ions was measured and in case of the presence of copper ions this value was $63 \pm 3 \%$. The present copper ions induced the pyoverdine synthesis and subsequently formed a complex with it. The absorption maximum of this complex (represented by the red chromatogram) was shifted against the maximum of “free” pyoverdine (the green chromatogram). On the other hand, a negative effect on production was observed in the presence of iron ions. In case of the combination of iron and copper ions was observed negative value of the percentage of released ions (see Fig. 7). This phenomenon could be caused by the simultaneous presence of both ions or by interactions of these ions with pyoverdine or the enzymatic apparatus of the cell.

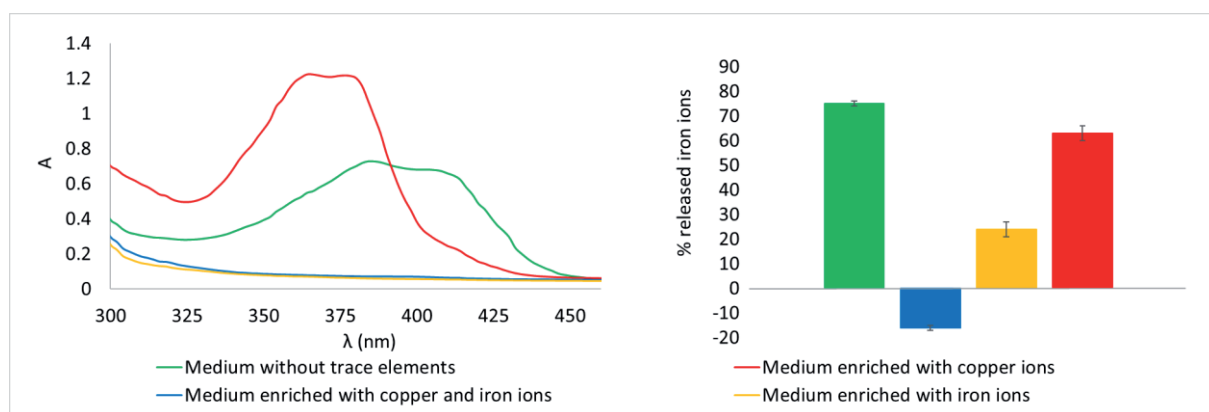


Figure 7. Absorption spectra of samples representing individual modified media (after completion of the cultivation process) and indirect quantification of the amount of pyoverdine (percentage of released iron ions from the structure of Chrom azurol S (CAS))

Conclusion

The studied microorganism produced a siderophore. The identification was performed according to the overlap of absorption and emission spectra of siderophore and standard. It was pyoverdine. The basis of a potential preparation could be a solution containing this producer, siderophores and other biologically active molecules or additives, or the preparation could be consisting only of a cell-free solution of the above-mentioned components. The production of pyoverdine was directly proportional to the cultivation time and the composition of the medium had a significant effect on its production. High productivity was observed in the absence of trace elements and in the presence of copper ions. Conversely, low productivity was observed in the presence of iron ions and in the case of a combination of iron and copper ions. This knowledge will be important for optimization of the cultivation process to maximize siderophore production at the lowest possible financial cost. The LiChrolut® SPE column had a higher sorption efficiency towards pyoverdine and rhamnolipids compared to the Strata® column and therefore it will be part of the downstream process in case of future experiments. The study of the sorption efficiency of the low molecular weight analytes (2,4-DAPG, pyocyanin and rhamnolipids) was performed with a more suitable HPLC system with UV detection (column: Watrex Nucleosil 100, C 18). The health and friendliness to plants and other organisms will need to be verified by phytotoxic and other tests before the preparation can be registered. Once the approval procedure is completed, the product could be officially applied (in terms of organic farming) on economically important crops.

Acknowledgement

This work was financially supported from the Internal Grant Agency of University of Chemistry and Technology – project number: A2_FPBT_2022_040

References

1. Singh G., Bhalla A., Bhatti J., Chandel S., Rajput A., Abdullah A. J.: *Microbiol. Biotechnol.* **3**, 27 (2013).
2. Liu X., Cao A., Yan D., Ouyang C., Wang Q., Li Y.: *Int. J. Pest Manag.* **67**, 65 (2021).
3. Volcão L. M., Halicki P. C. B., Christ-Ribeiro A., Ramos D. F., Badiale-Furlong E., Andreatza R.: *J. Toxicol. Environ. Health, Part A* **85**, 43 (2022).
4. Bradbury S. L., William J. B.: *Proc. Natl. Acad. Sci. U.S.A.* **69**, 2373 (1972).
5. Behnsen J., Raffatellu M.: *MBio.* **7**, 6 (2016).
6. Vindeirinho J. M., Soares H., Soares E. V.: *Appl. Biochem. Biotechnol.* **193**, 607 (2021).
7. Loudon B. C., Haarmann D., Lynne A. M.: *J. Microbiol. Biol. Educ.* **12**, 51 (2011).
8. Sultana S., Alam S., Karim M. M.: *J. Agric. Food Res.* **4**, 1 (2021).
9. Schwyn B., Neilands J. B.: *Anal. Biochem.* **160**, 47 (1987).
10. Chowdappa S., Jagannath S., Konappa N., Udayashankar A. C., Jogaiah S.: *Biomolecules* **10**, 1 (2020).

ANTIMICROBIAL ACTIVITY OF SILVER NANOPARTICLES PREPARED BY GREEN APPROACH

Miškovská A.¹, Čejková A.¹

¹University of Chemistry and Technology Prague, Technická 5, 166 28, Prague 6
anna.miskovska@vscht.cz

Abstract

Silver nanoparticles attract the attention of the scientific and commercial spheres because of their unique chemical, physical, and biological properties, including interesting antimicrobial effects, for which they are well known. In recent years, attention has been focused on nanoparticles prepared using the so-called "green" methods, which use natural materials to synthesize metal nanoparticles, and which work under mild conditions. The silver nanoparticles prepared by green approach are promising for many applications, including medicine. This work deals with the determination of antimicrobial effects of silver nanoparticles prepared using extract from agricultural waste (*Vitis vinifera* canes). The antimicrobial activities of two nanoparticle dispersions that differed in size and polydispersity against the opportunistic pathogenic yeast *Candida albicans* and the bacterium *Pseudomonas aeruginosa* were determined. The activity of the nanoparticles was monitored in the concentration range of 2.5–40.0 mg/L and their antimicrobial effects were confirmed against the planktonic cells of both tested microorganisms. While *P. aeruginosa* growth was more inhibited by smaller nanoparticles (MIC 10 mg/L), *C. albicans* growth was more inhibited by larger nanoparticles (MIC 20 mg/L).

Introduction

Green nanotechnology has provided many interesting opportunities, including the possibility of recycling waste products¹⁻³. Due to the ease of the use of waste parts of plants (such as leaves, canes, or peels) or plant extracts for the reduction of metal salts to nanoparticles, the application of these materials has attracted considerable attention in the last 30 years⁴. These products are generally very rich in useful phytochemicals, which can be used to synthesize and stabilize metal nanoparticles. The ability of plant extracts to reduce metal ions was known as early as the 19th century, although the nature of the reducing agents was not well studied. Nanoparticles of noble metals such as silver or platinum, were found to have antimicrobial activity⁵. The microbicidal effect of metal nanoparticles has been assigned to their small size and high specific surface, allowing them to interact with microbial membranes⁶. Multiple mechanisms of the AgNPs action have been proposed and their overall effect is most probably their combination. These are: release of Ag⁺ ions and their interaction with thiol groups, interaction of Ag⁰ with thiol groups and phosphorous groups, interaction of Ag₂O with biomolecules, generation of reactive oxygen species (ROS), and/or mechanical damage of cell membranes⁷. The antimicrobial properties of silver nanoparticles (AgNPs) find applications in various fields such as medical instruments, imaging systems, drug-delivery systems, water treatment, food processing or textile industry⁸.

The attractiveness of biosynthesized NPs lies in functionalization, capping, and stabilization through biological molecules (e.g., ascorbic acids, flavonoids, polyphenols, proteins, and terpenoids), which themselves may have antibacterial capabilities and therefore could enhance the antimicrobial properties of nanoparticles or allow the AgNPs to bind to the target cell surface⁸. In this work, the antimicrobial activity of silver nanoparticles synthesized using *Vitis vinifera* (grape vine) cane extract was studied. The beneficial effects and nutritional properties of *V. vinifera* have been known for thousands of years. All parts of this plant are rich in phenolic substances, which have antioxidant and antimicrobial effects⁹. As a result, we hypothesize that using *V. vinifera* extract for the biosynthesis of AgNPs could produce AgNPs with enhanced antimicrobial activity. In the present study, the antimicrobial activity was studied against two opportunistic pathogenic microorganisms, the bacteria *Pseudomonas aeruginosa* and the yeast *Candida albicans*. *P. aeruginosa* is a rod-shaped bacterium highly adaptive to various growth conditions that causes various human infections due to the numerous virulence factors it could produce¹⁰. These characteristics together with high antibiotic resistance make *P. aeruginosa* extremely difficult to combat. *C. albicans* is the most common pathogenic fungus isolated from bloodstream infections in hospitalized patients¹¹. The development of new strategies to combat these two human opportunistic pathogens is therefore a very current topic.

Experiment

Microorganisms, growth media and antimicrobials

Model strains *Pseudomonas aeruginosa* ATCC 1544 and clinical isolate strain *Candida albicans* ATCC 10231 originated from the American Type Culture Collection (ATCC) were used. The inoculum was pre-cultured before each experiment by adding the cryopreserved microorganism (stored at -70 °C) to a fresh growth medium – Lysogeny broth (LB) medium for the bacterium and yeast extract peptone dextrose broth medium (YPD) for the yeast and incubating for 24 h, at 37 °C, 150 rpm in an orbital shaker. The antimicrobial experiments were carried out in LB medium for *Pseudomonas* and Roswell Park Memorial Institute 1640 medium (RPMI-1640) with L-glutamine, without sodium bicarbonate for *C. albicans*.

Two green synthesized AgNPs dispersions were tested – monodisperse AgNPs (average diameter 12 ± 5 nm) and polydisperse AgNPs (average diameter 19 ± 14 nm). The AgNPs were collected from original reaction solution by centrifugation ($50\,000 \times g$, 30 min, 25 °C) and were resuspended in ultrapure water. The activity was tested in concentration range 2.5–40.0 mg/L.

Antimicrobial activity of AgNPs

The activity of AgNPs was tested against planktonic cells by the microdilution method. The cultivation of microorganisms was carried out in microtiter plates using BioscreenC analyser. Silver nanoparticles were added in concentration range 2.5–40.0 mg/L by dilution in phosphate buffered saline solution (PBS, pH = 7.4). After the antimicrobials, an aliquot of 162 μ l of fresh growth medium was added into each well. Each well was then filled up to a final volume by addition of 30 μ l of standard microbial inoculum with optical density $OD_{600\text{ nm}} = 0.100 \pm 0.010$. AgNPs-free control was filled with 130 μ l of PBS, 162 μ l of fresh growth medium and 30 μ l of standard inoculum. Each experiment was performed in 10 parallels.

Results and discussion

Antibacterial activity of AgNPs

Silver nanoparticles exhibit promising antibacterial effects against many clinically significant pathogenic bacteria (eg *Escherichia coli*, *Pseudomonas aeruginosa*, or *Staphylococcus aureus*), which makes them promising in several fields⁸. In the present study, the antibacterial activity of two AgNPs dispersions was tested against *P. aeruginosa* ATCC 15442 in concentration range 2.5–40.0 mg/L (Fig. 1). Complete inhibition of planktonic cell growth (MIC) of *P. aeruginosa* was achieved using 10 mg/L of smaller AgNPs (12 ± 5 nm). Larger polydisperse AgNPs (19 ± 14 nm) were found to be less effective and bacterial growth was inhibited using a four-fold higher concentration 40 mg/L. Our findings are consistent with scientific literature, when smaller AgNPs with larger surface to volume ratio usually exhibit stronger inhibition properties^{8,12}. However, even the lowest concentration tested of both AgNPs dispersions (2.5 mg/L) affected the growth dynamics of *P. aeruginosa* and caused a prolongation of the lag phase. This phenomenon was also reported in bacteria when using low concentrations of other antimicrobials (eg, antibiotics, metal nanoparticles)¹³. Similar observations, as in our study, were found by Otari et al. who tested the activity of biogenic AgNPs (5–50 nm) against *P. aeruginosa*. Similarly to our findings, the lowest concentration of AgNPs (10 mg/L) used extended the lag phase of bacteria from 5 to 10 hours, and while using 50 mg/L of AgNPs the growth of suspension cells was completely inhibited¹⁴.

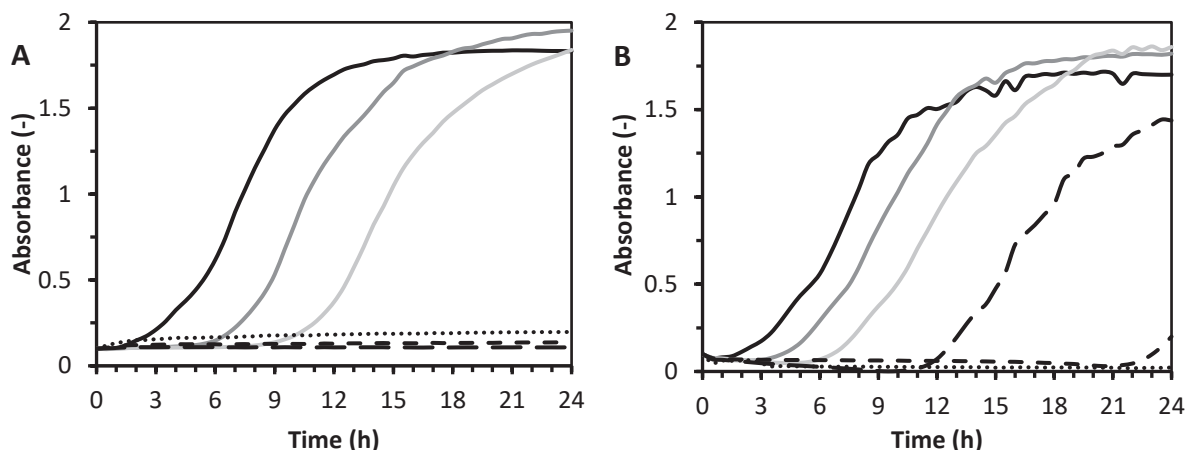


Figure 1. The antibacterial activity of biogenic AgNPs against suspension cells of *P. aeruginosa* ATCC 15442. **A** – monodisperse AgNPs, **B** – polydisperse AgNPs.

— control — 2.5 mg/l — 5 mg/l - - 10 mg/l - - - 20 mg/l 40 mg/l

Antifungal activity of AgNPs

Antifungal activity of biogenic silver nanoparticles against *C. albicans* ATCC 10231 was determined by microdilution method (Fig. 2). Smaller AgNPs showed to be effective against the yeast in concentration 20 mg/L and higher. Our results showed that larger AgNPs were more effective against the microorganism, and even 10 mg/L of AgNPs almost completely suppressed the growth of the yeast. Our observations indicate that the size of the AgNPs is not the only factor that influence the degree of the resulting antimicrobial effect. The difference in activity may be due to a fundamental difference between the structure of prokaryotic and eukaryotic cells and thus the different range of possible mechanisms of AgNPs action.

Similar results were obtained in the study investigating the antifungal activity of biogenic silver nanoparticles prepared by the green method using a cell-free extract of *Streptomyces xinghaiensis* culture, where the MIC 32 mg/L against *C. albicans* ATCC 10231 was found¹⁵. Nanoparticles used in the mentioned study were polydisperse (5–20 nm) and, like our AgNPs, had a predominantly spherical shape. Possible explanations for the higher activity of the nanoparticles used in our study include a possible synergy in the action of silver itself, and the phytochemicals derived from *V. vinifera* that surround the surface of the nanoparticles.

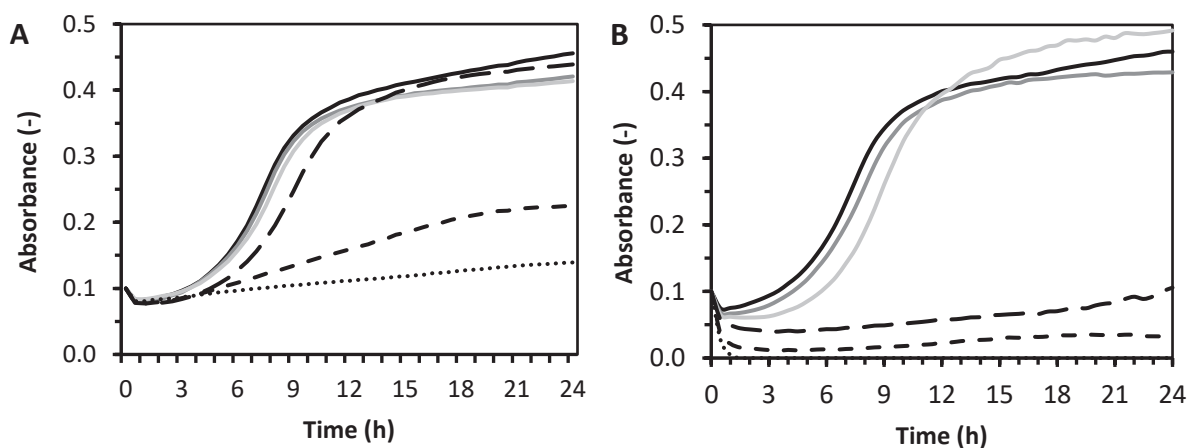


Figure 2. The antifungal activity of biogenic AgNPs against suspension cells of *C. albicans* ATCC 10231.

A – monodisperse AgNPs, **B** – polydisperse AgNPs

— control — 2.5 mg/l — 5 mg/l - - 10 mg/l - - - 20 mg/l 40 mg/l

Conclusion

The present study deals with the antimicrobial activity of silver nanoparticles prepared by green approach by using an extract of agricultural waste. Silver nanoparticles of varying size and polydispersity were tested against opportunistic pathogenic gram-negative bacteria *P. aeruginosa* and yeast *C. albicans*. The activity of AgNPs on

microbial growth was tested by microdilution method. Our results showed that both nanoparticle dispersions have inhibitory effects on both microorganisms. Although *Pseudomonas* was inhibited more by smaller nanoparticles (12 ± 5 nm), better inhibition of the yeast was observed by polydisperse nanoparticles (19 ± 14 nm). The difference in activity may be due to a fundamental difference between the structure of prokaryotic and eukaryotic cells and thus the different range of possible mechanisms of AgNPs action.

Acknowledgement

This work was supported from the grant of Specific university research – grant No. A2_FPBT_2022_018 (UCT Prague).

References

1. Gupta V., Chandra N.: Proc Natl Acad Sci India Sect B Biol Sci, *90*, 1093 (2020).
2. Zamani A., Marjani A. P., Mousavi Z.: Green Process. Synth., *8*, 421 (2019).
3. Sinsinwar S., Sarkar M. K., Suriya K. R., Nithyanand P., Vadivel V.: Microb. Pathog., *124*, 30 (2018).
4. Mittal A. K., Chisti Y., Banerjee U. C.: Biotechnol. Adv., *31*, 346 (2013).
5. Cho K.-H., Park J.-E., Osaka T., Park S.-G.: Electrochim. Acta, *51*, 956 (2005).
6. Ramyadevi J., Jeyasubramanian K., Marikani A., Rajakumar G., Rahuman A. A.: Mater. Lett., *71*, 114 (2012).
7. Rai M., Yadav A., Gade A.: Biotechnol. Adv., *27*, 76 (2009).
8. Maťátková O., Michailidu J., Miškovská A., Kolouchová I., Masák J., Čejková A.: Biotechnol. Adv. 107905 (2022), *in press*.
9. Asaduzzaman A., Chun B.-S., Kabir S. R.: J. Nanopart., *2016*, 49 (2016).
10. Wu W., Jin Y., Bai F., Jin S., v knize: *Molecular medical microbiology*, str. 753. Elsevier, 2015.
11. Lara H. H., Romero-Urbina D. G., Pierce C., Lopez-Ribot J. L., Arellano-Jiménez M. J., Jose-Yacamán M.: J. Nanobiotechnol., *13*, 1 (2015).
12. Szerencsés B., Igaz N., Tóbiás Á., Prucsi Z., Rónavári A., Bélteky P., Madarász D., Papp C., Makra I., Vágvölgyi C.: BMC microbiol., *20*, 1 (2020).
13. Theophel K., Schacht V. J., Schlüter M., Schnell S., Stingu C.-S., Schaumann R., Bunge M.: Front. Microbiol., *5*, 544 (2014).
14. Otari S., Patil R., Ghosh S., Thorat N., Pawar S.: Spectrochim. Acta, Part A, *136*, 1175 (2015).
15. Wypij M., Czarnecka J., Świecimska M., Dahm H., Rai M., Golinska P.: World J. Microbiol. Biotechnol., *34*, 1 (2018).

CHEMICAL PROCESSES AND DEVICES

THE VERIFICATION OF MATERIAL FLOW IN A BREWERY MALT TANK USING THE DEM METHOD

Likavčan A.¹, Peciar M.¹, Peciar, P.¹

¹*Slovak University of Technology in Bratislava, Faculty of Mechanical Engineering, Institute of Process Engineering, Námetie Slobody 17, 812 31 Bratislava 1, Slovakia*
e-mail: peter.peciar@stuba.sk

Abstract

Biotechnology is one of the fastest growing areas of research. In addition to the biotechnological process itself, it is also necessary to deal with the construction and design of devices. This paper deals with the design of a brewery malt tank with a closing element for a specific application in automated brewing equipment. An important part of the tank design, before its actual production, is the simulation of the emptying process in the EDEM Academic programme. For such a particular system the DEM method comes to the fore, where it is necessary to know the properties of the barley malt and mutual interactions during the simulation process.

Keywords: bulk solid, storage, brewery malt, tank design, DEM simulation

Introduction

Part of every technology that processes bulk materials is also their storage in tanks and their subsequent dosing. Bulk solids may change their properties over a long period of storage, which may be undesirable not only for the emptying and dosing process itself, but also in the subsequent process. Therefore, it is necessary to examine experimentally these properties and to design correctly the tank based on experimental measurements. This paper will deal with the design of a specific brewery malt tank of 25 litres capacity with a closing element. The tank will be used for dosing brewery malt in an automated mini brewery designed at the Institute of Process Engineering of the Faculty of Mechanical Engineering STU in Bratislava.

Theory of storage tanks

Particulate material is stored in tanks and their aim is short-term or long-term storage of material, or the creation of operational stocks, which are continuously taken into the production process. Bulk material tanks are divided according to the ratio of height to their width in bunkers and silos. Silos have height to width ratio greater than 2 (rather slim and tall thin-walled containers). They are used for long-term storage of large amount of loose non-stick material. They usually have conical bottoms with a certain type of feeder (e.g., turnstile, screw, etc.). Bunkers are defined as tanks with a height to width ratio of less than 2 (relatively wide and low containers) which are suitable for short-term storage of smaller quantities of material. They can have a wedge, rectangular or cylindrical shape. They are filled from above and emptied by a conical outlet located at the bottom of the container¹.

Emptying of storage tanks

From the point of view of the tank design, it is important to know the character of the material flow when emptying it. Material flow is affected not only by the geometry and material of the tank, but also by the mechanical-physical and flow properties of the stored particulate material, such as particle size and shape, bulk density, moisture, angle of repose, internal and external friction of the material. While emptying the tank by the influence of gravity, the material performs two types of main motion - material mass flow or material core flow. In addition to the main motion, there is also a secondary motion in the material, in which the particles rotate¹.

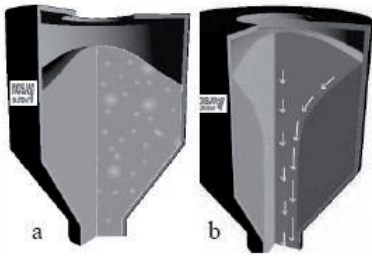


Figure 1. Types of main motion of a bulk material in a tank¹: a) mass flow, b) core flow.

Problems of storage tanks emptying

Different types of defects often occur during the discharge of material from a hopper. The area where the material does not flow but is retained at the walls of the tank is called a dead zone (Fig. 2a). The process, when the material is emptied only from the centre of the tank, is called ratholing (Fig. 2b). If the material flows out only from the lower part of the tank and the upper part is not emptied, a bridge is formed (Fig. 2c). In the extreme case an arch can appear which means that only a fractional amount of material flows out of the tank (Fig. 2d). In the event of material flow disturbances, emptying is abrupt or stops completely¹.

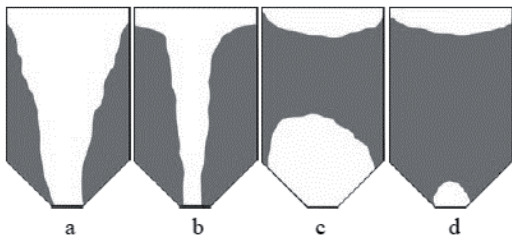


Figure 2. Flow problems¹: a) a dead zone forming, b) ratholing, c) bridging, d) arching.

Acquisition of mechanical-physical and flow properties of the experimental material

Ground brewing malt was used as experimental material during the measurements. Brewing malt is a sprouted and dried grain, which is one of the basic raw materials for beer production. In this case, it is a barley grain. The process of grinding brewing malt is a separate area and this process itself affects the entire process of brewing beer. Brewing malt was ground in the company SVOJEPIVO.SK with defined parameters for use in our brewing malt tank. A sample of ground brewing malt is shown in Figure 3.



Figure 3. A sample of ground brewing malt¹.

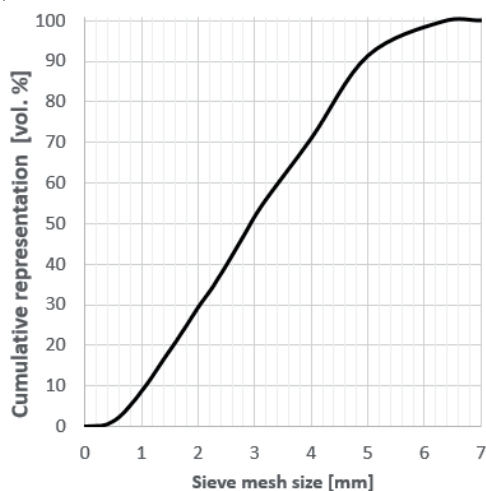
Analysis of experimental material properties

The basic measured properties of the experimental material were particle size analysis performed on the Microtrac PartAn 3D, unshaken and shaken bulk density of the material performed on the Sotax TD1. The results of individual measurements are shown in Table I and in Figure 4^{2,3,4,5}.

Table I

Results of experimental bulk density measurement on a Sotax TD1 device¹

GROUND BREWING MALT	
Initial weight [g]	108,2
Initial volume [ml]	230
1. number of vibrations/volume [-]/[ml]	10/218
2. number of vibrations/volume [-]/[ml]	490/200
3. number of vibrations/volume [-]/[ml]	750/197
Unshaken vol. weight [g/ml]	0,470
Shaken vol. weight [g/ml]	0,555
Compressibility factor [-]	15,22
Hausner ratio [-]	1,179

Figure 4. Results of experimental measurement of fraction composition on Microtrac PartAn 3D¹.

Storage tank design

It is important to correctly determine the angle of inclination of the hopper as well as the size of the outlet for tanks in which volumetric flow occurs. The design of the main dimensions of the tank and subsequently its mechanical design are derived from these parameters.

Design of the outlet and inclination of the hopper

A calculation method from Freeman Technology was used to determine the size of the outlet B of the hopper B and the angle of inclination of the hopper α . This method calculates the parameters B and α after entering the measured material properties, such as bulk density, internal and wall friction angle and flow function parameter. Freeman Technology is based on the Jenike's calculation method for volumetric flow. Its aim is to eliminate the stress $\bar{\sigma}_1$ creating an arch in the hopper^{6,7}.

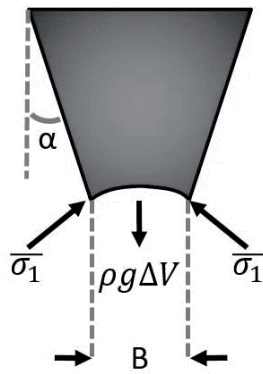


Figure 5. Stress $\bar{\sigma}_1$ forming an arch in the hopper⁷.

Design of the main dimensions of the tank

Since the tank and the dispenser will be connected to a container with a pre-existing malt inlet, it is necessary to adapt to this factual situation when designing this tank. The container has a neck at the top, which can be connected using a flange with a diameter of DN 50. The inner diameter of the flange is 0.05 m, which is also selected as the diameter of the outlet B. The maximum angle of inclination of the hopper wall α was calculated to 41° , but this value applies to the case of symmetrical placement of the hopper opening.

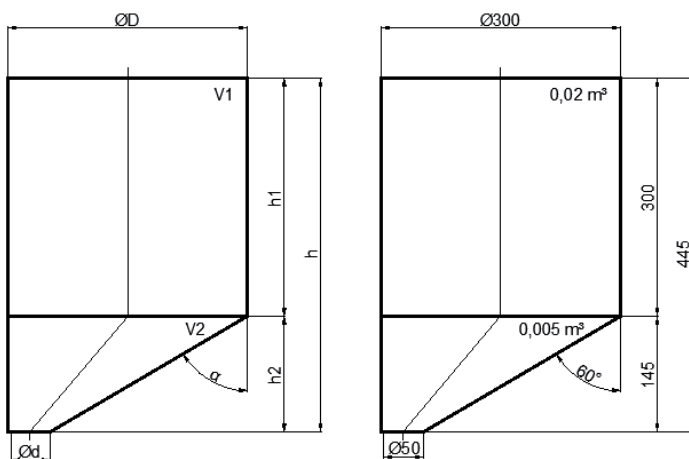


Figure 6. Tank diagram with designed dimensions.

In this case, it is necessary to state that the outlet cannot be designed in the axis of the tank and thus the angle of inclination of the hopper will not be constant. It will range from 0° to 60° , as the outlet is located asymmetrically on one side, as shown in Figure 6. Since the maximum slope of the hopper wall was calculated to 41° , it is necessary to check the given condition whether an arch or other defects during emptying would be formed. For this reason, the DEM simulation using the EDEM software was used. One of the design options to prevent the formation of an arch is also the design of an asymmetrical outlet. If the arch occurs in the simulations, it is possible to use other elements against the arching on the designed tank.

Particle flow simulation in EDEM programme

DEM method

DEM stands for Discrete Element Method. It is a numerical method used to calculate the motion and stress of large amounts of solid particles in a volume. It allows to work with the degrees of freedom of elements and to create interactions between them, even though the geometries of systems are often complicated. The basic structural element is a spherical particle and all other shapes (shapes of real particles) are laid out from such particles⁸.

Input data in the EDEM Academic programme

Initially, it was necessary to obtain all the material data needed to describe the particles, resp. particle material, as well as a description of the construction material and their mutual interactions. The mechanical-physical and flow properties from the experimental measurements used for the simulation are listed in Table I, while other data necessary for the simulation are obtained from the literature⁸.

Simulation in the EDEM Academic programme

The simulation of the whole process took place in several steps. The first step was to form barley malt particles in the upper part of the tank with a total weight of 10 kg, which was then deposited under the influence of gravity. After the material batch was formed, the slide gate valve on the outlet was opened and the material was allowed to fall from the hopper by gravity. For the analysis of the material flow in the tank, the experimental material was divided into 7 parts by height and the displacement of the individual layers was recorded at the given time points. This process is illustrated in Figure 7.

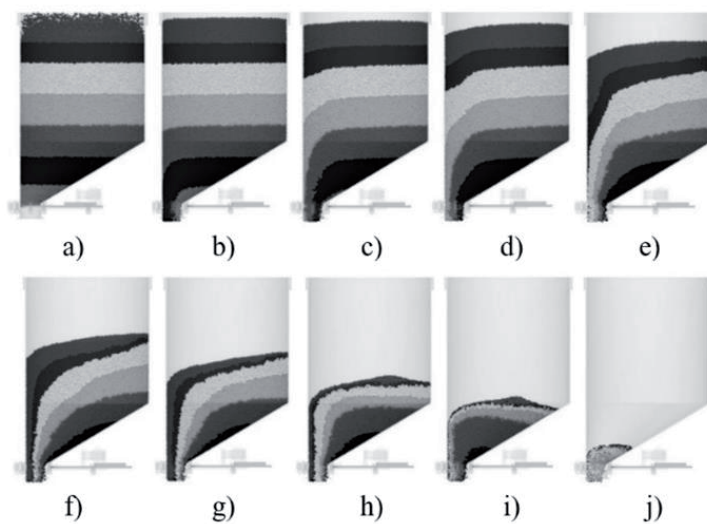


Figure 7. Material flow in the hopper at the given time point.
a) 3 s; b) 3,5 s; c) 5 s; d) 6 s; e) 10 s; f) 14 s; g) 20 s; h) 24 s; i) 28 s; j) 32 s

At the 15th second a cross-section of the hopper was made with creating of the velocity fields (Fig. 8). The aim of this illustration is to observe the movement of the particles during emptying.



Figure 8. Velocity fields in the hopper in the 15th second.

Conclusion

The aim of this article was to mechanically design a brewery malt tank with a closing element and to analyse the emptying process using the DEM method. Since the tank is to be mounted on a pre-existing container, it was necessary to adapt to this fact and build on it.

Since the mechanical-physical and flow properties of ground barley malt were obtained by experimental measurements, it was possible to determine the optimal shape and dimensions of the tank according to the assignment. As already mentioned, the layout of the mini brewery did not allow the creation of a tank with a symmetrical outlet, so it was necessary to come up with a different design solution. Assuming an asymmetrical outlet with a closing element, the slope of the tank wall was set to 60° in the maximum case, while the calculations determined the optimal slope as 41°. The use of such a slope had to be verified subsequently, for which the simulation in the EDEM Academic programme, using the DEM method, was used. The simulations proved that even though the material from the tank did not discharge evenly in the whole volume (on one side of the outlet the flow was affected by the 60° slope of the tank wall), no arch was formed and the whole amount of this material was easily discharged.

The simulation of the tank emptying process is only one way to verify the correct design of the tank. Therefore, it is necessary to perform the verification for the given barley malt samples on the pre-existing device. If the tank was not emptied optimally, elements preventing the formation of an arch would be applied.

Acknowledgement

The authors wish to acknowledge the Ministry of Education, Science, Research and Sport of the Slovak Republic for the financial support of this research by grants KEGA 016STU-4/2019, KEGA 036STU-4/2020 and the Nadácia Tatra banky by grant E-Talent 2019 (2019et011 – Smart Brewery).

References

1. Likavčan A.: Design of brewery malt tank with feeder, diploma thesis, STU (2021).
2. Peciar P., Juriga M., Gušťačík A., Kohútová M., Jezsó K.: Procesné strojnictvo: Príklady. Bratislava: Spektrum STU (2021). ISBN 978-80-227-5081-3. (In Slovak)
3. Macho O., Čierny M., Gabrišová Ľ., Juriga M., Ružinský R., Peciar P.: Dynamic Image Analysis to Determine Granule Size and Shape, for Selected High Shear Granulation Process Parameters. *Strojnícky časopis = Journal of Mechanical Engineering*. 69, 4 (2019). ISSN 0039-2472.
4. Fekete R., Peciar P., Kohútová M., Jirout T., Krátky L., Peciar M.: Flow Properties of Bulk Material as a Product of the Beech Chips Grinding. *Chemical Engineering Transactions*. 86 (2021). ISSN 2283-9216.
5. Peciar P., Jezsó K., Kohútová M., Gušťačík A., Krátky L., Fekete R., Jirout T., Peciar M.: Particle Size Distribution Analysis of Beech Chips Depending on the Measurement Method. *Chemical Engineering Transactions*. 92 (2022). ISSN 2283-9216.
6. Peciar P., Eckert M., Fekete R., Hrnčiar V.: Analysis of pharmaceutical excipient MCC Avicel PH102 using compaction equations. *Strojnícky časopis = Journal of Mechanical Engineering*. 66, 1 (2016). ISSN 0039-2472.
7. www.freemantech.co.uk/news/modern-tools-for-hopper-design
8. Peciar P., Macho O., Fekete R., Peciar M.: The Use of DEM Simulation for Confirming the Process of Particulate Material Mixing. *Acta Polytechnica*. 58, 6 (2018). ISSN 1805–2363.

INORGANIC TECHNOLOGY

DIFFERENCES IN COMPOSITION OF NAPLES YELLOW AND SYNTHESIS OF ITS MAIN PHASES

Dohnalová Ž.¹, Luxová J.¹, Šulcová P.¹, Šefců R.², Antušková V.²

¹University of Pardubice, Studentská 95, 532 10 Pardubice, Czech Republic

²National Gallery Prague, Staroměstské náměstí 12, 110 15 Prague 1, Czech Republic
Zaneta.dohnalova@upce.cz

Abstract

The main objective of the submitted work is to study the effect of reaction conditions on phase composition and colour parameters of $\text{Pb}_2\text{Sb}_2\text{O}_7$ and PbSb_2O_6 . These substances are the most often identified in composition of a historical pigment known as Naples yellow. The conditions of the calcination process as well as a molar Pb:Sb ratio were found to significantly influence the quality of multiphase $\text{Pb}_2\text{Sb}_2\text{O}_7$ product. Colour parameters of the products were compared with three commercial samples of the Naples yellow. The white powder of PbSb_2O_6 was synthesised in high purity in an opened tube furnace by calcination in two steps. The recommended calcining temperature of the first step is 600 °C with duration time of 12 hours and the temperature of the second step should be 850 °C for 72 hours.

Introduction

Naples yellow, is one of the oldest known synthetic pigments, which the small-scale production has been mentioned 3 500 years ago. In this time, it was widely used especially in Egypt, Mesopotamia and Babylon and mainly served as a colouring agent for colouring of glass and glaze. In the Middle Ages, it began to appear in a variety of European enamel pigments and from the end of the 14th century it became the main yellow pigment for colouring of ceramics and majolica. Its use in painting was discovered as early as the end of the 15th century, however, the presence of the Naples yellow in the painter colours is more frequented for the 17th century¹⁻⁴.

The Naples yellow with theoretical chemical formula $\text{Pb}_2\text{Sb}_2\text{O}_7$ belongs to the group of pyrochlore compounds. It is an isostructural anhydrous analogue to the natural mineral bindheimite $\text{Pb}_2\text{Sb}_2\text{O}_6(\text{O},\text{OH})$, which crystallizes in the cubic system. However, it is not clear whether this natural mineral has been used as a colouring agent in the past. In the description of the Naples yellow also other compositions with different Pb:Sb ratio including $\text{Pb}_3(\text{SbO}_4)_2$, $\text{Pb}(\text{SbO}_3)_2$, $\text{Pb}_8(\text{SbO}_4)_2$, PbSb_2O_4 , $\text{Pb}_2\text{Sb}_2\text{O}_6$ and other unidentified components have been given as well^{5,6}.

Many works studying the preparation of $\text{Pb}_2\text{Sb}_2\text{O}_7$ can be found in the current literature. These works can be divided into works that relating to the old-new synthesis of yellows according to the preserved recipes of individual workshops and modern synthesis, where preparation conditions of lead-yellows are studied. The work of the author Dik et al. can be included in the first group of old-new preparations³. They were engaged in the reconstruction of the preparation of the Naples yellow according to Marian's and Darduin's manuscripts (both 17th century). Although both ancient manuscripts contain "instructions" for the preparation of the Naples yellow, old producers did not specify exactly some of raw materials, firing temperatures or firing times. Therefore, the authors of this work dealt with the identification of suitable initial materials and subsequently the preparation conditions. As starting materials were used PbO, Sb_2O_3 , Sb_2S_3 , Sb; mineralizers NaCl and potassium tartrate. They also studied different weight ratios of raw materials. The starting materials were calcined in the temperature range 650–1100 °C for 24 h. The calcination was performed in high temperature unglazed crucibles. The result of the work is their specific recommendation, when they obtained the highest purity product of $\text{Pb}_2\text{Sb}_2\text{O}_7$ (>95 %), i.e., for synthesis to use PbO, Sb_2O_3 and NaCl as mineralizer in a weight ratio of 5: 3: 1; calcination temperature 750–1000 °C/24 h. The XRD records of the samples are not presented. Higher temperatures, up to 1100 °C, led to yellow colour of the pigments, while at lower temperatures the pigments had a more reddish tone. The research does not include spectrophotometric measurement of the pigment reflectivity. Pigment colour was only assessed based on a subjective colour rating.

Into the second group of "modern" works can include the works of the main authors Rosi and Hradil et al^{1,2,4}. In their work⁴, the Naples yellow was prepared from Pb_3O_4 , Sb_2O_3 or Sb_2S_3 in a Pb: Sb weight ratio of 1:1. NaCl and K_2CO_3 (10–20 wt. %) were used as flux agents. The calcination process was performed at temperatures of 700–1000 °C for 4-10 h. Since the authors evaluate the products primarily in comparison to another type of the Naples yellow, containing Pb-Sb-Sn, the work does not include the effect of the calcination mode on the phase composition and colour parameters of the products. In their next collective work¹, they continued in further research, where they synthesized $\text{Pb}_2\text{Sb}_2\text{O}_7$ under the previous best synthesis conditions (materials Pb_3O_4 , Sb_2O_3 ,

mineralizer NaCl 10 wt.%, $T = 900\text{ }^{\circ}\text{C}$) and investigated the effect of changing the molar ratio Pb:Sb (from 0.8:1 to 1.2:1) on the Naples yellow structure. The formation of major pyrochlore structures was detected, whose lattice parameters increase with the increasing Pb:Sb ratio. This ratio also modifies the Raman spectrum in its low-wavelength part. The next step in the research of the Naples yellow was the investigation of compounds which were prepared by repeated calcination². The first one was prepared from Pb_3O_4 and Sb_2O_3 (molar ratio Pb:Sb 1:1) and K_2CO_3 as mineralizer (10 wt.%) and the calcination process was carried out at $900\text{ }^{\circ}\text{C}/12\text{ h}$ and $900\text{ }^{\circ}\text{C}/12\text{ h}$ (double heating). The XRD measurement indicated the presence of $\text{Pb}_{3+x}\text{Sb}_2\text{O}_{8+x}$ as the major phase in the orange sample. The second sample was synthesized from Pb_3O_4 and Sb_2O_3 (molar ratio Pb:Sb 3:2) without the mineralizer. The calcination was performed at $800\text{ }^{\circ}\text{C}/12\text{ h}$ and $800\text{ }^{\circ}\text{C}/12\text{ h}$ (double heating). The XRD pattern of this sample also indicates the presence of the $\text{Pb}_{3+x}\text{Sb}_2\text{O}_{8+x}$ phase, but most of the diffraction lines were not identified. Colour of the samples was orange brown. Authors also prepared rosielite PbSb_2O_6 , by firing a homogenized mixture containing Pb_3O_4 and Sb_2O_3 in the Pb:Sb molar ratio of 1:2, to which no flux was added. The mixture was fired twice at $900\text{ }^{\circ}\text{C}$ for 10 h. The presence of bindheimite as an impurity next to the main rosielite phase was detected in the yellow final product.

Other work dealing with the search for conditions of the synthesis of the Naples yellow is a work from the collective Pelosi, Agresti et al. In their first work⁷, $\text{Pb}_2\text{Sb}_2\text{O}_7$ was synthesized from Pb_3O_4 and Sb_2O_3 in a Pb:Sb ratio of 1:1 and at temperatures of 900 and 950 $^{\circ}\text{C}$ with maintained time of 5 hours at maximum temperature. The authors of this work studied an effect of used ceramic crucibles (terracotta and porcelain) and an effect of cooling after calcination. Colour of the samples varies between yellow to brown. An analysis of the phase composition revealed a formation of multiphase products composed from $\text{Pb}_2\text{Sb}_2\text{O}_7$ as the main phase, but also other types of lead antimonate with different stoichiometry were detected, $\text{Pb}_{2.5}\text{Sb}_{1.5}\text{O}_{6.75}$, $\text{Pb}_{3+x}\text{Sb}_2\text{O}_{8+x}$ and PbSb_2O_6 . Next research of the Naples yellow uses various combinations of PbO and Pb_3O_4 with Sb_2O_3 and mineralizers NaCl and potassium tartrate⁸. In the terms of calcination conditions, it was a repeated firing - two-stage. Both firings were performed at temperature of 800 $^{\circ}\text{C}$ for 5 hours. Colour of the pigments was pale yellow, and their colour parameters varied in values $L^* = 61.1\text{--}71.1$; $a^* = 11.1\text{--}19.6$ and $b^* = 43.9\text{--}52.2$. Raman spectra were quite difficult to interpret, but the authors identified some common bands that can be attributed to the compound $\text{Pb}_2\text{Sb}_2\text{O}_7$ and to the rosielite.

None of the above publications contains clear information concerning the links between the conditions of the Naples yellow synthesis, the phase composition obtained and the colour parameters. Knowledge of these parameters can help to identification of historic pigments used in arts. Therefore, the main objective of the submitted work is to study the effect of reaction conditions on phase composition and colour parameters of $\text{Pb}_2\text{Sb}_2\text{O}_7$ and PbSb_2O_6 . The quality of the synthesized pigments is compared with the commercial pigments of the Naples yellow.

Experiment

Both pigments, $\text{Pb}_2\text{Sb}_2\text{O}_7$ and PbSb_2O_6 , were prepared by solid state reaction at high temperature. The samples of $\text{Pb}_2\text{Sb}_2\text{O}_7$ were prepared by calcination of a homogenised mixture of PbO and Sb_2O_3 in a different molar ratio of Pb:Sb (2:2; 1.9:2; 1.8:2) and NaCl mineralizer in amount of 10 % wt (all Lachema n.p., CZE). The reaction mixtures were calcined in a muffle furnace in two steps and in three calcination modes, in total 9 samples were prepared. The first step represents temperature of 800, 850 or 900 $^{\circ}\text{C}$ for 10 hours with rate $5\text{ }^{\circ}\text{C}\cdot\text{min}^{-1}$. After the first step, the mineralizer NaCl was removed from the samples by decantation in hot water and the dry samples were calcined in the second step under the same conditions as the first step. Three commercial Naples yellow pigments (Kremer Pigmente GmbH & Co. KG, DEU) were used as the comparative materials. The pigments are sold under names Naples yellow from Paris (order no. 10130), Naples yellow, dark (order no. 43125) and Naples yellow, reddish (order no. 43130).

Initial reagents Pb_3O_4 (Lachema n.p., CZE) and 99.5 % Sb_2O_3 (Bochemie s.r.o. CZE) in molar ratio Pb:Sb 1:2 were used for synthesis of PbSb_2O_6 . Homogenised reaction mixtures were placed into the alumina crucibles and heated at temperature of 600 and 850 $^{\circ}\text{C}$ in an electric muffle furnace or in a tube furnace opened to air atmosphere^{9,10}. Calcination rate of both steps was $10\text{ }^{\circ}\text{C}\cdot\text{min}^{-1}$. The details of the synthesis conditions are summarised in Table I.

Table I

Synthesis conditions of the pigments PbSb_2O_6

Sample	1 st calcination	2 nd calcination	Furnace
1.1	T=600 $^{\circ}\text{C}$ / 60 h	T=850 $^{\circ}\text{C}$ / 24 h	muffle
1.2	T=600 $^{\circ}\text{C}$ / 60 h	T=850 $^{\circ}\text{C}$ / 48 h	muffle
1.3	T=600 $^{\circ}\text{C}$ / 60 h	T=850 $^{\circ}\text{C}$ / 72 h	muffle
2.1	T=600 $^{\circ}\text{C}$ / 60 h	T=850 $^{\circ}\text{C}$ / 24 h	tube

Sample	1 st calcination	2 nd calcination	Furnace
2.2	T=600 °C / 60 h	T=850 °C / 48 h	tube
2.3	T=600 °C / 60 h	T=850 °C / 72 h	tube
3.1	T=600 °C / 12 h	T=850 °C / 24 h	tube
3.2	T=600 °C / 12 h	T=850 °C / 48 h	tube
3.3	T=600 °C / 12 h	T=850 °C / 72 h	tube

The elemental analysis was performed using a JEOL 6460 LA scanning electron microscope with an energy-dispersive X-ray detector in low-vacuum mode with a voltage of 20 kV and BSE detector. The particles of pigments were placed on a carbon tape on an aluminium stub and subsequently documented on a secondary electron (SE), under a high vacuum, at an accelerating voltage of 15 keV.

The phase composition of the samples was studied by X-ray diffraction analysis. The diffractograms of the samples were obtained by using a MiniFlex 600 (Rigaku, Japan) diffractometer working in Bragg-Brentano ($\theta/2\theta$) geometry with 1D d/teX Ultra silicon strip detector and K β filter. The data were collected within 2θ angle from 10–80 ° at a step size of 0.02 ° and a speed of 10 °C.min⁻¹ by using CuK α line. CuK α_1 ($\lambda=0.15418$ nm) radiation was used for the angular range of $2\theta < 35^\circ$, and CuK α_2 ($\lambda=0.15405$ nm) was used for the range of $2\theta > 35^\circ$. The identification of individual phases was based on the matching of the obtained diffraction patterns with the data contained in the JCPDS database.

Colour of the synthesized pigments was evaluated after their application to the organic matrix (dispersive acrylic paint Luxol, AkzoNobel). The slurry containing 1 g of the pigment and 0.5 g of the organic matrix was homogenized in an agate mortar. Coloured films were prepared by deposition of the slurries on the white non-absorbing paper. The thickness of the wet film was 100 μm . The colour properties of the films were objectively evaluated by measuring the spectral reflectance by using a spectrophotometer Ultra Scan VIS (HunterLab, USA). The measurement conditions were as follows: an Illuminant D65 and measuring geometry d/8°. For description of colour, the CIE L*a*b* colour space (also referred as CIELAB) was used¹¹. Parameter of chroma was calculated according to formula $C = (a^{*2} + b^{*2})^{1/2}$.

Discussion and results analysis

Characterization of the commercially available samples of the Naples yellow is given in Table II. Although, the chemical composition announced by the manufacturer is Pb(SbSn)O₃, Pb₂Sb₂O₇ and Pb₃(SbO₄)₂, also other elements were detected by EDS analysis. The results of X-ray diffraction analysis confirmed multiple phase compositions of all samples, including the presence of unidentified phases. This demonstrates a complicated situation when it comes to comparing the phase composition and colour parameters of the commercial pigments of Naples yellow with pigments used in art or with the synthesized pigments of Pb₂Sb₂O₇.

Table II

Chemical characterization of the commercially available Naples yellow pigments

Order no.	Chemical composition	EDS analysis [wt. %]							
		Al ₂ O	SiO ₂	ZnO	SnO ₂	Sb ₂ O ₃	CeO ₂	PbO	Total
10130	Pb(SbSn)O ₃	3.36	0	17.62	0.72	35.26	0	43.04	100
43125	Pb ₂ Sb ₂ O ₇	9.07	0	0	0	28.52	0	62.41	100
43130	Pb ₃ (SbO ₄) ₂	3.48	32.4	0	0	14.51	3.47	46.13	100

The synthesis of Pb₂Sb₂O₇ pigments did not produce a single-phase composition at any calcining temperature. In almost all cases, the cubic structure of Pb₂Sb₂O₇ was detected as the main phase, producing mainly the bindheimite, but also oxyplumboromeite phase. The increase of the calcining temperature supports the formation of the bindheimite phase, which is reflected in the increasing intensities of the diffraction lines. The sample (1.8:2) prepared by calcination at 800 °C did not contain the bindheimite phase, but next to oxyplumboromeite, also Pb₂Sb₂O₇ in its orthorhombic structure was detected by XRD analysis (Table III). Flux agent NaCl caused formation of sodium antimony oxides in several stoichiometric ratios. A lower molar ration of Pb:Sb than 2:2 is associated with the formation of the next phase, which is rosiite (PbSb₂O₆). The intensities of the diffraction lines of rosiite decrease with the increasing temperature. In addition, the diffraction lines with very low intensities that can be associated to the presence of lead oxide and antimony oxide were detected in all samples.

Table III

Main phases detected in the samples $\text{Pb}_2\text{Sb}_2\text{O}_7$

Molar ratio Pb:Sb	Temperature [°C]		
	800	850	900
2:2	$\text{Pb}_2\text{Sb}_2\text{O}_7$ (B+Oxy); $\text{Na}_2\text{Sb}_4\text{O}_7$; NaSb_5O_8 ;	$\text{Pb}_2\text{Sb}_2\text{O}_7$ (B+Oxy); $\text{Na}_2\text{Sb}_4\text{O}_7$;	$\text{Pb}_2\text{Sb}_2\text{O}_7$ (B+Oxy); $\text{Na}_2\text{Sb}_4\text{O}_7$;
1.9:2	$\text{Pb}_2\text{Sb}_2\text{O}_7$ (Oxy); PbSb_2O_6 ; $\text{Na}_4\text{Sb}_4\text{O}_7$;	$\text{Pb}_2\text{Sb}_2\text{O}_7$ (B+Oxy); PbSb_2O_6 ; $\text{Na}_2\text{Sb}_4\text{O}_7$; NaSbO_3 ;	$\text{Pb}_2\text{Sb}_2\text{O}_7$ (B+Oxy); PbSb_2O_6 ; $\text{Na}_2\text{Sb}_4\text{O}_7$;
1.8:2	$\text{Pb}_2\text{Sb}_2\text{O}_7$ (Oxy+ Orth); $\text{Na}_2\text{Sb}_4\text{O}_7$;	$\text{Pb}_2\text{Sb}_2\text{O}_7$ (B+Oxy); PbSb_2O_6 ; $\text{NaSb}_5\text{O}_{13}$;	$\text{Pb}_2\text{Sb}_2\text{O}_7$ (B+Oxy); PbSb_2O_6 ; $\text{Na}_2\text{Sb}_4\text{O}_7$;

* B = bindheimite; Oxy = oxylumboromeite; Orth = orthorhombic structure

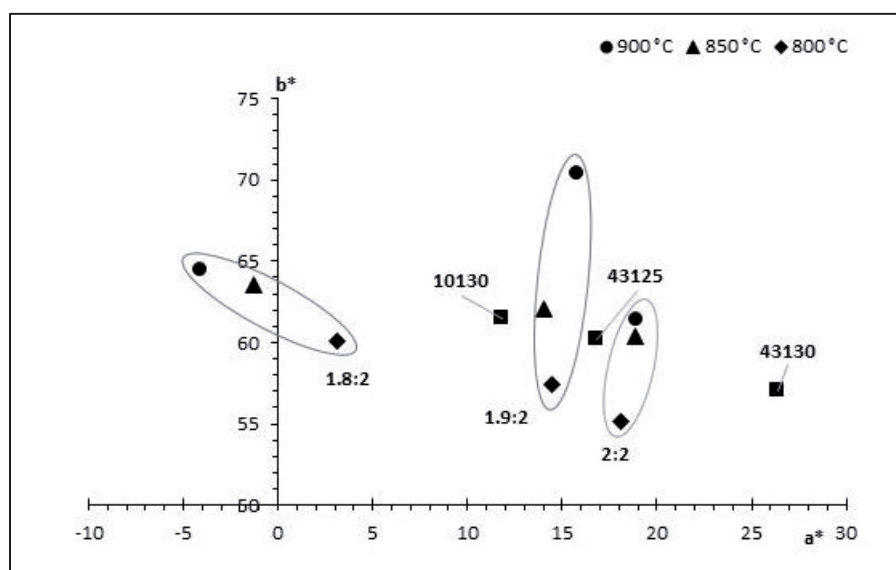
Although the elemental composition of the commercial samples of the Naples yellow is not in an agreement with the synthesised ones, their colour parameters were compared (Table IV, Figure 1). Elemental composition of the commercial samples of the Naples yellow does not affect values of chroma C, that varies between 62.5 to 62.8. Though the values of chroma are comparable, the bigger differences between parameters describing colour hues of the samples are visible in Figure 1. The Naples yellow no. 43130 contains the highest amount of red hue, its colour can be defined as reddish orange. This sample also has the lowest value of the b^* coordinate, expressing amount of yellow hue and the lowest value of lightness. The Naples yellows no. 43125 and no. 10130 have nearly the same lightness, chroma and the amount of yellow hue, the difference being the amount of red hue. Yellow pigments $\text{Pb}_2\text{Sb}_2\text{O}_7$ with similar colour parameters to the Naples yellow no. 43125 were synthesised at temperatures of 850 °C and 900 °C, mainly in the molar ratio of Pb:Sb 2:2. The lower molar ratios of Pb:Sb led to the formation of the powders with less red hue and higher lightness. This means that the samples are lighter, which may be due to phase composition, in particular the presence of the rosiate phase PbSb_2O_6 .

Table IV

Colour parameters of the commercial samples of the Naples yellow and synthesised $\text{Pb}_2\text{Sb}_2\text{O}_7$

Sample	800 [°C]		850 [°C]		900 [°C]	
	L^*	C	L^*	C	L^*	C
2:2	75.9	58.0	76.0	63.2	74.7	64.2
1.9:2	78.9	59.3	79.2	63.6	79.1	72.1
1.8:2	85.9	60.2	88.0	63.5	89.2	64.5

Sample	L^*a^*	C
10130	75.1	62.62
43125	75.4	62.54
43130	65.9	62.82

Figure 1. a^*b^* diagram of the samples $\text{Pb}_2\text{Sb}_2\text{O}_7$ and the commercial samples of Naples yellow.

Synthesis of the second type of mixed lead antimony oxide PbSb_2O_6 led to the formation of multi-phase products at all reaction conditions. The differences in phase composition of the prepared samples were already evident in their subjective observations, as the samples differed significantly from one another not only in colour, but also in the fineness of the powdered grains. Colour of the powders varied between light yellow to white. The samples with the finest particle size distribution were obtained by synthesis in the tube furnace in the case of samples no. 2.1-2.3. Only these samples contain one of the minority phases consisting of cubic $\text{Pb}_2\text{Sb}_2\text{O}_7$ in oxyplumboromeite modification, next to the main PbSb_2O_6 rosiate phase (Table V). Colour of the samples of no. 2.1-2.3 is the light yellow, which is also caused by the presence of cubic $\text{Pb}_2\text{Sb}_2\text{O}_7$. The darkest sample no. 2.1 ($L^* = 87.1$) was obtained by calcination in the tube furnace at 600 °C for 60 hours and consequently at 850 °C for 24 hours. Extending the calcining time at temperature of 850 °C from 24 hours to 48 and then up to 72 hours promotes the formation of rosiate and reduces the amount of produced $\text{Pb}_2\text{Sb}_2\text{O}_7$. This fact is visible also in Table V in the decreasing character of the values of colour parameter b^* , which expresses amount of yellow hue in final colouration. On the other hand, an increasing amount of rosiate phase raises of lightness of the samples. The same calcination conditions, but implemented in the muffle furnace, led to the formation of the desired rosiate phase, as the main phase, and in addition lead and antimony oxides were detected alongside it in the samples no. 1.1-1.3. Light yellow resultant colour is composed from yellow and green colour hues. The colour parameter a^* in negative values expresses amount of green colour hue and its value increases with calcination time at temperature of 850 °C. Amount of yellow colour hue can be considered as constant as well as chroma of the colour.

The best results were obtained by calcination of the reaction mixture containing Pb_3O_4 and Sb_2O_3 in the tube furnace for 12 hours at temperature of 600 °C and consequently at temperature of 850 °C. The pale yellow powder was obtained after a second calcination at 850°C and a duration time of 24 hours only. The major diffraction lines of PbSb_2O_6 and minor phases of PbO_2 and SbO_2 were detected in the sample 3.1. Longer calcination at 850 °C supported the reaction between lead and antimony oxides. Intensities of the diffraction lines of rosiate were higher and intensities of lead oxide and antimony oxide were very weak after calcination longer than 24 hours at temperature of 850 °C. The intensity of the PbO diffraction lines in sample 3.3 is at the noise limit. The change in the relative ratio of the individual phases detected in the samples 3.2 and 3.3 was also reflected by the change in their colour parameters. The amount of yellow hue and thus the values of the parameter b^* have decreased, as well as the value of chroma C. Resultant colour of the samples 3.2 and 3.3 is white with the high value of lightness L^* (Table V).

Table V

Main phases detected in the samples PbSb_2O_6 and their colour parameters.

Sample	Detected phases	L^*	a^*	b^*	C
1.1	PbSb_2O_6 (R); Sb_2O_4 , Pb_3O_4	90.23	-0.5	26.0	26.0
1.2	PbSb_2O_6 (R); PbO ; Sb_2O_4 ,	91.22	-2.5	26.5	26.6
1.3	PbSb_2O_6 (R); Sb_2O_4 ,	91.95	-3.3	25.4	25.6
2.1	PbSb_2O_6 (R); Sb_2O_5 ; $\text{Pb}_2\text{Sb}_2\text{O}_7$ (Oxy); Pb_3O_4	87.1	0.6	39.7	39.7
2.2	PbSb_2O_6 (R); $\text{P}_2\text{Sb}_2\text{O}_7$ (Oxy); PbO_2 ; Sb_2O_4	91.4	-3.3	26.4	26.6
2.3	PbSb_2O_6 (R); $\text{P}_2\text{Sb}_2\text{O}_7$ (Oxy); PbO_2 ; Sb_2O_4	92.2	-3.4	22.2	22.4
3.1	PbSb_2O_6 (R); PbO_2 ; SbO_2	87.1	-0.1	30.8	30.8
3.2	PbSb_2O_6 (R); Sb_6O_{13} ; PbO_2	92.1	-1.0	9.0	9.0
3.3	PbSb_2O_6 (R), PbO	92.6	-1.0	8.5	8.6

* R = rosiate; Oxy = oxyplumboromeite

Conclusion

The submitted work deals with the synthesis and characterization of the historical pigment known as the Naples yellow, whose composition is described by the formula $\text{Pb}_2\text{Sb}_2\text{O}_7$. The composition of the Naples yellow is highly complicated and heavily dependent on reaction conditions, which also affect its colour properties. In addition, commercially available samples of the Naples yellow contain other metal than the expected lead and antimony and therefore their use to identify the pigments used in fine art is very problematic.

$\text{Pb}_2\text{Sb}_2\text{O}_7$ in the modification of bindheimite and PbSb_2O_6 in the modification of rosiate are compounds which are the most often identified in phase composition of Naples yellow. Intensive yellow colour of $\text{Pb}_2\text{Sb}_2\text{O}_7$ is strongly affected by molar ration of Pb:Sb and by calcining conditions. The yellow pigment with the highest value of coordinate b^* is possible to prepare by calcination in two steps at temperature of 900 °C from the reaction mixture containing PbO and Sb_2O_3 in the molar ratio of Pb:Sb = 1.9:2 and 10 wt % of NaCl. The best result from

the point of phase composition is synthesis of the three-phase sample which contains $\text{Pb}_2\text{Sb}_2\text{O}_7$ in bindheimite and oxyplumboromeite modification and $\text{Na}_2\text{Sb}_4\text{O}_7$. This sample was prepared in molar ratio of Pb:Sb 2:2 and two calcination at 850 or 900 °C. Single phase powder of $\text{Pb}_2\text{Sb}_2\text{O}_7$ was not prepared at all.

White pigment PbSb_2O_6 were successfully synthesized by solid state reaction with calcination in the tube furnace in two steps. The first step of calcination was at temperature of 600 °C for 12 hours and the second calcination at the temperature of 850 °C for 72 hours. This calcination conditions lead to the formation of the rosiaite modification of PbSb_2O_6 with the presence of the PbO minor phase whose diffraction lines are at the noise limit of the equipment. The colour parameters of this sample are $L^*/a^*/b^* = 92.6/-1.0/8.5$.

Acknowledgement

This research has been supported by the programme of the Ministry of the Interior of the Czech Republic: Strategic Support for the Development of Security Research of the Czech Republic ČR 2021–2025 (IMPAKT 1), grant project: The Development of a Strategic Cluster for Effective Instrumental Technological Methods of Forensic Authentication of Modern Artworks, identification code VJ01010004.

References

- 1 Rosi F., Manuali V., Miliani C., Brunetti B. G., Sgamellotti A., Grygar T., Hradil D.: *J. Raman Spectrosc.*, **40**, 107 (2009).
- 2 Rosi F., Manuali V., Grygar T., Bezdička P., Brunetti B.G., Sgamellotti A., Burgio L., Seccaroni C., Miliani C.: *J. Raman. Spectrosc.*, **42**, 407 (2011).
- 3 Dik J., Hermens E.: *Archaeometry* **47**, 593 (2005).
- 4 Hradil D., Grygar T., Hradilová J., Bezdička P., Grúnwaldová V., Fogaš I., Miliani C.: *J. Cult. Herit.*, **8**, 377 (2007).
- 5 Feller R. L.: *Artists' Pigments: A Handbook of their History and Characteristics*, National Gallery of Art, Washington, 1986.
- 6 Eastaugh N., Walsh V., Chaplin T., Siddall R.: *Pigment Compendium: A Dictionary and Optical Microscopy of Historical Pigments*, Routledge, New York, 2013.
- 7 Pelosi C., Agresti G., Santamaria U., Mattei E.: *e-PS.*, **7**, 108 (2010).
- 8 Agresti G., Baraldi P., Pelosi C., Santamaria U., *Color Res. Appl.*, **41**, 226 (2016).
- 9 Zhang K.L., Lin X.P., Huang F.Q., Wang W.D.: *J. Mol. Catal. A Chem.* **258**, (2006) 185
- 10 Roper A. J., Leverett P., Murphy T. D., Williams P. A.: *Mineral. Mag.*, **79**, (2015) 537.
11. *Commission Internationale de l'Eclairage*, "Recommendations on uniform colour spaces, colour difference equations, psychometric colour terms", Supplement No.2 of CIE publication No. 15 (E1-1,31) 1971, Paris Bureau Central de la CIE, 1978.